Structure, Stability and Functioning of Food Webs

Kumulative Habilitationsschrift

vorgelegt der

Mathematisch-Naturwissenschaftlichen Fakultät der Universität Potsdam

von

Dr. Christian Guill

Dezember 2021

Summary

In this thesis, a collection of studies is presented that advance research on complex food webs in several directions. Food webs, as the networks of predator-prey interactions in ecosystems, are responsible for distributing the resources every organism needs to stay alive. They are thus central to our understanding of the mechanisms that support biodiversity, which in the face of increasing severity of anthropogenic global change and accelerated species loss is of highest importance, not least for our own well-being.

The studies in the first part of the thesis are concerned with general mechanisms that determine the structure and stability (in terms of persisting species) of food webs. It is shown in detail how the allometric scaling of metabolic rates with the species' body masses supports their persistence in size-structured food webs (where predators are larger than their prey), and how this interacts with the adaptive adjustment of foraging efforts by consumer species to create stable food webs that allow a large number of species to coexist. The importance of body mass as a master trait that is vital for structuring communities is further exemplified by demonstrating that the specific way the body masses of species engaging in empirically documented predator-prey interactions affect the predator's feeding rate dampens population oscillations, thereby helping both species to survive. In the first part of the thesis it is also shown that in order to understand certain dynamical phenomena observed in natural or experimental populations, e.g. a particular type of population oscillations, it is sometimes necessary to not only take the interactions of a focal species with other species (predators or resources) into account, but to also consider the internal structure of the population. This can refer for example to different abundances of age cohorts or developmental stages, or the way individuals of different age or stage interact with other species.

Building on these general insights, the second part of the thesis is devoted to exploring the consequences of anthropogenic global change on the persistence of species. The studies focus on warming, eutrophication and habitat change as three particularly important anthropogenic stressors on ecological communities. It is shown that warming decreases diversity in size-structured food webs. This is due to starvation of large predators on higher trophic levels, which suffer from a mismatch between their respiration rate and their maximum ingestion rate when temperature increases. In networks with a rather flat size structure, as in host-parasitoid networks, warming does not have these negative effects, but eutrophication destabilises the systems by inducing detrimental population oscillations. The studies on habitat change focus on the effects of increasing habitat isolation, i.e., the increasing distances between habitable patches embedded in an otherwise inhospitable landscape matrix. On the level of individual patches, increasing isolation has a similar effect as warming, as it leads to decreasing diversity due to the extinction of predators on higher trophic levels. In this case it is caused by the increasing dispersal mortality especially smaller (and therefore less mobile) species suffer when isolation increases. As a consequence, a higher fraction of their biomass production is lost to the inhospitable matrix surrounding the habitat patches and cannot be used as resources for the larger species. It is further shown that increasing habitat isolation desynchronises population oscillations between the patches, which in itself should help species to persist by dampening fluctuations on the landscape level. However, this is counteracted by an increasing strength of local population oscillations fueled by an indirect effect of dispersal mortality on the feeding interactions. Last, a study is

presented that introduces a novel mechanism for supporting diversity in metacommunities. It builds on the self-organised formation of spatial biomass patterns in the landscape, which leads to the emergence of spatially heterogeneous and temporally varying selection pressures that keep local communities permanently out of equilibrium and force them to continuously adapt. Because this mechanism relies on the spatial extension of the metacommunity, it is also sensitive to habitat change.

In the third part of the thesis, the consequences of biodiversity for the functioning of ecosystems are explored. The studies focus on standing stock biomass, biomass production, and trophic transfer efficiency as ecosystem functions. It is first shown that increasing the diversity of animal communities increases the total rate of intra-guild predation. However, the total biomass stock of the animal communities increases nevertheless, which also increases their exploitative pressure on the underlying plant communities. Despite this, the plant communities can maintain their standing stock biomass due to a shift of the body size spectra of both animal and plant communities towards larger species with a lower specific respiration rate. In another study it is further demonstrated that the generally positive relationship between diversity and the above mentioned ecosystem functions becomes steeper when not only the feeding interactions but also the numerous non-trophic interactions (like predator interference or competition for space) between the species of an ecosystem are taken into account. Finally, two studies are presented that demonstrate the power of an approach that does not build on taxonomic diversity (i.e., species richness) as the main explanatory variable, but on functional diversity. The latter is interpreted as the range spanned by functional traits of the species that determine their interactions. This approach allows to mechanistically understand how the ecosystem functioning of food webs with multiple trophic levels is affected by all parts of the food web and why a high functional diversity is required for efficient transportation of energy from primary producers to the top predators.

The general discussion draws some synthesising conclusions, e.g. on the predictive power of ecosystem functioning to explain diversity, and provides an outlook on future research directions.

Zusammenfassung

In dieser Habilitationsschrift wird eine Zusammenstellung wissenschaftlicher Arbeiten präsentiert, die die Forschung zu komplexen Nahrungsnetzen in verschiedene Richtungen weiterentwickeln. Nahrungsnetze sind die Netzwerke der Räuber-Beute-Interaktionen in einem Ökosystem und bestimmen damit über die Verteilung der von allen Arten zum Überleben benötigten Ressourcen. Sie sind daher ein zentrales Konzept für das Durchdringen der Mechanismen, die die stabile Koexistenz einer Vielzahl von Arten ermöglichen. Angesichts der zunehmenden Intensität des anthropogenen globalen Wandels und sich weiter beschleunigendem Artensterben ist ein solches Verständnis von zentraler Bedeutung, nicht zuletzt auch für das menschliche Wohlergehen.

Die Studien im ersten Teil der Habilitationsschrift befassen sich mit generellen Mechanismen, die die Struktur und Stabilität (gemessen an der Zahl persistenter Arten) von Nahrungsnetzen bestimmen. Es wird im Detail gezeigt, wie die allometrische Skalierung metabolischer Raten mit der Körpermasse der Individuen ihre Persistenz in größenstrukturierten Nahrungsnetzen (d.h. solchen, in denen Räuber signifikant größer sind als ihre Beutearten) unterstützt, und wie dies mit dem adaptiven Jagdverhalten von Räubern interagiert. Diese Interaktion erzeugt stabile Nahrungsnetzstrukturen, die die Koexistenz einer Vielzahl von Arten ermöglicht. Die Bedeutung der Körpermasse als ein physiologisches Merkmal, das die Struktur von Nahrungsnetzen mitbestimmt, wird auch dadurch gezeigt, dass die spezifische Art und Weise, wie die Körpermassen empirisch dokumentierter Räuber-Beute-Paare die Stärke der Fraßinteraktion beeinflusst, auftretende Populationsoszillationen abschwächt und damit das Überleben beider Arten ermöglicht. Es wird ferner gezeigt, dass es zum Verständnis bestimmter populationsdynamischer Phänomene, die in einer natürlichen oder experimentellen Population beobachtet wurden, notwendig sein kann, nicht nur die Interaktionen mit anderen Arten (Räubern oder Beuten) zu berücksichtigen, sondern auch die interne Struktur der betrachteten Population. Dies kann sich zum Beispiel auf die Größe von Alterskohorten beziehen oder darauf, wie Individuen unterschiedlichen Alters oder Entwicklungsstandes mit anderen Arten interagieren.

Auf diesen allgemeinen Erkenntnissen aufbauend werden im zweiten Teil der Habilitationsschrift Studien vorgestellt, die sich direkt mit den Auswirkungen von anthropogenem globalem Wandel auf die Persistenz von Arten befassen. Die Studien konzentrieren sich auf Erwärmung, Eutrophierung und Habitatveränderung, da diese Stressfaktoren im Allgemeinen besonders starke Auswirkungen auf ökologische Gemeinschaften haben. Erwärmung reduziert die Diversität in größenstrukturierten Nahrungsnetzen, indem sie zum Aussterben großer Räuberarten führt. Dies geschieht dadurch, dass die Respirationsrate wechselwarmer Tiere bei Erwärmung schneller ansteigt als ihre maximale Fraßrate, wodurch insbesondere große Arten ihren Energiebedarf nicht mehr decken können. In Netzwerken mit eher flacher Größenstruktur, wie z.B. Parasitoid-Wirt-Netzwerken, hat Erwärmung keinen derartigen negativen Effekt, allerdings führt Eutrophierung dort durch die Induktion starker Populationsoszillationen zu Destabilisierung und Artensterben.

Die Studien zum Thema Habitatveränderung konzentrieren sich auf die Auswirkungen zunehmender Habitatisolation. Damit ist der Effekt gemeint, dass in zunehmend anthropogen überformten Landschaften die Abstände zwischen hinreichend naturbelassenen Habitatflecken immer größer werden. In den einzelnen Habitatflecken führt zunehmende Isolation, ähnlich wie Erwärmung, zu einem Rückgang der Diversität aufgrund des Aussterbens von vorrangig großen

Räuberarten. In diesem Fall wird das durch die Zunahme der Mortalität kleinerer (und daher weniger mobiler) Arten bei der Wanderung zwischen entfernten Habitatflecken verursacht, welche dazu führt, dass ein immer größerer Anteil der Biomassenproduktion der kleineren Arten an die lebensfeindliche Matrix zwischen den Habitatflecken verloren geht, statt den größeren Räubern als Nahrung zur Verfügung zu stehen. Es wird weiterhin gezeigt, dass zunehmende Isolation zur Desynchronisierung von Populationsoszillationen zwischen den einzelnen Habitatflecken führt, was die Stärke der Oszillationen über die gesamte Landschaft gemittelt verringert und somit das Überleben der Arten erleichtern sollte. Allerdings führt die Zunahme der Wanderungsmortalität aufgrund eines indirekten Effektes auf die Fraßraten in den Habitatflecken zu einer Verstärkung der lokalen Populationsoszillationen, was den positiven Effekt der Desynchronisierung ausgleicht. Zuletzt wird in diesem Abschnitt ein neuartiger Mechanismus vorgestellt, der die Diversität in Meta-Gemeinschaften unterstützen kann. Er basiert auf selbstorganisierter Bildung räumlicher Muster in der Biomassenverteilung der Arten. Diese Muster erzeugen räumlich heterogene und zeitlich fluktuierende Selektionsdrücke, die die lokalen Artengemeinschaften in einem permanenten Nichtgleichgewichtszustand halten und dazu zwingen, sich ständig neu anzupassen. Da dieser Mechanismus auf der räumlichen Ausdehnung der Metagemeinschaften basiert, kann er ebenfalls empfindlich auf Habitatveränderungen reagieren.

Im dritten Teil der Habilitationsschrift werden die Effekte von Biodiversität auf Ökosystemfunktionen untersucht. Die entsprechenden Studien beziehen sich dabei vor allem auf den Biomassenbestand, die Produktionsrate von Biomasse sowie die trophische Transfereffizienz. Es wird zunächst gezeigt, dass zunehmende Diversität von Tiergemeinschaften die totale Rate intragilder Prädation (also des Fraßes innerhalb der Tiergemeinschaften) erhöht. Dennoch erhöht sich der Biomassenbestand der Tiergemeinschaften, wodurch ihr Fraßdruck auf die zugrundeliegenden Pflanzengemeinschaften zunimmt. Dessen ungeachtet können die Pflanzengemeinschaften ihren Biomassenbestand halten, was durch eine Verschiebung der Größenspektren von Pflanzen- und Tiergemeinschaften hin zu größeren Arten mit geringer spezifischer Respirationsrate ermöglicht wird. In einer weiteren Studie wird gezeigt, dass der im Allgemeinen positive Zusammenhang zwischen Biodiversität und den genannten Ökosystemfunktionen verstärkt wird, wenn neben den Fraßbeziehungen der Arten auch die zahlreichen weiteren Interaktionsmöglichkeiten der Arten (wie zum Beispiel Flächenkonkurrenz sessiler Arten) berücksichtigt werden. Abschließend werden zwei Studien präsentiert, die die Leistungsfähigkeit eines Ansatzes, der nicht auf der taxonomischen Diversität (also der Artenzahl) eines Systems basiert, sondern auf funktioneller Diversität. Letztere wird interpretiert als der Wertebereich, den funktionelle Merkmale, die die Interaktionen der Arten bestimmen, überspannen. Dieser Ansatz erlaubt es, mechanistisch nachzuvollziehen, wie die ökologischen Funktionen von Nahrungsnetzen von den einzelnen Teilen der Netzwerke beeinflusst werden, und warum eine hohe funktionelle Diversität für den effizienten Transport der Biomasse von den Primärproduzenten zu den Räubern an der Spitze der Nahrungskette notwendig ist.

In der allgemeinen Diskussion werden einige zusammenfassende Schlussfolgerungen gezogen, die zum Beispiel die Vorhersagekraft von Ökosystemfunktionen zum Erklären der Diversität betreffen, und es wird ein Ausblick auf künftige Forschungsansätze gegeben.

Contents

Chapter 1

Introduction

1.1 Modelling food webs

Ecology, as the scientific discipline devoted to the study of organisms and their interactions among each other and with their environment, is characterised by a remarkable degree of complexity that pervades every organisational level of the systems under consideration, from single organisms to the entire ecosphere. Insights in the factors determining the growth of populations or the coexistence of species in an ecological community are being gained first and foremost by observation and experiments. However, since its beginnings ecology as a discipline has also greatly benefited from theoretical considerations and mathematical modelling, which help to conceptualise ideas and reduce complexity by focusing on processes deemed most relevant for explaining a certain phenomenon.

Early examples of this are the works of Lotka (1925, 1932) and Volterra (1928), who independently developed mathematical models to describe predation and competition. With these models of two fundamental types of interactions they aimed at explaining the periodic changes in abundance observed in some animal populations and at establishing conditions that allow competitors of a single resource to coexist. At about the same time, Elton (1927) advanced the concepts of food chains and especially food webs as the network of all feeding interactions among the species of a biocoenosis, thereby bringing the need for understanding the dynamics of interacting populations and the conditions for their coexistence to a new level of complexity. Based upon empirical observation and phenomenological arguments, for several decades the consensus among ecologist was that complexity (in terms of number of species or interactions among them) would increase the stability of these systems. Stability could here either refer to the ability of communities to withstand invasions, or to the ability to dampen population oscillations following a perturbation (Odum, 1953; MacArthur, 1955; Elton, 1958). However, a rigorous mathematical proof of the assumed relation between food web-complexity and stability was not provided.

Linear stability analysis of multi-species predator-prey systems with generalised Lotka-Volterra dynamics (May, 1971) as well as numerical and analytical considerations of abstract random matrices (Gardener and Ashby, 1970; May, 1972) challenged the view that complexity begets stability by demonstrating that in fact both increasing the number of species or the number
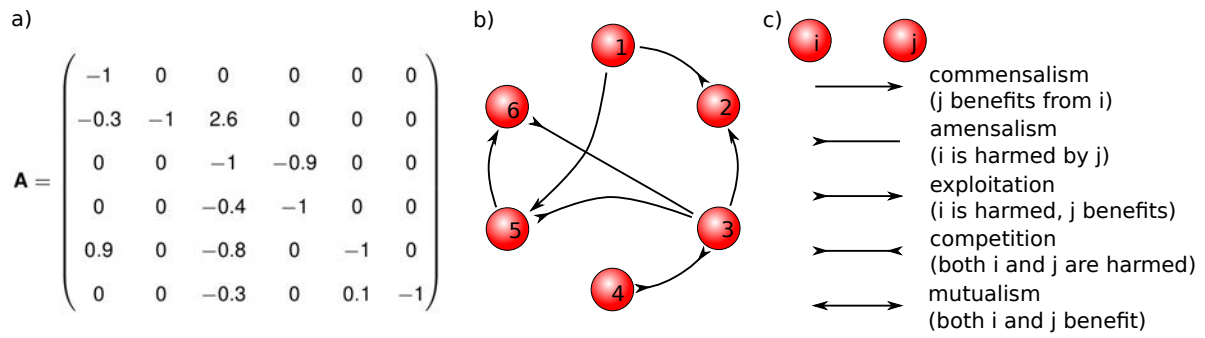
Figure 1.1: a) Example of a so called *community matrix* with random elements as in (May, 1972), with number of species $S = 6$, connectance $C = 0.2$ and mean squared interaction strength $\alpha = 1$, b) the corresponding graph of the random network, and c) an explanation of the types of ecological interactions encoded by the different arrow types. In the example shown, only commensalistic, amensalistic, and competitive interactions occur. The element a_{ij} in row i, column j of the community matrix $\mathbf{A}$ quantifies the effect species j has on species i at an equilibrium point of the population dynamics. The elements of $\mathbf{A}$ have a non-zero value with probability C. The actual value is drawn from a probability distribution with mean zero and mean square value α. The diagonal elements are set to -1 to account for self-dampening of the populations. Since by construction, the modelled systems do not only contain trophic (predator-prey or host-parasitoid) interactions, which would be characterised by pairs of non-zero matrix elements a_{ij} and a_{ji} with opposite sign, they do not represent food webs, but general ecological networks.

of interactions will actually destabilise the systems. In these studies, stability always referred to the linear stability of the population dynamics, i.e., it was measured how likely it was that the interacting populations approach a stable equilibrium instead of exhibiting oscillations. Especially the study by May (1972) proved hugely influential, as it covered ecological networks of arbitrary size and included as a testable prediction the result that ecological networks are *almost certainly* unstable if

$$\alpha\sqrt{S \cdot C} > 1 \, . \tag{1.1}$$

In this formula, S is the number of species, $C = L/S^2$ is the connectance (with L the number of interactions), and α is the mean square value of the interaction strengths. (More details on the methodology can be found in Fig. 1.1.) The study was particularly influential because its main result was generally interpreted not to mean that natural communities are either not complex or not stable, but that they must possess previously ignored or unknown properties that set them apart from the random networks studied by Gardener and Ashby (1970) and May (1972).

An important step forward was made by Yodzis (1981), who showed that when community matrices were parameterised using empirical food web data, the systems were far more likely to be stable than their random counterparts. Later, this was shown to be caused by the negative correlation of the values of pairs of elements, a_{ij} and a_{ji}, of the empirical community matrices representing food webs (Allesina and Tang, 2012). Empirical food webs (Briand, 1983) were also analysed regarding their general topological characteristics (throughout this thesis, *topology* refers to the binary network structure, i.e., only presence or absence of links are considered, but not the strength of interactions or the abundance of species). Certain scale-invariant properties

like the fraction of top species (which have no predator) or the fraction of basal species (which have no prey) were found (Briand and Cohen, 1984). Especially noteworthy is the so-called link-species scaling, i.e., the finding that in these early empirical food webs the total number of trophic links was proportional to the number of species. As this meant that in empirical food webs the connectance decreases with species number as $C \sim 1/S$, this seemed to provide an elegant way to avoid the destabilisation of larger food webs predicted by May's (1972) results (Eq. (1.1), see also (Cohen and Newman, 1985)). However, this was soon overturned, as larger and better resolved empirical food webs became available and it was shown that the number of trophic links increases faster than the number of species (Martinez, 1992; Riede *et al.*, 2010). Instead, it was shown that the stability of food webs is not determined by the pure number of interactions, but that it is intricately linked to the non-random distribution of interaction strengths in food webs (de Ruiter *et al.*, 1995; Neutel *et al.*, 2002; Rooney and McCann, 2012).

1.2 The bioenergetics approach of modelling food web dynamics

The studies discussed above mostly considered only the structure (topology) of food webs or treated population dynamics only implicitly by evaluating the linear stability of equilibrium points of the dynamics. Explicit models for the dynamics of interacting populations, formulated as systems of coupled ordinary differential equations (ODEs) in the form proposed by Lotka (1925) and Volterra (1928), where however also continuously developed. This was driven for example by the desire to understand the onset of population oscillations (Rosenzweig and MacArthur, 1963) or the transition to chaotic dynamics (Hastings and Powell, 1991).

Without aiming at explaining a certain phenomenon, Yodzis and Innes (1992) proposed an approach that ultimately proved to be highly influential. Their main goal was to develop an ecologically plausible model for consumer-resource dynamics by tying the terms that occur in the equations more explicitly to physiological processes. Within this approach, the dynamics of the biomass (i.e., population size times body mass of a typical individual) of a single species is given by

$$\frac{dB(t)}{dt} = eI - Q - L,\tag{1.2}$$

where B is the biomass, I is the total rate of ingestion, e is the fraction of ingested energy that is not excreted (such that eI is the intake rate of metabolisable energy), Q is the total respiration rate, and L is the rate of biomass loss due to other causes (mostly predation mortality). Starvation occurs when respiration, Q, surpasses the intake of metabolisable energy, eI, and new biomass is produced when the reverse is true. A population will then be at equilibrium if the rate of biomass production, $eI - Q$, equals the losses, L (Fig. 1.2).

A major advantage of the approach by Yodzis and Innes (1992) is that the actual parameters that are needed to turn Eq. (1.2) into a solvable model, like the assimilation efficiency e or the specific respiration rate $x = Q/B$, are based on the body mass and the metabolic type (e.g. vertebrate ectotherm or invertebrate) of the species or the type of resource that is ingested (animal or plant). This allowed for an easy generalisation and extension of the model, Eq. (1.2), to multi-species systems such as food webs. As an example, the corresponding differential equations
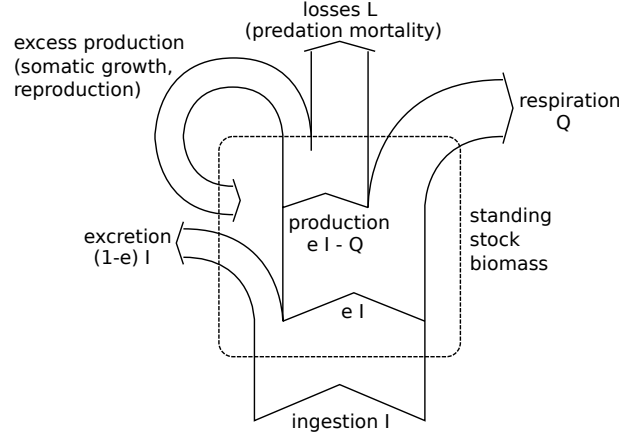
Figure 1.2: Schematic diagram of biomass flows in the bioenergetics approach of modelling biomass dynamics of a population (Yodzis and Innes, 1992). Ingested biomass is partly excreted (assimilation losses, fraction $1 - e$), and the remainder is used either for respiration (Q) or production ($eI - Q$). The latter balances mortality (e.g. by predators) and includes somatic growth and reproduction. In the example shown, the population is not at equilibrium, as losses do not equal the full production capabilities and excess production occurs, which leads to an increase in biomass. The dashed rectangle represents the standing stock biomass.

(in slightly adjusted form) used by Brose *et al.* (2006b) for describing the biomass dynamics of species in a food web are

$$\frac{dB_i(t)}{dt} = r_i(m_i) \left(1 - \frac{B_i}{K} \right) B_i - \sum_{j \in \text{ cons. of } i} x_j(m_j) y_j F_{ji}(\mathbf{B}) B_j \tag{1.3}$$

for producer species i and

$$\frac{dB_i(t)}{dt} = \sum_{j \in \text{res. of } i} e_j x_i(m_i) y_i F_{ij}(\mathbf{B}) B_i - \sum_{j \in \text{ cons. of } i} x_j(m_j) y_j F_{ji}(\mathbf{B}) B_j - x_i(m_i) B_i \tag{1.4}$$

for consumer species i. These equations are introduced in detail here as they serve as a template for most of the dynamic food web models analysed in this thesis. Here, $r_i(m_i)$ and $x_i(m_i)$ are the mass-specific maximum growth rate of producer species and the mass-specific respiration rate of consumer species, respectively. Both depend on the body mass m_i of typical individuals of the respective species in a negative quarter-power law relationship (allometric scaling, (Brown *et al.*, 2004)). The parameter y_i is maximum ingestion rate relative to the respiration rate. It does not depend on the body mass, but on the metabolic type of the consumer species (Yodzis and Innes, 1992). The assimilation efficiency e_j depends on the type (animal or plant) of resource j. The first terms on the respective right-hand sides of Eqs. (1.3) and (1.4) describe resource intake. For producer species this is modelled as logistic growth with carrying capacity K. This term already includes respiration losses. For consumer species, the first term represents feeding on other species (with functional response F_{ij}, see below). This term thus mirrors the second terms in Eqs. (1.3) and (1.4), which describe losses due to predation mortality. Finally, with the last term in Eq. (1.4) respiration losses of the consumers are explicitly accounted for.

The functional response F_{ij} describes how the realised feeding rate of consumer species i on prey species j depends on the biomass of all of its prey species as well as potentially on its own biomass. Various mathematical forms that differ in the biological processes they consider exist for this function (Volterra, 1928; Holling, 1959; Arditi and Ginzburg, 1989; Skalski and Gilliam, 2001). In (Brose *et al.*, 2006b), the following form is used:

$$F_{ij} = \frac{\omega_{ij} B_j^h}{B_0^h + \sum_{k \in \text{res. of } i} \omega_{ik} B_k^h + c_i B_0^h B_i} \, . \tag{1.5}$$

This accounts for the most important processes shaping the feeding rate: it increases monotonously with prey density B_j, but due to handling time constraints (Holling, 1959) saturates when any of the prey species k is very abundant. Via the Hill exponent h, refuge effects for the prey can be modelled, which for $h > 1$ suppress the feeding rate at low prey abundance and thereby stabilise the dynamics (Williams and Martinez, 2004; Rall *et al.*, 2008). With the parameters ω_{ij} preferences for the different prey species can be accounted for, which may be due to physiological constraints (Vucic-Pestic *et al.*, 2010; Schneider *et al.*, 2016) or attempts by the consumer to maximise its energy gains (Kondoh, 2003; Heckmann *et al.*, 2012). The parameter B_0 is called the half-saturation density and is here an inverse measure of the average attack rate of the consumer. Finally, the term proportional to the consumer biomass B_i in the denominator describes interference among the consumers, which limits their effective feeding rate at high consumer abundance and thereby also stabilises the dynamics (Beddington, 1975; DeAngelis, 1975; Rall *et al.*, 2008; Miele *et al.*, 2019).

The combination of the equations for multi-species biomass dynamics, Eqs. (1.3)–(1.5), with an algorithm for generating artificial food web topologies, is nowadays often referred to as an allometric trophic network (ATN) model (Boit *et al.*, 2012). In this thesis the flexibility of this framework is demonstrated by modifying it to account for the body mass- (Kalinkat *et al.*, 2013; Schneider *et al.*, 2016) or temperature-dependence (Binzer *et al.*, 2012, 2016) of model parameters, to turn the prey preferences ω_{ij} into dynamical variables (Heckmann *et al.*, 2012), to account for activity respiration (Kath *et al.*, 2018), or to include non-trophic interactions (Miele *et al.*, 2019). Other questions, regarding for example the internal age structure of populations (Guill *et al.*, 2014; Pfaff *et al.*, 2014) or dispersal dynamics in metacommunities (Ryser *et al.*, 2019; Stark *et al.*, 2021; Guill *et al.*, 2021) require dedicated models that are presented in detail in the respective publications.

1.3   Current developments and challenges for modelling food webs

The studies discussed in this thesis are all centred around the common theme of modelling food webs, but advance it in a number of different directions. They address the processes that shape the structure and dynamics of populations and communities, the determinants of food web stability, how (meta-)food webs respond to anthropogenic disturbances, and how characteristics of food webs in turn affect the functioning of ecosystems (Fig. 1.3).

i) Mechanistic models for
structure and stability
(1, 2, 3, 5, 8, 13)

ii) Food-web evolution (7)

iii) Adaptive and structured
populations (2, 4, 6)

iv) Anthropogenic global
change (9 - 12)

v) Metacommunity ecology
(11 - 13)

vi) Diversity-functioning
relationship (14 - 18)

vii) Non-trophic interactions (16)

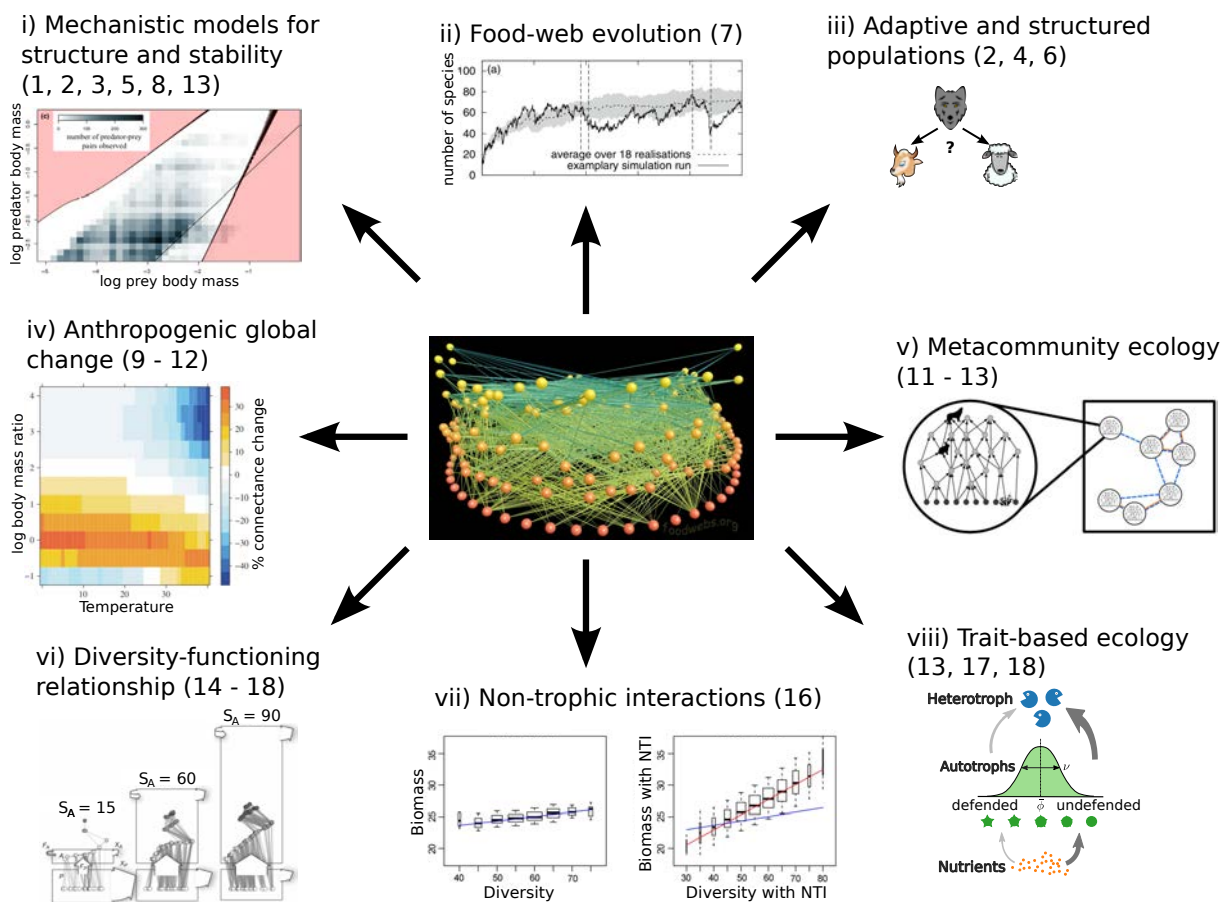viii) Trait-based ecology
(13, 17, 18)

Figure 1.3: Overview of the research topics discussed in this thesis, centred around the common theme of modelling food webs. The numbers in parentheses refer to the list of publications in chapter 2, double mentions indicate connections between the individual topics. The central panel is a depiction of the ElVerde rain forest-food web. Image produced with FoodWeb3D, written by R.J. Williams and provided by the Pacific Ecoinformatics and Computational Ecology Lab (www.foodwebs.org, (Yoon *et al.*, 2004)).

1.3.1 Structure and stability of food webs

One way of testing the ecological relevance of processes assumed to be important for determining the structure of food webs is to cast them into (stochastic) model algorithms that generate artificial food web topologies and to compare the statistical properties of these model-generated food webs with natural ones (Cohen and Newman, 1985; Williams and Martinez, 2000; Cattin *et al.*, 2004; Allesina *et al.*, 2008). A common feature of these algorithms is that they assume a more or less strict feeding hierarchy, which can be empirically motivated by the observation that predators are usually between 10 and 10000 times larger (in terms of average body mass) than their prey (Brose *et al.*, 2006a).

A mechanistic explanation for the observed predator-prey body-mass ratios is provided for example by experiments on terrestrial arthropods showing that the attack rate of predators varies

in a systematic way with the body mass of their (potential) prey (Vucic-Pestic *et al.*, 2010): attack rates are suppressed when the prey is either too small (due to increased prey agility or the presence of prey refuges that are inaccessible for the predator) or too large (because prey individuals become too fast or too strong to be effectively captured and subdued). The emerging unimodal relationship between the predator-prey body-mass ratio and the attack rate also provides an important link between the topology of the food web and the biomass dynamics of the species, as it can be included in the preference parameters in the feeding rates (ω_{ij} in Eq. (1.5)). Similarly, the body masses of the species can also be used to predict food web structures by using energetic reasoning based on the body-mass dependence of feeding rates (Petchey *et al.*, 2008).

This thesis contributes to the research on mechanistic models for dynamic food webs in general and the role of body mass in particular (Fig. 1.3i) by uncovering in detail how the allometric scaling of metabolic rates stabilises food webs (Kartascheff *et al.*, 2010), by determining how a stabilising body-mass structure emerges in a self-organised way when predators can adjust their foraging efforts (Heckmann *et al.*, 2012), and by demonstrating that the specific way in which the parameters of functional responses depend on the body masses of predator and prey supports the persistence of both species (Kalinkat *et al.*, 2013). Schneider *et al.* (2016) developed a food-web model in which both the structure of the food webs as well as the parametrisation of the dynamical equations are consistently based on empirically supported body-mass relations. This makes it a powerful and flexible modelling platform that can for example easily be extended to meta-food web scenarios (Ryser *et al.*, 2019). Furthermore, insights in the relation between the stability of the biomass dynamics in food webs and their complexity are gained by combining conventional numerical simulations of the biomass dynamics with a novel approach for determining the stability of fixed points (Plitzko *et al.*, 2012). Finally, the realism of the food-web structures generated by two variants of the widely used niche model (Williams and Martinez, 2000; Stouffer *et al.*, 2006) is tested using a method based on ordered three-species motifs (i.e., miniature sub-graphs of food webs consisting of three species that still exhibit a feeding hierarchy) (Guill and Paulau, 2016).

One of the shortcomings of the simple models for creating food web topologies like the niche or nested hierarchy model (Williams and Martinez, 2000; Cattin *et al.*, 2004) is that they do so in an ad-hoc manner and take the processes that in nature lead to the assembly of these complex systems, including their evolutionary history, only implicitly into account. That also means that the produced networks are not controlled for their stability (e.g. in terms of viability of all populations). While it is commonly made sure that all modelled consumer species have at least one resource, it is usually not possible to predict, based only on the network topology, whether a species can actually acquire enough resources to balance its losses (i.e., respiration and predation mortality). So-called evolutionary food-web models circumvent this problem by explicitly modelling the dynamical process by which complex food webs emerge (Drossel *et al.*, 2001; Loeuille and Loreau, 2005; Guill and Drossel, 2008). Starting from a single species, new species are added to the food web as variants of existing ones (speciation), which allows the model food webs to grow. By including differential equations for describing the population dynamics, species deterministically go extinct when their food intake is insufficient or the predation pressure is too high. The combination of these two processes can lead to a permanent species turnover, similarly to what is seen in natural communities. In this thesis, one such model is discussed (Fig. 1.3ii, Allhoff *et al.* (2015)), which focuses on the body mass of a species, its preferred prey

body mass and the width of its prey body mass spectrum as evolvable traits. With this setup, food webs with complex and realistic structures emerge, which nevertheless allow for continuous species turnover. This demonstrates again the importance body mass has for both the structure and dynamics of food webs.

Yet another perspective on the determinants of the dynamics of populations and the stability of communities is taken by studies that consider the internal structure of populations, e.g. in terms of age, size, developmental stage, phenotype or behavioural types (Fig. 1.3iii). The models discussed so far ignore the internal structure of populations, which is justified when the differences between the individuals of one population do not significantly affect the way they interact with other populations. In the bioenergetics framework it is, after all, not relevant whether the total biomass of a population increases due to the production of new individuals or due to somatic growth of existing individuals (Fig. 1.2). However, often the physiological or phenotypical differences between the individuals of a population are in fact quite significant: individuals may grow over several orders of magnitude in body mass and/or change their habitat during their ontogenetic development, with corresponding consequences for the range of prey, competitor, and predator species they interact with (Werner and Gilliam, 1984; Gaston *et al.*, 1997). Furthermore, individuals of a population may also pursue different foraging (Agrawal, 2001) or defence strategies (Yamamichi *et al.*, 2018) and adjust them adaptively, which not only increases the mean fitness of the populations, but also helps to stabilise the communities they are embedded in (Kondoh, 2003; Uchida and Drossel, 2007).

In this thesis, three different approaches for modelling the internal structure of populations are considered. In (Heckmann *et al.*, 2012), predators species can adapt their foraging efforts for their different prey species[1]. It is shown that the stabilising effect this has on food webs (e.g. in terms of persisting species) interacts with the stabilising effect of allometrically scaled metabolic rates by strengthening the size structure of the food webs. In (Guill *et al.*, 2014), the distinct 4-year oscillations in the abundances of certain populations of the Pacific sockeye salmon (*Oncorhynchus nerka*) are analysed. It is shown that this unique dynamic phenomenon can be explained by a model that takes the semelparous life cycle of the salmon (i.e., they reproduce only once before they die) and especially the predator-prey interactions in the food web of the nursery lakes of the salmon fry into account. Last, in (Pfaff *et al.*, 2014) a generic model of a single population with continuous age-structure (meaning that adult individuals continuously reproduce and that newborn individuals mature to adults after a fixed time span) is analysed with respect to different patterns of population oscillations that have been observed in this type of model.

1.3.2 Food webs under anthropogenic disturbances

Biodiversity is declining at unprecedented rates (Barnosky *et al.*, 2011; Pimm *et al.*, 2014), caused both directly and indirectly by human activities (Duraiappah *et al.*, 2005). Three of the most important anthropogenic stressors on ecosystems are warming, eutrophication, and habitat degradation (with the latter subsuming destruction and fragmentation of habitats). Warming directly affects many biological rates such as respiration, growth and feeding (Gillooly *et al.*,

---

[1]Note that these foraging efforts or strategies can be interpreted as variable fractions of individuals of a predator species that specialise on a given prey species.

2001; Brown *et al.*, 2004). As the maximum ingestion rate tends to increase not as strongly with temperature as the respiration rate (Rall *et al.*, 2012), one direct consequence of warming is that consumers may starve even in the presence of abundant resources, simply because they become too inefficient in using ingested energy. The direct effect of eutrophication (or enrichment) has also long been studied. While it has positive effects on the maximal potential biomass of producers, increasing eutrophication eventually destabilises the population dynamics of consumer-resource systems, leading to violent population oscillations that may even end in the extinction of the consumer (Rosenzweig and MacArthur, 1963; Rosenzweig, 1971).

The interaction of these two stressors is, however, not well studied, and it is far from trivial. While increasing eutrophication promotes population oscillations, warming tends to dampen them as it makes energy transfer from resource to consumer species less efficient (Rip and McCann, 2011). Furthermore, the effect warming has on biological rates that determine the interaction between resource and consumer species depends on the respective body masses, complicating predictions even further. In this thesis, two studies are presented that are concerned with the interactive effects of warming and eutrophication in food chains (Binzer *et al.*, 2012) and in food webs with different size structures (Binzer *et al.*, 2016) (Fig. 1.3iv). In food chains, extinction of top predators occurs at both very low temperatures (since energy transfer along the food chain is so efficient that it can cause strong population oscillations) and at very high temperatures (due to starvation). Both extinction thresholds are shifted towards higher temperatures as eutrophication increases. In food webs, the interactive effects of warming and eutrophication on diversity depend very much on the prevailing size structure. When consumers and resources have similar sizes (flat size structure, as in parasitoid-host systems), warming increases diversity and eutrophication decreases it, whereas in communities with a strong size structure (predator-prey systems) diversity declines strongly with warming, but has a mixed response to eutrophication.

In terrestrial systems, destruction and fragmentation of habitat due to changes in land use (e.g. transformation of previously undisturbed areas for agricultural use) have by far the largest negative impact on biodiversity (Brooks *et al.*, 2002; Pereira *et al.*, 2010). Considering that extinctions often occur much later than the habitat disturbance that caused them (Tilman *et al.*, 1994), studying the effects of decreasing habitat availability or quality on species-rich communities is of utmost importance. This calls for a metapopulation (Hanski, 1998) or metacommunity approach (Leibold *et al.*, 2004), where local populations or communities are thought to exist on more or less well-defined habitat patches and to interact via dispersal (Fig. 1.3v). Within this framework, various theoretical approaches exist that address a host of different questions, ranging from the conditions for coexistence of species with different competitive and dispersal abilities (Levins and Culver, 1971; Tilman, 1994) to the processes that synchronise population oscillations in space (Koenig, 1999; Sherratt *et al.*, 2000; Koelle and Vandermeer, 2005).

It is well established that a strong correlation between the size of a habitable area and the number of species within this area exist (Arrhenius, 1921), and that clear cause-effect relationships link habitat loss to declining diversity (Duraiappah *et al.*, 2005). Often, it is predicted that species on higher trophic levels are most vulnerable to habitat loss (Melian and Bascompte, 2002), but usually only relatively simple ecological communities are studied (Holt, 2002; Amarasekare, 2008; Holland and Hastings, 2008). This leaves questions regarding how species that are embedded in complex food webs react to habitat changes unanswered. In (Ryser *et al.*, 2019), we analysed for the first time actual meta-food webs, i.e., systems that combine

the complexity of species-rich communities with multiple trophic levels with equally complex networks of habitat patches. While the approach for modelling the biomass dynamics is not suitable for addressing the effect of habitat loss, it is shown that increasing habitat isolation (which is one aspect of habitat fragmentation) decreases the mean species richness per patch (α-diversity), but increases differences in species composition between patches (β-diversity). In line with previous predictions, it is further shown that the risk of local and regional extinction is highest for large species on higher trophic levels. This is mechanistically explained by the inability of small species on lower trophic levels, which suffer most from increased dispersal mortality in highly fragmented landscapes, to energetically support their predators.

Using the same approach for modelling complex habitat networks as Ryser *et al.* (2019), Stark *et al.* (2021) analysed in detail the dynamics of three-species meta-food chains. We showed that reduced dispersal rates due to increasing habitat isolation lead to less synchronous population oscillations, as expected (Sherratt *et al.*, 2000; Plitzko and Drossel, 2015). However, contrary to expectations (Schindler *et al.*, 2015), this did not translate into reduced regional (γ-) population variability. Instead, patch isolation increased local (α-) population variability via indirect effects on the local trophic interactions, which drove an increase in γ-variability.

The third metacommunity study presented in this thesis, (Guill *et al.*, 2021), is not directly concerned with effects of changing habitat availability, but proposes a novel mechanism for the maintenance of (functional) biodiversity. The mechanism is based on the self-organised formation of biomass patterns in the landscape, which supports well defended autotroph species on some patches and fast growing ones on others. Because this mechanism relies on the spatial extension of the habitat as well as on sufficiently high dispersal rates between the patches, it is also sensitive to habitat loss and fragmentation.

1.3.3   Ecological functioning of food webs

So far, questions regarding the stability of populations and communities and thus, ultimately, the determinants of biodiversity have been at the centre of most of the studies presented. However, diversity is not only a value of its own. Ecosystems provide important services and functions, like the production of biomass, and it has been a longstanding question how these functions are related to biodiversity (Hooper *et al.*, 2005; Loreau, 2010). Early studies were mostly concerned with the diversity and productivity of the plant level (Tilman and Downing, 1994; Hector *et al.*, 1999), usually showing a positive relation between species number and plant biomass (Tilman *et al.*, 2001). Including animal diversity, especially in the context of complex food webs, complicates predictions significantly, as effects are very context-dependent in this case (Duffy, 2002; Duffy *et al.*, 2007; Reiss *et al.*, 2009). On the one hand, increasing the diversity of a single trophic level of consumers (horizontal diversity) increases its exploitation pressure on its resources (Finke and Snyder, 2008). On the other hand, increasing the number of trophic levels in the animal community (vertical diversity) may lead to indirect positive effects on the plant level due to the emergence of trophic cascades (Pace *et al.*, 1999). However, omnivory (i.e., feeding on multiple trophic levels) is more common in diverse food webs (Riede *et al.*, 2010), which blurs the distinction of trophic levels and may make trophic cascades less likely again (Halaj and Wise, 2001).

In this thesis, five studies are presented that contribute to the research on the relation between

diversity and ecosystem functioning. In the body mass-based food-web model developed by Schneider *et al.* (2016), increasing the number of animal species increases horizontal and vertical diversity of the animal community simultaneously, similar to natural food webs. It is shown that increasing animal diversity leads to higher rates of intra-guild predation, but the animal community still accumulates more biomass and becomes more exploitative on the plant level. However, both animal and plant communities shift their size structure towards larger species with lower per-unit biomass respiration rates, which enables the plant level to maintain its biomass (Fig. 1.3vi). Kath *et al.* (2018) added to this by pointing out that ATN models like the one used in (Schneider *et al.*, 2016) need to take activity respiration (and not only basal respiration, as suggested by Yodzis and Innes (1992)) into account to avoid unrealistically high trophic transfer efficiencies.

Miele *et al.* (2019) complemented research on the biodiversity-ecosystem functioning relationship in complex food webs by an important observation. In natural ecological communities, there are often more non-trophic than trophic interactions between the species (Kéfi *et al.*, 2015). These non-trophic interactions can for example represent interference among predators or competition for space among sessile organisms. The joint effect of these diverse interactions is to increase the slope between diversity and functioning (Fig. 1.3vii), suggesting that studies that neglect non-trophic interactions underestimate the effect of species loss.

Finally, Ceulemans *et al.* (2019, 2021) took a somewhat different approach to studying the diversity-functioning relationship in food webs. The analysed systems are of intermediate complexity, with three distinct trophic levels, but only between one and four species per trophic level. Instead of taking species diversity as the main explanatory variable, these studies focus on functional diversity, i.e., the ranges spanned by functional traits of the species. These traits determine for example the selectivity of predators, the defence of prey species, or their maximal growth rate (Fig. 1.3viii). This trait-based approach facilitates a detailed mechanistic understanding of the observed patterns (Weithoff, 2003; Hillebrand and Matthiessen, 2009), like compensatory dynamics of species with complementary trait combinations. Both (Ceulemans *et al.*, 2019) and (Ceulemans *et al.*, 2021) highlight the importance of high functional diversity for a number of different ecosystem functions.

Chapter 2

Overview of the Publications

Publications with the first author(s) in italics are based on the master- or PhD-projects of students I supervised (as reflected by my last-authorship). The students received intensive guidance while conducting their projects, but were still granted first-authorship.

Reprints of the publications are provided in the Appendix.

2.1 Structure and stability of food webs

1 *Kartascheff, B., Heckmann*, L., Drossel, B. & **Guill, C.** (2010). Why allometric scaling enhances stability in food web models. *Theor. Ecol.*, 3, 195–208.

In this study we showed that allometric scaling of metabolic rates in size-structured food webs reduces predation mortality and increases intraspecific competition relative to baseline metabolic rates. These two effects have been identified as the main mechanisms by which allometric scaling stabilises complex food webs.

I lead the design of the study (60%) and contributed to the development of the model (50%), the interpretation of the results (40%) and the writing of the manuscript (30%).

2 *Heckmann, L.*, Drossel, B., Brose, U. & **Guill, C.** (2012). Interactive effects of body-size structure and adaptive foraging on food-web stability. *Ecol. Lett.*, 15, 243–250.

This study addresses the interaction of two important mechanisms that stabilise complex food webs, adaptive foraging of consumers and a body size-structure where consumers are on average larger than their prey. Most intriguingly, it is shown how stabilising body size structures emerge from random food web topologies via the dynamic adaptation of the consumers' foraging strategies.

I lead the design of the study (60%) and the development of the model (50%), and contributed to the interpretation of the results (50%) and the writing of the manuscript (40%).

3 *Plitzko, S.J.*, Drossel, B. & **Guill, C.** (2012). Complexity-stability relations in generalized food-web models with realistic parameters. *J. Theor. Biol.*, 306, 7–14.

This study provides novel insights into the relation between food web-stability and -complexity by combining two approaches of analysing models of complex food webs. The first is based on direct numerical integration of coupled ordinary differential equations describing the biomass dynamics of the species, the second is based on a powerful semi-analytical method for evaluating the local stability of fixed points of the population dynamics.

I lead the design of the study (60%) and contributed to the development of the models (50%), the interpretation of the results (35%), and the writing of the manuscript (25%).

4 **Guill, C.**, Carmack, E. & Drossel, B. (2014). Exploring cyclic dominance of sockeye salmon with a predator-prey model. *Can. J. Fish. Aquat. Sci.*, 71, 959–972.

This publication reviews several mechanism behind population oscillations in general and behind the conspicuous 4-year oscillations of the Pacific sockeye salmon spawning in the Fraser River basin in particular. It further demonstrates that for understanding this example of population oscillations a model that explicitly accounts for the complex life cycle of sockeye salmon is required.

I took the lead in the design of this study (80%), as well as in the development and implementation of the model (80%), the interpretation of the results (70%), and the writing of the manuscript (70%).

5 Kalinkat, G., Schneider, F.D., Digel, C., **Guill, C.**, Rall, B.C. & Brose, U. (2013). Body masses, functional responses and predator-prey stability. *Ecol. Lett.*, 16, 1126–1134.

In this study, the analysis of a large experimental data set on arthropod feeding rates demonstrated how all parameters of a generalised functional response model depend on the body masses of predator and prey species, thereby revealing a previously unrecognised effect of body mass on the persistence of predator-prey systems.

I influenced the design of the study (20%) by performing numerical model analyses (100%) that complemented the experimental data analysis. I made minor contributions to the manuscript text (<10%).

6 *Pfaff, T., Brechtel, A.*, Drossel, B. & **Guill, C.** (2014). Single generation cycles and delayed feedback cycles are not separate phenomena. *Theor. Pop. Biol.*, 98, 38–47.

In this publication it is shown that two types of population oscillations that occur in age-structured populations and that previously had been suggested to be caused by two different mechanisms, can in fact be understood as limiting cases of the same underlying mechanism. The publication thereby generalises important results on the interplay of life-history and population dynamics.

I contributed to the design of this study (60%), the development of the model (40%), the interpretation of the results (40%), and the writing of the manuscript (30%).

7 *Allhoff, K.T.*, Ritterskamp, D., Rall, B.C., Drossel, B. & **Guill, C.** (2015). Evolutionary food web model based on body masses gives realistic networks with permanent species turnover. *Sci. Rep.*, 5: 10955.

This study analyses a food web model on evolutionary time scales, where realistic food web structures emerge from an interplay of speciation and trophic interactions, thereby demonstrating the ecological importance of body mass as a master trait.

I contributed to the design of the study (40%), the development of the model (40%), the analysis and interpretation of the results (30%) and the writing of the manuscript (20%).

8 **Guill, C.** & Paulau, P. (2016). Prohibition rules for 3-node substructures in ordered food webs with cannibalistic species. *Israel J. Ecol. Evol.*, 61, 69–76.

This study contributes to our understanding of the structure of food webs by analysing the spectra of ordered three-species motifs in empirical food webs and in two frequently used stochastic models for generating artificial food web structures.

I lead the design of the study (80%) and the development of the analytical and numerical methods to investigate the spectra of the three-species motifs (70%). I produced the results (100%) and wrote most of the manuscript (80%).

2.2   Food webs under anthropogenic disturbances

9 Binzer, A., **Guill, C.**, Brose, U. & Rall, B.C. (2012). The dynamics of food chains under climate change and nutrient enrichment. *Phil. Trans. Royal. Soc. Lond. B*, 367, 2935–2944.

This study demonstrates the individual effects as well as the in parts surprising interactions of two important drivers of anthropogenic global change, warming and eutrophication, on the survivability of species in a three-species food chain.

I made some contributions to the design of the study (20%), but otherwise mostly contributed to the development and implementation of the model (40%) and the interpretation of the results (30%).

10 Binzer, A., **Guill, C.**, Rall, B.C. & Brose, U. (2016). Interactive effects of warming, eutrophication and size-structure: impacts on biodiversity and food-web structure. *Global Change Biol.*, 22, 220–227.

This comprehensive study shows that two important components of anthropogenic global change, eutrophication and warming, have antagonistic effects on the diversity of food webs, which further depend on whether the communities have a flat (as in host-parasitoid networks) or pronounced size structure (as in predator-prey networks).

For this study, I mainly contributed to the development and implementation of the model (50%) and to the interpretation of the results (25%).

11 *Ryser, R., Häussler, J., Stark, M.*, Brose, U., Rall, B.C. & **Guill, C.** (2019). The biggest losers: habitat isolation deconstructs complex food webs from top to bottom. *Proc. Roy. Soc. Lond. B*, 286: 20191177.

This study combines for the first time population dynamics of complex, species-rich food webs with dispersal dynamics on equally complex spatial networks of interconnected

habitat patches. This approach allowed us to obtain important mechanistic insights into how food webs are expected to lose stability under progressing habitat isolation.

This study was carried out as a collaborative project within the DFG-funded research unit FOR 1748: 'Networks on Networks', where I was one of the PIs. I contributed substantially to the design of the study (50%) and the development of the model (50%). I further contributed to the interpretation of the results (30%) and the writing of the manuscript (15%).

12 *Stark, M., Bach, M.* & **Guill, C.** (2021). Patch isolation and periodic environmental disturbances have idiosyncratic effects on local and regional population variability in meta-food chains. *Theor. Ecol.*, 14, 489–500.

In this publication it is shown how indirect effects of trophic interactions modify the effects of dispersal dynamics in metacommunities, thereby advancing our understanding of the relation between the synchrony of population oscillations on individual patches and the stability of metapopulations and -communities.

This study is directly based on my project within the research unit FOR 1748: 'Networks on Networks'. I lead the design of the study (80%) and contributed substantially to the development of the model (50%) and the interpretation of the results (50%). I wrote parts of the manuscript (30%).

13 **Guill, C.**, Hülsemann, J. & Klauschies, T. (2021). Self-organised pattern formation increases local diversity in metacommunities. *Ecol. Lett.*, 24: 2624–2634.

In this publication a novel mechanism for supporting functional diversity based on self-organised pattern formation is developed. These innovative results were obtained by combining state-of-the-art approaches of trait-based ecology and meta-community ecology.

I lead the design of the study (60%), the development of the model equations (50%) and the development of procedures for the data analysis (80%). I produced parts of the results (40%) and wrote substantial parts of the manuscript (50%).

2.3   Ecological functioning of food webs

14 *Schneider, F.D.*, Brose, U., Rall, B.C. & **Guill, C.** (2016). Animal diversity and ecosystem functioning in dynamic food webs. *Nat. Comm.* **7**: 12718.

This study is the first to systematically explore the effects of animal diversity on ecosystem functioning in complex food webs, which allows it to simultaneously capture implications of changing both vertical and horizontal diversity. With this novel approach, important insights on the consequences of animal species loss for fundamental ecosystem functions are gained.

I substantially contributed to the design of the study (50%) and lead the development and implementation of the model (70%). I further contributed to the evaluation and interpretation of the results (40%) as well as to the writing of the manuscript (25%).

15 Kath, N., Boit, A., **Guill, C.** & Gaedke, U. (2018). Accounting for activity respiration results in realistic trophic transfer efficiencies in allometric trophic network (ATN) models. *Theor. Ecol.*, 11, 453–463.

This study analyses in a very detailed manner the biomass dynamics predicted by so-called allometric trophic network models and demonstrates that it is necessary to account for two different modes of respiration (basal and activity) to obtain realistic estimates of the efficiency by which biomass is transferred from one trophic level to the next.

I contributed to the design of the study (40%), the development (50%) and implementation (40%) of the model, the interpretation of the results (35%) and the writing of the manuscript (20%).

16 Miele, V., **Guill, C.**, Ramos-Jiliberto, R. & Kéfi, S. (2019). Non-trophic interactions strengthen the diversity-functioning relationship in an ecological bioenergetic network model. *PLoS Comput. Biol.*, 15: e1007269.

In this study the effects of a large variety of ubiquitous non-trophic interaction pathways on species diversity and ecosystem functioning are explored. Among others it is shown that when these non-trophic interactions, which exist in great numbers among the species of a community, are not accounted for, the negative effects of declining biodiversity on ecosystem functioning are underestimated.

I contributed to the design of the study (35%), the development and implementation of the model (50%), the interpretation of the results (30%) and the writing of the manuscript (20%).

17 *Ceulemans, R.*, Gaedke, U., Klauschies, T. & **Guill, C.** (2019). The effects of functional diversity on biomass production, variability, and resilience of ecosystem functions in a tritrophic system. *Sci. Rep.* **9**: 7541.

We demonstrated the importance of functional trait diversity for the magnitude and stability of ecosystem functions by systematically analysing simple tri-trophic food webs with adjustable functional diversity on each trophic level. Additionally, a novel method for assessing the strength of top-down versus bottom-up control in non-equilibrium situations is developed in this study.

I substantially contributed to the design of the study (50%) and lead the development of the model (60%). I further contributed to the interpretation of the results (35%) and the writing of the manuscript (20%).

18 Ceulemans, R., **Guill, C.** & Gaedke, U. (2021). Top predators govern multitrophic diversity effects in tritrophic food webs. *Ecology*, 102: e03379.

In this study, an exceptionally large data set is generated and analysed with modern machine-learning methods, which allows to obtain generalisable results regarding the importance of functional diversity for ecosystem functioning in tri-trophic food webs.

I contributed to the design of the study (35%), the development of the model (40%) and the interpretation of the results (25%).

Chapter 3

Discussion

3.1 Synthesis

In this thesis, different facets of contemporary research on ecological networks, food webs in particular, have been presented. These revolved mainly around the general topics of i) mechanisms that explain the structure and the stability of natural food webs, ii) the reaction of food webs to anthropogenic global change, and iii) explaining the relationship between diversity (taxonomic or functional) and ecosystem functioning. These topics are not only connected by the common food web-theme, but also by recurrent concepts and methodological approaches.

One of these recurrent concepts is that of body mass as a master trait. As this thesis shows, body mass is relevant on different organisational, temporal, and spatial scales. In the studies concerned with the role of allometric scaling of metabolic rates for the stability of food webs (Kartascheff *et al.*, 2010; Heckmann *et al.*, 2012), it is shown how the body-mass structure of a network (i.e., the average predator-prey body-mass ratio) determines the broad patterns of energy transportation through the food web. On a smaller organisational level, Kalinkat *et al.* (2013) demonstrated how coexistence in predator-prey systems is facilitated by the specific way functional response parameters depend on the body masses of the two species. In these examples, body mass affects the interaction between species and their respiration rates, i.e., processes that take place on ecological time scales (defined by the life time of organisms). However, body mass is also a relevant trait for systems considering much longer time scales: Allhoff *et al.* (2015) used it as the main evolving trait in their model for food-web evolution and showed that with such an approach, food webs with realistic structures emerge. Finally, we demonstrated the (potential) importance of body mass for processes on larger spatial scales in two metacommunity studies (Ryser *et al.*, 2019; Stark *et al.*, 2021), where it is used to parametrise the dispersal dynamics. Based on the observation that larger animal species move generally faster than smaller ones (Peters, 1986; Hirt *et al.*, 2017), it was assumed that they also have a longer dispersal range and therefore have to endure less dispersal mortality (per distance travelled) than smaller species. However, while it was originally hypothesised that the longer dispersal range of larger animals would give them an advantage over smaller ones when habitat isolation increases, this turned out not to be the case. In fact, larger species have a higher extinction risk under increasing habitat isolation than smaller ones because the high dispersal mortality of the smaller species means

27

that they cannot support their larger predators energetically anymore when habitat isolation is too high. This shows that a certain body-mass related effect may be real (larger species are more mobile than smaller ones), but it may still be largely irrelevant for the eventual population dynamics and the survival of the species.

Methodological approaches create an interesting connection between the first and the third general topic. In the first one, specific mechanisms are analysed that stabilise food webs and thus explain their diversity (Kartascheff *et al.*, 2010; Heckmann *et al.*, 2012; Plitzko *et al.*, 2012). In the third one, in turn, the relation between diversity and ecosystem functioning is explored (Schneider *et al.*, 2016; Ceulemans *et al.*, 2019, 2021). It is therefore quite straight forward to ask whether the mechanisms identified in the first topic, like allometric scaling of metabolic rates in size-structured food webs, or adaptive foraging behaviour, also directly affect ecosystem functioning. Establishing such connections would lead to a more mechanistic understanding of the determinants of ecosystem functioning, similar to what approaches based on functional trait diversity are aiming at (Hillebrand and Matthiessen, 2009; Ceulemans *et al.*, 2019). Some degree of transitivity in the explanatory power of the fundamental mechanisms is of course to be expected. For example, adaptive foraging behaviour lets predator species focus on their most profitable prey species while at the same time minimising competition with other predator species, which should increase the efficiency of energy transfer through the food web and lead to overall higher rates of biomass production. However, for other mechanisms it is less clear how they might affect ecosystem functioning. The size structure of classical predator-prey food webs (where predators are several orders of magnitude larger than their prey) supports their diversity (Brose *et al.*, 2006b; Kartascheff *et al.*, 2010), but whether this means that they are also more productive than systems that lack such a size structure, like parasitoid-host networks, has not been shown. Extrapolating the conclusions from Schneider *et al.* (2016), I would hypothesise that parasitoid-host networks have lower standing stock biomasses than predator-prey networks, but more dedicated research is certainly needed to obtain a comprehensive picture of the effect of size structure of trophic networks on ecosystem functioning.

Another connection between the first and the third general topic of this thesis is related to the study of structured populations. Often, maturation of juvenile individuals to adults does not occur after a fixed time span (as in Guill *et al.* (2014); Pfaff *et al.* (2014)), but when individuals reach a certain size. Somatic growth, however, depends on resource intake and expenditure (cf. Fig. 1.2), which can create an ontogenetic bottleneck (de Roos *et al.*, 2007, 2008b). When the per-capita resource availability for the juveniles of a population is very low, they spend most of their ingested energy on respiration and very little on growth. As a consequence, the time to maturation is very long, the total juvenile sub-population accumulates lots of biomass, but its production rate of new biomass is extremely low (an analogous effect can occur in the adult stage when reproduction is resource dependent). The consequences of these population-level functioning effects for the functioning of entire ecosystems have not been systematically explored so far, only some indirect evidence exists. The occurrence of an ontogenetic bottleneck can facilitate the persistence of interacting species (de Roos *et al.*, 2008a), and ontogenetic stage structure of a high fraction of species has been shown to positively affect the diversity of food webs (Mougi, 2017). However, whether these positive effects on diversity translate into positive effects on the functioning of the entire community remains as a question for future research.

By looking at the individual studies of this thesis together, another conclusion regarding

ecosystem functioning can be drawn. The studies of the third general topic were concerned with the effect biodiversity has on ecosystem functioning. However, they do not show that there is actually a two-way relationship between diversity and functioning. This can be seen when interpreting the results of the second general topic, food webs under anthropogenic disturbances, in terms of ecosystem functioning. One important aspect of ecosystem functioning is how efficiently energy is transported from the primary producers to the top predators (Ceulemans *et al.*, 2021). The decreased stability of food chains (Binzer *et al.*, 2012) and food webs (Binzer *et al.*, 2016) under increasing warming or habitat isolation (Ryser *et al.*, 2019) (and notably the extinction of species on higher trophic levels) is a direct consequence of insufficient energy transfer efficiency. Higher ambient temperatures create a mismatch between respiration rates and maximum ingestion rates, as the former increases faster with temperature than the latter (Rall *et al.*, 2012). This means that every species along a food chain becomes less efficient at transferring energy. While this is usually tolerable for species on lower trophic levels, the combined effect of decreasing trophic transfer efficiency over multiple trophic levels means that top predators cannot acquire enough resources to balance their elevated respiration rate. Increasing habitat isolation in metacommunities has the same net effect, although the precise mechanism is somewhat different. As pointed out above, larger animals (which typically occupy the upper trophic levels) are quite mobile and may not be directly affected by increasing habitat isolation. However, less mobile, small species may suffer considerable mortality during dispersal between far away habitat patches. This means that a considerable fraction of their biomass production is 'lost' to the matrix surrounding the patches instead of being transferred up the food chain. In this case, the length of food chains is thus limited by a strong reduction of trophic transfer efficiency that occurs mostly at the lower trophic levels. Both examples thus demonstrate that a restriction of ecosystem functioning by external perturbations significantly affects diversity.

3.2   Outlook

The synopsis of the individual studies of this thesis also suggests interesting avenues for future research. For example, Guill *et al.* (2014) showed that in order to explain the large-scale population oscillations of some populations of a Pacific salmon species, it is necessary to take the age-structure of the populations into account. However, it is actually also essential for the proposed mechanism that the salmon individuals undergo a so-called ontogenetic habitat shift: after spending their first year in freshwater lakes, they migrate to the ocean, where they spend the majority of their life. Interestingly, the results of Guill *et al.* (2014) suggest that the interaction of the salmon fry with their predators (rainbow trout) in the nursery lakes is responsible for the observed population oscillations, and that the mechanism would break down if more than one salmon cohort at a time was subject to the predation by the trout. This calls for more systematic research on the effects of ontogenetic habitat shifts, i.e., a combination of models for age- or stage-structured populations with a metacommunity approach. Ryser *et al.* (2019) assumed that dispersal is triggered by poor growing conditions in a habitat, but it may also be triggered by ontogenetic development. Such complex life cycles are not uncommon among animal species (Werner and Gilliam, 1984), and it has already been shown for single populations that they can have far-reaching consequences like the emergence of alternative stable states (Schreiber and

Rudolf, 2008; Guill, 2009). These alternative states are related to the ontogenetic bottlenecks mentioned above. When juvenile and adult individuals of a species occupy different habitats and thus also have different resources, a bottleneck (associated with the accumulation of a high biomass stock, but a low biomass production rate) can occur in either of the states - but not in both at the same time. The crucial thing to note is that the stage that is *not* experiencing the bottleneck becomes a net producer of biomass, which it exports - via the ontogenetic link (maturation or reproduction) - to the habitat of the bottleneck stage, where it could be exploited by predators of that stage.

Extending this scenario to a trophically complex community on two patches that are dynamically coupled by the ontogenetic habitat shifts of a large proportion of the animal species might lead to some interesting phenomena. For example, if one of the habitats had a lower a-priori productivity (e.g. due to a reduced influx of nutrients), in that habitat the ontogenetic stages of species on lower trophic levels would presumably experience a bottleneck due to limited resource availability and start to accumulate biomass. This biomass would in part originate from the other habitat with higher productivity, via the mechanism described above. Due to these ontogenetic ecosystem subsidies, consumer species on the upper trophic levels might experience relatively even growth conditions in both habitats. This also means that if the ontogenetic biomass flows across the habitat boundaries are not accounted for, standing stock biomass and biomass production in the habitat with low a-priori productivity might appear higher than expected, and vice versa in the higher-productivity habitat.

Another promising direction for future research is to extend the study by Guill *et al.* (2021). In this study, a novel mechanism for supporting functional diversity in metacommunities based on self-organised formation of spatial biomass patterns has been described. However, in order to facilitate a detailed understanding of this mechanism, central model settings like the spatial arrangement of the habitat patches or the biodiversity throughout the food chain have been deliberately kept very simple. In order to establish the ecological relevance of self-organised pattern formation for the maintenance of diversity, it thus seems reasonable to extend the model to more realistic, but also more complex scenarios. This could be done by including complex networks of habitat patches (instead of a simple, one-dimensional ring formation), and by accounting for functional diversity on multiple trophic levels (instead of only at the producer level) to allow for co-adaptation of diverse prey and predator communities.

For modelling complex habitat networks, the approach developed by Ryser *et al.* (2019) could be adopted. There, habitat networks are created as so-called random geometric graphs by distributing the patches randomly across a two-dimensional landscape and creating dispersal links between any two patches whose distance is below a certain threshold. Whether or not self-organised pattern formation occurs in such a system depends among others on the eigenvalue spectrum of the so-called Laplacian matrix. The Laplacian is essentially a mathematical representation of the spatial patch network, encoding presence/absence and strength of dispersal links between patches (Nakao and Mikhailov, 2010). General mathematical results on these matrices suggest that the emerging patterns may be localised on small clusters of patches within the entire network (Brechtel *et al.*, 2018). Ecologically interpreted this may indicate that "islands of diversity" exist, i.e., single patches or densely connected clusters of a few patches that either harbour an elevated level of local (α-) functional diversity or that at least differ in community composition from the rest of the metacommunity, thereby contributing to regional (β-) diversity.

An important question would therefore be to determine whether such keystone patches (or clusters) actually exist, and if so, how much they contribute to diversity on the different spatial scales. To further elucidate the implications of this mechanism for nature conservation, one could then address how sensitive it is to habitat loss by sequentially removing habitat patches. This would change the eigenvalue spectrum of the corresponding Laplacian matrix in a discontinuous way and might lead to sudden shifts between metacommunity states with different spatial patterns or even without self-organised pattern formation.

As a step towards modelling realistic, trophically complex communities, the potential of self-organised pattern formation to support functional diversity on the level of consumers (in addition to the producer level) could be analysed. Even in non-spatial models, biomass-trait feedbacks between two functionally diverse trophic levels have been shown to lead to complex adaptation dynamics of the traits (Tirok *et al.*, 2011). By studying co-adaptation of consumer and resource species in an explicit metacommunity context it could therefore be investigated how this potential for complex local dynamics interacts with the non-equilibrium dynamics induced by self-organised pattern formation, and thus whether the mechanism for increasing functional diversity by self-organised pattern formation can be extended and generalised to multiple trophic levels.

Similar to what is done for the producers in the published model, the diversity of the consumers would be modelled as a continuous distribution of a functional trait that mediates for example a trade-off between the width of a given predator's prey spectrum and the efficiency with which it can attack prey species with different levels of defence (Tirok *et al.* (2011). Even though this would increase the mathematical complexity of the model only moderately, much more complex population- and trait dynamics can be expected to occur when both producer and consumer species are adaptive (Tirok *et al.*, 2011). However, producer and consumer species may have considerably different movement or dispersal modes. It is therefore not clear a priori whether the complex dynamics would translate into maintenance of functional diversity of the consumers. For example, actively moving consumers can be assumed to disperse much faster among habitats than producer species that rely on passive transport. While this can have important implications for the self-organised formation of patterns in the distribution of the species (Guill *et al.* (2021) showed that spatio-temporal patterns emerge when consumers have low to medium mobility, while static patterns emerge when they are highly mobile), very fast movement can also homogenise the trait distributions across the metacommunity. Over time this would lead to a loss of both regional and local functional diversity of the consumers, and potentially also the producers. It would therefore have to be explored very carefully, for which ranges of dispersal rates of the respective communities self-organised pattern formation occurs, and whether this leads to positive or negative effects on the functional diversity of producer and consumer communities.

The ideas for exploring the capabilities of self-organised pattern formation to increase functional diversity in metacommunities (Guill *et al.*, 2021) in both spatially and trophically more complex scenarios as described above are part of a research proposal submitted to the DFG and thus constitute a plan for my research in the near future.

Chapter 4

Bibliography

Agrawal, A.A. (2001). Phenotypic plasticity in the interactions and evolution of species. *Science*, 294, 321–326.

Allesina, S., Alonso, D., and Pascual, M. (2008). A general model for food web structure. *Science*, 320, 658–661.

Allesina, S. and Tang, S. (2012). Stability criteria for complex ecosystems. *Nature*, 483, 205–208.

Allhoff, K.T., D, R., Rall, B.C., Drossel, B., and Guill, C. (2015). Evolutionary food web model based on body masses gives realistic networks with permanent species turnover. *Sci. Rep.*, 5, 10955.

Amarasekare, P. (2008). Spatial dynamics of foodwebs. *Ann. Rev. Ecol. Evol. Syst.*, 39, 479–500.

Arditi, R. and Ginzburg, L.R. (1989). Coupling in predator-prey dynamics: ratio-dependence. *J. Theor. Biol.*, 139, 311–326.

Arrhenius, O. (1921). Species and area. *J. Ecol.*, 9, 95–99.

Barnosky, A.D., Matzke, N., Tomiya, S., Wogan, G.O.U., Swartz, B., Quental, T.B. *et al.* (2011). Has the earth's sixth mass extinction already arrived? *Nature*, 471, 51–57.

Beddington, J.R. (1975). Mutual interference between parasites or predators and its effects on searching efficiency. *J. Anim. Ecol.*, 44, 331–340.

Binzer, A., Guill, C., Brose, U., and Rall, B.C. (2012). The dynamics of food chains under climate change and nutrient enrichment. *Phil. Trans. R. Soc. Lond. B*, 367, 2935–2944.

Binzer, A., Guill, C., Rall, B.C., and Brose, U. (2016). Interactive effects of warming, eutrophication and size-structure: impacts on biodiversity and food-web structure. *Global Change Biol.*, 22, 220–227.

Boit, A., Martinez, N.D., Williams, R.J., and Gaedke, U. (2012). Mechanistic theory and modelling of complex food-web dynamics in lake constance. *Ecol. Lett.*, 15, 594–602.

Brechtel, A., Gramlich, P., Ritterskamp, D., Drossel, B., and Gross, T. (2018). Master stability functions reveal diffusion-driven pattern formation in networks. *Phys. Rev. E*, 97.

Briand, F. (1983). Environmental control of food web structure. *Ecology*, 64, 253–263.

Briand, F. and Cohen, J.E. (1984). Community food webs have scale-invariant structure. *Nature*, 307, 264–267.

Brooks, T.M., Mittermeier, R.A., Mittermeier, C.G., Da Fonseca, G.A.B., Rylands, A.B., Konstant, W.R. *et al.* (2002). Habitat loss and extinction in the hotspots of biodiversity. *Cons. Biol.*, 16, 909–923.

Brose, U., Jonsson, T., Berlow, E.L., Warren, P., Banasek-Richter, C., Bersier, L.F. *et al.* (2006a). Consumer-resource body-size relationships in natural food webs. *Ecology*, 87, 2411–2417.

Brose, U., Williams, R.J., and Martinez, N.D. (2006b). Allometric scaling enhances stability in complex food webs. *Ecol. Lett.*, 9, 1228–1236.

Brown, J.H., Gillooly, J.F., Allen, A.P., Savage, V.M., and West, G.B. (2004). Toward a metabolic theory of ecology. *Ecology*, 85, 1771–1789.

Cattin, M.F., Bersier, L.F., Banašek-Richter, C., Baltensperger, R., and Gabriel, J.P. (2004). Phylogenetic constraints and adaptation explain food-web structure. *Nature*, 427, 835–839.

Ceulemans, R., Gaedke, U., Klauschies, T., and Guill, C. (2019). The effects of functional diversity on biomass production, variability, and resilience of ecosystem functions in a tritrophic system. *Sci. Rep.*, 9, 7541.

Ceulemans, R., Wojcik, L.A., and Gaedke, U. (2021). Functional diversity alters the effects of a pulseperturbation on the dynamics of tritrophic foodwebs. *bioRxiv*, https://doi.org/10.1101/2021.03.22.436420.

Cohen, J.E. and Newman, C.M. (1985). A stochastic theory of community food webs: I. models and aggregated data. *Proc. R. Soc. Lond. B*, 224, 421–448.

DeAngelis, D.L. (1975). Stability and connectance in food web models. *Ecology*, 56, 238–243.

Drossel, B., Higgs, P.G., and McKane, A.J. (2001). The influence of predator-prey populations dynamics on the long-term evolution of food web structure. *J. Theor. Biol.*, 208, 91–107.

Duffy, J.E. (2002). Biodiversity and ecosystem function: the consumer connection. *Oikos*, 99, 201–219.

Duffy, J.E., Cardinale, B.J., France, K.E., McIntyre, P.B., Thébault, E., and Loreau, M. (2007). The functional role of biodiversity in ecosystems: incorporating trophic complexity. *Ecol. Lett.*, 10, 522–538.

Duraiappah, A., Naeem, S., Agardy, T., Ash, N., Cooper, H., Diaz, S. *et al.* (2005). *Ecosystems and human well-being: biodiversity synthesis; a report of the Millennium Ecosystem Assessment.* World Resources Institute, Washington, DC.

Elton, C.S. (1927). *Animal Ecology.* University of Chicago Press (reprint 2001), Chicago.

Elton, C.S. (1958). *The Ecology of Invasions by Animals and Plants.* Chapman & Hall, London.

Finke, D.L. and Snyder, W.E. (2008). Niche partitioning increases resource exploitation by diverse communities. *Science*, 321, 1488–1490.

Gardener, M.R. and Ashby, W.R. (1970). Connectance of large dynamic (cybernetic) systems: critical values for stability. *Nature*, 228, 784.

Gaston, K.J., Chown, S.L., and Styles, C.V. (1997). Changing size and changing enemies: the case of the mopane worm. *Acta Oecol.*, 18.

Gillooly, J.F., Brown, J.H., West, G.B., Savage, V.M., and Charnov, E.L. (2001). Effects of size and temperature on metabolic rate. *Science*, 293, 2248–2251.

Guill, C. (2009). Alternative dynamical states in stage-structured consumer populations. *Theor. Pop. Biol.*, 76, 168–178.

Guill, C., Carmack, E., and Drossel, B. (2014). Exploring cyclic dominance of sockeye salmon with a predator-prey model. *Can. J. Fish. Aquat. Sci.*, 71, 959–972.

Guill, C. and Drossel, B. (2008). Emergence of complexity in evolving niche-model food webs. *J. Theor. Biol.*, 251, 108–120.

Guill, C., Hülsemann, J., and Klauschies, K. (2021). Self-organised pattern formation increases local diversity in metacommunities. *Ecol. Lett.*, 24, 2624–2634.

Guill, C. and Paulau, P. (2016). Prohibition rules for 3-node substructures in ordered food webs with cannibalistic species. *Israel J. Ecol. Evol.*, 61, 69–76.

Halaj, J. and Wise, D.H. (2001). Terrestrial trophic cascades: how much do they trickle? *Am. Nat.*, 157, 262–281.

Hanski, I. (1998). Metapopulation dynamics. *Nature*, 396, 41–49.

Hastings, A. and Powell, T. (1991). Chaos in a three-species food chain. *Ecology*, 72, 896–903.

Heckmann, L., Drossel, B., Brose, U., and Guill, C. (2012). Interactive effects of body-size structure and adaptive foraging on food-web stability. *Ecol. Lett.*, 15, 243–250.

Hector, A., Schmid, B., Beierkuhnlein, C., Caldeira, M.C., Diemer, M., Dimitrakopoulos, P.G. *et al.* (1999). Plant diversity and productivity experiments in european grasslands. *Science*, 286, 1123–1127.

Hillebrand, H. and Matthiessen, B. (2009). Biodiversity in a complex world: consolidation and progress in functional biodiversity research. *Ecol. Lett.*, 12, 1405–1419.

Hirt, M.R., Jetz, W., Rall, B.C., and Brose, U. (2017). A general scaling law reveals why the largest animals are not the fastest. *Nat. Ecol. Evol.*, 1, 1116–1122.

Holland, M.D. and Hastings, A. (2008). Strong effect of dispersal network structure on ecological dynamics. *Nature*, 456, 792.

Holling, C.S. (1959). Some characteristics of simple types of predation and parasitism. *Can. Entom.*, 91, 385–399.

Holt, R.D. (2002). Food webs in space: on the interplay of dynamic instability and spatial processes. *Ecol. Res.*, 17, 261–273.

Hooper, D.U., Chapin III, F.S., Ewel, J.J., Hector, A., Inchausti, P., Lavorel, S. *et al.* (2005). Effects of biodiversity on ecosystem functioning: a consensus of current knowledge. *Ecol. Monog.*, 75, 3–35.

Kalinkat, G., Schneider, F.D., Digel, C., Guill, C., Rall, B.C., and Brose, U. (2013). Body masses, functional responses and predator-prey stability. *Ecol. Lett.*, 16, 1126–1134.

Kartascheff, B., Heckmann, L., Drossel, B., and Guill, C. (2010). Why allometric scaling enhances stability in food web models. *Theor. Ecol.*, 3, 195–208.

Kath, N., Boit, A., Guill, C., and Gaedke, U. (2018). Accounting for activity respiration results in realistic trophic transfer efficiencies in allometric trophic network (atn) models. *Theor. Ecol.*, 11, 453–463.

Kéfi, S., Berlow, E.L., Wieters, E.A., Joppa, L.N., Wood, S.A., Brose, U. *et al.* (2015). Network structure beyond food webs: mapping non-trophic and trophic interactions on chilean rocky shores. *Ecology*, 96, 291–303.

Koelle, K. and Vandermeer, J. (2005). Dispersal-induced desynchronization: from metapopulations to metacommunities. *Ecol. Lett.*, 8, 167–175.

Koenig, W.D. (1999). Spatial autocorrelation of ecological phenomena. *Trends Ecol. Evol.*, 14, 22 – 26.

Kondoh, M. (2003). Foraging adaptation and the relationship between food-web complexity and stability. *Science*, 299, 1388–1391.

Leibold, M.A., Holyoak, M., Mouquet, N., Amarasekare, P., Chase, J.M., Hoopes, M.F. *et al.* (2004). The metacommunity concept: a framework for multi-scale community ecology. *Ecol. Lett.*, 7, 601–613.

Levins, R. and Culver, D. (1971). Regional coexistence of species and competition between rare species. *Proc. Nat. Acad. Sci.*, 68, 1246–1248.

Loeuille, N. and Loreau, M. (2005). Evolutionary emergence of size-structured food webs. *Proc. Nat. Acad. Sci.*, 102, 5761–5766.

Loreau, M. (2010). *From populations to ecosystems: Theoretical foundations for a new ecological synthesis*. Princeton University Press, Princeton.

Lotka, A.J. (1925). *Elements of Physical Biology*. Williams & Wilkins Company, Baltimore.

Lotka, A.J. (1932). The growth of mixed populations: two species competing for a common food supply. *J. Washington Acad. Sci.*, 22, 461–469.

MacArthur, R.H. (1955). Fluctuations of animal populations, and a measure of community stability. *Ecology*, 36, 533–536.

Martinez, N.D. (1992). Constant connectance in community food webs. *Am. Nat.*, 139, 1208–1218.

May, R. (1971). Stability in multispecies community models. *Math. Biosci.*, 12, 59–79.

May, R.M. (1972). Will a large complex system be stable? *Nature*, 238, 413–414.

Melian, C.J. and Bascompte, J. (2002). Food web structure and habitat loss. *Ecol. Lett.*, 5, 37–46.

Miele, V., Guill, C., Ramos-Jiliberto, R., and Kéfi, S. (2019). Non-trophic interactions strengthen the diversity-functioning relationship in an ecological bioenergetic network model. *PLoS Comput. Biol.*, 15, e1007269.

Mougi, A. (2017). Persistence of a stage-structured food web. *Sci. Rep.*, 7, 11055.

Nakao, H. and Mikhailov, A.S. (2010). Turing patterns in network-organized activator–inhibitor systems. *Nat. Phys.*, 6, 544.

Neutel, A.M., Heesterbeek, J.A.P., and de Ruiter, P.C. (2002). Stability in real food webs: weak links in long loops. *Science*, 296, 1120–1123.

Odum, E.P. (1953). *Fundamentals of Ecology*. Saunders, Philadelphia.

Pace, M.L., Cole, J.J., Carpenter, S.R., and Kitchell, J.F. (1999). Trophic cascades revealed in diverse ecosystems. *Trends Ecol. Evol.*, 14, 483–488.

Pereira, H.M., Leadley, P.W., Proença, V., Alkemade, R., Scharlemann, J.P.W., Fernandez-Manjarrés, J.F. *et al.* (2010). Scenarios for global biodiversity in the 21st century. *Science*, 330, 1496–1501.

Petchey, O.L., Beckerman, A.P., Riede, J.O., and Warren, P.H. (2008). Size, foraging, and food web structure. *Proc. Nat. Acad. Sci.*, 105, 4191–4196.

Peters, R.H. (1986). *The ecological implications of body size*, vol. 2. Cambridge University Press.

Pfaff, T., Brechtel, A., Drossel, B., and Guill, C. (2014). Single generation cycles and delayed feedback cycles are not separate phenomena. *Theor. Pop. Biol.*, 98, 38–47.

Pimm, S.L., Jenkins, C.N., Abell, R., Brooks, T.M., Gittleman, J.L., Joppa, L.N. *et al.* (2014). The biodiversity of species and their rates of extinction, distribution, and protection. *Science*, 344, 1246752.

Plitzko, S.J. and Drossel, B. (2015). The effect of dispersal between patches on the stability of large trophic food webs. *Theor. Ecol.*, 8, 233–244.

Plitzko, S.J., Drossel, B., and Guill, C. (2012). Complexity-stability relations in generalized food-web models with realistic parameters. *J. Theor. Biol.*, 306, 7–14.

Rall, B.C., Brose, U., Hartvig, M., Kalinkat, G., Schwarzmüller, F., Vucic-Pestic, O. *et al.* (2012). Universal temperature and body-mass scaling of feeding rates. *Phil. Trans. R. Soc. Lond. B*, 367, 2923–2934.

Rall, B.C., Guill, C., and Brose, U. (2008). Food-web connectance and predator interference dampen the paradox of enrichment. *Oikos*, 117, 202–213.

Reiss, J., Bridle, J.R., Montoya, J.M., and Woodward, G. (2009). Emerging horizons in biodiversity and ecosystem functioning research. *Trends Ecol. Evol.*, 24, 505–514.

Riede, J.O., Rall, B.C., Banasek-Richter, C., Navarrete, S.A., Wieters, E.A., Emmerson, M.C. *et al.* (2010). Scaling of food-web properties with diversity and complexity across ecosystems. *Adv. Ecol. Res.*, 42, 139–170.

Rip, J. and McCann, K. (2011). Cross-ecosystem differences in stability and the principle of energy flux. *Ecol. Lett.*, 14, 733–740.

Rooney, N. and McCann, K.S. (2012). Integrating food web diversity, structure and stability. *Trends Ecol. Evol.*, 27, 40–46.

de Roos, A.M., Schellekens, T., van Kooten, T., and Persson, L. (2008a). Stage-specific predator species help each other to persist while competing for a single prey. 105, 13930–13935.

de Roos, A.M., Schellekens, T., van Kooten, T., van de Wolfshaar, K., Claessen, D., and Persson, L. (2007). Food-dependent growth leads to overcompensation in stage-specific biomass when mortality increases: the influence of maturation versus reproduction regulation. *Am. Nat.*, 170, E59–E76.

de Roos, A.M., Schellekens, T., van Kooten, T., van de Wolfshaar, K., Claessen, D., and Persson, L. (2008b). Simplifying a physiologically structured population model to a stage-structured biomass model. *Theor. Pop. Biol.*, 73, 47–62.

Rosenzweig, M.L. (1971). Paradox of enrichment: destabilization of exploitation ecosystems in ecological time. *Science*, 171, 385–387.

Rosenzweig, M.L. and MacArthur, R.H. (1963). Graphical representation and stability conditions of predator-prey interactions. *Am. Nat.*, 97, 209–223.

de Ruiter, P.C., Neutel, A.M., and Moore, J.C. (1995). Energetics, patterns of interaction strengths, and stability in real ecosystems. *Science*, 269, 1257–1260.

Ryser, R., Häussler, J., Stark, M., Brose, U., Rall, B.C., and Guill, C. (2019). The biggest losers: habitat isolation deconstructs complex food webs from top to bottom. *Proc. R. Soc. Lond. B*, 286, 20191177.

Schindler, D.E., Armstrong, J.B., and Reed, T.E. (2015). The portfolio concept in ecology and evolution. *Front. Ecol. Env.*, 13, 257–263.

Schneider, F.D., Brose, U., Rall, B.C., and Guill, C. (2016). Animal diversity and ecosystem functioning in dynamic food webs. *Nat. Comm.*, 7.

Schreiber, S. and Rudolf, V.H.W. (2008). Crossing habitat boundaries: coupling dynamics of ecosystems through complex life cycles. *Ecol. Lett.*, 11, 576–587.

Sherratt, T.N., Lambin, X., Petty, S.J., Mackinnon, J.L., Coles, C.F., and Thomas, C.J. (2000). Use of coupled oscillator models to understand synchrony and travelling waves in populations of the field vole *Microtus agrestis* in northern england. *J Appl Ecol*, 37, 148 – 158.

Skalski, G.T. and Gilliam, J.F. (2001). Functional responses with predator interference: viable alternatives to the holling type ii model. *Ecology*, 82, 3083–3092.

Stark, M., Bach, M., and Guill, C. (2021). Patch isolation and periodic environmental disturbances have idiosyncratic effects on local and regional population variability in meta-food chains. *Theor. Ecol.*, 14, 489–500.

Stouffer, D.B., Camacho, J., and Amaral, L.A.N. (2006). A robust measure of food web intervality. *Proc. Nat. Acad, Sci.*, 103, 19015–19020.

Tilman, D. (1994). Competition and biodiversity in spatially structured habitats. *Ecology*, 75, 2–16.

Tilman, D. and Downing, J.A. (1994). Biodiversity and stability in grasslands. *Nature*, 367, 363–365.

Tilman, D., May, R.M., Lehman, C.L., and Nowak, M.A. (1994). Habitat destruction and the extinction debt. *Nature*, 371, 65–66.

Tilman, D., Reich, P.B., Knops, J., Wedin, D., Mielke, T., and Lehman, C. (2001). Diversity and productivity in a long-term grasland experiment. *Science*, 294, 843–845.

Tirok, K., Bauer, B., Wirtz, K., and Gaedke, U. (2011). Predator-prey dynamics driven by feedback between functionally diverse trophic levels. *PloS One*, 6, e27357.

Uchida, S. and Drossel, B. (2007). Relation between complexity and stability in food webs with adaptive behavior. *J. Theor. Biol.*, 247, 713–722.

Volterra, V. (1928). Variations and fluctuations of the number of individuals in animal species living together. *ICES J Mar. Sci.*, 3, 3–51.

Vucic-Pestic, O., Rall, B.C., Kalinkat, G., and Brose, U. (2010). Allometric functional response model: body masses constrain interaction strengths. *J. Anim. Ecol.*, 79, 249–256.

Weithoff, G. (2003). The concepts of 'plant functional types' and 'functional diversity' in lake phytoplankton - a new understanding of phytoplankton ecology? *Freshw. Biol.*, 48, 1669–1675.

Werner, E.E. and Gilliam, J.F. (1984). The ontogenetic niche and species interactions in size-structured populations. *Ann. Rev. Ecol. Syst.*, 15, 393–425.

Williams, R.J. and Martinez, N.D. (2000). Simple rules yield complex food webs. *Nature*, 404, 180–183.

Williams, R.J. and Martinez, N.D. (2004). Stabilization of chaotic and non-permanent food-web dynamics. *Europ. Phys. J. B*, 38, 297–303.

Yamamichi, M., Klauschies, T., Miner, B.E., and van Velzen, E. (2018). Modelling inducible defences in predator–prey interactions: assumptions and dynamical consequences of three distinct approaches. *Ecol. Lett.*, 22, 390–404.

Yodzis, P. (1981). The stability of real ecosystems. *Nature*, 289, 674–676.

Yodzis, P. and Innes, S. (1992). Body size and consumer-resource dynamics. *Am. Nat.*, 139, 1151–1175.

Yoon, I., Williams, R.J., Levine, E., Yoon, S., Dunne, J.A., and Martinez, N.D. (2004). Webs on the web (wow): 3d visualization of ecological networks on the www for collaborative research and education. *Proc. IS&T/SPIE Symp. on El. Imag., Visual. and Data Anal.*, 5295, 124–132.

Chapter 5

Acknowledgements

First of all, I thank my mentor, Prof. Dr. Ursula Gaedke, for her professional guidance and encouragement during the past six years, for fruitful collaborations, for the family-friendly working conditions in her group and, last but not least, for her active support during the preparation of this thesis.

I wish to thank all my co-authors of the various projects for contributing their data, knowledge or unique skills, which were necessary to turn interesting ideas into cool results and ultimately into publications.

Dr. Ellen van Velzen and Dr. Toni Klauschies deserve my special gratitude for countless inspiring and insightful discussions on various scientific (and other) topics.

Over the years, I had the honour to supervise many students, for which I am very grateful. Their eagerness to gain knowledge, learn new methods and to contribute to science keeps inspiring me.

I thank all members of the working group "Ökologie und Ökosystemmodellierung" for creating a work environment that lets creativity flourish. Among them, Xenia Fahrentholz and Stefan Saumweber deserve a special mention for helping me with all the administrative and technical hurdles of the day-to-day work at the University of Potsdam.

My deepest gratitude, however, goes to Anke. To You I dedicate this thesis.

Chapter 6

Appendix: Reprints of the Publications

This appendix contains reprints of the 18 publications listed in chapter 2.

ORIGINAL PAPER

Why allometric scaling enhances stability in food web models

**Boris Kartascheff · Lotta Heckmann ·
Barbara Drossel · Christian Guill**

Abstract It has recently been shown that the incorporation of allometric scaling into the dynamic equations of food web models enhances network stability if predators are assigned a higher body mass than their prey. We investigate the underlying mechanisms leading to this stability increase. The dynamic equations can be written such that allometric scaling influences these equations at three places: the time scales of predator and prey dynamics become separated, the energy outflow to the predators is decreased, and intraspecific competition is increased relative to metabolic rates. For five food web topologies and various network sizes (i.e., species richness), we study the effect of each of these modifications on the percentage of surviving species separately and find that the decreased interaction strengths and the increased intraspecific competition are responsible for the enhanced stability. We also investigate the range of parameter values for which an enhanced stability is observed.

Keywords Metabolic theory · Population dynamics ·
Complexity–stability relation · Time scale effect ·
Interaction strength · Intraspecific competition

Introduction

Over the last few decades, there has been an intensive debate about why complex food webs persist in nature (McCann 2000). May (1972) demonstrated in an analytical approach for the dynamics of random networks near a fixed point that higher complexity inherently leads to less stability. This overturned the traditional view of ecologists that more complex ecosystems are more stable (MacArthur 1955; Elton 1958; Odum 1953), and initiated the so called complexity–stability debate. However, May's stability analysis did not remain uncriticized, mainly because of the linear stability concept, and because of the random choice of food web topology and consumer-resource coupling constants, which are not appropriate for empirical food webs (DeAngelis and Waterhouse 1987; Pimm 1984; Yodzis 1981).

Subsequent investigations of food web stability used more empirically realistic models with non-linear, saturating functional response of type II or III (Williams and Martinez 2004; Brose et al. 2006; Otto et al. 2007; Rall et al. 2008). These non-linear functional responses can be derived in a reasonably convincing way from first principles of time budgets (Koen-Alonso 2007), whereas they prevent analytic solutions of the resulting population dynamics. Further steps towards more realistic food web models introduced, among others, the concept of predator interference (Beddington 1975), more realistic food web structures (Williams and Martinez 2000; Martinez et al. 2006; Dunne 2006) and interaction strength patterns (McCann et al. 1998; Neutel et al. 2002; Paine 1980), or foraging adaptation (Kondoh 2003).

A variety of stability concepts have been used since May's work (McCann 2000). For the survival of a species, it is not necessary that the dynamics have a stable fixed point, and therefore, the concept of species persistence is often employed. We call the proportion

B. Kartascheff · L. Heckmann · B. Drossel · C. Guill (✉)
Institute of Condensed Matter Physics,
Darmstadt University of Technology, Hochschulstraße 6,
64289 Darmstadt, Germany
e-mail: guill@fkp.tu-darmstadt.de

of species that persist in a food web the "robustness" of the network.

In a recent study, Brose et al. (2006) demonstrated that the incorporation of mass-dependent metabolic rates into the nonlinear dynamical equations of food web models considerably increases food web robustness. Generally, metabolic rates of individuals are assumed to scale like power laws with body size, with the allometric exponents being either close to 3/4, as put forward by the metabolic theory (West et al. 1999; Enquist et al. 1999; Brown et al. 2004), or close to 2/3, as can be inferred from simple geometric arguments (Dodds et al. 2001; White and Seymour 2003). Recent studies, however, contest the universality of allometric scaling exponents (Bokma 2004; Glazier 2005; Price et al. 2009).

In the study by Brose et al. (2006), species were assigned a body mass according to their trophic level. The energy losses due to metabolism and the consumption rates thus became a function of the body mass. Using the modified cascade (Cohen et al. 1990), niche (Williams and Martinez 2000), and nested hierarchy model (Cattin 2004), Brose et al. (2006) showed that a predator–prey body mass ratio between 10 and 100 resulted in robustness values that approached 100% for large networks, and the authors presented empirical food web data that corroborated this optimum predator–prey body mass ratio. In a subsequent publication, Otto et al. (2007) showed how such predator–prey body mass ratios can stabilize three-species food chains. How food webs with a more general structure and with more species can be stabilized by such body mass ratios is, however, not explained at present.

It is the purpose of this paper to shed light on the mechanisms that lead to an increased stability of food webs in the presence of allometric scaling. We evaluate the robustness R as a function of the species number S within a wide range $20 \leq S \leq 80$, and for a fixed value of the initial connectance $C = 0.15$, which is the number of links in the network, divided by S^2. We chose Holling type-II functional responses and collected robustness data for five simple topological food web models that allow for fast data generation (see next section).

The differential equations of population dynamics with and without allometric scaling differ in three terms. Each of them was considered as a potential cause for the observed stability increase. In a simulation setup, we tested each of the potential causes separately and evaluated their effects on food web stability.

Compared to the model of Brose et al. (2006), our set of differential equations contains fewer parameters. This is because we bundled together empirical parameters such as the allometric coefficients taken from

Brown et al. (2004) and replaced products of parameters by one effective parameter wherever possible.

Food web models

The food web topologies in this study are the random, cascade (Cohen and Newman 1985), niche (Williams and Martinez 2000), nested hierarchy (Cattin 2004), and layered topology. In contrast to models that generate food webs by a dynamical process such as the Webworld (Drossel et al. 2001) or the matching model (Rossberg et al. 2006), these descriptive and rather simple models have distinctive topological features that allow to disentangle specific effects of the web topology on the stability of the webs under population dynamics. For the niche model, generalizations have been developed that predict empirical food web data even better (Allesina et al. 2008), but for the purpose of this work, it is sufficient to analyze the basic niche model with its very simple rules.

The random model imposes no restrictions on the web topology. Each link is realized with constant probability C. The cascade, niche, and nested hierarchy models all order the species along a single niche dimension and constrain predators to feed (mainly) on prey with a lower rank. The models differ by the amount of looping they permit, by the degree distributions, and by additional constraints such as diet contiguity in the niche model. In the layered model, species are placed on distinct trophic levels and are constrained to prey exclusively on those species on the next lower level. This creates a very strict feeding hierarchy that prohibits looping, cannibalism, and even omnivory. The species are evenly distributed on four trophic levels (we present only data for species numbers S that are multiples of 4).

Each simulation run started by randomly generating a food web consisting of S species according to the rules of the desired topology. The number of links L for fixed S and C varied between simulation runs; the average value, however, was fixed to $L = S^2 \cdot C$.

Two external resources with constant and identical size N_{res} were assigned to each model web. They serve as an inexhaustible pool of nutrients or other sources of energy, such as sunlight, that is consumed by the basal species (first trophic level). In the cascade model, these resources were assigned the lowest ranks, and in the niche and nested hierarchy models, they were assigned the smallest niche values. In niche model food webs, species with a feeding range that do not cover the resources are nevertheless assigned a link to the resources if their feeding range contains no species at all,

in accordance with the original algorithm by Williams and Martinez (Williams and Martinez 2000). In the random model, links to the resources are assigned in the same way as all other feeding links. In the layered model, all species on the first level received links to the two resources.

Introducing the resources as special nodes in the network has several advantages. First, it guarantees that, on average, a constant fraction of the trophic species has a link to the resources, independent of the size of the network. By this, we do not fix the number of basal species B, as was done by Brose et al. (2006), and the energy input per species to the network remains constant. This makes simulation results for small and large networks comparable. A constant number B would have a negative impact on the robustness of larger food webs. Both the slope and typical values of the robustness decrease, but we confirmed that changes in robustness caused by allometric scaling for the case of constant B remain qualitatively the same. Furthermore, empirical food web data do not suggest a fixed number of basal species that is independent from food web size.

Second, by representing the resources as nodes in the networks, we do not need to define special equations for the basal species. The implementation of constant resources leads to a logistic growth of the basal species that depends on the resources because we include intraspecific competition in the dynamical equations (see next section). Our equations are therefore formally equivalent to those used by Brose et al. (2006), where five primary producers (basal species) with logistic growth act as energy supply.

Population dynamics

The population dynamics is determined by a set of S-coupled ordinary differential equations (ODEs). We first introduce the ODEs for simulations without allometric scaling, followed by the ODEs for simulations with allometric scaling. The biomass density of species i, N_i changes with time according to

$$\frac{dN_i}{dt} = \lambda_i \sum_{j \in R_i} g_{ij}(\mathbf{N}) N_i - \sum_{k \in C_i} g_{ki}(\mathbf{N}) N_k - \alpha_i N_i - \beta_i N_i^2 ,$$

(1)

where R_i is the set of prey and C_i the set of predators of species i. λ_i denotes the assimilation efficiency ($\lambda_i < 1$). As long as λ_i was not too low ($\lambda_i > 0.1$), our simulation results did not depend qualitatively on the precise value of this parameter. We set assimilation

$\lambda_i = \lambda = 0.4$, close to values used by Brose et al. (2006) or Yodzis and Innes (1992). α_i is the biomass loss of species i due to respiration and mortality (we neglect other causes of biomass loss, e.g., due to death caused by diseases or accidents) and β_i is the intraspecific competition coefficient. Intraspecific competition depends on the density of the respective population. It limits the growth of a species due to a limited availability of nesting sites or territory. We set the respiration rate to $\alpha_i = \alpha = 0.05$ and the competition strength to $\beta_i = \beta = 0.4$, as chosen by Ushida and Drossel (2007). We found that a variation of α and β can have a quantitative and qualitative influence on the effect of allometric scaling on food web stability when these parameters are too large. We discuss the parameter ranges for which population dynamics with allometric scaling enhance stability in the conclusion. The functional response g_{ij} was of Holling type-II form,

$$g_{ij}(\mathbf{N}) = \frac{a_{ij} f_{ij} N_j}{1 + \sum_{l \in R_i} a_{il} f_{il} h_{il} N_l} ,$$

(2)

with constant foraging efforts $f_{ij} = 1/\omega_i$, where ω_i is the number of prey of species i. f_{ij} reduces the interaction strength between predator i and prey j if i is a generalist, i.e., if i forages for many different prey species, because it has to divide its available searching time among its different prey. a_{ij} is the encounter rate of predator i and prey j and h_{il} denotes the handling time, i.e., the time a consumer i needs to digest a unit biomass of prey l. Encounter rates and handling times of a predator i are assumed to be the same for all its prey species, i.e., $a_{ij} = a_i$ and $h_{ij} = h_i$ for all j. With this, the functional response Eq. 2 can be rewritten as

$$g_{ij}(\mathbf{N}) = \frac{1}{h_i} \frac{f_{ij} N_j}{\frac{1}{a_i h_i} + \sum_{l \in R_i} f_{il} N_l} .$$

(3)

In this notation, $1/h_i$ can be interpreted as maximal ingestion rate of a predator individual and $1/h_i a_i$ is the half-saturation density. Following Yodzis and Innes (1992) and Brose et al. (2006), we modelled the latter to be constant. Since the maximal ingestion rate depends on the body size of the predator (see below), this also implies that the encounter rate depends on the predator body size such that $a_i h_i =$const. It should be noted that, although it is quite common, the assumption of a constant half-saturation density is theoretically not well justified. However, abandoning this assumption would limit comparability of our results with previous studies.

The encounter rate was set to $a_i = 5$ for all links and the handling time was set to $h_i = 0.3$. Simulation results were qualitatively robust against variations of h_i and a_i within a tested parameter range of $0.1 < h_i < 0.5$

and $1 < a_i < 10$. We do not include explicit prey size dependence of the encounter rates as is suggested by several recent studies (Brose et al. 2008; Weitz and Levin 2006) because, implicitly, the food web models partially account for this by their bias at selecting the prey species a predator can successfully feed on. However, note that predator- and prey-size dependency of the encounter rates would not only influence the diet of consumers but might also change the dynamic behavior of the system (Weitz and Levin 2006).

With these parameter values and the large size of the resource pools ($N_{\text{res}} = 700$), basal species realize about 99.9% of their maximal ingestion rate. To emphasize the size of the resource pools, consider that the hypothetical maximal biomass density of an unpredated basal species is approximately 3.2, i.e., more than two orders of magnitude smaller than the size of the resource pools (this can be shown by a simple fixed-point calculation). Therefore, any species that has feeding links to both the resources and another trophic species in the network will always receive the vast majority of its food from the resources.

The total biomass density N_i of the population is the product of the density of individuals and the biomass per individual (the body mass). Up to now, we have not yet considered the fact that body mass varies between species. As mentioned above, the metabolic rates of individuals are assumed to increase with body mass according to a power law. The exponent of this allometric relationship is highly controversial and may even not be universal (Bokma 2004; Glazier 2005; Price et al. 2009). However, in order to keep our model simple and because the value seems to establish as a standard approximation, we take individual metabolic rates to increase with body mass with a single exponent of 3/4 (but note that our results do not rely on the precise value of the allometric exponent; see last paragraph of this section). The metabolic rate per unit biomass decreases, therefore, with the body mass M as $M^{-1/4}$. Since the metabolic rate affects the ingestion and respiration rates, the dynamic equations take the form

$$\frac{dN_i}{dt} = \lambda \sum_{j \in R_i} \frac{g_{ij}(\mathbf{N}) N_i}{M_i^{0.25}} - \sum_{k \in C_i} \frac{g_{ki}(\mathbf{N}) N_k}{M_k^{0.25}} - \frac{\alpha N_i}{M_i^{0.25}} - \beta N_i^2 \quad (4)$$

when different body masses are accounted for (Brose et al. 2006; Brown et al. 2004; Enquist et al. 1999). Intraspecific competition is not a directly metabolically based process; therefore, it is not scaled allometrically. As indicated before, this notation implies that a_i scales inversely with body mass as h_i, so that $a_i h_i = $const (Brose et al. 2006; Yodzis and Innes 1992).

We set the body mass of individuals of basal species to 1; therefore, M_i represents the mass of one individual of species i, divided by the mass of a basal individual. With this choice, the ingestion and respiration rates of basal species do not change when scaled allometrically. Therefore, the energy entering the food webs, which depends only on the ingestion of the basal species, is constant whether or not allometric scaling is considered. The body masses of the other species were assigned according to the rules given in Table 2. In the cascade, niche, and nested hierarchy models, the species are ordered along a single niche dimension, which we assume to be related to the average body mass of the species. The higher the index or niche value of a species is, the higher its trophic level (defined as the length of the shortest path from the species to the resources via feeding links) is on average. The scaling factor x introduced in Table 2 denotes how strongly body mass increases (or decreases, if $x < 0$) along the niche axis. Although there is no unique mapping between a species' position on the niche axis (and, thereby, its mass) and its trophic level, there is still a strong positive correlation. Therefore, x can be used as a proxy for the body-mass ratio of predator–prey pairs. In the layered model, there are only four niches that are identical to the trophic levels of the species, and in the random model, the trophic level is the only measure by which species can be ordered. In these two models, we therefore relate the body mass of the species directly to their trophic level and the scaling factor x is the log_{10} of the body-mass ratio of species on neighboring trophic levels. When the scaling factor $x = 0$, Eq. 4 reduces to Eq. 1.

With these rules we apply for assigning body masses to the species, our results do not rely on the precise value of the scaling exponent of the metabolic rate. A change of the scaling exponent can be mapped onto a change of the scaling factor x. Our results obtained with a scaling exponent of $-1/4$ are equivalent to results obtained with an exponent $-1/3$, but with the scaling factor x reduced by a factor 3/4. Since our results are robust against such changes in x, as will be shown later in the results section (Fig. 3), they are also robust against changes of the scaling exponent of the metabolic rates.

Simulation setup

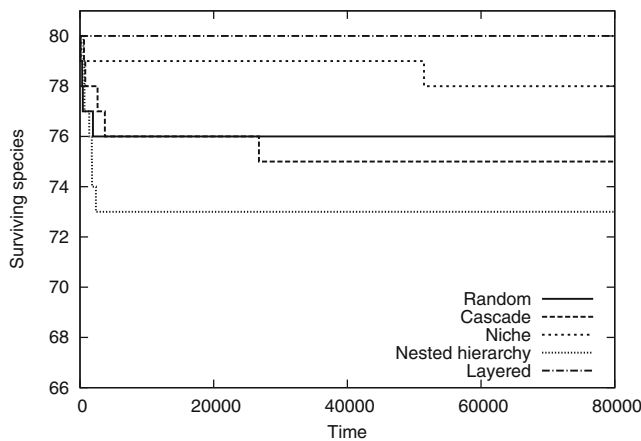We evaluated the robustness R for the five food web topologies, varying the species number between 20 and

Fig. 1 Number of surviving species in representative simulation runs with allometric scaling and $x = 2$ for all five topological models as a function of time. All parameters are at their default values (Table 1)

80 and the scaling factor x (see Table 2) between -2 and 4. Positive values for x mean that predators are, in most cases, larger than their prey.

Initial biomass densities of the species were randomly chosen from the interval $[0, 1]$. If a biomass density dropped at some time during the simulation below the value of 10^{-6} (the extinction threshold), the species was considered extinct and removed from the community by permanently setting its biomass value to 0.

Each simulation run with $x = 0$ was performed according to Eq. 1 for 2,500 time units, which is 125 times longer than the life span of individuals, $1/\alpha_i$. Simulations with larger x needed more time since species with large body mass have a longer life span (e.g., $\max_i(1/\alpha_i) = 2000$ for $x = 2$), and their dynamics are slow. Therefore, these species approach the extinction threshold very slowly. We used a maximum duration of 80,000 time units for simulations that involved large body masses. Tests with a few selected simulation runs

showed that far less than 1% of the species present at the end of these 80,000 time units would become extinct even later (see Fig. 1, where we plot the number of surviving species over time for single simulation runs of each of the five food web models). The robustness data shown in the following are therefore very close to the (hypothetical) exact values.

The numerical integration of the dynamical equations was performed using the Runge–Kutta–Fehlberg algorithm with an absolute local error tolerance $\epsilon_{abs} = 10^{-5}$ and a relative local error tolerance $\epsilon_{rel} = 10^{-8}$. For each data point, we averaged the data obtained from 500 runs that used the same network model (i.e., random, cascade, niche, nested hierarchy, or layered topology) and the same values of all parameters, in particular of S and x. Individual runs differed by the actual network topology generated within the constraints of the respective model and by the randomly chosen initial biomass densities of the species.

Results

We first show that the general effects of allometric scaling of metabolic rates observed by Brose et al. (2006) are also found here, despite some differences in the dynamic equations. This also holds for the two more artificial network topologies (random and layered) that have not been analyzed by Brose et al. (2006). When predators are, on average, larger than their prey, food web robustness is enhanced by allometric scaling. In Fig. 2, the robustness obtained using Eq. 1, i.e., without allometric scaling, is compared with the robustness obtained with allometric scaling (Eq. 4). The data shown are those for the niche model with scaling exponent $x = 2$, those for the other topological models are shown in Fig. 5. Note that, in contrast to Brose et al. (2006), we

Table 1 Parameters and variables used in this study

Parameters are set to their default values unless it is explicitly stated otherwise. A numerical value is only given if it is constant in all simulations. The unit of biomass densities is 1/area and not mass/area because mass is made dimensionless by normalizing it to basal species body mass

| Parameter	Unit	Default value	Meaning
S	Dimensionless		Species richness
C	Dimensionless	0.15	Directed connectance
N_{res}	1/area	700	Size of the resource pools
N_i	1/area		Biomass density of species i
λ_i, λ	Dimensionless	0.4	Assimilation efficiency
α_i, α	1/time	0.05	Respiration rate
β_i, β	Area/time	0.4	Intraspecific competition
a_{ij}, a_i	Area/time	5	Encounter rate
h_{ij}, h_i	Time	0.3	Handling time
f_{ij}	Dimensionless	$1/\omega_i$	Foraging effort of predator i directed to prey j
ω_i	Dimensionless		Number of prey of predator species i
M_i	Dimensionless		Body mass of species i relative to basal body mass
x	Dimensionless		$\log_{10}$ of predator–prey size ratio
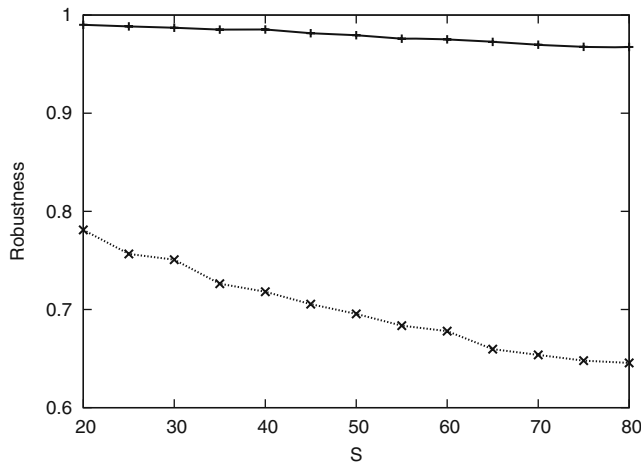
Fig. 2 Robustness vs number of species (S) with (*solid line*, $x = 2$) and without (*dotted line*) allometric scaling in the niche model. All parameters are at their default values (Table 1)

did not observe that the implementation of allometric scaling changes the slope of the robustness vs S curves.

Figure 3 presents robustness results for different predator–prey body mass ratios in all topological models. Food web robustness is enhanced as long as predator size increases with the trophic level or with the niche value (i.e., when x is positive). In the opposite case ($x < 0$), a significant decrease of robustness is found, in line with the results reported by Brose et al. (2006). The small decrease in robustness for large values of x is due to decreasing biomass densities of species on the upper trophic levels. Not enough energy is transported through the food webs to permit survival of all top
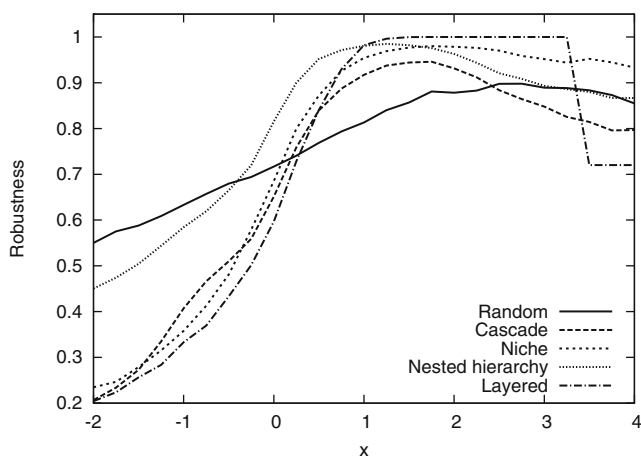
Fig. 3 Robustness as function of the predator–prey body mass ratio. The value of x (see Table 2) varied between −2 (predator 100 times smaller than prey) and 4 (predator 10^4 times larger than prey). Results are shown for $S = 50$. The duration of simulation runs with $x > 2$ was set to 10^6 time units. All parameters are at their default values (Table 1)

predators. From now on, we carry out all simulations where we consider allometric scaling with body mass ratio $x = 2$ since, for this value, robustness is close to its maximal value in all topological food web models, and our results are robust to changes of x by ±1. Furthermore, empirical data suggest that this is a typical value for body mass ratios of predator–prey pairs (Brose et al. 2006) (but note that, in empirical food webs, the $\log_{10}$ of body mass ratios of individual predator–prey pairs can be as large as 16 or as small as −6).

In systems with positive values of x, links from small predators to large prey rarely persisted after population dynamics because the prey became extinct. For instance, in the random model, feeding links connecting predators from the second trophic level to prey on the third trophic level almost always resulted in the extinction of the prey species. However, species on the second trophic level that are eaten by species on the first trophic level have a higher chance of survival. This can be understood as follows: The resources appear in the denominator of every functional response of a predator on the first trophic level. Due to their large size, they drastically decrease the functional response to prey other than the resources. Theoretical considerations of the survivability of prey species that are much larger than their predators are provided by Yodzis and Innes (1992) and by Weitz and Levin (2006).

In the following, we focus on the reasons for the stability increase due to allometric scaling. To this purpose, we multiply Eq. 4 by $M_i^{0.25}$ and obtain

$$\frac{dN_i}{dt} \cdot M_i^{0.25} = \lambda \sum_{j \in R_i} g_{ij}(\mathbf{N}) N_i - \sum_{k \in C_i} \frac{M_i^{0.25}}{M_k^{0.25}} g_{ki}(\mathbf{N}) N_k$$
$$- \alpha N_i - M_i^{0.25} \beta N_i^2 . \qquad (5)$$

This notation, which is mathematically equivalent to Eq. 4 (i.e., it gives rise to exactly the same dynamics) leads to a new interpretation of the effects of allometric scaling. Formally, Eq. 5 differs at three places from Eq. 1:

1. The time increment dt is multiplied by a factor $M^{-0.25}$, which means that the dynamics of species

Table 2 Rules for assignment of body mass to species

Random, layered model	$M_i = 10^{x \cdot (\mathrm{TL}_i - 1)}$.
Cascade model	$M_i = 10^{4 \cdot x \cdot (n_i/S)}$.
Niche & nested-hierarchy model	$M_i = 10^{4 \cdot x \cdot nv_i}$

x defines the relationship between species properties and logarithm of body mass, TL_i is the trophic level, n_i the species index (Cohen and Newman 1985), and nv_i the niche value of species i. The factor 4 was inserted in order to make cascade, niche, and nested-hierarchy models comparable to random and layered models, which usually consist of max. four trophic levels

with larger body mass is much slower than that of basal species.

2. The factor $M_i^{0.25}/M_k^{0.25}$ on the right-hand side reduces the biomass outflow from prey to predator when the predator has a larger body mass than the prey.

3. The competition parameter β is increased by a factor $M_i^{0.25}$ for non-basal species.

In order to identify the cause for the increasing stability, we included the mass dependence only at one of the three places and investigated each of the three possible cases separately. We compared the simulation results for each of the three cases with those obtained from Eq. 1, i.e., without mass effects, and with those obtained with Eq. 4, i.e., with allometric scaling. In order to make the notation shorter, we denote the case without mass effects as the case $x = 0$, and the case with allometric scaling as the case $x = 2$, since we always chose this value of the exponent x.

In the following three subsections, we present the simulation results for the three cases.

Different time scales for species with different body masses

First, we investigated systems with the dynamical equation

$$\frac{dN_i}{dt} \cdot M_i^{0.25} = \lambda \sum_{j \in R_i} g_{ij}(\mathbf{N}) N_i - \sum_{k \in C_i} g_{ki}(\mathbf{N}) N_k$$
$$- \alpha N_i - \beta N_i^2 . \tag{6}$$

Species with a larger body mass have slower dynamics. We expected this to have a positive impact on robustness as the slower dynamics of top species gives species on the lower trophic levels more time to adjust to predator biomasses, thus reducing oscillations.

However, we found that this intuition appears to be wrong. The allometric slowing down of the dynamics of larger species does not increase the robustness of food webs. Moreover, for most models, it even has a small negative impact on the food web robustness (Fig. 6). For this reason, we do not discuss the diversity–robustness relations for this case in detail.

Mass-dependent intraspecific competition

Next, we investigated systems with the dynamical equation

$$\frac{dN_i}{dt} = \lambda \sum_{j \in R_i} g_{ij}(\mathbf{N}) N_i - \sum_{k \in C_i} g_{ki}(\mathbf{N}) N_k$$
$$- \alpha N_i - M_i^{0.25} \cdot \beta N_i^2 . \tag{7}$$

One can expect that the mass-dependent factor in the last term increases robustness, as it reduces predator biomass densities and, thus, increases the survival chances of prey. As a preliminary investigation, we used Eq. 1 to study how the robustness depends on β when all species have the same value of β (Fig. 4). Higher intraspecific competition enhances stability by controlling the biomass densities of the species, but at high values of β, it may reduce the biomasses of species too strongly to permit survival of species on the upper trophic levels (cf. results for the layered model).
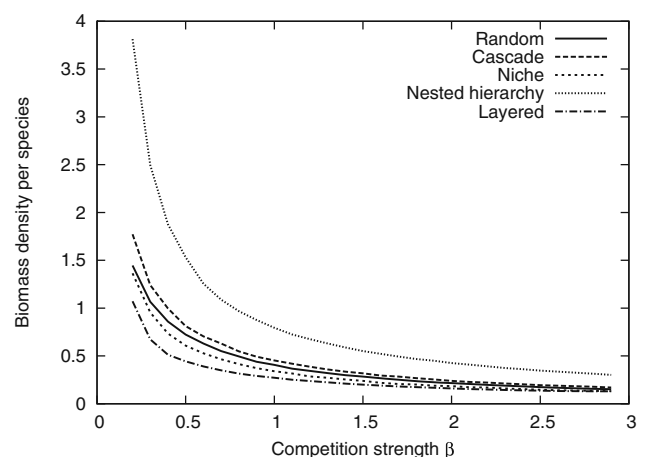
Fig. 4 Robustness and average biomass density per species for all network types as a function of the competition strength β. Higher intraspecific competition enhances robustness by reducing the biomass density per species. All other parameters are at their default values (Table 1); $S = 50$
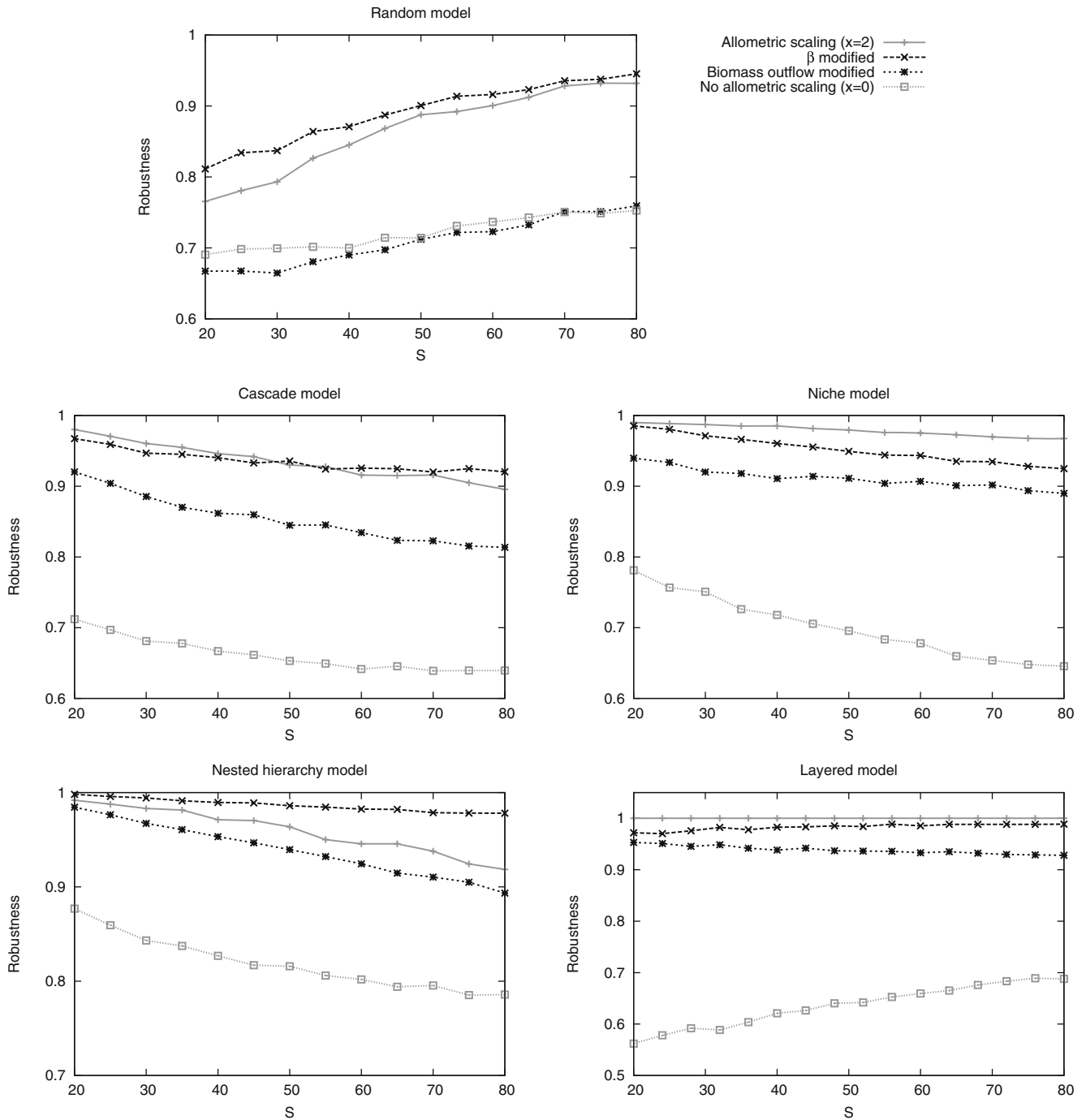
Fig. 5 Effect of mass-dependent competition coefficients (*black long-dashed lines*) and biomass outflow terms (*black short-dashed lines*) on robustness for five different network topologies, compared to the case $x = 0$ (*grey dotted lines*) and to the case $x = 2$ (*grey solid lines*). All parameters are at their default values (Table 1)

Let us see next how robustness is changed when β is multiplied by $M_i^{0.25}$. The simulation results for the different foodweb topologies are shown in Fig. 5 and compared to the cases $x = 0$ and $x = 2$. For all topologies, robustness was increased compared to the case $x = 0$. The extent of the increase depends on the foodweb architecture. It is largest in the random and nested hierarchy models, where the robustness even exceeds that for the case $x = 2$ when S is high. For the other models, robustness is close to that for $x = 2$.

Springer
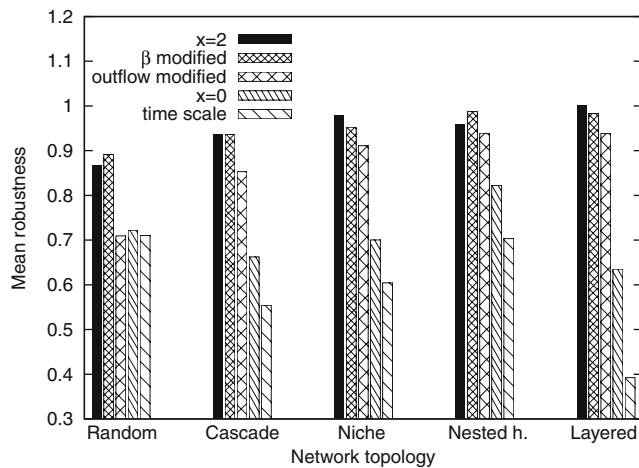
Fig. 6 Robustness values averaged over all species numbers considered for five different network topologies and the five dynamical scenarios

Mass-dependent biomass outflow

Last, we investigated systems with the dynamical equation

$$\frac{dN_i}{dt} = \lambda \sum_{j \in R_i} g_{ij}(\mathbf{N})N_i - \sum_{k \in C_i} \frac{M_i^{0.25}}{M_k^{0.25}} g_{ki}(\mathbf{N})N_k$$
$$- \alpha N_i - \beta N_i^2 . \qquad (8)$$

Biomass outflow from prey to predator is smaller when the body-mass ratio between predator and prey is larger. The robustness data are also shown in Fig. 5, which allows to compare them with the cases $x = 2$ and $x = 0$. While the niche, nested-hierarchy, cascade, and layered models again show a large increase in robustness compared to the case $x = 0$, robustness in the random model is not increased and even appears to decrease slightly for small S.

The simulation results for the three cases that include the mass dependence only at one place in the equations, as well as for the cases $x = 0$ and $x = 2$ are summarized in Fig. 6. For this bar chart, the robustness results have been averaged over all foodweb sizes S.

Discussion

Increasing intraspecific competition, and a reduced biomass outflow to predators that are larger than their prey are both found to increase the robustness of food webs. However, these mechanisms do not enhance stability to the same extent; the magnitude of their impact depends on the topology of the respective food web. For example, in randomly connected webs, the modification of

the biomass outflow has almost no effect. In order to understand the simulation results, we therefore focus our discussion on the random and layered topologies. These two rather artificial food web models do not reflect empirical food web patterns very well, but they represent extreme topologies whose characteristics can be found in empirical food webs in alleviated form. The layered model has the strictest feeding hierarchy. There are no feeding loops, omnivory is excluded (that means all predator-prey pairs have body mass ratio x), and the number of trophic levels (at initialization) is fixed to four. The random topology, on the other hand, does not implement any hierarchy, but it allows for various types of loops and omnivorous links (i.e., feeding links that connect predator–prey pairs with body mass ratios that deviate strongly from the ideal ratio x). We hypothesize that the extent to which these topological characteristics are found in food webs determines the mechanism by which allometric scaling enhances the robustness. The other models are between these two extreme topologies; therefore, the effects we discuss are also intermediate to those observed in random and layered food webs. We restrict our discussion to cases 2 and 3 (mass-dependent competition and mass-dependent energy outflow), since the mass-dependent time scale has almost no positive effect on robustness.

Let us first discuss the results obtained for the random topology. Remarkably, robustness is not affected at all by changing the biomass outflow term. This can be understood by the fact that predators are often not larger than their prey. There is a high number of links connecting small predators to large prey, and in contrast to the feeding loops that occur in the niche and nested hierarchy models, the body mass ratios in these links can be rather extreme in the random model (in the case $x = 2$, a predator two levels under its prey is 10^4 times smaller than its prey). The modification of the biomass outflow term is beneficial only if predators are larger than their prey, and it is highly disadvantageous in the opposite case. Positive and negative effects on stability cancel each other in this case.

In order to understand the simulation results in more detail, we first show the average biomass density per species on each trophic level for the four cases under consideration ($x = 0$, $x = 2$, body-mass-dependent energy outflow, body-mass-dependent competition) after computing the population dynamics; see Fig. 7.

The average biomass density per species on all four trophic levels is significantly larger for the simulations with mass-dependent biomass outflow, compared to the case $x = 0$, indicating that the majority of surviving links connect large predators to small prey. As we have mentioned before, links from small predators to large
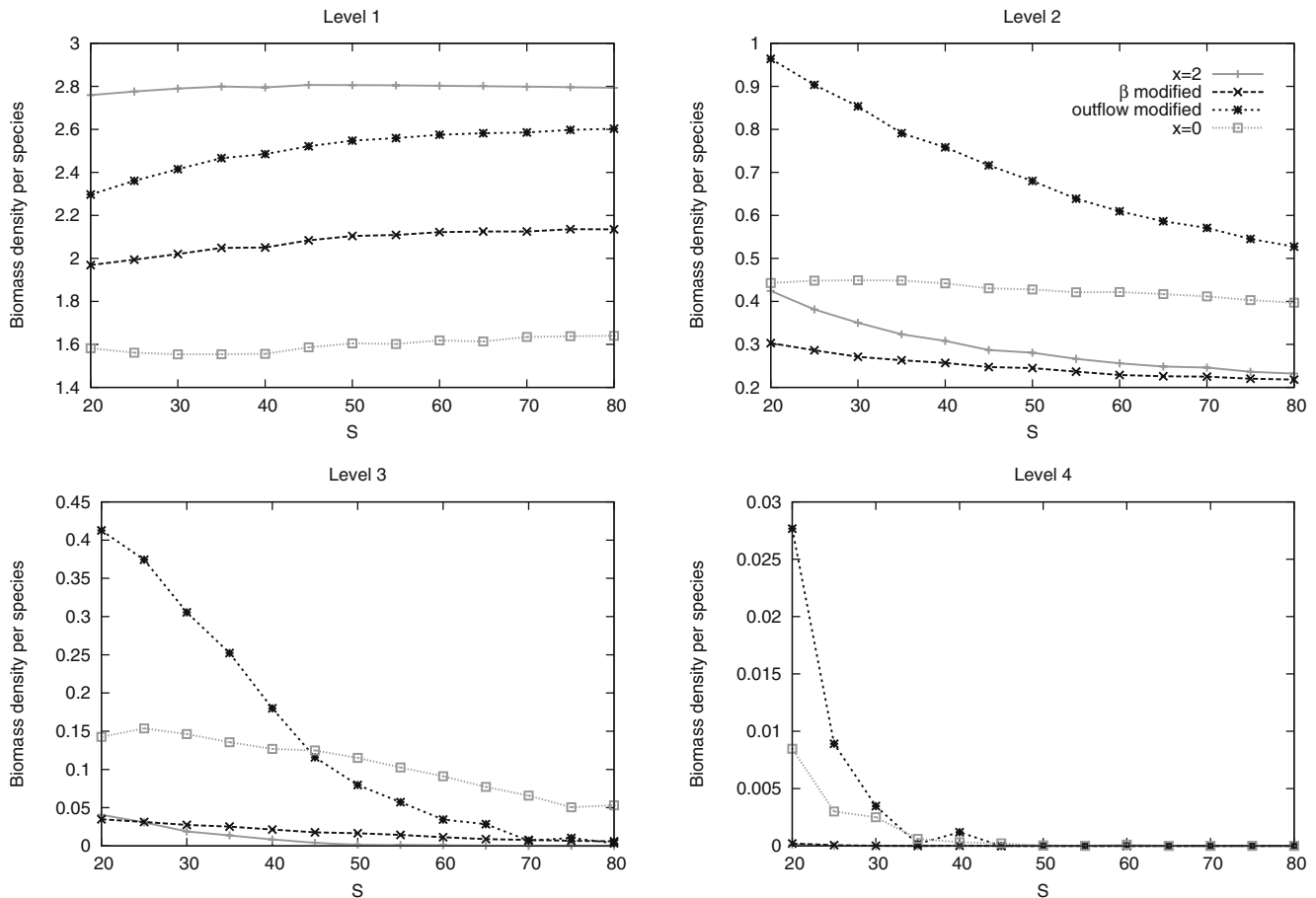
Fig. 7 Average biomass density per species on the four trophic levels of the random model. We show results for the cases $x = 2$ (*grey solid lines*), $x = 0$ (*grey dotted lines*), with mass-dependent competition coefficients (*black long-dashed lines*), and with mass-dependent biomass outflow (*black short-dashed lines*). All parameters are at their default values (Table 1)

prey tend to vanish because the predators drive their prey to extinction. For the case $x = 2$, the biomass density per species on the first trophic level is considerably higher than for the other cases. Apparently, the combined effect of mass-dependent competition and reduced energy outflow strongly decreases the predation pressure on basal species, which, therefore have an increased biomass density.

Now, we turn to the robustness results obtained for the layered model. In order to understand why the mass-dependent biomass outflow has such a strong effect on robustness in this food web topology, we consider again the distribution of average biomass density per species on the four trophic levels, shown in Fig. 8.

In contrast to food webs with random topology, layered foodwebs clearly benefit from the mass-dependent outflow term because of the absence of feeding loops. Compared to simulations with $x = 0$, basal species have a higher average biomass density because of the decreased predation pressure. Species on the fourth

trophic level do not have predators; therefore, their dynamic equations are not changed. Their biomass density increases because their prey becomes more abundant. Species on the intermediate levels benefit from both effects: Their prey becomes more abundant, and their biomass is less reduced by predation. This explains the high values of average biomass density per species and the high robustness for the case of mass-dependent energy outflow in the layered model.

When the competition coefficient is made mass-dependent, this has a negative impact on the average biomass density per species on all trophic levels but the first (compared to the case $x = 0$). The biomass density of the basal species increases because, on the first level, β_i does not change (because $M_i = 1$ for basal species), but predator abundance and, therefore, predation pressure is reduced. Note that, for $x = 2$, $\beta_i M_i^{0.25}$ is ten times larger for species on the third level than for basal species. For even higher values of the competition strength or of the body mass ratio x, competition on the
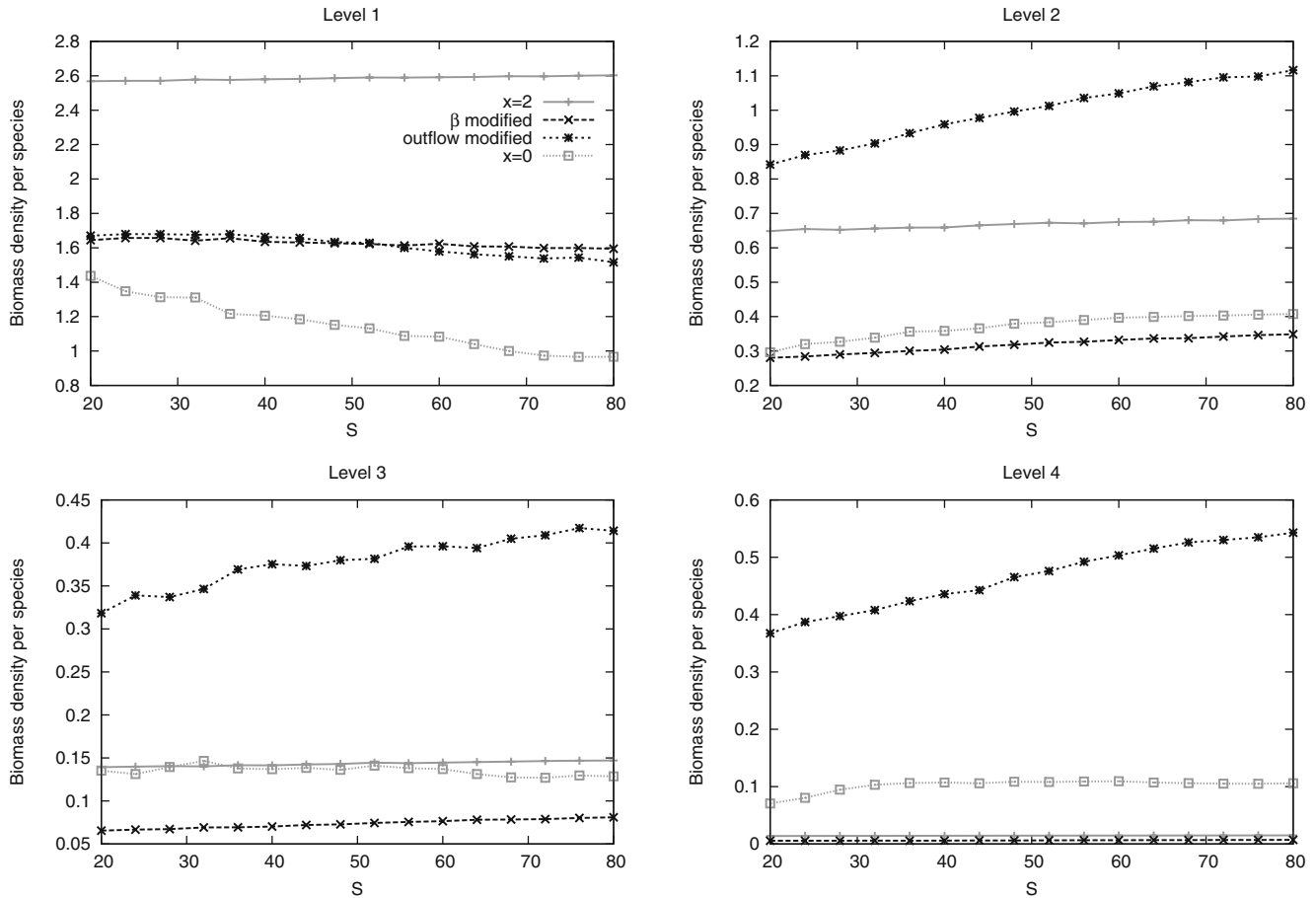
Fig. 8 Average biomass density per species on the four trophic levels of the layered model. We show results for the cases $x = 2$ (*grey solid lines*), $x = 0$ (*grey dotted lines*), with mass-dependent competition coefficients (*black long-dashed lines*), and with mass-dependent biomass outflow (*black short-dashed lines*). All parameters are at their default values (Table 1)

upper two trophic levels would decrease prey biomass density to values too low to permit species survival. The mass-dependent competition coefficient would thereby decrease the positive impact of allometric scaling on robustness (see lines for the layered model in Figs. 3 and 4).

In the case $x = 2$, the effects of increased competition and decreased interaction strength act together. On the lower two levels, this leads to an increase in biomass density compared to simulations without $x = 0$. Here, the reduced biomass outflow to predators is the dominant effect. However, on the third and the fourth levels, the increased competition coefficient becomes very prominent. Note the very low biomass density of the top predators, which is close to that in the case of modified competition coefficient.

The main conclusions from these considerations are, thus, the following: when loops are absent, a mass-dependent outflow term has a positive impact on the biomass densities of all species apart from basal species.

A body-mass-dependent competition coefficient, on the other hand, reduces their biomass density. In the niche and nested hierarchy models, loops can occur, but in contrast to the random model, the unfavorable body mass ratios in these links tend to be moderate. Mass-dependent biomass outflow therefore also increases robustness in these models (Fig. 5).

Finally, let us briefly assess the possible impact of food web connectance on our robustness results. As we wrote in the "Introduction," we initialized food webs with average connectance $C = 0.15$. We confirmed that the average value of final connectance, i.e., after computation of the population dynamics, was still close to this value. However, the realized value of C in individual simulation runs could differ significantly from this average, especially in the niche model. It is well established that different levels of network complexity (measured by C) influence the stability of food webs (Kartascheff et al. 2009) and could, therefore, be responsible for part of the differences in robustness

we observed. We tested for this and found changes in robustness caused by different values of realized connectance to be small compared to the differences caused by allometric scaling.

Conclusion

We have identified two main mechanisms by which allometric scaling of metabolic rates enhances the ro-bustness of food webs. (1) Allometric scaling increases intraspecific competition relative to metabolic rates for species with higher body mass. (2) Allometric scaling leads to a reduced biomass outflow from prey to preda-tor when the predator is larger than the prey. The second effect is less pronounced when there are more feeding loops in the food web, and a mass-dependent outflow does, therefore, not enhance the robustness of food webs with a random topology. The first effect becomes less beneficial when the biomass density of
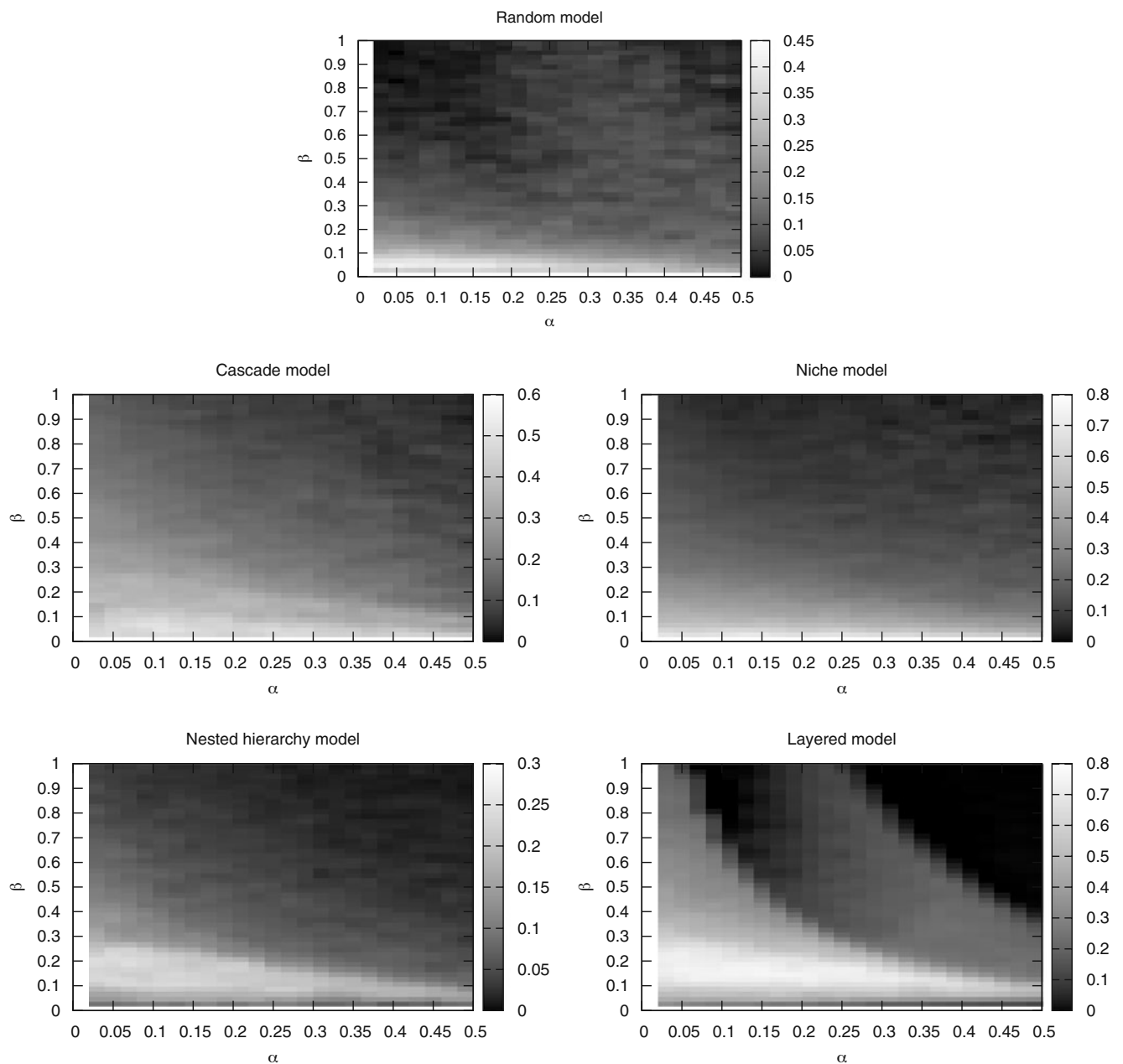
Fig. 9 Increase in robustness in the case $x = 2$ compared to the case $x = 0$ for varying α and β. All other parameters are at their default values (Table 1); $S = 20$

Author's personal copy

top predators is reduced to the extent that they become extinct, as it was observed in models with the layered topology for large values of x or β.

The more realistic cascade, niche, and nested-hierarchy food web models respond strongly to both mechanisms. While they allow for omnivory and, except for the cascade model, also for feeding loops, there is still a more or less strict feeding hierarchy, and the reduced predator–prey interaction strength has a positive effect on robustness. This is consistent with the results by Brose et al. (2006), Otto et al. (2007), and Rall et al. (2008). These results display a robustness increase of the same order of magnitude as observed by us. In contrast to our work, their model does not include intraspecific competition (except for Rall et al. 2008). However, they have not investigated the two topologies where this difference becomes most visible.

We conclude by discussing the limits of validity of our findings. Clearly, allometric scaling will not enhance robustness for all possible choices of parameters. The values of the respiration rate α and the competition strength β must be such that species on higher trophic levels still have a sufficiently large biomass density to be able to persist. The constraints on α and β differ among the topological food web models (Fig. 9). For example, in the niche model, the increase in robustness caused by allometric scaling seems to be nearly independent of α in the tested parameter range, while in the layered model, allometric scaling only increases robustness when $\beta \lesssim 1.7 - 2.8\alpha$. When this condition is not satisfied, the effect of allometric scaling on robustness is neutral or might even become negative.

The size of external resources also has an effect on the robustness increase. If resource biomass was reduced by two orders of magnitude compared to the value chosen by us so that food uptake by the basal species is no longer close to its metabolically determined maximal value, allometric scaling would not be able to increase stability, and it would even decrease stability in some cases, because biomass flow to the upper trophic levels would be too small.

The chosen value of the extinction threshold can affect food web robustness when the average biomass density of the persisting species becomes lower than the extinction threshold. At constant biomass density, large-bodied species have a smaller population density than small species. We nevertheless assumed a constant extinction threshold in our simulations because larger individuals are more mobile than small organisms and can therefore stand smaller population densities when searching for a mating partner before the species becomes extinct. This need not be exact; therefore, we also performed simulations with the extinction thresh-old increasing linearly with the species body mass. We found that our simulation results are valid as long as the maximal extinction threshold is not larger than 10^{-6}.

References

Allesina S, Alonso D, Pascual M (2008) A general model for food web structure. Science 320:658–661

Beddington JR (1975) Mutual interference between parasites or predators and its effect on searching efficiency. J Anim Ecol 44:331–340

Bokma F (2004) Evidence against universal metabolic allometry. Funct Ecol 18:184–187

Brose U, Williams RJ, Martinez ND (2006) Allometric scaling enhances stability in food web models. Ecol Lett 9:1228–1236

Brose U, Ehnes RB, Rall BC, Vucic-Pestic O, Berlow EL, Scheu S (2008) Foraging theory predicts predator–prey energy fluxes. J Anim Ecol 77:1072–1078

Brown JH, Gillooly JF, Allen AP, Savage VM, West GB (2004) Toward a metabolic theory of ecology. Ecology 85:1771–1789

Cattin MF, Bersier LF, Banašek-Richter C, Baltensperger R, Gabriel JP (2004) Phylogenetic constraints and adaptation explain food-web structure. Nature 427:835–839

Cohen JE, Newman CM (1985) A stochastic theory of community food webs. Models and aggregated data. Proc R Soc Lond B 224:421–448

Cohen JE, Briand, EF, Newman, CM (1990) Community food webs: Data and theory. Springer, New York

DeAngelis DL, Waterhouse JC (1987) Equilibrium and nonequilibrium concepts in ecological models. Ecol Monogr 57:1–21

Dodds PS, Rothman DH, Weitz JS (2001) Re-examination of the "3/4-law" of metabolism. J Theor Biol 209:9–27

Drossel B, Higgs PG, McKane AJ (2001) The influence of predator-prey dynamics on the long-term evolution of food web structure. J Theor Biol 208:91–107

Dunne JA (2006) The network structure of food webs. In: Pascual M, Dunne JA (eds) Ecological networks: linking structure to dynamics in food webs. Oxford University Press, Oxford, pp 27–86

Elton CS (1958) Ecology of invasions by animals and plants. Chapman & Hall, London.

Enquist BJ, West GB, Charnow EL, Brown JH (1999) Allometric scaling of production and life-history variation in vascular plants. Nature 401:907–911

Glazier DS (2005) Beyond the '3/4-power law': variation in the intra- and interspecific scaling of metabolic rate in animals. Biol Rev 80:611–662

Kartascheff B, Guill C, Drossel B (2009) Complexity-stability relations in complex model food webs without foraging adaptation. J Theor Biol 259:12–23

Koen-Alonso M (2007) A process-oriented approach to the multispecies functional response. In: Rooney N, McCann KS, Noakes DLG (eds) From energetics to ecosystems: the dynamics and structure of ecological systems. Springer, Dordrecht

Kondoh M (2003) Foraging adaptation and the relationship between food-web complexity and stability. Science 299:1388–1391

Martinez ND, Williams, RJ, Dunne, JA (2006) Diversity, complexity, and persistence in large model ecosystems. In: Pascual M, Dunne JA (eds) Ecological networks: linking structure to dynamics in food webs. Oxford University Press, Oxford, pp 163–185

May RM (1972) Will a large complex system be stable? Nature 238:413–414

MacArthur RH (1955) Fluctuations of animal populations and a measure of community stability. Ecology 36:533–536

McCann K, Hastings A, Huxel GR (1998) Weak trophic interactions and the balance of nature. Nature 395:794–798

McCann KS (2000) The diversity-stability debate. Nature 405:228–233

Neutel AM, Heesterbeek JAP, de Ruiter PC (2002) Stability in real food webs: weak links in long loops. Science 296:1120–1123

Odum E (1953) Fundamentals of ecology. Saunders, Philadelphia

Otto SB, Rall BC, Brose, U (2007) Allometric degree distributions facilitate food-web stability. Nature 450:1226–1230

Paine RT (1980) Food webs, linkage interaction strength, and community infrastructure. J Anim Ecol 49:667–685

Pimm SL (1984) The complexity and stability of ecosystems. Nature 307:321–326

Price CA, Ogle K, White EP, Weitz JS (2009) Evaluating scaling models in biology using hierarchical Bayesian approaches. Ecol Lett 12:641–651

Rall BC, Guill C, Brose U (2008) Food-web connectance and predator interference dampen the paradox of enrichment. Oikos 117:202–213

Rossberg AG, Matsuda H, Amemiya T, Itoh K (2006) Food webs: experts consuming families of experts. J Theor Biol 241:552–563

Ushida S, Drossel B (2007) Relation between complexity and stability in food webs with adaptive behaviour. J Theor Biol 247:713–722

Weitz JS, Levin SA (2006) Size and scaling of predator-prey dynamics. Ecol Lett 9:548–557

West CB, Brown JH, Enquist BJ (1999) The fourth dimension of life: fractal geometry and allometric scaling of organisms. Science 284:1677–1679

White CR, Seymour RS (2003) Mammalian basal metabolic rate is proportional to body mass$^{\frac{2}{3}}$. Proc Natl Acad Sci 100:4046–4049

Williams RJ, Martinez ND (2000) Simple rules yield complex food webs. Nature 404:180–183

Williams RJ, Martinez ND (2004) Stabilizaton of chaotic and non-permanent food web dynamics. Eur Phys J B 38:297–303

Yodzis P (1981) The stability of real ecosystems. Nature 289:674–676

Yodzis P, Innes S (1992) Body size and consumer-resource dynamics. Am Nat 139:1151–1175

LETTER

Interactive effects of body-size structure and adaptive foraging on food-web stability

Lotta Heckmann,[1]* Barbara Drossel,[1] Ulrich Brose[2] and Christian Guill[2]

[1]Institut fur Festkörperphysik, TU Darmstadt, Hochschulstraße 6, 64289 Darmstadt, Germany

[2]Systemic Conservation Biology, J.F. Blumenbach Institute of Zoology and Anthropology, Georg-August-University Göttingen, Berliner Str. 28, 37073 Göttingen, Germany

*Correspondence: E-mail: lotta@fkp.tu-darmstadt.de

Abstract

Body-size structure of food webs and adaptive foraging of consumers are two of the dominant concepts of our understanding how natural ecosystems maintain their stability and diversity. The interplay of these two processes, however, is a critically important yet unresolved issue. To fill this gap in our knowledge of ecosystem stability, we investigate dynamic random and niche model food webs to evaluate the proportion of persistent species. We show that stronger body-size structures and faster adaptation stabilise these food webs. Body-size structures yield stabilising configurations of interaction strength distributions across food webs, and adaptive foraging emphasises links to resources closer to the base. Moreover, both mechanisms combined have a cumulative effect. Most importantly, unstructured random webs evolve via adaptive foraging into stable size-structured food webs. This offers a mechanistic explanation of how size structure adaptively emerges in complex food webs, thus building a novel bridge between these two important stabilising mechanisms.

Keywords

Body mass, networks, optimal foraging, population dynamics, predator–prey, simulation.

Ecology Letters (2012) **15**: 243–250

INTRODUCTION

Despite several decades of research, the stability of complex food webs is not yet completely understood (McCann 2000; Montoya *et al.* 2006). May (1972) demonstrated that randomly connected food webs with random interaction strengths are unstable with respect to perturbations of an equilibrium point if the number of species, the number of links or the interaction strengths are too high. This contradicted the perception of field ecologists (MacArthur 1955) and thus raised the so-called complexity stability debate, since empirical food webs can be very complex and yet seem to be stable.

May's assumptions of random topologies and random interaction strengths do not lead to ecologically plausible models, however, even with more empirically motivated topologies (Cohen & Newman 1985; Williams & Martinez 2000; Cattin *et al.* 2004; Stouffer *et al.* 2005), empirically consistent interaction strength distributions (Yodzis 1981; de Ruiter *et al.* 1995; Neutel *et al.* 2002, 2007) and other notions of stability (e.g. Williams & Martinez 2004; Brose *et al.* 2006b; Kartascheff *et al.* 2010), it was observed that the stability of model food webs typically decreases with increasing connectance of the networks or with the number of species. It increases only when resources are abundant and the functional response satisfies certain requirements (Williams & Martinez 2004; Rall *et al.* 2008; Kartascheff *et al.* 2009). Two effects that were reported to enhance the stability of food webs are those of body-size structure and adaptive foraging (Kondoh 2003; Brose *et al.* 2006b; Uchida & Drossel 2007; Rall *et al.* 2008; Kartascheff *et al.* 2009). The interplay of these two mechanisms in determining food-web stability is the focus of the present paper.

Ecological communities generally possess a clear body-size structure with predators being typically 0.5–4 orders of magnitude larger in body mass than their prey (Brose *et al.* 2006a,b; Riede *et al.* 2011). Many species traits vary across different species with their average body size as a power law with exponent different from one, which creates a specific pattern of interaction strengths in food webs. This mechanism is often paraphrased as allometric scaling of metabolic rates. Building on these allometric relationships, Brose *et al.* (2006b) and Rall *et al.* (2008) showed that model food webs exhibit positive relationships between species number or connectance and stability if they possess an empirically consistent body-size structure of predators being larger than their prey. A mechanistic explanation for the stabilising effect of allometric scaling was provided by Kartascheff *et al.* (2010).

Adaptive foraging, which is the ability of species to adapt their foraging efforts to changing prey abundances, is a widely used concept in ecological modelling (Uchida *et al.* 2007; Abrams 2010; Loeuille 2010; Valdovinos *et al.* 2010) which can also have a positive effect on food-web stability (Kondoh 2003, 2006; Uchida & Drossel 2007; Berec *et al.* 2010). However, few studies include both the effects of allometric scaling and adaptive processes, notable examples being Loeuille & Loreau (2005) and Rossberg *et al.* (2008) where adaptation on evolutionary time scales in size-structured communities is studied.

In this work, the combined influence of body-size structure and adaptive foraging on the stability of model food webs is investigated. Our results show that allometry of metabolic rates stabilises food webs only if predators are larger than their prey, and that adaptive foraging can stabilise food webs if adaptation occurs sufficiently fast. On top of that, by the analysis of randomly connected food webs, we demonstrate for the first time that an interactive effect between allometric scaling and adaptive foraging exists: adaptive foraging dynamically emphasises those predator–prey body-size structures that favour ecosystem stability. This leads to even higher food-web stability if both mechanisms act together.

MATERIALS AND METHODS

The model food webs consist of S species, Z of which are *basal species* that only feed on a nutrient pool with constant size (called 'resource'

in the following), while $S-Z$ species feed on other species but not on the resource. The *trophic level* of a species denotes its minimal distance to the resource measured in predator–prey links. The *connectance C* is the average number of links divided by S^2.

We used two different stochastic models with input parameters S, Z and C to create the network structure of the food webs. In the random model, the Z basal species are assigned only a link to the resource, all other links are realised with the same probability $p = CS^2/S(S-Z)$. In the niche model (Williams & Martinez 2000) each species is assigned a niche value $n_i \in [0,1]$, which together form an ordered set. Trophic links are set such that the prey species of a predator have consecutive niche values that are in general smaller than the predator's niche value. In this model, species without prey are basal species, which are assigned a link to the resource. Only webs with Z basal species are accepted. Cannibalistic links are never profitable for adaptive foragers in both models, we therefore do not allow such links for non-adaptive species either.

The dynamical model is based on the bioenergetics approach of Yodzis & Innes (1992). The time evolution of the biomass densities B_i of the S species is described by S coupled ordinary differential equations (Brose *et al.* 2006b; Kartascheff *et al.* 2010), a detailed derivation of which is given in the Appendix S1:

$$\dot{B}_i = \lambda \sum_{j \in R_i} m_i^{-0.25} \frac{af_{ij}B_j}{1 + \sum_{l \in R_i} af_{il}hB_l} B_i$$
$$- \sum_{k \in C_i} m_k^{-0.25} \frac{af_{ki}B_i}{1 + \sum_{n \in R_k} af_{kn}hB_n} B_k - \alpha m_i^{-0.25} B_i - \beta m_i^{-0.25} B_i^2.$$

(1)

R_i denotes the set of prey species, C_i the set of predator species and m_i the mean body mass of species i. The expression in the first sum describes the per unit biomass consumption rate of a predator individual, which follows a Holling Type II functional response with prey biomass density B_j, multiplied by the total biomass density of the predator population. The parameters a and h are the mass-corrected attack rate and handling time, respectively. f_{ij} denotes a foraging effort describing the percentage of time species i spends on foraging for species j, which requires $\sum_{j \in R} f_{ij} = 1$ (Kondoh 2003, 2006). λ is the assimilation efficiency of consumers, i.e. the capability of converting consumed biomass into own biomass. The parameters α and β describe mass-corrected respiration rate and intraspecific competition, respectively. Intraspecific competition provides a self damping effect stabilising population dynamics and thereby allowing for more coexisting species. For basal species, the first term in eqn 1 gives a constant growth rate, leading together with the last two terms to logistic growth.

Respiration rate and maximum ingestion rate of individuals scale allometrically with body mass, the exponent of the corresponding power law relations is often recorded to be around 3/4 (Peters 1983; Brown *et al.* 2004). Consequently, mass-specific consumption rate (the first term in eqn 1) and mass-specific respiration rate (the third term in eqn 1) scale with $m_i^{-0.25}$. However, the value of the exponent is controversial: a scaling exponent of 2/3 would correspond to a geometrical mechanism (White & Seymour 2003), and recently it was suggested that both exponents may be correct in certain regimes (Kolokotrones *et al.* 2010; Ehnes *et al.* 2011). For simplicity, we confine ourselves to the exponent 3/4, while lower exponents lead to qualitatively consistent results. Following the 'Metabolic Theory of Ecology' (West *et al.* 1997; Brown *et al.* 2004), equilibrium biomass

densities increase with a 1/4-power law with body mass such that the last term of eqn 1 also scales with $m_i^{-0.25}$.

In our simulations, the body-size structure of food webs is created by assigning the species a body mass $m_i = 10^{xn_i}$, where n_i is a random number between 0 and 1 in the random model and is identical to the niche value in the niche model. Basal species are exempted from this rule; to guarantee comparable energy input into the webs for both topologies, we impose $m_{\text{basal}} = 1$. The parameter x fixes the maximum (minimum for $x < 0$) possible predator–prey body-mass ratio in a web, which is 10^x. The body-mass ratio of a blue whale to krill, for example, is $c.\ 10^8$ and could only appear in food webs with $x \geq 8$.

The network model, niche or random, thereby defines whether there is an initial size structure in the network with predators being either consistently larger or smaller than their prey or not. The parameter x determines how strong this body-size structure of the food webs is. In the niche model, $x > 0$ means that predators are typically larger than their prey, and for $x < 0$, they are mostly smaller than their prey. In random networks, this holds only for the trophic relations to the basal species. All other predator–prey pairs have random body-mass ratios, therefore random food webs have (apart from the basal species) no body-size structure. To shorten notation, we refer to x as the allometry coefficient in the following.

We chose parameter values that are motivated empirically (Yodzis & Innes 1992; Brose *et al.* 2006b; Williams *et al.* 2007; Berec *et al.* 2010; Kartascheff *et al.* 2010) and set $\lambda = 0.65$, $a = 6$, $h = 0.35$ and $\alpha = 0.3$ for all simulations. The biomass density of the resource, $B_{res} = 500$, and the strength of the intraspecific competition, $\beta = 0.5$, were fixed such that the maximum biomass density of a basal species remains much smaller than the biomass density of the resource. With our choice of parameters, we have $B_{basal}^{max} \approx 3$. All parameters, their physical dimensions, and, where applicable, allometric scaling relationships are summarised in Table A1 in the Appendix S1.

The dynamics of the foraging efforts is described by replicator equations, which is a commonly used form (Kondoh 2003, 2006; Garcia-Domingo & Saldana 2007; Uchida *et al.* 2007; Uchida & Drossel 2007). The differential equation for foraging effort f_{ij} has the form

$$\dot{f}_{ij} = \kappa f_{ij} \left(\frac{\partial G_i}{\partial f_{ij}} - \sum_{k \in R_i} f_{ik} \frac{\partial G_i}{\partial f_{ik}} \right),$$

(2)

where G_i is the net growth rate of population i: $\dot{B}_i = G_i B_i$. To avoid that links that are initially present disappear completely, efforts that fall below a value of 10^{-4} are set to this value such that they can increase again later (Uchida & Drossel 2007). It was tested that our results do not qualitatively depend on this assumption (see Appendix S2). The parameter κ defines the time scale on which foraging efforts can be adapted to changing prey biomass densities. In the following, we refer to κ as the adaptation rate.

We used two measures of stability that are widespread in the food-web literature (Brose *et al.* 2003; Kondoh 2003; Brose *et al.* 2006b; Kondoh 2006; Uchida & Drossel 2007). The *robustness R* is the percentage of species that survive population dynamics, averaged over many realisations of food webs constructed using the same parameter values. The second stability measure is the *persistence P* of food webs: For an ensemble of food webs, it describes the fraction of webs in which all species survived population dynamics.

For our simulations, we set $S = 30$, $Z = 5$ and $C = 0.15$, and we averaged over 100 food-web realisations for each combination of x

and κ. Initial values for biomass densities are chosen randomly from the interval [0,1]. Foraging efforts are initialised with $f_{ij}{}^0 = 1/p(i)$, where $p(i)$ is the number of prey species of species i. A species is considered to be extinct if its biomass density falls below the extinction threshold $B_{ext} = 10^{-6}$, and its density is then set to zero permanently. The time evolution of the dynamics is run until a fixed time t_{end} at which the number of surviving species and the links between them are evaluated. Since larger body-mass ratios lead to slower dynamics for larger species (cf. eqn A4 in the Appendix S1), we set $t_{end} = 20\,000$ for allometry coefficients $x \leq 2$ and $t_{end} = 10\,000 \cdot x$ for larger values of the coefficient. We checked exemplarily that this time is sufficiently long such that it is unlikely that further extinctions occur. The computer simulations were performed with C-programs, using the Runge–Kutta–Fehlberg algorithm provided by the gnu scientific library, with an absolute local error tolerance $\varepsilon_{abs} = 10^{-6}$ and a relative local error tolerance $\varepsilon_{rel} = 10^{-8}$.

RESULTS

We first present results for the stability of model food webs with random and niche topologies and then analyse the structure of the persistent networks.

Stability of the food webs

We evaluated the robustness and persistence of the two topological models for different values of the allometry coefficient x, where $-12 \leq x \leq 16$ with $\Delta x = 0.8$, and different adaptation rates κ of the

foraging efforts. The adaptation rate was varied logarithmically between 10^{-3} and 10^2 with a factor of 10, and an additional set of simulation runs for $\kappa = 0$, i.e. without adaptation, was performed (Fig. 1). The main results here are (1) that a larger adaptation rate κ (horizontal direction in the plots in Fig. 1) generally has a stabilising effect on both models and (2) that predator–prey body-mass ratios larger than 1 (allometry coefficient $x > 0$) always stabilise niche model food webs but not random models. Notably, in random model food webs a robustness close to 1 is only observed if the allometry coeffiecient is positive and if the adaptation of foraging efforts occurs at least on the time scale of the population dynamics (i.e. for adaptation rates $\kappa \geq 1$). For negative values of the allometry coefficient, only around 30% of the species survive, and the persistence falls to zero in both models.

An interesting feature of the robustness data shown in Fig. 1 is the local minimum of stability for allometry coefficients $x \lesssim 0$ and intermediate adaptation rates ($\kappa \approx 0.1$). This can be understood by analysing the robustness for each trophic level separately (Fig. 2). In both models and for all combinations of allometry coefficient and adaptation rate, species on lower trophic levels have a higher probability to survive than species on higher trophic levels, which means that the average trophic level of all surviving species in the food web closely follows the robustness patterns shown in Fig. 1.

Species on trophic level 3 or higher hardly ever survive if body masses decrease with niche value (i.e. for negative allometry coefficients) irrespective of the value of the adaptation rate κ, while for species on trophic level 2, survival depends on the value of the
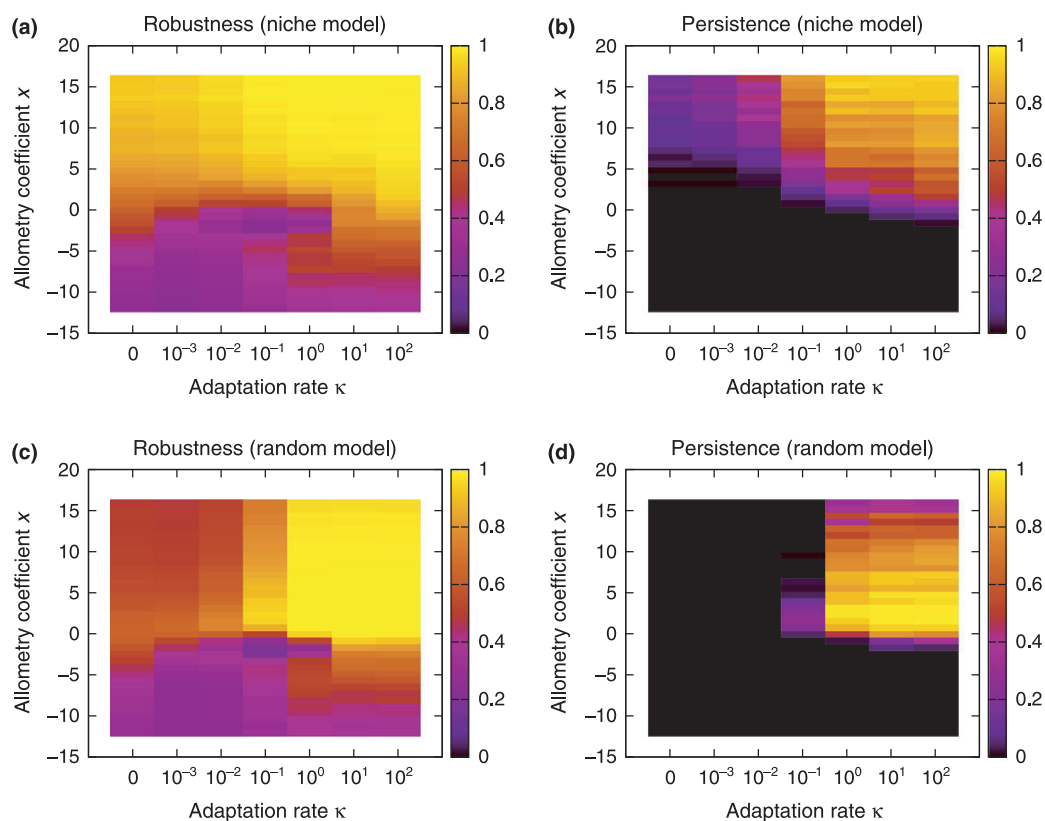

Figure 1 Robustness (left) and persistence (right) for niche (top) and random model (bottom). For each model and each combination of the allometry coefficient x (slope of the $\log_{10}$ increase of body mass with niche value) and adaptation rate κ (speed of foraging adaptation), 100 food webs were evaluated. The abscissae are scaled logarithmically except for the leftmost columns which correspond to $\kappa = 0$ (no adaptation).
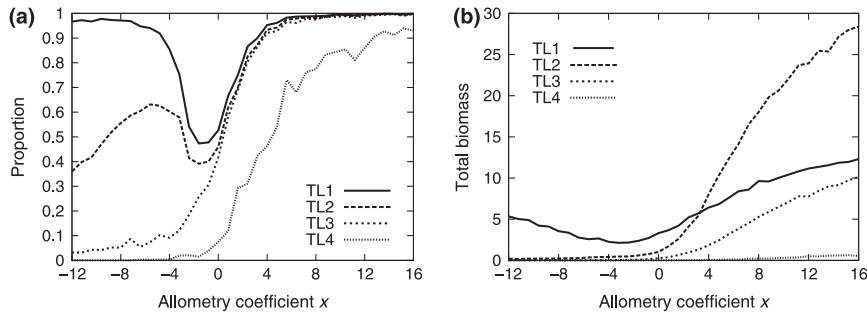
Figure 2 The percentage of surviving species (a) and the total biomass (b) on different trophic levels for the niche model with adaptation rate $\kappa = 1$ as an example of the non-monotonous behaviour of the robustness of species on the first and second trophic level for intermediate adaptation rates. These graphs also illustrate how allometry stabilises food webs: Increasing predator–prey body-mass ratios limit the per unit biomass flow from prey to predators and thus allows all species to accumulate more biomass and thereby enhance their survivability. For each value of the allometry coefficient x, the data points are averaged over 300 realisations.

adaptation rate: if $\kappa \lesssim 1$, species on trophic level 2 benefit from small negative allometry coefficients, while for very large and very small adaptation rates, their survivability decreases monotonously with the coefficient x. The robustness of basal species is, irrespective of the adaptation rate κ, close to 1 if the absolute value of the allometry coefficient is sufficiently large (i.e. if body masses vary over a wide range).

In the niche model, we find that for large allometry coefficients x and small adaptation rates κ the robustness of the networks is close to 1 while the persistence is close to zero. This is due to the small fraction of species on the fourth or a higher trophic level, which only survive if they can adapt sufficiently fast to their most profitable prey (see Appendix S2).

Structure of the food webs after population dynamics

In order to further investigate the interplay of allometric scaling and adaptive foraging with respect to their positive influence on food-web stability, we analysed the structure of these food webs, i.e. the properties of the persistent species and of the remaining links after population dynamics. We did this only for positive allometry coefficients, because the stability results shown in Figs 1 and 2 suggest that for negative allometry coefficients the persistent parts of the food webs have a trivial network structure with mainly basal species and their direct predators surviving.

We consider the average trophic level of prey species, compared to the trophic level of their predators:

$$\langle \text{TL}_{\text{prey}} \rangle := \frac{1}{S' - Z'} \sum_{i=1}^{S'} \sum_{j \in R_i} f_{ij}(\text{TL}(j) - \text{TL}(i)). \qquad (3)$$

Here, $\text{TL}(i)$ is the trophic level of species i, S' is the number of surviving species and Z' is the number of surviving basal species. The links are weighted with the values of the respective foraging efforts at t_{end} to account for the dynamically realised network structure.

For food webs with a random topology, we also investigated the average predator–prey body-mass ratio, as in contrast to the niche model, in random models trophic level and body mass of a species are initially not correlated, except for basal species which are either the smallest ($x > 0$) or the largest ($x < 0$) species in the network. Instead of directly evaluating the body-mass ratios, we evaluated the

niche values of the prey species compared to those of their predators. They are proportional to the $\log_{10}$ of the body-mass ratio, but do not explicitly contain the allometry coefficient x (see Appendix S2).

$$\langle n_{\text{prey}} \rangle := \frac{1}{S' - Z'} \sum_{i=1}^{S'} \sum_{j \in R_i} f_{ij}(n_j - n_i). \qquad (4)$$

For allometry coefficients $x > 0$ this is negative if predators prefer prey that is smaller than themselves. In Fig. 3 we show the final average prey trophic level (relative to that of the respective predators) for the niche (a) and the random model (b) as well as the final average prey niche values for the random model (c). For all values of the allometry coefficient x and the adaptation rate κ these final values are smaller than the corresponding initial values that are evaluated with the initial foraging efforts f_{ij}. This indicates that predators tend to focus on prey species on lower trophic levels and with smaller body masses.

If in the calculation of the average trophic level or the body mass of the prey species the links are not weighted with the corresponding foraging effort f_{ij}, additional insight on the survivability of predator–prey pairs can be gained. These final unweighted values are also smaller than the corresponding initial unweighted values for all allometry coefficients and adaptation rates showing that predator–prey pairs have a higher chance to persist if the predator is larger and on a higher trophic level than the prey (results not shown).

If the food webs are stable, i.e. for allometry coefficients $x \geq 0$ and adaptation rates $\kappa \geq 1$, the final network structures resemble empirical food webs fairly well (cf. Table 1; Dunne *et al.* 2004). Not surprisingly, the niche model performs better than the random model (Williams & Martinez 2000). The average predator–prey body-mass ratio varies consistently with the allometry coefficient x. In natural food webs the most typical mass ratios are between $10^{0.5}$ and 10^4 (Brose *et al.* 2006b; Riede *et al.* 2011), which corresponds roughly to allometry coefficients between $x = 2$ and $x = 10$.

DISCUSSION

In the following, we argue that body-size structure and foraging adaptation provide a mechanism for dynamical ordering and self-
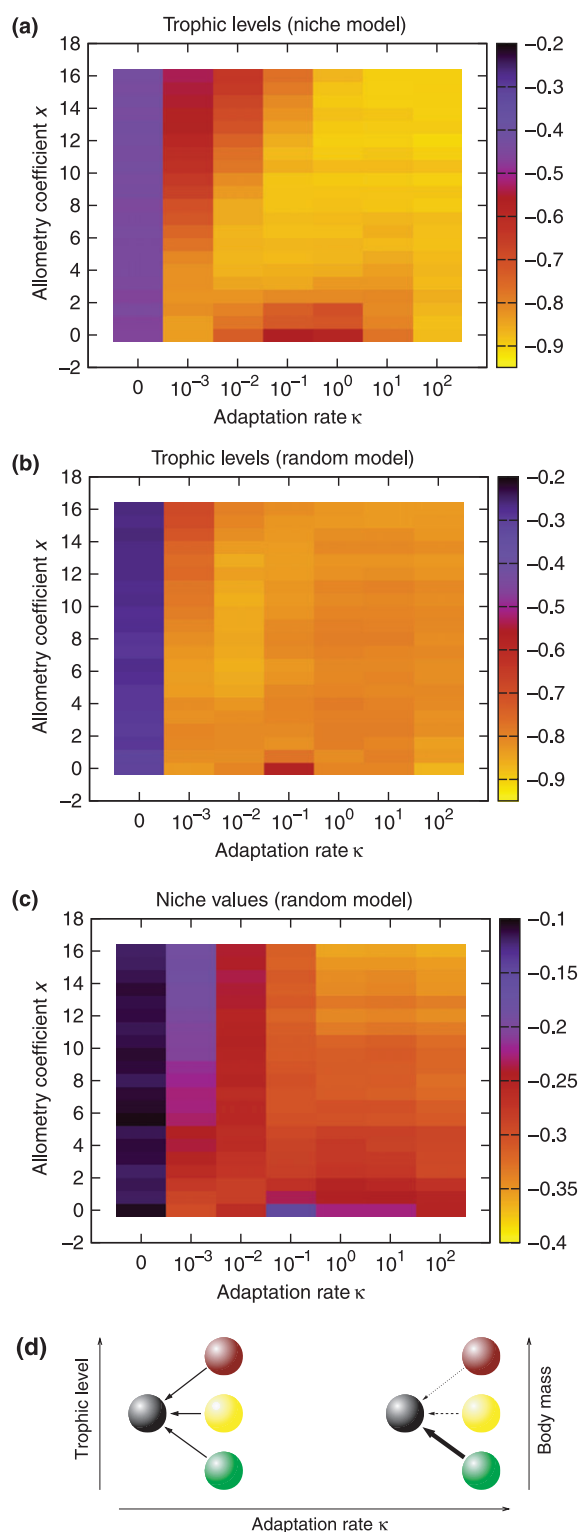
Figure 3 Average prey trophic level relative to that of the predators after population dynamics for the niche model (a) and the random model (b) and average prey niche value relative to that of the predators after the population dynamics for the random model (c). The initial values of average prey trophic level and average prey niche value are independent of κ and x. For the niche model, we have $\langle TL^{ini}_{prey} \rangle = -0.420$, and for the random model, we have $\langle TL^{ini}_{prey} \rangle = -0.241$ and $\langle n^{ini}_{prey} \rangle = -0.086$. The final values shown are all smaller than the initial values, which indicates that adaptive foragers focus on prey on lower trophic levels and with smaller body mass (d).

stabilisation of food webs. If foraging adaptation is fast enough, even in networks with initially random structure stabilising body-size structures with large predators and small prey emerge dynamically. We start with a separate analysis of the influence of body-size structure and adaptive foraging on food webs, before we discuss the interactive effect.

Effects of body-size structure

Let us first consider network structures that cannot change via adaptive foraging (adaptation rate $\kappa = 0$) and focus on the case in which body masses increase with niche value (allometry coefficient $x > 0$). In the random model, predators are initially equally often larger and smaller than their prey, since body masses are assigned randomly, while in the niche model, in most predator–prey relationships the predator is larger than the prey. Our finding that larger average body-mass ratios (larger values of the allometry coefficient x) stabilise niche model food webs (Fig. 1a,b, in vertical direction) thus confirms the well-known result that the allometry of metabolic rates stabilises model food webs with a strong body-size structure where species on higher trophic levels have larger body masses than species on lower levels (Brose *et al.* 2006b; Kartascheff *et al.* 2010). If on the other hand there is no clear body-mass structure in the food webs, like in the random model, and there are many links connecting smaller predators to larger prey, we find no stabilisation of the networks for large allometry coefficients x (Fig. 1c,d). Similarly, if the allometry coefficient is negative, the persistence falls to zero in all models (Fig. 1b,d), and robustness decreases in general, too, which shows that small predators foraging for large prey are not favourable for stability. These theoretical results are in agreement with the fact that in empirical (stable) food webs predators are mostly larger than their prey (Woodward *et al.* 2005; Brose *et al.* 2006a,b).

The stabilisation of food webs with strong body-mass structure and positive allometry coefficient x was mechanistically explained by Kartascheff *et al.* (2010). When multiplying eqn 1 with $m_i^{0.25}$, one can see that the outflow of biomass from species i to a predator species k scales with $(m_i/m_k)^{0.25}$ (cf. eqn A4 in the Appendix S1), implying that this outflow is smaller and that the prey survives with higher probability when m_i/m_k is smaller. Here, we have shown that this explanation also holds in networks with adaptive link structure.

The robustness results for the random model are not symmetric with respect to the sign of the allometry coefficient x because the body mass of basal species is always $m_{basal} = 1$. For $x > 0$ this makes them the smallest species in the food webs and for $x < 0$ the largest. This has either a positive ($x > 0$) or a negative ($x < 0$) effect on the stability of the networks via the mechanism described above. The niche model allows a few exceptions from the strict body-mass structure, but these do not have a qualitative effect on the results as comparative simulations with the generalised cascade model (Stouffer *et al.* 2005) that excludes these exceptions have confirmed.

We therefore conclude that allometric scaling has a stabilising effect on food webs only if species on higher trophic levels are larger than species on lower trophic levels. Our results are in agreement with prior studies concerning the body-size structure of food webs (Brose *et al.* 2006b; Kartascheff *et al.* 2010) that report quantitatively similar increases in the robustness of non-random networks, and with studies analysing the evolutionary emergence of size-structured communities (Loeuille & Loreau 2005; Rossberg *et al.* 2008). Furthermore, the

Table 1 Structural properties of stable model food webs with adaptation rate $\kappa = 10$. Evaluated are the average predator–prey body-mass ratio, the normalised standard deviations of vulnerability and generality distributions, the fractions of basal, intermediate, and top species, the average trophic level, and the average number of links per species for different values of the allometry coefficient x. For comparison, we also show minimum and maximum of empirically observed values reported by Brose *et al.* (2006b; typical body-mass ratios), Dunne *et al.* (2004; average trophic levels), and Williams & Martinez (2000; all other quantities). Note that the definition of trophic level used by Dunne *et al.* (2004) slightly differs from the one used in this study

	x	$\langle m_{pred}/m_{prey} \rangle$	σ_V^{norm}	σ_G^{norm}	%B	%I	%T	$\langle TL \rangle$	$\langle L/S \rangle$
Niche	0	1.0	0.65	1.01	19.1	72.3	8.7	2.078	3.627
	4	$7.21 \cdot 10^1$	0.63	1.01	17.2	75.6	7.2	2.163	4.392
	8	$4.95 \cdot 10^3$	0.65	1.02	16.9	74.9	8.2	2.159	4.355
	12	$3.00 \cdot 10^5$	0.65	1.04	16.8	75.7	7.4	2.148	4.529
	16	$2.11 \cdot 10^7$	0.65	1.02	16.8	74.4	8.8	2.187	4.553
Random	0	1.0	0.44	0.62	16.8	82.3	0.9	2.178	4.237
	4	$4.44 \cdot 10^1$	0.44	0.63	16.7	82.2	1.1	2.168	4.188
	8	$2.12 \cdot 10^3$	0.44	0.62	16.8	82.2	0.9	2.172	4.149
	12	$1.22 \cdot 10^5$	0.45	0.62	17.0	81.9	1.1	2.146	4.165
	16	$5.94 \cdot 10^6$	0.46	0.63	17.3	81.3	1.4	2.128	4.046
Empirical	Min	$10^{0.5}$	0.54	0.73	0.04	0.52	0	1.5	2.2
	Max	10^4	1.41	1.42	0.32	0.92	0.32	3.2	10.8

range of body-mass ratios for which stabilisation occurs in our simulation fits well to observed ecosystem data (Brose *et al.* 2006b; Riede *et al.* 2011). However, we only considered body masses via the allometry of metabolic rates, although there is evidence that for example attack rates exhibit hump-shaped dependencies on predator–prey body-mass ratios (Wahlstroem *et al.* 2000; Brose *et al.* 2008; Vucic-Pestic *et al.* 2010). The influences of such more complex and more realistic assumptions on food-web stability would require further investigations that are beyond the scope of this work.

Adaptive foraging

We found that adaptive foraging allows for more surviving species in both niche and random model food webs if adaptation occurs sufficiently fast (adaptation rate $\kappa > 1$), in agreement with existing results (Uchida & Drossel 2007; Guill & Drossel 2008): adaptive species can focus on their most profitable prey and release unprofitable prey with low biomass from predation. If the adaptation is sufficiently fast, species that come close to the extinction threshold are not preyed upon any more and have therefore a higher chance to regain biomass and survive. In size-structured ecosystems, predators will thus preferably focus on small prey species because they have larger per unit biomass production rates.

If the adaptation rate is very small ($\kappa = 10^{-3}$), the time scale of foraging adaptation is by far slower than that of population dynamics. Adaptation to changing prey abundances is therefore very inefficient and can hardly stabilise webs compared to the situation of no adaptation ($\kappa = 0$). For intermediate adaptation rates ($\kappa = 10^{-2} \ldots 1$), the effects of body-mass structure and adaptive foraging interact. Adaptation is fast enough for predators to be able to focus on prey on lower trophic levels, but if body masses are sufficiently different within a network (allometry coefficient $x \gtrsim 3$), only niche model food webs are stable and random food webs are not, because the effects of body-mass structure dominate. When predator–prey body-mass ratios are smaller, the energetic demands of predators relative to the per unit biomass production rates of their prey increase which leads to overexploitation of species on the lower two trophic levels and at the same time to starvation of the predators. This leads to the minimum of robustness around $\kappa = 10^{-1}$ and $x \lesssim 0$ (Fig. 2). The

robustness of the food webs increases again slightly at even lower negative values of the allometry coefficient when the species on the second trophic level are released from predation due to the extinction of their predators. This top-down release process leads to stable flat food webs consisting of only basal species and their direct predators.

From these considerations follows that fast foraging adaptation of predators always stabilises food webs. To our knowledge, however, it is not known to which extent foraging adaptation occurs in nature as a fast or slow process. Adaptation may occur through evolution or through a change in behaviour (i.e. learning), and the relative time scales of these processes are still discussed (Hairston *et al.* 2005). It is possible that the adaptation rate κ depends on the body mass and is thus not independent of the allometry coefficient x. Adaptation rate might be high for both the smallest and the largest species, but small for intermediate species: small species can have a high evolutionary potential for fast adaptation due to their larger populations sizes and short generation times, while larger species might benefit from a fast learning capability due to their larger brains (Kondoh 2010). The effect of interspecific variation of adaptation rates is thus another open question.

Food-web structure

Next, we discuss the resulting structure of stable food webs, i.e. those with allometry coefficients ≥0. Structurally, we observed in both models the trend that a predator–prey pair is more likely to persist if the prey is on a lower trophic level and has a smaller body mass than its predator. A low average trophic level of the prey corresponds to the fact that it is favourable for a species to feed on prey close to the external resource ('food chains are short'). This general result has to be qualified if, other than we assumed in our dynamical model, different prey species that are assimilated with low or high efficiency like plants and animal prey, respectively, have to be considered. In this case, omnivorous predators would adaptively focus on the resource that yields the highest net energy gain (consumption rate times assimilation efficiency).

Evaluating which prey are preferred dynamically, i.e. via the adaptation of foraging efforts, shows a pronounced preference of

predators towards smaller prey species on lower trophic levels in both random and niche model food webs (Fig. 3). This effect is larger in the random model than in the niche model, since in the niche model most predators are in the initial networks already larger than their prey. This finding means that predators do not exploit all of their potential prey species equally, but focus on prey species on lower trophic levels and with smaller body masses. This is in agreement with the result that species in stable food webs should possess few strong and several weak links if the food web is to be stable (McCann *et al.* 1998; Kondoh 2006; Scotti *et al.* 2009).

More precisely, our results are coherent with the finding reported in Gross *et al.* (2009) that the stability of niche model food webs is correlated with the average difference of the niche values of predators and prey, and that weak links may promote stability in this model only if these links correspond to predator–prey pairs with a large difference in niche values. However, for a randomly connected web no such connection between body masses and stability was established yet. Thus, our results show that an initially randomly connected web without body-size structure evolves towards an ordered web with clear, stabilising body-size structure during population dynamics via extinctions of unfavourably connected species and via dynamical focusing of predators on profitable prey species.

CONCLUSIONS

We conclude that body-size structure and adaptive foraging can both independently stabilise food webs if predator–prey body-mass ratios are in a range that is also found in real ecosystems (Brose *et al.* 2006b) and if adaptation occurs on a time scale faster than population dynamics. When both mechanisms are accounted for in the model, the two mechanisms together lead to even more stable food webs showing that the stabilising influences of both effects interact positively (Fig. 4).

Most importantly, our results show that even networks with random linkage patterns and random interaction strengths can be dynamically
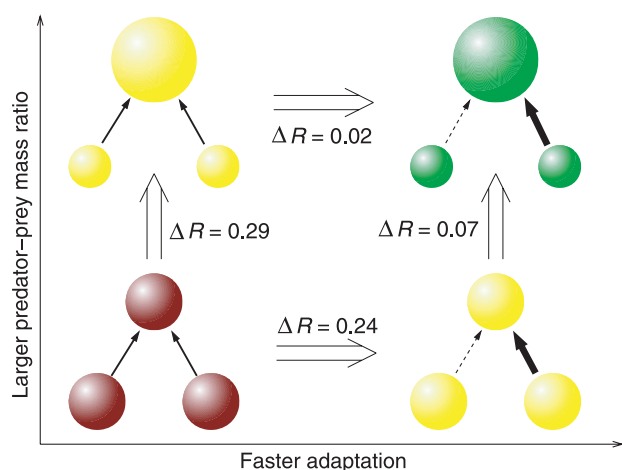
Figure 4 Combined effect of body-size structure and adaptive foraging on the robustness in the niche model as obtained from Fig. 1. The colours indicate the stability of the networks, where green corresponds to highest and red to lowest stability. The robustness increases by $\Delta R = 0.31$ from 63% for food webs where the body masses of all species are identical and without adaptive foraging (bottom left) to 94% for the case of large predator–prey body-mass ratios (allometry coefficient $x = 16$) and fast foraging adaptation ($\kappa = 10^2$) (top right). Both mechanisms also lead separately to enhanced stability (top left and bottom right).

stabilised: if a food web initially does not have a body-size structure, adaptive foraging provides a dynamical mechanism that emphasises links with favourable connection strengths (i.e. those that are associated with predator–prey mass ratios larger than 1) and weaken unfavourable links. By this, stable network topologies with strong, empirically consistent body-size structure occur (Fig. 3d). This is one further reason for why May's results (May 1972), which built on random networks, may not apply to real ecosystems in which non-random patterns emerge dynamically. In conclusion, the work presented here demonstrates that the combination of body-size structure and adaptive foraging provides a synergetic mechanism that leads dynamically to the emergence of stable food webs.

REFERENCES

Abrams, P. (2010). Implications of flexible foraging for interspecific interactions: lessons from simple models. *Funct. Ecol.*, 24, 7–17.

Berec, L., Eisner, J., and Krivan, V. (2010). Adaptive foraging does not always lead to more complex food webs. *J. Theor. Biol.*, 266, 211–218.

Brose, U., Williams, R., and Martinez, N. (2003). Comment on foraging adaptation and the relationship between food-web complexity and stability. *Science*, 301, 918–919.

Brose, U., Jonsson, T., Berlow, E., and Warren, P. (2006a). Consumer-resource body-size relationships in natural food webs. *Ecology*, 87, 2411–2417.

Brose, U., Williams, R., and Martinez, N. (2006b). Allometric scaling enhances stability in complex food webs. *Ecol. Lett.*, 9, 1228–1236.

Brose, U., Ehnes, R., Rall, B., Vucic-Pestic, O., Berlow, E., and Scheu, S. (2008). Foraging theory predicts predator–prey energy fluxes. *J. Anim. Ecol.*, 77, 1072–1078.

Brown, J., Gillooly, J., Allen, A., Savage, V., and West, G. (2004). Toward a metabolic theory of ecology. *Ecology*, 85, 1771–1789.

Cattin, M., Bersier, L.-F., Banasek-Richter, C., Baltensperger, R., and Gabriel, J.-P. (2004). Phylogenetic constraints and adaptation explain food-web structure. *Nature*, 427, 835–839.

Cohen, J. and Newman, C. (1985). A stochastic theory of community food webs: I. Models and aggregated data. *Proc. R. Soc. Lond.* B, 224, 421–448.

Dunne, J., Williams, R.J., and Martinez, N.D. (2004). Network structure and robustness of marine food webs. *Mar. Ecol. Prog. Ser.*, 273, 291–302.

Ehnes, R., Rall, B., and Brose, U. (2011). Phylogenetic grouping, curvature and metabolic scaling in terrestrial invertebrates. *Ecol. Lett.*, 14, 993–1000.

Garcia-Domingo, J. and Saldana, J. (2007). Food-web complexity emerging from ecological dynamics on adaptive networks. *J. Theor. Biol.*, 247, 819–826.

Gross, T., Rudolf, L., Levin, S., and Dieckmann, U. (2009). Generalized models reveal stabilizing factors in food webs. *Science*, 325, 747–750.

Guill, C. and Drossel, B. (2008). Emergence of complexity in evolving niche-model food webs. *J. Theor. Biol.*, 251, 108–120.

Hairston, N., Ellner, S., Geber, M., Yoshida, T., and Fox, J. (2005). Rapid evolution and the convergence of ecological and evolutionary time. *Ecol. Lett.*, 8, 1114–1127.

Kartascheff, B., Guill, C., and Drossel, B. (2009). Positive complexity–stability relations in food web models without foraging adaptation. *J. Theor. Biol.*, 259, 12–23.

Kartascheff, B., Heckmann, L., Drossel, B., and Guill, C. (2010). Why allometric scaling enhances stability in food web models. *Theor. Ecol.*, 3, 195–208.

Kolokotrones, T., Savage, V., Deeds, E., and Fontana, W. (2010). Curvature in metabolic scaling. *Nature*, 464, 753–756.

Kondoh, M. (2003). Foraging adaptation and the relationship between food-web complexity and stability. *Science*, 299, 1388–1391.

Kondoh, M. (2006). Does foraging adaptation create the positive complexity–stability relationship in realistic food-web structure? *J. Theor. Biol.*, 238, 646–651.

Kondoh, M. (2010). Linking learning adaptation to trophic interactions: a brain size-based approach. *Funct. Ecol.*, 24, 35–43.

Loeuille, N. (2010). Consequences of adaptive foraging in diverse communities. *Funct. Ecol.*, 24, 18–27.

Loeuille, N. and Loreau, M. (2005). Evolutionary emergence of size-structured food webs. *Proc. Natl Acad. Sci. USA*, 102, 5761–5766.

MacArthur, R. (1955). Fluctuations of animal populations and a measure of community stability. *Ecology*, 36, 533–536.

May, R. (1972). Will a large complex system be stable? *Nature*, 238, 413–414.

McCann, K. (2000). The diversity–stability debate. *Nature*, 405, 228–233.

McCann, K., Hastings, A., and Huxel, G. (1998). Weak trophic interactions and the balance of nature. *Nature*, 395, 794–798.

Montoya, J., Pimm, S., and Sole, R. (2006). Ecological networks and their fragility. *Nature*, 442, 259–264.

Neutel, A.-M., Heesterbeek, J., and de Ruiter, P. (2002). Stability in real food webs: weak links in long loops. *Science*, 296, 1120–1123.

Neutel, A., Heesterbeek, J., de Koppel, J., Hoenderboom, G., Vos, A., Kaldeway, C., Berendse, F. *et al.* (2007). Reconciling complexity with stability in naturally assembling food webs. *Nature*, 449, 599–602.

Peters, R.H. (1983). *The Ecological Implications of Body Size*. Cambridge University Press, pp. 24–44.

Rall, B., Guill, C., and Brose, U. (2008). Food-web connectance and predator interference dampen the paradox of enrichment. *Oikos*, 117, 202–213.

Riede, J., Brose, U., Ebenman, B., Jacob, U., Thompson, R., Townsend, C., and Jonsson, T. *et al.* (2011). Stepping in elton's footprints: a general scaling model for body masses and trophic levels across ecosystems. *Ecol. Lett.*, 14, 169–178.

Rossberg, A., Ishii, R., Amemiya, T., and Itoh, K. (2008). The top-down mechanism for body-mass-abundance scaling. *Ecology*, 89, 567–580.

de Ruiter, P., Neutel, A.-M., and Moore, J. (1995). Energetics, patterns of interaction strengths, and stability in real ecosystems. *Science*, 269, 1257–1260.

Scotti, M., Bondavallia, C., and Bodinia, A. (2009). Linking trophic positions and flow structure constraints in ecological networks: energy transfer efficiency or topology effect? *Ecol. Model.*, 220, 3070–3080.

Stouffer, D., Camacho, J., Guimera, R., Ng, C., and Nunes Amaral, L. (2005). Quantitative patterns in the structure of model and empirical food webs. *Ecology*, 86, 1301–1311.

Uchida, S. and Drossel, B. (2007). Relation between complexity and stability in food webs with adaptive behaviour. *J. Theor. Biol.*, 247, 713–722.

Uchida, S., Drossel, B., and Brose, U. (2007). The structure of food webs with adaptive behaviour. *Ecol. Model.*, 206, 263–276.

Valdovinos, F., Ramos-Jiliberto, R., Garay-Narvaez, L., Urbani, P., and Dunne, J. (2010). Consequences of adaptive behaviour for the structure and dynamics of food webs. *Ecol. Lett.*, 13, 1546–1559.

Vucic-Pestic, O., Rall, B., Kalinkat, G., and Brose, U. (2010). Allometric functional response model: body masses constrain interaction strengths. *J. Anim. Ecol.*, 79, 249–256.

Wahlstroem, E., Persson, L., Diehl, S., and Bystroem, P. (2000). Size-dependent foraging efficiency , cannibalism and zooplankton community structure. *Oecologia*, 123, 138–148.

West, G., Brown, J., and Enquist, B. (1997). A general model for the origin of allometric scaling laws in biology. *Science*, 276, 122–126.

White, C. and Seymour, R. (2003). Mammalian basal metabolic rate is proportional to body mass2/3. *Proc. Natl Acad. Sci. USA*, 100, 4046–4049.

Williams, R. and Martinez, N. (2000). Simple rules yield complex food webs. *Nature*, 404, 180–183.

Williams, R. and Martinez, N. (2004). Stabilization of chaotic and non-permanent food-web dynamics. *Eur. Phys. J.* B, 38, 297–303.

Williams, R., Brose, U., and Martinez, N. (2007). Homage to yodzis and innes 1992: scaling up feeding-based population dynamics to complex ecological networks. In: *From Energetics to Ecosystems: The Dynamics and Structure of Ecological Systems* (eds Rooney, N., McCann, K.S., & Noakes, D.L.G.). Springer, Dordrecht, pp. 37–52.

Woodward, G., Ebenman, B., Emmerson, M., Montoya, J.M., Olesen, J.M., Valido, A., and Warren, P.H. *et al.* (2005). Body size in ecological networks. *Trends Ecol. Evol.*, 20, 402–409.

Yodzis, P. (1981). The stability of real ecosystems. *Nature*, 289, 674–676.

Yodzis, P. and Innes, S. (1992). Body-size and consumer-resource dynamics. *Am. Nat.*, 139, 1151–1173.

SUPPORTING INFORMATION

Complexity–stability relations in generalized food-web models with realistic parameters

Sebastian J. Plitzko [a,*], Barbara Drossel [a], Christian Guill [b]

[a] Institut für Festkörperphysik, TU Darmstadt, Hochschulstraße 6, D-64289 Darmstadt, Germany
[b] Systemic Conservation Biology, J.F. Blumenbach Institute of Zoology and Anthropology, Georg-August-University Göttingen, Berliner Straße 28, D-37073 Göttingen, Germany

A B S T R A C T

We investigate the relation between complexity and stability in model food webs by evaluating the local stability of fixed points of the population dynamics using the recently developed method of generalized modeling. We first determine general conditions that lead to positive complexity–stability relations. These include (1) high resource abundance and (2) strong density-dependent mortality effects that limit consumer populations. The parameters that constitute a generalized model have clear biological meanings. In this work, emphasis is placed on using realistic values for these generalized parameters. They are derived from conventional ordinary differential equations which are commonly used to describe population dynamics and for which empirical parameter estimates exist. We find that the empirically supported generalized parameters fall in regions of the parameter space that allow for a positive relation between food-web complexity and stability.

© 2012 Elsevier Ltd. All rights reserved.

1. Introduction

Considering the pace of global biodiversity loss and its impact on ecosystem services (Dobson et al., 2006), understanding the mechanisms that stabilize ecological communities is of critical importance. However, this is often hampered by the high complexity of the considered systems. Early theoretical studies have shown that complexity (in terms of species diversity or connectance of the interaction networks) does not increase stability by simply providing alternative interaction pathways, but rather decreases the dynamical stability of the communities (Gardner and Ashby, 1970; May, 1972). More recent studies have highlighted the importance of realistic network topologies (Yodzis, 1981; Martinez et al., 2006), non-random patterns of interaction strengths (McCann et al., 1998; Neutel et al., 2002; Berlow et al., 2004; Gross et al., 2009), and effects mediated by natural body size (Yodzis and Innes, 1992; Brose et al., 2006; Kartascheff et al., 2010).

Theoretical results concerning the population dynamics of interacting species always depend to some extent on the mechanistic assumptions and the specific form of the equations used in the respective study. For example, dynamical patterns and the stability of food webs are often highly sensitive to the exact mathematical form of the functional response that describes the interaction rate between predator and prey species (Williams and Martinez, 2004; Rall et al., 2008) or to the precise values of the parameters characterizing these rates (McCann et al., 1998).

These limitations are avoided by the method of generalized modeling (GM) recently developed by Gross and Feudel (2006) and successfully applied to ecological problems (Gross et al., 2005, 2009). This method builds on a rescaling of the dynamical equations describing the population dynamics such that the fixed points (equilibrium values) of all populations are 1. It avoids the need to calculate the population dynamics explicitly and determines instead the stability of the fixed point of dynamics directly from the Jacobian of the dynamical system. In contrast to May's seminal work, which also evaluates the stability of fixed points (May, 1972), the elements of the Jacobian in GM are not random numbers, but depend on parameters whose values can be directly interpreted in terms of simple, but very general statements such as "prey is abundant" or "mortality is dominated by density-dependent effects". The method can also be extended to studying the stability of periodic solutions (Kuehn and Gross, 2011). However, GM can give no information on species persistence when the considered fixed point or periodic solution is unstable.

In contrast, the conventional modeling approach, which is based on integrating differential equations for the population dynamics, can also evaluate the stability of food webs with regular or chaotic oscillations by determining the fraction of species that are able to persist in these dynamical states. These non-stationary dynamics have been shown to play a crucial role

* Corresponding author. Tel.: +49 6151 16 4969; fax: +49 6151 16 3681.
E-mail addresses: plitzko@fkp.tu-darmstadt.de (S.J. Plitzko),
drossel@fkp.tu-darmstadt.de (B. Drossel), guill@fkp.tu-darmstadt.de (C. Guill).

in preserving biodiversity in systems that depend only on a few different limiting nutrients (Huisman and Weissing, 1999). Nevertheless, it appears that in general the conditions for local stability, such as the one derived by May (1972) for randomly connected networks, and the conditions for species persistence are very similar (Sinha and Sinha, 2005). The great advantage of GM is the ability to derive stability criteria from a more abstract perspective, which does not rely on specific assumptions concerning the interactions between populations.

Despite their simple biological meaning, direct estimates for the values of the parameters used in GM studies are not available since experimental studies normally focus on quantifying explicit functional relationships. In this study, we advance the ecological applicability of GM by first establishing the conditions for a positive relation between complexity (measured either as species diversity or as network connectance) and dynamical stability of communities with realistic network topologies. The latter are created with the niche model (Williams and Martinez, 2000), which successfully reproduces empirical food-web patterns. We then derive values for the generalized parameters from conventional population dynamics equations for which parameter estimates based on empirical and experimental knowledge exist. We demonstrate that the generalized parameters derived from this procedure fall in regions of the parameter space that allow for a positive relation between food-web complexity and stability.

2. The model

In the following, we first describe the food-web topology used in this study. Then, we introduce the generalized modeling equations. In order to make the method as transparent as possible, we start from a broadly used form of conventional population dynamics equations and explicitly carry out the generalization procedure.

2.1. Topology of the food-web model

Our investigations are based on the widely used niche model (Williams and Martinez, 2000). The species in the network are ordered on a one-dimensional niche axis. A predator species i preys on all species j whose niche values n_j (the position on the niche axis) are within an interval on the niche axis with width $n_i r_i$ and center c_i (see Fig. 1). The "feeding range" of a predator is therefore given by the interval $c_i \pm n_i r_i / 2$. The parameters n_i and r_i are chosen at random from probability distributions on the interval $[0;1]$, and c_i is drawn with constant probability from the interval $[n_i r_i / 2; n_i]$. The probability distribution used for the niche value n_i is a constant distribution, while the distribution of the relative width r_i is a β-distribution $P(r|1,\beta) = \beta(1-r)^{\beta-1}$. We define $\beta = (1-2C)/2C$ including the connectance C, which is the number of present links divided by the number of possible links.

Species with a feeding range that contains no prey species are considered as basal species, which obtain their energy from an external resource pool that is not affected by the dynamics of the food web.
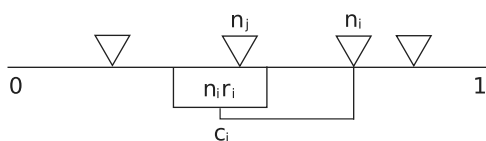

Fig. 1. Sketch of the niche model, after Williams and Martinez (2000). Species j with niche value n_j is prey of species i.

2.2. Conventional food-web dynamics

The biomass dynamics of S interacting species is generally described by a system of S coupled ordinary differential equations. Here, we use the bio-energetics approach developed by Yodzis and Innes (1992) as a standard model of the conventional population dynamics (Brown et al., 2004; Brose et al., 2006; Kartascheff et al., 2010; Heckmann et al., 2012). The nonlinear differential equations for the biomass densities $\mathbf{B} = (B_1, B_2, \ldots, B_S)$ of the species include terms for (in the order of appearance) food ingestion, losses due to predation, mortality and respiration, and intraspecific competition

$$\frac{dB_i(t)}{dt} = \lambda \sum_{j \in R_i} G_{ij}(\mathbf{B}, M_i) B_i - \sum_{k \in C_i} G_{ki}(\mathbf{B}, M_k) B_k - \alpha_i(M_i) B_i - \beta_i(M_i) B_i^2. \quad (1)$$

Here, R_i and C_i are the sets of prey species and predators, respectively, of species i, which are determined by the rules of the niche model. The parameter λ is the assimilation efficiency, α_i summarizes respiration and mortality, and β_i is the strength of intraspecific competition. The latter represents a simplified concept of general self limitation at high population densities without accounting for more specific behavioral mechanisms involved. Basal species have a constant growth rate $q_i > \alpha_i$, which models primary production, instead of the food ingestion term. In combination with the term for intraspecific competition, this leads to a logistic net growth rate of the basal species with a carrying capacity proportional to $1/\beta_i$.

The trophic interaction between predator species i and its prey j is described by a Holling type II functional response

$$G_{ij}(\mathbf{B}, M_i) = \frac{a_i(M_i) f_i B_j}{1 + \sum_{l \in R_i} a_i(M_i) f_i h_i(M_i) B_l}, \quad (2)$$

with a_i being the prey capture rate, $f_i = 1/$(number of predator i's prey species) denoting the fractional foraging effort invested into each prey species, and h_i being the handling time that a predator needs to deal with and digest a unit biomass of prey. The constant growth rate q_i of basal species can also be written in the form (2) by setting $q_i = a_i R / (1 + a_i h_i R)$, with a constant resource pool of size R.

The parameters a_i, h_i, α_i, and β_i all scale allometrically with body mass M_i according to the following power laws: $a_i = a M_i^{-0.25}$, $h_i = h M_i^{0.25}$, $\alpha_i = \alpha M_i^{-0.25}$ and $\beta_i = \beta M_i^{-0.25}$ (Peters, 1986; West et al., 1997; Brown et al., 2004). Multiplying Eq. (1) with $M_i^{0.25}$ enables us to write it in a form that is more convenient for the derivation of the generalized model

$$\frac{dB_i(t)}{dt} M_i^{0.25} = \lambda \sum_{j \in R_i} G_{ij}(\mathbf{B}) B_i - \sum_{k \in C_i} \frac{M_i^{0.25}}{M_k^{0.25}} G_{ki}(\mathbf{B}) B_k - \alpha B_i - \beta B_i^2. \quad (3)$$

We link the body masses of the species to their niche values according to $M_i = 10^{x \cdot n_i}$, where n_i is the niche value of species i, and x is a parameter that quantifies the change of body mass with niche value, here set to $x = 8$, which means that the ratio between the largest and smallest body mass of a species is 10^8. The body mass of basal species is set to $M_i = 1$.

When evaluating the stability of a fixed point, a linear analysis in the neighborhood of a fixed point is sufficient, leading to the linearized set of equations

$$\delta \dot{\mathbf{B}} = J(\mathbf{B}^*) \cdot \delta \mathbf{B},$$

where $\delta \mathbf{B}$ is the deviation of the population sizes from their fixed point values, and $J(\mathbf{B}^*)$ is the Jacobian matrix, i.e., the derivative of the right-hand side of the population dynamics equations with respect to the population sizes B_i at the fixed point B_i^*. If all eigenvalues of the Jacobian have negative real parts,

perturbations approach asymptotically zero, and the fixed point is locally stable.

2.3. Generalized food-web model

Next we will use Eq. (3) to derive the generalized model introduced by Gross and Feudel (2006). The biomass densities B_i and functions U_i that depend on biomass densities are normalized such that their fixed point values becomes 1, by defining the dimensionless quantities

$$b_i = \frac{B_i}{B_i^*}; \quad u_i(b_1, b_2, \ldots, b_S) = \frac{U_i(B_1^* b_1, B_2^* b_2, \ldots, B_S^* b_S)}{U_i^*},$$

where the function at the fixed point is denoted as $U_i^* = U_i(B_1^*, B_2^*, \ldots, B_S^*)$. In the following we will need three such functions. The first function is the total biomass density of the prey of predator i, denoted as T_i or, in its dimensionless form, $t_i = T_i/T_i^*$. The second function is $g_i(t_i)$, which is the dimensionless version of the first term on the right side of Eq. (3), i.e., of the biomass gain due to feeding. The third dimensionless function is $m_i(b_i)$, which describes all biomass loss incurred due to causes other than predation, i.e., due to the last two terms on the right-hand side of Eq. (3). They cover respiration, background mortality, diseases, and competition for all resources other than food.

In order to illustrate how the elements of the Jacobian result from the population dynamics equations, we derive them starting from Eq. (3) with the functional response (2). We do not allow cannibalism, and therefore every species either gains biomass due to consumption or due to primary production. The latter is being modeled by a logistic growth function. The negative quadratic part of this function, which contains the carrying capacity, is associated with the mortality term. With these simplifications, the elements of the Jacobian can be written as

$$J_{ij} = \tau_i \left[\vartheta_i \gamma_i \chi_{ij} - \delta_i \left(\rho_{ji} + \sum_{l=1}^{S} \rho_{li}(\gamma_l - 1)\chi_{lj} \right) \right] \tag{4}$$

and

$$J_{ii} = \tau_i \left[1 - (1-\delta_i)\mu_i - \delta_i \left(\sum_{l=1}^{S} \rho_{li}[(\gamma_l - 1)\chi_{li} + 1] \right) \right]. \tag{5}$$

The seven parameters in Eqs. (4) and (5) can be classified as scale parameters and exponent parameters. The scale parameters describe the relative weights of biomasses or biomass fluxes, or measure the time scale. These are the parameters τ_i, ϑ_i, δ_i, ρ_{ji}, and χ_{ji}. The exponent parameters μ and γ measure the extent of nonlinearity of the functions m_i and g_i with respect to the normalized biomass densities b_i at the fixed point.

In the following, we will explain all these parameters in more detail. The parameter τ_i refers to the characteristic time scale of the population dynamics of species i and denotes the biomass turnover rate. The fractions of biomass gain due to consumption of prey and of biomass loss due to being preyed upon, of species i are represented by the parameters ϑ_i and δ_i. This means that $(1-\vartheta_i)$ describes the fraction of biomass gain due to primary production, and that $(1-\delta_i)$ is the fraction of all other sources of biomass loss apart from being eaten. The parameter χ_{ij} measures the relative weight of population j to the total amount of available food to species i. ρ_{ji} measures the relative contribution of species j to the predative loss of species i.

The expressions for these scale parameters in terms of those of the conventional model are the following:

$$\tau_i = (\lambda q_i) + \left(\sum_{j \in R_i} \frac{\lambda a f_i B_j^*}{1 + \sum_{j' \in R_i} h a f_i B_{j'}^*} \right)$$

$$= \left(\sum_{k \in C_i} \left(\frac{M_i}{M_k} \right)^{0.25} \frac{a f_k B_k^*}{1 + \sum_{i' \in R_k} h a f_k B_i^*} \right) + (\alpha + \beta B_i^*),$$

$$\vartheta_i = \frac{1}{\tau_i} \sum_{j \in R_i} \frac{\lambda a f_i B_j^*}{1 + \sum_{j' \in R_i} h a f_i B_{j'}^*},$$

$$(1 - \vartheta_i) = \frac{1}{\tau_i} \lambda q_i,$$

$$\delta_i = \frac{1}{\tau_i} \sum_{k \in C_i} \left(\frac{M_i}{M_k} \right)^{0.25} \frac{a f_k B_k^*}{1 + \sum_{i' \in R_k} h a f_k B_i^*},$$

$$(1 - \delta_i) = \frac{1}{\tau_i}(\alpha + \beta B_i^*),$$

$$\chi_{ij} = \frac{B_j}{\sum_{j' \in R_i} B_{j'}},$$

$$\rho_{ji} = \frac{1}{\tau_i \delta_i} \left(\frac{M_i}{M_j} \right)^{0.25} \frac{a f_j B_j^*}{1 + a h f_j T_j}.$$

The first exponent parameter, μ_i, denotes the extent of non-linearity of the mortality effects of species i. We assume it to be in the interval [1, 2]. $\mu_i = 1$ means that mortality and respiration are linear in b_i (i.e., density-independent), while density-dependent effects such as diseases and intraspecific competition are associated with a value $\mu_i = 2$. A value between 1 and 2 implies that both types of effects are important at the fixed point. The last parameter, γ_i, measures predation sensitivity to prey density. It is identical to the slope of the normalized functional response. We assume that its value is in the interval $(0, 1)$, which is the range of values for Holling Type II functional responses. A value of γ close to 1 denotes scarce prey biomass, while $\gamma = 0$ means that prey is abundant and that the functional response is saturated.

The mathematical expressions of these exponent parameters are

$$\mu_i := \left. \frac{\partial}{\partial b_i} m_i(b_i) \right|_{\mathbf{b} = \mathbf{b}^* = 1} \tag{6}$$

and

$$\gamma_i := \left. \frac{\partial}{\partial t_i} g_{ij}(t_i) \right|_{\mathbf{b} = \mathbf{b}^* = 1}. \tag{7}$$

3. Evaluating the stability of generalized webs

We investigated how the stability of generalized food webs depends on the generalized parameters. To this purpose, we evaluate niche model food webs with five basal species ($Z = 5$). By fixing the number of basal species, we keep the energy input into the food web constant when the number of species or links is changed. The seven parameters that occur in Eqs. (4) and (5) are chosen as follows. A species is either a primary producer ($\vartheta_i = 0$) or it is only preying on other species ($\vartheta_i = 1$). We assume that every prey species j of a predator i contributes the same to its diet, such that χ_{ij} does not depend on j and is given by the inverse of the number of prey species of predator i. Similarly, we assume that every predator i of species j contributes the same to the predative losses of this species, such that ρ_{ij} is given by the inverse of the predator count for species j. Finally, we set the time scale parameter $\tau_i = 1$, because we found that there is no connection between the average stability of a food web and the parameter τ_i, as was shown recently for conventional models, too (Kartascheff et al., 2010).

The remaining parameters are varied in an appropriate range. The value of δ_i has to be chosen from the interval [0, 1) since it describes the fraction of biomass loss due to predation. Top

predators have $\delta_i = 0$. A value $\delta_i = 1$ is not realistic because respiration and background mortality are present for every species. The nonlinearity parameter of the mortality term μ_i is chosen from the interval $[1, 2]$. We set both parameters to three different values, $\delta = \{1/3; 1/2; 2/3\}$ and $\mu = \{4/3; 3/2; 5/3\}$, resulting in nine parameter combinations for each value of γ. For the sake of simplicity, we assume in this section that the parameters are identical for all species (Gross et al., 2009). In the next section, we will evaluate how these parameters vary within and between trophic levels. The parameter γ depends on the amount of available prey, which may vary continuously. We therefore vary γ nearly continuously, too (in steps of 0.01), from 0 to 1.

For each set of parameter values, 10 000 network structures were generated randomly using the niche model. We accepted only networks that had no disconnected parts and that had a connectance that deviated at most by 0.01 from the expected value of C. The eigenvalues of the Jacobian were evaluated and when all eigenvalues had negative real parts, a food web was stable.

We varied the number of species, $S = \{20; 30; 40; 60\}$ for a fixed connectance $C = 0.15$, and in a second computation we varied the connectance, $C = \{0.10; 0.15; 0.20; 0.30\}$ for a fixed species number $S = 30$. Figs. 2 and 3 show the results for these computations. In general, a larger proportion of food webs is stable if total mortality is dominated by nonlinear effects such as intraspecific
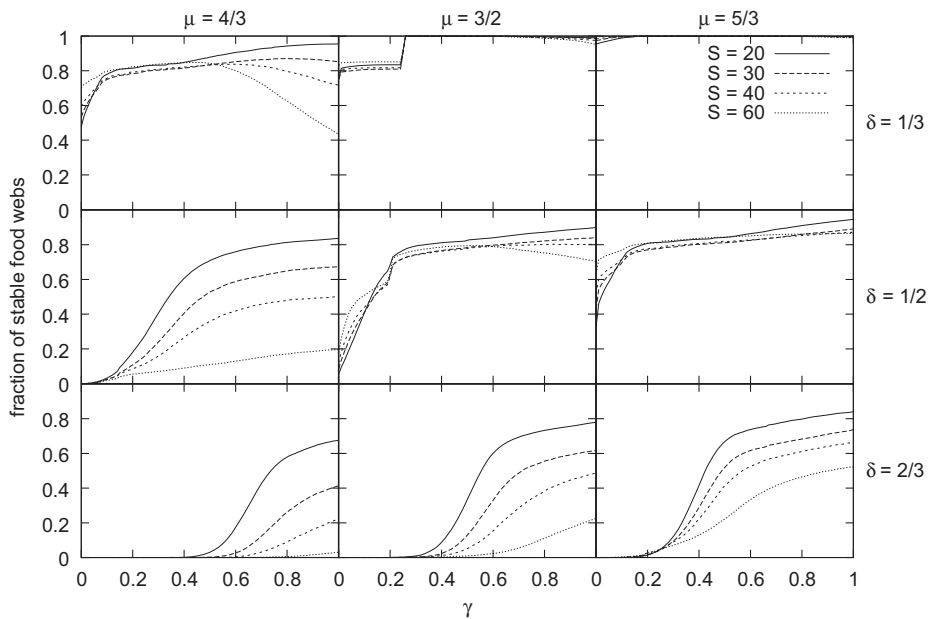
Fig. 2. Fraction of stable food webs for different configurations of δ and μ for varied S. δ is the fraction of biomass loss due to predation and μ the strength of density-dependent mortality effects. All graphs are evaluated for $\gamma \in [0, 1]$ which is the slope of the normalized functional response.
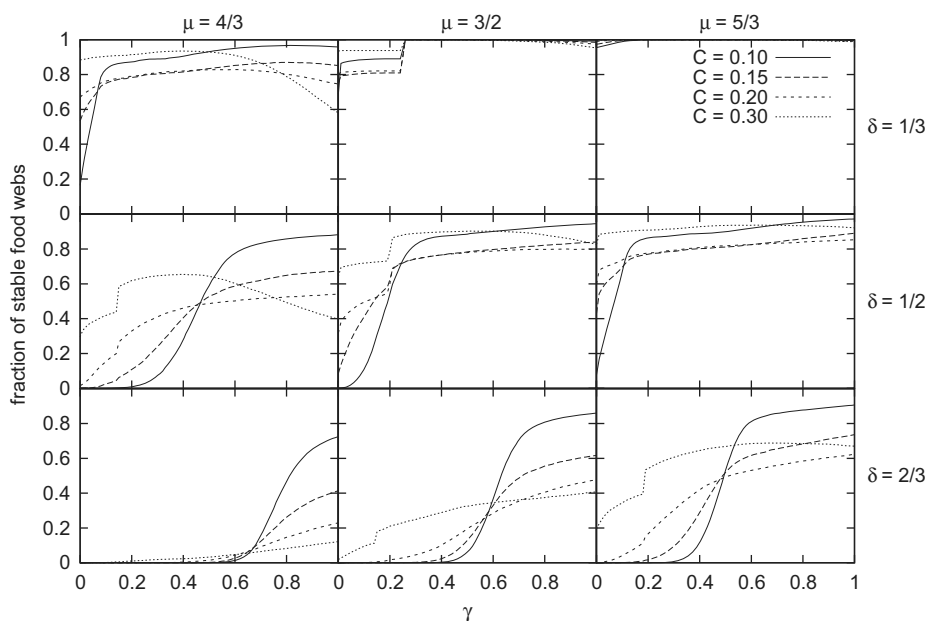

Fig. 3. Fraction of stable food webs for different configurations of δ and μ for varied C. δ is the fraction of biomass loss due to predation and μ the strength of density-dependent mortality effects. All graphs are evaluated for $\gamma \in [0, 1]$ which is the slope of the normalized functional response.

competition (large values of μ) and if these effects are more important than mortality due to predation (low values of δ). Indeed, the product $(1-\delta)\mu$ indicates the importance of mortality and is the leading negative part in Eq. (5). Negative diagonal elements in the Jacobian are known to be important for the local stability of food webs (Takeuchi, 1996). The importance of non-linear mortality for stabilizing food webs was emphasized for instance by Gross et al. (2005).

Further, higher sensitivity of the consumption rate g_{ij} to prey density b_j (i.e., higher values for γ) also increases the proportion of locally stable food webs. This general observation was already reported by Gross et al. (2004), but is supplemented here with some additional results. While in Gross et al. (2004), γ approaching 1 always meant stable food webs, here we find that for some combinations of the generalized parameters stability is highest for intermediate values of γ, especially if food-web complexity is high. Also, the sensitivity of the consumption rate to prey density has a qualitative impact on the relation between food-web connectance and stability: most graphs in Fig. 3 show a positive complexity–stability relation for low values of γ, i.e., stability increases with increasing connectance, and a negative complexity–stability relation for high values of γ.

An increase of stability with the species number S is much harder to obtain than an increase with C, compare Fig. 2 with Fig. 3, and can only be found for very small values of γ. This is in agreement with earlier findings that stability is more likely to increase with complexity when the latter means more prey species per predator instead of simply a larger total number of species (Uchida and Drossel, 2007; Kartascheff et al., 2009).

Our results obtained by the generalized formalism agree also in other respects with those obtained using other stability criteria. For instance, the positive effect of a density-dependent mortality on the stability of a system was previously reported by Kartascheff et al. (2010) for different food-web models (random, niche, cascade, nested hierarchy, layer) when evaluating the network robustness, which is the proportion of species that survive when the population dynamics are run for a long time. Earlier, it was found that robustness satisfies a positive complexity–stability relation in random food webs with a sufficiently large supply of resources (Kartascheff et al., 2009), which agrees with our finding that a small value of γ, i.e., very abundant prey for Holling type II functional response, leads to positive complexity–stability relations. Results obtained by other authors can also be interpreted as implying stability at low values of γ. A study by Uchida and Drossel (2007) has shown that adaptive behavior can result in positive complexity–stability relations when higher complexity means more potential prey per species. Since adaptive behavior leads to larger weights on links to more abundant prey species, it decreases γ. McCann shows in a paper on the dynamical stability of food webs that a Holling type II functional response together with weak links has a stabilizing effect (McCann et al., 1998). A Holling type II functional response means that γ take values between 0 and 1 (in contrast to a Lotka–Volterra functional response where $\gamma=1$), and that the per capita consumption rate is limited. Additional weak links that are associated with small attack rates or scarce prey species effectively increase γ. Together with the above-mentioned stabilizing effect of decreasing γ, this explains the large proportion of stable food webs observed for intermediate values of γ.

A striking feature of some curves in Figs. 2 and 3 is the rapid change in stability, which is more pronounced when S or C is larger. By evaluating the eigenvalues of the Jacobian, we could see that several saddle node or Hopf bifurcations occur close to each other for certain parameter values of δ and μ. The occurrence of several bifurcations in a small parameter range was also pointed out by Gross et al. (2005) for food chains.

In the next section, we will determine the values of the generalized parameters from an evaluation of dynamically stable conventional food web models to obtain a general idea of realistic parameter regions for our model.

4. Evaluation of the generalized parameters based on stable conventional webs

So far, we established general conditions for dynamically stable food webs, assuming that all species have the same values of the generalized parameters. We will now investigate which values of the generalized parameters occur in realistic food-web models and to what extent they differ among species. To this purpose, we choose a plausible set of parameters for Eq. (3), summarized in Table 1.

We generated niche model food webs that had only one component and that had a connectance of $C \pm 0.01$. We used the realistic parameter set listed in Table 1, and we retained 10 000 webs that were locally stable and had at most four trophic levels. The fixed points were determined by running computer simulations until the absolute sum of relative changes of biomass densities ($\sum_i |dB_i/B_i\, dt|$) had become less than 10^{-8}. We define the trophic level as the shortest distance through feeding links to the external resource which is the food source for basal species. The majority of species ($\approx 57.6\%$) in such webs are on trophic level 2. Trophic level 3 contains about 24.9% of all species, and level 4 about 0.8%. We computed the population dynamics according to Eq. (3), with the parameter values given in Table 1, and then calculated the generalized parameters from the obtained population densities for every single food web.

Fig. 4 shows the probability distribution of the parameter γ, evaluated for each trophic level separately. The values of γ span a wide range between 0.14 and 0.83, and the mean value increases with the trophic level. Note that basal species are not included, since they have a constant growth term and thus the parameter γ is not defined for them.

Table 1
Realistic values for the standard conventional food-web dynamical equations with Holling Type II dynamic (Eqs. (2) and (3)) to determine the dynamical behavior (Brose et al., 2006; Heckmann et al., 2012).

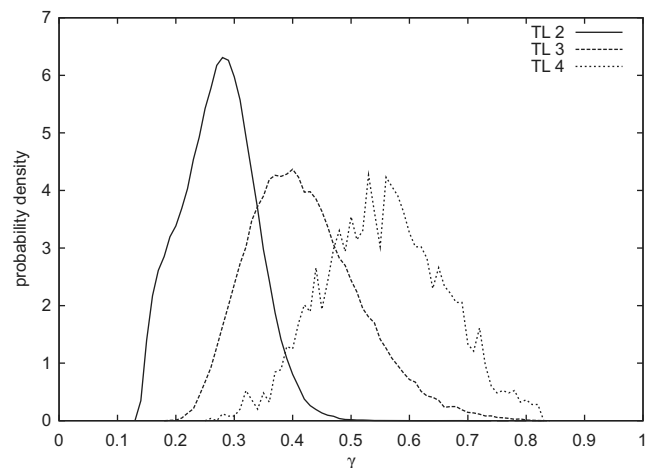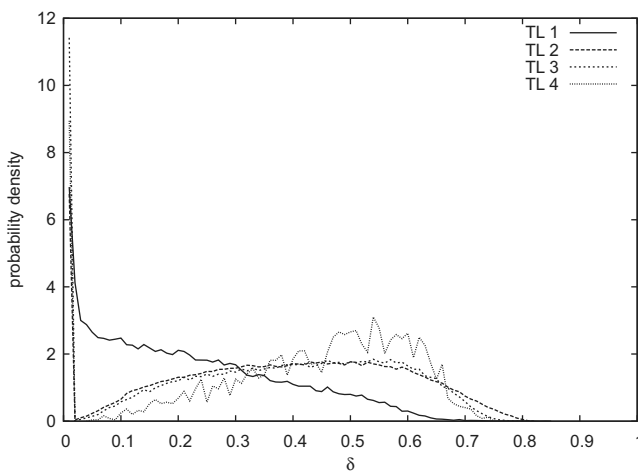| S	Z	C	a	λ	h	α	β	R
30	5	0.15	6	0.65	0.35	0.30	0.50	500

Fig. 4. The probability distribution for the values of γ for trophic levels 2, 3, and 4. The curves are based on the evaluation of 10 000 food webs with 30 species each.

The increase of γ with the trophic level is due to its dependence on prey biomass,

$$\gamma_i = \frac{1}{1 + haf_i T_i^*}, \tag{8}$$

derived from Eq. (7). Fig. 5 shows that the biomass at the fixed point decreases with the trophic level. This is due to the energy loss from one trophic level to the next. Therefore, γ increases with decreasing prey biomass and thus with increasing trophic level of predator and prey.

Since the majority of species is on trophic level 2, the overall mean value of $\overline{\gamma} \approx 0.32$ is dominated by the values of species on this level. We have seen in the previous section (Fig. 3) that such values of γ are likely to be associated with a positive complexity–stability relation.

As we have seen in the previous section, the stability of the food webs increases with an increasing value of the product $(1-\delta)\mu$, where δ is the fraction of biomass loss due to predation and μ is the nonlinearity of the mortality function. The probability distributions of the two parameters δ and μ are shown in Figs. 6 and 7. Part of the species have a value $\delta_i = 0$, those are top predators. The probability distribution of δ on trophic level 1 is dominated by small values (the mean is close to 0.2), while
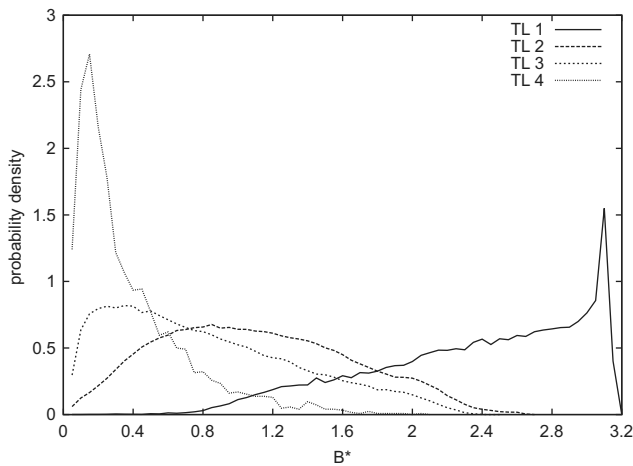
Fig. 5. Probability distribution for the biomass densities at the fixed point B^* in the different trophic levels, obtained by evaluating 10 000 food webs with 30 species each.

Fig. 6. The probability distribution for the values of δ in the different trophic levels. The curves are based on the evaluation of 10 000 food webs with 30 species each.
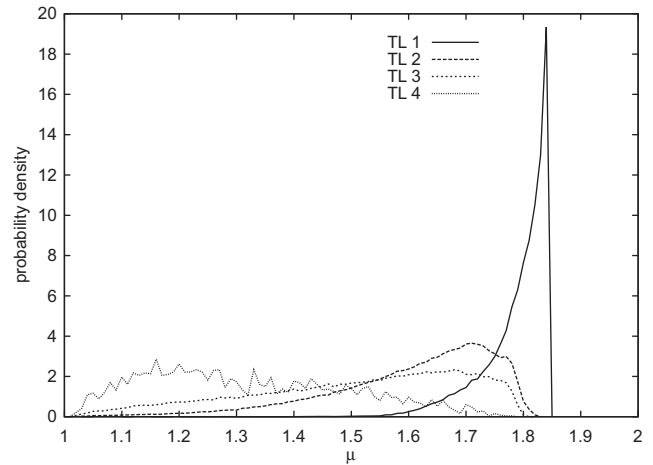

Fig. 7. The probability distribution for the values of μ for the different trophic levels. The curves are based on the evaluation of 10 000 food webs with 30 species each.

the distribution on the higher trophic levels is very wide with a mean close to 0.4, bell-shaped and similar for all levels. The reason for the small values of δ on level 1 is that the biomass of basal species is close to saturation and therefore essentially regulated by intraspecific competition and mortality. There is a constant pool of resources available for them. The basal species are therefore best interpreted as plants, which gain energy directly from the sun. By taking the average over all trophic levels, we have $\overline{\overline{\delta}} \approx 0.35$. In the previous section, we used three different values of δ between 0 and 1, and by comparison we find that the parameter configurations in the top rows of Figs. 2 and 3, where we have $\delta = 1/3$, are good representatives for this section's results. For those configurations we have a high percentage of stable food webs ($\approx 80\%$) for most values of γ, and a positive complexity–stability relation for small values of γ.

The parameter μ depends only on the biomass of species i and is given by the equation

$$\mu_i = 1 + \frac{\beta B_i^*}{\alpha + \beta B_i^*}, \tag{9}$$

which is obtained from Eq. (6). The distribution of biomass is shown in Fig. 5. As we can see in Fig. 7, species on trophic level 1 mostly have large values of μ (max. $\mu_i = 1.84$), corresponding to a high importance of density-dependent effects. The mean of μ decreases monotonously with increasing trophic level, since the average biomass per species decreases and density-dependent effects are thus less important. The value of μ decreases with increasing C or S, due to smaller population sizes.

If we compare the calculated average values of μ for each trophic level (1.78, 1.60, 1.50, 1.31 on levels 1–4) and the overall average of $\overline{\mu} = 1.59$ with the figures from the last section, the food webs simulated by us are best represented by the two columns on the right in Figs. 2 and 3, where we have $\mu = 3/2$ and $\mu = 5/3$. Similarly to what we found for δ, we also have a high percentage of stable food webs ($\approx 80\%$) for a wide parameter range of γ, and for low values of γ a positive complexity–stability relation. Combining the realistic values of δ and μ we find that the realistic configurations are the upper configuration in the middle and on the right of Figs. 2 and 3 with the fraction of stable food webs about 95%.

To conclude, we have found that the generalized parameters depend strongly on the trophic level and have broad distributions. The increase of γ and δ and the decrease of μ with trophic level is due to the decrease in biomass. We also found that the typical values of these parameters are such that a large percentage of

food webs are stable and that positive complexity–stability relations are possible.

The results of this section show that the values of the generalized parameters chosen by Gross et al. (2009) are such that the resulting food webs are less stable than food webs that we found to be realistic. Their value $\gamma = 0.95$ implies scarce prey, leading to negative complexity–stability relations throughout that study. Their choice of $\delta = 0$ for top predators and $\delta = 1$ for all other species means that species that are not top predators have negligible respiration and negligible intraspecific competition. This decreases again the stability compared to more realistic parameter choices. Further, Gross et al. chose $\mu = 1$, which is the exponent of closure that regulates the biomass loss of top predators. This value means that intraspecific competition is neglected, which again has a destabilizing effect. The reasons behind the difference between the parameter choice by Gross et al. (2009) and our work is that Gross et al. considered marine systems and defined biomass in terms of nitrogen, which is a limiting resource. Maintenance costs can be neglected for most species if biomass corresponds to nitrogen. In contrast, we refer to terrestrial food webs, with biomass corresponding to energy. Our findings are valid as long as population dynamics is not constrained by a limiting resource apart from energy.

5. Conclusion

By using a generalized modeling approach, which is based on evaluating the stability of fixed points of population dynamics, we obtained general conditions for food-web stability and positive complexity–stability relations. These conditions can be expressed in terms of the values of generalized parameters, which can in turn be formulated as very general statements about food-web properties. The generalized parameters can be written as a function of the conventional parameters and functional relationships used in explicit population dynamics equations, but they do not rely on a particular modeling approach. They stand for a whole class of systems. For example, if the generalized parameter γ, which quantifies the response of predation intensity to prey density, is set to 1, this can be interpreted as Lotka–Volterra dynamics but also as Holling Type II dynamics with low prey density.

One of our main findings is that higher density-dependent mortality effects (higher μ) or a smaller biomass loss due to predation (lower δ) increase stability. This is due to the fact that intraspecific competition prevents population sizes from becoming too large, which reduces population oscillations and relieves the predation pressure on the prey of these species. Furthermore, we found that in general stability increases with increasing γ. A fact found earlier by Gross et al. (2004) studying the influence of the parameter γ on the stability on the system in detail for different functional forms of the functional response. This is because a larger γ implies a stronger response of feeding rates to changes in the prey populations. A small value of γ implies a very high energy input into the system. Its destabilizing effect is known as the paradox of enrichment, first described by Rosenzweig (1971), which states that enrichment can lead to oscillations (but not necessarily to extinctions). On the other hand, when complexity, i.e., S or C, is large, food-web stability decreases again when γ becomes too large, because larger values of γ imply less energy input into the system, which can have a destabilizing effect when the energy is distributed among too many species, i.e. when the network is large. Networks with high complexity are most stable at intermediate values of γ, for which the consumption rates of predators are partially saturated, which means that predator populations are capable of responding to

changes in prey populations, while the energy input into the food web through the basal species is sufficiently large. The stabilizing effect of a sufficiently high energy input was also found by Kartascheff et al. (2009).

From Figs. 2 and 3 we have obtained a positive complexity–stability relation for low values of γ. These findings agree with previous results (Uchida and Drossel, 2007; Kartascheff et al., 2009, 2010; Brose et al., 2006) obtained for conventional food-web dynamics with other stability criteria. This agreement can be explained by the fact that the local stability of fixed points (which is investigated in GM) is related to the extent to which oscillations are dampened, which in turn prevents species from fluctuating so much that they go extinct. In fact, the May–Wigner criterion, which was formulated by May for the local stability of population dynamics of biological species (May, 1972), has been shown to be also valid for species persistence by Sinha and Sinha (2005).

In the second part of the paper, we evaluated the typical range of the values of the generalized parameters for realistic food-web models with Holling type II dynamics. We found that the generalized parameter γ shows a trend towards larger values with increasing trophic level, with a mean of $\overline{\gamma} = 0.32$, which is an intermediate value that leads to high stability. Such values of γ imply that prey with a large biomass is available and that predators obtain most of their energy from such abundant prey. For predators on higher trophic levels the biomass of prey species is smaller, and therefore it is important for food-web stability that these predators can feed on several prey (i.e, connectance C must not bee too small).

In our realistic food-web models, we implemented the effect of allometric scaling of metabolic rates with body mass, which is known to be an important factor for food-web stability, due to reducing the biomass flow from prey to predator on higher trophic levels (Brose et al., 2006; Kartascheff et al., 2009). Without allometric scaling, the generalized parameter γ would take higher values on the higher trophic levels.

The generalized parameter δ, which measures the fraction of biomass loss due to predation, has a broad distribution on all trophic levels but the first. The mean value is $\overline{\delta} \lesssim 0.4$, which is in the range of values leading to high food-web stability. The generalized parameter μ, which measures density-dependent effects on mortality, decreases with increasing trophic level, as expected. Nevertheless, the stabilizing effect of nonlinear contributions to mortality is important also on the highest trophic levels, where μ is sometimes called the "exponent of closure" (Gross et al., 2005).

Apart from demonstrating that realistic food-web models show a high degree of stability, our results for the typical values of the generalized parameters serve also as an important input that can be used in future GM studies. Previous work on GM (Gross et al., 2009) did not have this information available. We believe that it should even be possible to obtain some of the generalized parameters directly from empirical observations. For instance, the parameter δ gives the proportion of deaths due to predation, which should easily be measurable in field or laboratory studies. It would also be worthwhile to investigate the typical range of generalized parameters in more comprehensive food-web models. Such models can include the effects of predator interference, of type III functional responses, or of adaptive foraging. We expect both effects to increase stability even more since they reduce oscillations.

Our findings imply that the most crucial stabilizing factor is an intermediate value of the generalized parameter γ, which is obtained when the total energy input into the food web is large enough. This means that the restriction of ecosystems by human interference is a serious threat to food-web stability, because it decreases the total amount of resources available at the bottom

level. Such a decrease is most detrimental in large food webs, leading to a negative complexity–stability relation.

We conclude that GM is a very powerful tool to investigate factors that stabilize ecosystems, due to its independence of the detailed model features, and due to the low computational effort, which makes it possible to scan a huge range of parameter values and network structures. This method can be used to classify different types of functional responses and dynamical equations with respect to the range of values of their generalized parameters, which are the main determinants of food-web stability. For a given class of dynamical equations, the GM method can be used to express the generalized parameters in terms of the original parameters and to identify parameter ranges for which the food webs are stable. If, additionally, direct empirical estimates of the generalized parameters became available, the GM method could become a universal tool for answering questions related to food-web stability and the relation between complexity and stability.

References

Berlow, E.L., Neutel, A.M., Cohen, J.E., de Ruiter, P.C., Ebenman, B., Emmerson, M., Fox, J.W., Jansen, V.A.A., Jones, J.I., Kokkoris, G.D., Logofet, D.O., McKane, A.J., Montoya, J.M., Petchey, O., 2004. Interaction strengths in food webs: issues and opportunities. J. Anim. Ecol. 73, 585–598.

Brose, U., Williams, R.J., Martinez, N.D., 2006. Allometric scaling enhances stability in complex food webs. Ecol. Lett. 9, 1228–1236.

Brown, J.H., Gillooly, J.F., Allen, A.P., Savage, V.M., West, G.B., 2004. Toward a metabolic theory of ecology. Ecology 85, 1771–1789.

Dobson, A., Lodge, D., Alder, J., Cumming, G.S., Keymer, J., McGlade, J., Mooney, H., Rusak, J.A., Sala, O., Wolters, V., Wall, D., Winfree, R., Xenopoulos, M.A., 2006. Habitat loss, trophic collapse, and the decline of ecosystem services. Ecology 87, 1915–1924.

Gardner, M.R., Ashby, W.R., 1970. Connectance of large dynamic (cybernetic) systems—critical values for stability. Nature 228, 784.

Gross, T., Feudel, U., 2006. Generalized models as a universal approach to the analysis of nonlinear dynamical systems. Phys. Rev. E 73, 016205.

Gross, T., Ebenhoh, W., Feudel, U., 2004. Enrichment and foodchain stability: the impact of different forms of predator–prey interaction. J. Theor. Biol. 227, 349–358.

Gross, T., Ebenhoh, W., Feudel, U., 2005. Long food chains are in general chaotic. Oikos 109, 135–144.

Gross, T., Rudolf, L., Levin, S.A., Dieckmann, U., 2009. Generalized models reveal stabilizing factors in food webs. Science 325, 747–750.

Heckmann, L., Drossel, B., Brose, U., Guill, C., 2012. Interactive effects of body-size structure and adaptive foraging on food-web stability. Ecol. Lett. 15, 243–250.

Huisman, J., Weissing, F.J., 1999. Biodiversity of plankton by species oscillations and chaos. Nature 402, 407–410.

Kartascheff, B., Guill, C., Drossel, B., 2009. Positive complexity–stability relations in food web models without foraging adaptation. J. Theor. Biol. 259, 12–23.

Kartascheff, B., Heckmann, L., Drossel, B., Guill, C., 2010. Why allometric scaling enhances stability in food web models. Theor. Ecol. 3, 195–208.

Kuehn, C., Gross, T., 2011. Nonlocal generalized models of predator–prey systems arXiv:1105.3662v1.

Martinez, N.D., Williams, R.J., Dunne, J.A., 2006. Ecological Networks: Linking Structure to Dynamics in Food Webs. Oxford University Press.

May, R.M., 1972. Will a large complex system be stable. Nature 238, 413–414.

McCann, K., Hastings, A., Huxel, G.R., 1998. Weak trophic interactions and the balance of nature. Nature 395, 794–798.

Neutel, A.M., Heesterbeek, J.A.P., de Ruiter, P.C., 2002. Stability in real food webs: weak links in long loops. Science 296, 1120–1123.

Peters, R.H., 1986. The Ecological Implications of Body Size. Cambridge University Press.

Rall, B.C., Guill, C., Brose, U., 2008. Food-web connectance and predator interference dampen the paradox of enrichment. Oikos 117, 202–213.

Rosenzweig, M., 1971. Paradox of enrichment—destabilization of exploitation ecosystems in ecological time. Science 171, 385–387.

Sinha, S., Sinha, S., 2005. Evidence of universality for the May–Wigner stability theorem for random networks with local dynamics. Phys. Rev. E 71, 020902.

Takeuchi, Y., 1996. Global Dynamical Properties of Lotka–Volterra Systems, 1st edition World Scientific Publishing Company.

Uchida, S., Drossel, B., 2007. Relation between complexity and stability in food webs with adaptive behavior. J. Theor. Biol. 247, 713–722.

West, G.B., Brown, J.H., Enquist, B.J., 1997. A general model for the origin of allometric scaling laws in biology. Science 276, 122–126.

Williams, R.J., Martinez, N.D., 2000. Simple rules yield complex food webs. Nature 404, 180–183.

Williams, R.J., Martinez, N.D., 2004. Stabilization of chaotic and non-permanent food-web dynamics. Eur. Phys. J. B 38, 297–303.

Yodzis, P., 1981. The stability of real ecosystems. Nature 289, 674–676.

Yodzis, P., Innes, S., 1992. Body size and consumer–resource dynamics. Am. Nat. 139, 1151–1175.

Exploring cyclic dominance of sockeye salmon with a predator–prey model

Christian Guill, Eddy Carmack, and Barbara Drossel

Abstract: We explain in an intuitive and detailed way a predator–prey model that generates cyclic dominance in Fraser River sockeye salmon. In contrast with usual predator–prey models, this model includes four distinct prey lines and thus a combination of continuous and discrete dynamics, reflecting the particular freshwater and marine life cycle features of sockeye salmon (*Oncorhynchus nerka*) populations. The predator–prey interaction causing the oscillations takes place in the rearing lakes, rather than in the ocean. The values of most parameters of this model can be estimated from empirical data that are available for the large salmon-rearing lakes in the Fraser River basin. The mechanism that produces the oscillations in this model is compared with other mechanisms that can generate population oscillations, and we argue that predator–prey dynamics is the most likely mechanism to produce the observed patterns. We explain why the period of the oscillation is exactly 4 years, and we explore how the dynamical pattern is affected by changes in external conditions or by management decisions.

Résumé : Nous expliquons de manière intuitive et détaillée un modèle prédateurs–proies qui produit une dominance cyclique chez le saumon rouge du fleuve Fraser. Contrairement aux modèles prédateurs–proies habituels, ce modèle comprend quatre lignées de proies distinctes et, donc, une combinaison de dynamique continue et discrète qui reflète des caractéristiques précises des portions marines et d'eau douce du cycle biologique des populations de saumons rouges (*Oncorhynchus nerka*). L'interaction prédateurs–proies qui cause les oscillations a lieu dans les lacs d'alevinage plutôt que dans l'océan. Les valeurs de la plupart des paramètres de ce modèle peuvent être estimées à partir de données empiriques disponibles pour les grands lacs d'alevinage dans le bassin du fleuve Fraser. Le mécanisme qui produit les oscillations dans ce modèle est comparé à d'autres mécanismes qui peuvent produire des oscillations de la population, et nous arguons que la dynamique prédateurs–proies est le mécanisme le plus susceptible de produire les distributions observées. Nous expliquons pourquoi la période d'oscillation est d'exactement quatre ans et nous examinons l'incidence de variations de conditions externes ou de décisions de gestion sur cette dynamique. [Traduit par la Rédaction]

Introduction

The 4-year oscillation in the number of spawning sockeye salmon (*Oncorhynchus nerka*) that return to their native streams within the Fraser River basin in Canada is a striking example of oscillations in fish populations (Ricker 1950, 1997; Townsend 1989). The period of oscillation corresponds to the dominant generation time of these fish, which led to the term "cyclic dominance". These oscillations were reported as early as the 19th century and remain evident in the extremely high catches by fisheries every fourth year (Rounsefell and Kelez 1938).

The special life history of the sockeye salmon sets their population oscillations apart from those observed in other populations, many of which have already been understood and implemented successfully in mathematical models. Sockeye salmon spawn in freshwater habitats that discharge into the Pacific Ocean. Sockeye salmon originating from the Fraser River in British Columbia, which is one of the most productive river systems for sockeye salmon in the world, predominantly spawn at the age of 4 years after returning to the streams in which they hatched. After hatching and overwintering in the gravel, they rear for 1 year in large lakes found in the Fraser River system. They migrate to the ocean in the following spring and stay there for 2 full years. Most sock-

eye salmon then migrate back to their natal spawning grounds where they die after spawning. This particular life cycle of non-overlapping generations, in combination with a dominant age at maturity, gives rise to four largely separated brood lines in each local, lake-specific population of sockeye salmon. A small minority of the sockeye (at most 10%) spawns at the age of 5 years, thereby resulting in some mixing between the brood lines.

In addition to involving four different salmon brood lines, the oscillations in population abundance observed in Fraser River sockeye salmon show two other features that make them unique and that represent a challenge for population modelling. One feature is that the population oscillation period is exactly 4 years (with the subdominant year being sometimes stronger than the dominant one owing to environmental fluctuations), although the mean generation time of these fish is longer than 4 years. The other feature is that the magnitude of the oscillation is extremely large, with the difference between dominant and weak years being a factor of 100 or even 1000.

In the literature, different explanations and mathematical models for cyclic dominance can be found, such as dampened oscillations that are sustained by stochastic influences (Myers et al. 1998), depensatory predation (Larkin 1971), fishing (Walters and Staley 1987), or genetic effects (Levy and Wood 1992; Walters

C. Guill.* Department of Zoology and Anthropology, University of Göttingen, Berliner Straße 28, 37073 Göttingen, Germany.
E. Carmack. Institute of Ocean Sciences, 9860 West Saanich Road, Sidney, BC V8L 4B2, Canada.
B. Drossel. Institut für Festkörperphysik, TU Darmstadt, Hochschulstraße 6, 64289 Darmstadt, Germany.

Corresponding author: Christian Guill (e-mail: C.P.Guill@uva.nl).
*Present address: Institute for Biodiversity and Ecosystem Dynamics, University of Amsterdam, P.O. Box 94248, 1090 GE Amsterdam, the Netherlands.

➥ Published at www.nrcresearchpress.com/cjfas on 2 March 2014.

960

Can. J. Fish. Aquat. Sci. Vol. 71, 2014

and Woodey 1992), but none of these explanations are fully convincing (Levy and Wood 1992; Ricker 1997). Recently, we took a different approach and introduced a three-species model for the dynamics of the salmon fry, their predator (for instance, rainbow trout (*Oncorhynchus mykiss*)), and their food (mainly *Daphnia*) in the rearing lake (Guill et al. 2011). This model reproduces the dynamical pattern of cyclic dominance with a period of exactly 4 years and generates the correct sequence of a dominant, a subdominant, and two low years, which is seen in three of the largest sockeye salmon stocks in the Fraser River basin (late Stuart, Quesnel, and Shuswap stocks; Guill et al. 2011).

Building upon this approach, we here propose an even simpler model, which is a two-species predator–prey model. Similar to other predator–prey models, the food of the prey (i.e., of the sockeye fry) is taken into account only indirectly by specifying the carrying capacity of the juvenile-rearing lake. Owing to the relatively small number of parameters, we can estimate most model parameter values from empirical data. We do not assume a priori differences between salmon from different brood lines of the same stock or even between salmon of different stocks to determine whether or not a stock exhibits cyclic dominance or, if it does, which line will be dominant and which will be weak. Furthermore, empirical abundance data of the sockeye or the predator are not required to parameterize the model. Instead, environmental conditions such as the productivity of the rearing lake or the degree to which the predator relies on sockeye fry as its main resource determine the dynamics of the sockeye stock. Since the various sockeye stocks from the Fraser River basin and also other areas such as Bristol Bay (Alaska) or the coastal areas of British Columbia show a wide variety of environmental conditions and population dynamics, we can use this approach to estimate conditions under which a salmon stock can be expected to be cyclic or not. A particularly interesting case is the sockeye population that originates from the Kvichak River (Alaska). This is another highly productive stock that exhibited cyclic dominance, but with a period near 5 years.

We begin by a brief comparison of simple models that show population oscillations, such as classic predator–prey models and single-species models with density-dependent feedback. This elucidates different mechanisms that can, in principle, generate population oscillations and demonstrates the requirements that need to be fulfilled for each of these mechanisms to occur. Since the classical models cannot, however, adequately reproduce the unique type of population oscillations of sockeye salmon, we discuss the general model features (i.e., biological mechanisms captured by the model equations) that are essential to obtain cyclic dominance. Such an approach of using models that account for only a few central features of the natural system to be described has proven successful in explaining other iconic population oscillations, such as the lynx–hare (*Lynx canadensis* – *Lepus americanus*) oscillations in Canada (Elton and Nicholson 1942; Odum 1953; Blasius et al. 1999) or the cyclic outbreak dynamics of the spruce budworm (*Choristoneura fumiferana*) (Ludwig et al. 1978; Royama 1984). In each of these cases, a set of general, realistic model features was sufficient to explain the observed phenomenon.

We conclude by using the model to explore different scenarios of environmental conditions or conservation and management measures. Even though the model is not sufficiently detailed to make precise predictions (within the limits set by stochastic environmental perturbations), it allows us to assess the robustness of cyclic dominance and related impacts in the face of various natural and anthropogenic disturbances.

General mechanisms behind population oscillations

In this section we describe several mechanisms that are known to produce population oscillations, and we argue that of these mechanisms the coupling to a predator is the most likely one to be

the cause of cyclic dominance of sockeye salmon. When the predominantly 4-year life cycle of the sockeye salmon is not accounted for, however, even predator–prey interactions cannot generate the oscillation pattern characteristic of cyclic dominance.

Fundamentally, when a population shows a regular oscillation, there must exist a mechanism that causes the population to become smaller than the average value some time after it has been larger than the average value, and vice versa. This effect must be sufficiently robust that the oscillation does not weaken with time and go to an equilibrium point. Three general classes exist for such mechanisms. The first one is external periodic forcing. In this case, the population is influenced by an abiotic or biotic factor that shows an oscillation and that causes the population to oscillate at the same period (or a multiple of it). In the simplest case, this could be the change of abundance of a species during the course of a year due to the change of the seasons. If an external periodic driving force was the cause of cyclic dominance (for example, a 4-year oscillation in ocean temperatures or currents that affects salmon survival), then all salmon populations would be required to oscillate in a synchronous manner. Since this is not observed across all Fraser River stocks, an external forcing of cyclic dominance of Fraser River sockeye salmon can be ruled out (Levy and Wood 1992). Furthermore, an external periodic forcing would most likely lead to an evolutionary response in the life history of the weaker cycle lines (e.g., an increase of the relative time spent in fresh water or in the ocean) that could allow them to benefit from the favourable environmental conditions supporting the dominant line. This would lead to systematic differences of the age at maturity between the different cycle lines, which are also not observed in Fraser River sockeye salmon.

The second type of mechanism that can cause population oscillations is a direct density-dependent feedback, which can best be observed in certain laboratory populations (Kendall et al. 1999). Juveniles that grow up at high densities may experience a large mortality or slow growth and give rise to few or small adults that lay fewer eggs. In principle, such a mechanism could also cause an oscillation in the density of sockeye salmon. It has been observed, for example, that the fry produced by a dominant brood line are on average smaller than those of less abundant years (Hume et al. 1996), probably because of stronger competition for food. This may have a strong effect on their survival during migration to the ocean and in the ocean, leading to a smaller spawning population in the next generation. The diminished population produces fewer eggs, leading to better growth conditions and higher marine survival for its offspring, and the cycle repeats. If this mechanism was relevant for the sockeye salmon, however, it would lead not to cyclic dominance, but to an oscillation with a period of 8 years, because the offspring of an abundant salmon year would return after 4 years and cause a weak salmon year, leading again to an abundant year after an additional 4 years. In fact, this is the mechanism that causes sustained oscillations in the widely used Ricker model (Ricker 1954; Myers et al. 1998).

The third type of mechanism that can cause population oscillations is a time delay in the dynamics, which can be caused, for example, by a coupling to a second species (e.g., a predator). The origin of oscillations in such systems has been recognized since Lotka (1925), and Volterra (1926) introduced the first mathematical predator–prey model. However, a predator–prey oscillation only occurs if the two species interact strongly with each other and the influence of other species, which can be alternative food sources for the predator or other enemies of the prey species, is sufficiently weak. If the population dynamics of other species interfered with the predator–prey system, the simple oscillation pattern would be destroyed. A second requirement for predator–prey oscillations is that the environment provides the capacity for a considerable variation in the population densities of predator and prey. This means that there must be a sufficient amount of food available for the prey and that factors that limit predator

density (e.g., the availability of spawning grounds or diseases) must not be dominant over the effects of its prey (Rall et al. 2008).

Sometimes, depensation (the Allee effect, or inverse density dependence) due to predation or fishing is proposed as a cause of cyclic dominance in Fraser River sockeye salmon. The idea behind this concept is that the predator (or the fisheries) tries to take an amount of prey that decreases slower than proportionally for small prey population densities. This causes very high per-capita mortality in weak salmon lines, thus preventing them from becoming stronger. However, this mechanism has been shown to be very uncommon in fish populations, and in fact it would lead to the extinction of the weak lines rather than stabilization at low levels (Myers et al. 1995). Moreover, such a strong interaction between predator and prey would also affect the predator population, and we therefore pursue below the more general idea of coupled population dynamics of predator and prey.

Other possibilities for the generation of time delays in the dynamics are also possible, for example, a shift in the composition of the prey species in edible and inedible subtypes or a shift in the genetic composition of a species that is related to growth, but these are essentially special cases of interactions between two species or two subpopulations of the same species.

Predator–prey models can be either continuous or discrete in time. Those that are continuous in time, such as the Lotka–Volterra and Rosenzweig–MacArthur models (Rosenzweig and MacArthur 1963), are only appropriate if the population density changes smoothly in time. Populations with discrete generations, however, have a discontinuous change in density when adults, such as salmon, produce offspring and die at the same time. In this case, one must use a description with discrete time steps. The model for sockeye salmon and their predator that we consider here belongs to this latter category. We emphasize that the predator–prey interaction causing the oscillation must take place in the rearing lakes and not in the ocean, since the latter would once again lead to all salmon populations of the same river system cycle in phase.

To illustrate and compare mechanism two (direct density-dependent feedback) and mechanism three (time delay in the dynamics due to coupling to a second species), Table 1 shows the Ricker model together with two predator–prey models. The first, known as the Rosenzweig–MacArthur model (Rosenzweig and MacArthur 1963), is continuous in time, and the second is essentially a time-discrete version of the Rosenzweig–MacArthur model. Both predator–prey models satisfy the two conditions mentioned above for oscillations to occur. They also satisfy basic biological requirements such as predator saturation at large prey density and limited maximum prey biomass.

All three models show the transition from an equilibrium to an oscillation as a parameter is changed to increase the maximum (prey) population density. These parameters are the maximum reproductive success a for the Ricker model and the carrying capacity K for the two predator–prey models. For a complete bifurcation analysis of the Ricker model, see for example May and Oster (1976). The transition from an equilibrium to an oscillation is a so-called flip bifurcation in the Ricker model, a Hopf bifurcation in the continuous predator–prey model, and a Neimark–Sacker bifurcation in the discrete predator–prey model. In contrast with the continuous model, the oscillation in the discrete models is not continuous in time; the population densities change from one year to the next by a finite amount, which can be large. The population density in the Ricker model oscillates between two values only, while the oscillation in discrete predator–prey models is usually "quasiperiodic". This means that the pattern of points is never exactly repeated and that the number of points that fit into one oscillation period is generally not a rational number. Thus, when the oscillation becomes strictly periodic, as observed, there must be a specific reason, and this is why it is such a puzzle that the salmon oscillation appears to have a period of

exactly 4 years. It would be more general to find an oscillation that has a period somewhere between 4 and 5 years, which is the mean generation time of the salmon. In this case there would not be one cycle line that is dominant for all times, but a continuous turnover of lines that become dominant only for a number of years and then decline again.

We finally note that the period of the predator–prey oscillations shown by the two corresponding models is much longer than the generation time of the sockeye salmon. In general, the period of the oscillation depends on the values of the parameters and changes when the parameters are changed. In the continuous predator–prey model, even a period of about 4 years can be obtained. However, as we have argued above, such a model cannot, by its very nature, adequately describe the discrete life history of sockeye salmon. For the discrete predator–prey model, it has been shown that predator–prey oscillations almost always have oscillation periods longer than two times the generation time of the prey plus four times the generation time of the predator (Murdoch et al. 2002), which contrasts with the observed 4-year period of cyclic dominance. This discrepancy can only be resolved if the discrete, anadromous life cycle of the sockeye salmon is accounted for.

The model for salmon and its predator

We argued in the previous section that standard predator–prey models (second and third model in Table 1) cannot produce the oscillation pattern of cyclic dominance (i.e., a clear 4-year cycle with one dominant line, followed by a subdominant line and two nondominant lines). We now present a new model that combines a predator–prey interaction with minimum information on the life cycle of the sockeye salmon. This model is similar to a three-species model introduced earlier (Guill et al. 2011), but here the food of the sockeye fry is taken into account only indirectly through the carrying capacity of the juvenile-rearing lake.

During a given growth season in the rearing lakes, from early summer to fall, the sockeye fry interact with a population of predators. This interaction is described using a continuous-time dynamical model with equations for the biomass density of the sockeye fry ($F_n(t)$) and the predators ($P_n(t)$). Here, t denotes the time during the growth season and n is the year. The dynamics during the growth season are given by the equations

$$(1) \quad \begin{aligned} \frac{dF_n(t)}{dt} &= r \cdot F_n \cdot \left(1 - \frac{F_n}{K}\right) - f(F_n, P_n) \cdot P_n \\ \frac{dP_n(t)}{dt} &= e \cdot f(F_n, P_n) \cdot P_n - d \cdot P_n \end{aligned}$$

with the maximum growth rate r of the sockeye fry, the carrying capacity K of the rearing lake, the feeding rate $f(F_n, P_n)$ of the predators, the biomass assimilation efficiency e of the predators, and the respiration and mortality rate d of the predators. The feeding rate generally is a nonlinear function of both prey and predator density. Thus, instead of taking a type II feeding rate, as in the Rosenzweig–MacArthur model (Table 1), which only depends on the prey density, we use the Beddington–DeAngelis form (Beddington 1975; Skalski and Gilliam 2001):

$$(2) \quad f(F_n, P_n) = \frac{I \cdot F_n}{B_0 + F_n + c \cdot P_n}$$

which includes not only the effect of predator saturation at high prey density (through the term F_n in the denominator), but also interference of predators (through the term $c \cdot P_n$). I is the maximum rate at which the predator can ingest food, and B_0 is the half-saturation density (i.e., the prey density at which the predators consume at half of their maximum rate). All terms occurring

Table 1. Three simple models that generate population oscillations: top row: direct density-dependent feedback (Ricker model); middle row: continuous predator–prey model (Rosenzweig–MacArthur model); bottom row: discrete predator–prey model.

Model	Time series	Bifurcation diagram
Direct density-dependent feedback $S_{n+4} = a \cdot S_n \cdot e^{-S_n}$		
Continuous predator–prey $\dfrac{dS}{dt} = r \cdot S \cdot \left(1 - \dfrac{S}{K}\right) - \dfrac{I \cdot S \cdot P}{B_0 + S}$ $\dfrac{dP}{dt} = e \cdot \dfrac{I \cdot S \cdot P}{B_0 + S} - d \cdot P$		
Discrete predator–prey $S_{n+1} = r \cdot S_n \cdot \left(1 - \dfrac{S_n}{K}\right) - \dfrac{I \cdot S_n \cdot P_n}{B_0 + S_n}$ $P_{n+1} = e \cdot \dfrac{I \cdot S_n \cdot P_n}{B_0 + S_n} + (1 - d) \cdot P_n$		

Note: The first column shows the equation for the considered species (S) and, if applicable, its predator (P), with n counting the years in the two discrete models. The second column shows a time series for a dampened and a sustained oscillation, and the third column shows the bifurcation diagram, which gives all values for S that occur in the stationary state (i.e., after a sufficiently long transient time) as a function of a control parameter. In the Ricker model, a is the reproductive parameter, with $a = 1.6$ (8.5) in the upper (lower) time series. In the continuous predator–prey model, $r = 1$ is the growth rate of S, K is the carrying capacity with $K = 1.5$ (2.8) in the upper (lower) time series, $I = 0.6$ is the maximum rate at which P can consume and digest S, $B_0 = 1$ is the half-saturation density of the predator feeding rate, $e = 0.85$ is the assimilation efficiency, and $d = 0.15$ is the rate of biomass loss of the predator due to metabolism and death. In the discrete predator–prey model, the parameters have a similar meaning as in the continuous model. Their values are $r = 3$, $K = 1.8$ (2.2), $I = 1.2$, $B_0 = 1$, $e = 0.85$, and $d = 0.32$.

in eqs. 1 and 2 were introduced in the previous section, and we chose them because they are the simplest form of these terms that nevertheless take into account the most important effects known to be present.

To bridge sequential brood lines, the continuous equations of eq. 1 need to be supplemented by a discrete step that connects the biomass densities at the end of the growth season (time T) in year n to the biomass densities at the beginning of subsequent seasons (time 0). After spending their second winter in the rearing lakes, most sockeye salmon then spend 2 years in the ocean, migrating back to their original spawning locations at the age of 4 years. A certain fraction of each generation, however, stays in the ocean

one additional year and spawns at the age of 5 years, resulting in some mixing between the brood lines. We assume that the number of sockeye spawners that produce the fry of the year $n + 1$ (S_{n+1}) is proportional to the number of fry at the end of the respective earlier growth seasons in the rearing lakes:

$$(3) \qquad S_{n+1} = a_1 \cdot a_2 \cdot (1 - h) \cdot [(1 - \epsilon) \cdot F_{n-3}(T) + \epsilon \cdot F_{n-4}(T)]$$

The proportionality factors represent conversion of the biomass density of the fry at the end of the growth season (time $t = T$) to number density (a_1), marine survivability (a_2), and the probability

to survive fishing $(1 - h)$, where h represents the harvest rate. ϵ is the fraction of salmon spawning at the age of 5 years.

The biomass density of fry at the beginning of the growth season (time $t = 0$) produced from a given number density of spawners is given by a saturating Beverton–Holt recruitment function:

$$(4) \qquad F_{n+1}(0) = \frac{b \cdot S_{n+1}}{1 + \dfrac{b \cdot S_{n+1}}{K_S}}$$

The constant b is the maximum fry biomass per spawner. It includes the number of eggs per female spawner, the sex ratio among the spawners, the mass of the eggs, and the egg-to-fry survival probability. The parameter K_S denotes the carrying capacity of the spawning grounds, which is the maximum biomass of fry per square metre lake surface that can be produced on the spawning grounds. Finally, we assume that a constant fraction s_w of the predators survives over the winter:

$$(5) \qquad P_{n+1}(0) = s_w \cdot P_n(T)$$

We assume that details of the life cycle of the predators such as its age at maturity or the timing of spawning are not important for the generation of cyclic dominance.

The continuous equations of eq. 1, together with the discrete step (eqs. 3–5), belong to the class of systems that may display a Neimark–Sacker bifurcation (Kuznetsov 2004). (For a Hopf bifurcation, one would need a fully continuous model.) In fact, our model can be turned into a discrete model, because the biomass densities of the two species in the fall of year $n + 1$ are uniquely determined from the biomass densities in the fall of the years $n - 4$ to n. To calculate these biomass densities, however, the equations must be numerically evaluated on a computer (cf. Guill et al. (2011) for further details on the mathematical procedure).

Parametrization

We chose model parameter values, summarized in Table 2, based on published empirical data. The majority of the growth of the sockeye fry in the rearing lakes occurs when temperature, light, and nutrient conditions allow phytoplankton and zooplankton to grow. This is mainly from mid-May to mid-October, a growth season of $T = 150$ days. The maximum net growth rate r of the sockeye fry in the rearing lake is the difference between their maximum food ingestion rate and their metabolic rate. Following Yodzis and Innes (1992), the maximum ingestion rate of ectotherm vertebrates is approximately 3.9 times larger than their metabolic rate. Metabolic data taken from White et al. (2006) suggest that the maximum growth rate of sockeye fry with an approximate body mass of 1 g is around 0.03 per day. The carrying capacity K of the rearing lake limits the availability of food when sockeye fry is very abundant. Hume et al. (2005) report that in both Quesnel and Shuswap lakes (two of the most important juvenile-rearing lakes in the Fraser River system), the biomass density of sockeye fry during the growth season never exceeds 1.4 g·m⁻² and saturates at around 0.8 g·m⁻². This saturation value, however, already includes the losses to predators, so we assume a somewhat higher value of $K = 2$ g·m⁻² for the carrying capacity.

The assimilation efficiency e of the predators is set to 0.85, which is a standard value for carnivores (Yodzis and Innes 1992). The metabolic rate of the predators d is estimated from data by White et al. (2006). Assuming a mean body mass of 500 g for the predators, we obtain $d = 0.0046$ per day, and for the maximum

**Table 2.** Summary of parameters of the predator–prey model.

Symbol	Parameter	Value
T	Length of growth season	150 days
r	Sockeye maximum net growth rate	0.03 day⁻¹
K	Juvenile-rearing lake carrying capacity	2 g·m⁻²
e	Predator assimilation efficiency	0.85
d	Predator metabolic rate	0.0046 day⁻¹
I	Predator maximum ingestion rate	0.018 day⁻¹
B_0	Predator half-saturation density	0.02 g·m⁻²
c	Predator interference competition	0.5
s_w	Predator overwinter survivability	0.85
ϵ	Fraction of sockeye spawning at age 5	0.1
a_1	Fry biomass density to number density conversion	$0.\overline{3}$ g⁻¹
a_2	Marine survivability	0.1
h	Harvest rate	0.7
b	Fry biomass produced per spawner	12.8 g
K_S	Spawning ground carrying capacity	0.1 g·m⁻²

ingestion rate, which is again 3.9 times larger than the metabolic rate, we thus obtain $I = 0.018$ per day. The half-saturation density B_0 of the feeding rate depends on the attack rate of the predators on the sockeye fry. Since experimental data for this parameter are notoriously difficult to transfer to natural environments, we choose the value of B_0 such that it leads to realistic results, namely that the predator is able to live on the prey but does not always feed at maximum rate. We therefore set $B_0 = 0.02$ g·m⁻² and explore the robustness of the results with respect to the value of B_0 in the Supplementary Material S1[1]. The same applies to the strength of interference competition among the predators, specified by the parameter c. We set it to $c = 0.5$ so that predators interfere with each other to some extent and again explore the robustness of the results with respect to the value of c in the Supplementary Material S1[1]. With all other parameters as in Table 2, cyclic dominance is predicted by the model for $0.15 \lesssim c \lesssim 0.85$ and for $0 \le B_0 \lesssim 0.04$.

The constant a_1 converts the biomass density of sockeye fry at the end of the growth season into number density. We set $a_1 = 0.\overline{3}$ g⁻¹, assuming an average body mass of 3 g of the sockeye fry at the end of the growth season (Hume et al. 1996). The probability for an individual fry to return as an adult to the spawning ground is given by the marine survivability a_2, which is close to 0.1 (Hume et al. 1996), and the probability to survive fishing (1 minus the harvest rate h). The harvest rate varied considerably during the last century and is usually not the same for the four lines of a cycle. To simplify the analyses, we nevertheless begin by assuming a constant harvest rate of $h = 0.7$ (English et al. 2011) and explore the effects of variable harvest rates in the Supplementary Material S2[1]. The age composition of the sockeye spawners can be directly observed. We assume a fraction of $\epsilon = 0.1$ of salmon that spawn at the age of 5 years (Kim Hyatt, personal communication). The parameter b, which gives the biomass of fry at the beginning of a growth season derived from one spawner, is set to 12.8 g. It includes a fraction of roughly 0.5 of effective female spawners among all spawners (Hume et al. 1996), on average 3200 eggs per female spawner in the upper Fraser region with a mean mass of 0.1 g (Beacham and Murray 1993), and an egg-to-fry survival rate of 0.08, approximated from data shown by Hume et al. (1996). These data also show that when there are many spawners, the number of fry that emerge in the rearing lake at the beginning of the growth season does not increase indefinitely, but saturates at approximately $K_S = 0.1$ g·m⁻². Finally, the overwinter survivability of the predators (s_w) is set to 0.85 (Carl Walters, personal communication).

Fig. 1. Overview of the dynamics of the predator–prey model: (*a*) Bifurcation diagram of the density of sockeye spawners when varying the carrying capacity *K* of the juvenile-rearing lake. Note that small biomass densities are shown on a logarithmic scale. Also note that to make our simulation results easier to compare with empirical data, we plot the number of spawners per hectare instead of a biomass density (measured in g·m^{-2}). The dashed vertical lines indicate the values of the carrying capacity that were used to generate the time series of sockeye spawner densities in the subsequent panels. (*b*) Stable equilibrium at *K* = 0.3 g·m^{-2}. (*c*) Quasiperiodic oscillations at *K* = 0.53 g·m^{-2}. (*d*) Cyclic dominance at *K* = 2.0 g·m^{-2}. All other parameters are as described in the text. Different symbols in the close-ups of the time series denote the four cycle lines: dominant (squares), subdominant (diamonds), and two nondominant lines (upright and inverted triangles). For the quasiperiodic oscillations (*c*), this assignment refers only to the initial part of the time series, as the four cycle lines change their role continuously over time.
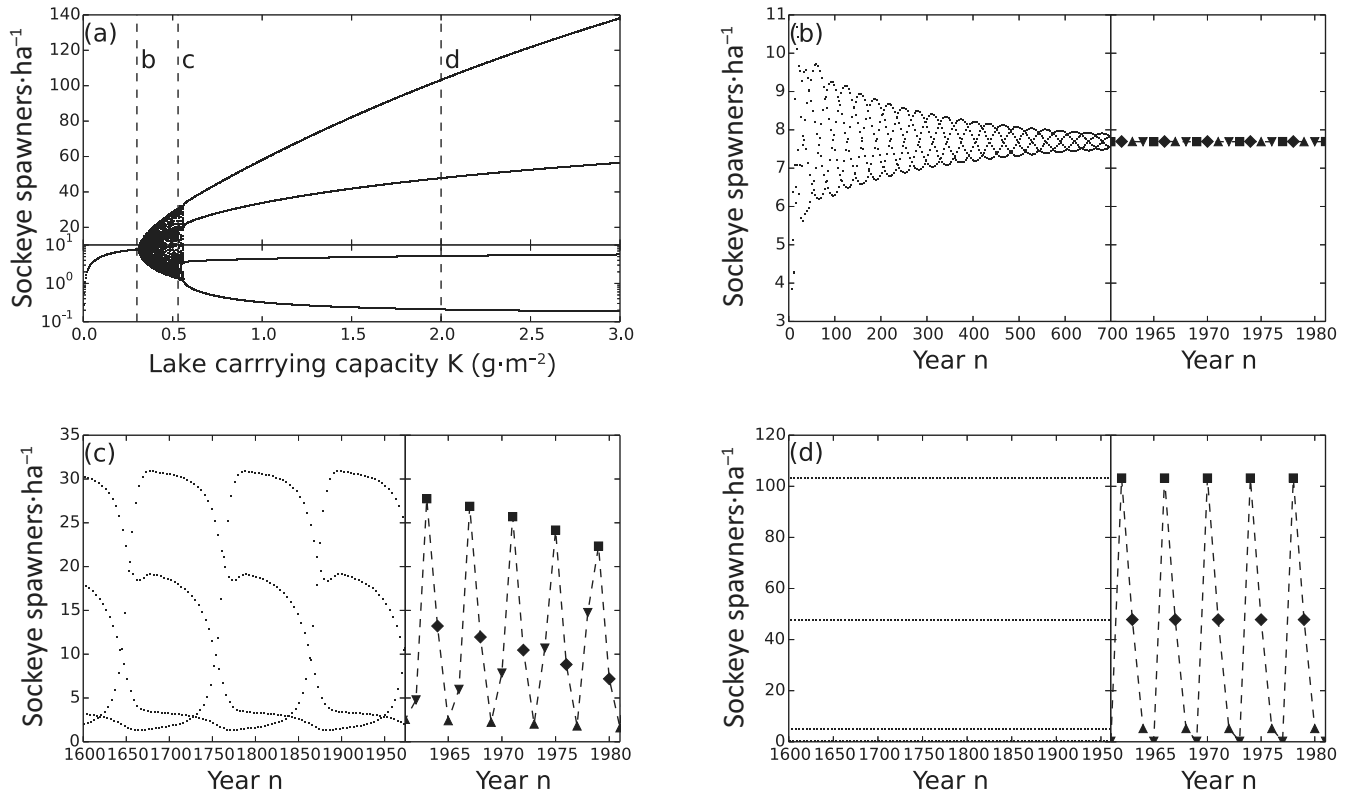
Dynamic regimes

Depending on the parameter values, the model for sockeye prey and its trout predator produces qualitatively different dynamical patterns (Fig. 1). If, for example, the carrying capacity *K* of the rearing lake is very low, the salmon fry cannot develop sufficiently large biomass densities, and so no oscillations occur. Instead, even if initially some differences exist between the four salmon lines, they are soon dampened away (Fig. 1*b*). When *K* is increased, the stable equilibrium becomes unstable because of a Neimark–Sacker bifurcation, and quasiperiodic oscillations occur. When only short parts of the time series are considered (Fig. 1*c*, right side of panel), a pattern that is very similar to cyclic dominance can be observed; every fourth year, the number of spawning salmon is much higher than in the other years. However, the pattern changes slowly over time, as is typical for quasiperiodic oscillations, and each successive dominant line reaches a slightly different level than that of 4 years earlier. Only when considering very long time intervals can it be seen that dominance switches in a regular fashion between the four brood lines (Fig. 1*c*, left side of panel).

At increasingly higher values of *K*, the period of the oscillation suddenly becomes locked at exactly four (Fig. 1*d*). The mathematical mechanism behind this period locking is the so-called strong resonance, which can occur if the oscillation period subsequent to a Neimark–Sacker bifurcation is close to two, three, or four (Kuznetsov 2004). If no stochastic perturbations occur, a brood line that is dominant will stay dominant for all time. The dominant line is followed by an intermediate or subdominant line and two subsequent nondominant or off lines, just as it is observed in some of the largest sockeye populations in the Fraser River region (Hume et al. 1996; Ricker 1997).

The values of several of the parameters of the model, especially the rearing lake carrying capacity *K* and the spawning ground carrying capacity *K*$_S$, have been adapted to roughly represent the situation of the sockeye salmon populations in Quesnel, Shuswap, and Stuart lakes. Other parameters like the length of the growth season (*T*) and the fraction of sockeye spawning at age 5 (*ε*) represent also most other sockeye stocks (cyclic or not) in the Fraser River system. The remaining parameters, like the growth rate of the sockeye fry (*r*) or the physiological rates of the predator (*I* and *d*) characterize sockeye salmon and their predator in general and are not specific for certain stocks. We note that none of the parameters have been fitted numerically to the observed time series of spawner abundances in lakes that show cyclic dominance. Nevertheless, the spawner abundances predicted by the predator–prey model match the numbers observed in nature quite well (Figs. 2*a* and 2*b*). This degree of not only qualitative but also quantitative agreement with empirical data is, indeed, remarkable for a strategic model that uses very little system-specific information.

Nevertheless, the model is sufficiently flexible to produce a variety of dynamical patterns that, in similar form, can also be found in different natural sockeye stocks. In Fig. 2 we contrast

Fig. 2. Comparison of model dynamics (left column) with time series of sockeye spawners from different stocks that show a similar behaviour (right column). (*a*) Standard set of parameters (Table 2) leading to persistent cyclic dominance. Adding stochastic perturbations to the model increases the similarity to the dynamics of the Shuswap Lake stock even further (Schmitt et al. 2012). (*b*) Shuswap (Adams River) stock. (*c*) Dampened oscillations due to strong spawning ground limitations (K_S = 0.01 g·m^{-2}). (*d*) Harrison Lake stock. (*e*) High lake productivity (K = 4 g·m^{-2}) and spawning ground capacity (K_S = 0.2 g·m^{-2}) leading to high abundance of a competitor (threespine stickleback) of the sockeye fry, which in turn leads to a levelling off of cyclic dominance. (*f*) Alastair Lake stock. (*g*) The majority of the sockeye spawns at the age of 5 years (ϵ = 0.9), leading to irregular, persistent cycles with a period close to 5 years. T = 120 days, I = 0.036·day^{-1}, d = 0.0092·day^{-1}. (*h*) Kvichak River stock. Unless stated otherwise, all model parameters are as in Table 2.

966

Can. J. Fish. Aquat. Sci. Vol. 71, 2014
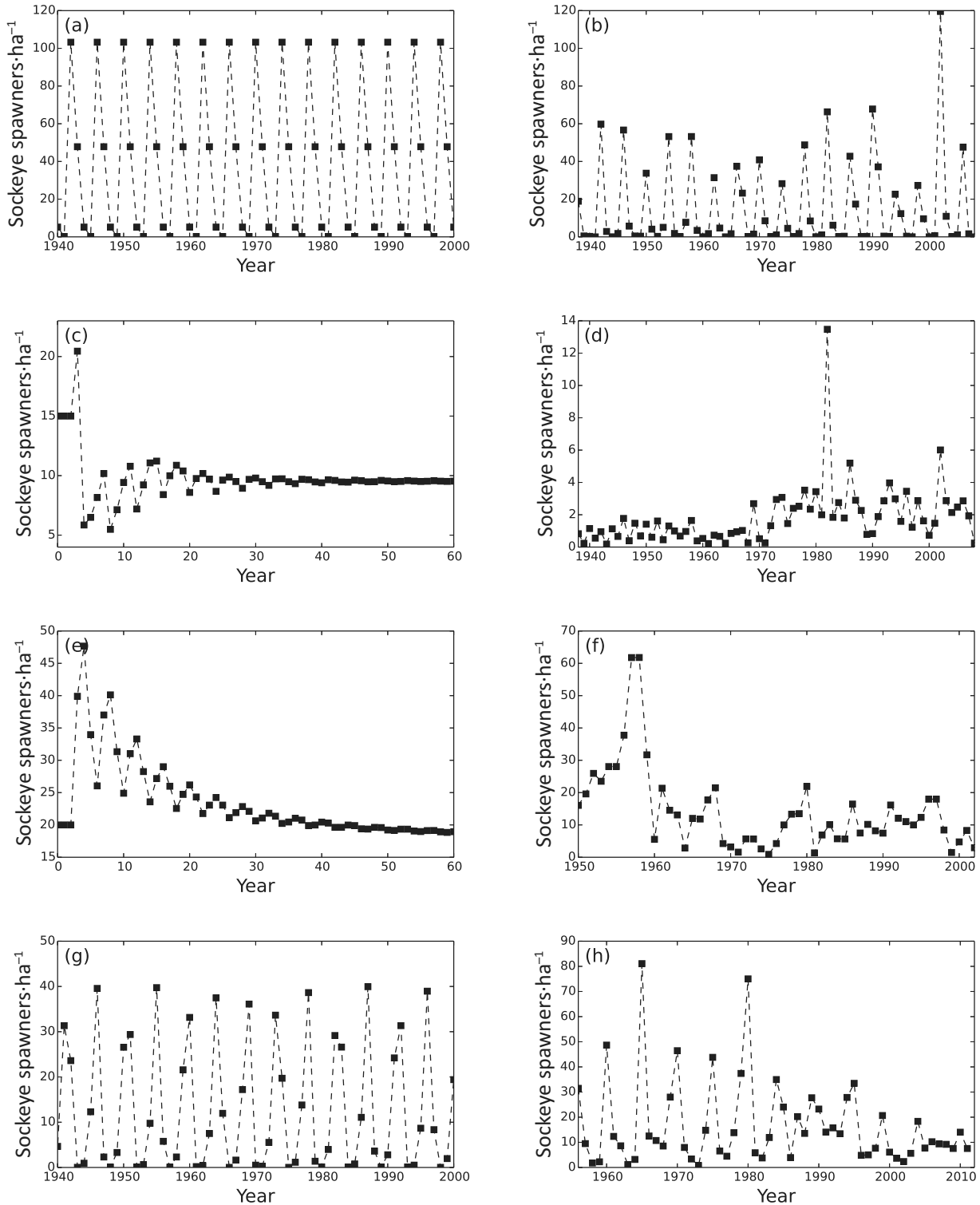
model simulations with different parameter values (left column) with escapement data of four very different sockeye stocks from the Fraser River and other regions (right column). Aside from the classic cyclic dominance case (Fig. 2a, parameters as in Table 2, and Fig. 2b, Shuswap lake stock), we also show what happens if the salmon population is strongly limited by K_S. Figure 2c shows a simulation run with $K_S = 0.01$ g·m^{-2}, or ten times less than the standard value for this parameter. This reflects the situation of the Harrison Lake stock (Fig. 2d), which shows no cyclic dominance despite favourable growth conditions for the sockeye fry in the rearing lake (Ricker 1950). Importantly, this simulation overestimates the natural spawner densities by a factor of two to five, indicating that spawning ground limitations for the Harrison Lake stock might be even more severe than has been assumed.

One of the core assumptions of our predator–prey model is that the rearing lake is oligotrophic and species-poor (see also Guill et al. 2011). This ensures a strong coupling of the predator to the sockeye fry. If the assumption of oligotrophy is violated, other fish species may occur in the rearing lake and serve as an alternative food source for the predator, thereby reducing its coupling to the sockeye fry and impairing the potential for cyclic dominance. This could be the case in Alastair Lake (Fig. 2f), which is among the most productive lakes in British Columbia and hosts a large population of threespine stickleback (*Gasterosteus aculeatus*) in addition to a noncyclic stock of sockeye salmon (Shortreed et al. 2001). For the corresponding simulation run, we doubled the lake K to 4 g·m^{-2} and the spawning ground K_S to 0.2 g·m^{-2}. Both factors in principle increase the potential for cyclic dominance. However, we also introduced a competitor species (stickleback) that grows according to the same logistic equation as the sockeye fry (cf. eq. 1) and is also eaten by the predator. We assume that the predator prefers sockeye fry and spends two-thirds of its time foraging for them and one-third foraging for stickleback. Competition between sockeye fry and stickleback is mediated only via the predator, not via their resources. In this case, the time series of sockeye spawner density shows some initial cycles, which, however, are soon dampened away, and the spawner density settles at a value comparable to that recorded for the Alastair Lake stock.

The Kvichak River in Alaska is another highly productive river for sockeye salmon, and its salmon population is also known to display cyclic dominance. However, the cycles are not as regular as, for example, in the Shuswap Lake stock, and the period of the oscillation is often closer to 5 years instead of 4 (Fig. 2h). The reason for this relates to the spawning age distribution of the Kvichak River sockeye salmon. A variable but usually high fraction of them spends an additional year in the rearing lakes (Iliamna and Clark lakes) or at sea (Isakov et al. 2000) (i.e., the most common age at spawning of Kvichak River sockeye salmon is approximately 5 years). We can account for this in the model by increasing the fraction of spawners returning at the age of 5 years (ϵ) from 0.1 to 0.9 (Fig. 2g). For this simulation we also decreased the length of the growth season (T) from 150 to 120 days to account for latitude and assumed that the predator is on average smaller and thus has higher mass-specific metabolic rates ($I = 0.036$ g·m^{-2} and $d = 0.0092$ g·m^{-2}). The simulated time series is more variable than in the classic case of cyclic dominance (Fig. 2a), the oscillation period varies between 4 and 5 years as in the empirical data, and even the so-called precycle (a cycle line with intermediate abundance that precedes the dominant line) is predicted by the model.

Exploring scenarios

The predator–prey model given here allows us to examine the system's response to certain natural and anthropogenic scenarios by varying some of its parameters in ways that mimic changing environmental conditions or imposing new management measures. We discuss in the following four different scenarios how

internal dynamical behaviour is affected by certain changes in external forcing conditions. In contrast with the study by Schmitt et al. (2012), which investigates the role of fluctuating parameters, we use here constant parameter values and investigate how the dynamical attractors depend on these values. Taken together, the two studies show that that pattern of cyclic dominance is very robust to changes in the environment or management practices.

Scenario 1: warming

Global warming has been identified as a major driver of ecosystem changes (Nelson 2005; Pörtner and Farrell 2008; Brose et al. 2012). We test how the coupled system of sockeye salmon and its predator respond to warming by applying two simple changes to the model. First, we assume that warming changes the length of the growth season, and second, we assume that warming increases mortality during stressful phases in the life cycle of the salmon, especially during migration to or from the ocean. Let the impact of warming be quantified by some dimensionless parameter x, ranging from 0 to 1, which influences the length of the growth season T and the total smolt to adult survival $a = a_1 \cdot a_2 \cdot (1 - h)$ as follows:

$$T = (120 + 120 \cdot x) \text{ days}$$

$$a = (0.0125 - 0.01 \cdot x)/\text{g}$$

We lack sufficient empirical data to give an exact quantitative relation between the lengthening of the growth season and the increase of the migration mortality that is implied by these equations. Instead, we have chosen the parameter values such that warming has a marked influence on both the length of the growth season and the smolt-to-adult survival.

The response of the salmon is shown in Fig. 3. A small temperature increase has a similar effect as an increase in carrying capacity. It leads to higher spawner numbers in the dominant line, but to lower spawner numbers in the two nondominant lines (which, however, can be regarded as negligible because of the low absolute numbers of spawners in these two lines). If warming increases the length of the growth season to more than approximately 160 days and decreases smolt-to-adult survival by more than 10% (corresponding to $x > 0.35$), any further warming has a negative effect on all four brood lines. Eventually, cyclic dominance becomes replaced by quasiperiodic oscillations.

This is, of course, only a very simple analysis of a possible response of the system to changing climate conditions. Other responses are also possible. For example, while the length of the growth season increases, the productivity of the rearing lakes might still decrease because of increased thermal stratification and reduced vertical mixing in the lakes or altered river flows that may lead to lower nutrient influxes. This would lead to even lower sockeye abundances and hasten the breakdown of the cyclic or quasiperiodic behaviour.

Scenario 2: spawning channels

In several lakes spawning channels are operated in some years to enhance the production of sockeye fry. Spawning channels have a twofold effect on the parameters of our model, since they increase K_S and the egg survivability b by excluding predators from the spawning grounds.

The simplest way to take these two effects into account is by introducing a factor of spawning ground improvement y and to relate it to K_S and b via the following equations:

$$K_S = K_S^* \cdot y$$

$$b = b^* \cdot y$$

Fig. 3. Effect of warming on the sockeye salmon population (scenario 1). The bifurcation diagram (*a*) summarizes the response of the salmon population over a gradient of environmental conditions. For better visibility of the nondominant lines, small spawner densities are shown on a logarithmic scale. Higher values of the abstract warming parameter *x* correspond to higher temperatures. The curved dotted line marks the mean spawner density during one cycle. In the time series (*b*), it can be seen that the general pattern of the oscillation remains the same and that mainly the dominant (squares) and the subdominant (diamonds) lines suffer from warming (*x* = 0.8, open symbols, dash-dotted lines in both panels) compared with the standard conditions (*x* = 0.25, filled symbols, dashed lines in both panels).
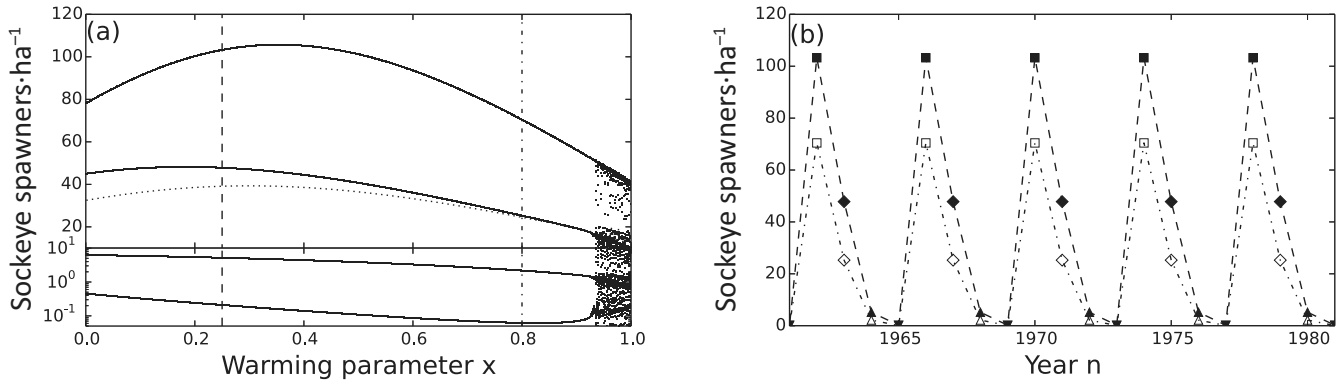
Fig. 4. Effect of improving the spawning ground quality by operating spawning channels (scenario 2). (*a*) Bifurcation diagram over a gradient of spawning ground quality. For better visibility of the nondominant lines, small spawner densities are shown on a logarithmic scale. The curved dotted line corresponds to the mean spawner density during one cycle. (*b*) Time series for standard conditions (*y* = 1, filled symbols, dashed lines) and for threefold higher spawning ground quality (*y* = 3, open symbols, dash-dotted lines).
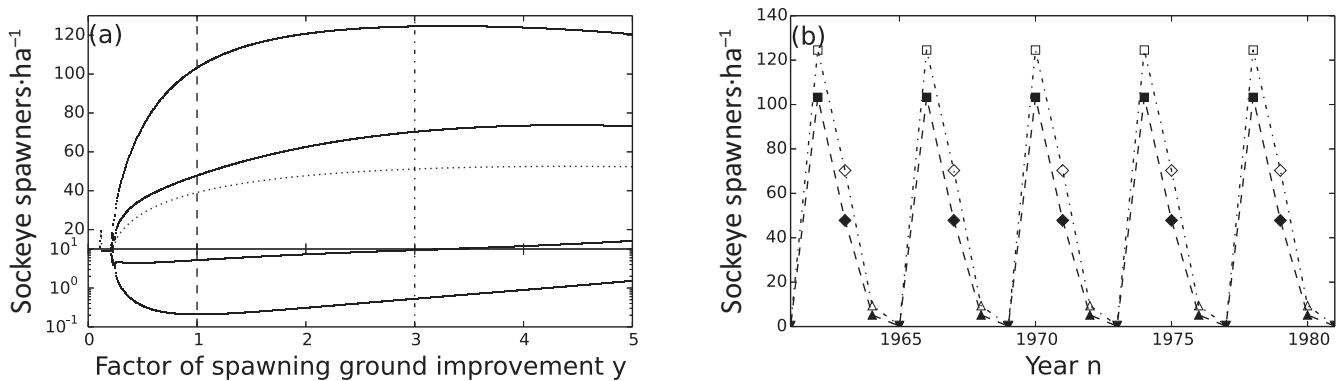
where $K_S^* = 0.1$ g·m^{-2} and $b^* = 12.8$ g are the standard values for these parameters.

If modelled in this way, spawning channels have little effect on the dominant brood line (Fig. 4). Doubling or even tripling the spawning ground quality increases spawner abundance by less than 20%, and higher efforts even have a negative effect. In absolute numbers the subdominant line benefits most from the spawning channels (diamond symbols in Fig. 4*b*), although the nondominant lines (triangle symbols) show a stronger relative increase. The mean spawner density during one cycle increases from approximately 40 spawners per hectare at standard conditions to 52 spawners per hectare if the quality of the spawning grounds is increased by a factor five. In reality, one can expect the effect on the dominant line to be even smaller, since salmon can also spawn in the lake when they are very abundant, and the spawning channels then constitute a smaller proportion of their spawning grounds.

These simulations demonstrate that if the salmon fry in the rearing lake are controlled by a predator or by the availability of food, then the productivity of the stock is increased only marginally by the addition of spawning channels and only by a very high effort to improve the conditions for egg deposition and development. This result depends, however, to some extent on the parameter values we used in the simulations. If, for example, the carrying capacity of the rearing lake is much higher than we

estimated (larger *K*) or the predator is less efficient in catching sockeye fry (larger B_0), the above conditions do not apply, and increasing the availability of spawning grounds could substantially increase the biomass density of sockeye fry. If, however, the quality of the spawning grounds is even lower than we have assumed for standard conditions, the mean spawner density quickly decreases to values below 10 spawners per hectare, and cyclic dominance does not occur. This may indicate why some rearing lakes, which should have the capacity to host large populations of salmon fry, have developed only small sockeye stocks that lack cyclic dominance. This mechanism was hypothesized by Ricker (1950) to explain the relatively small sockeye population of Harrison Lake.

Scenario 3: predator culling and stock management

Removal of predators (e.g., by increasing sport fishery quotas on in-lake trout) has been suggested as one possibility to enhance the abundance of sockeye salmon in all four cycle lines to the level of the dominant line (Larkin 1971). This would greatly enhance the biomass of sockeye that could later be harvested by the marine fisheries. We test this idea by increasing the parameter *d* of the model, which contains the mortality and the respiration rate of the predator (Fig. 5).

Increasing the predator mortality rate to intermediate levels (*d* ≈ 0.007) has nearly no effect on the dominant line, but the other

Fig. 5. Effect of increasing the predator mortality rate (scenario 3) on the sockeye salmon (*a*, *c*) and on the predators (*b*, *d*). The curved dotted lines in the bifurcation diagrams (*a*, *b*) correspond to the mean spawner density and the mean predator biomass density during one cycle, respectively. In the time series (*c*, *d*), filled symbols and dashed lines denote standard conditions (*d* = 0.0046, no additional predator mortality), and open symbols and dash-dotted lines denote intermediate levels of additional predator mortality (*d* = 0.0075). Symbols in the predator time series (*d*) correspond to those of the same year in the sockeye spawner time series (*c*).
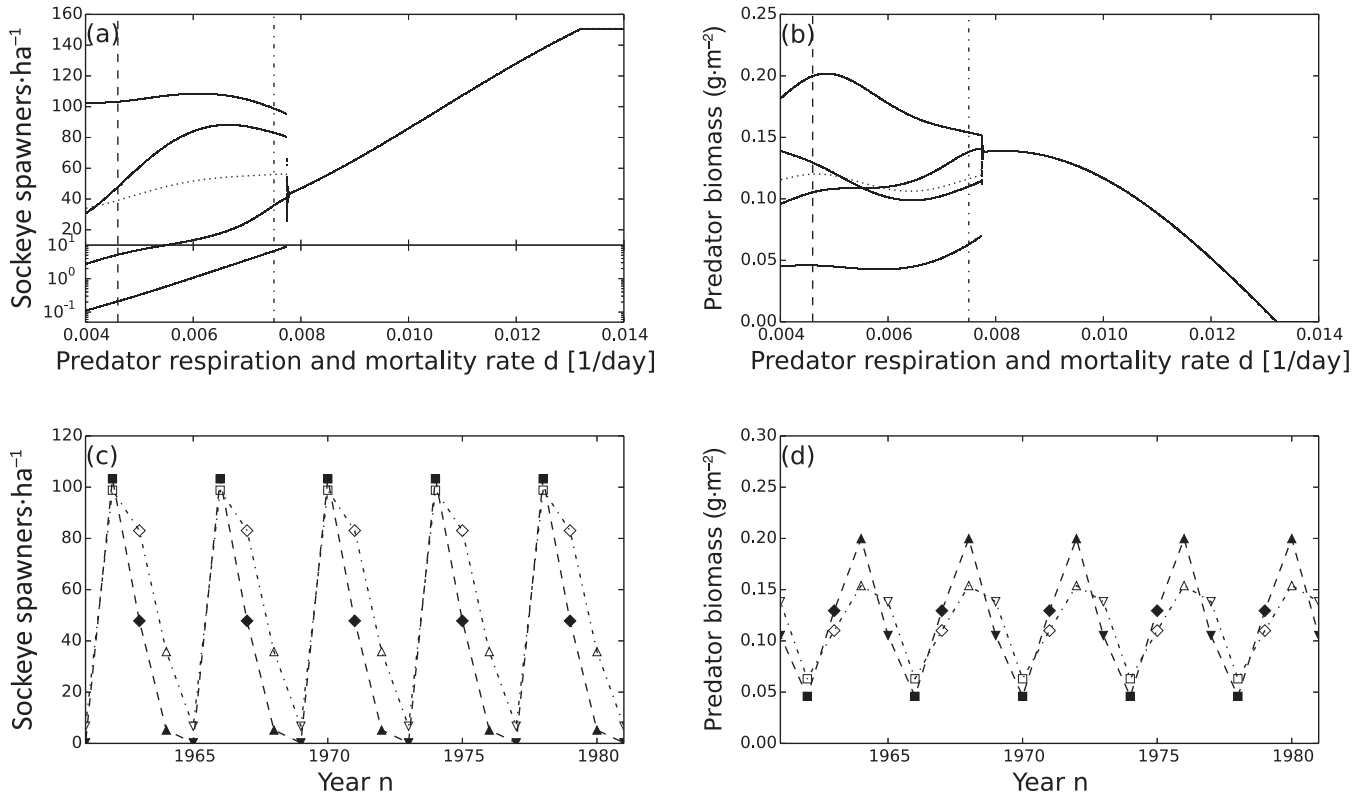
lines (especially the subdominant line and the first nondominant line) increase considerably in abundance (Fig. 5*c*). This also increases the average spawner abundance significantly. When *d* is further increased, cyclic dominance becomes replaced by quasi-periodic oscillations in a very narrow range of parameters. At *d* ≈ 0.0078, these break down, too, and the four salmon lines settle down at a stable equilibrium. However, in this population state, the four lines are only at a level comparable to the subdominant line in the unperturbed system, not at the level of the dominant line.

Based on the data published by Sebastian et al. (2003) on rainbow trout in Quesnel Lake, we estimated a total number of about 40 000 rainbow trout weighing approximately 500 g each and about half that number weighing 1000 g or more. This results in a predator biomass density in Quesnel Lake (surface area: 270 km^2) of approximately 0.15 g·m^{-2}. The predator biomass density predicted by our model is in very good agreement with this estimate (Fig. 5*d*). Our simulations also reveal that when the sockeye salmon display cyclic dominance, the difference between the strongest and the weakest line of the predator is only a factor four, while in the salmon population it is close to a factor 1000. Such a rather small numerical response of the predators to highly variable prey abundance, which will most likely be difficult to detect in nature, has been suggested before (Ricker 1997). Interestingly, the parameter *d*, which summarizes mortality and respiration rate of the predator, can be nearly doubled without reducing the mean biomass density of the predator. This phenomenon has been called the hydra effect (Abrams 2009) and is due to the increased availability of food. Only when *d* is increased beyond 0.01 does the predator biomass density decline to levels lower than in

the unperturbed system, and the predator is finally driven to extinction at *d* ≈ 0.013. This decrease of predator biomass density allows the sockeye population to increase in all four brood lines to levels even higher than that of the original dominant line.

This strategy to increase the abundance of sockeye salmon is, however, extremely ill-advised. First, our model does not account for the life history of the predator. It only accounts for the positive effect of salmon biomass density on the predator that leads to a delayed increase in predation mortality of the sockeye fry. While this is sufficient to generate cyclic dominance, more detailed models have demonstrated a differential effect of predator mortality. If competition among adult predators is strong, moderately increasing their mortality might actually increase their recruitment rate (De Roos et al. 2007), which could have negative effects on the salmon population. Only high levels of additional predator mortality are guaranteed to negatively affect the predator and thus benefit the sockeye salmon. More detailed information about the predator is therefore crucially important, for example about potential bottlenecks in its life cycle dynamics, to obtain reliable quantitative predictions concerning the outcome of such a predator-removal program. Second, the most important predator of sockeye salmon fry in the rearing lakes in the Fraser River system is the rainbow trout, which have their own ecological and economic value. As top predators they have a prominent role in controlling the structure and the dynamics of the rearing lake ecosystem (Duffy 2003; Casini et al. 2009). Removing them from the rearing lakes would cause considerable economic losses for the local tourism industry because of their importance for sport fishing.

Fig. 6. Effects of adjusting the harvest rate (scenario 4) on the abundance of spawners (*a*), the catch (*b*), the total return (*c*), and on the predators (*d*). The curved dotted lines correspond to the mean values during one cycle, and the dashed vertical lines mark the standard conditions. Time series of spawner abundance (*e*) and fisheries yield (*f*) are shown for standard conditions (harvest rate $h = 0.7$, filled symbols, dashed lines) and for an overfishing scenario ($h = 0.94$, open symbols, dash-dotted lines).
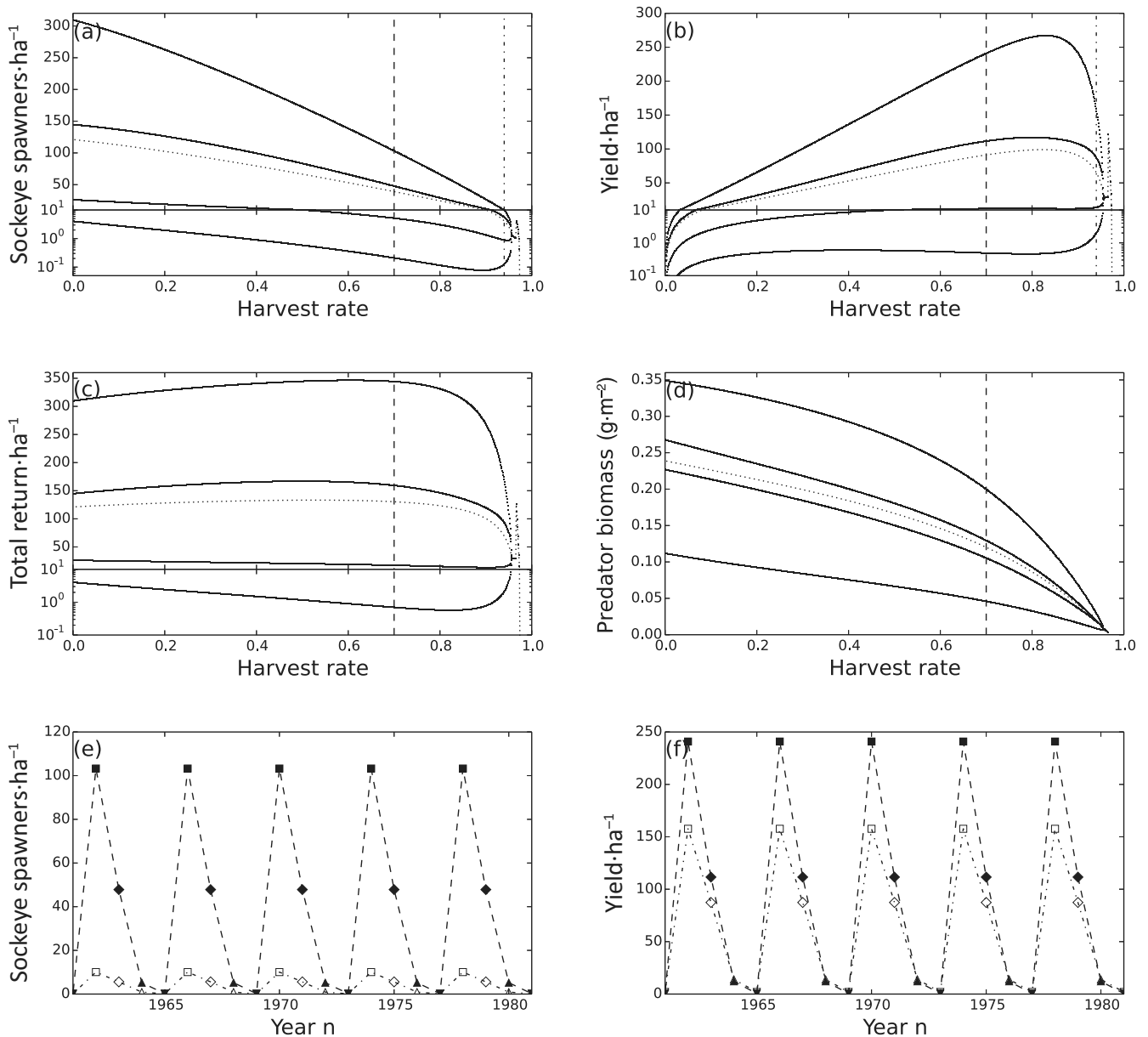
Scenario 4: adjusting harvest rates

With the value of the annual catch of Fraser River sockeye salmon previously exceeding CAN\$100 million in dominant years (Hume et al. 1996), a major motivation to investigate the population dynamics of sockeye salmon is to provide a scientific basis for management decisions. Our model also allows us to explore the effects of varying the harvest rate *h* (eq. 3). For simplicity we have chosen it to be the same for all four lines of a cycle, with a standard value of 0.7.

We can, however, vary the harvest rate between 0 and 1 to explore the consequences for the sockeye population (Fig. 6). The response of the number of spawners to varying harvest rates is quite straightforward; the higher the fraction of adult salmon that are caught, the fewer the fish that reach the spawning grounds (Fig. 6*a*). This is true for all four brood lines. At the same

time, higher harvest rates also means that higher absolute numbers of fish are caught, as long as the rate is not too high (Fig. 6*b*). The yield peaks at a harvest rate of approximately 0.83. This value appears to near a population threshold, and only slightly higher rates lead to a drastic decline of the absolute yield in dominant as well as subdominant years. However, the decrease in the yield is not as strong as the decrease of the spawner abundance (Figs. 6*e*, 6*f*). Eventually, cyclic dominance breaks down as the stock collapses. This increases the yield from the formerly nondominant lines, but this can by far not compensate the much smaller yield from the formerly dominant and subdominant lines.

The total return (catch plus spawners; Fig. 6*c*) is close to its maximum at the standard value of fishing mortality we have used in this study. Increasing the harvest rate above 0.85 leads to a rapid collapse of the stock because of overfishing. Lower harvest

970

Can. J. Fish. Aquat. Sci. Vol. 71, 2014

rates, however, do not increase the total return, because this only leads to higher competition on the spawning grounds and higher predation mortality during the first year in the rearing lake. This demonstrates that a certain degree of "managed" mortality is necessary to maximize the production of a salmon stock.

Our model also allows us to estimate some consequences of fishing at the ecosystem level. Every sockeye salmon that is removed from the system because of fishing is essentially lost to the freshwater ecosystem, causing a continuous decrease of the predator biomass density with increasing harvest rate (Fig. 6d). If the rate is too high (above approximately 0.95), the predator is driven to extinction. This leads to an increase of the fisheries yield in a narrow parameter range, but at only slightly higher harvest rates the sockeye are driven to extinction, too.

With harvest rates regularly exceeding 0.50, the management strategy applied can be expected to have a strong impact on the overall population dynamics of the salmon. Here we have assumed that the harvest rate is the same for all four cycle lines. Other strategies like a constant-escapement policy would lead to different fishing mortalities in different years of the cycle, which might either enhance or suppress cyclic dominance. In the Supplementary Material S2[1], we present simulation results for two alternative harvest strategies (constant escapement and constant harvest goal). In either case cyclic dominance still occurs over a wide parameter range, demonstrating once again the robustness of this phenomenon to anthropogenic disturbances.

Discussion and conclusions

We have demonstrated that the phenomenon of cyclic dominance of Fraser River sockeye salmon can be explained by a predator–prey interaction in the juvenile-rearing lakes of the salmon, as has been hypothesized before (Ricker 1997). It correctly predicts the sequence of one dominant year, followed by one subdominant year and two nondominant years, which is observed in the Shuswap, Quesnel, and late Stuart stocks, three of the largest sockeye stocks in the Fraser River basin. Unlike other mathematical models that have explored this mechanism, our model predicts cyclic dominance as a stable state of the system that is robust to perturbations (Schmitt et al. 2012) and to a broad range of variations in environmental conditions. In the last decades, however, the cyclic patterns of the Quesnel and late Stuart stocks have begun to show signs of weakening. The dominant lines are decreasing and one of the weaker lines might take over as a new dominant line. This might indicate that the stocks are now actually in or near the quasiperiodic regime (Fig. 1c), possibly because of a change in environmental conditions that negatively affect the productivity of the lakes (cf. Fig. 1a and scenario 1, warming). It is, however, also possible that dominance shifts to another line in those stocks following stochastic perturbations instead of a permanent change of environmental conditions (Schmitt et al. 2012).

In contrast with an earlier paper based on a three-species model (Guill et al. 2011), the present model includes only two species, thereby specifying the trophic interaction in the rearing lakes that is likely to be relevant for the occurrence of cyclic dominance. The former study included the zooplankton food of the sockeye fry. The zooplankton can be neglected as an independent dynamic variable, as in this study, because its dynamics are usually much faster than those of the fish species, meaning that the zooplankton will closely follow a moving equilibrium that is determined by the biomass density of the sockeye fry.

The model results are robust to varying the growth efficiency of the sockeye fry. This can be tested by introducing an exponent (g) in the growth term of the sockeye fry in eq. 1 (i.e., $r \cdot F_n \cdot (1 - F_n/K)^g$). Values of g smaller than 1 imply higher growth efficiencies of the sockeye fry, but as long as g is not too small (e.g., g > 0.2), this has no impact on the dynamics other than to increase the abundance of the dominant line. We interpreted the parameter e in eq. 1 as

the assimilation efficiency of the predator (i.e., as the fraction of ingested food that is not excreted as faeces or urine). Alternatively, it can be interpreted as growth efficiency, which also accounts for metabolic costs due to specific dynamic action and higher activity associated with foraging. In this case, e would have a smaller value of around 0.55 (instead of 0.85), but the metabolic rate d of the predator would have a smaller value too, because parts of the total metabolic demands are already included in e. In this case, realistic limits for the metabolic rate are 0.002 per day ≤ d ≤ 0.003 per day, which leads to the same qualitative behaviour as before.

The oscillation pattern of cyclic dominance belongs to the class of single generation cycles, because the period of the oscillation matches the dominant generation time. Classically, generation cycles are assumed to be caused by a direct density-dependent feedback of the dominating cohort on the competing cohorts (De Roos and Persson 2003). This is seen, for example, in Nicholson's sheep blowfly (*Lucilia cuprina*) populations (Kendall et al. 1999). In sockeye salmon populations, however, the situation is quite different. Because the sockeye salmon leave the freshwater habitat after 1 year, they cannot compete directly — in-lake — with the subsequent brood lines. Instead, we observe an indirect competition, which is mediated by the predators. Further, the mechanism behind the oscillations is also different from classic predator–prey oscillations, which are characterized by an oscillation period that is much longer than the generation time of the prey or the predators (Murdoch et al. 2002). The population oscillations of snowshoe hare and lynx are a typical example for this kind of oscillations (Elton and Nicholson 1942).

We thus conclude that cyclic dominance is a unique type of population oscillation that is caused by a subtle interplay between the life history of the sockeye salmon and its interaction with a highly piscivorous predator. Owing to the special life history of sockeye salmon, each brood line experiences predation in the rearing lakes only for 1 year and feeds a predator population the size of which will affect the brood line of the following year. The species-poor food web in the rearing lakes ensures that the state of the predators is tightly coupled to the abundance of their prey, the sockeye salmon. The slower life cycle and population dynamics of the predator leads to a delayed response of the predators to changing prey abundances; after 2 nondominant years, the predator population is in a very weak state and it requires 2 years to reach its maximum value again. This delay allows the dominant and, to a lesser degree, the subdominant brood lines to express the observed high abundances and subsequently leads to the suppression of the following brood lines.

Such a delayed effect of a predator population on the sockeye salmon has also been proposed by Larkin (1971). He introduced coefficients of delayed density dependence (i.e., a negative effect of high densities of salmon fry not only on their own survival, but also on that of following cycle lines) to mimic the effect of a predator. However, the population dynamics of the predator was not included explicitly in his model, and the predator was only represented by its effect on the salmon. This required implementing specific assumptions, for example, that the dominant line is not (or only weakly) affected by predation. This is also predicted by our model, but the assumption breaks down as soon as there are multiple dominant cycle lines. In this case, the higher availability of food during a whole cycle period would feed back on the predator population and allow it to increase to levels high enough to also affect dominant lines. By ignoring this feedback, the model of Larkin was able to frequently produce cycles with at least two dominant lines.

The predator–prey model we have proposed here allows us to explore scenarios of changing environmental conditions or human intervention with the natural system. These model-based experiments are not of sufficient detail to apply them strictly to management decisions or protection measures. For example, we

neglected that warming (scenario 1) also affects physiological rates and thus the predator–prey dynamics (Binzer et al. 2012; Rall et al. 2012). Nevertheless, these investigations demonstrate the advantage mechanistic modelling approaches have over mere statistical or descriptive ones. The analyses further show that cyclic dominance appears under a wide range of environmental conditions, as long as neither the spawning grounds nor the food availability are too strongly limiting, and the predator cannot switch to alternative food sources that completely substitute the sockeye fry in nondominant years. These conditions are met for some of the largest salmon stocks in the upper Fraser River region, implying that cyclic dominance can indeed be the natural state of several of the sockeye salmon populations in the Fraser River basin.

Strong empirical evidence for the mechanism we proposed for the generation of cyclic dominance could be provided by observations of piscivorous predator populations in the rearing lakes. We would expect to find an oscillation of the total predator biomass with a period of 4 years only in rearing lakes of sockeye stocks that exhibit cyclic dominance, but more constant or even completely absent predator populations in rearing lakes of noncyclic stocks. Our simulations, however, predict a comparably small amplitude of the oscillation in the predator population, which makes detection of the oscillation (and of distinguishing it from random environmental perturbations) difficult. So far we can demonstrate that the biomass density of rainbow trout in Quesnel Lake, where they are the main predator of sockeye fry, is in the range of what is predicted by our simulations. This is only a first step, and better and especially time-resolved data on potential predator populations is needed. This encouraging result, however, suggests that enhancing empirical research on the ecological processes in the freshwater habitat of sockeye salmon might be the key to understanding one of the most intriguing phenomena of the population dynamics of sockeye salmon.

Acknowledgements

References

Abrams, P.A. 2009. When does greater mortality increase population size? The long history and diverse mechanisms underlying the hydra effect. Ecol. Lett. **12**: 462–474. doi:10.1111/j.1461-0248.2009.01282.x.

Beacham, T.D., and Murray, C.B. 1993. Fecundity and egg size variation in North American Pacific salmon (*Oncorhynchus*). J. Fish. Biol. **42**: 485–508. doi:10.1111/j.1095-8649.1993.tb00354.x.

Beddington, J.R. 1975. Mutual interference between parasites or predators and its effect on searching efficiency. J. Anim. Ecol. **44**(1): 331–340. doi:10.2307/3866.

Binzer, A., Guill, C., Brose, U., and Rall, B.C. 2012. The dynamics of food chains under climate change and nutrient enrichment. Philos. Trans. R. Soc. B Biol. Sci. **367**: 2935–2944. doi:10.1098/rstb.2012.0230.

Blasius, B., Huppert, A., and Stone, L. 1999. Complex dynamics and phase synchronization in spatially extended ecological systems. Nature, **399**: 354–359. doi:10.1038/20676. PMID:10360572.

Brose, U., Dunne, J.A., Montoya, J.M., Petchey, O.L., Schneider, F.D., and Jacob, U. 2012. Climate change in size-structured ecosystems. Philos. Trans. R. Soc. B Biol. Sci. **367**: 2903–2912. doi:10.1098/rstb.2012.0232.

Casini, M., Hjelm, J., Molinero, J.-C., Lövgren, J., Cardinale, M., Bartolino, V., Belgrano, A., and Kornilovs, G. 2009. Trophic cascades promote threshold-like shifts in pelagic marine ecosystems. Proc. Natl. Acad. Sci. **106**: 197–202. doi:10.1073/pnas.0806649105. PMID:19109431.

De Roos, A.M., and Persson, L. 2003. Competition in size-structured populations: mechanisms inducing cohort formation and population cycles. Theor. Popul. Biol. **63**: 1–16. doi:10.1016/S0040-5809(02)00009-6. PMID:12464491.

De Roos, A.M., Schellekens, T., van Kooten, T., van de Wolfshaar, K., Claessen, D., and Persson, L. 2007. Food-dependent growth leads to overcompensation in stage-specific biomass when mortality increases: the influence of maturation versus reproduction regulation. Am. Nat. **170**: E59–E76. doi:10.1086/520119. PMID:17879182.

Duffy, J.E. 2003. Biodiversity loss, trophic skew and ecosystem functioning. Ecol. Lett. **6**: 680–687. doi:10.1046/j.1461-0248.2003.00494.x.

Elton, C.S., and Nicholson, M. 1942. The ten-year cycle in numbers of the lynx in Canada. J. Anim. Ecol. **11**: 215–244. doi:10.2307/1358.

English, K.K., Edgell, T.C., Bocking, R.C., Link, M., and Raborn, S. 2011. Fraser River sockeye fisheries and fisheries management and comparison with Bristol Bay sockeye fisheries [online]. LGL Ltd. Cohen Commission Tech. Rep. 7. Vancouver, B.C. Available from www.cohencommission.ca.

Guill, C., Drossel, B., Just, W., and Carmack, E. 2011. A three-species model explaining cyclic dominance of Pacific salmon. J. Theor. Biol. **276**(1): 16–21. doi:10.1016/j.jtbi.2011.01.036. PMID:21291894.

Hume, J.M.B, Shortreed, K.S., and Morton, K.F. 1996. Juvenile sockeye rearing capacity of three lakes in the Fraser River system. Can. J. Fish. Aquat. Sci. **53**(4): 719–733. doi:10.1139/f95-237.

Hume, J.M.B., Shortreed, K.S., and Whitehouse, T. 2005. Sockeye fry, smolt, and nursery lake monitoring of Quesnel and Shuswap lakes in 2004 [online]. Available from http://www.unbc.ca/sites/default/files/sections/quesnel-river-research-centre/frp3hume.pdf [accessed 12 August 2013].

Isakov, A.G., Mathisen, O.A., Ignell, S.E., and Quinn, T.J., II. 2000. Ocean growth of sockeye salmon from the Kvichak River, Bristol Bay based on scale analysis. N. Pac. Anadr. Fish Comm. Bull. **2**: 233–245.

Kendall, B.E., Briggs, C.J., Murdoch, W.W., Turchin, P., Ellner, S.P., McCauley, E., Nisbet, R.M., and Wood, S.N. 1999. Why do populations cycle? A synthesis of statistical and mechanistic modeling approaches. Ecology, **80**(6): 1789–1805. doi:10.2307/176658.

Kuznetsov, Y.A. 2004. Elements of applied bifurcation theory. Springer, New York.

Larkin, P.A. 1971. Simulation studies of the Adams River sockeye salmon (*Oncorhynchus nerka*). J. Fish. Res. Board Can. **28**(10): 1493–1502. doi:10.1139/f71-230.

Levy, D.A., and Wood, C.C. 1992. Review of proposed mechanisms for sockeye salmon population cycles in the Fraser River. Bull. Math. Biol. **54**: 241–261. doi:10.1007/BF02464832.

Lotka, A.J. 1925. Elements of physical biology. Williams & Wilkins Company, Baltimore.

Ludwig, D., Jones, D.D., and Holling, C.S. 1978. Qualitative analysis of insect outbreak systems: the spruce budworm and forest. J. Anim. Ecol. **47**: 315–332. doi:10.2307/3939.

May, R.M., and Oster, G.F. 1976. Bifurcations and dynamic complexity in simple ecological models. Am. Nat. **110**: 573–599. doi:10.1086/283092.

Murdoch, W.W., Kendall, B.E., Nisbet, R.M., Briggs, C.J., McCauley, E., and Bolser, R. 2002. Single-species models for many-species food webs. Nature, **417**: 541–543. doi:10.1038/417541a. PMID:12037520.

Myers, R.A., Barrowman, N.J., Hutchings, J.A., and Rosenberg, A.A. 1995. Population dynamics of exploited fish stocks at low population levels. Science, **269**: 1106–1108. doi:10.1126/science.269.5227.1106. PMID:17755535.

Myers, R.A., Mertz, G., Bridson, J.M., and Bradford, M.J. 1998. Simple dynamics underlie sockeye salmon (*Oncorhynchus nerka*) cycles. Can. J. Fish. Aquat. Sci. **55**(10): 2355–2364. doi:10.1139/f98-059.

Nelson, G.C. 2005. Millennium ecosystem assessment: drivers of ecosystem change: summary chapter. World Resources Institute, Washington, D.C.

Odum, E.P. 1953. Fundamentals of ecology. W.B. Saunders, Philadelphia.

Pörtner, H.O., and Farrell, A.P. 2008. Physiology and climate change. Science, **322**: 690–692. doi:10.1126/science.1163156. PMID:18974339.

Rall, B.C., Guill, C., and Brose, U. 2008. Food-web connectance and predator interference dampen the paradox of enrichment. Oikos, **117**: 202–213. doi:10.1111/j.2007.0030-1299.15491.x.

Rall, B.C., Brose, U., Hartvig, M., Kalinkat, G., Schwarzmüller, F., Vucic-Pestic, O., and Petchey, O.L. 2012. Universal temperature and body-mass scaling of feeding rates. Philos. Trans. R. Soc. B Biol. Sci. **367**: 2923–2934. doi:10.1098/rstb.2012.0242.

Ricker, W.E. 1950. Cycle dominance among the Fraser sockeye. Ecology, **31**(1): 6–26. doi:10.2307/1931356.

Ricker, W.E. 1954. Stock and recruitment. J. Fish. Res. Board Can. **11**(5): 559–623. doi:10.1139/f54-039.

Ricker, W.E. 1997. Cycles of abundance among Fraser River sockeye salmon (*Oncorhynchus nerka*). Can. J. Fish. Aquat. Sci. **54**(4): 950–968. doi:10.1139/f97-047.

Rosenzweig, M.L., and MacArthur, R.H. 1963. Graphical representation and stability conditions of predator–prey interactions. Am. Nat. **97**: 209–223. doi:10.1086/282272.

Rounsefell, G.A., and Kelez, G.B. 1938. The salmon and salmon fisheries of Swiftsure Bank, Puget Sound, and the Fraser River. Bull. Bur. Fish. **49**: 692–823.

Royama, T. 1984. Population dynamics of the spruce budworm *Choristoneura fumiferana*. Ecol. Monogr. **54**: 429–462. doi:10.2307/1942595.

Schmitt, C.K., Guill, C., and Drossel, B. 2012. The robustness of cyclic dominance under random fluctuations. J. Theor. Biol. **308**: 79–87. doi:10.1016/j.jtbi.2012.05.028. PMID:22677399.

Sebastian, D., Dolighan, R., Andrusak, H., Hume, J., Woodruff, P., and Scholten, G. 2003. Summary of Quesnel Lake kokanee and rainbow trout biology with reference to sockeye salmon. Ministry of Water, Land, and Air Protection, Province of British Columbia. Stock Management Report No. 17.

Shortreed, K.S., Morton, K.F., Malange, K., and Hume, J.M.B. 2001. Factors limiting juvenile sockeye production and enhancement potential for selected B.C. nursery lakes. Research Document 2001/098 for the Canadian Science Advisory Secretariat.

Skalski, G.T., and Gilliam, J.F. 2001. Functional responses with predator interference: viable alternatives to the Holling type II model. Ecology, **82**(11): 3083–3092. doi:10.1890/0012-9658(2001)082[3083:FRWPIV]2.0.CO;2.

Townsend, C.R. 1989. Population cycles in freshwater fish. J. Fish Biol. **35**(Suppl. A): 125–131. doi:10.1111/j.1095-8649.1989.tb03053.x.

Volterra, V. 1926. Variations and fluctuations of the number of individuals in animal species living together. ICES J. Mar. Sci. (1928), **3**: 3–51. [Reprint and translation into English.] doi:10.1093/icesjms/3.1.3.

Walters, C.J., and Staley, M.J. 1987. Evidence against the existence of cyclic dominance in Fraser River sockeye salmon (*Oncorhynchus nerka*). *In* Sockeye salmon (*Oncorhynchus nerka*) population biology and future management. *Edited by* H.D. Smith, L. Margolis, and C.C. Wood. Can. Spec. Publ. Fish. Aquat. Sci. **96**: 375–384.

Walters, C., and Woodey, J.C. 1992. Genetic models for cyclic dominance in sockeye salmon (*Oncorhynchus nerka*). Can. J. Fish. Aquat. Sci. **49**(2): 281–292. doi:10.1139/f92-032.

White, C.R., Phillips, N.F., and Seymour, R.S. 2006. The scaling and temperature dependence of vertebrate metabolism. Biol. Lett. **2**: 125–127. doi:10.1098/rsbl.2005.0378. PMID:17148344.

Yodzis, P., and Innes, S. 1992. Body size and consumer–resource dynamics. Am. Nat. **139**(6): 1151–1175. doi:10.1086/285380.

LETTER

Body masses, functional responses and predator–prey stability

Gregor Kalinkat,[1,2]* Florian D. Schneider,[1,2,3] Christoph Digel,[2] Christian Guill,[2,4] Björn C. Rall[2] and Ulrich Brose[2]

Abstract

The stability of ecological communities depends strongly on quantitative characteristics of population interactions (type-II vs. type-III functional responses) and the distribution of body masses across species. Until now, these two aspects have almost exclusively been treated separately leaving a substantial gap in our general understanding of food webs. We analysed a large data set of arthropod feeding rates and found that all functional-response parameters depend on the body masses of predator and prey. Thus, we propose generalised functional responses which predict gradual shifts from type-II predation of small predators on equally sized prey to type-III functional-responses of large predators on small prey. Models including these generalised functional responses predict population dynamics and persistence only depending on predator and prey body masses, and we show that these predictions are strongly supported by empirical data on forest soil food webs. These results help unravelling systematic relationships between quantitative population interactions and large-scale community patterns.

Keywords

Allometric scaling, body size, consumer-resource, ecological modelling, feeding rate, food webs, interaction strength, metabolic theory.

INTRODUCTION

The stability of populations, communities and ecosystem functions depends critically on the strengths, distributions and characteristics of the interactions connecting species in complex food webs (McCann *et al.* 1998; Neutel *et al.* 2002; Rooney *et al.* 2006). Traditionally, consumer–resource interactions have been categorised according to their functional response as hyperbolic (type-II) or sigmoid (type-III) increases in the consumer's *per capita* feeding rate with the resource density (Holling 1959; Murdoch & Oaten 1975; Sarnelle & Wilson 2008). Historically, the quest for type-III functional responses has been fuelled by their severe consequences for population dynamics: they promote stable equilibria by accelerating predation risk at low resource densities which prevents unstable population oscillations (Murdoch & Oaten 1975; Williams & Martinez 2004; Fryxell *et al.* 2007; Rall *et al.* 2008). Despite their dynamical importance, however, characterising these functional-response types for each of the myriads of interactions in natural communities by tedious individual experiments is unfeasible thus rendering a generalised understanding of natural population dynamics virtually or nearly impossible.

An alternative approach employs body masses and their *allometric* relationships with ecologically important traits of species and their interactions (Peters 1983; Brown *et al.* 2004; Brose 2010). This allometric approach predicts the biological rates of populations such as respiration, consumption and growth by population-averaged body masses (Peters 1983; Brown *et al.* 2004) that are often available for consumer-resource pairs (Digel *et al.* 2011; Riede *et al.* 2011). Moreover, this constrains the universe of possible combinations of biological rates into those that are probable given that they all scale with species' body masses (Brose 2010). In this vein, systematic scaling relationships of the functional-response parameters handling time and capture rate (see Methods for detailed functional-response models) have been documented (Wahlström *et al.* 2000; Aljetlawi *et al.* 2004; Vonesh & Bolker 2005; Vucic-Pestic *et al.* 2010b; McCoy *et al.* 2011; Rall *et al.* 2011). Recently, it was shown that predatory beetles exhibited type-II or type-III functional responses when feeding on a small or a large prey species, respectively (Vucic-Pestic *et al.* 2010b), but this pattern has not been generalised across different predator and prey species. Allometric scaling of handling time and capture rate (also known as attack rate, see Methods) were included in population dynamic models demonstrating that variance in body masses has profound effects on population dynamics (Yodzis & Innes 1992; Weitz & Levin 2006; Otto *et al.* 2007) and food-web persistence (Loeuille & Loreau 2005; Brose *et al.* 2006; Rall *et al.* 2008; Heckmann *et al.* 2012). However, as none of these models addressed relationships between body masses and functional-response types, they could not explain the radical dynamic shifts associated with differences between these types (e.g. Williams & Martinez 2004; Brose *et al.* 2006; Rall *et al.* 2008).

We investigated how allometric scaling models can be integrated into functional-response types. These generalised allometric functional responses go beyond traditional functional-response types by including a body mass dependency for the capture exponent causing a gradual transition between hyperbolic and sigmoid functional responses. After parameterising allometric functional-response models employing data of terrestrial arthropod consumer–resource interactions, we show in dynamical analyses that allometric scaling of the capture exponent causes severe differences in population dynamics. In consequence, this model predicts a more realistic domain of

[1]*Department of Biology, Darmstadt University of Technology, Schnittspahnstr. 10, Darmstadt, 64287, Germany*

[2]*J.F. Blumenbach Institute of Zoology and Anthropology, Georg-August University of Göttingen, Berliner Str. 28, Göttingen, 37073, Germany*

[3]*Institut des Sciences de l'Evolution, CNRS, Université Montpellier 2 - CC065, Montpellier Cedex 05, 34095, France*

[4]*Institute for Biodiversity and Ecosystem Dynamics, University of Amsterdam, P.O. Box 94248, Amsterdam, 1090 GE, The Netherlands*

Correspondence: E-mail: kalinkat@bio.tu-darmstadt.de

stable coexistence for consumer-resource pairs than previous models, as we show by comparing the match with body-mass data from an entirely independent data base on natural food webs.

MATERIAL AND METHODS

Functional responses

The functional-response model framework established by Holling (1959) has been used in a plethora of studies (reviewed in Rall *et al.* 2012), where the per capita consumption rate of the predator, F, depends on the density of the prey, N:

$$F = \frac{aN}{1 + ahN}, \tag{1}$$

with the handling time, h [s], needed to kill, ingest and digest a prey individual (Jeschke *et al.* 2002) and the capture rate, a [m^2 s^{-1}], as a measure of the predator's hunting efficiency (originally termed 'rate of successful search'; Holling 1959). The capture rate was also termed 'attack rate' in other studies, a term that we consider as deprecated because of its ambiguity in excluding or including unsuccessful attempts of attack (Koen-Alonso 2007). This model framework is suitable for a wide range of consumer–resource interactions but as our experimental work was exclusively based on terrestrial invertebrate predators and their prey we will subsequently adhere to the terminology of predators and prey. Several functional-response studies have addressed allometric scaling and showed that capture rates follow hump-shaped relationships with predator–prey body-mass ratios while handling times decrease with increasing predator body mass and increase with prey body mass which can be explained by functional morphological constraints and allometric arguments based on metabolic theory (Wahlström *et al.* 2000; Aljetlawi *et al.* 2004; Vonesh & Bolker 2005; Vucic-Pestic *et al.* 2010b; McCoy *et al.* 2011; Rall *et al.* 2011; more references in Brose 2010).

The type-II functional response with a constant capture rate (eqn 1) can be modified to account for capture rates that vary with prey density, $a = bN^q$ (Williams & Martinez 2004; Rall *et al.* 2008; Vucic-Pestic *et al.* 2010b), which yields type-III functional responses:

$$F = \frac{bN^{1+q}}{1 + bhN^{1+q}}, \tag{2}$$

where b is a capture coefficient (sometimes also referred to as search coefficient), and q is a scaling exponent (hereafter: capture exponent) that converts hyperbolic type-II ($q = 0$) into sigmoid type-III ($q > 0$) functional responses. Subsequently, we aim to demonstrate that the inclusion of allometric dependencies for the capture coefficient, b, and capture exponent, q, substantially improve and generalise functional-response models.

Feeding rate experiments

We integrated data of prior feeding and functional-response studies (Brose *et al.* 2008; Vucic-Pestic *et al.* 2010b; Rall *et al.* 2011) with additional feeding experiments. These experiments used different treatment designs, but where all employing exactly the same microcosm set-up and environmental conditions (see Table S2 in Supplementary Material for a list of predator–prey pairs and reference to previous publications). In total, this yielded *per capita* feeding rates

of 25 species of generalist arthropod predators (Coleoptera: Carabidae, Staphylinidae; Araneae: Lycosidae, Pisauridae, Salticidae; Chilopoda: Lithobiidae) on eight differently sized prey species [Collembola; Diptera (larvae and adults); Coleoptera (larvae); Isopoda; Orthoptera) varying between one and 1000 prey individuals per arena (0.04 m², see Table S1 for species names and density levels for each predator–prey pair]. All experimental units comprised a single predator individual and prey density was varied systematically (e.g. 1, 3, 5, 10, 30, 50 individuals per arena). Here, the definition of a predator includes its taxonomy and size class (narrow size ranges). Predators were sampled in the field, and only a small fraction of juvenile centipedes and lycosid spiders were reared in the laboratory until they reached the designated size. Prey populations were reared in the laboratory. Body masses of predators were determined individually. Prey body masses were estimated as averages across prey populations (see Table S2 for predator and prey species with ranges of body masses). Prey density levels were replicated two to eight times resulting in a total number of 2564 experimental units (see Table S2).

The predator individuals were kept separate in plastic jars dispersed with water and were deprived of food for at least 48 h before the start of the experiments. The experiments were performed in acrylic glass arenas (0.2 × 0.2 × 0.1 m) covered with lids permeable to air. The arena was floored with moist plaster of Paris (200 g dry weight) to provide constant humidity during the experiments. Habitat structure in the arenas was provided by moss (*Polytrichum formosum*, 2.35 g dry weight) that was first dried for 3 days at 40 °C to exclude animals and then re-moisturised prior to the experiments. Prey individuals were placed in the arenas half an hour in advance of the predators to allow them to disperse in the arenas. The experiments were run for 24 h with 12 h dark and 12 h light at a constant temperature of 15 °C in temperature cabinets. Initial and final prey densities were used to calculate the number of prey eaten. Predators were weighted before and after the experiments to calculate mean body mass. Control experiments without predators showed that prey mortality or escape was negligible.

Functional-response models

Different candidate functional-response models were fitted to the feeding-rate data that were evaluated according to their ΔAIC (difference in Akaike Information Criterion). As null models, we estimated constant parameters for non-allometric models of type-II (h and a in eqn 1) and type-III (h, b and q in eqn 2) functional responses. The first allometric model was a type-II functional response (eqn 1) with fixed allometric-scaling exponents according to Yodzis & Innes (1992), where the handling time,

$$h = h_0 m_r m_c^{-0.75}, \tag{3a}$$

as well as the capture rate,

$$a = a_0 m_r^{-1} m_c^{0.75}, \tag{3b}$$

are described with h_0 and a_0 as constants and the body masses [g], m_c and m_r, of the predator c, and the prey r, respectively. These null models of allometric relations are based on the simplifying assumption that interaction parameters should scale with body masses in the same way as metabolic rates with a ¾ power law (Peters 1983; Brown *et al.* 2004; Brose 2010; see Supplementary Information for a detailed description of the derivation of functional-response

parameters from the models in Yodzis & Innes 1992). Subsequently, we will refer to this first model (inserting eqns 3a,b into eqn 1) as the allometric type-II functional response.

In the second model, allometric relationships were included according to a prior study (Rall *et al.* 2011) where handling time, *h*, follows power-law relationships with predator and prey body mass:

$$h = h_0 m_r^{\alpha_r} m_c^{\alpha_c}, \tag{4a}$$

where and α_c and α_r are allometric exponents (Rall *et al.* 2011). As capture rates follow hump-shaped relationships with predator–prey body-mass ratios (Wahlström *et al.* 2000; Aljetlawi *et al.* 2004; Vonesh & Bolker 2005; Vucic-Pestic *et al.* 2010b; McCoy *et al.* 2011) we estimated the allometry of the capture rate, *a*, using a combined equation comprising a power-law relationship with prey body mass and an exponential Ricker function that describes a humped curve with increasing body-mass ratios of the predator to the prey:

$$a = a_0 m_r^{\beta_r} \frac{m_c}{m_r} e^{\varepsilon \frac{m_c}{m_r}}, \tag{4b}$$

where a_0 is a constant, β_r is the exponent for the scaling of m_r, and ε is a constant which determines the width of the hump (Rall *et al.* 2011). This pattern of decreases and increases in capture rates at low and high prey body mass yields a hump-shaped attack model (Wahlström *et al.* 2000; Aljetlawi *et al.* 2004; Vucic-Pestic *et al.* 2010b; McCoy *et al.* 2011). We will refer to this second model as the hump-shaped allometric functional response.

Finally, we extended the second model by including a sigmoid scaling of the capture exponent, *q*, with the predator–prey body-mass ratio *R*:

$$q = \frac{q_{max} R^2}{q_0^2 + R^2}, \tag{5a}$$

where q_{max} and q_0 are scaling parameters defining the sigmoid relationship. The capture coefficient, *b*, follows the same allometric scaling relationships as the capture rate, *a*, in the previous model (eqn 4b), with the constant b_0 instead of a_0:

$$b = b_0 m_r^{\beta_r} \frac{m_c}{m_r} e^{\varepsilon \frac{m_c}{m_r}}. \tag{5b}$$

Inserting eqns 4a, 5a,b into eqn 2 yielded our third model, the generalised allometric functional response, accounting for hyperbolic as well as sigmoid forms of the response in dependence on predator and prey body masses.

Fitting the models to the data set of experimental observations by nonlinear least squares methods requires integrating the functional response to predict N_e, the number of prey individuals eaten during the experimental time as a function of the initial prey density ('nls' in R; Bolker 2008; R Development Core Team 2010). The application of Rogers' random predator equation accounts for decreasing prey densities during the experiment (Rogers 1972; Vonesh & Bolker 2005; McCoy & Bolker 2008) and can be solved using the Lambert W function (implemented in the package 'emdbook' for the statistical software R; Bolker 2008; R Development Core Team 2010 see Supplementary Information for details on equations and fitting procedure).

Model analyses

To illustrate the different consequences of these functional-response models for population dynamics, we performed bioenergetic simula-

tions of simple predator–prey pairs (Yodzis & Innes 1992; Otto *et al.* 2007; Heckmann *et al.* 2012; Schneider *et al.* 2012) for each of the three different functional response models: the allometric type-II, the hump-shaped allometric and the generalised allometric functional response (see Supplementary Information for methodological details of the model simulations). We compared the resulting persistence domains of the model simulations (i.e. the combinations of prey and predator body masses at which the predator is predicted to persist) to a new data base on predator and prey body masses of terrestrial soil food webs from a large biodiversity research project in Germany (see Supplementary Information for details on food-web assembly). On basis of the predicted persistence domains, the three models were compared using a dimensionless score value, *S*. We defined this value to be a product of two ratios calculated within to the total area of the comparison, A_{total} (see Supplementary Information, Fig. S1 for the definition of this comparison envelope):

$$S = \frac{L_{pers}}{L_{emp}} \times \frac{A_{total} - A_{pers}}{A_{total}}. \tag{6}$$

The first fraction is the percentage of predator–prey pairs for which persistence is predicted by the model, L_{pers}, among all empirically observed links, L_{emp}. It is multiplied with the fraction of the area where no persistence of the predator is possible (total area, A_{total}, minus the persistence domain, A_{pers}). Thus, *S* penalises large persistence domains, which *per se* include larger proportions of the empirical links. For the same set of empirical predator–prey pairs, the score is maximised for a model that includes a maximal number of predator–prey pairs while predicting a minimal persistence domain.

RESULTS

The comparison via AIC revealed that the generalised functional-response model with allometric scaling of all parameters including *q* was the best-fitting model (AIC = 34087.74; ΔAIC = 0.0; d.f. = 9) compared to the hump-shaped allometric functional response (ΔAIC = 566.54; d.f. = 7) and the allometric type-II functional response (ΔAIC = 1586.69; d.f. = 3). The application of non-allometric type-II and type-III functional-response models to the data set scored worst (ΔAIC = 1688.54, d.f. = 3 and ΔAIC = 2134.58, d.f. = 3 respectively; see Table 1 for an overview of all parameter estimates). Together, these results imply that the generalised allometric functional-response model provides a substantially better fit to the feeding data over a wide variety of species, and the subsequent results will be based on this best-fitting model.

For handling time *h*, we found a significant negative power-law scaling with predator body mass ($h_0 = 43\ 280$; standard error = 8.364; $P < 0.001$; $\alpha_c = -0.283$; SE = 0.0218; $P < 0.001$; Fig. 1a), and a positive power-law scaling with prey body mass ($\alpha_r = 0.568$; SE = 0.022; $P < 0.001$; Fig. 1a). Hence, handling times are highest at very low predator–prey body-mass ratios (i.e. the prey is larger than the predator, Fig. 1a). Furthermore, we found a hump-shaped relationship for the capture coefficient *b* with the predator–prey body-mass ratio ($b_0 = 1.680 \times 10^{-8}$; SE = 4.469×10^{-9}; $P < 0.001$; $\beta_r = 0.0033$; SE = 0.0371; $P = 0.378$; $\varepsilon = -0.0182$; SE = 0.0008; $P < 0.001$; Fig. 1b). Finally, the capture exponent *q* scaled positively with the predator–prey body-mass ratio *R* following a sigmoid relationship ($q_0 = 1.009$; SE = 21.84; $P < 0.001$; $q_{max} = 3.306$; SE = 0.148; $P < 0.001$; Fig. 1c) implying that the higher the body-mass ratio the more sigmoid the functional

Table 1 Summary of the fitted parameters for the competing functional-response models

Parameter	Estimate	SE	t	P
Type-II functional response (ΔAIC = 1688.54, d.f. = 3)				
a	$8.478 \cdot 10^{-8}$	$2.703 \cdot 10^{-9}$	31.37	<0.0001***
h	$1.475 \cdot 10^{2}$	$2.321 \cdot 10^{1}$	6.35	<0.0001***
Type-III functional response, $q = 1$ (ΔAIC = 2134.58, d.f. = 3)				
b	$1.609 \cdot 10^{-11}$	$7.812 \cdot 10^{-13}$	20.60	<0.0001***
h	$5.999 \cdot 10^{2}$	$1.632 \cdot 10^{1}$	36.76	<0.0001***
Traditional allometric type-II functional response (ΔAIC = 1586.69, d.f. = 3)				
a_0	$1.673 \cdot 10^{-10}$	$7.305 \cdot 10^{12}$	22.90	<0.0001***
h_0	$4.084 \cdot 10^{5}$	$1.853 \cdot 10^{4}$	22.04	<0.0001***
Hump-shaped allometric functional response (ΔAIC = 566.54, d.f. = 7)				
a_0	$1.074 \cdot 10^{-7}$	$3.305 \cdot 10^{-8}$	3.25	0.0012**
h_0	$8.263 \cdot 10^{4}$	$2.101 \cdot 10^{4}$	3.93	<0.0001***
ε	$-1.892 \cdot 10^{-3}$	$1.116 \cdot 10^{-4}$	-16.96	<0.0001***
β_r	$5.218 \cdot 10^{-1}$	$4.069 \cdot 10^{-2}$	12.82	<0.0001***
α_r	$6.936 \cdot 10^{-1}$	$3.056 \cdot 10^{-2}$	22.70	<0.0001***
α_c	$-3.116 \cdot 10^{-1}$	$5.363 \cdot 10^{-2}$	-5.81	<0.0001***
Generalised allometric functional response (ΔAIC = 0, d.f. = 9)				
b_0	$1.680 \cdot 10^{-8}$	$4.469 \cdot 10^{-9}$	3.76	0.0002***
β_r	$3.276 \cdot 10^{-2}$	$3.711 \cdot 10^{-2}$	0.883	0.3775
ε	$-1.821 \cdot 10^{-2}$	$8.122 \cdot 10^{-4}$	-22.43	<0.0001***
q_{max}	3.306	$1.482 \cdot 10^{-1}$	22.30	<0.0001***
q_0	$1.009 \cdot 10^{3}$	$2.184 \cdot 10^{1}$	46.20	<0.0001***
h_0	$4.328 \cdot 10^{4}$	$8.364 \cdot 10^{3}$	5.18	<0.0001***
α_r	$5.681 \cdot 10^{-1}$	$2.183 \cdot 10^{-2}$	26.02	<0.0001***
α_c	$-2.825 \cdot 10^{-1}$	$2.177 \cdot 10^{-2}$	-12.98	<0.0001***

ΔAIC: difference in Akaike Information Criterion, AIC, to the generalised allometric functional response (AIC = 34 087.74); d.f.: degrees of freedom used by the model, SE: standard error; t: students t; P: two-sided P-value.
*$P < 0.05$.
**$P < 0.01$.
***$P < 0.001$.

response. This translates into type-II-like responses for small predators consuming relatively large prey, while large predators should be feeding on small prey following type-III-like responses according to the traditional categorisation of functional responses.

These general allometric scaling relationships of handling time, capture coefficient and capture exponent with predator and prey body masses allow predicting feeding rates for any combination of predator and prey body mass, and thus for any predator–prey pair (shown as solid lines in Fig. 2a-c for three exemplary taxonomic predator–prey pairs, see Fig. S1 for more examples). Embedding the parameters of these generalised allometric functional responses in population models yield predictions of predator–prey biomass dynamics (shown exemplarily in Fig. 2d-f for the taxonomic pairs of a-c). Subsequently, we have used one aspect of these biomass dynamics, predator survival, to compare the predictions of the three allometric functional-response models. We found that the simulations of the dynamic population model with the three functional responses predict very different persistence domains of predator and prey body masses enabling predator survival (non-red areas in Fig. 3). While the predator in the allometric type-II functional-response model only persists at very low prey body masses (Fig. 3a), the other two models produce a more band-shaped persistence domain across the range of predator–prey masses (Fig. 3b-c). However, these two domains exhibit pronounced differences

including that under the hump-shaped allometric functional responses large predators can persist across a wide range of prey body masses (Fig. 3b), whereas the generalised allometric functional responses produces a cone-shaped persistence domain where the largest predators can only persist on a very small range of prey body masses (Fig. 3c).

We compared the persistence domains predicted by the dynamic population models to empirical body-mass data of forest soil invertebrates. These data were selected for model evaluation, because they include many of the predator and prey taxa that were used in the functional-response experiments and thus in the models' parameterisation. We evaluated the three models according to the percentage of natural predator–prey links (grey-shaded squares in Fig. 3a-c) that fall within the persistence domains. This comparison revealed that the allometric type-II functional-response model yielded a persistence domain that included only 21.9% of the natural body-mass combinations (Fig. 3a), which is considerably less than the persistence domain of the hump-shaped allometric functional-response model including 95.8% of the interaction pairs (Fig. 3b). The generalised allometric functional-response model performed best by yielding a persistence domain matching 97.7% of the links in the food-web data base (Fig. 3c). However, as the sizes of the predicted persistence domains differ (19.9, 66.0 and 50.8% of the total area for the allometric type-II, the hump-shaped and the generalised functional-response model respectively), the chances of correctly including a predator–prey pair in the domain are not equal. To account for these differences between the models, we penalise for the size of the predicted persistence domain in the score S (see Methods). This yielded score values of $S = 0.17$ for the allometric type-II model, $S = 0.32$ for the hump-shaped allometric model and $S = 0.48$ for the generalised allometric functional-response model. Hence, the generalised model predicts the persistence domains substantially better than the other models, even after accounting for the different sizes of persistence domains.

DISCUSSION

We examined how the body masses of predators and prey constrain their interaction strengths. Corroborating prior functional-response studies (Wahlström *et al*. 2000; Aljetlawi *et al*. 2004; Vonesh & Bolker 2005; Vucic-Pestic *et al*. 2010b; McCoy *et al*. 2011; Rall *et al*. 2011), we found power-law relationships between handling time and predator as well as prey mass and hump-shaped relationships between capture rates and predator–prey body-mass ratios. In addition, our study demonstrates for the first time a systematic body-mass dependency of the capture exponent, converting hyperbolic (type-II) into sigmoid (type-III) functional responses with increasing predator body mass and decreasing prey body mass. This suggests that these functional-response types are not strict categories but rather gradually shift from type-II predation of small predators on equally sized prey to type-III functional responses of large predators on small prey. Thus, we were able to support prior findings that sigmoid type-III responses can come about in simple one predator – one prey systems (Sarnelle & Wilson 2008; Vucic-Pestic *et al*. 2010a,b) and are not necessarily related to the multi-prey environments as most previous studies on type-III responses and switching behaviour suggested (Murdoch *et al*. 1975; Kalinkat *et al*. 2011). Hence, our study represents an incremental advancement of prior studies on allometric constraints on functional responses
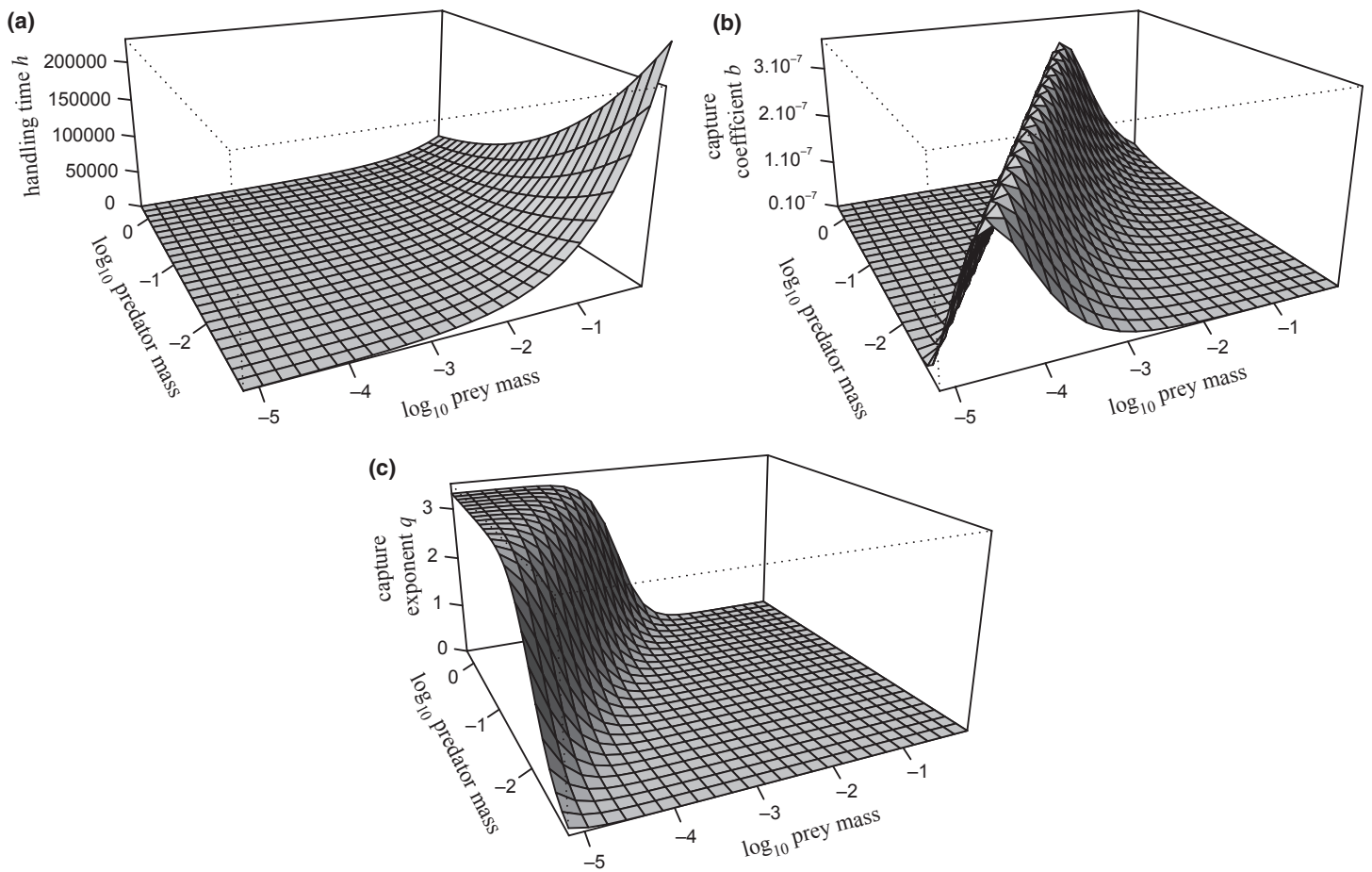
(a)

(b)

(c)

Figure 1 The generalised allometric functional-response model includes dependencies of the three fundamental functional-response parameters (a) handling time h, (b) capture coefficient b and (c) the capture exponent q on predator mass and prey mass. These relationships were estimated by fitting functional-response models to feeding data of terrestrial arthropods ($n = 2{,}564$).

(Wahlström *et al.* 2000; Aljetlawi *et al.* 2004; Vonesh & Bolker 2005; Brose 2010; Vucic-Pestic *et al.* 2010b; McCoy *et al.* 2011; Rall *et al.* 2011) but additionally entails far-reaching and important consequences for population and community ecology.

The allometric scaling of handling time is consistent with prior studies (Aljetlawi *et al.* 2004; Vucic-Pestic *et al.* 2010b; Rall *et al.* 2011, 2012). Compared to established null models based on the metabolic theory of ecology (Yodzis & Innes 1992; Brown *et al.* 2004), our results suggest that the power-law exponent of the relationship between handling time and predator mass (-0.28) is much shallower than the expected negative ¾ exponent. Moreover, the power-law increase in handling time with prey mass is also shallower (0.56) than the expected isometric scaling. These shallow scaling relationships of handling time with predator and prey masses are consistent with the findings from a recent and comprehensive meta-study on the allometry of feeding rates (Rall *et al.* 2012). Together, these results suggest that handling time is constrained by more complex processes and not solely by metabolism. For instance, the scaling relationship for predator mass might be biased by different feeding modes such as sucking or chewing that shift with increasing body masses. In our data set, liquid-feeding spiders (mean body mass: 0.036 g; $n = 618$) and centipedes (0.082 g; $n = 903$) are generally smaller than chewing beetles (0.126 g;

$n = 1044$). Therefore, small liquid feeders that ingest less unpalatable parts of their prey such as sclerotised cuticles have relatively quicker handling times than larger chewers ingesting whole prey items, which could explain the shallower relationships. On the basis of a large data base, our results suggest that the assumption of negative ¾ power-laws should be replaced by shallower scaling relationships for handling time.

The intentional exclusion of the taxonomic information in our generalised modelling approach is supported by previous work that has shown how allometric functional-response models can explain a large part of the variation in empirically observed feeding rates of taxonomically different predator–prey pairs with a minimal number of parameters (Rall *et al.* 2011). Nonetheless, generalised allometric models can be easily integrated with taxonomic approaches by making one or several parameters (e.g. the optimal prey body mass) dependent on predator taxonomy (Rall *et al.* 2011). In contrast, traditional taxonomy-based approaches describe each particular predator–prey pair with a set of parameters (e.g. Vucic-Pestic *et al.* 2010b). This traditional approach might produce more precise predictions (see examples in Fig. 2a-c and Fig. S1 in the Supplementary Information), but it comes at the cost of using more parameters: While the generalised model is very efficient in the use of parameters (eight parameters, d.f. = 9), a taxonomic model would have
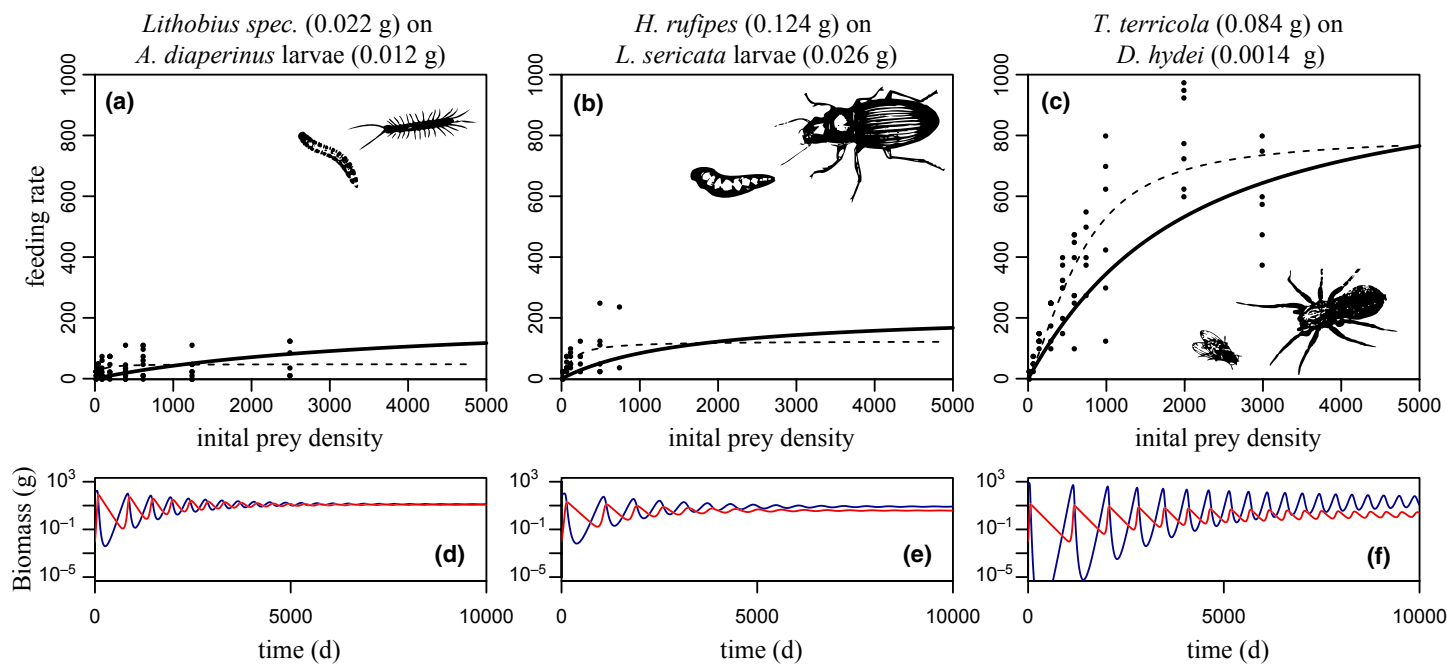
Figure 2 (a-c) The generalised allometric functional-response model (solid line) describes experimentally observed feeding rates (black dots) as a function of initial prey density and predator and prey body mass. The generalised model predicts similar feeding rates as independent models for the particular predator–prey pairs (dashed lines) without the necessity of taking taxonomic differences into account. (d-f) Simulated dynamics of predator (red line) and prey (blue line) population biomasses as predicted by a generalised model for the predator–prey pairs of panels a-c.

required 216 parameters for 72 taxonomic predator–prey pairs (72 times the three parameters h, b and q, d.f. = 217). In a prior study, we have shown that focussing on these taxonomic differences while lumping individuals of the same species but different body size yield less accurate predictions of feeding rates than allometric models that lump species of different taxonomies (Rall *et al*. 2011). Furthermore, generalised models are applicable to predict the feeding rates of predator–prey pairs depending on their body size, whereas classical taxonomic models are restricted to predict feeding of those predator–prey pairs that were used for parameterisation. This last feature is of high relevance when it comes to estimating feeding rates for the innumerable trophic interactions in natural communities, where an experimental measurement of all pairwise interactions is impossible. Accordingly, increased application of such 'purely allometric approaches' in community ecology has recently been demanded (e.g. Blanchard 2011), but until now such taxonomy-neglecting allometric approaches have exclusively been used in the description of pelagic communities ('size spectra', e.g. Sheldon *et al*. 1972; Jennings & Mackinson 2003; but see Reuman *et al*. 2008 for an application to soil food webs). The allometric functional-response approach of our study thus gives up accuracy in predicting feeding strengths of specific interactions while allowing generalising across the myriads of interactions in natural ecosystems.

This generality of allometric models also allows investigating how body masses constrain population dynamics of a wide range of predator and prey pairs. Indeed, allometric scaling of metabolism, growth and maximum feeding (i.e. the inverse of handling time) with average individual body masses are the core assumptions of a bioenergetic model that predicts population dynamics of simple predator–prey modules (Yodzis & Innes 1992; McCann *et al*. 1998; Otto *et al*. 2007) and complex food webs (Brose *et al*. 2006; Stouffer

& Bascompte 2010; Heckmann *et al*. 2012). The early applications of this model retained some shortcomings such as an arbitrary choice of free parameters, the basal carrying capacity and the capture exponent determining the functional-response type, and an unrealistic power-law scaling of capture rates. A prior model improvement included an allometric scaling relationship of carrying capacities and more realistic scaling relationships of capture rates (Weitz & Levin 2006). In recent years, hump-shaped scaling of capture rates with predator–prey body-mass ratios became widely accepted (Wahlström *et al*. 2000; Aljetlawi *et al*. 2004; Vonesh & Bolker 2005; Vucic-Pestic *et al*. 2010b; McCoy *et al*. 2011; Rall *et al*. 2011). Altogether, these efforts helped to eliminate biologically unrealistic trait combinations (Brose 2010) and implementations of these improved allometric constraints into the bioenergetic model were successfully employed to predict population dynamics in complex multi-predator communities (Boit *et al*. 2012; Schneider *et al*. 2012). The generalised allometric functional-response models of the present study allow dropping assumptions on the functional-response type (II or III) in future studies, which will have far-reaching consequences for stability analyses (e.g. Brose *et al*. 2006; Rall *et al*. 2008).

The biological mechanisms that can lead to type-III functional responses include prey refuges and optimal foraging processes (Murdoch & Oaten 1975). Subsequently, we will discuss how they fit into the allometric framework of our study. The habitat structure of the moss in our feeding experiments provides refuges for small prey that are not accessible for large predators. Thus, at very low prey densities, small prey individuals will have a reduced risk of predation and the population will not be over-exploited, as it is characteristic for type-III responses (Crawley 1992, p. 53). Consequently, this would imply that we would not have found type-III responses

in treatments without habitat structure which was corroborated by one prior study (Vucic-Pestic *et al.* 2010a). However, this represents an extremely artificial environment for the litter-dwelling arthropods of our experiments, which does not characterise natural ecosystems that should generally exhibit sufficient habitat structure to provide refuges for small prey. As a second possibility, sigmoid predation curves might arise due to behavioural responses of the predators to the level of prey densities (Sih 1984). Especially at high predator–prey body-mass ratios it might not be energetically profitable to pursue relatively small prey individuals at very low densities. Due to evolutionary optimisation, the predator might 'activate' its 'foraging mode' aimed at small prey species only if their overall density is reaching a certain threshold (Sih 1984). It is important to note that these active mechanisms of size-driven prey selection evolved in the context of having alternative prey species available, but nonetheless will influence the predator individuals' behaviour in the experiments with only one prey species present. Overall, both processes, the availability of prey refuges and optimal foraging, may contribute to the allometric functional-response patterns documented here.

The functional-response data used for our analyses are obtained under simplified laboratory conditions which include the restriction that only combinations of single predator and single prey species were used here. However, predators exhibit active prey selection in environments with two prey species present (Kalinkat *et al.* 2011).

Moreover, these active preferences go beyond the expectations derived from single-prey experiments and are by themselves functions of predator and prey body masses (Kalinkat *et al.* 2011). In reverse, predators should tend to disregard prey whose individual body mass is too far from this optimum as exemplified by several zero-consumption replicates in our data set. This is especially important for the comparison of our model results (i.e. predator persistence domain) with the soil food-web data (Fig. 3) as the first was parameterised on base of the 'single-prey world' in our experimental setting, whereas the second represents the 'real, multi-prey world'. Specifically, our model employs simple predator–prey structures that in some cases lead to predator extinction if the prey as the only resource does not support the predator population. However, this would rarely be observed in natural ecosystems, in which predators have multiple prey. Hence, we assume that the empirically observed feeding links should represent those interactions that provide the major energy channels supporting predator biomass. We acknowledge that this is a reductionist test for the validity of allometric constraints on feeding rates since in nature predator populations rely on multiple prey species of different mean body masses that often also comprise intraspecific size-structure. Prior studies including these features such as ontogenetic niche differentiation or cannibalism (e.g. Rudolf 2008; Rudolf & Armstrong 2008) have demonstrated their importance for population dynamics. Neverthe-
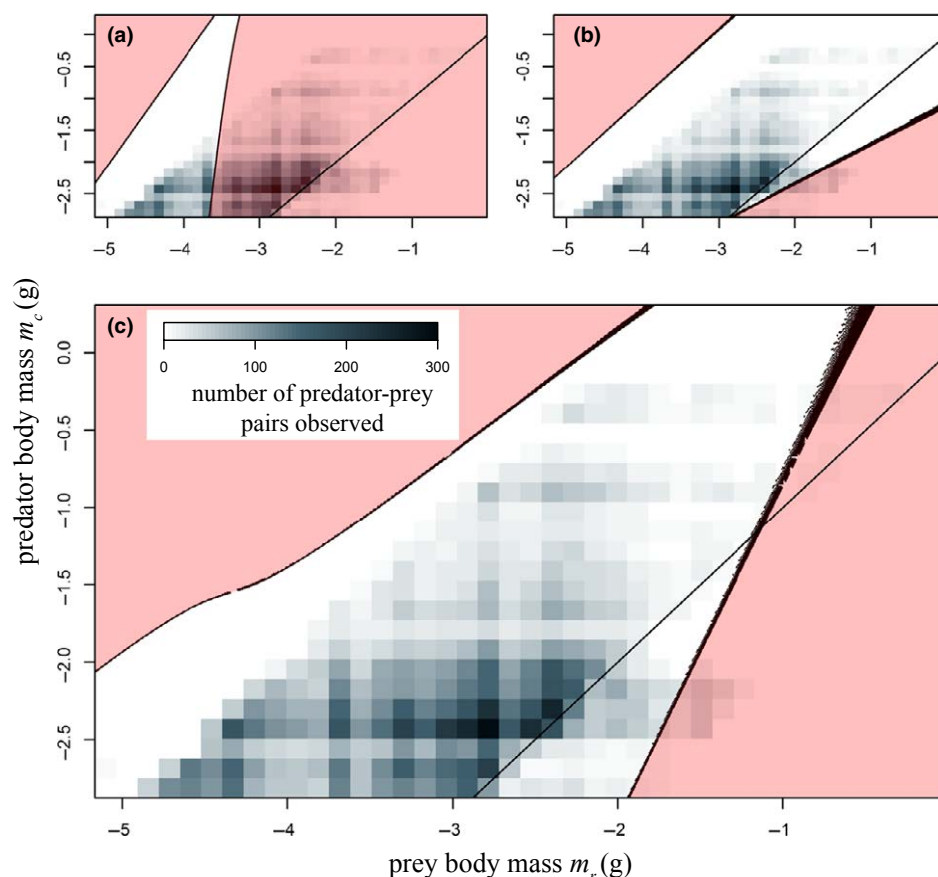
Figure 3 Densities of 18 713 empirically observed predator–prey pairs from the soil food web and predicted persistence domains for predators ($Bc > 10^{-30}$ non-red areas, black border of persistence domain appears non-continuous due to oscillating dynamics) for (a) traditional allometric type-II functional-response model (score $S = 0.17$), (b) hump-shaped allometric functional-response model ($S = 0.33$) and (c) the generalised allometric functional-response model ($S = 0.48$). S is the proportion of the predator–prey pairs that lie within the predicted persistence domain times the proportion of the area predicted as non-persistent (red areas). The thin black line represents equal body masses of predator and prey.

less, McCoy *et al.* (2011) have demonstrated recently how size-dependent functional-response models might successfully predict prey mortality in short-term experiments with large variation in prey size although the models were developed from experiments with homogenous prey-size cohorts invigorating the reliability of our approach.

Interestingly, our intrinsic assumptions yield relatively small persistence domains for large predators (Fig. 3c). Analyses of empirical food webs have shown that larger predators tend to be more generalised than smaller predators (Digel *et al.* 2011), which could be an evolutionary response to balance their smaller persistence domains by more diverse diets. Hence, the cone-shaped persistence domain we found in our model simulations (i.e. large persistent prey size range for small predators and small persistent prey size range for large predators) complements with findings from food-web studies that generality increases with predator mass. While the allometric functional-response models may represent an important step towards a generalised understanding of natural interaction strengths, it will remain an important challenge to cope with other dimensions of natural complexity such as coexistence of multiple prey (Kalinkat *et al.* 2011) and habitat structure (Vucic-Pestic *et al.* 2010a; Kalinkat *et al.* 2013). Furthermore, the allometric scaling relationship of the capture exponent that we found for terrestrial arthropods of forest floors still has to be corroborated in studies on other organism groups and ecosystem types.

Meanwhile, we suggest employing the generalised allometric functional responses in future analyses of population dynamics (Otto *et al.* 2007), food-web persistence (Brose *et al.* 2006) or network structure (Petchey *et al.* 2008) to obtain more realistic predictions and avoid uncertainty caused by the strict distinction into type-II and -III functional-response models. Ultimately, by providing a general framework of feeding interactions that is applicable to entire communities the generalised allometric approach may bridge the gap between quantitative studies of population interactions (Holling 1959; Rall *et al.* 2011) and large-scale comparisons of community patterns (Riede *et al.* 2011).

AUTHORSHIP

The authors have made the following declarations about their contributions: GK and FDS contributed equally to this study. Conceived and designed the experiments: GK, FDS, BCR, UB. Performed the experiments: GK, FDS, BCR, UB. Analysed the data: GK, FDS, BCR. Provided data/analytical tools: CD CG. Wrote the paper: GK, FDS, BCR, UB, with minor contributions of CG and CD.

REFERENCES

Aljetlawi, A.A., Sparrevik, E. & Leonardsson, K. (2004). Prey-predator size-dependent functional response: derivation and rescaling to the real world. *J. Anim. Ecol.*, 73, 239–252.

Blanchard, J.L. (2011). Body size and ecosystem dynamics: an introduction. *Oikos*, 120, 481–482.

Boit, A., Martinez, N.D., Williams, R.J. & Gaedke, U. (2012). Mechanistic theory and modelling of complex food-web dynamics in Lake Constance. *Ecol. Lett.*, 15, 594–602.

Bolker, B. (2008). *Ecological Models and Data in R*. Princeton University Press, Princeton.

Brose, U. (2010). Body-mass constraints on foraging behavior determine population and food-web dynamics. *Funct. Ecol.*, 24, 28–34.

Brose, U., Williams, R.J. & Martinez, N.D. (2006). Allometric scaling enhances stability in complex food webs. *Ecol. Lett.*, 9, 1228–1236.

Brose, U., Ehnes, R.B., Rall, B.C., Vucic-Pestic, O., Berlow, E.L. & Scheu, S. (2008). Foraging theory predicts predator-prey energy fluxes. *J. Anim. Ecol.*, 77, 1072–1078.

Brown, J.H., Gillooly, J.F., Allen, A.P., Savage, V.M. & West, G.B. (2004). Toward a metabolic theory of ecology. *Ecology*, 85, 1771–1789.

Crawley, M.J. (1992). *Natural Enemies: The Population Biology of Predators, Parasites, and Diseases*. Blackwell Scientific Publications, Oxford.

Digel, C., Riede, J.O. & Brose, U. (2011). Body sizes, cumulative and allometric degree distributions across natural food webs. *Oikos*, 120, 503–509.

Fryxell, J.M., Mosser, A., Sinclair, A.R.E. & Packer, C. (2007). Group formation stabilizes predator-prey dynamics. *Nature*, 449, 1041–1043.

Heckmann, L., Drossel, B., Brose, U. & Guill, C. (2012). Interactive effects of body-size structure and adaptive foraging on food-web stability. *Ecol. Lett.*, 15, 243–250.

Holling, C.S. (1959). The components of predation as revealed by a study of small-mammal predation of the European pine sawfly. *Canad. Entomol.*, 91, 293–320.

Jennings, S. & Mackinson, S. (2003). Abundance–body mass relationships in size-structured food webs. *Ecol. Lett.*, 6, 971–974.

Jeschke, J.M., Kopp, M. & Tollrian, R. (2002). Predator functional responses: discriminating between handling and digesting prey. *Ecol. Monogr.*, 72, 95–112.

Kalinkat, G., Rall, B.C., Vucic-Pestic, O. & Brose, U. (2011). The allometry of prey preferences. *PLoS ONE*, 6, e25937.

Kalinkat, G., Brose, U. & Rall, B.C. (2013). Habitat structure alters top-down control in litter communities. *Oecologia*, 172, 877–887.

Koen-Alonso, M. (2007). A process-oriented approach to the multispecies functional response. In *From Energetics to Ecosystems: The Dynamics and Structure of Ecological Systems, the Peter Yodzis Fundamental Ecology Series* (eds Rooney, N., McCann, K.S. & Noakes, D.L.G.). Springer, Dordrecht, pp. 1–36.

Loeuille, N. & Loreau, M. (2005). Evolutionary emergence of size-structured food webs. *Proc. Natl Acad. Sci. USA*, 102, 5761–5766.

McCann, K.S., Hastings, A. & Huxel, G.R. (1998). Weak trophic interactions and the balance of nature. *Nature*, 395, 794–798.

McCoy, M.W. & Bolker, B.M. (2008). Trait-mediated interactions: influence of prey size, density and experience. *J. Anim. Ecol.*, 77, 478–486.

McCoy, M.W., Bolker, B.M., Warkentin, K.M. & Vonesh, J.R. (2011). Predicting predation through prey ontogeny using size-dependent functional response models. *Am. Nat.*, 177, 752–766.

Murdoch, W.W. & Oaten, A. (1975). Predation and population stability. *Adv. Ecol. Res.*, 9, 1–131.

Murdoch, W.W., Avery, S. & Smyth, M.E.B. (1975). Switching in predatory fish. *Ecology*, 56, 1094–1105.

Neutel, A.-M., Heesterbeek, J.A.P. & de Ruiter, P.C. (2002). Stability in real food webs: weak links in long loops. *Science*, 296, 1120–1123.

Otto, S., Rall, B.C. & Brose, U. (2007). Allometric degree distributions stabilize food webs. *Nature*, 450, 1226–1229.

Petchey, O.L., Beckerman, A.P., Riede, J.O. & Warren, P.H. (2008). Size, foraging, and food web structure. *Proc. Natl Acad. Sci. USA*, 105, 4191–4196.

Peters, R.H. (1983). *The Ecological Implications of Body Size*. Cambridge University Press, New York.

R Development Core Team (2010). *R: A Language and Environment for Statistical Computing*. Austria, Vienna.

Rall, B.C., Guill, C. & Brose, U. (2008). Food-web connectance and predator interference dampen the paradox of enrichment. *Oikos*, 117, 202–213.

Rall, B.C., Kalinkat, G., Ott, D., Vucic-Pestic, O. & Brose, U. (2011). Taxonomic versus allometric constraints on non-linear interaction strengths. *Oikos*, 120, 483–492.

Rall, B.C., Brose, U., Hartvig, M., Kalinkat, G., Schwarzmüller, F., Vucic-Pestic, O. *et al.* (2012). Universal temperature and body-mass scaling of feeding rates. *Phil. Trans. R. Soc. B*, 367, 2923–2934.

Reuman, D.C., Mulder, C., Raffaelli, D. & Cohen, J.E. (2008). Three allometric relations of population density to body mass: theoretical integration and empirical tests in 149 food webs. *Ecol. Lett.*, 11, 1216–1228.

Riede, J.O., Brose, U., Ebenman, B., Jacob, U., Thompson, R., Townsend, C.R. *et al.* (2011). Stepping in Elton's footprints: a general scaling model for body masses and trophic levels across ecosystems. *Ecol. Lett.*, 14, 169–178.

Rogers, D. (1972). Random search and insect population models. *J. Anim. Ecol.*, 41, 369–383.

Rooney, N., McCann, K., Gellner, G. & Moore, J.C. (2006). Structural asymmetry and the stability of diverse food webs. *Nature*, 442, 265–269.

Rudolf, V.H.W. (2008). Consequences of size structure in the prey for predator-prey dynamics: the composite functional response. *J. Anim. Ecol.*, 77, 520–528.

Rudolf, V.H.W. & Armstrong, J. (2008). Emergent impacts of cannibalism and size refuges in prey on intraguild predation systems. *Oecologia*, 157, 675–686.

Sarnelle, O. & Wilson, A.E. (2008). Type III functional response in Daphnia. *Ecology*, 89, 1723–1732.

Schneider, F.D., Scheu, S. & Brose, U. (2012). Body mass constraints on feeding rates determine the consequences of predator loss. *Ecol. Lett.*, 15, 436–443.

Sheldon, R.W., Sutcliff, W.H. Jr & Prakash, A. (1972). The size distribution of particles in the ocean. *Limnol. Oceanogr.*, 17, 327–340.

Sih, A. (1984). Optimal behavior and density-dependent predation. *Am. Nat.*, 123, 314–326.

Stouffer, D.B. & Bascompte, J. (2010). Understanding food-web persistence from local to global scales. *Ecol. Lett.*, 13, 154–161.

Vonesh, J. & Bolker, B. (2005). Compensatory larval responses shift trade-offs associated with predator-induced hatching plasticity. *Ecology*, 86, 1580–1591.

Vucic-Pestic, O., Birkhofer, K., Rall, B.C., Scheu, S. & Brose, U. (2010a). Habitat structure and prey aggregation determine the functional response in a soil predator-prey interaction. *Pedobiologia*, 53, 307–312.

Vucic-Pestic, O., Rall, B.C., Kalinkat, G. & Brose, U. (2010b). Allometric functional response model: body masses constrain interaction strengths. *J. Anim. Ecol.*, 79, 249–256.

Wahlström, E., Persson, L., Diehl, S. & Bystrom, P. (2000). Size-dependent foraging efficiency, cannibalism and zooplankton community structure. *Oecologia*, 123, 138–148.

Weitz, J.S. & Levin, S.A. (2006). Size and scaling of predator–prey dynamics. *Ecol. Let.*, 9, 548–557.

Williams, R.J. & Martinez, N.D. (2004). Stabilization of chaotic and non-permanent food-web dynamics. *Eur. Phys. J. B*, 38, 297–303.

Yodzis, P. & Innes, S. (1992). Body size and consumer-resource dynamics. *Am. Nat.*, 139, 1151–1175.

SUPPORTING INFORMATION

Additional Supporting Information may be downloaded via the online version of this article at Wiley Online Library (www.ecologyletters.com).

Single generation cycles and delayed feedback cycles are not separate phenomena

T. Pfaff [a], A. Brechtel [a], B. Drossel [a], C. Guill [b,*]

[a] *Institute of Condensed Matter Physics, Hochschulstraße 6, 64289 Darmstadt, Germany*
[b] *Institute for Biodiversity and Ecosystem Dynamics, P.O. Box 94248, 1090 GE Amsterdam, The Netherlands*

ABSTRACT

We study a simple model for generation cycles, which are oscillations with a period of one or a few generation times of the species. The model is formulated in terms of a single delay-differential equation for the population density of an adult stage, with recruitment to the adult stage depending on the intensity of competition during the juvenile phase. This model is a simplified version of a group of models proposed by Gurney and Nisbet, who were the first to distinguish between single-generation cycles and delayed-feedback cycles. According to these authors, the two oscillation types are caused by different mechanisms and have periods in different intervals, which are one to two generation times for single-generation cycles and two to four generation times for delayed-feedback cycles. By abolishing the strict coupling between the maturation time and the time delay between competition and its effect on the population dynamics, we find that single-generation cycles and delayed-feedback cycles occur in the same model version, with a gradual transition between the two as the model parameters are varied over a sufficiently large range. Furthermore, cycle periods are not bounded to lie within single octaves. This implies that a clear distinction between different types of generation cycles is not possible. Cycles of all periods and even chaos can be generated by varying the parameters that determine the time during which individuals from different cohorts compete with each other. This suggests that life-cycle features in the juvenile stage and during the transition to the adult stage are important determinants of the dynamics of density limited populations.

© 2014 Elsevier Inc. All rights reserved.

1. Introduction

Ecological models which involve the age or size structure of a population have been studied for almost one century now (Kermack and McKendrick, 1927). It is known that the detailed age or size structure of populations can have a major influence on the dynamics of ecological systems. Vital rates, such as growth rate, death rate and fecundity are in general dependent on the age of an individual (de Roos et al., 2003a). The structure of a population is important for effects such as generation cycles (Gurney and Nisbet, 1985; Knell, 1998; Ruxton and Gurney, 1992), juvenile bottle necks (Neill, 1988), life boat mechanisms (Bosch et al., 1988), host–parasite interaction (Godfray and Hassell, 1989; Gordon et al., 1991; Godfray, 1987) or emergent Allee effects (Courchamp et al., 1999; de Roos et al., 2003b), as well as for the effects of environ-

mental stochasticity (Bjørnstad et al., 2004). A population can either be structured by age or size. In the first case the development of an individual always follows the same time course, while in the second case development depends on food intake and metabolism. Mathematical models can capture the population structure in different ways, the three most prominent being stage structured models that divide a population into several stages in which the vital rates are uniform among all individuals (Gurney et al., 1980, 1983), matrix models that use discrete time steps and a matrix as the update function of a state vector (Caswell, 2001), and finally physiologically structured models that define the vital rates as functions of the continuous structure parameter (de Roos, 1996).

In this paper, we focus on generation cycles and investigate age-structured stage models. Generation cycles are a consequence of population structure that has been observed in a wide spectrum of field and laboratory populations. Even a single species in a constant laboratory environment can exhibit population density oscillations, as has been shown by Nicholson in the famous blow-fly experiments (Nicholson, 1954, 1957). A population of blow flies was kept under constant conditions with a constant daily amount of resource and it was observed that the population fluctuated with

a period slightly larger than the generation time. Such an oscillation period of the order of the generation time is the indicator of generation cycles. In contrast to this, other types of population cycles, like predator–prey cycles, have larger periods depending on the life cycle of predator and prey (Murdoch et al., 2002). Generation cycles are frequently observed in natural populations (NERC, 2010) and they can occur in isolated species as well as in generalist species that are likely to have a stable resource basis, whereas predator–prey cycles are more common for specialist predators (Murdoch et al., 2002).

Gurney and Nisbet (Gurney and Nisbet, 1985; Gurney et al., 1983) investigated generation cycles by a comprehensive stage structured population model and identified mechanisms behind these cycles. The model was inspired by the laboratory situation of constant food supply. The population was divided into a juvenile and an adult stage. The cycles were found to be driven by density dependent competition of juveniles. According to the model, this competition can be due to four different effects: a direct death of juveniles (*Larval Death LD*), increased development time of juveniles (*Maturation Time MT*), decreased survival of pupae (*Pupal Survival PS*), or a decreased fecundity in the adult stage (*Adult Fecundity AF*). Gurney and Nisbet studied 4 different versions of their model, each of which contained one of these effects. They evaluated these models in the vicinity of the Hopf bifurcation that marks the onset of oscillations in parameter space. The main findings were that a competition that has a direct influence on the population dynamics (LD and MT) leads to cycles of 1–2 times the maturation time τ, while competition that has a delayed influence on the dynamics (PS and AF) leads to cycles of 2–4 times the maturation time. These two disjoint intervals of one octave led to a classification of generation cycles into *single generation cycles* for cycles with periods between τ and 2τ, and *delayed feedback cycles* for periods from 2τ to 4τ. This theory has been considered to be among the "most important advancements in the theory about the life history-population dynamic interplay" (de Roos et al., 2003a).

The findings of Gurney and Nisbet thus suggest that the oscillation period does not depend on all details of the model but essentially on the time period during which density-dependent competition affects a population. In this respect their results appear to be very general. On the other hand, their investigation is constrained by the strict coupling between the maturation time and the time delay between competition and its effect on the population. This delay is either zero (LD and MT models) or one generation (PS and AF models). However, the effect of competition is usually a combination of several of the above-mentioned phenomena. Additionally, competition can have effects over time periods other than zero and the maturation time, if, for instance, the food consumption of one cohort affects the food available to another cohort, or if the duration of the non-competing egg and pupal stages cannot be neglected.

In this paper, we present and investigate a model that fills these gaps. Our model considers the time period over which competition is felt by a cohort as a separate parameter, different from the maturation time, and variable within realistic limits. The model has the same general form as the PS model, but includes a simpler expression for the density-dependent probability to survive from birth into the adult stage. It contains the situations described by the PS and LD models as special cases, and we find in these cases a dynamical behavior similar to that of the LD and PS models, thus confirming again that the main determinant of the oscillation period is the relation between the maturation time and the time delay over which competition is felt. We corroborate this finding further by briefly studying two additional model versions that have a complexity intermediate between our simple model and the LD and PS models by Gurney and Nisbet and display a similar dynamica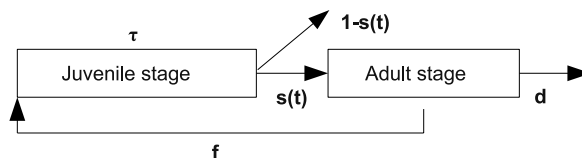l behavior. Due to the greater computer power and new numerical solvers, we were able to investigate the original LD and PS models beyond the parameter range originally studied by Gurney and Nisbet, revealing oscillation periods much larger than four times the maturation time in the PS model and even chaos. We also study our model for general values of the competition time, confirming and complementing all these results. Typically, the periods of generation cycles cover a broad range of values and can be continuously changed by changing the competition time. It follows that periods do not lie in disjoint intervals of one octave, which makes a clear distinction between single-generation cycles and delayed-feedback cycles impossible. Furthermore, we find chaotic behavior in almost all model versions.

Our general model is described in detail in the next section. Section 3.1 presents the results for the two parameter sets that show a similar behavior to the LD and PS models by Gurney and Nisbet, which are also studied. Section 3.2 discusses the model dynamics for general values of the parameters. The conclusions are drawn in Section 4.

Fig. 1. Sketch of the model.

2. Model

The model is of the same form as the PS model by Gurney and Nisbet (1985). A sketch of the model is given in Fig. 1. The population is divided into two stages, the juvenile stage, which is not explicitly modeled, and the adult stage with a population density $A(t)$. Our fundamental equation for the population dynamics is

$$\frac{dA(t)}{dt} = s(t) \cdot f \cdot A(t - \tau) - d \cdot A(t). \tag{1}$$

New individuals are born with a rate f ("fecundity") that is proportional to the number of adults. The newborn juveniles need a time τ to mature to adults. Only a proportion $s(t)$ of the juveniles survive maturation. The survival function $s(t)$ depends on competition for food during the competitive part of the juvenile stage. The adults die with a constant death rate d. As we show in Appendix A, the general model described by Eq. (1) is identical to the PS model by Gurney and Nisbet (1985). Other model versions by Gurney and Nisbet are obtained by introducing a density dependent death rate for the juvenile stage, or by making the maturation time τ or the fecundity f density dependent. These versions however are not considered in the following.

In the PS model, the survival function $s(t)$ depends via a double integral on the population densities between time $t - 2\tau$ and t. In general, the survival function is a decreasing function of the strength of competition that an individual has experienced during the juvenile stage, as indicated in Fig. 2(a). In order to make the model more transparent, while preserving its most important features, we use a simpler form for $s(t)$ with less parameters than in the PS model. We assume a linear dependence of the survival function $s(t)$ on the birth rate of competitors $C(t)$ (to be specified below) of the cohort that matures at time t, see also Fig. 2(a):

$$s(t) = \max\left(r_{max} \cdot \left(1 - \frac{C(t)}{C_{max}}\right), 0\right). \tag{2}$$

The survival function is r_{max} without competitors and 0 for $C(t) \geq C_{max}$. A linear form is a good approximation if the system is close to a fixed point. In fact, we will see that even far away from the fixed
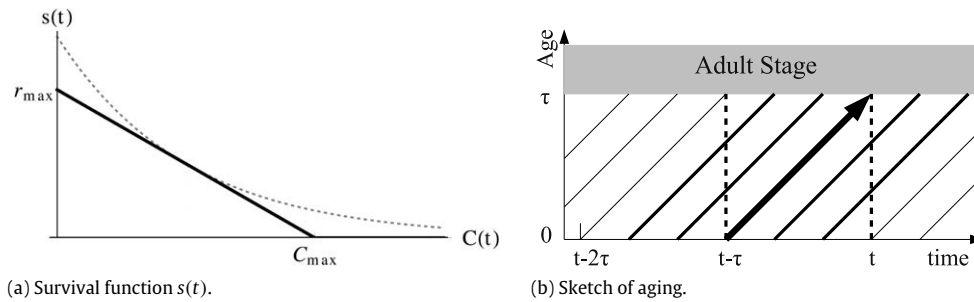
(a) Survival function $s(t)$.

(b) Sketch of aging.

Fig. 2. (a) Survival function $s(t)$ in dependence on competition $C(t)$. A nonlinear relation (dotted line) is approximated by a function with constant slope $s(t)$ (black solid line). (b) Age of cohorts at a given time. Juveniles born at $t - \tau$ mature at time t (thick arrow). Other juveniles born between $t - 2\tau$ and t have a time overlap with this cohort and are thus competitors, if the juveniles compete during their whole life up to the maturation.

point the linear term is sufficient to reproduce the characteristic periods and amplitudes of generation cycles.

The strength of competition the cohort that matures at time t experiences is determined by the average birth rate of juveniles in a time window of length $T = T_{max} - T_{min}$. It is given by

$$C(t) = \frac{f}{T} \int_{t-T_{max}}^{t-T_{min}} A(t')dt'. \tag{3}$$

The time parameters in this expression have the following definition: Individuals maturing at time t were born at $t - \tau$, their oldest competitors were born at time $t - T_{max}$ and their youngest competitors were born at $t - T_{min}$. Thus the oldest juveniles that compete with the considered cohort are older by a time $T_{max} - \tau$, while the youngest juveniles are younger by $\tau - T_{min}$. In any case, the relation

$$0 \leq T_{min} \leq \tau \leq T_{max} \tag{4}$$

(together with $0 < \tau$ and $T_{min} < T_{max}$) must hold since the individuals of one cohort always compete with themselves.

Different values of T_{max} and T_{min} reflect different life histories of juveniles: If juveniles compete with all other juveniles present between their birth at $t - \tau$ and their maturation at t, we obtain $T_{min} = 0$ and $T_{max} = 2\tau$ (see Fig. 2(b)). This is a situation similar to the PS model by Gurney and Nisbet, and the dynamics described in the next section are indeed similar to those of the PS model. To simplify the notation, we therefore refer to the parameter set $T_{min} = 0$ and $T_{max} = 2\tau$ as a special model version which we call the *Simplified Pupal Survival (SPS)* model. Another important situation is given by $T_{min} = 0$ and $T_{max} = \tau$. In this case only younger juveniles are considered as competitors. This corresponds to a situation where most of the older juveniles already died through competition before reaching the pupal stage, so that their contribution to the juvenile density is low. As we will see in the next section, the dynamics of this system is very similar to the "Larval Death model" (LD) of Gurney and Nisbet. The parameter set $T_{min} = 0$ and $T_{max} = \tau$ is therefore referred to as the *Simplified Larval Death (SLD)* model.

Other values of T_{min} and T_{max} also have a biological significance:

If the life history includes non competing stages before the adult stage, such as the egg or pupal stage, we obtain $T_{min} > 0$, with the value of T_{min} being the total duration of the egg and pupal stages. This is because individuals that differ in age by more than $\tau - T_{min}$ cannot be in the larval stage at the same time.

If the resources are not supplied at a constant rate on the other hand, resource availability depends on resource consumption at earlier times by older cohorts. This means that the maturing juveniles experience an indirect competition from cohorts that have already left the larval stage. This effect results in values of T_{max} higher than 2τ. We will see below that T_{max} has an important influence on the oscillation period, which means that the resource plays a vital role in determining the periods of generation cycles.

Finally, we simplify the model by introducing effective parameters and natural units. Time is measured in units of τ (i.e., $\tau = 1$),

which gives the new parameters $\tilde{f} = f \cdot \tau$ and $\bar{d} = d \cdot \tau$. The population density is given in terms of the natural unit C_{max}/f, which can be thought of as the effective carrying capacity. Furthermore, the product $r_{max} \cdot \tilde{f}$ is the effective fecundity $\bar{f}$. For better readability, we drop the bar on the new parameters in the following. We thus obtain the equation

$$\frac{dA}{dt} = \begin{cases} r(t) \cdot A(t-1) - d \cdot A(t) & \text{for } r(t) > 0 \\ -d \cdot A(t) & \text{otherwise} \end{cases} \tag{5}$$

with

$$r(t) = f \left[1 - \frac{1}{T} \int_{t-T_{max}}^{t-T_{min}} A(t')dt' \right].$$

This is a model with one delay differential equation and the four parameters f, d, T_{min}, and T_{max}. The recruitment rate $r(t)$ is obtained by combining Eqs. (2) and (3).

3. Results

First, we investigate the two cases $T_{min} = 0$ and $T_{max} = 1$ (SLD model) and $T_{min} = 0$ and $T_{max} = 2$ (SPS model), which are close in behavior to the LD and PS models by Gurney and Nisbet (1985).

We focus on the influence of the death rate d and the effective fecundity f on the dynamics. In the second subsection, we study the influence of the maximum and minimum delays T_{max} and T_{min} on the dynamics to obtain more general results. The simulations were performed by solvers that are implemented by Mathematica®8 and Euler algorithms with delays, which were both sufficiently tested to exclude numerical errors.

3.1. Simplified larval death and pupal survival models

Let us first discuss the dynamics of the SLD model, i.e., the case $T_{min} = 0$ and $T_{max} = 1$. The graphs 3(a) and (c) show the different types of dynamical behavior and the periods of the periodic oscillations. The occurring dynamical behaviors of the model are very similar to the LD model of Gurney and Nisbet. Depending on the parameters f and d, the dynamical regimes are extinction, a stable equilibrium, and regular oscillations. Obviously, the species goes extinct if the effective fecundity is smaller than the adult death rate, $f < d$. At $f = d$, a transcritical bifurcation occurs, and for $f > d$ the non-trivial fixed point $A^* = (f - d)/f$ becomes positive and stable. At even higher values of f, a Hopf bifurcation occurs. This bifurcation can be investigated analytically by variational calculus, as performed in Appendix B, giving the exact bifurcation line and the oscillation periods close to the bifurcation. Both bifurcation lines in Fig. 3(a) were calculated analytically. The period of the oscillation (Fig. 3(c)) mainly depends on the death rate d and is almost independent of f. All periods are in the interval [1, 2], just as for the LD model by Gurney and Nisbet, for which

(a) Dynamics SLD model.

(b) Dynamics SPS model.

(c) Periods SLD model.

(d) Periods SPS model.
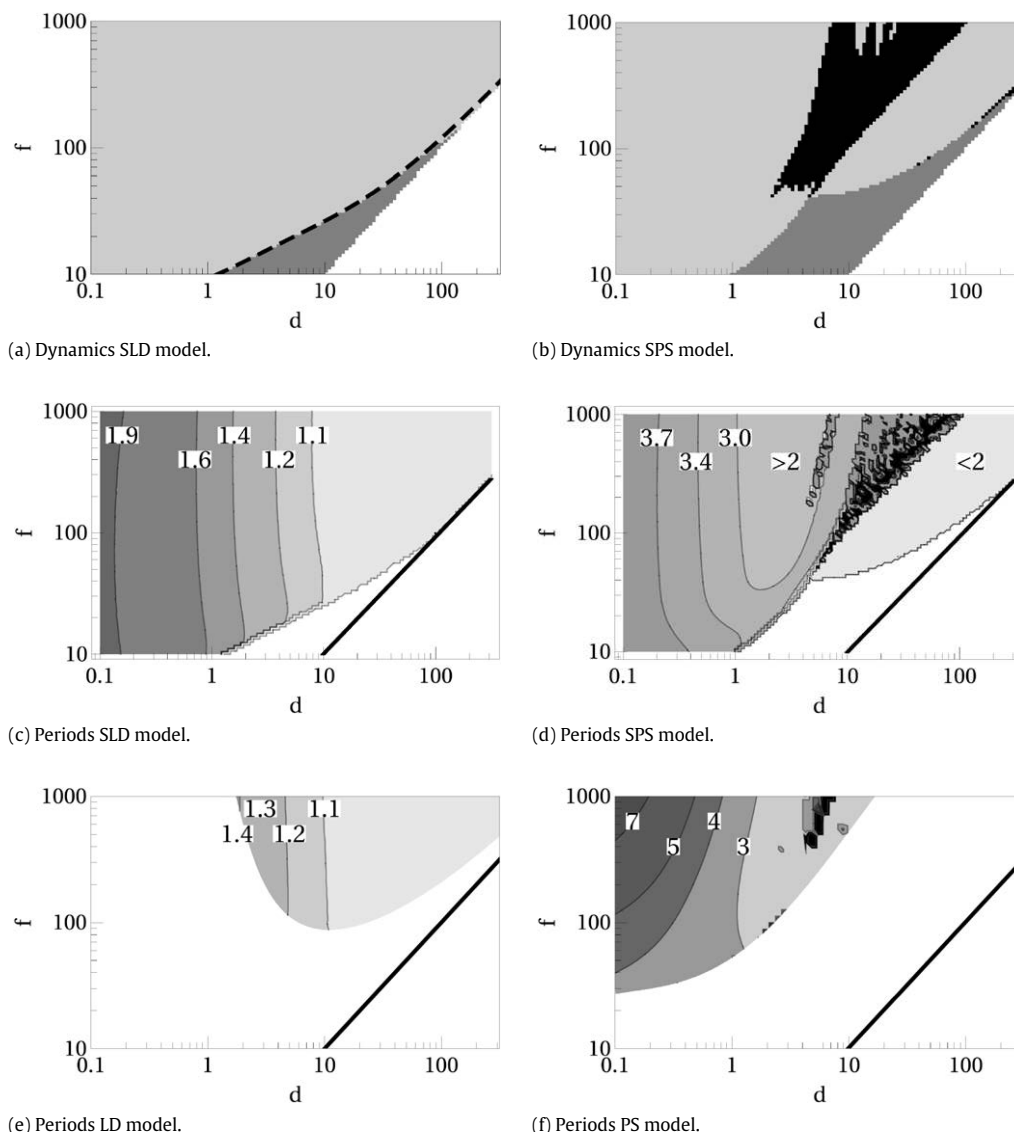
(e) Periods LD model.

(f) Periods PS model.

Fig. 3. Dynamical behavior and periods of the model—(a) and (b): dynamical behavior of our models, white: extinction, dark gray: stable, light gray: oscillation, black: chaos, (c) and (d): periods of our models in units of τ, (e) and (f): periods derived from our new simulations of the original models by Gurney and Nisbet (see Appendix A), (e) $W'_M = 0.05$, $W'_H = 1$, $\Gamma' = 0.05$, (f) $X' = 0.01$, $Y' = 0.1$. Black line in (c)–(f): extinction boundary ($f = d$).

we also performed computer simulations, shown in Fig. 3(e). The periods of the two models are almost identical at the same value of d. Only the stability border differs for low values of the death rate d: while the LD model is stable for small d, the SLD model oscillates, but with a very small relative amplitude (see Section 3.2).

The SPS model with $T_{\min} = 0$ and $T_{\max} = 2$ shows more complex dynamics. Fig. 3(b) shows a chaotic region in addition to a stable equilibrium (fixed point) and regular oscillations. Chaos has not been reported so far in models for generation cycles, however, we find it also in our simulations of the original PS model by Gurney and Nisbet, see Fig. 3(f). The periods of the oscillations in the SPS model are shown in Fig. 3(d). There are two types of periodic regions, which are separated by the chaotic region. For smaller values of d, the periods are in the interval [2, 4], as reported by Gurney and Nisbet. At higher values of d, the periods approach the value 1, just as for single generation cycles. We also find short periods for other competition times, as discussed in the next subsection. Our computer simulations of the original PS model revealed not only the existence of a chaotic region, but also of oscillations with larger periods of up to 7 generation times in the investigated parameter range. They appear when the fecundity f is increased, i.e., further away from the Hopf bifurcation line (see Fig. 3(f)).

In order to illustrate the dynamics in the different dynamical regimes, we show in Fig. 4 different time series of the model. An oscillation at a small value of d is shown in Fig. 4(a). It has a long period and a small relative amplitude. With increasing d the amplitude increases and the period decreases (Fig. 4(b)). The PS model gives rise to similar time series, as shown in Fig. 4(e) for an intermediate case between 4(a) and (b). Also the chaotic behavior of the SPS and PS models, shown in Fig. 4(c) and (f), looks very similar. The distance between maxima of the time series is approximately constant while the amplitude is chaotic. These features of uniform phase evolution and chaotic amplitude (UPCA) have been observed in predator–prey interactions with ordinary differential equations (Blasius et al., 1999). The fast oscillation that is shown in Fig. 4(d) is not observed in the PS model.

The main observations of this section can be summed up as follows: (i) Our simplified model shows dynamical features very similar to the PS and LD models by Gurney and Nisbet. (ii) The SLD and LD models have almost identical periods at equal values of d (or δ' in the LD model). The dynamical behaviors of both models are very similar, even though the balance equations are quite different. This suggests that single generation cycles are very robust against changes of mathematical details in the model. In
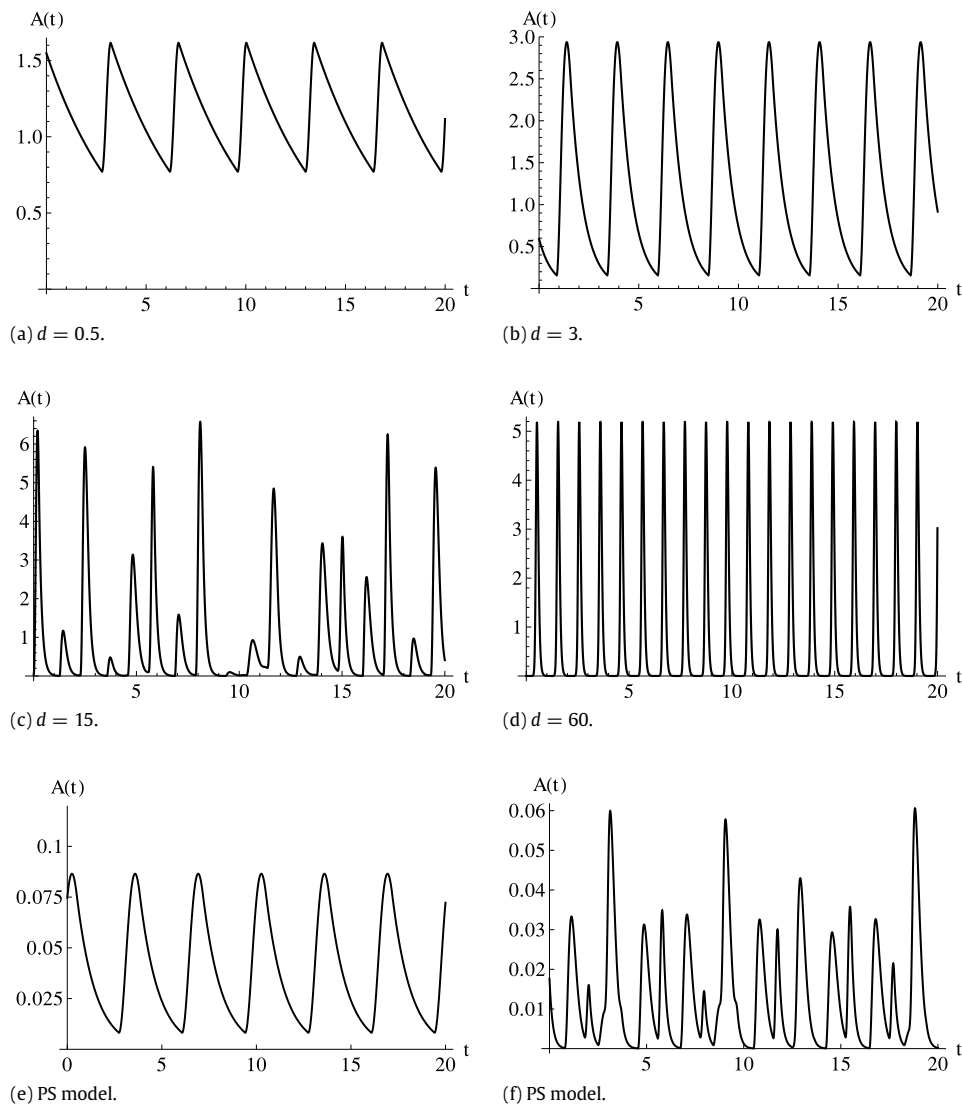
Fig. 4. Time series of the models: (a)–(d): SPS model with parameters $f = 200$, $T_{min} = 0$, $T_{max} = 2$, (e) and (f): PS model by Gurney and Nisbet, (e) $\delta' = 1.0$, $f' = 400$, $X' = 0.01$ $Y' = 0.1$, (f) $\delta' = 6.1$, $f' = 700$, $X' = 0.01$ $Y' = 0.1$. $A(t)$ is normalized to different natural units in the PS and SPS models, respectively.

fact, we also investigated another model version that includes a competition-dependent death rate of juveniles instead of the survival function, and we found the same behavior. (iii) The SPS and PS models have equal periods at the stability boundary, but differ further away from the Hopf bifurcation. (iv) We observed chaos in the PS and SPS models. As shown in the following subsection, model versions without chaos, such as the SLD and LD models appear to be the exception.

3.2. General T_{min} and T_{max}

Next, we investigate how the findings reported in the previous subsection depend on T_{max} and T_{min}. We found that in general the value of T_{max} has a much larger effect on the dynamical behavior than the value of T_{min}. This is illustrated in Fig. 5, where the phases with different dynamical behavior and the periods of the oscillations are given for all possible combinations of $T_{min} = 0$ or 0.5 and $T_{max} = 1$, 1.4 or 8. As discussed in the model section, the cases $T_{max} < 1$ and $T_{min} > 1$ are not biologically meaningful, as one cohort would not compete with itself in this case. We found that the dynamics lack chaotic behavior only for the case $T_{max} = 1$, where the maximum delay and the generation time are in resonance.

Fig. 5 shows the oscillation periods in units of the maximum delay T_{max}, as this proves to be the natural time scale for gener-

ation cycles. In the SLD model ($T_{max} = 1$) the periods are in the range 1–2, and in the SPS model ($T_{max} = 2$) in the range 2–4 for the main mode. In general, the periods of the oscillations appear to be mostly between T_{max} and $2T_{max}$, but they can take much higher values near to the chaotic regime. As argued in Section 2, the recovery time of the resource increases the maximum delay T_{max}, which can therefore take any value larger than 1. Values between 1 and 2 represent direct competition between the cohort under consideration and cohorts born up to one generation earlier, while values larger than 2 model indirect competition mediated by resources with a long recovery time. As T_{max} can vary continuously, there is a smooth transition between dynamical regimes usually classified a single-generation cycles ($T_{max} = 1$) and delayed-feedback cycles ($T_{max} = 2$). As the periods lie in a range T_{max} to $2T_{max}$ (and even higher), model versions with intermediate values of T_{max} give rise to both types of periods: those that belong to the interval assigned to single generation cycles and those that belong to the interval of delayed feedback cycles. This makes a clear distinction of both types of cycles impossible. For example at $T_{max} = 1.4$ the periods have values of 1.4τ and up to 10τ in the main part of the parameter space. There are no strict borders between single generation cycles (τ to 2τ) and delayed feedback cycles (2τ to 4τ), i.e. the dynamics cannot be classified based on this distinction.
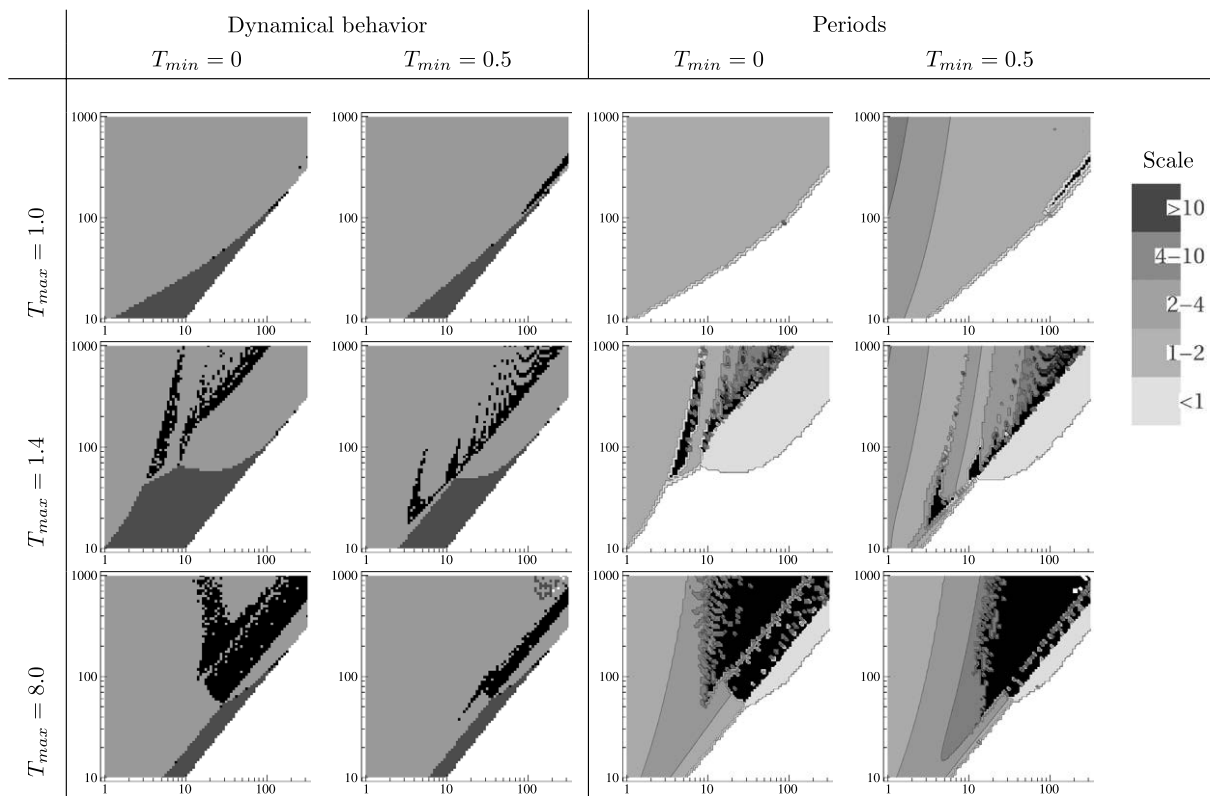
Fig. 5. Dynamical behavior—white: extinction, dark gray: stable, light gray: oscillation, black: chaos; Periods (in units of $T_{\max}$), system is quasi periodic or chaotic in black regime.

(a) $T_{\min} = 0$, $T_{\max} = 1$.

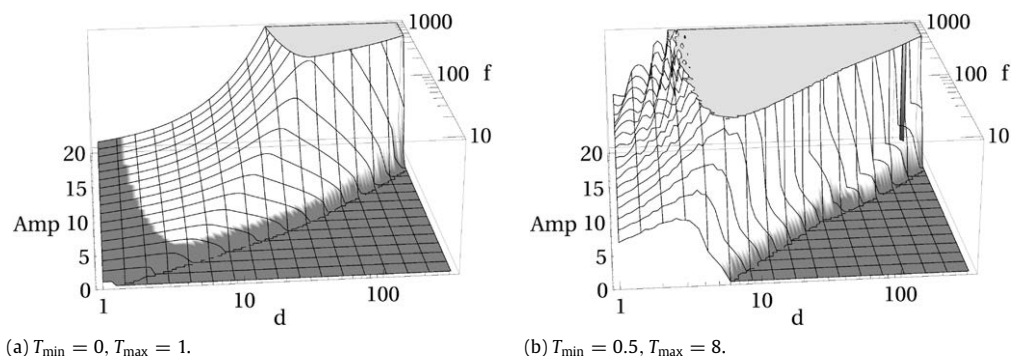(b) $T_{\min} = 0.5$, $T_{\max} = 8$.

Fig. 6. Relative amplitude of oscillation for two sets of parameters. Relative amplitudes lower than 2 are shaded in gray.

Furthermore, there are also regions in parameter space where oscillations have periods smaller than $T_{\max}$ (except for $T_{\max} = 1$). In this case the periods take values near $T_{\max} - \tau$, $T_{\max} - T_{\min}$ or $T_{\min}$, apparently with a preference for the shorter periods. The period of these short period generation cycles can take unrealistic values shorter than 0.1τ. However, there are also sets of parameters where this mode can be important. For example for $T_{\max} = 2$ the $T_{\max} - \tau$ mode is equal to the maturation time. This means again that the same model can show periods between 1 and 2 and periods between 2 and 4, i.e., single generation cycles and delayed feedback cycles occur in the same model.

We complete our investigation of the dynamical behavior of the model by studying oscillation amplitudes. Fig. 6 shows the relative amplitude $(A_{\max} - A_{\min})/A_{\text{mean}}$ of the oscillations. A harmonic (sinusoidal) oscillation has a relative amplitude smaller than 2. An oscillation with a relative amplitude larger than 2 has pronounced peaks, corresponding to discrete generations, as in the time series of Fig. 4. Large relative amplitudes occur in a large part of parameter space. The amplitudes increase with f and with d. Remarkably, they have the highest values close to the stability boundary.

4. Conclusions

In this paper we investigated a very basic model for generation cycles. This model considers only one population, which is divided into a juvenile and an adult stage. Of the four independent parameters of the model, the effective fecundity f and the death rate d of adults were found to be most important for the dynamical behavior. Generation cycles are driven by density dependent competition within the juvenile stage. The time scale of the dynamics is set by the maturation time τ. We did not impose a strict coupling between maturation time and the time delay of the competition effect, but instead introduced two parameters $T_{\min}$ and $T_{\max}$ that determine the time interval during which competitors of a focal cohort are born. A juvenile cohort of a given age is in competition with all juveniles that are younger by at most $\tau - T_{\min}$ or older by at most $T_{\max} - \tau$. A value $T_{\min} > 0$ means that there is a noncompeting stage, such as an egg stage. A value $T_{\max} > 2\tau$ means that juveniles feel the competition of cohorts that have matured before the juveniles were born, because these cohorts have left behind exploited resources, which need time to recover.

Contrary to earlier results, we found that periods of generation cycles are not within a range of one octave when d and f are varied. Only for $T_{\min} = 0$ and close to the Hopf bifurcation are the periods of the dominant mode in the interval of one octave, which was already observed by Gurney and Nisbet (1985). A strict distinction between single generation cycles and delayed competition cycles is therefore not possible but for a few special cases.

Gurney and Nisbet observed single generation cycles and delayed feedback cycles as a result of different models with different mechanisms of competition, such as the direct death of juveniles (LD model) and the death during pupation (PS model). These models assume a strict coupling between the maturation time and the time delay of the effect of competition on the population dynamics, which can be either zero (LD model) or one generation (PS model). We showed that if this constraint is relaxed, both types of generation cycles can be obtained from one model and in fact can be smoothly transformed into another by varying the time delay of the effect of competition. It is thus not possible to infer the exact mechanism of competition acting in a population only from the oscillation period in an observed time series.

Decoupling maturation time and the time delay of the effect of competition allowed us to explore a wide range of time delays. Instead of the maturation time τ the maximum delay $T_{\max}$ turned out to be the best measure for the periods of the main oscillation mode. Further oscillation modes with periods around $T_{\max} - \tau$, $T_{\max} - T_{\min}$, and $T_{\min}$ also occur, and we observed a region of chaotic dynamics for all combinations of $T_{\max}$ and $T_{\min}$, except for the case $T_{\max} = \tau$ where the competition time and the maturation time are in resonance. The chaotic region separates the main oscillation mode, which has the longest periods close to the chaotic region, from the aforementioned oscillation modes with periods shorter than $T_{\max}$.

We observed all these patterns not only in the simplified model, but also in the original models by Gurney and Nisbet, for which we also performed computer simulations. The effective fecundity f and the adult death rate d have a major influence on the dynamical behavior of the system, which is largely independent of the time delay of the effect of competition. For $f < d$ the species goes extinct. At small values of d and f the population dynamics are at a stable equilibrium. For larger values of f, generation cycles occur. The amplitude of the oscillation increases with f and d and the periodic oscillation eventually becomes unstable and gives rise to chaotic dynamics.

In the simplified model, we considered maximum delays $T_{\max}$ of up to eight times the maturation time τ, which we motivated by resources with a very long recovery time. The periods of the oscillations exceeded 40 times the maturation time for some values of fecundity f and death rate d. These long periods are indeed not characteristic of generation cycles but of consumer-resource cycles (Murdoch et al., 2002), thus supporting our interpretation of a (hidden) consumer-resource dynamics. It is important to note that in our model the resource is taken into account only indirectly. Further investigations will show if our results hold when resource dynamics are modeled explicitly. The dynamical behavior of such a model was investigated by Ruxton and Gurney (1992), but the influence of the resource on the periods is still unknown. An important question of this approach is whether there is a smooth transition between generation cycles, predator–prey cycles and prey escape cycles, as our current results suggest. Furthermore, we neglected the influence of competition on maturation time and fecundity, just as it was done in the PS model by Gurney and Nisbet, and modeled the effect on direct death of juveniles only indirectly. An interesting question is thus what happens if several effects are taken into account explicitly at the same time. The study by Gurney and Nisbet implicitly assumes that there will always be only one dominant effect of juvenile competition, which determines the type of generation cycles that will be observed. We suggest that ei-

ther the longest delay $T_{\max}$ is still the predominant factor for cycles or periods in the range of one generation time are predominant as they were observed to be very robust. However, we note that it is also possible that the different effects interact and result in an effective delay that is neither identical to the maturation time τ nor to the maximal delay $T_{\max}$. Such a mixed effect would further challenge the simple picture of either single-generation cycles or delayed-feedback cycles, as our results suggest that in such a scenario the effective delay would determine the oscillation period. Finally, we found fast frequency generation cycles which have not been reported yet. It is important to determine whether these cycles exist in more complex models as well and prove to be a realistic concept.

Acknowledgments

Appendix A. Mathematical relation to the PS model of Gurney and Nisbet (1985)

With time normalized to the maturation time τ (i.e., $\tau = 1$), the pupal survival model is given by

$$\dot{L}'(t') = f'A'(t') - f'A'(t' - 1) \tag{A.1}$$

$$\dot{A}'(t') = f'\alpha(t')A'(t' - 1) - \delta'A'(t') \tag{A.2}$$

$$\dot{W}'(t') = g'(t') - g'(t' - 1) \tag{A.3}$$

with the larval density L', adult density A', individual weight at maturation W'. The parameter f' is the fecundity and δ' is the death rate. The growth rate g' and the survival α are defined by:

$$g'(t) = \begin{cases} 1/(1 + L'(t')) - \Gamma' & \text{if } L' < 1/\Gamma' - 1 \\ 0 & \text{otherwise} \end{cases} \tag{A.4}$$

and

$$\alpha(t) = \begin{cases} (W'(t') - W'_M)/\left(W'(t') - W'_M + W'_H\right) & \text{if } W' \geq W_M \\ 0 & \text{otherwise.} \end{cases} \tag{A.5}$$

Eqs. (A.1) and (A.3) can be solved by integration, yielding

$$L(t') = f' \int_{t'-1}^{t'} A(\bar{t})d\bar{t} \quad \text{and} \tag{A.6}$$

$$W(t') = \int_{t'-1}^{t'} g(\bar{t})d\bar{t}. \tag{A.7}$$

Writing the four functions $L = L(A)$, $g = g(L)$, $W = W(g)$ and $\alpha = f(W)$ as one function $\alpha = \alpha(A)$ gives

$$\alpha(t') = f\left[\int_{t'-1}^{t'} g\left(\int_{\bar{t}-1}^{\bar{t}} A(\bar{\bar{t}})d\bar{\bar{t}}\right) d\bar{t}\right]. \tag{A.8}$$

Plugging $\alpha(t')$ into Eq. (A.2) finally leads to the single model equation

$$\dot{A}'(t') = f'\alpha(t')A'(t' - 1) - \delta'A'(t'). \tag{A.9}$$

At this point no simplification has been done. We just integrated two equations and used simple algebra. Our basic model equation (1) is identical to this form, except that we denote the share of larvae surviving until the maturation with $s(t)$ instead of $\alpha(t)$.

We tested different models with linear functions for g and a weighting function of the form $w(t')A(t')dt'$ to take into account that competition strength depends on the age difference of cohorts. We found that the exact form of the integral has a minor influence on dynamical properties such as periods and amplitudes. The essential parameter of this function is the maximum delay that we introduced as a parameter T_{max}. The maximum delay of Eq. (A.8) is 2. We approximate the double integral by a simple integral $\alpha = \alpha[\int_{t'-2}^{t'} A(\bar{t})d\bar{t}]$. If the survival α is now approximated by a linear function (Eq. (2)) then our model in the form given by Eq. (5) is obtained.

Appendix B. Fixed point and variational calculus of the model

We performed calculations for our model along the same lines as in the following earlier publications: A variational calculus of the model by Gurney and Nisbet is given in the appendix of Gurney and Nisbet (1985). A linearization of a more general system is given in Jones et al. (1988). For further linearizations see Cooke and Driessche (1986) and references therein. In this section the fixed point of our model is calculated and a variational calculus in the environment of the fixed point is performed using a linearization of the model at the fixed point. This leads to a better mathematical understanding of the periods.

The fixed point A^* of a delayed differential equation

$$\frac{dA(t)}{dt} = f\left[1 - 1/T \int_{t-T_{max}}^{t-T_{min}} A(t')dt'\right] A(t-1) - dA(t) \quad (B.1)$$

is calculated just as in the case of ordinary differential equations, i.e., it satisfies the condition

$$0 = f\left[1 - 1/T \int_{t-T_{max}}^{t-T_{min}} A^*dt'\right] A^* - dA^*. \quad (B.2)$$

This gives the two fixed points

$$A_0^* = 0 \quad \text{and} \quad (B.3)$$

$$A^* = 1 - \frac{d}{f}. \quad (B.4)$$

For $d > f$ the trivial fixed point A_0^* is stable while A^* is negative and unstable. At $d = f$ a transcritical bifurcation occurs. Both fixed points change stability and the nontrivial fixed point becomes positive.

The transition from stable dynamics to oscillations can be treated by variational calculus. The solution $A(t)$ of the balance equation is divided into the fixed point share A^* and a small deviation $a(t)$ around the fixed point, i.e. $A(t) = A^* + a(t)$. Plugging this into the model equation (B.1) yields:

$$\frac{da(t)}{dt} = f(1 - A^*)A^* - dA^*$$
$$+ f\left[-1/T \int a(t')dt'\right] a(t-1) + f(1-A^*)a(t-1)$$
$$+ f\left[-1/T \int a(t')dt'\right] A^* - d \cdot a(t). \quad (B.5)$$

The first part of this equation equals zero and the second part is neglected, as only linear terms in a are taken into account. For the linear equation the exponential ansatz $a(t) = e^{\lambda t}$ with complex λ is chosen. This gives

$$\lambda^2 e^{\lambda t} = \lambda d\left[e^{\lambda(t-1)} - e^{\lambda t}\right] - \frac{fA^*}{T}\left[e^{-\lambda(t-T_{min})} - e^{-\lambda(t-T_{max})}\right]. \quad (B.6)$$

This equation can be divided by $e^{\lambda t}$. Furthermore the complex number λ is divided into a real part α and a complex part $i\beta$ with real numbers α and β. This yields two equations—one for the real and one for the imaginary part:

(a) $T_{max} = 1$, $T_{min} = 0$.

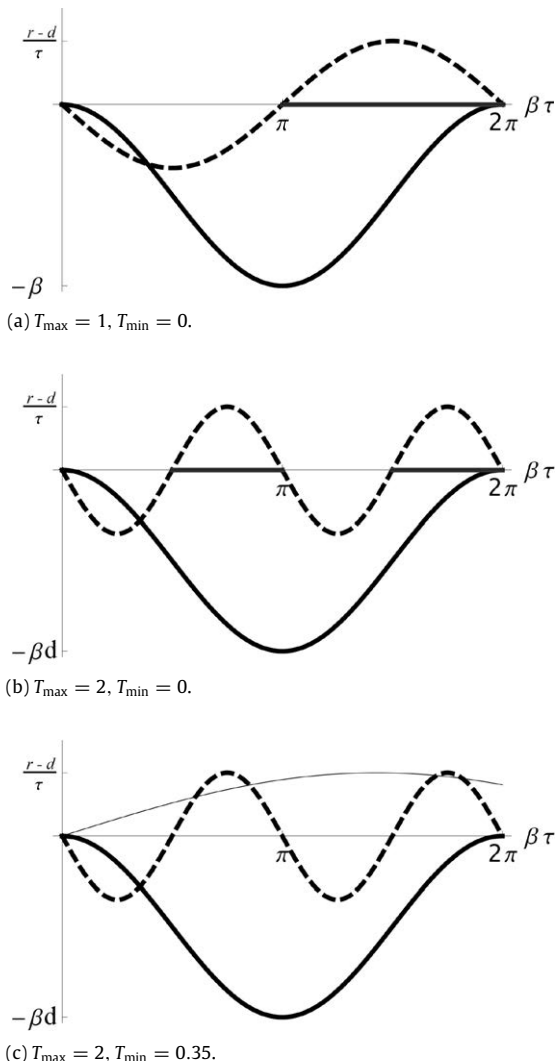(b) $T_{max} = 2$, $T_{min} = 0$.

(c) $T_{max} = 2$, $T_{min} = 0.35$.

Fig. B.7. Sketches of Eq. (B.10) for $T_{min} = 0$. (a) and (b): $\sin(\beta T_{max})$-term (dashed), $\cos(\beta) - 1$-term (solid), the two terms must add up to zero. This is only possible if both phases have opposite signs. (c) With additional $\sin(\beta T_{min})$-term (fine).

$$\alpha^2 - \beta^2 = \alpha d(e^{-\alpha}\cos\beta - 1) + \beta de^{-\alpha}\sin\beta$$
$$- \frac{fA^*}{T}\left[e^{-\alpha T_{min}}\cos(\beta T_{min}) - e^{-\alpha T_{max}}\cos(\beta T_{max})\right] \quad (B.7)$$

and

$$2\alpha\beta = \alpha d(-e^{-\alpha}\sin\beta) + \beta d(e^{-\alpha}\cos\beta - 1)$$
$$- \frac{fA^*}{T}\left[-e^{-\alpha T_{min}}\sin(\beta T_{min}) + e^{-\alpha T_{max}}\sin(\beta T_{max})\right]. \quad (B.8)$$

At a Hopf bifurcation two complex conjugate eigenvalues cross the imaginary axis. At this point the real part α of the solution vanishes. Setting $\alpha = 0$ finally results in

$$\beta^2 = -\beta d\sin\beta + \frac{f-d}{T}\left[\cos(\beta T_{min}) - \cos(\beta T_{max})\right] \quad (B.9)$$

$$0 = -\beta d(\cos\beta - 1) + \frac{f-d}{T}\left[-\sin(\beta T_{min}) + \sin(\beta T_{max})\right]. \quad (B.10)$$

These equations are symmetric, i.e. for any real valued β the complex conjugate solution $-\beta$ is another solution of the system. The results can be understood by sketching equation (B.10). The factor $(f-d)/T$ is positive in the considered interval and βd is positive as one positive β is involved in the Hopf bifurcation. The three summands of Eq. (B.10) are plotted in Fig. B.7 for the three
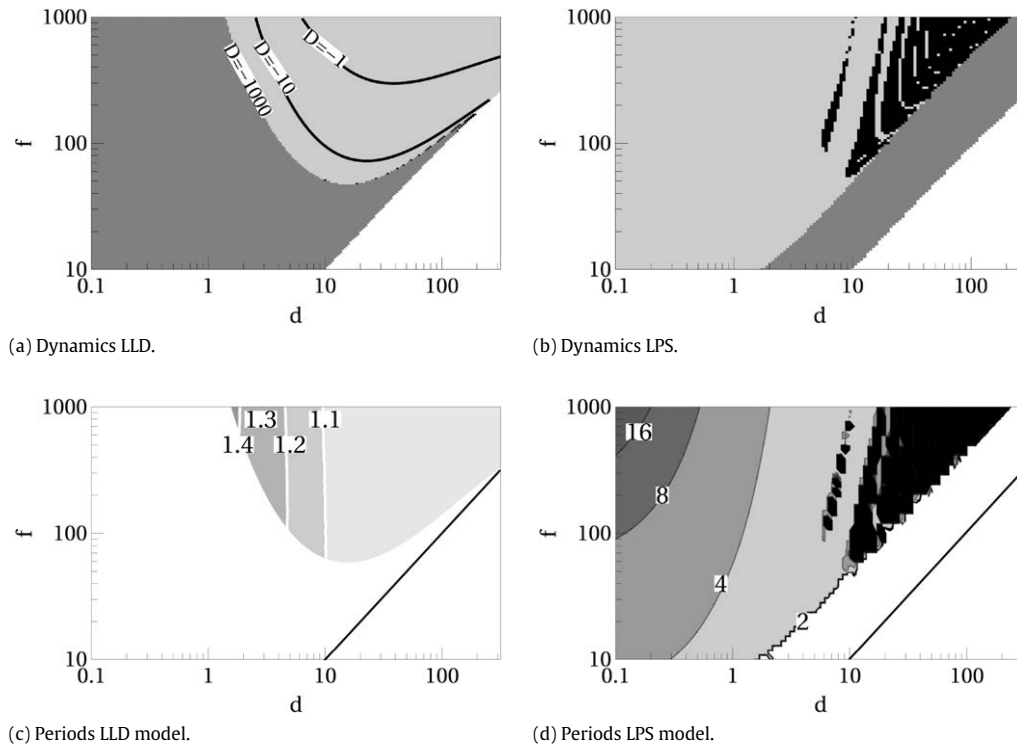
Fig. C.8. Dynamical behavior and periods—(a) and (b): dynamical behavior of our models, white: extinction, dark gray: stable, light gray: oscillation, black: chaos, (c) and (d): periods of our models in units of τ. The black solid lines mark the extinction boundary ($f = d$).

combinations of T_{max} and T_{min}. They must add up to zero. This is only positive if at least two summands have opposite signs. For $T_{min} = 0$ the solutions for β turn out to be restricted to certain intervals. Using $T = 2\pi/\beta$ the lowest possible periods are

$$T = \{T_{max}, 2T_{max}\}. \tag{B.11}$$

This is the main mode of generation cycles. For $T_{min} > 0$ the discussion becomes more complex. It is a common sense in the literature that noncompetitive stages in generation models play a minor role. Fig. 5 promotes this idea for $T_{max} > 1$. Yet, the linearization shows that dynamics might become much more complex with $T_{min} > 0$ (see Fig. B.7(c)).

Appendix C. Linearizations of the LD and PS models

In this section we present two more models. These models have exactly the same form as the original Larval Death model (LD) and the Pupal Survival model (PS), respectively. The only difference to the models by Gurney and Nisbet is, that we take linearized functions for the density dependent competition. We observe that the linearization of this term has no influence on the dynamics of the LD model, but changes the dynamics of the PS model. These findings again promote the result, that the LD dynamics are robust against changes in the mathematical details of the model, while the PS dynamics are not robust.

Linearized Larval Death model (LLD). The Linearized Larval Death model is given by

$$\frac{dL}{dt} = f \cdot A(t) - f \cdot A(t-1) \cdot s(t) \tag{C.1}$$

$$- d_L(t)J(t) \tag{C.2}$$

$$\frac{dA}{dt} = f \cdot A(t-1) \cdot s(t) - d \cdot A(t) \tag{C.3}$$

$$s(t) = \exp\left[-\int_{t-1}^{t} d_L(t')dt'\right] \tag{C.4}$$

$$d_L(t) = \text{Max}[0, D + L(t)] \tag{C.5}$$

with the larval death rate $d_L(t)$ and the linear larval death rate D. This model is equal to the LD model, except that the instantaneous death of juveniles due to competition is linearized to

$$\text{Death}_L(t) = \text{Max}\left[0, \left(D_0 + D_S L(t)\right)J(t)\right]. \tag{C.6}$$

Linearized Pupal Survival model (LPS). The balance equations of the LPS model are:

$$\frac{dA}{dt} = \begin{cases} s(t) \cdot A(t-1) - d \cdot A(t) & \text{for } s(t) > 0 \\ -d \cdot A(t) & \text{otherwise} \end{cases} \tag{C.7}$$

with

$$s(t) = r - r \int_{t-2}^{t} (1 - |t' - t + 1|)A(t')dt'.$$

This model is similar to the PS model, the basic form is identical to system (A.1)–(A.3) and Eq. (1), respectively. The recruitment rate of juveniles in dependence of the number of competitors has been linearized to

$$r(t) \propto r_{max}\left(1 - \frac{C(t)}{C_{max}}\right). \tag{C.8}$$

The number of competitors $C(t)$ can be calculated as an integral over the time-dependent birth rate, weighted by a time function $(1 - |t' - t + 1|)$. This time function reflects that a single larva has a longer period of competition with larvae of the same age. On the other hand side it has only small time overlap in the larva stage with much younger or older individuals. A sketch of this time overlap is given in Fig. 2(b). No further simplifications have been used except for the linearization of the recruitment rate term.

Results of the linearized models. The dynamical behavior and periods of the linearized models are shown in Fig. C.8. Comparing these simulations with the simplified models and the full Gurney–Nisbet dynamics (Fig. 3) leads to the following results: (i) There is no

visible difference between the LLD dynamics and the LD dynamics. The bifurcations, dynamical features and periods are equal within observable precision. (ii) The dynamical features of the LPS and PS models are similar. Yet, the exact bifurcation lines, the parameter space of chaotic behavior and the periods differ in their details. Thus (iii) we once again find the oscillations in the region of one generation time to be very robust, while models for delayed feedback cycles are less generic.

References

Bjørnstad, O.T., Nisbet, R.M., Fromentin, J.-M., 2004. Trends and cohort resonance in age-structured populations. J. Anim. Ecol. 73, 1157–1167.

Blasius, B., Huppert, A., Stone, L., 1999. Complex dynamics and phase synchronization in spatially extended ecological systems. Nature 399 (May), 354–359.

Bosch, F., de Roos, A.M., Gabriel, W., 1988. Cannibalism as a life boat mechanism. J. Math. Biol. 26, 619–633.

Caswell, H., 2001. Martix Population Models, Construction, Analysis and Interpretation, second ed. Sinauer Associates Inc., Sunderland, MA.

Cooke, K.L., Driessche, P.vd., 1986. On zeroes of some transcendental equations. Funkcial. Ekvac. 29, 77–90.

Courchamp, F., Clutton-Brock, T., Grenfell, B., 1999. Inverse density dependence and the Allee effect. Trends Ecol. Evol. 14 (1984), 405–410.

de Roos, A.M., 1996. A gentle introduction to physiologically structured populations models. In: Structured-Population Models in Marine, Terrestrial and Freshwater Systems. Chapman & Hall, pp. 119–204.

de Roos, A.M., Persson, L., McCauley, E., 2003a. The influence of size-dependent life-history traits on the structure and dynamics of populations and communities. Ecol. Lett. 6 (5), 473–487.

de Roos, A.M., Persson, L., Thieme, H.R., 2003b. Emergent Allee effects in top predators feeding on structured prey populations. Proc. R. Soc. Biol. Sci. Ser. B 270 (1515), 611–618.

Godfray, H.C.J., 1987. Natural enemies may be a cause of discrete generations in tropical insects. Nature 327.

Godfray, H.C.J., Hassell, M.P., 1989. Discrete and continuous insect populations in tropical environments. J. Anim. Ecol. 58 (1), 153–174.

Gordon, D.M., Nisbet, R.M., de Roos, A.M., 1991. Discrete generations in host–parasitoid models with contrasting life cycles. J. Anim. Ecol. 60 (1), 295–308.

Gurney, W.S.C., Blythe, S.P., Nisbet, R.M., 1980. Nicholson's blowflies revisited. Nature 287, 17–21.

Gurney, W.S.C., Nisbet, R.M., 1985. Fluctuation periodicity, and the expression of larval competition. Theor. Popul. Biol. 28, 150–180.

Gurney, W.S.C., Nisbet, R.M., Lawton, J.H., 1983. The systematic formulation of tractable single-species population models incorporating age structure. J. Anim. Ecol. 52 (2), 479–495.

Jones, A.E., Nisbet, R.M., Gurney, W.S.C., Blythe, S.P., 1988. Period to delay ratio near stability boundaries for systems with delayed feedback. J. Math. Anal. Appl. 135 (1), 354–368.

Kermack, W.O., McKendrick, A.G., 1927. A contribution to the mathematical theory of epidemics. Proc. R. Soc. A: Math. Phys. Eng. Sci. 115 (772), 700–721.

Knell, R.J., 1998. Generation cycles. Trends Ecol. Evol. 13 (5), 186–190.

Murdoch, W.W., Kendall, B.E., Nisbet, R.M., Briggs, C.J., McCauley, E., Bolser, R., 2002. Single-species models for many-species food Webs. Nature 417 (6888), 541–543.

Neill, W.E., 1988. Community responses to experimental nutrient perturbations in oligotrophic lakes: the importance of bottlenecks in size-structured populations. In: Size-Structured Populations—Ecology and Evolution. Springer, Berlin, Heidelberg.

NERC Centre for Population Biology—Imperial College, 2010. The Global Population Dynamics Database Version 2. http://www.sw.ic.ac.uk/cpb/cpb/gpdd.html.

Nicholson, A.J., 1954. An outline of the dynamics of animal populations. Aust. J. Zool. 2, 9–65.

Nicholson, A.J., 1957. The self-adjustment of populations to change. Cold Spring Harb. Symp. Quant. Biol. 22, 153–172.

Ruxton, G.D., Gurney, W.S.C., 1992. Interference and generation cycles. Theor. Popul. Biol. 253, 235–253.

SCIENTIFIC REP♦RTS

Evolutionary food web model based on body masses gives realistic networks with permanent species turnover

K.T. Allhoff[1], D. Ritterskamp[2], B.C. Rall[3], B. Drossel[4] & C. Guill[5]

The networks of predator-prey interactions in ecological systems are remarkably complex, but nevertheless surprisingly stable in terms of long term persistence of the system as a whole. In order to understand the mechanism driving the complexity and stability of such food webs, we developed an eco-evolutionary model in which new species emerge as modifications of existing ones and dynamic ecological interactions determine which species are viable. The food-web structure thereby emerges from the dynamical interplay between speciation and trophic interactions. The proposed model is less abstract than earlier evolutionary food web models in the sense that all three evolving traits have a clear biological meaning, namely the average body mass of the individuals, the preferred prey body mass, and the width of their potential prey body mass spectrum. We observed networks with a wide range of sizes and structures and high similarity to natural food webs. The model networks exhibit a continuous species turnover, but massive extinction waves that affect more than 50% of the network are not observed.

Classical models addressing the structure and stability of food webs are based on stochastic algorithms that produce structural patterns similar to empirically measured food webs[1], such as the niche model[2] or the cascade model[3]. A more recent approach is to use the empirically found allometries of body size and foraging behaviour of individual consumers to predict the links between species on a more biological basis[4].

However, real food webs are not produced by a generative algorithm, but have been shaped by their evolutionary history and show an ongoing species turnover. New species in a food web occur by immigration and speciation, and species vanish due to extinction. Currently, the world faces one of the largest extinction waves ever, which is thought to be caused by anthropogenic drivers such as climate change and land use[5]. Even without human interference or other catastrophic causes, and apart from evolutionary suicide due to runaway selection[6], biological extinctions occur due to intrinsic processes, i.e., the dynamic trophic and competitive interactions among species[7,8]. The stability of food webs in terms of resistance to extinction waves after a perturbation (such as the removal or addition of a species), thus also depends on the network structure of these interactions between the species[9,10], and conversely the

[1]Institute for Condensed Matter Physics, Technische Universität Darmstadt, Germany. [2]Institute for Chemistry and Biology of the Marine Environment, Carl von Ossietzky University of Oldenburg, Germany. [3]German Centre for Integrative Biodiversity Research (iDiv) Halle-Jena-Leipzig, Germany; Institute of Ecology, Friedrich Schiller University Jena, Germany; Netherlands Institute of Ecology (NIOO-KNAW), Wageningen, The Netherlands; J.F. Blumenbach Institute of Zoology and Anthropology, Georg-August-University Göttingen, Germany. [4]Institute for Condensed Matter Physics, Technische Universität Darmstadt, Germany. [5]Institute for Biodiversity and Ecosystem Dynamics, University of Amsterdam, The Netherlands; Institute of Biochemistry and Biology, University of Potsdam, Germany. Correspondence and requests for materials should be addressed to K.T.A. (email: allhoff@fkp.tu-darmstadt.de)

network structure results from species extinctions and additions. Understanding the interplay of food web structure and stability has therefore been identified as one of the most important questions in ecology[11].

Over the last decade, several models were introduced that include evolutionary rules on a longer time scale, in addition to population dynamics on shorter time scales: The former enables new species to enter the system, whereas the latter determines which species are viable and which go extinct. The newly emerging species can be modelled and interpreted either as invaders from another, not explicitly considered region or as "mutants" of existing species. The emerging network structures evolve in a self-organising manner, giving rise to complex, species-rich communities even when starting from initial networks with very few species[1].

A particularly simple and often cited evolutionary food web model was introduced in 2005 by Loeuille and Loreau[12] and subsequently modified by several other authors[13–15]. Each species is characterised by its body mass, which is the only evolving trait. Feeding and competition interactions are determined via differences in body mass. The fact that body mass is an ecologically interpretable trait makes the results from this model easily comparable to empirical data. This major advantage has been pointed out in the review on large community-evolution models by Brännström *et al.*[16]. The evolutionary process in this model generates large networks that show an almost static behaviour, with clearly defined niches all of which are and remain occupied. Even if a newly emerging species is slightly better adapted to the resources and therefore displaces a species of similar body mass, it has the same feeding preferences and hence the same function in the food web, leading to a very low species turnover without secondary extinctions[15]. The network structure is robust with respect to various changes in the population dynamics rules, indicating that some simple, robust mechanism structuring these food webs is at work[12,15].

Complex networks with a less rigid structure emerge in the evolutionary version of the niche model[17]. The model allows for the evolution of three traits instead of just one, namely the niche value, the centre and the width of the feeding range. Other authors describe a species in a more abstract way by a vector of many traits, as implemented in the matching model[18,19] and in the webworld model[20,21]. Recently, also several individual-based models for evolving food webs were introduced[22–24]. The emergence of complex food webs in these models is highly nontrivial. Some past attempts to set up an evolutionary model lead to repeated network collapse instead of persisting complex networks[25]. Other attempts lead to trivial network structures, like simple food chains in the evolving niche model[17] or a single trophic level in the webworld model[21]. In both models, adaptive foraging was required in order to obtain more complex networks.

Allhoff and Drossel[15] suggested that an evolutionary food web model has to fulfil two conditions to be able to generate diverse and complex networks. First, it should allow for the evolution of more traits in addition to body mass in order to generate several possible survival strategies like for example specialists and omnivores. This idea is consistent with results from a recent empirical study by Rall *et al.*[26], who found that predators of similar body mass differ significantly in their feeding preferences. Second, the evolution of each trait has to be restricted in order to prevent unrealistic trends, for example towards extremely small or large body masses or towards extremely broad or narrow feeding ranges. In this context, the stabilising effect of adaptive foraging in previous models could be explained by the fact that a predator can focus on its most profitable prey without losing adaptation to other prey.

In this paper, we propose a new evolutionary food web model that includes the restriction of trait evolution in a more direct way. Similarly to the evolutionary niche model[17] and supported by empirical data regarding the body-mass ratios of predator-prey pairs[27,28], we characterise a species by three traits with clear biological meaning: its own body mass (which determines its metabolic rates), its preferred prey body mass, and the width of its potential prey body mass spectrum. The evolutionary rules in our model confine the traits within certain boundaries, without the requirement to include adaptive foraging.

The model most similar to our model is the one by Loeuille and Loreau[12]. It also has body mass as a key trait and a similar concept for setting the feeding preferences. Our model differs from the model by Loeuille and Loreau in the number of traits that characterize a species (3 instead of 1), the functional response (Beddington-deAngelis instead of linear), the competition rules (based on link overlap instead of body mass differences), the possibility of cannibalism and loops (included only in our model) and the resource dynamics. Moreover, we consider body mass ratios instead of body mass differences so that the body masses in our model spread over several orders of magnitude instead of only one. The bio-energetics of the species in our model follow well documented allometric scaling relationships[29], leading to networks with realistic body-mass scaling relations that can be tested directly against empirical data.

We demonstrate the capabilities of our model by evaluating 18 common food web properties and compare them to a data set of 51 empirical food webs from a large variety of different ecosystems. We further use the well-known evolutionary model by Loeuille and Loreau[12] as a benchmark to assess the quality of the predictions of our model. In principle, both models are able to produce diverse networks. However, we obtain a higher variability in the feeding preferences and survival strategies and therefore more realistic values for the corresponding network properties. Moreover, while the network structures of Loeuille and Loreau are static, species turnover and extinction avalanches occur naturally in our model.
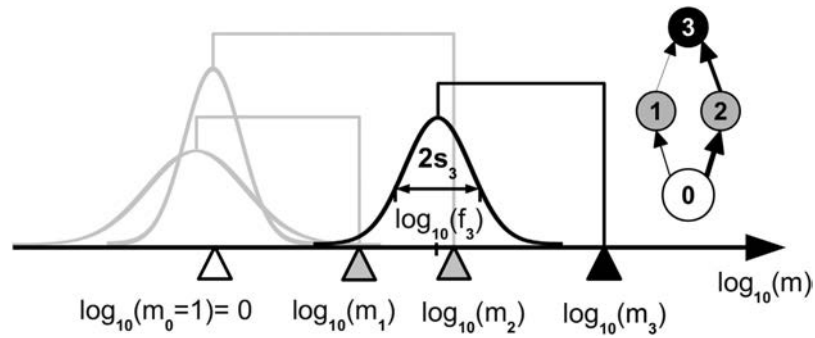
Figure 1. Model illustration using 4 species . Species 3 (black triangle) is characterised by its body mass m_3, the centre of its feeding range f_3, and the width of its feeding range s_3. The Gaussian function (black curve) describes its attack rate kernel N_{3j} on potential prey species. Here, species 3 feeds on species 2 and 1 (grey triangles) with a high resp. low attack rate. Species 1 and 2 are consumers of the external resource, represented as species 0 with a body mass $m_0 = 1$ (white triangle). Also shown is the corresponding network graph.

The Model

The model includes fast ecological processes (population dynamics), which determine whether a species is viable in a given environment that is created by the other species, and slow evolutionary processes (speciation events), which add new species and enable the network to grow and produce a self-organised structure. A species i is characterised by its body mass, m_i, the centre of its feeding range, f_i, and the width of its feeding range, s_i. These traits determine the feeding interactions in the community (see Fig. 1) and thereby the population dynamics. A summary of all model parameters and variables is given in table 1.

Population dynamics. The population dynamics follows the multi-species generalisation of the bio-energetics approach by Yodzis and Innes[30,31]. The rates of change of the biomass densities B_i of the populations are given by

$$\dot{B}_0 = G_0 B_0 - \sum_{j=\text{consumers}} g_{j0} B_j \tag{1}$$

for the external resource (species 0) and

$$\dot{B}_i = \sum_{j=\text{resources}} e_j g_{ij} B_i - \sum_{j=\text{consumers}} g_{ji} B_j - x_i B_i \tag{2}$$

for consumer species. $G_0 = R(1 - B_0/K)$ is the logistic growth rate of the external resource, e_j is the efficiency with which biomass of species j can be assimilated by its consumers, g_{ij} is the mass-specific rate with which species i consumes species j, and x_i is i's mass-specific respiration rate. The mass-specific consumption rate is given by

$$g_{ij} = \frac{1}{m_i} \frac{a_{ij} B_j}{1 + \sum_{k=\text{res.}} h_i a_{ik} B_k + \sum_{l=\text{comp.}} c_{il} B_l}, \tag{3}$$

where

$$a_{ij} = a_i \cdot N_{ij} = a_i \cdot \frac{1}{s_i \sqrt{2\pi}} \cdot \exp\left[-\frac{\left(\log_{10} f_i - \log_{10} m_j \right)^2}{2 s_i^2} \right] \tag{4}$$

is the rate of successful attacks of species i on individuals of species j, with the Gaussian feeding kernel N_{ij} as shown in Fig. 1. The parameter h_i is the handling time of species i for one unit of prey biomass, and c_{il} quantifies interference competition among predators i and l[32–34]. It depends on their similarity, as measured by the overlap $I_{il} = \int N_{ij} \cdot N_{lj} d\left(\log_{10} m_j \right)$ of their feeding kernels, via

$$c_{il} = c_{\text{food}} \cdot \frac{I_{il}}{I_{ii}} \text{ for } i \neq l. \tag{5}$$

111

parameter	meaning
resource	
$m_0 = 1$	body mass
$R = 1$	maximum mass-specific growth rate
$K = 100$	carrying capacity
B_0	biomass density
species i	
m_i	body mass
f_i	centre of feeding range
s_i	standard deviation of feeding range
B_i	biomass density
population dynamics	
$e_j = 0.85\ (0.45)$	assimilation efficiency for animal (plant) resources
g_{ij}	functional response of predator i on prey j
a_{ij}	attack rate of predator i on prey j
$a_i = 1 \cdot m_i^{0.75}$	attack rate parameter
$h_i = 0.398 \cdot m_i^{-0.75}$	handling time of predator i
c_{il}	competition on species i from species l
c_{food}	competition parameter for food
c_{intra}	intraspecific competition parameter
$x_i = 0.314 \cdot m_i^{-0.25}$	respiration rate of species i
evolutionary rules	
$\omega = 10^{-4}$	mutation probability
$\varepsilon = \frac{2}{10^4}$	initial population density of a new species and extinction threshold

Table 1. A summary of all model parameters. The values of the population parameters are based on the work by Yodzis and Innes[30]. If no value is given for a parameter, it is variable.

The normalisation of the competition with I_{ii} was proposed by Scheffer *et al.*[35] and accounts for the fact that the competition matrix is not symmetric. More specialised species exert a higher competition pressure than species with broad feeding ranges. The overlap I_{il} is similar to the niche overlap discussed by May[36].

We assume that interference competition is significantly higher within a species than between different species, e.g. due to territorial or mating behaviour. To account for this, we introduce an intraspecific competition parameter c_{intra} and set $c_{ii} = c_{\text{food}} + c_{\text{intra}}$.

Speciation events. Each simulation starts with a single ancestor species with body mass $m_1 = 100$ and feeding parameters $f_1 = 1$ and $s_1 = 1$, which is thus feeding on the external resource with its maximum attack rate. The initial biomass densities are $B_0 = K = 100$ for the resource and $B_1 = m_1 \cdot \varepsilon = 2 \cdot 10^{-2}$ for the ancestor species. The parameter ε is the extinction threshold, i.e., the minimum population density required for a population to survive. At each unit time step, species below this extinction threshold get removed from the system.

A speciation event occurs with probability $\omega = 0.0001$ per unit time. This is so rare that the system is typically close to a fixed point before the next mutation occurs. Then, one of the currently existing species (but not the external resource) is chosen randomly as parent species i for a "mutant" species j. Thus, every species has the same probability ω/S to "mutate", where S is the number of currently viable species. The logarithm of the mutant's body mass, $\log_{10}(m_j)$, is chosen randomly from the interval $[\log_{10}(0.5m_i), \log_{10}(2m_i)]$, meaning that the body masses of parent and mutant species differ at most by a factor of 2. The mutant's initial biomass density is set to $B_j = m_j \cdot \varepsilon$ and is taken from the parent species.

The mutant's feeding traits f_j and s_j are independent of the parent species. The logarithm of the feeding centre, $\log_{10} f_j$, is drawn randomly from the interval $[(\log_{10}(m_j) - 3), (\log_{10}(m_j) - 0.5)]$, meaning that the preferred prey body mass is 3 to 1000 times smaller than the consumer's body mass, and following the results from Brose *et al.*[27]. The width of the feeding range, s_j, is drawn randomly from the interval $[0.5, 1.5]$. A small value of s_j corresponds to a more specialised consumer, while a large value of s_j characterises a consumer with a broad feeding range and lower attack rates. A combination of large preferred prey mass f_j and a wide feeding range enables a consumer to prey on species with a larger body mass

than its own. This enables the emergence of cannibalism and feeding loops. The fixed intervals keep the evolving traits in reasonable ranges and prevent unrealistic trends, following the results by Allhoff and Drossel[15].

When testing the robustness of the model predictions with respect to the model details, we used alternative rules, where the probability for choosing a parent species is proportional to its biomass (similar to the model by Loeuille and Loreau[12]) or to its inverse generation time $m_i^{-1/4}$ so that the mutation rate is proportional to the reproduction rate. Furthermore, we tested Gaussian distributions of mutant body masses around the parent with a standard deviation between 0.09 and 1. We used a cutoff at two standard deviations resulting in a maximum body mass factor between parent and daughter species between $10^{2 \cdot 0.09} \approx 1.5$ and $10^{2 \cdot 1} \approx 100$. The former describes local speciation events, whereas the latter describes species invasions from not explicitly modelled regions. We also compared the results to simulations where the mutants body mass is drawn randomly from the interval $[10^{-0.5}, 10^6]$. Finally, with a similar approach, we also included heredity into the feeding parameters s_i and f_i by combining Gaussian distributions around the parent's traits with the above given mutation intervals.

Methods

The computer code for our simulations was written in C. We used the Runge-Kutta-Fehlberg algorithm provided by the GNU Scientific library[37] for the numerical integration of the differential equations. Simulations were run for $5 \cdot 10^8$ time units. For comparison, the generation time of the initial ancestor species with body size $m_1 = 100$ is of the order of $\frac{1}{x_1} = \frac{100^{0.25}}{0.314} \approx 10$ time units.

The competition parameters c_{food} and c_{intra} have a strong effect on the diversity of the emerging food webs. To obtain the network variability observed in nature, we performed computer simulations with all four combinations of $c_{\text{food}} = 0.6$ or 0.8 and $c_{\text{intra}} = 1.4$ or 1.8. The time series of these simulations are shown in the online supplementary material. From each simulation run, we collected 80 food webs obtained after every $5 \cdot 10^6$ time units from $t = 10^8$ to $t = 5 \cdot 10^8$, resulting in a total of 320 different networks. Due to the initial build-up of the network, the first 10^8 time units were not taken into account.

The structure of the emerging food webs is compared both to food webs produced with the model by Loeuille and Loreau[12] and to empirical food webs. For the empirical data, we re-evaluated 51 of the 65 food webs from different ecosystem types analysed by Riede *et al.*[38] for which we had body-mass data for all species in the network (for the complete list see online supplementary material). For the model by Loeuille and Loreau, we evaluated the final network structures obtained with 75 combinations of different parameter values. Due to the static network structure, we could not obtain different networks from one evolutionary simulation. The niche width was set to $nw = \frac{s^2}{d} = 0.5, 1.0, 1.5, 2.0, 2.5$ and the competition strength to $\alpha_0 = 0.1, 0.2, 0.3, 0.4, 0.5$, similar to the original work. To get networks of comparable size we decreased the competition range, $\beta = 0.025, 0.05, 0.075$.

Both models use Gaussian feeding kernels with in principle infinite width to describe the feeding interactions, meaning that each species can prey on every other species. Thus, for analysis, very weak links have to be cut off in order to obtain meaningful network structures. In our networks, we removed all links that contribute less than 75% of the average link to the total resources of a consumer. This criterion is weaker than it might seem, because most of the links of a predator are very weak, and so is the average link strength. Our cutoff measure depends on both the attack rate and the prey's biomass density. It thereby mimics unavoidable sampling limits in empirical food-web studies. For the networks produced by the algorithm of Loeuille and Loreau we used the cutoff criterion of the original work and removed all links with an attack rate that is smaller than 15% of the respective predator's potential maximum attack rate, disregarding the prey's biomass density. Since the value of the cutoff criterion is to some extent arbitrary, we report its effects on the predicted network properties in the online supplementary material. There we also show results obtained for the model by Loeuille and Loreau with our cutoff rule.

Results

A typical simulation run. A typical simulation run with the competition parameters $c_{\text{intra}} = 1.4$ and $c_{\text{food}} = 0.8$ is shown in Fig. 2. After an initial period of strong diversification, the system reaches a size of approximately 60 species (panel (a)) on 3 to 4 trophic levels above the resource (panel (c)). The species form clusters of similar body masses, as shown in panel (b). New predator and prey species emerge preferentially within these clusters: A prey species in a cluster experiences less predation pressure due to the saturation of the functional response of the predator, and the predation input of a predator is larger if its feeding preferences match such a cluster. Therefore, we observe a trend towards strong specialisation on these clusters, resulting in the following network structure. Species in the first cluster have a body mass of approximately 10^1, specialise on the resource and represent most of the second trophic level. Species in the second cluster with a body mass of approximately $10^2 - 10^3$ feed either on the resource (TL ≈ 2) or on the first cluster (TL ≈ 3). Species in the top cluster with a body mass greater than 10^3 specialise either on the first or on the second cluster and therefore have intermediate trophic positions ($3 \leq$ TL ≤ 4). Some species have even higher trophic positions due to cannibalism and loops.

The initial build-up of the network continues until the species in the top cluster are close to the extinction threshold. Once all clusters have emerged, the system shows a continuous turnover of species. We suppose the following turnover mechanism. Mutants with very few predators can occur occasionally
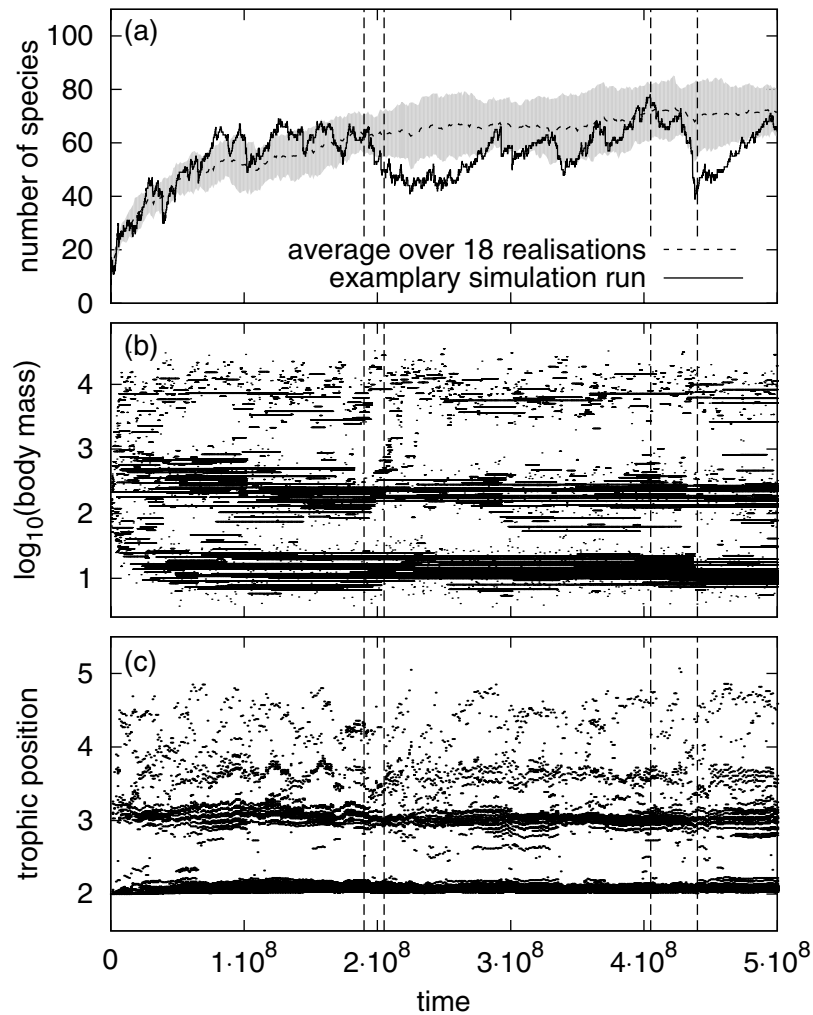
Figure 2. Network size, body masses and flow-based trophic positions[60] of all species occurring during one exemplary simulation run with competition parameters $c_{intra} = 1.4$ and $c_{food} = 0.8$. Panel (a) also shows the average network size and its standard deviation for 18 simulations with identical parameters but different random numbers. Body masses and trophic positions were plotted at every 25th mutation event. Network visualisations for the time points indicated by vertical lines are shown in the online supplementary material.

if their body mass is between two clusters and if the other species are specialised on the clusters. If such a mutant has viable feeding parameters, it can grow a large population and displace many other species at once, potentially even causing secondary extinctions. Examples for such extinction events are visible at $t \approx 2 \cdot 10^8$ and $t \approx 4.3 \cdot 10^8$. After an extinction event, the network rearranges, and temporally also species with broader feeding ranges appear, before the trend towards specialisation followed by an extinction event starts again.

Network evaluation and comparison. We compared 320 networks from our model with 51 empirical networks and 75 networks from the model by Loeuille and Loreau[12], see Fig. 3. Panels (a)–(c) show the distributions of body masses of all three data sets. The observed peaks in our simulated data correspond to the body mass clusters mentioned before. The distance between the peak maxima is determined by the upper boundary of the mutation interval of the feeding centre. Single empirical food webs show a similar peak pattern (not shown). In contrast, the body mass distribution of the model by Loeuille and Loreau looks blurred, due to our choice of the niche width $nw = \frac{s^2}{d}$. With smaller values of the feeding range s, the network structure is strongly layered and clusters of body masses that are multiples of the feeding distance d occur, where each species feeds on those in the cluster below and is prey to those in the cluster above[15]. We also observed that because we based the network structure on predator-prey body-mass ratios instead of body-mass differences, the resulting community-size spectra from our model

114
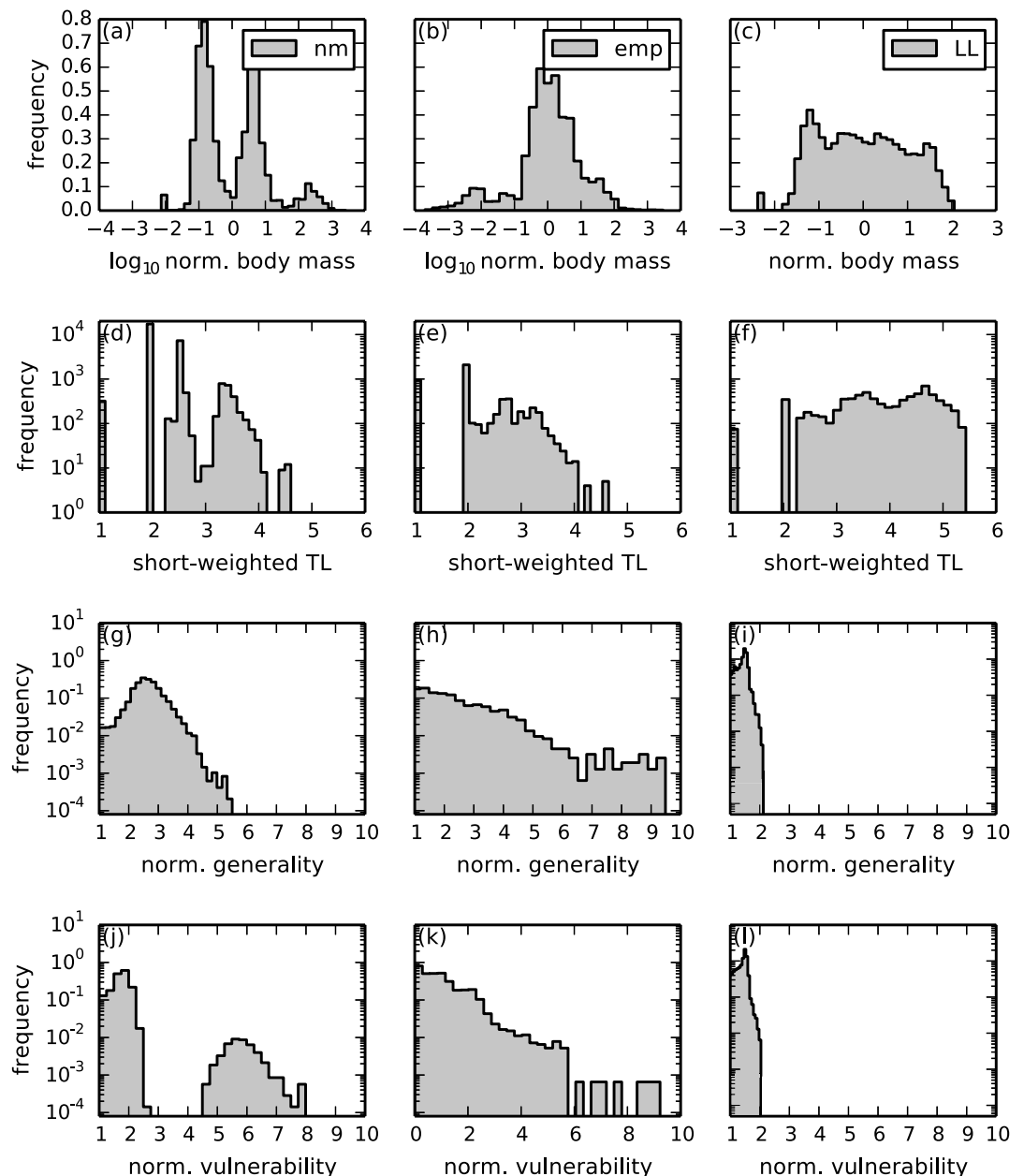
Figure 3. Frequency distributions of body masses and short-weighted trophic level[60], as well as the distributions of generality (number of prey species) and vulnerability (number of predators). The latter two are normalised by the average number of links per species. **nm**: 320 networks from 4 simulations of our new model with all four combinations of $c_{food} = 0.6$ or 0.8 and $c_{intra} = 1.4$ or 1.8. **emp**: Average over 51 empirical food webs. **LL**: Average over 75 simulations of the model by Loeuille and Loreau[12]. Note that panel (c) shows absolute body masses, since in this model all body masses are in the same order of magnitude. See *Methods* for more information.

follow empirical observations and theoretical predictions more closely than those from the model by Loeuille and Loreau, as shown in the online supplementary material.

Panels (d)–(f) show the distributions of trophic levels of all three data sets. Here, we use the short-weighted instead of the flow-based trophic level. This allows for better comparison with the empirical data for which the population sizes are often not available. The comparison between the two models reveals the main difference between the two different cutoff rules. A link with intermediate attack rate to a small prey population represents only a small proportion of the predator's diet, and is therefore neglected when using our cutoff threshold (75% of the average link). However, it is not recognised as a weak link with the cutoff rule by Loeuille and Loreau (15% of the maximum attack rate). On the other hand, a link with small attack rate to a big prey population (especially to the resource) is deleted in their

115
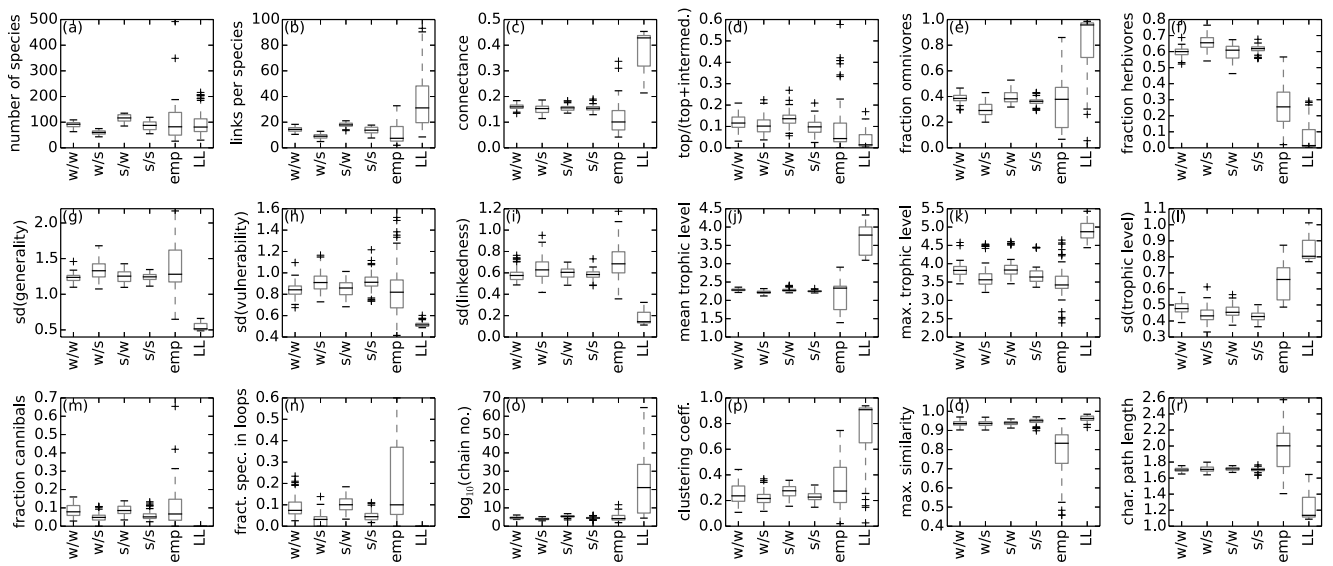
Figure 4. Network properties of four realisations with different values of the competition parameters.
w/w: Weak competition, $c_{intra} = 1.4 / c_{food} = 0.6$. **w/s**: Weak intraspecific competition and strong competition for food, $c_{intra} = 1.4 / c_{food} = 0.8$. **s/w**: Strong intraspecific competition and weak competition for food, $c_{intra} = 1.6 / c_{food} = 0.6$. **s/s**: Strong competition, $c_{intra} = 1.6 / c_{food} = 0.8$. **emp**: Average over 51 empirical food webs. **LL**: Average over 75 simulations of the model by Loeuille and Loreau[12]. See *Methods* for more information. Details on the calculation of these network characteristics can be found in the online supplementary material.

model. Thus, trophic levels are overestimated, whereas our model with our cutoff rule results in a quite realistic distribution.

Both models have difficulties reproducing the empirical distributions of generality (number of prey species) and vulnerability (number of predators), which are much broader than the distributions produced by the models (panels (g)–(l)). For the model by Loeuille and Loreau, the distribution results from the fact that the species in the model feed only on prey with smaller body masses. The situation is similar to the cascade model[3], which also constrains predators to feed only on prey with a lower rank. Consequently, both generality and vulnerability cannot be larger than twice the average number of links per species. In our new model, the distribution of the vulnerability shows two humps. The first hump contains the carnivores in the higher trophic levels that feed on herbivores or on other carnivores. They have a high generality and a small vulnerability. The second hump contains the herbivores that feed on the resource. They are prey to many other species and hence have a high vulnerability.

We ascribe the differences between the models and the empirical distributions to the fact that both models have only one resource, which means that all herbivores feed on the same resource, whereas in empirical networks herbivores can have more than one resource. Furthermore, both models ignore the within-species body-mass distribution by assigning to each species a precise value of the body mass. This also narrows down the range of body sizes a species can feed on or is vulnerable to.

By analysing the 320 networks from the 4 simulations separately (see Fig. 4), we found two trends concerning the network size (panel (a)): First, the stronger the intraspecific competition c_{intra}, the smaller are the population sizes and the more populations can survive on the same amount of energy provided by the resource. Second, the stronger the competition for food c_{food} is, the sooner species can displace others resulting in rather small networks with fast evolutionary species turnover.

Both models are able to produce networks of realistic sizes, but tend to overestimate the number of links per species (panel (b)) and hence the connectance (panel (c)). The effect is much larger in the model by Loeuille and Loreau due to their original cutoff rule. This also explains the high fraction of omnivores and the low fraction of top and herbivorous species (panels (d)–(f)), as well as the high values of the number of chains and the clustering coefficient (panel (o) and (p)) and the small value of the characteristic path length (panel (r)). In the online supplementary material, we show that the model by Loeuille and Loreau provides more realistic predictions when using our cutoff rule.

Both models fail to reproduce the maximum similarity (panel (q)), due to the same reasons that also lead to the narrow distributions of generality and vulnerability. For the remaining panels, the model by Loeuille and Loreau performs worse than our model regardless which cutoff rule is used. For example, the short-weighted trophic levels (panel (j)–(l)) are not only overestimated due to the cutoff rule, but also reflect the regular network structure. As mentioned above, these networks are layer-like structures,

where each cluster represents one trophic level. Since all clusters accommodate a similar number of species instead of heaving more species on lower levels like in our model, the mean trophic level is overestimated. Moreover, the model does not include cannibalism (panel (m)) and loops (panel (n)), for which our model provides good predictions.

Due to the evolution of three instead of one trait, we obtain more diverse network structures than Loeuille and Loreau. We observe a higher standard deviation of the generality, the vulnerability and the linkedness (panel (g)–(i)), reflecting different feeding preferences and survival strategies.

Robustness of the results against variations of the evolutionary rules.

In order to ensure that our findings are no artefacts of the specific choice of evolutionary rules, we tested the robustness of our results against the changes outlined at the end of the model section. We found that making mutation probabilities dependent on biomass or body mass influences the time dependency of the network development but leaves the averaged network properties, like the total network size, the distribution of body masses and the fraction of species or biomasses per trophic level, mostly unchanged. Also the trend towards strong specialisation with subsequent extinctions still occurs in these variants.

When changing the degree to which the parent's body mass is inherited by the mutant, the main effect was that species turnover became slower with stronger inheritance. In this case it is less likely that mutants with body masses between two clusters occur, which have few predators and cause extinction avalanches. The probability for such mutants increases with a decreasing degree of inheritance, which is consistent with our oberservation that the body mass clusters appear to be blurred in case of a very low degree of inheritance. The same is true for randomly chosen body masses. However, we still obtain large, complex networks.

If the parent species i and the mutant j have similar feeding centres, $f_i \approx f_j$, the initial build-up of different trophic levels and their recovery after an extinction avalanche is also slowed down. With very strong inheritance of the feeding centre, all species will focus on the resource and no mutant emerges with a feeding centre matching the first body mass cluster, leading to trivial structures with only one trophic level. If parent and mutant have a similar degree of specialisation, $s_i \approx s_j$, all species exert and experience a similar competition pressure. Thus, instead of one species displacing another, both populations stay small and hence more populations per trophic level can survive. However, small or intermediate degrees of inheritance in the feeding traits leave the network characteristics again mostly unchanged. The situation is different, when either the feeding range or the feeding centre is chosen from an interval around the parent's trait without any body mass dependent constraint. In consistency with the predictions of Allhoff and Drossel[15], these variants lead to unrealistic trends and trivial instead of complex network structures.

Discussion

We introduced a new evolutionary food web model where the feeding links are based on body mass, and where species differ by body mass, feeding centre, and feeding range. By iterating population dynamics and speciation events for a sufficiently long time, we obtained complex networks, which show a high degree of commonality with empirical food webs. The new model is able to produce more realistic and more diverse network structures than the model by Loeuille and Loreau[12].

Both models use a very similar approach of Gaussian feeding kernels to determine the interactions between the species, which by construction leads to perfectly interval networks. Following the results of Stouffer et al.[39], we assume this to be a reasonable approximation. In contrast to the model by Loeuille and Loreau, the new model allows for cannibalism and loops, since the feeding range can extend to body masses larger than that of the predator. The species in our model can have different feeding preferences and survival strategies, due to the larger number of evolving traits in our model. This leads to a higher variability in network characteristics such as linkedness, generality and vulnerability, even though natural variability is still larger, which we ascribe to the facts that our model has only one basal resource and no body-size structure within species. We showed that an appropriate choice of the cutoff rule for weak links is essential for obtaining realistic results for connectance and trophic structure.

The increased number of evolving traits compared to the model by Loeuille and Loreau has also a large effect on the evolutionary trends. The networks show an ongoing species turnover and are subject to constant restructuring. The species in our model form body mass clusters and the evolutionary process is characterised by a trend towards increased specialisation on these clusters. Similar specialisation trends have also been observed in other studies[15,17]. We assume the following explanation for the continuous species turnover. The evolved specialists gradually replace less efficient species with broader feeding ranges that cover also the gaps between the body mass clusters. Those broad ranged species have the role of keystone species that stabilise the networks against the occurrence of large extinction avalanches[40,41]. In the absence of control by such predators, new mutants (or invaders) can find niches between two clusters with very little predation pressure, where they can grow to high abundance and cause extinction avalanches propagating from lower to higher trophic levels. After such extinction events, the empty niches can be reoccupied also by species with broader feeding ranges, before the speciation process starts again.

This corresponds to the results of Binzer et al.[8], who identified specialised species on high trophic levels to be prone to secondary extinctions, and to the results of Rossberg[42], who suggested a very similar turnover mechanism for the results of his model. In consistence with the described mechanism, also

Mellard and Ballantyne[43] reported that co-evolution of species does not necessarily lead to high levels of resilience for the ecosystem as a whole. However, such a turnover mechanism is missing in the model by Loeuille and Loreau. There, a displaced species is always replaced by a new species of a very similar body mass. And since the body mass is the only evolving trait, the new species has automatically the same predators and the same prey, excluding the possibility of secondary extinctions or major changes in the network structure[15]. The same is true for the model version by Brannström *et al.*, which led to evolutionary equilibria, where no more mutants are able to invade the system[14]. Ingram *et al.* reported that also their model extension with evolving feeding ranges, but with fixed predator-prey body mass ratios, tends to reach dynamically stable configurations with little structural change[13].

However, real ecosystems do show extinction events of different sizes, and their distribution evaluated over geological times resembles a power law[44]. For this reason, it has been suggested that ecosystems show self-organised criticality (SOC)[45], which means that the intrinsic dynamics of the systems is responsible for the power-law size distribution of extinctions. However, the question remains open due to sparse and ambiguous data[46,47]. Some previous evolutionary food web models, for example the evolutionary niche model[17], exhibit SOC, whereas other models like the webworld model[20] or the model by Loeuille and Loreau[12] do not. The size distribution of extinction avalanches in our model is a power law with an exponent around 4 (not shown). Because of its steepness, this power law covers only approximately one decade, meaning that extinction events of more than 10 species are extremely rare. This is not the type of SOC required to explain the large extinction events in earth history, where up to 90 percent of all species went extinct. Regarding the time span a species is present in the system, our model is consistent with paleobiological data concerning the fact that higher trophic level species stay in the system for a shorter time span than lower level species[46], although it should be mentioned that the exact distribution of these time spans in our model depends on the relation between a species' body mass and its mutation probability.

The evolutionary rules implemented in our model are simplified and to some extent artificial. To make sure that our results do not depend on these simplified rules, we tested several variations concerning the mutation and inheritance rules. Our general finding is that minor changes in the evolutionary algorithm have only minor effects on the results. The overall mechanism with a trend towards specialisation followed by an extinction event as explained above is robust to changes in the evolutionary rules. Also the time averaged network structures remain mostly unchanged. However, the typical time period for a specialisation-extinction cycle can change with extinction events being triggered sooner or later.

The fact that our networks show realistic patterns concerning many common food web properties suggests that our model provides a valuable tool to discuss urgent topics in ecological research. For example, the allometric equations are extendable by temperature terms (e.g.[48–51]). This approach would allow to model how warming might change evolution and extinction waves, in order to discuss current global change questions.

Another idea would be to address habitat loss and habitat fragmentation as a prominent example of an external driver of extinction events[52,53]. Recently, various approaches have been made to study the influence of the spatial environment on the food web composition and stability. If space has the structure of discrete habitats, these food webs can be interpreted as "networks of networks"[54,55]. However, most of the studies on such metacommunities so far focus on spatial aspects under the assumption that the species composition is static, although it has been emphasised that combining the spatial and the evolutionary perspective is essential for a better understanding of ecosystems[56–58]. Recently, Allhoff *et al.* studied a spatial version of the model by Loeuille and Loreau[59]. However, their findings were associated with the applied competition rules and the remarkable stability of the original model, highlighting the assumption that a more dynamic species turnover as in our new model would lead to a better understanding of the interplay between evolving food web structure and spatial structure.

References

1. Drossel, B. & McKane, A. J. *Handbook of Graphs and Networks: From the Genome to the Internet*, **Ch. 10,** 218–247 (Wiley-VCH Verlag GmbH & Co. KGaA, Weinheim, 2005).
2. Williams, R. J. & Martinez, N. D. Simple rules yield complex food webs. *Nature* **404,** 180–182 (2000).
3. Cohen, J. & Newman, C. A stochastic theory of community food webs: I. models and aggregated data. *Proceedings of the Royal society of London. Series B. Biological sciences* **224,** 421–448 (1985).
4. Petchey, O. L., Beckerman, A. P., Riede, J. O. & Warren, P. H. Size, foraging, and food web structure. *Proceedings of the National Academy of Sciences* **105,** 4191–4196 (2008).
5. Barnosky, A. D. *et al.* Has the earth's sixth mass extinction already arrived? *Nature* **471,** 51–57 (2011).
6. Parvinen, K. Evolutionary suicide. *Acta Biotheoretica* **53,** 241–264 (2005).
7. Riede, J. O. *et al.* Size-based food web characteristics govern the response to species extinctions. *Basic and Applied Ecology* **12,** 581–589 (2011).
8. Binzer, A. *et al.* The susceptibility of species to extinctions in model communities. *Basic and Applied Ecology* **12,** 590–599 (2011).
9. May, R. M. Will a large complex system be stable? *Nature* **238,** 413–414 (1972).
10. Otto, S. B., Rall, B. C. & Brose, U. Allometric degree distributions facilitate food-web stability. *Nature* **450,** 1226–1229 (2007).
11. May, R. Unanswered questions in ecology. *Philos. Trans. R. Soc. London B Biol. Sci.* **354,** 1951–1959 (1999).
12. Loeuille, N. & Loreau, M. Evolutionary emergence of size-structured food webs. *PNAS* **102,** 5761–5766 (2005).
13. Ingram, T., Harmon, L. J. & Shurin, J. B. Niche evolution, trophic structure, and species turnover in model food webs. *The American Naturalist* **174,** 56–67 (2009).
14. Brännström, Å., Loeuille, N., Loreau, M. & Dieckmann, U. Emergence and maintenance of biodiversity in an evolutionary food-web model. *Theoretical Ecology* **4,** 467–478 (2011).

15. Allhoff, K. T. & Drossel, B. When do evolutionarty food web models generate complex structures? *Journal of Theoretical Biology* **334,** 122–129 (2013).

16. Brännström, Å. *et al.* Modelling the ecology and evolution of communities: a review of past achievements, current efforts, and future promises. *Evolutionary Ecology Research* **14,** 601–625 (2012).

17. Guill, C. & Drossel, B. Emergence of complexity in evolving niche-model food webs. *Journal of Theoretical Biology* **251,** 108–120 (2008).

18. Rossberg, A., Matsuda, H., Amemiya, T. & Itoh, K. Food webs: Experts consuming families of experts. *Journal of Theoretical Biology* **241,** 552–563 (2006).

19. Rossberg, A., Ishii, R., Amemiya, T. & Itoh, K. The top-down mechanism for body-mass-abundance scaling. *Ecology* **89,** 567–580 (2008).

20. Drossel, B., Higgs, P. G. & McKane, A. J. The influence of predator-prey population dynamics on the long-term evolution of food web structure. *Journal of Theoretical Biology* **208,** 91–107 (2001).

21. Drossel, B., McKane, A. J. & Quince, C. The impact of nonlinear functional responses on the long-term evolution of food web structure. *J. Theor. Biol.* **229,** 539–548 (2004).

22. Bell, G. The evolution of trophic structure. *Heredity* **99,** 494–505 (2007).

23. Yamaguchi, W., Kondoh, M. & Kawata, M. Effects of evolutionary changes in prey use on the relationship between food web complexity and stability. *Popul. Ecol.* **53,** 59–72 (2011).

24. Takahashi, D., Brännström, Å., Mazzucco, R., Yamauchi, A. & Dieckmann, U. Abrupt community transitions and cyclic evolutionary dynamics in complex food webs. *Journal of Theoretical Biology* **337,** 181–189 (2013).

25. Takahashi, D., Brännström, Å., Mazzucco, R., Yamauchi, A. & Dieckmann, U. Cyclic transitions in simulated food-web evolution. *J. Plant. Interact.* **6,** 181–182 (2011).

26. Rall, B. C., Kalinkat, G., Ott, D., Vucic-Pestic, O. & Brose, U. Taxonomic versus allometric constraints on non-linear interaction strengths. *Oikos* **120,** 483–492 (2011).

27. Brose, U. *et al.* Consumer-resource body-size relationships in natural food webs. *Ecology* **87,** 2411–2417 (2006).

28. Riede, J. O. *et al.* Stepping in elton's footprints: a general scaling model for body masses and trophic levels across ecosystems. *Ecology Letters* **14,** 169–178 (2011).

29. Brown, J. H., Gillooly, J. F., Allen, A. P., Savage, V. M. & West, G. B. Toward a metabolic theory of ecology. *Ecology* **85,** 1771–1789 (2004).

30. Yodzis, P. & Innes, S. Body size and consumer-resource dynamics. *The American Naturalist* **139,** 1151–1175 (1992).

31. Brose, U., Williams, R. J. & Martinez, N. D. Allometric scaling enhances stability in complex food webs. *Ecol. Lett.* **9,** 1228–1236 (2006).

32. Beddington, J. R. Mutual interference between parasites or predators and its effect on searching efficiency. *Journal of Animal Ecology* **44,** 331–340 (1975).

33. DeAngelis, D. L., Goldstein, R. A. & O'Neill, R. V. A model for tropic interaction. *Ecology* **56,** 881–892 (1975).

34. Skalski, G. T. & Gilliam, J. F. Functional responses with predator interference: viable alternatives to the holling type ii model. *Ecology* **82,** 3083–3092 (2001).

35. Scheffer, M. & van Nes, E. H. Self-organized similarity, the evolutionary emergence of groups of similar species. *Proceedings of the National Academy of Sciences* **103,** 6230–6235 (2006).

36. May, R. M. On the theory of niche overlap. *Theoretical Population Biology* **5,** 297–332 (1974).

37. Galassi, M. *et al. GNU Scientific Library Reference Manual* (Network Theory Ltd, 2009).

38. Riede, J. O. *et al.* Scaling of food-web properties with diversity and complexity across ecosystems. *Advances In Ecological Research* **42,** 139–170 (2010).

39. Stouffer, D. B., Camacho, J. & Amaral, L. A. N. A robust measure of food web intervality. *Proceedings of the National Academy of Sciences* **103,** 19015–19020 (2006).

40. Power, M. E. *et al.* Challenges in the quest for keystones. *Bioscience* **46,** 609–620 (1996).

41. Eklöf, A. & Ebenmann, B. Species loss and secondary extinctions in simple and complex model communities. *Journal of Animal Ecology* **75,** 239–246 (2006).

42. Rossberg, A. G. *Food webs and biodiversity: foundations, models, data*, Ch. 22, 287–309 (John Wiley & Sons, 2013).

43. Mellard, J. P. & Ballantyne IV, F. Conflict between dynamical and evolutionary stability in simple ecosystems. *Theoretical Ecology* **7,** 273–288 (2014).

44. Raup, D. Biological extinction in earth history. *Science* **231,** 1528–1533 (1986).

45. Sneppen, K., Bak, P., Flyvbjerg, H. & Jensen, M. H. Evolution as a self-organized critical phenomenon. *Proceedings of the National Academy of Sciences* **92,** 5209–5213 (1995).

46. Newman, M. E. & Palmer, R. G. *Modeling extinction* (Oxford University Press, 2003).

47. Drossel, B. Biological evolution and statistical physics. *Advances in Physics* **50,** 209–295 (2001).

48. Vasseur, D. A. & McCann, K. S. A mechanistic approach for modeling temperature-dependent consumer-resource dynamics. *The American Naturalist* **166,** 184–198 (2005).

49. Binzer, A., Guill, C., Brose, U. & Rall, B. C. The dynamics of food chains under climate change and nutrient enrichment. *Philosophical Transactions of the Royal Society B: Biological Sciences* **367,** 2935–2944 (2012).

50. Norberg, J., Urban, M. C., Vellend, M., Klausmeier, C. A. & Loeuille, N. Eco-evolutionary responses of biodiversity to climate change. *Nature Climate Change* **2,** 747–751 (2012).

51. Stegen, J. C., Ferriere, R. & Enquist, B. J. Evolving ecological networks and the emergence of biodiversity patterns across temperature gradients. *Proceedings of the Royal Society of London B: Biological Sciences* **279,** 1051–1060 (2012).

52. Hagen, M. *et al.* Biodiversity, species interactions and ecological networks in a fragmented world. *Advances in Ecological Research* **46,** 89–210 (2012).

53. Gonzalez, A., Rayfield, B. & Lindo, Z. The disentangled bank: How loss of habitat fragments and disassembles ecological networks. *American Journal of Botany* **98,** 503–516 (2011).

54. Amarasekare, P. Spatial dynamics of foodwebs. *Annual Review of Ecology, Evolution, and Systematics* **39,** 479–500 (2008).

55. Leibold, M. A. *et al.* The metacommunity concept: a framework for multi-scale community ecology. *Ecology letters* **7,** 601–613 (2004).

56. Logue, J. B., Mouquet, N., Peter, H. & Hillebrand, H. Empirical approaches to metacommunities: a review and comparison with theory. *Trends in Ecology & Evolution* **26,** 482–491 (2011).

57. Urban, M. C. *et al.* The evolutionary ecology of metacommunities. *Trends in Ecology & Evolution* **23,** 311–317 (2008).

58. Loeuille, N. & Leibold, M. Ecological consequences of evolution in plant defenses in a metacommunity. *Theoretical population biology* **74,** 34–45 (2008).

59. Allhoff, K. T., Weiel, E. M., Rogge, T. & Drossel, B. On the interplay of speciation and dispersal: An evolutionary food web model in space. *Journal of Theoretical Biology* **366,** 46–56 (2014).

60. Williams, R. J. & Martinez, N. D. Limits to trophic levels and omnivory in complex food webs: Theory and data. *The American Naturalist* **163,** 458–468 (2004).

119

Acknowledgements

Author Contributions

All authors designed the model. K.T.A. performed the simulations. K.T.A. and C.G. analysed the results. K.T.A. wrote the manuscript with minor contributions from the other authors. All authors reviewed the manuscript.

Additional Information

Supplementary information accompanies this paper at http://www.nature.com/srep

Competing financial interests: The authors declare no competing financial interests.

How to cite this article: Allhoff, K.T. *et al.* Evolutionary food web model based on body masses gives realistic networks with permanent species turnover. *Sci. Rep.* **5**, 10955; doi: 10.1038/srep10955 (2015).

120

Prohibition rules for three-node substructures in ordered food webs with cannibalistic species

Christian Guill [a]*[†] and Pavel Paulau[b]

[a]Institute for Biodiversity and Ecosystem Dynamics (IBED), University of Amsterdam, Amsterdam, The Netherlands; [b]Institute for Chemistry and Biology of the Marine Environment (ICBM), Carl-von-Ossietzky University of Oldenburg, Oldenburg, Germany

We evaluate the spectrum of ordered three-node substructures in food webs taking self-links (cannibalism) into account. If the order of nodes in the network cannot be neglected, 512 substructures can be distinguished. Simple statistical models of networks impose constraints on the structure that prohibit a large number of substructures completely. We analyse two variants of the widely used niche model, the original niche model and the generalised niche model, and show analytically and numerically that they exclude 344 and 320 substructures, respectively. The prohibition rules for three-node substructures in the two niche-model variants are further contrasted with a large set of empirical food webs, which reveals that up to about 30% of the three-node substructures that occur in empirical food webs are prohibited by the model algorithms.

Keywords: motif analysis; food webs; cannibalism; node ordering; body mass; niche model

Introduction

Networks are a powerful tool to describe systems as different as transportation and power systems, social communities, or the World Wide Web (Albert & Barabási 2002; Newman 2003). In the biological sciences, networks are used to analyse e.g. metabolic pathways in cells (Jeong et al. 2000), neural systems (Varshney et al. 2011), or the interactions of species in an ecosystem (Dunne et al. 2002a). In this article, we are interested in the structure of food webs, which are the networks of predator−prey interactions in ecological communities (Drossel & McKane 2005). Understanding the structure of these networks is of great importance to unravel the factors that determine the resistance or vulnerability of ecosystems against accelerating species loss (Dunne et al. 2002b; Binzer et al. 2011). The analysis of substructures has been used successfully to identify important building blocks or functional units of larger networks. We follow the convention of Milo et al. (2002) and call such a building block that occurs significantly more often than in suitably randomised networks a motif. In theoretical ecology, the dynamics of interconnected populations that form a motif (or *module*, if the population size associated with a node in the motif is considered as a dynamic quantity) is a frequently studied subject (McCann et al. 1998). While in most types of networks self-links are not important, they naturally occur in food webs as cannibalistic interactions within species (Fox 1975; Polis 1981). They are, however, usually neglected even in the ecological literature on motif analysis (Stouffer et al. 2007), despite the intricate effects cannibalism can have on the population dynamics in food-web modules (Persson et al. 2003; Claessen et al. 2004).

Several models exist that generate artificial food-web structures using stochastic algorithms. These artificial networks resemble certain aspects of natural food webs, but usually also impose constraints on the links among the species. Often the existence of an order of the nodes (species) is assumed, e.g. induced by the mean body masses of the species, such that species with a higher index have a higher mean body mass. In the cascade model (Cohen & Newman 1985) and the generalised cascade model (Stouffer et al. 2005), the species form a completely ordered set, and predators are prohibited from having prey with a higher index (body mass) than themselves. This has obvious effects on the number of substructures that may occur in these types of networks. The niche model (Williams & Martinez 2000) is one of the most widely used models for food-web structures. It also assumes that the species form a completely ordered set. It constrains predators to take their prey from a contiguous interval on the niche axis, but up to half of the interval may extend above the niche position of the predator. This makes links that point in the direction of the node order possible, but the contiguity of the feeding ranges imposes constraints regarding the presence of cannibalistic links. The generalised niche model (Stouffer et al. 2006) relaxes the contiguity constraint of the feeding ranges by assigning predators a certain number of prey species with a lower index at random. We use here the convention that links point from predator to prey (Milo et al. 2002; Newman 2003; Camacho et al. 2007; Stouffer et al. 2007), while part of the literature about food webs uses another convention, where the links point in the direction of the resource flow (Drossel & McKane 2005).

The structure of the article is as follows. In the second section, we describe the full set of ordered three-node substructures including cannibalism, we present the simple statistical model allowing us to define the spectrum of
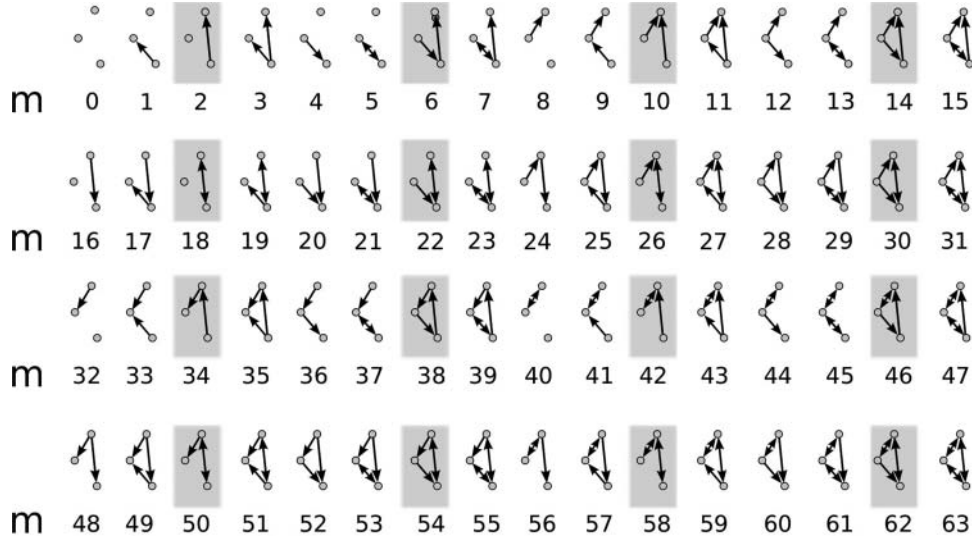

Figure 1. The 64 ordered three-node substructures without self-links. The index (rank or niche position) of a node increases from bottom to top for each substructure. The horizontal displacement of nodes is only for illustrative purposes. Shaded rectangles mark the substructures that are always prohibited in both the original and the generalised niche model, irrespective of the cannibalistic configuration. The integer index $m \in [0; 63]$ is a decimal form of the binary number formed by the off-diagonal elements of the adjacency matrix.

substructures (i.e., the frequencies of their occurrence) analytically, and we compare it with the results obtained with our numerical algorithms. In the third section we build analytically the binary spectra of three-node substructures for food webs generated with the (generalised) niche model and we compare them with a data set of empirical food webs. We further determine the quantitative importance of prohibited substructures in the empirical food webs. The results are discussed in the last section.

The spectrum of ordered three-node substructures

In this article, we consider only simple networks that are characterised by one type of nodes (biological species in the context of food webs) and one type of links (feeding interactions among species). This is indeed a simplification, as non-trophic interactions can be very common in food webs (Kéfi et al. 2012). A link between two species i and j is considered directed. Furthermore, the networks are ordered, i.e., between any two arbitrarily chosen nodes i and j, we can define a relation such that one of the nodes is higher than the other. In food webs, the average adult body mass of the species can be used to define such a relation.

In a recent paper (Paulau et al. 2015), the motif analysis of food webs has been extended by taking the anisotropy of ecological niche space and the order of species into account. In the simplest case, the niche space (a niche axis) is one-dimensional (Cohen and Stephens 1978) and, following Elton (1927), the position on this axis defines the feeding interactions of a species. If this one-dimensional niche space is anisotropic, species with a high position on the niche axis feed on those with a low position with a different probability than vice versa. Since in food webs it has been reported that predators are commonly larger than their prey (at least when parasites are excluded), body mass is indeed a useful proxy for niche position (Brose et al. 2006).

In such an anisotropic situation, the members of the 13 isomorphism classes of connected three-node

substructures (Milo et al. 2002) that are formed by cyclic and mirror permutations of nodes are no longer statistically equivalent and the extended spectrum of three-node substructures must be analysed (Figure 1). In each substructure, the nodes are ordered in such a way that the lowest index corresponds to the bottom node, the intermediate index corresponds to the middle node, and the highest index to the top node. A three-node substructure can be fully described by a 3×3 adjacency matrix M with elements M_{ij} that are 1 if i is a predator of j and 0 else. The six non-diagonal elements correspond to links between the nodes and there are $2^6 = 64$ different three-node substructures, as shown in Figure 1.

A lot of literature about networks is focused only on connected substructures (Milo et al. 2002; Stouffer et al. 2007). If one considers a network of only three nodes and one of them (i) is isolated, i.e., $M_{ij} = M_{ji} = 0 \; \forall \; j \neq i$, then this isolated node has no effect on the others and only the connected nodes are important. But the consideration of only three-node substructures of larger networks is a rather rough limitation. If we would study substructures with one more node, then some of the previously ignored isolated nodes could be not isolated anymore and could play an important role in the functioning of the network. Therefore, we include substructures with isolated nodes in our analysis, because their frequencies are also a relevant measure of ordered networks.

Usually, the diagonal elements of M are ignored, too, but as we have pointed out in the introduction, self-links are important in food webs. We use the diagonal elements of M to distinguish eight configurations, corresponding to three cannibalistic links that can be either present or absent (Figure 2). This leads to a total of 512 different three-node substructures. We index them using (k, m) indices, where k (given in binary format for convenience, see Figure 2) is the cannibalistic configuration and m (given in decimal format) refers to the configuration of links between the species (Figure 1).
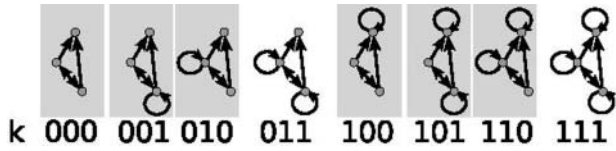
Figure 2. All substructures of Figure 1 have 8 possible configurations describing the presence and absence of self-links. It is illustrated for substructure 15. Shaded rectangles mark the substructures that are prohibited in both the original and the generalised niche model.

To illustrate the properties of the spectrum of ordered substructures and to test our numerical algorithms, we consider here a modified version of the directed random graph discussed in more detail by Paulau et al. (2015). Assume that we have a set of N indexed nodes and the directed link between each two of them has the probability $p\uparrow$, if the source node index is smaller than target node index, and $p\downarrow$ for an inversely directed link. In addition each node is cannibalistic (self-linked) with probability p_s. Analogously to (Paulau et al. 2015), one can define the conditional probabilities for any ordered three-node substructure. For example, the probability $P_{k,m}$ of substructure $k = 011$ and $m = 15$ in Figure 2 is

$$P_{011,15} = p_\uparrow (1-p_\downarrow) p_\uparrow (1-p_\downarrow) p_\uparrow p_\downarrow p_s p_s (1-p_s), \quad (1)$$

where the first two multipliers describe the link between middle and top nodes, the third and fourth multipliers describe the link between bottom and top nodes, the fifth and sixth multipliers describe the double link between bottom and middle nodes. Finally, the last three multipliers describe the presence or absence of cannibalistic links. The number of all possible different combinations of ordered triplets in a network with N nodes is the binomial coefficient $C_3^N = \frac{1}{6} N(N-1)(N-2)$ and hence the mean frequency of each substructure can be defined as

$$\eta_{k,m} = P_{k,m} C_3^N. \quad (2)$$

We numerically generated a large number of initialisations of the directed random graph with cannibalistic links. Our counting algorithm allows us to compute the mean spectrum of ordered substructures numerically. The

last is in perfect agreement with the analytical prediction, Equation (2) (see Figure 3, this figure is given to demonstrate the agreement of analytical and numerical results, rather than to distinguish densities of every separate substructure). We would like to note here, that in the directed random graph the probabilities $P_{k,m}$ do not depend on the size of the network, while frequencies $\eta_{k,m}$ do depend.

Three-node substructures of food-web models and empirical data

One of the prerequisites of food-web models to be able to reproduce empirical food-web topologies is that the niche values of the species form a totally ordered set (Stouffer et al. 2005). Very simple early models like the cascade model (Cohen & Newman 1985) comply with this, but also more recent and complex models like the niche model (Williams & Martinez 2000) assume the ordering of the species. The cascade model constrains predators to feed only on prey with a lower niche index than itself, which prohibits every substructure with an upwards arrow in Figure 1, i.e., there are only eight allowed substructures (the first and fifth columns of the figure). One of the main improvements of the niche model over the cascade model is that it allows for the possibility of upward links. However, the niche model assumes that a predator species preys on all species from a contiguous interval on the niche axis, and the centre of this interval is constrained to be not higher than the predator's niche value. Due to this constraint, a predator that feeds on a prey with higher niche index is for example always assumed to be a cannibal. For three species i, j, k with ordering $i < j < k$, a substructure is prohibited due to the intervality constraint if at least one of the following conditions is fulfilled:

$$M_{ik} = 1 \text{ and } (M_{ii} = 0 \text{ or } M_{ij} = 0) \quad (C1)$$

$$M_{ij} = 1 \text{ and } M_{ii} = 0 \quad (C2)$$

$$M_{jk} = 1 \text{ and } M_{jj} = 0 \quad (C3)$$

$$M_{ki} = 1 \text{ and } M_{kk} = 1 \text{ and } M_{kj} = 0. \quad (C4)$$

The first condition prohibits substructures where the bottom species feeds on the top species but not on the intermediate species or itself, the second condition prohibits substructures where the bottom species feeds on the
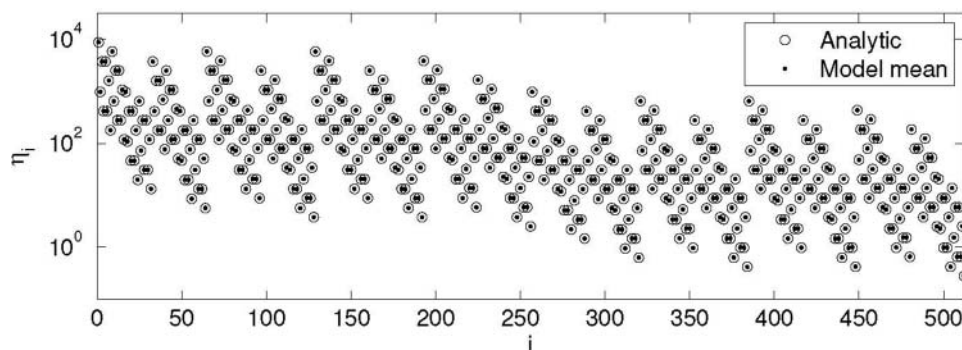

Figure 3. The spectrum of the directed random graph with cannibalistic links. Circles − analytical prediction, dots − numerical results obtained from 40,000 initialisations of the random graph with $N = 100$, $p_\uparrow = 0.3$, $p_\downarrow = 0.4$, and $p_s = 0.1$. The index i is the decimal form of binary number formed by 0s and 1s of the adjacency matrix.

intermediate species but not on itself, the third condition prohibits substructures where the intermediate species feeds on the top species but not on itself, and the fourth condition prohibits substructures where the top species preys on the bottom species and on itself but not on the intermediate species. The generalised niche model (Stouffer et al. 2006) was introduced as an interpolation between the niche model and the generalised cascade model that, in contrast to the niche model, has no constraints regarding diet contiguity, but prohibits upward feeding links. To this end, a parameter $c \in [0, 1]$ is introduced that reduces the contiguous feeding range of a predator. To correct for the decreased expected number of prey, a corresponding number of prey species is selected at random from the pool of species with a lower niche index than the predator that are not already prey of the predator. This removes the diet-contiguity constraint for downward links, i.e., condition (C4), but substructures that fulfil either of the conditions (C1)−(C3) are prohibited in the generalised niche model, too.

With these conditions, we can compute the binary spectra of allowed and prohibited three-node substructures in the niche model and the generalised niche model (Figure 4(a) and 4(b)). Of the 512 potential substructures, only 168 are allowed in the niche model and only 192 are allowed in the generalised niche model. Numerical simulations of the two models (Figure 4(c) and (d)) confirmed the analytical predictions for the binary spectra, but several of the allowed substructures were found to occur extremely rarely in the niche model (e.g. substructure ($k = 111$, $m = 11$)).

Natural feeding relations also underly some constraints, although they may be not as strict as in the niche model algorithms. To determine whether the substructures that are prohibited by the two niche model variants occur in empirical food webs, we evaluated 63 food webs from

different habitat types that we obtained from a large food-web database (Riede et al. 2010; Digel et al. 2014). Only food webs for which body masses of all species were available were used. Species numbers in these food webs ranged from 26 to 492. The food webs in our analysis included 21 river or stream food webs, 19 lake food webs, 15 terrestrial food webs, 5 marine food webs, and 3 estuary food webs.

Prior to computing the spectrum of three-node substructures, we ordered the food webs according to the body masses of the species (with the lowest index for the lightest species). This was not always possible unambiguously because in some webs species with identical body masses (within the limits of experimental accuracy) were present. Of all possible three-node substructures we found that all but one occur in the empirical food webs (the exception is substructure (101,45)). Three-hundred and forty three (319) of the 511 present substructures are prohibited in the (generalised) niche model (see Figure 5). The niche model provides qualitatively good agreement with experimental webs for some properties such as the fraction of top species or omnivore species, as well as for Z-scores of motifs (Stouffer et al. 2007); however, the frequencies of substructures of empirical food webs are often (e.g. for the most frequently occurring connected substructure (000, 48), see Figure 6 and Paulau et al. (2015)) more than two standard deviations away from the mean of the niche-model prediction. Some limitations of the niche model are discussed in (Williams & Martinez 2008), and more recently other variants of the niche model have been proposed that relax the assumption of diet contiguity. The latter include the extended generalised niche model (Capitán et al. 2013) and the probabilistic niche model (Williams & Purves 2011), which both allow for non-contiguous diets both below and above a predator's niche position. This will apparently resolve the problem of
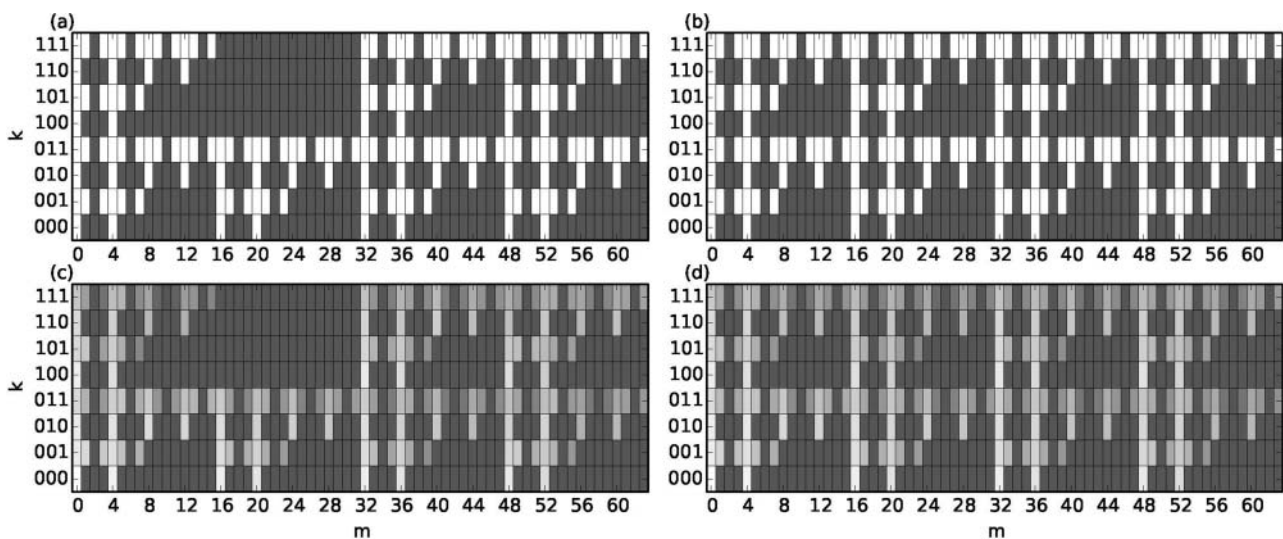

Figure 4.   Spectra of three-node substructures in the niche model (a) and (c) and the generalised niche model (b) and (d). (a) and (b) Substructures that appear with nonzero (zero) probability are marked with white (grey) boxes. (c) and (d) Cumulative spectra in logarithmic representation ($\log(1 + \eta_{km})$) of 10,000 initialisations of both niche model variants with $N = 100$ species and connectance $C = 0.1$. In the generalised niche model, the factor that reduces the contiguous feeding range of predators is set to $c = 0.8$. Dark grey corresponds to zero probability, white corresponds to maximal probability.
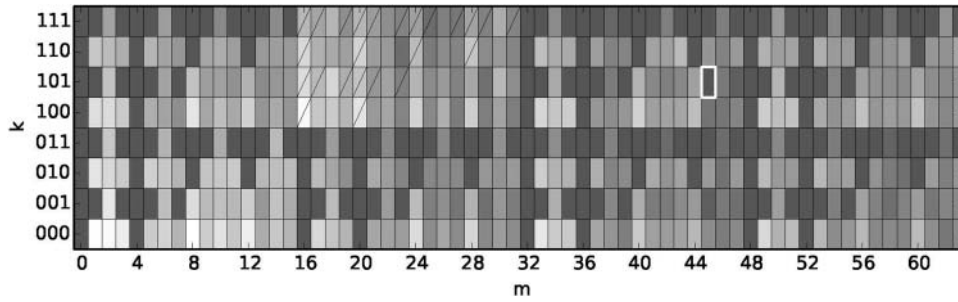
Figure 5. Cumulative spectrum of empirical food webs in logarithmic representation ($\log(1 + \eta_{km})$). Substructures that are prohibited in both variants of the niche model but present in the empirical data are emphasised. Substructures that are allowed in the niche model or that occur with zero density are marked by dark grey colour, and substructures that are allowed in the generalised niche model but prohibited in the niche model are crossed out with a single line. The only substructure that is not observed in the empirical data-set, (101,45), is emphasised with a white frame. Dark grey corresponds to zero occurrence $\eta_{k,m}$, white corresponds to maximal occurrence $\eta_{k,m}$. All substructures that are allowed in the models are also observed in the empirical data (cf. Figure 6).

prohibited substructures, while it maintains to be a challenge to have all frequencies of substructure within ± 2 standard deviations around the mean of the model prediction.

The empirical food webs have relatively small connectance (median $C \approx 0.1$); therefore, the substructures with isolated nodes have very high frequencies. The trivial substructure ($k = 000$, $m = 0$) occurs approximately 10 times more often than any other substructure and nearly all connected substructures may look like quantitatively unimportant. Therefore, we discuss quantitative details only for connected substructures. In total, 3,702,652 connected substructures exist in the empirical food webs. Of these, 31.3% are prohibited in the niche model and 27.9% are prohibited in the generalised niche model. The three quantitatively most important of them, (000,48), (000,20), and (100,48), are allowed in both niche model variants, but of the 12 substructures that appear with a frequency of at least 0.1 relative to substructure (000,48), 5 (4) are prohibited in the (generalised)
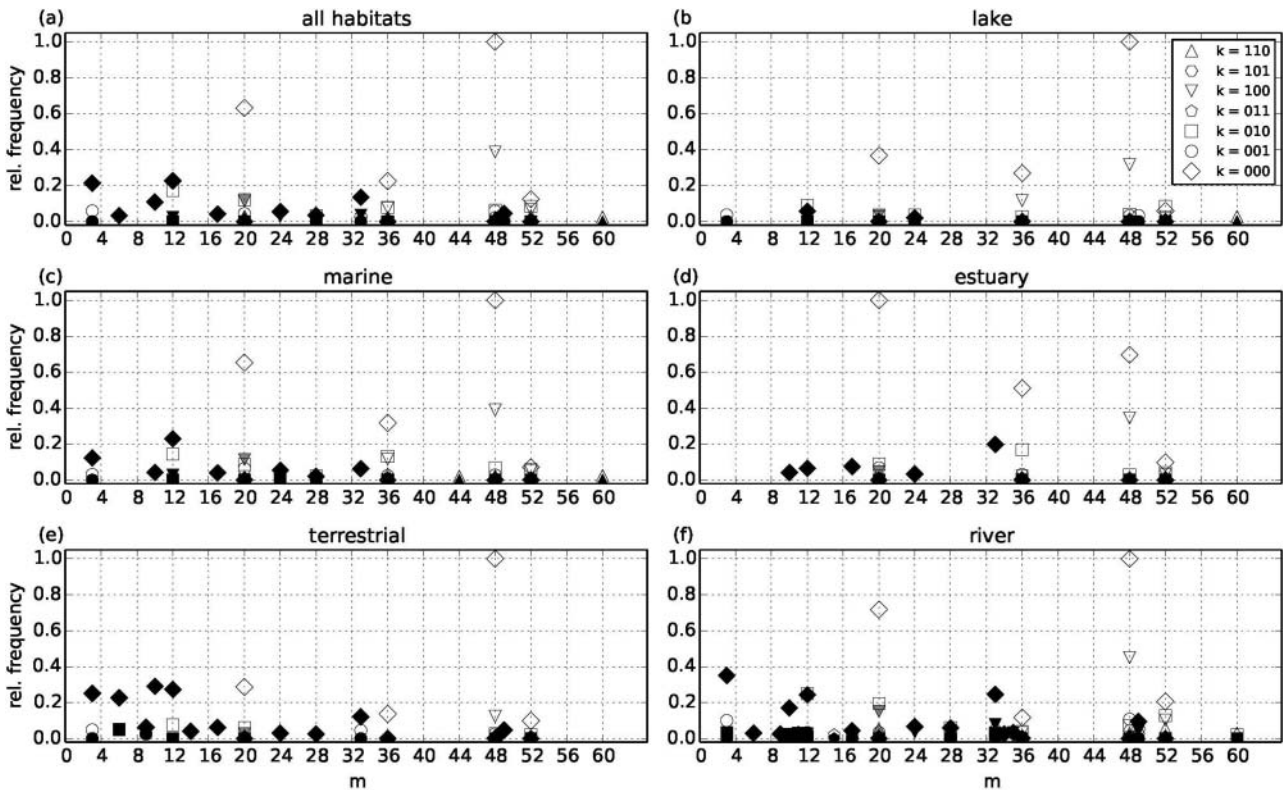
Figure 6. Quantitative spectra of connected three-node substructures in (a) the entire data-set of 63 natural food webs, (b) lake food webs, (c) marine food webs, (d) estuary food webs, (e) terrestrial food webs, and (f) river or stream food webs. Substructures that are prohibited in the niche model and in the generalised niche model are marked with black symbols, substructures that are allowed in the generalised niche model but prohibited in the niche model are marked with grey symbols, and substructures that are allowed in both models are marked with open symbols. Substructures that appear with relative frequency < 0.02 are omitted in this plot. Frequencies are normalised to the occurrence of the most frequent connected substructure, (000,20) in estuary food webs and (000,48) in all other cases.

niche model (Figure 6a). The only connected substructure of high quantitative importance that is allowed by the generalised niche model but prohibited by the original niche model is (100,20).

When the empirical food webs are grouped according to their habitat type, considerable differences can be found in the fraction of substructures that are prohibited by the two model algorithms (Figure 6(b)−6(f)). It ranges from 8.9% (7.2%) in lake food webs up to 37.7% (33.9%) in river food webs and even 45.0% (44.0%) in terrestrial food webs (numbers in parentheses refer to the generalised niche model).

Discussion

In ecological networks such as food webs, self-links have a very specific meaning that cannot be ignored. This has consequences for the spectrum of three-node substructures in these networks, which consists of 512 different elements, including 432 connected substructures. The niche model is a simple, but nevertheless highly successful and widely accepted model for the prediction of food web structures. Here we have shown that due to the assumption of contiguous feeding intervals, which is a central building block of the niche model, most of the sub structures cannot occur in the niche model. This is in sharp contrast with the frequent occurrence of some of these prohibited substructures in empirical food webs.

The problem of diet contiguity in the niche model has raised prior criticism (Cattin et al. 2004) and several variants of the niche model have been developed specifically to address this issue. The generalised niche model is an example for this, as it allows to create model food webs with a tunable bias towards diet contiguity. It may, therefore, seem surprising that the generalised niche model prohibits almost as many substructures as the original niche model. The reason is that the generalised niche model lifts the intervality constraint only for downward links where the prey has a lower niche index than the predator.

The relatively small advantage of the generalised niche model over the original one indicates that in order to accurately predict the full spectrum of ordered three-node substructures in natural food webs, removing the intervality constraint alone might not be sufficient. It seems to be necessary to also break the strict connection between feeding on prey with a higher niche position and cannibalism that is built into both the original and the generalised niche model. Considering that cannibalism likely occurs between differently sized individuals of the same species, there is no actual mechanism that makes such a connection between these ecologically quite different processes necessary. In fact, the high frequencies of occurrence of substructures with upward feeding links but no cannibalism suggest that there is no such connection. In more recent variants of the niche model like the probabilistic niche model (Williams & Purves 2011), no diet contiguity at either end of the feeding range is assumed. This model therefore does not prohibit any substructures, but it still assumes a positive correlation between cannibalism

and upward feeding links. Whether or not this is justified could be revealed by a quantitative comparison of the predicted and the empirically observed spectrum of three-node substructures.

The quantitative evaluation of the spectrum of (connected) three-node substructures in empirical food webs revealed that approximately 30% of all substructures are prohibited in both the original and the generalised niche model. Between different habitat types, this fraction of prohibited substructures varied considerably and ranged from less than 9% of the three-node substructures found in lake food webs up to 45% of those found in terrestrial food webs. These differences might indicate that in terrestrial ecosystems body mass is not as important for generating feeding hierarchies as it is in lake ecosystems. In Brose et al. (2006) similar results have been found and it was hypothesised that this is due to physical and morphological constraints on trophic interactions. For example, if a lack of hard surfaces (as in pelagic systems) requires predators to consume their prey in one piece, gape limitation determines the maximal prey size. However, this should affect river and stream food webs in a similar way as lake food webs, which is in contrast to our finding that more than 33% of the connected three-node substructures in river or stream food webs are prohibited by the model algorithms. At this point, we, therefore, cannot rule out the possibility that methodological differences in the assembly of the food webs are responsible for the different fractions of prohibited substructures in food webs from different habitats. The lake food webs in our database were on average the smallest networks. This might be due to lower taxonomic resolution or less complete sampling, which makes direct comparison of the quantitative spectra of food webs from different habitats difficult.

The extent of the disagreement between predictions by the two niche model variants and relative frequency of substructures in empirical food webs still might in part be due to inaccurate data. In a number of food webs, several species had identical body masses, which in reality should not be the case. This lead to some ambiguity in the order of species we used to calculate the spectrum of substructures. In our data-set of empirical food webs, 31.2% of the species had a non-unique body mass in their respective food webs. While this seems like a lot, we calculated that only 2.3% of all three-node substructures contained species that could not be ordered unambiguously. For the results presented in this manuscript, we, therefore, decided to use the empirical data 'as is', i.e., the order of species with identical body mass was set randomly. We also tried to order the species in a conservative way with respect to prohibited substructures. Whenever a unique feeding hierarchy existed between species with identical body mass (e.g. species i feeds on species j, but not vice versa) we assumed that i had a higher index (niche position) than j. Because the majority of the species with non-unique body mass are basal species between which such a hierarchy cannot exist, this decreased the fraction of three-node substructures with two or three species with

identical body mass only marginally to 2.1%. A further literature search for more accurate body-mass data could further attenuate this issue, but limited taxonomic resolution of the food webs, especially at the basal level, will also limit the success of such an effort.

Our results might also be affected by another aspect of limited resolution in the empirical data. Nodes in food webs often represent average individuals of a population (Digel et al. 2014). This means that a node summarises the feeding relations of individuals with different body masses, e.g. due to different developmental status. Feeding links between (on average) small predator and large prey species could thus actually occur only between the largest individuals of the predator species and the smallest individuals of the prey species. If the size ranges of the two species overlap, this would reverse the direction of the feeding link relative to the niche axis and could turn a prohibited substructure into an allowed one. Given the prevalence of ontogenetic diet shifts in natural populations (Werner & Gilliam 1984), resolving the size or stage dependency of feeding interactions in both models and empirical data thus seems advisable (see (Rudolf & Lafferty 2011), for an example of a modelling study that resolves the stage dependency of feeding links).

Finally, our results have implications for the rich body of literature that studies the population dynamics of small modules of (usually two to four) interacting populations (McCann et al. 1998; Hastings & Powell 1991; Polis & Holt 1992; Gjata et al. 2012). Due to the allometric relationship between body mass and metabolic rates (Brown et al. 2004), the dynamics of interacting populations depends on their relative niche positions (i.e., predator−prey body-mass ratios, Yodzis and Innes 1992) and stable configurations that allow for the persistence of all species are usually found if predators are larger than their prey (Otto et al. 2007; Kartascheff et al. 2010; Heckmann et al. 2012). Most of the three-node substructures that are prohibited by the niche model include links between a small predator and a large prey, and our results suggest that these substructures are more common in natural food webs than previously assumed. For the three-species food chain (substructures $k = 000$, $m = 6, 9, 17, 24, 34$, and 36), it has been shown that almost all instances that are found in a number of empirical food webs have predator−prey body-mass ratios that allow for coexistence of all three species in an isolated food chain (Otto et al. 2007). It might be interesting to see whether this also applies for other three-node substructures, or if additional mechanisms that promote species coexistence (such as coupling to the surrounding food web, or cannibalistic links) are required.

Disclosure statement
No potential conflict of interest was reported by the authors.

ORCID
Christian Guill http://orcid.org/0000-0002-5955-9998

References

Albert R, Barabási AL. 2002. Statistical mechanics of complex networks. Rev Mod Phys. 74:47−97.

Binzer A, Brose U, Curtsdotter A, Eklöf A, Rall BC, Riede JO, de Castro F. 2011. The susceptibility of species to extinctions in model communities. Basic Appl Ecol. 12:590−599.

Brose U, Jonsson T, Berlow EL, Warren PH, Banasek-Richter C, Bersier LF, Blanchard JL, Brey T, Carpenter SR, Blandenier M-FC, et al. 2006. Consumer-resource body-size relationships in natural food webs. Ecology. 87:2411−417.

Brown JH, Gillooly JF, Allen AP, Savage VM, West GB. 2004. Toward a metabolic theory of ecology. Ecology. 85:1771−1789.

Camacho J, Stouffer DB, Amaral, LAN. 2007. Quantitative analysis of the local structure of food webs. J Theor Biol. 246:260−268.

Capitán JA, Arenas A, Guimerà R. 2013. Degree of intervality of food webs: from body- size data to models. J Theor Biol. 334:35−44.

Cattin MF, Bersier LF, Banasek-Richter C, Baltensperger R, Gabriel JP. 2004. Phylogenetic constraints and adaptation explain food-web structure. Nature. 427:835−839.

Claessen D, de Roos AM, Persson, L. 2004. Population dynamic theory of size-dependent cannibalism. Proc Biol Sci. 271:333−340.

Cohen JE, Newman CM. 1985. A stochastic theory of community food webs: I. Models and aggregated data. Proc Biol Sci. 224:421−448.

Cohen JE, Stephens DW. 1978. Food Webs and Niche Space. Princeton (NJ): Princeton University Press.

Digel C, Curtsdotter A, Riede JO, Klarner B, Brose U. 2014. Unravelling the complex structure of forest soil food webs: higher omnivory and more trophic levels. Oikos. 123:1157−1172.

Drossel B, McKane AJ. 2005. Modelling food webs. In: Bornholdt S, Schuster HG, editors. Handbook of graphs and networks: from the genome to the internet. Weinheim: Wiley-VCH Verlag GmbH & Co. KGaA; p. 218−247.

Dunne JA, Williams RJ, Martinez ND. 2002a. Food-web structure and network theory: the role of connectance and size. Proc Natl Acad Sci USA. 99:12917−12922.

Dunne JA, Williams RJ, Martinez ND. 2002b. Network structure and biodiversity loss in food webs: robustness increases with connectance. Ecol Lett. 5:558−567.

Elton CS. 1927. Animal ecology. New York (NY): Macmillan Co.

Fox LR. 1975. Cannibalism in natural populations. Ann Rev Ecol Syst. 6:87−106.

Gjata N, Scotti M, Jordán F. 2012. The strength of simulated indirect interaction modules in a real food web. Ecol Complex. 11:160−164.

Hastings A, Powell T. 1991. Chaos in a three species food chain. Ecology. 72:896−903.

Heckmann L, Drossel B, Brose U, Guill C. 2012. Interactive effects of body-size structure and adaptive foraging on food-web stability. Ecol Lett. 15:243−250.

Jeong H, Tombor B, Albert R, Oltvai ZN, Barabási AL. 2000. The large-scale organization of metabolic networks. Nature. 407:651−654.

Kartascheff B, Heckmann L, Drossel B, Guill C. 2010. Why allometric scaling enhances stability in food web models. Theor Ecol. 3:195−208.

Kéfi S, Berlow EL, Wieters EA, Navarrete SA, Petchey OL, Wood SA, Boit A, Joppa LN, Lafferty KD, Williams RJ, et al. 2012. More than a meal... integrating non-feeding interactions into food webs. Ecol Lett. 15:291−300.

McCann K, Hastings A, Huxel GR. 1998. Weak trophic interactions and the balance of nature. Nature. 395:794−798.

Milo R, Shen-Orr S, Itzkovitz S, Kashtan N, Chklovskii D, Alon U. 2002. Network motifs: simple building blocks of complex networks. Science. 298:824−827.

Newman MEJ. 2003. The structure and function of complex networks. SIAM Rev. 45:167−256.

Otto SB, Rall BC, Brose U. 2007. Allometric degree distributions facilitate food-web stability. Nature. 450: 1226−1229.

Paulau P, Feenders C, Blasius B. 2015. Extended structural analysis of ordered networks. (Unpublished manuscript, available upon request from P. Paulau.)

Persson L, de Roos AM, Claessen D, Bystrom P, Lovgren J, Sjogren S, Svanback R, Wahlström E, Westman E. 2003. Gigantic cannibals driving a whole-lake trophic cascade. Proc Natl Acad Sci USA. 100:4035−4039.

Polis GA. 1981. The evolution and dynamics of intraspecific predation. Ann Rev Ecol Syst. 12:225−251.

Polis GA, Holt RD. 1992. Intraguild predation: the dynamics of complex trophic interactions. Trends Ecol Evol. 7:151−154.

Riede JO, Rall BC, Banasek-Richter C, Navarrete SA, Wieters EA, Emmerson MC, Brose U. 2010. Scaling of food-web properties with diversity and complexity across ecosystems. Adv Ecol Res. 42:139−170.

Rudolf VHW, Lafferty KD. 2011. Stage structure alters how complexity affects stability of ecological networks. Ecol Lett. 14:75−79.

Stouffer DB, Camacho J, Guimera R, Ng CA, Amaral LAN. 2005. Quantitative patterns in the structure of model and empirical food webs. Ecology. 86:1301−1311.

Stouffer DB, Camacho J, Amaral LAN. 2006. A robust measure of food web intervality. Proc Natl Acad Sci USA. 103:19015−19020.

Stouffer DB, Camacho J, Jiang W, Amaral LAN. 2007. Evidence for the existence of a robust pattern of prey selection in food webs. Proc Biol Sci. 274:1931−1940.

Varshney LR, Chen BL, Paniagua E, Hall DH, Chklovskii DB. 2011. Structural properties of the *Caenorhabditis elegans* neuronal network. PLoS Comput Biol. 7:e1001066.

Werner EE, Gilliam JF. 1984. The ontogenetic niche and species interactions in size- structured populations. Ann Rev Ecol Syst. 15:393−425.

Williams RJ, Martinez ND. 2000. Simple rules yield complex food webs. Nature. 404:180−183.

Williams RJ, Martinez ND. 2008. Success and its limits among structural models of complex food webs. J Anim Ecol. 77:512−519.

Williams RJ, Purves DW. 2011. The probabilistic niche model reveals substantial variation in the niche structure of empirical food webs. Ecology. 92:1849−1857.

Yodzis P, Innes S. 1992. Body size and consumer resource dynamics. Am Naturalist. 139:1151−1175.

Research

The dynamics of food chains under climate change and nutrient enrichment

Amrei Binzer*, Christian Guill, Ulrich Brose and Björn C. Rall

*J. F. Blumenbach Institute of Zoology and Anthropology, Georg-August University Göttingen,
Göttingen, Germany*

Warming has profound effects on biological rates such as metabolism, growth, feeding and death of organisms, eventually affecting their ability to survive. Using a nonlinear bioenergetic population-dynamic model that accounts for temperature and body-mass dependencies of biological rates, we analysed the individual and interactive effects of increasing temperature and nutrient enrichment on the dynamics of a three-species food chain. At low temperatures, warming counteracts the desta-bilizing effects of enrichment by both bottom-up (via the carrying capacity) and top-down (via biological rates) mechanisms. Together with increasing consumer body masses, warming increases the system tolerance to fertilization. Simultaneously, warming increases the risk of starvation for large species in low-fertility systems. This effect can be counteracted by increased fertilization. In combination, therefore, two main drivers of global change and biodiversity loss can have positive and negative effects on food chain stability. Our model incorporates the most recent empirical data and may thus be used as the basis for more complex forecasting models incorporating food-web structure.

Keywords: global warming; metabolism; paradox of enrichment; fertilization;
biodiversity loss; temperature

1. INTRODUCTION

Current changes in our planet's ecosystems have the potential to cause species extinctions [1]. The changes in nutrient availability (enrichment) and temperature (climate warming) were identified by the Millennium Ecosystem Assessment as two major direct drivers of biodiversity loss [2]. They predict the impact of both these drivers to increase very rapidly in all biomes [3, p. 9]. To predict accurately the community effects of enrichment and warming, it is important to understand their interactive impact on biological rates. This helps in developing community protection measures and in conserving important ecosystem functions.

Both enrichment and warming have wide-ranging implications for food-web and ecosystem structure, many of which are mediated by changes in population dynamics [4–11]. Rosenzweig [6] analytically investigated the effect of increased energy input on the dynamics of a predator–prey system and coined the term 'paradox of enrichment': enrichment drives a predator–prey system from stable equilibria into oscillations and finally into extinction when population minima hit extinction boundaries [6]. This has recently been generalized as the principle of energy flux: any process increasing energy fluxes relative to consumer loss rate will destabilize systems by shifting biomass up the trophic levels [12]. This moves the isoclines of the

species towards unstable equilibria. Interestingly, when consumer mass systematically increases with trophic levels [13], the destabilizing effects of enrichment are ameliorated [11].

Warming has profound effects on biological rates such as organism metabolism [14–16], growth [17], feeding [18,19] and death [20]. However, the interplay of these physiological effects at the population level is not yet entirely clear, and there are several possibilities. Warming might simply accelerate population dynamics. In a seminal study of population dynamics, Vasseur & McCann [5] found that increasing temperature destabilizes systems and increases the amplitudes of oscillations. These findings are based on assumptions such as temperature invariance of the system carrying capacity (the maximum biomass the system can support) and the consumer's half saturation density. While the former is certainly not supported by empirical data [21], the latter characterizes the consumer's efficiency at attacking resources and more recent studies showed that it is likely to change with temperature [19,22,23]. Additionally, Vasseur & McCann [5] assumed that in most natural communities, the species ingestion increases more with warming than does their metabolism. However, feeding interactions among terrestrial and marine invertebrates indicate the opposite [18,19,24]. These studies found that warming increases species metabolism more strongly than ingestion rates. The decreasing energetic efficiencies (the ratio of ingestion rate to metabolism) lead to increasing energetic restrictions for predators and decreasing predator biomasses. This stabilizes the system dynamics and

reduces biomass oscillations. These studies emphasize the possibility of predator starvation at high temperatures when metabolism exceeds ingestion rates [18,19]. However, dynamic model analyses of these empirical patterns are still lacking.

Here, we fill this void by developing a nonlinear bioenergetic population-dynamic model that includes empirical body-mass and temperature dependencies for the major biological rates affecting population dynamics such as carrying capacity [21], production [17], metabolism [16] and functional response parameters [25]. With this model, we numerically investigated the solitary and interactive effects of two major drivers of global change, enrichment and warming, on the population dynamics of a three-species food chain. We were particularly interested in the following questions: (i) What are the individual effects of enrichment and warming on the dynamics of the food chain? (ii) What are the combined effects of enrichment and warming on these dynamics? and (iii) Does the community size structure with systematically increasing body mass ratios influence these effects?

2. METHODS

The bioenergetic dynamic model used is based on Yodzis and Innes' [26] consumer–resource model and is updated with allometric coefficients and temperature dependencies of the biological rates. In the three-species food chain, the basal species (B) is fed on by the intermediate species (I) which in turn is consumed by the top species (T). The biomass changes of the species ($\dot{B}_B$, $\dot{B}_I$ and $\dot{B}_T$, respectively) are described by the following differential equations:

$$\dot{B}_B = r_B G_B B_B - B_I f_{IB},$$ (2.1)

$$\dot{B}_I = e_{IB}(B_I f_{IB}) - B_T f_{TI} - x_I B_I$$ (2.2)

$$\text{and} \quad \dot{B}_T = e_{TI}(B_T f_{TI}) - x_T B_T.$$ (2.3)

Here, r_B is the basal species' mass and temperature-specific maximum growth rate, G_B is the basal species' logistic growth term and B_B is its population biomass density. The functional responses f_{IB} and f_{TI} describe the feeding dynamics of the feeding links in the food chain. The assimilation efficiencies (efficiency of conversion of prey biomass into predator biomass), e_{IB} and e_{TI}, are both set to 0.85 because both species are carnivores [26]. The metabolism of the intermediate and top species, x_I and x_T, also depend on their masses and the temperature of the system.

We used a logistic growth term where the potential growth of the population depends on its current population biomass and its body-mass and temperature-dependent carrying capacity, K_B:

$$G_B = \left(1 - \frac{B_B}{K_B}\right).$$ (2.4)

The functional response, f_{ji}, describes the feeding dynamics between consumer j and its prey i. It depends on the consumer's maximum consumption rate when feeding on species i, y_{ji}, which depends on the body-masses of both species j and i and the temperature, the Hill exponent, h, which determines the

shape of the function and the half saturation density B_0. B_0 gives the prey population density at which half the maximum consumption of the consuming species is reached and depends on the body-masses of species j and i and the temperature of the system:

$$f_{ji} = \frac{y_i B_i^h}{B_{0_{ji}}^h + B_i^h}.$$ (2.5)

The mass and temperature dependencies of the maximum growth rate of the basal species r_B (s^{-1}) is calculated as follows:

$$r_B = e^{I_r} m_B^{s_{rB}} e^{Ea_r(T_0 - T/kTT_0)}.$$ (2.6)

Here, e^{I_r} is the rate-specific constant, calculated for a species' body mass of 1 g and a temperature of 20°C (= 293.15K). Its value is modified by the second term, the body-mass dependency, expressed by the mass of the species m and a rate-specific scaling coefficient, s. The term of the temperature dependency is an extended notation of the Arrhenius equation, where Ea is the activation energy (eV), T_0 the normalization temperature, T the temperature of the system and k (eV K^{-1}) the Boltzmann constant.

The mass and temperature dependent metabolism of the intermediate and top species x_i (s^{-1}) and the carrying capacity of the basal species K_B (g m^{-2}) are calculated accordingly:

$$x_i = e^{I_x} m_i^{s_{xi}} e^{Ea_x(T_0 - T/kTT_0)}.$$ (2.7)

and

$$K_B = e^{I_K} m_B^{s_{KB}} e^{Ea_K(T_0 - T/kTT_0)}.$$ (2.8)

Both terms of the functional response, the maximum ingestion, y_{ji}, and the half saturation density, $B_{0_{ji}}$, depend not only on the temperature of the system and the body mass of species i, but also on the body mass of its predator j:

$$y_{ji} = e^{I_y} m_j^{s_{yj}} m_i^{s_{yi}} e^{Ea_y(T_0 - T/kTT_0)}$$ (2.9)

and

$$B_{0_{ji}} = e^{I_{B_0}} m_j^{sB_{0j}} m_i^{sB_{0i}} e^{Ea_{B_0}(T_0 - T/kTT_0)}.$$ (2.10)

Analyses of extensive databases [25] revealed additional dependencies of the parameters of the functional response. To understand these, it is best to refer to the traditional Holling type II functional response model [27]:

$$f_{ji} = \frac{\alpha_{ji} B_i^h}{(1 + \alpha_{ji} t h_{ji}) B_i^h}.$$ (2.11)

Instead of using the maximum ingestion and half saturation density of the other notation (equation (2.5)), this uses α_{ji}, the attack rate of the consumer when it feeds on i, and the handling time, $t_{h_{ji}}$, the time the consumer needs to process one prey item before it can start looking for another one. The attack rate and the handling time both show a hump-shaped relationship with the body-mass ratio of the consumer and its prey. The exponential equations for these dependencies follow the same principle as

already introduced (see equations (2.6)–(2.10)):

$$\alpha_{\mathrm{m}ji} = e^{I_{am}+s1_{ai}\ln(m_j/m_i)+s2_{ai}(\ln(m_j/m_i))^2} \qquad (2.12)$$

and

$$th_{\mathrm{m}ji} = e^{I_{thm}+s1_{thi}\ln(m_j/m_i)+s2_{thi}(\ln(m_j/m_i))^2}. \qquad (2.13)$$

Here, I_m is the intercept, and the consumer–prey mass ratio has a twofold influence on the feeding parameters: the slope $s1$ is the ratio's scaling coefficient in its simple form, whereas $s2$ is the scaling coefficient for its quadratic form.

The handling time also displays a hump shape with temperature:

$$th_{\mathrm{T}ji} = e^{I_{thT}+s1_{thTi}T+s1_{thTi}T^2}. \qquad (2.14)$$

These additional scaling relationships of the functional response parameters can be incorporated into the equations for the maximum consumption and half saturation density by using the interrelation of the parameters of the two different notations of the functional response:

$$B_0 = \frac{1}{\alpha t_h}, \qquad (2.15)$$

and

$$y = \frac{1}{t_h}. \qquad (2.16)$$

This yields the following equations to express the body-mass and temperature scaling of the functional response parameters:

$$y_{ji} = e^{I_y} m_j^{s_{yj}} m_i^{s_{yi}} e^{Ea_y(T_0-T/kTT_0)} \frac{1}{th_{\mathrm{m}ji}} \frac{1}{th_{\mathrm{T}ji}}, \qquad (2.17)$$

and

$$B_{0ji} = e^{I_{B_0}} m_j^{sB_{0j}} m_i^{sB_{0i}} e^{Ea_{B_0}(T_0-T/kTT_0)} \frac{1}{\alpha_{\mathrm{m}ji} th_{\mathrm{m}ji}} \frac{1}{1 th_{\mathrm{T}ji}}. \qquad (2.18)$$

Inserting all equations accounting for the allometric and temperature scaling of the biological rates (equations (2.6)–(2.8), (2.17) and (2.18)) into the differential equations (2.1)–(2.3) yields a nonlinear bioenergetic population-dynamic model of a three-species food chain.

In this study, we modelled a food chain parametrized solely for invertebrates. Whenever possible, we incorporated values extracted from extensive empirical databases. These parameters represent a wide range of different species and ecosystem types. The scaling relationships for the biological rates and their sources are summarized in tables 1 and 2. Using these relationships yields a model with five free parameters: (i) the body mass of the basal species, (ii) the body-mass structure of the species in the food chain, (iii) the temperature of the system, (iv) the Hill coefficient shaping the functional response, and (v) the intercept of the carrying capacity (basic fertilization level). We used constants for the basal body mass (0.01 g) and the Hill coefficient (1, yielding type-II functional responses). A species was considered extinct and removed from the system when its biomass fell below

Table 1. The parameter values of the model's mass and temperature dependencies of the carrying capacity (K in g m^{-2}), from Meehan (2006) [21], growth (r in s^{-1}), from Savage *et al.* [17], maximum ingestion (y in s^{-1}), from Rall *et al.* [25], half saturation density (B_0 in g m^{-2}), from Rall *et al.* [25] and metabolism (x in s^{-1}), from Ehnes *et al.* [16]. Generally, the parameters scale with the body mass of the resource species (i) of the considered species pair; only the feeding parameters scale additionally with the body mass of the consumer species (j). The conversion factor used to transform the metabolism of the species from Joule per hour to s^{-1} was taken from Peters [28].

	K_i	r_i	y_{ji}	B_{0ji}	x_i
intercept (I)		-15.68	-9.66	3.44	-16.54
slope resource species i (s_i)	0.28	-0.25	0.45	0.2	-0.31
slope consumer species j (s_j)			-0.47	0.33	
activation energy (Ea)	0.71	-0.84	-0.26	0.12	-0.69

Table 2. The parameter values for the body-mass ratio and temperature-dependent hump shape of the functional response parameters, attack rate and handling time. The mass ratio and temperature dependencies of the attack rate (in m^{2}s^{-1}, mass dependency a_{m}) and handling time (in s, mass dependency th_{m}, temperature dependency th_{T}).

	a_{m}	th_{m}	th_{T}
intercept (I)	-1.81	1.92	0.5
slope term 1 ($s1$)	0.39	-0.48	-0.055
slope term 2 ($s2$)	-0.017	0.0256	0.0013

10^{-12} g m^{-2}. To investigate the individual and combined effects of enrichment and warming, we systematically varied the intercept of the carrying capacity (fertilization gradient, range from 1 to 20), temperature (range from 0°C to 40°C) and the size structure of the community in three levels: (i) all species equally sized (no size structure), or consumers (intermediate or top) are (ii) 10 times larger or (iii) 100 times larger than their resources. Every species started with a biomass density (g m^{-2}) equal to half the carrying capacity of the system with that particular enrichment and temperature combination. All simulations ran for 100 000 years and we recorded species biomasses and survival.

3. RESULTS
(a) *Single effects of enrichment and warming*
Increasing system fertility at a constant temperature increases the carrying capacity linearly (see figure 1*a*, for an example at 20°C). The growth rate, the relative metabolism of the species and its ingestion efficiency are not affected (figure 1*b–d*). However, there is an inverse proportional decrease in the half saturation density relative to the carrying capacity (figure 1*e*). This implies that fertilization increases the efficiency of
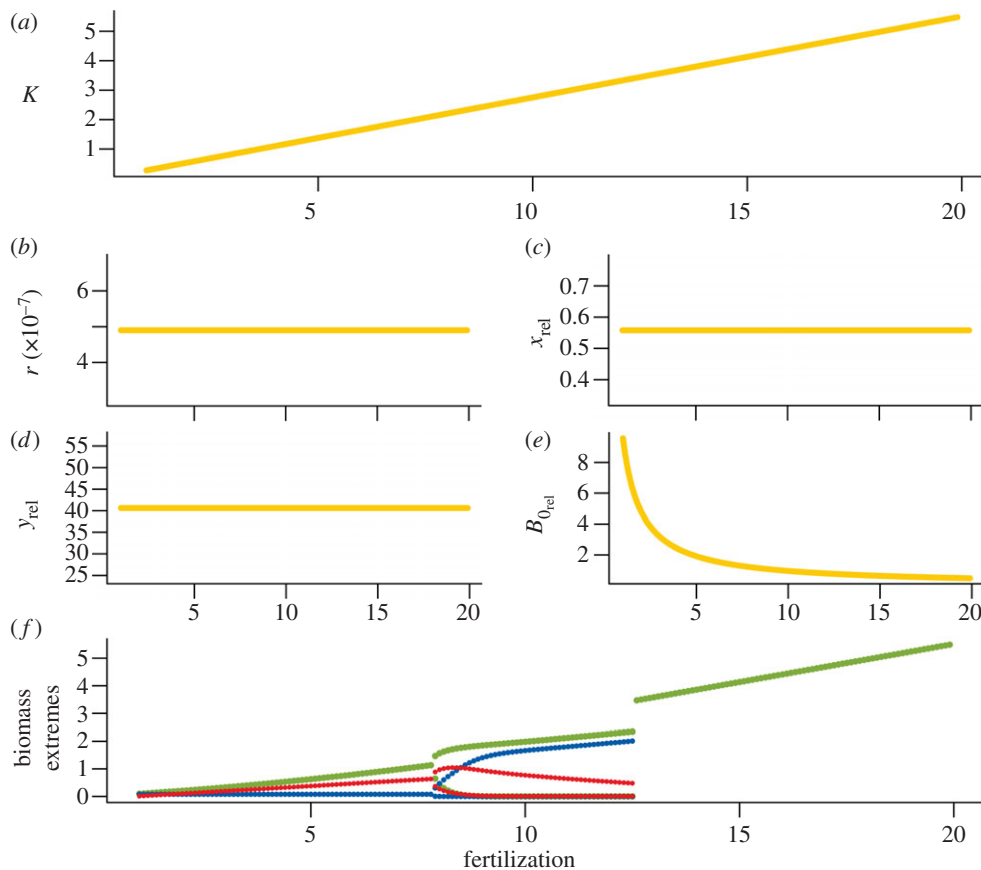
Figure 1. The mass- and temperature-dependent parameters of the model and a bifurcation diagram on a fertilization gradient. All parameter values are calculated for species with a body mass of 0.01 g at a temperature of 20°C. Shown are (*a*) the carrying capacity of the basal species (K (g m^{-2})), (*b*) the growth rate of the basal species (r (s^{-1})), (*c*) the metabolism of a consumer relative to the basal species' growth rate ($x_{\mathrm{rel}} = xr^{-1}$, dimensionless), (*d*) the maximum consumption of the species relative to their metabolism ($y_{\mathrm{rel}} = yx^{-1}$, dimensionless), (*e*) the species' half saturation density relative to the carrying capacity ($B_{0_{\mathrm{rel}}} = B_0 K^{-1}$, dimensionless) and (*f*) the biomass extremes of the three species (basal species: green; intermediate species: blue, top species: red, (g m^{-2}) on a fertilization gradient.

consumers in attacking resources. The bifurcation diagram shows the classical pattern of the 'paradox of enrichment'. At low fertility, all species coexist in an equilibrium at low densities; the equilibrium biomasses increase as fertility increases until the biomasses start cycling (figure 1*f*). The amplitude of these cycles increases until both the top and the intermediate species are driven into extinction and only the basal species survives, growing up to its carrying capacity. Increasing the fertility thus destabilizes the system. Both increasing bottom-up supply (figure 1*a*) and increasing top-down pressure (figure 1*e*) contribute to this progressive instability of the system.

Increasing the temperature of the system at a constant fertilization level decreases the carrying capacity exponentially (see figure 2*a* for an example at a fertilization value of 3). At the same time, the growth rate of the basal species increases (figure 2*b*). The metabolism of the species increases with temperature at a slower rate, resulting in a decrease in the relative metabolism (metabolism relative to basal production) of the species (figure 2*c*). The ingestion efficiency (ratio of ingestion and metabolism of a species) decreases with temperature: a species' metabolism increases more strongly with temperature than its ingestion (figure 2*d*). At the same time, the relative half saturation density of the species increases (figure 2*e*). This

results in a reduced flux of energy from the base to the top of the food chain. Warming has a marked effect on species biomasses (figure 2*e*). At low temperatures, only the basal species survives, growing up to its carrying capacity. At higher temperatures, the biomasses of the species oscillate with decreasing amplitudes along the temperature gradient. Finally, the system crosses over an inverse Hopf bifurcation and reaches equilibrium dynamics. A further temperature increase pushes the top species beyond the point where its ingestion cannot keep up with its metabolism and it dies as a result of a poor ingestion efficiency. At even higher temperatures, the same happens to the intermediate species and it also dies of starvation. Warming up the system thus stabilizes population dynamics, with a pattern of a reversed enrichment gradient, but very high temperatures can lead to the extinction of species.

(b) *Interactive effect of enrichment and warming*
The carrying capacity increases with fertilization and decreases with warming. This leads to the highest carrying capacities at combinations of high fertilization and low temperature and the lowest carrying capacities at combinations of low fertilization and high temperature (figure 3*a*). The number of species extant
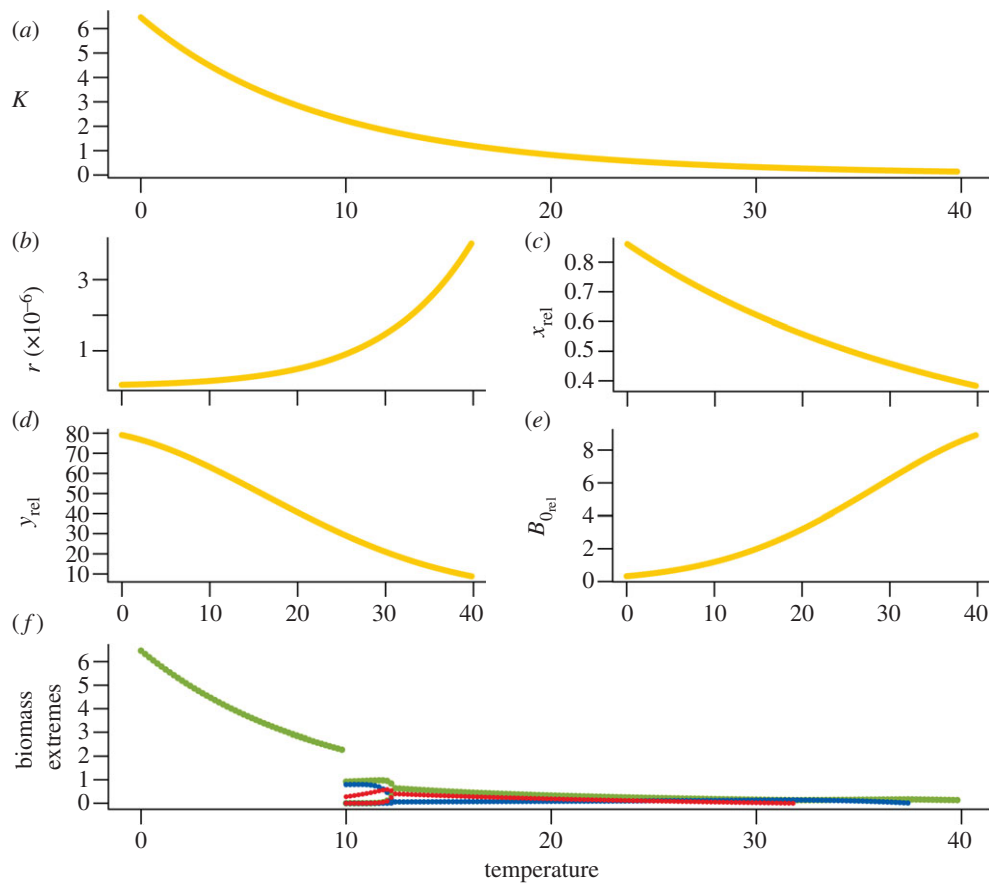
Figure 2. The mass- and temperature-dependent parameters of the model and a bifurcation diagram on a temperature gradient. All parameter values are calculated for species with a body mass of 0.01 g at an artificial fertilization level of 3. Shown are (*a*) the carrying capacity of the basal species (K (g m^{-2})), (*b*) the growth rate of the basal species (r (s^{-1})), (*c*) the metabolism of a consumer relative to the basal species' growth rate ($x_{rel} = xr^{-1}$, dimensionless), (*d*) the maximum consumption of the species relative to their metabolism ($y_{rel} = yx^{-1}$, dimensionless), (*e*) the species' half saturation density relative to the carrying capacity ($B_{0_{rel}} = B_0 K^{-1}$, dimensionless) and (*f*) the biomass extremes of the three species (basal species: green; intermediate species: blue, top species: red, (g m^{-2})) on a temperature gradient.

after 10 000 years across all combinations of fertilization and temperature is shown in the remaining panels of figure 3. In the scenario without body-mass structure, increasing fertility at low temperatures leads to species extinctions (figure 3*b*). Warming counteracts these detrimental effects of enrichment: the higher the temperature, the more the system can be fertilized before it loses species. The exceptions are high temperature, low fertility systems (upper left corner, same panel) where warming decreases the relative ingestion and increases the relative half saturation density of the consumer, reducing its efficiency. Consequently, first the top and then the intermediate species cannot ingest as much energy as they need to survive and become extinct. These extinctions at high temperatures are prevented by higher levels of fertilization. The lower two panels show the surviving species in a scenario with size structure (figure 3*c*, consumer 10 times larger than its prey; basal species: 0.01 g, intermediate species: 0.1 g, top species: 1 g; figure 3*d*, consumer 100 times larger than its prey; basal species: 0.01 g, intermediate species: 1 g, top species: 100 g). A three-species food chain with a structured body-size distribution, as is likely in nature [13,29], is generally less susceptible to the paradox of enrichment, and at low temperatures, the

extinctions are postponed to higher fertilization levels. The rescuing effect of warming that prevents extinctions caused by unstable oscillations is more pronounced in size-structured food chains, but the top and intermediate species are more vulnerable to starvation and, in the low fertility region, extinctions occur at lower temperatures. At high temperatures, it takes more fertilization to rescue the consumers from starvation due to lower ingestion efficiencies. Warming thus counteracts the paradox of enrichment at low temperatures but increases the starvation risk of species with higher trophic levels in high temperature, low fertility systems. At high temperatures, increasing fertility prevents consumer extinctions. The stabilizing and destabilizing effects of warming are more pronounced the larger consumers are.

Increasing enrichment increases the carrying capacity and destabilizes the biomass dynamics of the species. Extinctions occur when the carrying capacity exceeds a certain threshold. Warming, in contrast, reduces the carrying capacity and stabilizes species biomass dynamics. No further extinctions occur when the carrying capacity falls below a certain threshold. If both enrichment and warming would act entirely through the carrying capacity (i.e. via bottom-up effects), these thresholds would be the same across all
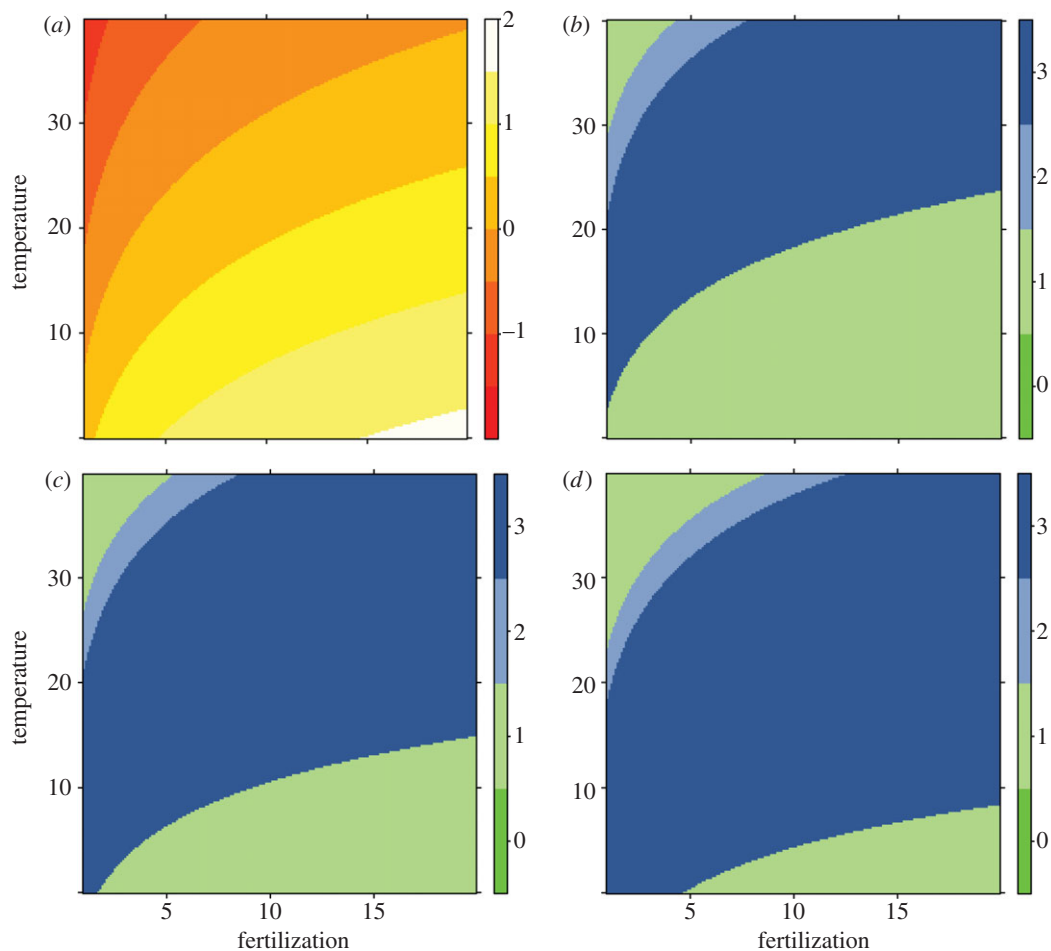
Figure 3. The $\log_{10}$ of the carrying capacity of the three-species system ((*a*), colour-coded, see colour key) and the number of species surviving after 10 000 years ((*b*): no body-mass structure; (*c*): consumer 10 times larger than its prey; (*d*): consumer 100 times larger than its prey, colour-coded, see colour-key) on a combined gradient of fertilization (*x*-axis) and temperature (*y*-axis (°C)).

temperature and fertilization combinations. A carrying capacity value above this threshold would lead to extinctions, whereas none would occur at lower carrying capacities. We refer to this threshold as the maximum feasible carrying capacity: it is the maximum carrying capacity the system can be subjected to without losing species. However, instead of being constant, the maximum feasible carrying capacity follows a nonlinear curve with temperature, with a maximum at approximately 38°C (figure 4, all curves). This indicates a 'top-down' component in the impact temperature has on the dynamics of the system. Additionally, applying a body-mass structure to the food-chain increases the maximum feasible carrying capacity (no structure: 1.47–5.24; consumers ten times larger: 3.65–20.42; consumers 100 times larger: 10.09–92.04). Warming operates via both bottom-up and top-down effects. This increases the maximum carrying capacity that the system can tolerate without losing species. Again, the effect of temperature is more pronounced in size-structured food chains.

4. DISCUSSION

Using a nonlinear bioenergetic population-dynamic model for a three-species food chain parametrized with the latest body-mass and temperature dependencies

for biological rates, we investigated the individual and combined effects of two main drivers of biodiversity loss, nutrient enrichment and warming, in food chains with different body size structures. Consistent with expectations [6,30], enrichment destabilizes the system and ultimately leads to extinctions. Warming stabilizes the system by reducing the carrying capacity and the ingestion efficiency and increasing the relative half saturation density of the species. When the ratio between maximum ingestion and metabolism of a species falls below a critical threshold, it becomes extinct as a result of starvation. Thus, high temperature surprisingly counteracts the destabilizing effects of enrichment. High temperatures, however, also increase the risk of consumers starving in oligotrophic and low fertility systems. Higher levels of fertilization, in turn, counteract these detrimental effects of warming. Larger consumer body masses enhance the stabilizing as well as the destabilizing effect of warming and postpone the effects of fertilization. Additionally, warming increases the maximum carrying capacity at which the system retains all its species, and again, increasing consumer body masses enhance this effect drastically. This implies novel interactions between two drivers of global change: nutrient enrichment and warming. Moreover, we found striking effects of the community size structure amplifying the impacts of warming.
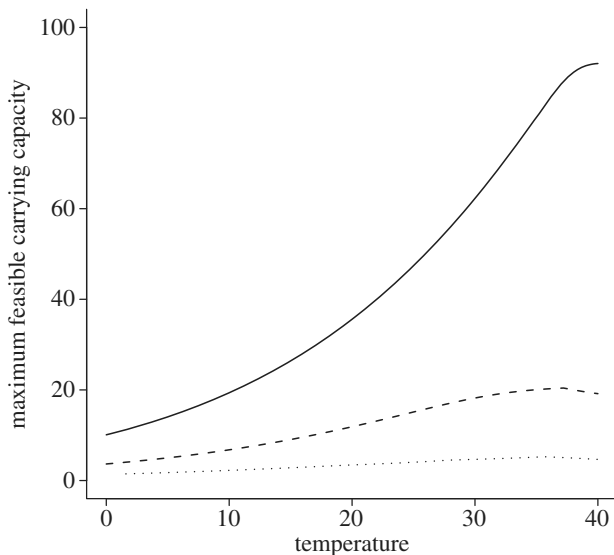
Figure 4. The maximum feasible carrying capacity able to sustain all three species in the system (*y*-axis), depending on the temperature (*x*-axis (°C)) for the approach without body-mass structure (dotted line), with the respective consumer 10 times larger than its prey (dashed line) and with the respective consumer 100 times larger (solid line).

(a) Single effects of enrichment and warming

The carrying capacity of the three-species food chain increases with enrichment. This decreases the ratio of half saturation density to carrying capacity and consequently increases the energy flux from the basal to the top species [5,26]. This direct conversion of bottom-up supply into top-down pressure destabilizes the system along the fertilization gradient and results in the biomass patterns of the 'paradox of enrichment' [6]. Consistent with prior studies [11], simulations with differently sized consumers and prey display a reduced severity of this effect (figure 3*b*–*d*). Inedible, invulnerable or unpalatable prey and inducible defences can alleviate the paradox of enrichment in natural and laboratory environments [31–35]. These are not accounted for in our model.

Warming stabilizes the biomass oscillations within the food chain, leading to a pattern of an inverse 'paradox of enrichment'. This corroborates recent feeding studies of terrestrial arthropods [18,19] and is contrary to the predictions of Vasseur & McCann [5]. This discrepancy is explained by differences in the temperature dependencies of the biological rates. We assumed that the carrying capacity of the system decreases with temperature. Simultaneously, the half saturation density of the species relative to the carrying capacity increases with warming, decreasing the flux of energy to the top of the chain and stabilizing the dynamics. Vasseur & McCann [5] assumed the carrying capacity, the half saturation density and therefore also their ratio to be temperature independent. The parameter values of our system suggest that the growth rate of the basal species increases faster with warming than with the consumers' metabolism. The increase in production outpaces the increasing metabolic demands of the consumers, enhancing the system's ability to keep energy at the lower trophic levels [5]. This reduces biomass oscillations. Also,

the temperature dependencies of ingestion and metabolism [16,25] suggest that a species metabolism increases faster with warming than with its maximum ingestion, reducing its ingestion efficiency and thus biomass oscillations. Vasseur & McCann [5] discussed all possibilities but then assumed that warming induces faster increases in species metabolism than in basal species growth rate and the increase in ingestion to outpace the increase in metabolism. Together, this leads to the destabilization of the system they found. The parametrization of our study is well supported by empirical data [16,17,21,25], suggesting a broad generality of the results presented here. There are, however, cases where warming destabilizes population dynamics. Warming increased population oscillations of the rotifer *Brachionus calyciflorus* [36] and also induced the development of defensive spines [37]. Inducible defences thus might attenuate not only the detrimental effects of enrichment [33,35] but also the effects of temperature we found. Similarly, warming can disrupt species interactions [38] and thus dynamics in many ways, for example via changing developmental schedules [39] or dissimilar range shifts [40]. Our model is based solely on energetic considerations and does not account for other effects that can modify a system's response to warming.

At high temperatures, the metabolism of the consumers exceed their ingestion rates; so their metabolic demands are higher than the energy gained by ingestion. In consequence, they can be surrounded by prey but starve to death. This phenomenon was observed in terrestrial [18,19] and aquatic [8] microcosm experiments, where high trophic level species were found to be at risk of starvation at high temperatures. A three-species laboratory system involving plankton was destabilized at a high temperature [41,42]. The data indicate no oscillations though, and temperature-induced changes of population rates are likely to have led to consumer starvation [42]. Moreover, increased risk of starvation might help to explain the warming-induced shift towards smaller species in aquatic systems [43,44]. Through changing size distributions, warming can indirectly have profound effects on species communities and ecosystem functioning (see Brose *et al.* [45] and citations within).

(b) Interactive effect of enrichment and warming

Fertilization and warming together have interactive effects on the dynamics of the food chain. At low temperatures, warming counteracts the degrading effects of enrichment: both the onset of the oscillations and the occurrence of extinctions connected to increasing fertilization are delayed. Kratina *et al.* [46] corroborate our findings and showed for pond mesocosms that fertilization destabilized chlorophyll biomass dynamics at ambient temperature but not under three degrees of warming. Interestingly, this stabilizing effect of a small amount of warming was observed in a temperate seasonal environment with an annual range of about 20°C in daily average temperature. Moreover, Shurin *et al.* [47] found a negative interaction between nutrient content and warming in the experimental ponds: warming

reduced the effects of eutrophication. A study of a host–parasitoid community, however, showed no interactive effect of temperature and nitrogen levels [48]. This might be due to the different nature of host–parasitoid feeding relationships and their different body-size structure. We found that the rescuing effect of temperature was more pronounced when the consumers were larger than their prey. Larger species are more susceptible to the effect of temperature on their biological rates. A fundamental difference between terrestrial (without interactive effect) and aquatic (with interactive effect) systems is not supported by our data because the parametrization of the model incorporates data of different ecosystems.

At high temperatures, higher fertility counteracts the detrimental effects of warming. Fertilization increases the attack efficiency of the consumers and can thus save species from warming-induced starvation. In size-structured communities, this rescuing effect is delayed to higher fertilization levels. The biological rates of large species react more strongly to warming and so need more fertilization to antagonize its effect. Laboratory studies could test this model prediction, but it should be kept in mind that at different temperatures, varying resource quality affects small species differently than larger species [49].

The increasing maximum feasible carrying capacity with warming is a sign for a top-down component in the effect of warming. Warming has been shown to strengthen top-down control in food webs [46,50,51], explaining the increase in the maximum carrying capacity. Also, warming has stronger effects on larger species. This increases the maximum feasible carrying capacity in size-structured food chains. Its slight decrease at high temperatures is caused by the curve of the maximum ingestion (maximum around 30°C). The decreasing maximum consumption at higher temperatures accelerates the decrease of the species' ingestion efficiency and decreases the maximum feasible carrying capacity after its maximum.

5. CONCLUSIONS

In this study, we show that it is important to understand the interactive effects of drivers of global change. On the basis of our simulations, we expect climate change to have different effects on nutrient-poor and nutrient-rich communities, and nutrient enrichment to act differently in different climates. Warming in both nutrient-poor and nutrient-rich communities generally decreases biomass oscillations and stabilizes population dynamics, with nutrient-poor communities being more stable at low temperatures than their nutrient-rich counterparts. At high temperatures, however, consumers in nutrient-poor communities run a risk of starvation because of an unfavourable ratio of ingestion to metabolism. This does not happen in nutrient-rich communities within the temperature range we simulated. Both the stabilizing and the destabilizing effect of increasing temperatures are more pronounced when the consumers are larger than their prey. Consequently, nutrient-poor biomes are fragile, and, especially, large consumers are at risk of starvation when temperatures increase. Nutrient-rich systems are stabilized by increasing temperatures.

Enrichment has different effects on communities in cold and warm environments. In cold climates, nutrient enrichment has the detrimental effects described by the 'paradox of enrichment'. This harmful impact of nutrient loading is attenuated by an increasing body-size structure in the food chain. Hence, large top consumers of cold climates are less prone to extinction by nutrient enrichment than small consumers. In warm environments, increasing nutrient levels save the consumer species from starvation, and we observe a beneficial effect of nutrient enrichment. Increasing consumer body masses delay the onset of this rescuing effect of enrichment. Therefore, a small body size is advantageous for consumers at high temperatures, but this advantage is lost with increasing enrichment.

With our simulations, we have taken an important step to disentangle the effects of two main direct drivers of global change. We have shown that the combined effects of warming and nutrient enrichment are far from trivial and can, depending on the situation, be supportive or detrimental for the stability of food chains. Increasing body-mass ratios generally accentuate the effects of changing temperatures. This knowledge will help us to develop conservation measures that are tailored to the specific conditions of the species environment.

REFERENCES

1 Barnosky, A. D. *et al.* 2011 Has the Earth's sixth mass extinction already arrived? *Nature* **471**, 51–57. (doi:10.1038/nature09678)

2 Nelson, G. C. 2005 *Millennium ecosystem assessment: drivers of ecosystem change: summary chapter.* Washington, DC: World Resources Institute.

3 Nelson, G. C. 2005 *Millennium ecosystem assessment, ecosystems and human well-being: biodiversity synthesis.* Washington, DC: World Resources Institute.

4 Tylianakis, J. M. 2008 Understanding the web of life: the birds, the bees, and sex with aliens. *PLoS Biol.* **6**, e47. (doi:10.1371/journal.pbio.0060047)

5 Vasseur, D. A & McCann, K. S. 2005 A mechanistic approach for modeling temperature-dependent consumer–resource dynamics. *Am. Nat.* **166**, 184–198. (doi:10.1086/431285)

6 Rosenzweig, M. L. 1971 Paradox of enrichment: destabilization of exploitation ecosystems in ecological time. *Science* **171**, 385–387. (doi:10.1126/science.171.3969.385)

7 Yvon-Durocher, G., Jones, J. I., Trimmer, M., Woodward, G. & Montoya, J. M. 2010 Warming alters the metabolic balance of ecosystems. *Phil. Trans. R. Soc. B* **365**, 2117–2126. (doi:10.1098/rstb.2010.0038)

8 Petchey, O. L., McPhearson, P. T., Casey, T. M. & Morin, P. J. 1999 Environmental warming alters food-web structure and ecosystem function. *Nature* **402**, 69–72. (doi:10.1038/47023)

9 Parmesan, C. 2006 Ecological and evolutionary responses to recent climate change. *Annu. Rev. Ecol. Evol. Syst.* **37**, 637–669 (doi:10.1146/annurev.ecolsys. 37.091305.110100)

10 Brose, U. 2008 Complex food webs prevent competitive exclusion among producer species. *Proc. R. Soc. B* **275**, 2507–2514. (doi:10.1098/rspb.2008.0718)

11 Rall, B. C., Guill, C. & Brose, U. 2008 Food-web connectance and predator interference dampen the paradox of enrichment. *Oikos* **117**, 202–213. (doi:10. 1111/j.2007.0030-1299.15491.x)

12 Rip, J. M. K. & McCann, K. S. 2011 Cross-ecosystem differences in stability and the principle of energy flux. *Ecol. Lett.* **14**, 733–740. (doi:10.1111/j.1461-0248. 2011.01636.x)

13 Riede, J. O., Brose, U., Ebenman, B., Jacob, U., Thompson, R., Townsend, C. R. & Jonsson, T. 2011 Stepping in Elton's footprints: a general scaling model for body masses and trophic levels across ecosystems. *Ecol. Lett.* **14**, 169–178. (doi:10.1111/j.1461-0248. 2010.01568.x)

14 Hansen, P., Bjornsen, P. & Hansen, B. 1997 Zooplankton grazing and growth: scaling within the 2–2,000-μm body size range. *Limnol. Oceanogr.* **42**, 687–704.

15 Gillooly, J. F., Brown, J. H., West, G. B., Savage, V. M. & Charnov, E. L. 2001 Effects of size and temperature on metabolic rate. *Science* **293**, 2248–2251. (doi:10.1126/ science.1061967)

16 Ehnes, R. B., Rall, B. C. & Brose, U. 2011 Phylogenetic grouping, curvature and metabolic scaling in terrestrial invertebrates. *Ecol. Lett.* **14**, 993–1000. (doi:10.1111/j. 1461-0248.2011.01660.x)

17 Savage, V. M., Gillooly, J. F., Brown, J. H., West, G. B. & Charnov, E. 2004 Effects of body size and temperature on population growth. *Am. Nat.* **63**, 429–441. (doi:10. 1086/381872)

18 Rall, B. C., Vucic-Pestic, O., Ehnes, R. B., Emmerson, M. & Brose, U. 2010 Temperature, predator–prey interaction strength and population stability. *Glob. Change Biol.* **16**, 2145–2157. (doi:10.1111/j.1365-2486.2009. 02124.x)

19 Vucic-Pestic, O., Ehnes, R., Rall, B. C. & Brose, U. 2011 Warming up the system: higher predator feeding rates but lower energetic efficiencies. *Glob. Change Biol.* **17**, 1301–1310. (doi:10.1111/j.1365-2486.2010.02329.x)

20 Brown, J. H., Gillooly, J. F., Allen, A. P., Savage, V. M. & West, G. B. 2004 Toward a metabolic theory of ecology. *Ecology* **85**, 1771–1789. (doi:10.1890/03-9000)

21 Meehan, T. D. 2006 Energy use and animal abundance in litter and soil communities. *Ecology* **87**, 1650–1658. (doi:10.1890/0012-9658(2006)87[1650:EUAA AI]2.0.CO;2)

22 Lang, B., Rall, B. C. & Brose, U. 2011 Warming effects on consumption and intraspecific interference competition depend on predator metabolism. *J. Anim. Ecol.* **81**, 516–523. (doi:10.1111/j.1365-2656.2011.01931.x)

23 Englund, G., Öhlund, G., Hein, C. L. & Diehl, S. 2011 Temperature dependence of the functional response. *Ecol. Lett.* **14**, 914–921. (doi:10.1111/j.1461-0248. 2011.01661.x)

24 Twomey, M., Brodte, E., Jacob, U., Brose, U., Crowe, T. P. & Emmerson, M. C. 2012 Idiosyncratic species effects confound size-based predictions of responses to climate change. *Phil. Trans. R. Soc. B* **367**, 2971–2978. (doi:10.1098/rstb.2012.0244)

25 Rall, B. C., Brose, U., Hartvig, M., Kalinkat, G., Schwarzmüller, F., Vucic-Pestic, O. & Petchey, O. L. 2012 Universal temperature and body-mass scaling of feeding rates. *Phil. Trans. R. Soc. B* **367**, 2923–2934. (doi:10.1098/rstb.2012.0242)

26 Yodzis, P. & Innes, S. 1992 Body size and consumer–resource dynamics. *Am. Nat.* **139**, 1151–1175. (doi:10. 1086/285380)

27 Holling, C. S. 1965 The functional response of predators to prey density and its role in mimicry and population regulation. *Mem. Entomol. Soc. Can.* **45**, 1–60. (doi:10. 4039/entm9745fv)

28 Peters, R. H. 1983 *The ecological implications of body size*. Cambridge, UK: Cambridge University Press.

29 Brose, U. *et al.* 2006 Consumer–resource body-size relationships in natural food webs. *Ecology* **87**, 2411–2417. (doi:10.1890/0012-9658(2006)87[2411:CBR INF]2.0.CO;2)

30 Fussmann, G. F., Ellner, S. P., Shertzer, K. W. & Hairston Jr, N. G. 2000 Crossing the Hopf bifurcation in a live predator–prey system. *Science* **290**, 1358–1360. (doi:10.1126/science.290.5495.1358)

31 Abrams, P. A. & Walters, C. J. 1996 Invulnerable prey and the paradox of enrichment. *Ecology* **77**, 1125–1133.

32 Genkai-Kato, M & Yamamura, N. 1999 Unpalatable prey resolves the paradox of enrichment. *Proc. R. Soc. Lond. B* **266**, 1215–1209. (doi:10.1098/rspb.1999.0765)

33 Vos, M., Kooi, B. W., DeAngelis, D. L. & Mooij, W. M. 2004 Inducible defences and the paradox of enrichment. *Oikos* **105**, 471–480. (doi:10.1111/j.0030-1299.2004. 12930.x)

34 Roy, S. & Chattopadhyay, J. 2007 The stability of ecosystems: a brief overview of the paradox of enrichment. *J. Biosci.* **32**, 421–428. (doi:10.1007/s12038-007-0040-1)

35 Van Donk, E., Ianora, A. & Vos, M. 2011 Induced defences in marine and freshwater phytoplankton: a review. *Hydrobiologia* **668**, 3–19. (doi:10.1007/s10750-010-0395-4)

36 Halbach, U. 1970 Einfluss der Temperatur auf die Populationsdynamik des planktischen Raedertieres *Brachionus calyciflorus* Pallas (influence of temperature on the population dynamics of the rotifer *Brachionus calyciflorus* Pallas). *Oecologia* **4**, 176–207. (doi:10.1007/BF00377100)

37 Halbach, U. 1970 Die Ursachen der Temporalvariation von *Brachionus calyciflorus* Pallas (Rotatoria). *Oecologia* **4**, 262–318. (doi:10.1007/BF00377250)

38 Harley, C. D. G. 2011 Climate change, keystone predation, and biodiversity loss. *Science* **334**, 1124–1127. (doi:10.1126/science.1210199)

39 Tuda, M. & Shimada, M. 1995 Developmental schedules and persistence of experimental host–parasitoid systems at two different temperatures. *Oecologia* **103**, 283–291. (doi:10.1007/BF00328616)

40 Voigt, W. *et al.* 2003 Trophic levels are differentially sensitive to climate. *Ecology* **84**, 2444–2453. (doi:10.1890/ 02-0266)

41 Beisner, B., Mccauley, E. & Wrona, F. 1996 Temperature-mediated dynamics of planktonic food chains: the effect of an invertebrate carnivore. *Freshw. Biol.* **35**, 219–232. (doi:10.1046/j.1365-2427.1996.00492.x)

42 Beisner, B., McCauley, E. & Wrona, F. 1997 The influence of temperature and food chain length on plankton predator–prey dynamics. *Can. J. Fish. Aquat. Sci.* **54**, 586–595. (doi:10.1139/cjfas-54-3-586)

43 Daufresne, M., Lengfellner, K. & Sommer, U. 2009 Global warming benefits the small in aquatic ecosystems. *Proc. Natl Acad. Sci. USA* **106**, 12 788–12 793. (doi:10. 1073/pnas.0902080106)

44 Yvon-Durocher, G., Montoya, J. M., Trimmer, M. & Woodward, G. 2011 Warming alters the size spectrum and shifts the distribution of biomass in freshwater ecosystems. *Glob. Change Biol.* **17**, 1681–1694. (doi:10. 1111/j.1365-2486.2010.02321.x)

45 Brose, U., Dunne, J. A., Montoya, J. M., Petchey, O. L., Schneider, F. D. & Jacob, U. 2012 Climate change in

size-structured ecosystems. *Phil. Trans. R. Soc. B* **367**, 2903–2912. (doi:10.1098/rstb.2012.0232)

46 Kratina, P., Greig, H., Thompson, P. L., Carvalho-Pereira, T. S. A. & Shurin, J. B. 2012 Warming modifies trophic cascades and eutrophication in experimental freshwater communities. *Ecology* **93**, 1421–1430. (doi:10.1890/11-1595.1]

47 Shurin, J. B., Clasen, J. L., Greig, H. S., Kratina, P. & Thompson, P. L. 2012 Warming shifts top-down and bottom-up control of pond food web structure and function. *Phil. Trans. R. Soc. B* **367**, 3008–3017. (doi:10.1098/rstb.2012.0243)

48 de Sassi, C., Staniczenko, P. P. A. & Tylianakis, J. M. 2012 Warming and nitrogen affect size structuring and density dependence in a host–parasitoid food web.

Phil. Trans. R. Soc. B **367**, 3033–3041. (doi:10.1098/rstb.2012.0233)

49 Ott, D., Rall, B. C. & Brose, U. 2012 Climate change effects on macrofaunal litter decomposition: the interplay of temperature, body masses and stoichiometry. *Phil. Trans. R. Soc. B* **367**, 3025–3032. (doi:10.1098/rstb.2012.0240)

50 O'Connor, M. I., Piehler, M. F., Leech, D. M., Anton, A. & Bruno, J. F. 2009 Warming and resource availability shift food web structure and metabolism. *PLoS Biol.* **7**, pe1000178. (doi:10.1371/journal.pbio.1000178)

51 Hoekman, D. 2010 Turning up the heat: temperature influences the relative importance of top-down and bottom-up effects. *Ecology* **91**, 2819–2825. (doi:10.1007/s00442-010-1802-2)

Interactive effects of warming, eutrophication and size structure: impacts on biodiversity and food-web structure

AMREI BINZER[1,2], CHRISTIAN GUILL[2,3,4], BJÖRN C. RALL[2,5,6] and ULRICH BROSE[2,5,6]

[1]*Department of Physics, Chemistry and Biology (IFM), Linköping University, SE-581 83 Linköping, Sweden,* [2]*J.F. Blumenbach Institute of Zoology and Anthropology, University of Göttingen, Berliner Str. 28, 37073 Göttingen, Germany,* [3]*Institute of Biochemistry and Biology, University of Potsdam, Maulbeerallee 2, 14469 Potsdam, Germany,* [4]*Institute for Biodiversity and Ecosystem Dynamics (IBED), University of Amsterdam, P.O. Box 94248, 1090 GE, Amsterdam, The Netherlands,* [5]*German Centre for Integrative Biodiversity Research (iDiv) Halle-Jena-Leipzig, Deutscher Platz 5e, 04103 Leipzig, Germany,* [6]*Institute of Ecology, Friedrich Schiller University Jena, Dornburger-Str. 159, 07743 Jena, Germany*

Abstract

Warming and eutrophication are two of the most important global change stressors for natural ecosystems, but their interaction is poorly understood. We used a dynamic model of complex, size-structured food webs to assess interactive effects on diversity and network structure. We found antagonistic impacts: Warming increases diversity in eutrophic systems and decreases it in oligotrophic systems. These effects interact with the community size structure: Communities of similarly sized species such as parasitoid–host systems are stabilized by warming and destabilized by eutrophication, whereas the diversity of size-structured predator–prey networks decreases strongly with warming, but decreases only weakly with eutrophication. Nonrandom extinction risks for generalists and specialists lead to higher connectance in networks without size structure and lower connectance in size-structured communities. Overall, our results unravel interactive impacts of warming and eutrophication and suggest that size structure may serve as an important proxy for predicting the community sensitivity to these global change stressors.

Keywords: complex food webs, extinctions, generalists, global change, size structure, specialists

Received 10 June 2015 and accepted 7 August 2015

Introduction

Global change and the resulting changes in biodiversity are a major threat to the world's ecosystems. However, even though the main stressors for biodiversity have been identified, their interactions remain poorly understood (Peñuelas *et al.*, 2013; but see de Sassi *et al.*, 2012; Sentis *et al.*, 2014). The impact of two of these stressors, climate warming and eutrophication, is predicted to become increasingly important, rendering research on their interactive effects critical.

Despite accumulating evidence on the independent effects of warming and eutrophication (Petchey *et al.*, 1999; Vasseur & McCann, 2005; Rall *et al.*, 2008, 2010; Amarasekare & Coutinho, 2014; Amarasekare, 2015), their interactions have so far only been investigated for simplified community modules (Binzer *et al.*, 2012; Gilbert *et al.*, 2014; Sentis *et al.*, 2014). They both increase short-term per capita energy fluxes due to higher activity (warming) or resource availability (eutrophication). In consequence, eutrophication increases the bottom-up energy supply, which may result in unstable oscillations and consumer extinctions ('paradox of enrichment,' Rosenzweig, 1971; Rall *et al.*, 2008). While

Correspondence: Amrei Binzer, tel. +4613282965, fax +4613-14 94 03, e-mail: amrei.binzer@liu.se

similar effects could be expected for warming (Vasseur & McCann, 2005), empirical studies showed that warming causes disproportionally stronger metabolic losses yielding lower consumer densities and long-term population-level energy fluxes (Rall *et al.*, 2010, 2012; Fussmann *et al.*, 2014; Gilbert *et al.*, 2014). Consistent with theoretical predictions, warming thus stabilizes population dynamics (Johnson *et al.*, 2010; Fussmann *et al.*, 2014) and causes consumer starvation (Fussmann *et al.*, 2014), which explains high trophic level consumer extinctions in experiments (Petchey *et al.*, 1999; Shurin *et al.*, 2012). In the same vein, food-chain models demonstrated that warming prevents species loss by enrichment-driven unstable oscillations at low temperatures, but causes extinctions due to starvation at high temperatures (Binzer *et al.*, 2012). In more complex communities, however, these results may differ due to shifts in the relative strengths of feeding links (Petchey *et al.*, 2010; Sentis *et al.*, 2014; Tunney *et al.*, 2014). Together, these results suggest that warming and eutrophication may have strong interactive effects on ecological community structure and diversity, but their interplay in complex communities remains to be addressed.

In addition, warming alters the body-mass distribution of natural communities by favouring small over

large species (e.g., Daufresne *et al.*, 2009; O'Gorman *et al.*, 2012). Warming and species body masses also interactively affect network body-mass structure of ecological networks (Gibert & DeLong, 2014). As the inverted body-mass pyramid (i.e., increases in body mass with trophic levels, Riede *et al.*, 2011) is critically important for food-web stability (Brose *et al.*, 2006; Heckmann *et al.*, 2012), a shift in food-web size structure may severely undermine the stability of natural communities. Moreover, the warming and eutrophication effects on population dynamics in simple three-species models are also modified by the community size structure (Binzer *et al.*, 2012; Brose *et al.*, 2012). Higher consumer-resource body-mass ratios enhance the stabilizing and destabilizing effects of warming (Binzer *et al.*, 2012). Consistently, experimental studies demonstrated positive and negative interactions between warming and eutrophication at low and high body-mass ratios, respectively (de Sassi *et al.*, 2012; Shurin *et al.*, 2012). Accordingly, warming and eutrophication effects on population dynamics and extinctions in complex food webs may strongly depend on the community size structure.

Here, we expanded our previous models of simple modules (Rall *et al.*, 2010; Binzer *et al.*, 2012) by investigating the effects of warming and eutrophication on complex food webs of varying body-mass structures. We expected that the opposite effects on consumer-resource energy fluxes should lead to antagonistic impacts of eutrophication and warming on species persistence (fraction of surviving species). In addition, we also hypothesized strong interactions between stressors and consumer-resource body-mass ratios (i.e., size of consumers relative to their prey) in the food webs, leading to stability impacts of warming. For the first time, we also address the consequences of the stressors for the network structure of the food webs (connectance, generality, vulnerability). This study thus provides a comprehensive analysis of how warming, eutrophication and network body-size structure interactively affect the structure and diversity of natural communities.

Methods

The model

First, we created food-web structures according to the niche model (Williams & Martinez, 2000) with an initial species richness of 30 and a connectance (the connection probability in the feeding matrix) of 0.1. This yielded static, fully connected network structures of who eats whom in the community.

Subsequently, we assigned ordinary differential equations (ODE) to each species *i* of the food web to calculate changes in the species biomasses, B_i, over time, *t*, (Yodzis & Innes, 1992;

Brose *et al.*, 2006). A basal species (eqn. 1) grows logistically with an intrinsic net growth rate, r_i, and a carrying capacity, K_i. The species in the food webs gain and lose biomass by feeding, F_{ij}, and assimilate consumed biomass with a ratio of $e_s = 0.85$ (assimilation efficiency, Yodzis & Innes, 1992):

$$\frac{dB_i}{dt} = r_i B_i \left(1 - \frac{B_i}{K_i}\right) - \sum_m F_{mi} B_{mi} \tag{1}$$

Consumers (eqn. 2) additionally lose biomass through respiration, x_i:

$$\frac{dB_i}{dt} = \sum_s e_s F_{is} B_i - \sum_m F_{mi} B_m - x_i B_i \tag{2}$$

The feeding function, F_{ij}, follows a resource density-dependent functional response:

$$F_{ij} = \frac{a_{ij} B_k^q}{1 + \sum_k \mathrm{Th}_{ik} a_{ik} B_k^q}, \tag{3}$$

with a link-specific attack rate, a_{ij}, the handling time, Th, and the Hill exponent, *q = 1.2*, determining the shape of the functional response (type II while *q = 1*; type III while *q = 2*).

Parameterization

The body mass, m_i, of a species *i* in the food web scales according to the following:

$$m_i = m_0 R^{L_i - 1 + \varepsilon_i}, \tag{4}$$

where m_0 is the body mass of the basal species in the food web ($m_0 = 0.01$ g), *R* is the average body-mass ratio of all species in the food web and L_i is the prey-averaged trophic level of the species *i* (see Williams & Martinez, 2004). To avoid that all species of a trophic level (e.g., herbivores of trophic level 2) are equally sized, we added random deviations from these strict scaling relationships by sampling ε_i for each species *i* independently from a normal distribution with a mean of zero and a standard deviation of 1. All parameters, except for the assimilation efficiency, *e*, and the hill exponent, *h*, scale with body mass and temperature (Brown *et al.*, 2004; Savage *et al.*, 2004; Ehnes *et al.*, 2011; Binzer *et al.*, 2012; Rall *et al.*, 2012):

$$a_{ij}, \mathrm{Th}_{ij} = f(m_i, m_j, T) = d m_i^b m_j^c e^{E \frac{T_0 - T}{k T T_0}} \tag{5a}$$

$$r_i, K_i, x_i = f(m_i, T) = d m_i^b e^{E \frac{T_0 - T}{k T T_0}} \tag{5b}$$

where *d* and T_0 are constants, *k* is the Boltzmann constant, m_i and m_j are the average body masses of species *i* and *j*, respectively, *b* and *c* are allometric exponents, *E* is the activation energy and *T* is the temperature in Kelvin. Note that due to the availability of high-quality data, the parameterization is based on actively hunting invertebrates. The units and values of the parameters are given in Table 1.

Model simulations

We set the initial biomass densities of the basal species equal to their carrying capacities and the initial consumer biomasses

Table 1 Model mass and temperature scaling parameters: carrying capacity (K in [g m^{-2}] (Meehan, 2006)), growth (*r* in [1/s], (Savage *et al.*, 2004)), metabolism (*x* in [1/s], (Ehnes *et al.*, 2011)), attack rate (a in [m^2 s^{-1}]) and handling time (Th in [s], both calculated from (Rall *et al.*, 2012)). The parameters scale with the body mass of the resource species (*i*) of the species pair considered, attack rate and handling timescale additionally with the body mass of the consumer species (*j*). We calculated the species metabolism using the conversion factor from Peters (1983)

	K_i	r_i	a_{ji}	Th_{ji}	x_i
Intercept (*I*)		−15.68	−13.1	9.66	−16.54
Body mass scaling species *i* (b)	0.28	−0.25	0.25	−0.45	−0.31
Body mass scaling predator (c)			−0.8	0.47	
Activation energy (E)	0.71	−0.84	−0.38	0.26	−0.69

to 1/8 of the mean of the carrying capacities of the basal species in the food web. The carrying capacities vary with body mass and temperature (see eqn. 5b), and varying the initial biomasses accordingly prevented basal extinctions during transient dynamics. Changing these initial biomasses within ecologically plausible boundaries does not affect the results, unless basal biomasses are too low to provide sufficient energy input into the food web. To reach stable attractors of population dynamics, we ran simulations for an equivalent of 1000 years. During these time series, a species was considered extinct and removed from the simulation when its biomass density fell below 10^{-12}.

We analyzed food-web dynamics across gradients of temperature *T* (0–40 °C in steps of 1 °C), eutrophication (varying the intercept of the carrying capacity, *d*, between 1 and 20 in steps of 1 to manipulate the energy input into the food webs) and community size structures by varying the log$_{10}$ consumer-resource body-mass ratio between −1 (consumers ten times smaller than their prey) and 4 (consumers 10^4 times larger than their resources) in steps of 1. For each combination of these parameters, the simulations were replicated 100 times.

At the end of the time series, we monitored (1) persistence as the fraction of species that survived, (2) connectance (C = L/S², L = number of feeding links, S = number of species), (3) the average generality (number of links to resource species) and (4) the average vulnerability (number of links to consumer species) across all species. As vulnerability and generality depend on species richness and connectance that change after extinctions during time series, they cannot be compared to the initial values. Hence, as a null expectation, we created 10 000 reference niche food webs according to the final species richness (thus accounting for extinctions) and initial connectance (assuming random extinctions that are independent of the species' linkedness and thus without effect on connectance) of each replicate. To test for nonrandom extinctions, we calculated the log$_{10}$ ratio between the simulated and reference food-web values of generality and vulnerability.

Results

Interactive effects of warming and eutrophication on species persistence

In our complex model food webs, warming, eutrophication and the body-size structure have interactive effects on species persistence (Figs 1 and 2). In food webs without body-mass structure, in which all species are of equal size, persistence decreases with eutrophication and increases with warming (Fig. 1a), except for very low eutrophication (<2.5) and high temperature (>35 °C), where persistence decreases with warming (Fig. 1a). These results suggest that the diversity of networks without size structure (e.g., parasitoid–host communities) should increase with warming and strongly decrease with eutrophication.

We compared these results to those of food webs with a size structure of consumers that are on average hundred times larger than their resources (Fig. 1b, similar results were obtained for other positive log$_{10}$ body-mass ratios, see Fig. 2). Here, warming strongly decreases persistence, most notably at low eutrophication. Eutrophication itself has only a slightly negative effect at low temperatures and even increases persistence at intermediate and high temperatures (Fig. 1b). Hence, the diversity of typical predator–prey communities with consumers that are larger than their resources should be severely reduced by warming, whereas eutrophication has only weak effects that depend on temperature.

Generally, the interaction between the stressors creates hump-shaped responses of persistence along the eutrophication gradient. Here, the entire humps along the eutrophication axis are, for example, visible for food webs with an average body-mass ratio of 100 at 10 °C (Fig. 1b), whereas for most other combinations of body-mass ratios and temperature only the left half of the hump is visible.

Our findings can be generalized across different body-mass ratios: Warming decreases persistence at medium to high body-mass ratios, but increases persistence at low body-mass ratios (Fig. 2). Moreover, increasing body-mass ratios yield higher persistence at low and intermediate temperatures, whereas a more complex relationship with two maxima in persistence at high (R~10^4) and low body-mass ratios (R~10^1) emerges at the highest temperatures. Interestingly, these results suggest the structural stability of arctic and temperate communities is maximized at the highest body-mass ratios, whereas tropic ecosystems should have their maximum stability at either low or high body-mass ratios. The stable high body-mass ratios, however, do not sustain over longer time series (e.g., 10 000 years).
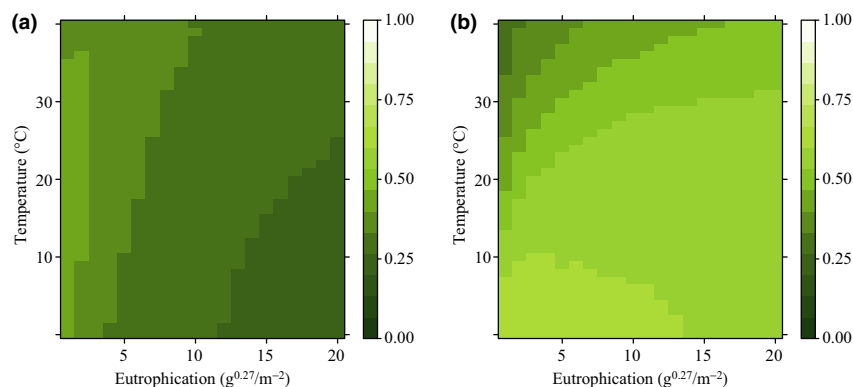
Fig. 1 The influence of eutrophication (intercept of carrying capacity, x-axes) and temperature (y-axes) on the persistence of species (averaged over 100 food webs; as a fraction, color coded, see color key) in food webs with (a) predators on average of the same age as their prey ($\log_{10}$ body mass ratio = 0) and (b) predators on average 100 times larger than their prey ($\log_{10}$ body mass ratio = 2).
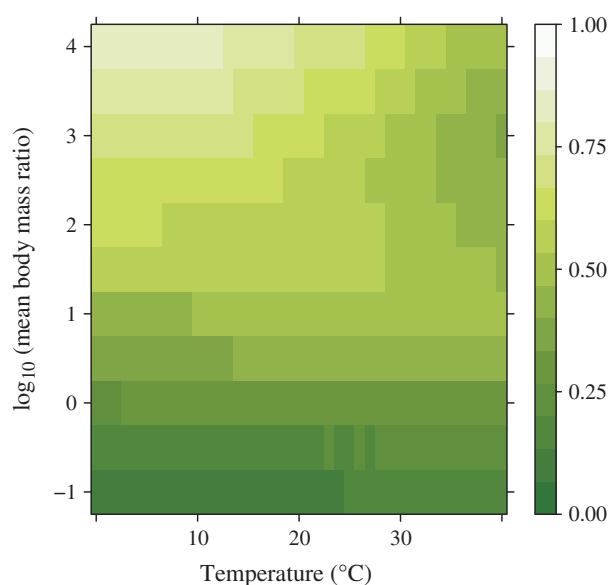

Fig. 2 The influence of temperature (x-axes) and $\log_{10}$ body mass structure (y-axes) on the persistence of species (averaged over 100 food webs; as a fraction, color coded, see color key) in food webs of intermediate eutrophication (intercept of carrying capacity of 10).

Effects on connectance and link distributions

Generally, the extinctions in our time series are not random and cause changes in connectance of the food web that interactively depend on the body-mass ratio of the community and temperature (Fig. 3). Connectance increased in communities with low body-mass ratios, most notably at low temperatures. Note that the exception to this pattern at body-mass ratios (R) of 10^{-1} (Fig. 3) may be caused by the low persistence (Fig. 2) that led to final food webs of low diversity and

connectance. In contrast, connectance decreased in communities with high body-mass ratios, in particular at high temperatures (Fig 3). We found that warmer food webs generally have a lower connectance than their cooler counterparts with the same size structure, with the exception of food webs with very low body-mass ratios ($R < 10^0$). This pattern suggests that warming increased the likelihood that highly linked species become extinct, thus decreasing connectance.

In our subsequent analyses, we disentangled whether this loss in highly linked species was driven by losses of the most vulnerable or most general species that are highly linked to consumers or resources, respectively. We calculated the ratio between the final vulnerability and generality of the simulated food webs and reference webs built with the final species richness, but the initial connectance (see Methods). These ratios thus represent deviations from the null assumption of random extinctions that do not depend on linkedness. We found that the increases in connectance at low temperatures and low body-mass ratios (Fig. 3) are driven by increases in vulnerability (Fig. 4a). The decreases in connectance at high temperatures and high body-mass ratios (Fig. 3), however, are similarly affected by decreases in vulnerability (Fig. 4a) and generality (Fig. 4b). Warming thus causes a dominance of specialists, lowering the number of resources (lower generality, Fig. 4b) and also the number of consumers (lower vulnerability, Fig. 4a).

Discussion

We analyzed dynamic models of complex food webs and showed that warming, eutrophication and body-mass structure interactively determine their diversity and network structure. Consistent with our initial expectations, we found that warming and eutrophica-

tion have opposite effects on species persistence. Interestingly, the effect of these antagonistic stressors depends strongly on the body-mass ratio of the community. In the following, we discuss these outcomes by disentangling the interplay of opposing population parameters that determine the strengths of the energetic pathways and subsequently population stability (Yodzis & Innes, 1992; Rall *et al.*, 2010; Rip & McCann, 2011; Fussmann *et al.*, 2014). Combining these
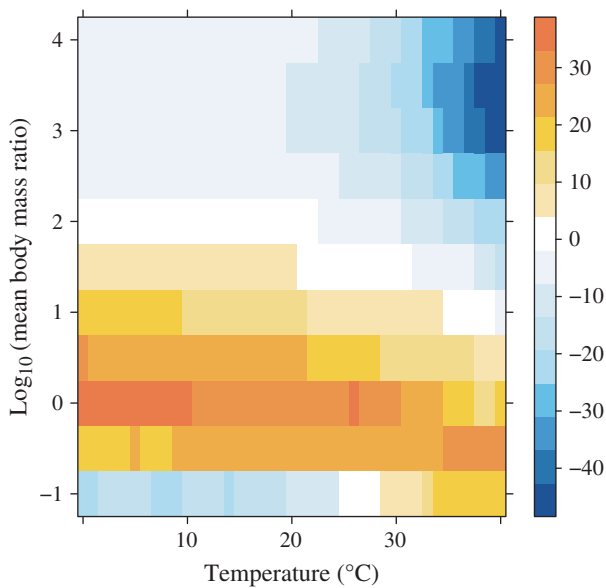
principles with food-web theory on consumer-resource body-mass ratios (Brose *et al.*, 2006) and biomass ratios (Gilbert *et al.*, 2014) allows a mechanistic understanding of how these antagonistic stressors interactively determine the diversity and network structure of species communities.

Warming, eutrophication and community size-structure effects on species persistence

The classic instability of complex and diverse food webs can be overcome by increasing predator–prey body-mass ratios that reduce the consumers' relative rates of consumption and metabolism (Yodzis & Innes, 1992), thereby lowering interaction strengths and top-down pressure and therefore increasing species persistence (Brose *et al.*, 2006; Kartascheff *et al.*, 2009; Heckmann *et al.*, 2012). Our results generalize this finding across gradients in eutrophication and temperature except for the highest temperatures, where strong metabolic losses impose strong constraints on highly linked species (see Discussion below for more mechanistic details).

Eutrophication boosts energy input into the food web yielding higher biomass densities of resources and their consumers. These higher densities cause higher population-level consumption rates that strengthen top-down control and lead to unstable oscillations and extinctions ('paradox of enrichment,' Rosenzweig, 1971; Rall *et al.*, 2008; Rip & McCann, 2011). The lower top-down pressure in size-structured food webs counteracts this mechanism of unstable oscillations. This provides an explanation for our novel result that networks without size structure (e.g., parasitoid–host communities) are more prone to detrimental eutrophication effects than size-structured communities (e.g., predator–prey
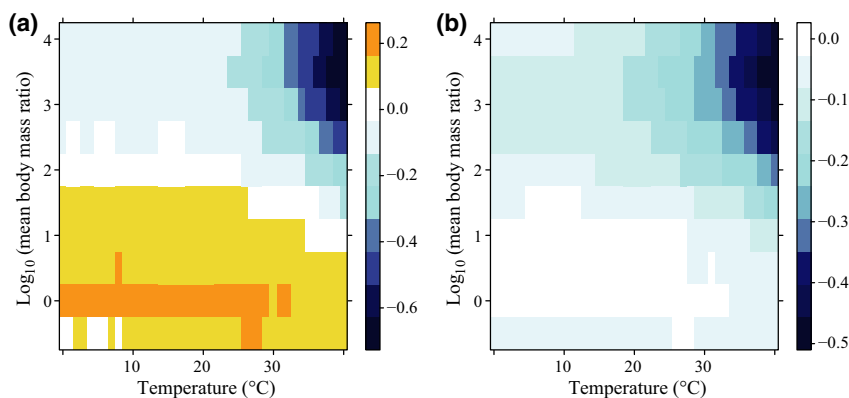

Fig. 3 Influence of temperature (*x*-axis) and log$_{10}$ body mass structure (*y*-axis) on the deviation of final to initial connectance (C = 0.1), in percentage (color coded, see color key) and averaged for 100 food webs at intermediate eutrophication (compare Fig. 2).

Fig. 4 Influence of temperature (*x*-axis) and log$_{10}$ body mass structure (*y*-axis) on the deviation of the mean food web: a) vulnerability b) and generality from the expected mean values derived from 10 000 food webs of the same species number but initial connectance (see Methods for further details), expressed in standard deviations of the expected link distributions.

communities). Although this result still needs to be reconciled with prior findings on the stabilizing effects of inducible defences, sigmoidal functional responses and predator interference (e.g., Vos *et al.*, 2004; Rall *et al.*, 2008), it offers an empirically testable prediction.

Warming increases metabolism more strongly than it increases feeding rates (Rall *et al.*, 2010; Vucic-Pestic *et al.*, 2011; Fussmann *et al.*, 2014). In oscillating systems, warming thus stabilizes the population dynamics by lowering the top-down pressure, but these reduced energy fluxes ultimately lead to starvation when consumers cannot meet their metabolic demand anymore (Binzer *et al.*, 2012; Fussmann *et al.*, 2014). The antagonistic interaction of warming and eutrophication is caused by their opposite effects on consumer-resource energy fluxes that drive population stability (Yodzis & Innes, 1992; Rip & McCann, 2011; Fussmann *et al.*, 2014). In consequence, warming can stabilize dynamics in eutrophic ecosystems, whereas it should cause extinctions due to starvation in oligotrophic systems (Binzer *et al.*, 2012). Interestingly, in more resident species, temperature has no effect on predator–prey interaction strengths (Vucic-Pestic *et al.*, 2011; Novich *et al.*, 2014). For them, temperature should only increase their metabolic demands, leading to more severe starvation problems.

Our results indicate that the interactive effects between warming and eutrophication found in simple community modules (Binzer *et al.*, 2012) can also be found in complex food webs. Additionally, we addressed the entirely new question of how these stressors interact with the community size structure. As an increasing consumer-resource body-mass ratio decreases per unit biomass energy fluxes (Yodzis & Innes, 1992) and top-down control, it should be synergistic with warming (which decreases fluxes) and antagonistic to eutrophication (which increases fluxes). Consistent with this hypothesis, we found that an increasing size structure enforced the stabilizing and destabilizing effects of warming and buffered against eutrophication. In consequence, warming increases persistence in communities without size structure (e.g., parasitoid–host communities), whereas it decreases persistence in size-structured networks (e.g., predator–prey communities). Consistent with our results that warming can induce extinctions in highly size-structured webs, microcosm experiments demonstrated that warming increased biomass of bacteria and their consumers, but led to extinction of larger predators (Petchey *et al.*, 1999). These results suggest that both the consumer-resource body-mass ratios of natural communities and the eutrophication level interact with temperature and may serve as a proxy for estimating the sensitivity to detrimental warming effects.

Effects on community diversity, connectance and linkedness

Our model results demonstrated an interesting emergent pattern: While persistence increased with body-mass ratios at low-to-intermediate temperatures, it exhibited two maxima at higher temperatures. However, one of these, the maximum at high body-mass ratios and high temperatures, becomes less and less pronounced the longer the simulations run (data not shown). This suggests that large-bodied species are to some extent – over ecological timescales such as the 1000 years of our study – buffered against the detrimental effect of increased temperatures, but will still be affected in the long term over more evolutionary timescales. Consistent with emergent empirical patterns (Daufresne *et al.*, 2009; and for small marine species Gibert & DeLong, 2014), this suggests a systematic distribution of consumer-resource body-mass ratios along global gradients: They should be high in arctic and temperate ecosystems and low in tropic habitats.

Our model analyses suggested that final food-web connectance decreases with increasing body-mass ratios and warming. In our simulations, all 100 food-web replicates were exposed to every body mass ratio–temperature combination. The clear pattern in final connectance is thus caused by a systematic effect of body-mass ratios and temperature on the extinction risk of generalists (with many links) and specialists (with few links). In our model, each additional feeding link of a consumer decreases the strength of each of its individual links, because they distribute their feeding efforts across their resources. As a result, specialists have few, strong feeding links, whereas generalists have many, weak links to resources. At high body-size ratios and high temperatures, specialists have an advantage, because their strong feeding interactions save them from starvation, whereas generalists die due to the lower energy supply through their weaker interactions.

Unfortunately, data that relate body-size ratios and temperature to species degree of generalism are rare or absent. However, species richness increases from the poles to the tropics, and increasing species specialization has been suggested to account for it (MacArthur, 1972). Subsequent studies, however, have given mixed results, but they employed data on mutualistic networks (Schleuning *et al.*, 2012), included many endotherm species (Davey *et al.*, 2012), spiders (Birkhofer & Wolters, 2012) or fish (González-Bergonzoni *et al.*, 2012). Our model is dedicated to describe actively hunting invertebrates, which is least partially inconsistent with these data compilations. Hence, future studies will need to compile data for testing our prediction that

specialism of actively hunting invertebrates should increase with temperature.

The low species vulnerability at high temperatures and body-mass ratios is caused by the loss of generalists in the webs, whose extinction decreases the number of top consumers. Low mean generality and low mean vulnerability thus go hand in hand. The increased connectance in webs with low body-mass ratios, however, is due to the increased vulnerability of the species in those webs. These food webs at low temperatures combine high interaction strengths (caused by low body-mass ratios) with low respiration rates (caused by low temperatures). Consequently, species can use relatively more of the energy obtained from feeding to build up own biomass because less of it is lost to respiration. This leads to higher biomass densities and oscillations. Less vulnerable species with only a few consumers accumulate more biomass than vulnerable species with more consumers. Hence, these oscillations are particularly strong for the less vulnerable species, which increases their probability of extinction. Warming increases the respiration rate of the species, and more energy is lost to metabolism. This results in decreasing biomass oscillations and fewer species extinctions. The combination of these processes determines the final connectance of the food webs. At low body-mass ratios, connectance increases with warming because species with few predators (i.e., low vulnerability) are lost preferentially as a result of their unstable oscillations. At high body-mass ratios, and especially high temperatures, connectance decreases because generalist species become extinct due to the limited energy supply through their weak interactions.

Future directions

Of course, the effects found in our study depended strongly on the values of the model's scaling coefficients. Especially, different scaling relationships for metabolism and feeding rates could change the behavior of the model (Vasseur & McCann, 2005). However, our parameterization for these rates is based on the largest and most comprehensive empirical databases compiled so far (Ehnes *et al.*, 2011; Rall *et al.*, 2012) and thus represents the currently most realistic response of biological parameters to warming and eutrophication. However, future studies may also include more complex scaling relationships of metabolism and functional responses with temperature (Pörtner & Farrell, 2008; Kolokotrones *et al.*, 2010; Ehnes *et al.*, 2011; Colinet *et al.*, 2015), the temperature dependence of other biological processes (Dell *et al.*, 2011), asymmetry in species responses to warming (Dell *et al.*, 2014), the dynamics of nutrients and their effect on plant growth

(Brose, 2008), the interactive effects of temperature and predator body masses on body-size structure (Gibert & DeLong, 2014) and adaptations of the network structure to warming (Petchey *et al.*, 2010; Sentis *et al.*, 2014; Tunney *et al.*, 2014). Moreover, our approach was based on constant temperature, whereas increasing temperature variation may be an even more important threat of global change to natural populations (Sentis *et al.*, 2013; Vasseur *et al.*, 2014; Colinet *et al.*, 2015). Despite our simplifying assumptions, the modeling approach presented here is flexible to include these factors, thus providing a general signature of how natural ecosystems may respond to these interacting global change drivers.

Our results provide strong evidence that two of the most important global change stressors, warming and eutrophication, should have antagonistic effects on the diversity and structure of natural communities. In addition, their effects also depend strongly on the size structure of the community. Energy flux models explain that increasing average consumer-resource body-mass ratios are synergistic with warming and antagonistic to eutrophication. In this vein, we found that communities of similarly sized species such as parasitoid–host systems are stabilized by warming and destabilized by eutrophication. In contrast, the diversity of size-structured predator–prey networks decreases strongly with warming, but is less responsive to eutrophication. Additionally, warming increased species persistence in eutrophic systems, whereas it imposed negative effects on persistence in oligotrophic systems. Interestingly, our model analyses also reveal that the extinctions driven by these two global change stressors are nonrandom. Specifically, warming should lead to higher connectance in networks without size structure and lower connectance in size-structured communities. These multifarious interactions between warming, eutrophication and the community size structure render responses in the real world extremely varied. Models like ours can help disentangling these complex effects of global change and build theory that can be tested in the field. Overall, our results do not only unravel interactive impacts of warming and eutrophication on the diversity and structure of natural communities, and they also suggest that size structure interacts with these global change stressors and may serve as an important proxy for predicting the community sensitivity to them.

References

Amarasekare P (2015) Effects of temperature on consumer–resource interactions. *Journal of Animal Ecology*, **84**, 665–679.

Amarasekare P, Coutinho RM (2014) Effects of temperature on intraspecific competition in ectotherms. *The American Naturalist*, **184**, E50–E65.

Binzer A, Guill C, Brose U, Rall BC (2012) The dynamics of food chains under climate change and nutrient enrichment. *Philosophical Transactions of the Royal Society B: Biological Sciences*, **367**, 2935–2944.

Birkhofer K, Wolters V (2012) The global relationship between climate, net primary production and the diet of spiders. *Global Ecology and Biogeography*, **21**, 100–108.

Brose U (2008) Complex food webs prevent competitive exclusion among producer species. *Proceedings of the Royal Society B: Biological Sciences*, **275**, 2507–2514.

Brose U, Williams RJ, Martinez ND (2006) Allometric scaling enhances stability in complex food webs. *Ecology Letters*, **9**, 1228–1236.

Brose U, Dunne JA, Montoya JM, Petchey OL, Schneider FD, Jacob U (2012) Climate change in size-structured ecosystems. *Philosophical Transactions of the Royal Society B: Biological Sciences*, **367**, 2903–2912.

Brown JH, Gillooly JF, Allen AP, Savage VM, West GB (2004) Toward a metabolic theory of ecology. *Ecology*, **85**, 1771–1789.

Colinet H, Sinclair BJ, Vernon P, Renault D (2015) Insects in fluctuating thermal environments. *Annual Review of Entomology*, **60**, 123–140.

Daufresne M, Lengfellner K, Sommer U (2009) Global warming benefits the small in aquatic ecosystems. *Proceedings of the National Academy of Sciences of the United States of America*, **160**, 12788–12793.

Davey CM, Chamberlain DE, Newson SE, Noble DG, Johnston A (2012) Rise of the generalists: evidence for climate driven homogenization in avian communities. *Global Ecology and Biogeography*, **21**, 568–578.

Dell AI, Pawar S, Savage VM (2011) Systematic variation in the temperature dependence of physiological and ecological traits. *Proceedings of the National Academy of Sciences of the United States of America*, **108**, 10591–10596.

Dell AI, Pawar S, Savage VM (2014) Temperature dependence of trophic interactions are driven by asymmetry of species responses and foraging strategy. *Journal of Animal Ecology*, **83**, 70–84.

Ehnes RB, Rall BC, Brose U (2011) Phylogenetic grouping, curvature and metabolic scaling in terrestrial invertebrates. *Ecology Letters*, **14**, 993–1000.

Fussmann KE, Schwarzmueller F, Brose U, Jousset A, Rall BC (2014) Ecological stability in response to warming. *Nature Climate Change*, **4**, 206–210.

Gibert JP, DeLong JP (2014) Temperature alters food web body-size structure. *Biology Letters*, **10**, 20140473.

Gilbert B, Tunney TD, McCann KS *et al.* (2014) A bioenergetic framework for the temperature dependence of trophic interactions. *Ecology Letters*, **17**, 902–914.

González-Bergonzoni I, Meerhoff M, Davidson TA, Mello FT, Baattrup-Pedersen A, Jeppesen E (2012) Meta-analysis shows a consistent and strong latitudinal pattern in fish omnivory across. *Ecosystems*, **15**, 492–503.

Heckmann L, Drossel B, Brose U, Guill C (2012) Interactive effects of body-size structure and adaptive foraging on food-web stability. *Ecology Letters*, **15**, 243–250.

Johnson DM, Büntgen U, Frank DC *et al.* (2010) Climatic warming disrupts recurrent Alpine insect outbreaks. *Proceedings of the National Academy of Sciences of the United States of America*, **107**, 20576–20581.

Kartascheff B, Guill C, Drossel B (2009) Positive complexity-stability relations in food web models without foraging adaptation. *Journal of Theoretical Biology*, **259**, 12–23.

Kolokotrones T, Savage Van, Deeds EJ, Fontana W (2010) Curvature in metabolic scaling. *Nature*, **464**, 753–756.

MacArthur RH (1972) *Geographical Ecology: Patterns in the Distribution of Species*. Princeton University Press, Princeton, NJ.

Meehan TD (2006) Energy use and animal abundance in litter and soil communities. *Ecology*, **87**, 1650–1658.

Novich RA, Erickson EK, Kalinoski RM, DeLong JP (2014) The temperature independence of interaction strength in a sit-and-wait predator. *Ecosphere*, **5**, art137.

O'Gorman EJ, Pichler DE, Adams G *et al.* (2012) Chapter 2 - Impacts of warming on the structure and functioning of aquatic communities: individual- to ecosystem-level responses. In: *Advances in Ecological Research*, Vol. 47 (eds Guy Woodward UJ and EJO), pp. 81–176. Academic Press, Oxford.

Peñuelas J, Sardans J, Estiarte M *et al.* (2013) Evidence of current impact of climate change on life: a walk from genes to the biosphere. *Global Change Biology*, **19**, 2303–2338.

Petchey OL, McPhearson PT, Casey TM, Morin PJ (1999) Environmental warming alters food-web structure and ecosystem function. *Nature*, **402**, 69–72.

Petchey OL, Brose U, Rall BC (2010) Predicting the effects of temperature on food web connectance. *Philosophical Transactions of the Royal Society B: Biological Sciences*, **365**, 2081–2091.

Peters RH (1983) *The Ecological Implications of Body Size*. Cambridge University Press, Cambridge.

Pörtner HO, Farrell AP (2008) Physiology and climate change. *Science*, **322**, 690–692.

Rall BC, Guill C, Brose U (2008) Food-web connectance and predator interference dampen the paradox of enrichment. *Oikos*, **117**, 202–213.

Rall BC, Vucic-Pestic O, Ehnes RB, Emmerson M, Brose U (2010) Temperature, predator-prey interaction strength and population stability. *Global Change Biology*, **16**, 2145–2157.

Rall BC, Brose U, Hartvig M, Kalinkat G, Schwarzmüller F, Vucic-Pestic O, Petchey OL (2012) Universal temperature and body-mass scaling of feeding rates. *Philosophical Transactions of the Royal Society of London. Series B, Biological sciences*, **367**, 2923–2934.

Riede JO, Brose U, Ebenman B, Jacob U, Thompson R, Townsend CR, Jonsson T (2011) Stepping in Elton's footprints: a general scaling model for body masses and trophic levels across ecosystems. *Ecology Letters*, **14**, 169–178.

Rip JMK, McCann KS (2011) Cross-ecosystem differences in stability and the principle of energy flux. *Ecology Letters*, **14**, 733–740.

Rosenzweig ML (1971) Paradox of enrichment: destabilization of exploitation ecosystems in ecological time. *Science*, **171**, 385–387.

de Sassi C, Lewis OT, Tylianakis JM (2012) Plant-mediated and nonadditive effects of two global change drivers on an insect herbivore community. *Ecology*, **93**, 1892–1901.

Savage VM, Gillooly JF, Brown JH, West GB, Charnov E (2004) Effects of body size and temperature on population growth. *The American Naturalist*, **163**, 429–441.

Schleuning M, Fründ J, Klein A-M *et al.* (2012) Specialization of mutualistic interaction networks decreases toward tropical latitudes. *Current Biology: CB*, **22**, 1925–1931.

Sentis A, Hemptinne J-L, Brodeur J (2013) Effects of simulated heat waves on an experimental plant–herbivore–predator food chain. *Global Change Biology*, **19**, 833–842.

Sentis A, Hemptinne J-L, Brodeur J (2014) Towards a mechanistic understanding of temperature and enrichment effects on species interaction strength, omnivory and food-web structure. *Ecology Letters*, **17**, 785–793.

Shurin JB, Clasen JL, Greig HS, Kratina P, Thompson PL (2012) Warming shifts top-down and bottom-up control of pond food web structure and function. *Philosophical Transactions of the Royal Society B: Biological Sciences*, **367**, 3008–3017.

Tunney TD, McCann KS, Lester NP, Shuter BJ (2014) Effects of differential habitat warming on complex communities. *Proceedings of the National Academy of Sciences of the United States of America*, **111**, 8077–8082.

Vasseur DA, McCann KS (2005) A mechanistic approach for modeling temperature-dependent consumer–resource dynamics. *The American Naturalist*, **166**, 184–198.

Vasseur DA, DeLong JP, Gilbert B *et al.* (2014) Increased temperature variation poses a greater risk to species than climate warming. *Proceedings of the Royal Society B: Biological Sciences*, **281**, 20132612.

Vos M, Kooi BW, DeAngelis DL, Mooij WM (2004) Inducible defences and the paradox of enrichment. *Oikos*, **105**, 471–480.

Vucic-Pestic O, Ehnes R, Rall BC, Brose U (2011) Warming up the system: higher predator feeding rates but lower energetic efficiencies. *Global Change Biology*, **17**, 1301–1310.

Williams RJ, Martinez ND (2000) Simple rules yield complex food webs. *Nature*, **404**, 180–183.

Williams RJ, Martinez ND (2004) Limits to trophic levels and omnivory in complex food webs: theory and data. *The American Naturalist*, **163**, 458–468.

Yodzis P, Innes S (1992) Body size and consumer-resource dynamics. *The American Naturalist*, **139**, 1151–1175.

Research

Authors for correspondence:
Remo Ryser
e-mail: remo.ryser@idiv.de
Christian Guill
e-mail: guill@uni-potsdam.de

†These authors contributed equally to this study.

The biggest losers: habitat isolation deconstructs complex food webs from top to bottom

Remo Ryser[1,2,†], Johanna Häussler[1,2,†], Markus Stark[3,†], Ulrich Brose[1,2], Björn C. Rall[1,2] and Christian Guill[3]

[1]EcoNetLab, German Centre for Integrative Biodiversity Research (iDiv) Halle-Jena-Leipzig, Deutscher Platz 5e, 04103 Leipzig, Germany
[2]Institute of Biodiversity, Friedrich Schiller University Jena, Dornburger-Strasse 159, 07743 Jena, Germany
[3]Institute of Biochemistry and Biology, University of Potsdam, Maulbeerallee 2, 14469 Potsdam, Germany

RR, 0000-0002-3771-8986; JH, 0000-0003-1729-954X; CG, 0000-0002-5955-9998

Habitat fragmentation threatens global biodiversity. To date, there is only limited understanding of how the different aspects of habitat fragmentation (habitat loss, number of fragments and isolation) affect species diversity within complex ecological networks such as food webs. Here, we present a dynamic and spatially explicit food web model which integrates complex food web dynamics at the local scale and species-specific dispersal dynamics at the landscape scale, allowing us to study the interplay of local and spatial processes in metacommunities. We here explore how the number of habitat patches, i.e. the number of fragments, and an increase of habitat isolation affect the species diversity patterns of complex food webs (α-, β-, γ-diversities). We specifically test whether there is a trophic dependency in the effect of these two factors on species diversity. In our model, habitat isolation is the main driver causing species loss and diversity decline. Our results emphasize that large-bodied consumer species at high trophic positions go extinct faster than smaller species at lower trophic levels, despite being superior dispersers that connect fragmented landscapes better. We attribute the loss of top species to a combined effect of higher biomass loss during dispersal with increasing habitat isolation in general, and the associated energy limitation in highly fragmented landscapes, preventing higher trophic levels to persist. To maintain trophic-complex and species-rich communities calls for effective conservation planning which considers the interdependence of trophic and spatial dynamics as well as the spatial context of a landscape and its energy availability.

1. Introduction

Understanding the impact of habitat fragmentation (habitat loss, number of fragments and isolation) on biodiversity is crucial for ecology and conservation biology [1–3]. A general observation and prediction is that large-bodied predators at high trophic levels which depend on sufficient food supplied by lower trophic levels are most sensitive to fragmentation, and thus, might respond more strongly than species at lower trophic levels [4,5]. However, most conclusions regarding the effect of fragmentation are based on single species or competitively interacting species (see references within [6–8], but see for example [9–11] for food chains and simple food web motifs). There is thus limited understanding how species embedded in complex food webs with multiple trophic levels respond to habitat fragmentation [4,12–15], even though these networks are a central organizing theme in nature [16,17].

The stability of complex food webs is, among others, determined by the number and strength of trophic interactions [18]. While it is broadly recognized that habitat fragmentation can have substantial impacts on such feeding relationships [19,20],

we lack a comprehensive and mechanistic understanding of how the disruption or loss of these interactions will affect species persistence and food web stability [15,19,21,22]. Assuming that a loss of habitat, a decreasing number of fragments, and increasing isolation of the remaining fragments disrupt or weaken trophic interactions [7], thereby causing species extinctions [15,20], population and community dynamics might change in unexpected and unpredictable ways. This change in community dynamics might lead to secondary extinctions which potentially cascade through the food web [23,24].

Habitat loss, i.e. the decrease of total habitable area in the landscape or a reduction in patch size, can limit population sizes and biomass production, which might drive energy-limited species extinct [25,26] and subsequently entail cascading extinctions [23]. Successful dispersal among habitat patches might prevent local extinctions (spatial rescue effects), and thus, ensure species persistence at the landscape scale [27,28]. Whether dispersal is successful or not depends, among other factors, on the distance an organism has to travel to reach the next habitat patch and on the quality of the matrix the habitat patches are embedded in (in short: the habitat matrix) [29]. With progressing habitat fragmentation, suitable habitat becomes scarce and the remaining habitat fragments increasingly isolated [3,30], affecting the dispersal network of a species. As a consequence, organisms have to disperse over longer distances to connect habitat patches, which in turn might increase dispersal mortality and thus promote species extinctions [2]. Also, habitat fragmentation often increases the hostility of the habitat matrix, e.g. owing to human land use and landscape degeneration [3,31,32]. The increased matrix hostility might further reduce the likelihood of successful dispersal between habitat patches as the movement through a hostile habitat matrix is energy intensive, and thus, population biomass is lost [29,31]. This loss depends on the distance an organism has to travel and its dispersal ability, i.e. its dispersal range and the energy it can invest into movement. Finally, the detrimental effects of habitat loss and increasing isolation are likely to interact, as dispersal mortality can be expected to have a larger *per capita* effect when a population is already declining owing to decreasing habitat.

In this context, superior dispersers might have an advantage over species with restricted dispersal abilities if the distances between habitat patches expand to a point where dispersal-limited species can no longer connect habitat patches. If this is the case, increasing habitat isolation impedes the ability of organisms to move across a fragmented landscape and prevents spatial rescue effects buffering against local extinctions. Increasing habitat isolation might result in increased extinction rates and ultimately lead to the loss of dispersal-limited species from the regional species pool. As large animal species are, at least up to a certain threshold, faster than smaller ones [33,34], they should also be able to disperse over longer distances [4,35,36]. In fragmented landscapes, this body mass-dependent scaling of dispersal range might favour large-bodied consumers such as top predators, and thus, increase top-down pressure resulting in top-down regulated communities.

Empirical evidence and results from previous modelling approaches, however, suggest that species at higher trophic positions are most sensitive to isolation [9,15,37–39]. Modelling tri-trophic food chains in a patch-dynamic framework, Liao *et al.* [9,10], for example, show that increasing habitat fragmentation leads to faster extinctions of species at higher trophic levels, which they ascribe to reduced availability of prey [9]. In the

fragmentation experiment by Davies *et al.* [39], on the other hand, the observed loss of top species is attributed to the unstable population dynamics of top species under environmental change.

Despite its relevance, a realistic picture and comprehensive understanding of how natural food webs might respond to different aspects of fragmentation such as habitat loss or increasing isolation, and any alteration to the spatial configuration of habitat in general, are lacking. To understand how fragmentation affects the diversity of communities organized in complex food webs requires knowledge of the interplay between their local (trophic) and spatial (dispersal) dynamics. The latter are determined by the number of fragments in the landscape and the distance between them, which can potentially affect the local trophic dynamics. We address this issue using a novel modelling approach which integrates local population dynamics of complex food webs and species-specific dispersal dynamics at the landscape scale (which we hereafter refer to as the meta-food-web model, see figure 1 for a conceptual illustration). Our spatially explicit dynamic meta-food-web model allows us to explore how direct and indirect interactions between species in complex food webs together with spatial processes that connect sub-populations in different habitat patches interact to produce diversity patterns across increasingly fragmented landscapes. Specifically, we ask how the number of fragments and increasing habitat isolation impact the diversity patterns in complex food webs. We further ask which species or trophic groups shape these patterns.

Following general observations and predictions, we expect species diversity within complex food webs to decrease along a gradient of isolation. Based on the substantial variation in both dispersal abilities and energy requirements among species and across trophic levels [4,25,39], we expect species at different trophic levels to strongly vary in their response to isolation. Specifically, we expect certain trophic groups such as consumer species at lower trophic ranks with limited dispersal abilities or top predators with strong resource constraints to be particularly sensitive to isolation. Additionally, with a larger number of fragments we expect more potential for rescue effects, thus fostering survival. This might especially apply to species with large dispersal ranges, which allow them to connect many habitat patches. We test our expectations using Whittaker's classical approach of α-, β- and γ-diversity [40], where α- and γ-diversity describe species richness at the local (patch) and regional (metacommunity) scale, respectively, and β-diversity accounts for compositional differences between local communities.

2. Methods

In the following, we outline a methods summary, for detailed information on equations and parameters see the methods section in the electronic supplementary material. We consider a multitrophic metacommunity consisting of 40 species on a varying number of randomly positioned habitat patches (the meta-food-web, figure 1b). All patches have the same abiotic conditions and each patch can potentially harbour the full food web, consisting of 10 basal plant and 30 animal consumer species. The potential feeding links (i.e. who eats whom) are constant over all patches (figure 1a,b) and are as well as the feeding dynamics determined by the allometric food web model by Schneider *et al.* [41]. We use a dynamic bioenergetic model formulated in terms of ordinary differential equations that describe the feeding and dispersal dynamics. The rate of change in biomass density of a species depends on its biomass gain by feeding and immigration and its biomass loss by
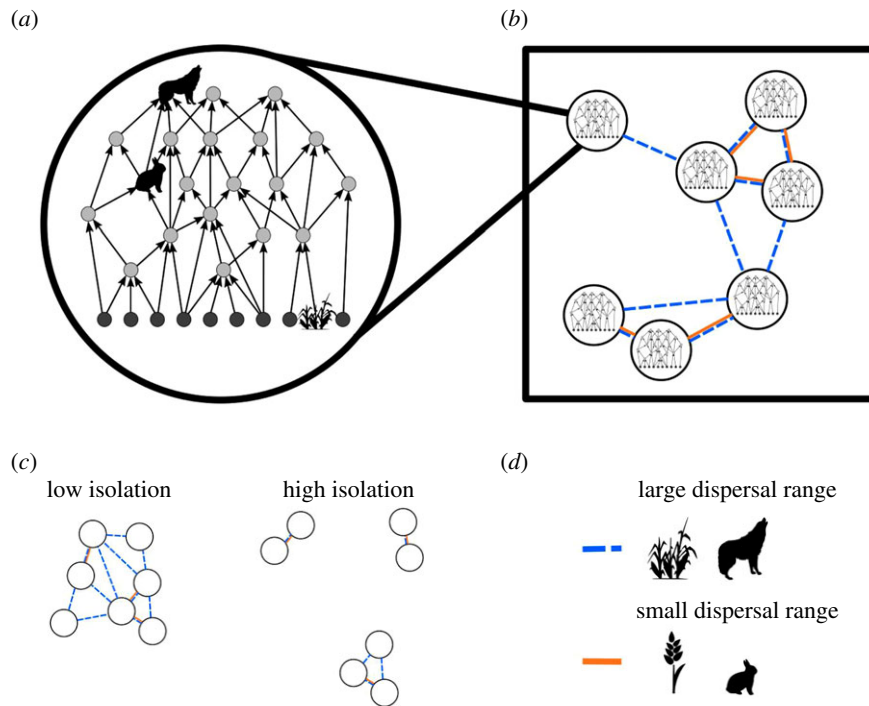
Figure 1. Conceptual illustration of our modelling framework. In our meta-food-web model (*b*), we link local food web dynamics at the patch level (*a*) through dynamic and species-specific dispersal at the landscape scale (*d*). We consider landscapes with identical but randomly distributed habitat patches, i.e. all patches have the same abiotic conditions, and each patch can potentially harbour the full food web. We model fragmented landscapes which differ in the number of habitat patches and the mean distance between patches (*c*).

metabolism, being preyed upon and emigration. We integrate dispersal as species-specific biomass flow between habitat patches (figure 1*b,d*). Based on empirical observations (e.g. [35]) and previous theoretical frameworks (e.g. [4,12,34,42]), we assume that the maximum dispersal distance of animal species increases with their body mass. As plants are passive dispersers, we model their maximum dispersal distance as random and body mass independent. We model emigration rates as a function of each species' *per capita* net growth rate, which is summarizing local conditions such as resource availability, predation pressure, and inter- and intraspecific competition [43]. During dispersal, distance-dependent mortality occurs, i.e. the further two patches are apart, the more biomass is lost to the hostile matrix separating them. We constructed 30 model food webs and simulated each food web on 72 different landscapes. For each simulation, we generated landscapes on two independent gradients covering two aspects of fragmentation, namely number of patches and habitat isolation (figure 1*c*). We achieved a full range for the gradient of habitat isolation (landscape connectance ranging from 0 to 1, figure 3*c*). Additionally, we performed dedicated simulation runs to reference the two extreme cases, i.e. (i) landscapes in which all patches are direct neighbours without a hostile matrix, and thus, no dispersal mortality and (ii) fully isolated landscapes, in which no species can bridge between patches, and thus, a dispersal mortality of 100%. Additionally, we tested a null model in which all species have the same maximum dispersal distance. To visualize the impact of number of patches and habitat isolation on species diversity, we used generalized additive mixed models from the mgcv package in R [44,45]. See the electronic supplementary material for detailed information on the maximum dispersal distance, the additional simulations and the statistical analysis.

3. Results

(a) Species diversity patterns

Our simulation results identify habitat isolation (defined as the mean distance between habitat patches, $\overline{\tau}$, figure 2, *x*-axis)

as the key factor driving species diversity loss. As expected, we find fewer species on patches (the averaged local diversity, $\overline{\alpha}$) in landscapes in which habitats are highly isolated (figure 2*a*). In contrast to the decrease in $\overline{\alpha}$-diversity, β-diversity (figure 2*b*), which describes differences in the community composition between patches, increases with habitat isolation. This increase starts around the inflection point of the landscape connectance at a mean patch distance of $\log_{10} \overline{\tau} \approx$ of -0.5, at which 50% of all possible patch to patch connections are lost (figure 3*c* and the electronic supplementary material, figure S4). γ-diversity, the species diversity in the landscape, shows a more complicated pattern. First it decreases owing to the loss of $\overline{\alpha}$-diversity with habitat isolation. This decrease is then reversed by the increase of β-diversity and the γ-diversity increases again with habitat isolation (figure 2*c*). The number of habitat patches in a landscape, Z (figure 2, *y*-axis), only marginally affects the diversity patterns. The additional simulations of the two extreme cases (i.e. joint scenario with no dispersal loss and fully isolated scenario with 100% dispersal mortality) support these patterns (see the electronic supplementary material, section S7 for the corresponding results). We further show that the isolation-induced species loss also translates into a loss of trophic complexity, i.e. isolated landscapes are characterized by reduced food webs with fewer species and fewer trophic levels (see the electronic supplementary material, figure S2).

(b) Differences among trophic levels

As the number of patches only marginally affects the species diversity patterns, we hereafter focus on the effects of habitat isolation on trophic-dependent differences among species (figure 3). In figure 3, biomass densities, B_i, and landscape connectances, ρ_i, represent the average of each species *i* over all food webs. Species are ranked according to their body
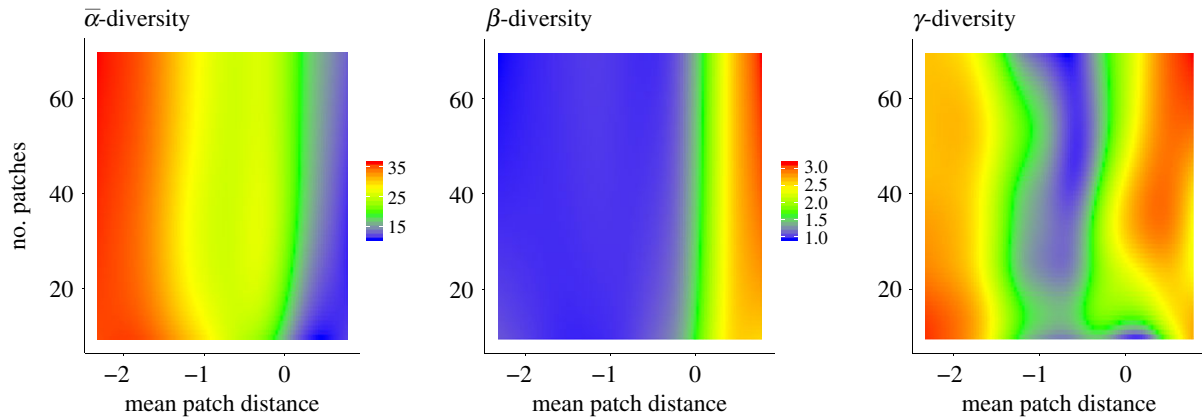
Figure 2. Heatmaps visualizing $\overline{\alpha}$-, β- and γ-diversity (colour-coded; *z*-axis) in response to habitat isolation, i.e. the mean patch distance ($\overline{\tau}$, $\log_{10}$-transformed; *x*-axis) and the number of habitat patches (*Z*; *y*-axis), respectively. We generated the heatmaps based on the statistical model predictions (see the electronic supplementary material).
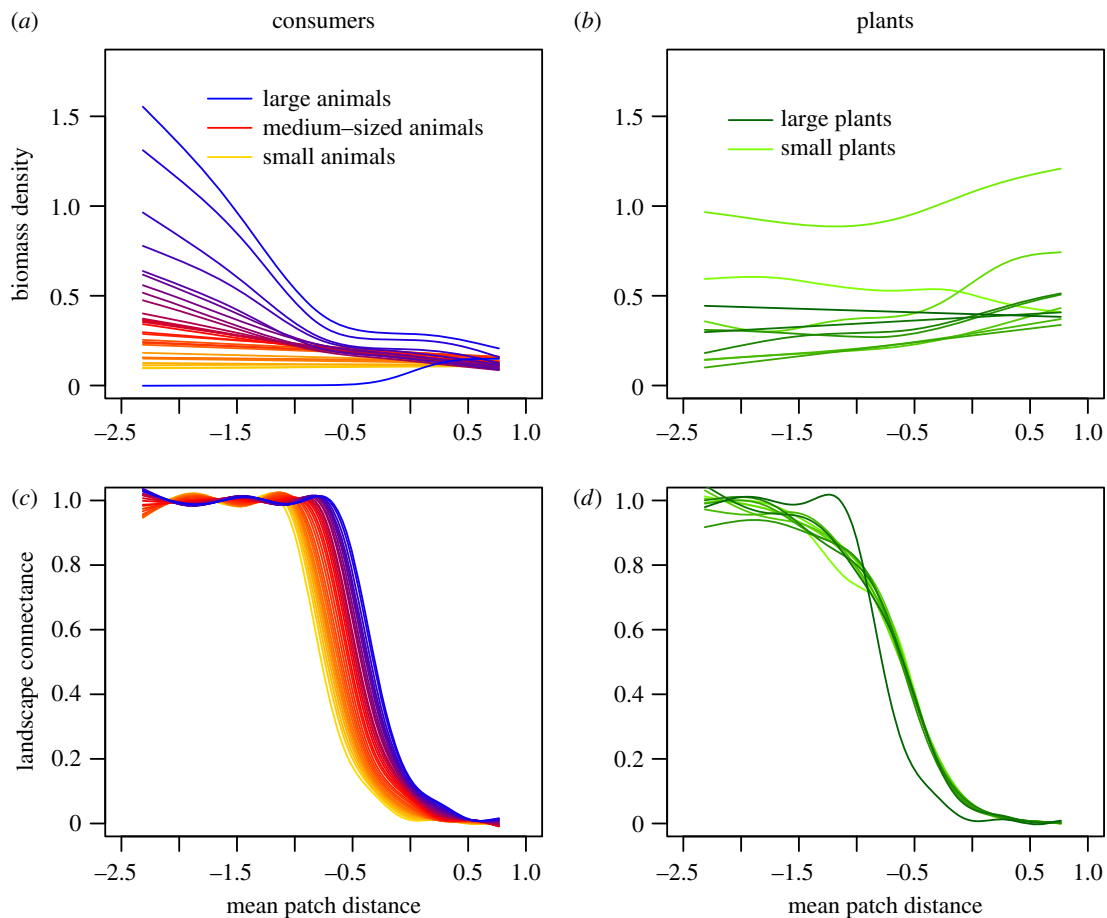

Figure 3. Top row: Mean biomass densities [$\log_{10}$(biomass density + 1)] of animal consumer species (*a*) and basal plant species (*b*) over all food webs (B_i, $\log_{10}$-transformed; *y*-axis) in response to habitat isolation, i.e. the mean patch distance ($\overline{\tau}$, $\log_{10}$-transformed; *x*-axis). Each colour depicts the biomass density of species *i* averaged over all food webs: (*a*) colour gradient where orange represents the smallest, red the intermediate and blue the largest consumer species; (*b*) colour gradient where light green represents the smallest and dark green the largest plant species. Bottom row: Mean species-specific landscape connectance (ρ_i; *y*-axis) for consumer (*c*) and plant species (*d*) over all food webs as a function of the mean patch distance ($\overline{\tau}$, $\log_{10}$-transformed; *x*-axis). See the electronic supplementary material, figure S9 for standard errors in biomass densities for four exemplary species.

mass. Thus, although species body masses differ between food webs, species 1 is always the smallest, species 2 the second smallest and so forth. The same applies to ρ_i, where the landscape connectance of consumer species is body mass dependent, but the connectance of plant species is body mass independent (see the methods section). In well-connected landscapes (i.e. landscapes with small mean patch distances, $\overline{\tau}$), large and medium-sized consumer species (except the

very largest) have higher population biomass densities than smaller consumers (figure 3*a,c*). With expanding distances between habitat patches, large-bodied consumers at high trophic positions (figure 3*a*, red to blue lines) show a particularly strong decrease in population biomass densities. Small consumer species (figure 3*a*, orange lines) are generally less affected by increasing habitat isolation. Plant species show a less consistent response to increased isolation, with most

species slightly increasing their biomass density (figure 3b). Based on our assumption that the maximum dispersal distance of animals scales with body mass, the ability to connect a landscape follows the same allometric scaling (figure 3c). Despite this dispersal advantage, intermediate-sized and large animal species (figure 3a, red to blue lines) lose biomass in landscapes in which they still have the potential to fully connect (almost) all habitat patches (figure 3c). The differences in plant species biomass densities cannot be attributed to body mass dependent species-specific dispersal distances as for plants maximum dispersal distances were randomly assigned, and thus, there is no connection between body mass and landscape connectance (ρ_i, figure 3d). Additional simulations, in which we assumed a constant maximum dispersal distance for all species of $\delta_i = \delta_{max} = 0.5$, support the negligibility of species-specific differences in dispersal ability for the emerging diversity patterns (see the electronic supplementary material, figure S3).

4. Discussion

Habitat fragmentation is a major driver of global biodiversity decline. To date, a comprehensive understanding of how the different aspects of habitat fragmentation, i.e. habitat loss [6], number of fragments and isolation, affect the diversity patterns of species embedded in complex ecological networks such as food webs is lacking (see e.g. meta-analysis by Martinson & Fagan [15], and references therein). Our simulation experiment allows us to independently explore the effects of number of fragments (i.e. number of habitat patches in the landscape), and of habitat isolation (i.e. distance between patches) on persistence and biomass densities of species in complex communities. We identified habitat isolation to be responsible for species diversity decline both at the local and regional scale.

The rate at which a species loses biomass density strongly depends on its trophic position. Large-bodied consumer species at the top of the food web are most sensitive to isolation although they are dispersing most effectively (i.e. for them, increasing distances between habitat patches do not necessarily result in the loss of dispersal pathways or a substantial increase of dispersal mortality). Surprisingly, we find top species to lose biomass density and sometimes even go extinct in landscapes they can still fully connect, whereas the biomass densities of small consumer species at lower trophic levels and plant species are only marginally affected by increasing habitat isolation. We attribute the accelerated loss of top species to the energy limitation propagated through the food web: with increasing habitat isolation an increasing fraction of the biomass production of the lower trophic levels is lost owing to mortality during dispersal and is thus no longer available to support the higher trophic levels. Additionally, the reduced top-down pressure on smaller consumers seems to compensate for their increased dispersal loss. Our model adds a complementary perspective to previous research pointing towards a trophic-dependent extinction risk owing to constraints in resource availability with increasing habitat fragmentation [9,38].

(a) Habitat isolation drives species loss

The increasing isolation of habitat fragments poses a severe threat to species persistence (but see [46,47]). We demonstrate in our simulation experiment that the generally observed pattern of species loss with increasing habitat isolation (e.g. [3])

also holds for species embedded in large food webs. The loss of species occurs both at the local ($\overline{\alpha}$-diversity) and regional (γ-diversity) scale. For the latter, however, an increase in β-diversity compensates the loss in local diversity ($\overline{\alpha}$) when landscapes become very isolated and γ-diversity increases again (see section below: Habitat isolation promotes β-diversity).

We modelled dispersal between habitat patches by assuming an energy loss for the dispersing organisms—a biologically realistic assumption as landscape degeneration, which often occurs concurrently with habitat fragmentation, increases the hostility of the habitat matrix [3]. Consequently, the dispersal mortality, and thus, biomass loss of populations to the habitat matrix increases substantially when dispersal distances between habitat patches expand. To account for the variation in dispersal ability among trophic groups, we incorporated species-specific maximum dispersal distances. For animal species, this maximum dispersal distance increases like a power law with body mass, therefore weakening the direct effect of habitat isolation the larger a species is. Despite this, top predators and other large consumer species respond strongly to isolation. These species exhibit a dramatic loss in biomass density or even go extinct in landscapes they still perceive as almost fully connected (landscape connectance, ρ_i, close to one), which indicates that their response to habitat isolation is mediated by indirect effects originating from the local food web dynamics.

(b) Local food web dynamics and energy limitation drive top predator loss

In local food webs, energy is transported rather inefficiently from the basal to the top species, with transfer efficiency in natural systems often only around 10% [48]. This energy limitation effectively controls the food chain length [26] and renders large species at high trophic levels vulnerable to extinction owing to resource shortage [49]. In our model, energy availability decreases if habitat isolation is high as this increases biomass loss during dispersal. This affects particularly small species at lower trophic levels because they generally have the highest metabolic costs per unit biomass and therefore the highest biomass losses per distance travelled [33,41]. The biomass loss during dispersal consequently reduces the net biomass production at the bottom of the food web and severely threatens species at higher trophic positions that already operate on a very limited resource supply.

Moreover, owing to the feedback mechanisms regulating the community dynamics within complex food webs, a loss of top consumer species can have severe consequences for the functioning and stability of the network [21,22]. A loss of top-down regulation can, for instance, lead to secondary extinctions resulting in simpler food webs [21,50]—an additional mechanism that can foster the loss of biodiversity as observed in our simulations. However, we also see a much more direct effect of the changing community composition: the biomass densities of small species that suffer most from increased dispersal mortality do not, as one might expect, decline much as isolation progresses. We attribute this to a release from top-down control as their consumers lose biomass or even go extinct, which counters the negative direct effect of habitat isolation. These arguments suggest that differential dispersal capabilities are less important than energetic limitations in explaining the strong negative response of large consumers to habitat isolation. This claim is supported

by the additional simulations where all species experienced the same level of dispersal mortality, which yielded similar results (see the electronic supplementary material, figure S3).

We did not find an effect of the number of patches on $\bar{\alpha}$-, β- and γ-diversity. As we model biomass densities on patches without defined area (see section below: Model specifications), fewer patches do not reflect habitat loss, but rather the loss of fragments, i.e. stepping stones in the dispersal network. Thus, the energy limitation in our simulated landscapes derives from direct dispersal loss and cascading effects of dispersal losses of resources. For plant and small animal species, this can be understood easily, as these species are less energy limited and thus are able to persist on a single habitat patch. For larger animal species the situation is more subtle: while they can integrate over multiple patches, feeding interactions still always occur on one patch at a time. If the biomass densities of their resources (and thus also the realized feeding rate) is too low on a particular patch to cover their metabolic requirements, they gain no advantage from the addition of more patches with equally low resource abundance.

(c) Habitat isolation promotes β-diversity

Contrary to the decline in $\bar{\alpha}$-diversity with increasing habitat isolation, we find an increase in β-diversity starting from around $\log_{10}$ mean patch distance $\bar{\tau} \approx -0.5$. We assumed identical abiotic conditions on all habitat patches, i.e. there are no differences in nutrient availability or background mortality rates. Therefore, any differences in conditions experienced by the species on different patches can only originate from the initial community composition and the structure of the dispersal network. One way for such different conditions to emerge is the disintegration of the dispersal network into several smaller clusters. Up to a $\log_{10}$ mean patch distance $\bar{\tau} \approx -0.5$, the species with the largest maximum dispersal distance (which could be both large animals that have not already gone extinct and plants with a randomly selected large dispersal distance) have a landscape connectance (ρ_i) of at least 0.5. This dispersal advantage easily allows them to connect all patches to a single network component, thereby providing homogenization for the meta-food-web. However, as the mean patch distance increases further, even these species cannot bridge all gaps in the habitat matrix any more and clusters of patches emerge that are for all species disconnected from the other patches. As these clusters vary in the number of patches and mean patch distance within the cluster, the level of dispersal mortality experienced by the species on the different clusters can also vary considerably. Any further increase in mean patch distance causes the landscape connectance to drop to nearly zero for all species and all patches within the landscape approach complete isolation. With no immigration into isolated patches, non-resident species cannot colonize them and initial community compositions drive dissimilarities among patches. However, the initial β-diversity is not sufficient in explaining the high β-diversity in strongly isolated landscapes (electronic supplementary material, figure S4). This suggests that different food web positions of initial species lead to different cascading effects in local food web dynamics with more or less secondary extinctions on isolated patches further increasing differences in local community compositions. The increase in β-diversity is even stronger than the loss of local diversity resulting in an increase in γ-diversity in highly isolated landscapes. However, species contributing to this high γ-diversity tend to occur on fewer patches and thus are more prone to go extinct in the whole landscape owing to stochastic extinction events.

(d) Model specifications

The framework we propose here for modelling meta-food-webs is very general and allows for a straightforward implementation of future empirical insight where we so far had to rely on plausible assumptions. The trophic network model for the local food webs is based on a tested and realistic allometric framework [41] with a fixed number of 40 species—a typical value in dynamic food web modelling (e.g. [51,52]). We based all model parameters on allometric principles [33,53] allowing for a simple adaptation of our modelling approach to other trophic networks such as empirically sampled food webs [54] or other food web models such as the niche model [55]. Moreover, empirical patch networks (e.g. the coordinates of meadows in a forest landscape) or other dispersal mechanisms [6,56] may be incorporated in the future. In our simulations, biomass loss during dispersal is predominantly responsible for the decline in species diversity. We linked the maximum dispersal distance of animals and thereby also their mortality during dispersal to body mass, which is plausible because larger animal species can move faster [34], and thus, have to spend less time in the hostile habitat matrix. Interestingly, however, we did not find any empirical study relating body mass directly to mortality or biomass loss during migration. If such information becomes available in the future, it can be easily incorporated into our modelling framework. Further, we deliberately assumed all habitat patches to share the same abiotic conditions [57] as we wanted to focus on the general effects of the interaction of complex food web and dispersal dynamics. Adding habitat heterogeneity among patches, e.g. by modifying nutrient availability or mean temperature, however, is straightforward and can be expected to yield additional insight into the mechanisms for the maintenance of species diversity in meta-food-webs. Finally, by using a dynamical model formulated in terms of biomass densities instead of absolute biomasses (or population sizes), we make the implicit assumption that patches do not have an absolute size. Thus, the number of patches in a landscape cannot be directly linked to the total amount of habitat but rather reflects the number of fragments, i.e. stepping stones in the dispersal network of a species. A decreasing number of patches thus does not necessarily imply habitat loss. In order to also address effects of habitat loss (in terms of area), the model could be adapted to include, for example, area-specific extinction thresholds and absolute biomasses in dispersal dynamics, but this was beyond the scope of this study.

(e) Synthesis and outlook

Our simulation experiment demonstrates that habitat isolation reduces species diversity in complex food webs in general, with differences in the effect across trophic levels. In increasingly isolated landscapes, energy becomes limited, which decreases the biomass density of large consumers or even drives them extinct. These primary extinctions may result in a cascade of secondary extinctions, given the importance of top predators for food web stability [24,58]. The increased risk of network downsizing, i.e. simple food webs with fewer and smaller species [14,59], stresses the importance to consider both direct and indirect trophic interactions as well as dispersal when assessing the extinction risk of species embedded in complex food webs and other ecological networks.

To date, most conservation research focuses on single species and does not consider the complex networks of interactions in natural communities [7,14]. However, the patterns we presented here clearly support previous studies highlighting the importance of trophic interactions (e.g. [9,37,38]). We show that the fragmentation-induced extinction risk of species strongly depends on their trophic position, with top species being particularly vulnerable. Given that top-down regulation can stabilize food webs [24,58], the loss of top predators might entail unpredictable consequences for adjacent trophic levels, destabilize food webs, reduce species diversity and trophic complexity and ultimately compromise ecosystem functioning [23,24]. In addition to the trophic position of a species, the trophic structure of the food web has also been shown to be an important aspect [11]. Our results suggest that bottom-up energy limitation caused by dispersal mortality owing to habitat isolation can be a critical factor driving species loss and the reduction of trophic complexity. The extent of this loss strongly depends on the spatial context (see also [6]). Thus, to maintain species-rich and trophic-complex natural communities under future environmental change, effective conservation planning must consider this interdependence of spatial and trophic dynamics. Notably, conservation planning should also consider habitat isolation and matrix hostility (and consequently dispersal mortality) to ensure sufficient biomass exchange between local populations, capable of inducing spatial rescue effects and to alleviate bottom-up energy limitation of large consumers. Energy limitations can also result from habitat loss (which we did not model here), decreasing energy availability at the bottom of the food web affecting local dynamics intrinsically independent of dispersal. Thus, avoiding habitat loss remains a crucial aspect [2,47]. We highlight the need to explore food webs and other complex ecological networks in a spatial context to achieve a more holistic understanding of biodiversity and ecosystem processes.

References

1. Tilman D, May RM, Lehman CL, Nowak MA. 1994 Habitat destruction and the extinction debt. *Nature* **371**, 65–66. (doi:10.1038/371065a0)

2. Fahrig L. 2003 Effects of habitat fragmentation on biodiversity. *Annu. Rev. Ecol. Evol. Syst.* **34**, 487–515. (doi:10.1146/annurev.ecolsys.34.011802.132419)

3. Haddad NM *et al*. 2015 Habitat fragmentation and its lasting impact on Earth's ecosystems. *Sci. Adv.* **1**, e1500052. (doi:10.1126/sciadv.1500052)

4. Holt RD. 2002 Food webs in space: on the interplay of dynamic instability and spatial processes. *Ecol. Res.* **17**, 261–273. (doi:10.1046/j.1440-1703.2002.00485.x)

5. Henle K, Davies KF, Kleyer M, Margules C, Settele J. 2004 Predictors of species sensitivity to fragmentation. *Biodivers. Conserv.* **13**, 207–251. (doi:10.1023/B:BIOC.0000004319.91643.9e)

6. Melián CJ, Bascompte J. 2002 Food web structure and habitat loss. *Ecol. Lett.* **5**, 37–46. (doi:10.1046/j.1461-0248.2002.00280.x)

7. Valiente-Banuet A *et al*. 2015 Beyond species loss: the extinction of ecological interactions in a changing world. *Funct. Ecol.* **29**, 299–307. (doi:10.1111/1365-2435.12356)

8. Rybicki J, Hanski I. 2013 Species-area relationships and extinctions caused by habitat loss and fragmentation. *Ecol. Lett.* **16**, 27–38. (doi:10.1111/ele.12065)

9. Liao J, Bearup D, Blasius B. 2017 Diverse responses of species to landscape fragmentation in a simple food chain. *J. Anim. Ecol.* **86**, 1169–1178. (doi:10.1111/1365-2656.12702)

10. Liao J, Bearup D, Wang Y, Nijs I, Bonte D, Li Y, Brose U, Wang S, Blasius B. 2017 Robustness of metacommunities with omnivory to habitat destruction: disentangling patch fragmentation from patch loss. *Ecology* **38**, 42–49. (doi:10.1002/ecy.1830)

11. Liao J, Bearup D, Blasius B. 2017 Food web persistence in fragmented landscapes. *Proc. R. Soc. B* **284**, 20170350. (doi:10.1098/rspb.2017.0350)

12. Holt R, Hoopes M. 2005 *Food web dynamics in a metacommunity context: modules and beyond. October 2016*. Chicago, IL: The University of Chicago Press.

13. Amarasekare P. 2008 Spatial dynamics of foodwebs. *Annu. Rev. Ecol. Evol. Syst.* **39**, 479–500. (doi:10.1146/annurev.ecolsys.39.110707.173434)

14. Hagen M *et al*. 2012 Biodiversity, species interactions and ecological networks in a fragmented world. *Adv. Ecol. Res.* **46**, 89–210. (doi:10.1016/B978-0-12-396992-7.00002-2)

15. Martinson HM, Fagan WF. 2014 Trophic disruption: a meta-analysis of how habitat fragmentation affects resource consumption in terrestrial arthropod systems. *Ecol. Lett.* **17**, 1178–1189. (doi:10.1111/ele.12305)

16. Elton CSCS. 1927 *Animal ecology*. Chicago, IL: University of Chicago Press.

17. Dunne JA. 2005 The network structure of food webs. In *Ecological networks linking structure to dynamics in food webs* (eds M Pascual, JA Dunne), pp. 27–90. Oxford, UK: Oxford University Press.

18. May RM. 1972 Will a large complex system be stable? *Nature* **238**, 413–414. (doi:10.1038/238413a0)

19. Kondoh M. 2003 Habitat fragmentation resulting in overgrazing by herbivores. *J. Theor. Biol.* **225**, 453–460. (doi:10.1016/S0022-5193(03)00279-0)

20. Valladares G, Salvo A, Cagnolo L. 2006 Habitat fragmentation effects on trophic processes of insect-plant food webs. *Conserv. Biol.* **20**, 212–217. (doi:10.1111/j.1523-1739.2006.00337.x)

21. Dobson A *et al*. 2006 Habitat loss, trophic collapse, and the decline of ecosystem services. *Ecology* **87**, 1915–1924. (doi:10.1890/0012-9658(2006)87[1915:HLTCAT]2.0.CO;2)

22. Rooney N, Mccann K, Gellner G, Moore JC. 2006 Structural asymmetry and the stability of diverse food webs. *Nature* **442**, 265–269. (doi:10.1038/nature04887)

23. Dunne JA, Williams RJ. 2009 Cascading extinctions and community collapse in model food webs. *Phil. Trans. R. Soc. B* **364**, 1711–1723. (doi:10.1098/rstb.2008.0219)

24. Curtsdotter A, Binzer A, Brose U, de Castro F, Ebenman B, Eklöf A, Riede JO, Thierry A, Rall BC. 2011 Robustness to secondary extinctions:

comparing trait-based sequential deletions in static and dynamic food webs. *Basic Appl. Ecol.* **12**, 571–580. (doi:10.1016/J.BAAE.2011.09.008)

25. Post DM. 2002 The long and short of food-chain length. *Trends Ecol. Evol.* **17**, 269–277. (doi:10.1016/S0169-5347(02)02455-2)

26. Takimoto G, Post DM. 2013 Environmental determinants of food-chain length: a meta-analysis. *Ecol. Res.* **28**, 675–681. (doi:10.1007/s11284-012-0943-7)

27. Brown JH, Kodric-Brown A. 1977 Turnover rates in insular biogeography: effect of immigration on extinction. *Ecology* **58**, 445–449. (doi:10.2307/1935620)

28. Hanski I. 1998 Metapopulation dynamics. *Nature* **396**, 41–49. (doi:10.1038/23876)

29. Bonte D *et al.* 2012 Costs of dispersal. *Biol. Rev. Camb. Philos. Soc.* **87**, 290–312. (doi:10.1111/j.1469-185X.2011.00201.x)

30. Fahrig L. 1997 Relative effects of habitat loss and fragmentation on population extinction. *J. Wildl. Manage* **61**, 603–600. (doi:10.2307/3802168)

31. Prugh LR, Hodges KE, Sinclair ARE, Brashares JS. 2008 Effect of habitat area and isolation on fragmented animal populations. *Proc. Natl Acad. Sci. USA* **105**, 20 770–20 775. (doi:10.1073/pnas.0806080105)

32. LeCraw RM, Kratina P, Srivastava DS. 2014 Food web complexity and stability across habitat connectivity gradients. *Oecologia* **176**, 903–915. (doi:10.1007/s00442-014-3083-7)

33. Peters RH. 1983 *The ecological implications of body size*. Cambridge, UK: Cambridge University Press.

34. Hirt MR, Jetz W, Rall RC, Brose U. 2017 A general scaling law reveals why the largest animals are not the fastest. *Nat. Ecol. Evol.* **1**, 1116–1122. (doi:10.1038/s41559-017-0241-4)

35. Jenkins DG *et al.* 2007 Does size matter for dispersal distance? *Glob. Ecol. Biogeogr.* **16**, 415–425. (doi:10.1111/j.1466-8238.2007.00312.x)

36. van Noordwijk CGET *et al.* 2015 Species-area relationships are modulated by trophic rank, habitat affinity, and dispersal ability. *Ecology* **96**, 518–531. (doi:10.1890/14-0082.1)

37. Holyoak M. 2008 Habitat subdivision causes changes in food web structure. *Ecol. Lett.* **3**, 509–515. (doi:10.1111/j.1461-0248.2000.00180.x)

38. van Nouhuys S. 2005 Effects of habitat fragmentation at different trophic levels in insect communities. *Ann. Zool. Fennici* **42**, 433–447. (doi:10.2307/23735888)

39. Davies KF, Margules CR, Lawrence JF. 2000 Which traits of species predict population declines in experimental forest fragments? *Ecology* **81**, 1450–1461. (doi:10.1890/0012-9658(2000)081[1450:WTOSPP]2.0.CO;2)

40. Whittaker RH. 1972 Evolution and measurement of species diversity. *Taxon* **21**, 213–251. (doi:10.2307/1218190)

41. Schneider FD, Brose U, Rall BC, Guill C. 2016 Animal diversity and ecosystem functioning in dynamic food webs. *Nat. Comm.* **7**, 3–8. (doi:10.1038/ncomms12718)

42. Jetz W, Carbone C, Fulford J, Brown JH. 2004 The scaling of animal space use. *Science* **306**, 266–268. (doi:10.1126/science.1102138)

43. Fronhofer EA *et al.* 2018 Bottom-up and top-down control of dispersal across major organismal groups. *Nat. Ecol. Evol.* **2**, 1859–1863. (doi:10.1038/s41559-018-0686-0)

44. R Core Team. 2016 *R: a language and environment for statistical computing*. Vienna, Austria: R Foundation for Statistical Computing. See https://www.R-project.org.

45. Wood SN. 2006 *Generalized additive models: an introduction with R*. Boca Raton, FL: CRC Press/Chapman and Hall.

46. Fahrig L. 2017 Ecological responses to habitat fragmentation per se. *Annu. Rev. Ecol. Evol. Syst.* **48**, 1–23. (doi:10.1146/annurev-ecolsys-110316-022612)

47. Fahrig L *et al.* 2019 Is habitat fragmentation bad for biodiversity? *Biol. Conserv.* **230**, 179–186. (doi:10.1016/j.biocon.2018.12.026)

48. Lindeman RL. 1942 The trophic-dynamic aspect of ecology. *Ecology* **23**, 399–417. (doi:10.2307/1930126)

49. Binzer A, Guill C, Brose U, Rall BC. 2012 The dynamics of food chains under climate change and nutrient enrichment. *Phil. Trans. R. Soc. B* **367**, 2935–2944. (doi:10.1098/rstb.2012.0230)

50. Brose U, Dunne JA, Montoya JM, Petchey OL, Schneider FD, Jacob U. 2012 Climate change in size-structured ecosystems. *Phil. Trans. R. Soc. B* **367**, 2903–2912. (doi:10.1098/rstb.2012.0232)

51. Brose U *et al.* 2006 Consumer-resource body-size relationships in natural food webs. *Ecology* **87**, 2411–2417. (doi:10.1890/0012-9658(2006)87[2411:CBRINF]2.0.CO;2)

52. Rall BC, Guill C, Brose U. 2008 Food-web connectance and predator interference dampen the paradox of enrichment. *Oikos* **117**, 202–213. (doi:10.1111/j.2007.0030-1299.15491.x)

53. Rall BC, Brose U, Hartvig M, Kalinkat G, Schwarzmüller F, Vucic-Pestic O, Petchey OL. 2012 Universal temperature and body-mass scaling of feeding rates. *Phil. Trans. R. Soc. B* **367**, 2923–2934. (doi:10.1098/rstb.2012.0242)

54. Brose U, Williams RJ, Martinez ND. 2006 Allometric scaling enhances stability in complex food webs. *Ecol. Lett.* **9**, 1228–1236. (doi:10.1111/j.1461-0248.2006.00978.x)

55. Williams RJ, Martinez ND. 2000 Simple rules yield complex food webs. *Nature* **404**, 180–183. (doi:10.1038/35004572)

56. Eklöf A, Kaneryd L, Münger P, Eklof A, Kaneryd L, Munger P. 2012 Climate change in metacommunities: dispersal gives double-sided effects on persistence. *Phil. Trans. R. Soc. B* **367**, 2945–2954. (doi:10.1098/rstb.2012.0234)

57. Leibold MA *et al.* 2004 The metacommunity concept: a framework for multi-scale community ecology. *Ecol. Lett.* **7**, 601–613. (doi:10.1111/j.1461-0248.2004.00608.x)

58. Brose U. 2008 Complex food webs prevent competitive exclusion among producer species. *Proc. R. Soc. B* **275**, 2507–2514. (doi:10.1098/rspb.2008.0718)

59. Duffy JE. 2003 Biodiversity loss, trophic skew and ecosystem functioning. *Ecol. Lett.* **6**, 680–687. (doi:10.1046/j.1461-0248.2003.00494.x)

60. Ryser R, Häussler J, Stark M, Brose U, Rall BC, Guill C. 2019 Data from: The biggest losers: habitat isolation deconstructs complex food webs from top to bottom. Dryad Digital Repository. (https://doi.org/10.5061/dryad.c624907)

ORIGINAL PAPER

Patch isolation and periodic environmental disturbances have idiosyncratic effects on local and regional population variabilities in meta-food chains

Markus Stark[1] · **Moritz Bach**[1] · **Christian Guill**[1]

Abstract

While habitat loss is a known key driver of biodiversity decline, the impact of other landscape properties, such as patch isolation, is far less clear. When patch isolation is low, species may benefit from a broader range of foraging opportunities, but are at the same time adversely affected by higher predation pressure from mobile predators. Although previous approaches have successfully linked such effects to biodiversity, their impact on local and metapopulation dynamics has largely been ignored. Since population dynamics may also be affected by environmental disturbances that temporally change the degree of patch isolation, such as periodic changes in habitat availability, accurate assessment of its link with isolation is highly challenging. To analyze the effect of patch isolation on the population dynamics on different spatial scales, we simulate a three-species meta-food chain on complex networks of habitat patches and assess the average variability of local populations and metapopulations, as well as the level of synchronization among patches. To evaluate the impact of periodic environmental disturbances, we contrast simulations of static landscapes with simulations of dynamic landscapes in which 30 percent of the patches periodically become unavailable as habitat. We find that increasing mean patch isolation often leads to more asynchronous population dynamics, depending on the parameterization of the food chain. However, local population variability also increases due to indirect effects of increased dispersal mortality at high mean patch isolation, consequently destabilizing metapopulation dynamics and increasing extinction risk. In dynamic landscapes, periodic changes of patch availability on a timescale much slower than ecological interactions often fully synchronize the dynamics. Further, these changes not only increase the variability of local populations and metapopulations, but also mostly overrule the effects of mean patch isolation. This may explain the often small and inconclusive impact of mean patch isolation in natural ecosystems.

Keywords Metacommunity dynamics · Dispersal · Patch isolation · Stability · Synchronization · Disturbance

Introduction

Anthropogenic habitat degradation and loss are strong negative drivers of biodiversity on local and global scales (Butchart et al. 2010; Pereira et al. 2010; Pimm et al. 2014). While habitat loss has a clear cause–effect relationship with declining diversity induced by, e.g., lack of resources, habitat size restrictions or increased mortality (Brooks et al. 2002; Duraiappah et al. 2005), the effect of other modifications of the landscape such as fragmentation is still intensely debated (Hanski 2015; Fahrig 2017; Fletcher et al. 2018;

Fahrig et al. 2019). Following Fahrig (2003), habitat fragmentation comprises three main components: the number of patches, patch isolation and patch size, but excludes habitat loss. Their respective effects are more difficult to assess because they are usually weaker than the effects of habitat loss (Fahrig 2003) and often confounded with the latter (Didham et al. 2012).

In metacommunities, patch isolation determines to which extent individuals can disperse through the landscape and thereby contribute to the regional distribution and persistence of species. Empirical and experimental studies report, however, conflicting results of patch isolation at different spatial scales: Negative effects on regional diversity have been attributed to the prevention of rescue effects (Levins 1969; Gotelli 1991), but also positive effects on local diversity have been recorded (Fahrig 2017). On the local scale dispersal can

✉ Markus Stark
mstark@uni-potsdam.de

1   Institute of Biochemistry and Biology, University
of Potsdam, Maulbeerallee 2, Potsdam 14469, Germany

also alter biotic interactions among species directly, emphasizing the interplay between local and regional dynamics in metacommunities (Walting and Donnelly 2006). Recent modeling approaches on metacommunities try to integrate more details of local and regional aspects regarding landscape attributes and species interactions, but mainly focus on species persistence and diversity (Pillai et al. 2011; Ryser et al. 2019) and ignore effects of dispersal on local population dynamics and its relevance for stability (LeCraw et al. 2014).

A major concern of models that include explicit population dynamics are mechanisms that synchronize population cycles between habitat patches. Such synchronous oscillations destabilize metapopulations by amplifying the amplitude of oscillations in their regional abundances and increasing the extinction risk of species in entire regions due to correlated local extinction events. Conversely, asynchronous oscillations can promote regional persistence and stability through rescue effects (Levins 1969; Blasius et al. 1999) or the portfolio effect (Schindler et al. 2015; Thorson et al. 2018). These models, which are often limited to either a small number of patches or to regular, rectangular lattices (Briggs and Hoopes 2004), have established that the synchronicity of population oscillations between patches generally increases with dispersal rate (Sherratt et al. 2000; Jansen 2001). Other factors affecting synchronicity are adaptive dispersal (Abrams 2007; Abrams and Ruokolainen 2011), inter- and intraspecific density dependence of dispersal rates (Hauzy et al. 2010), and costliness or distance dependence of dispersal (Koelle and Vandermeer 2005). In larger networks of habitat patches, an irregular network structure favors asynchronous dynamics (Holland and Hastings 2008), but high dispersal rates again lead to synchronous oscillations that are detrimental for species persistence (Plitzko and Drossel 2015). At larger effective distance between patches, dispersal between them is limited (Koelle and Vandermeer 2005; Fletcher et al. 2016), linking the results regarding synchronization of population oscillations to research on the effect of patch isolation. Indeed, it has been shown that synchronization among natural populations declines with increasing distance between them (Ranta et al. 1995).

While synchronization is often linked to dispersal rate and thereby implicitly to landscape properties like patch isolation, it can also be directly affected by correlated environmental fluctuations (Moran 1953; Ranta et al. 1995; Koenig 1999; Kahilainen et al. 2018). These fluctuations can affect demographic rates of the species via changing environmental conditions (like ambient temperature or resource availability), but they can also directly influence the availability of patches as habitable areas. As an example for the latter, a landscape in which both a temporally variable environment and a pronounced spatial structure strongly affect ecological communities is kettle holes in formerly glaciated regions (Kalettka and Rudat 2006). These small ponds are typically

formed in large clusters, and seasonal changes of temperature and precipitation cause some of them to be only temporally filled with water. The local aquatic communities of these temporary ponds thus periodically become completely extinct, and recolonization through dispersing species from permanent ponds is a key element to reestablish the communities (De Meester et al. 2005). As the recolonization happens in a temporally correlated manner at the beginning of the wet season, a synchronizing effect on the population dynamics can be expected. However, this is again contingent on the spatial structure of the landscape, as lower dispersal rates due to higher mean patch isolation can impede the recolonization process.

So far, the interaction between these drivers of synchronization and population variability in general remains largely unexplored (but see (Gouhier et al. 2010)), despite the fact that anthropogenic activity continues to increase both habitat degradation and environmental variability. In order to fill this gap, we examine the dynamics of a meta-food chain in large, spatially explicit networks of habitat patches and analyze its stability with respect to the mean patch isolation of the landscape and environmental disturbances that periodically render a subset of the patches uninhabitable. We chose a food chain as model system because it has, on the one hand, a simple and tractable structure that, on the other hand, already allows for indirect effects mediated by feeding interactions on different trophic levels. In order to obtain a complete picture of the effects of patch isolation and periodic environmental disturbances on the extent and synchronicity of population oscillations in food chains, we analyze two parameterizations of the food chain that correspond to contrasting oscillation patterns. These patterns are characterized either by a relatively even distribution of biomass along the food chain (weak trophic cascade) or by marked differences among the species (strong trophic cascade), both of which are common in natural ecosystems (Estes and Duggins 1995; Carter and Rypstra 1995).

Our model setup explicitly addresses one aspect of fragmentation, namely patch isolation, while keeping other potentially confounding drivers such as the total amount of habitat or the number of patches constant. We consider both static landscapes, where all patches are constantly available as habitats, and dynamic landscapes, where periodic environmental disturbances regularly render some of the patches uninhabitable. The stability of the dynamics of the metacommunity is evaluated within the framework of Wang and Loreau (2014) that divides population variability into an α-, β-, and γ-component (similar to the classical diversity indices by Whittaker (1972)): α-variability is the average coefficient of variation of a species' local abundances, γ-variability is the coefficient of variation of the regional (metapopulation) abundance, and β-variability quantifies differences in oscillations between patches, i.e., how synchronously the local populations oscillate. Generally, it is

assumed that higher dispersal rates synchronize population dynamics (e.g., Gouhier et al. (2010)). When mean patch isolation increases, mortality during dispersal increases, too. We expect that this decreases net dispersal flows and thus also decreases synchrony of population dynamics among patches (i.e., increases β-variability). This may, however, be counteracted by (synchronous) periodic disturbances of patch availability. Furthermore, we expect local (α-) variability to decrease, as increasing mortality allows less biomass to flow up the food chain, thus weakening (and thereby stabilizing) the trophic interactions (Rip and McCann 2011). If the local population oscillations indeed become less synchronous, this will also decrease regional (γ-) variability as habitats become more isolated.

Methods

The model comprises a tri-trophic food chain including an autotroph (A), a consumer (C) and a predator (P) species. As basis for the growth of the autotroph, a dynamic resource (R) serves as essential energy source and can be seen as a universal nutrient. This food chain is extended to a metacommunity by placing copies of it on habitat patches that are randomly distributed in space and connected via species-specific dispersal links (Fig. 1). Where applicable, the individual parameters are derived from empirical data, largely from invertebrate communities.

Trophic interactions

We first describe only the trophic interactions between the populations on a single patch and disregard dispersal. The local dynamics of the food chain follow a generalization of the bioenergetics approach (Yodzis and Innes 1992; Brose et al. 2006), supplemented with an equation for the resource. Adapted from chemostat dynamics, the rate of change of the resource density R is expressed as

$$\frac{dR}{dt} = D \cdot (R_0 - R) - G_{AR}A \tag{1}$$

with the resource turnover rate D and the supply concentration R_0. Uptake of resources by the autotroph A is described by a Monod function $G_{AR} = r\frac{R}{K+R}$ with maximum uptake rate r and half saturation constant K. The rates of change in biomass density for each species (A, C and P) are expressed by

$$\begin{aligned}\frac{dA}{dt} &= G_{AR}A - F_{CA}C - x_A A = g_A A \\ \frac{dC}{dt} &= e_C F_{CA}C - F_{PC}P - x_C C = g_C C \\ \frac{dP}{dt} &= e_P F_{PC}P - x_P P = g_P P\end{aligned} \tag{2}$$

where the first terms in all three equations represent growth due to consumption, the last terms denote metabolic losses, and the middle terms in the equations for the autotroph and the consumer describe mortality through predation. The terms are summarized by the net per capita growth rates g_i ($i = A, C, P$). The parameters e_i and x_i are assimilation efficiencies and per capita respiration rates, respectively. The per capita feeding rate of species i on species j is described by a Beddington–DeAngelis functional response (DeAngelis et al. 1975; Beddington 1975):

$$F_{ij} = \frac{1}{m_i}\frac{a_{ij}B_j}{1 + a_{ij}h_{ij}B_j + c_i B_i} \tag{3}$$

with the attack rate a_{ij}, the handling time h_{ij}, the interference coefficient c_i, and B_i and B_j as placeholders for the respective consumer's or resource's biomass density. Since the model is formulated in terms of biomass densities (as opposed to population densities), the functional response is scaled with $\frac{1}{m_i}$, the inverse of the respective consumer's body mass (Heckmann et al. 2012).

The parameters of the trophic dynamics scale allometrically with the body mass of the species. Mass-specific

Fig. 1 **a)** simplified example of a spatial network of habitat patches. Dashed lines of different grey tones indicate dispersal links of the respective species. The resource does not disperse between patches. **b)** local food chain on each patch comprising three trophic levels (autotrophs, A, consumers, C, and predators, P) plus a dynamic resource, R
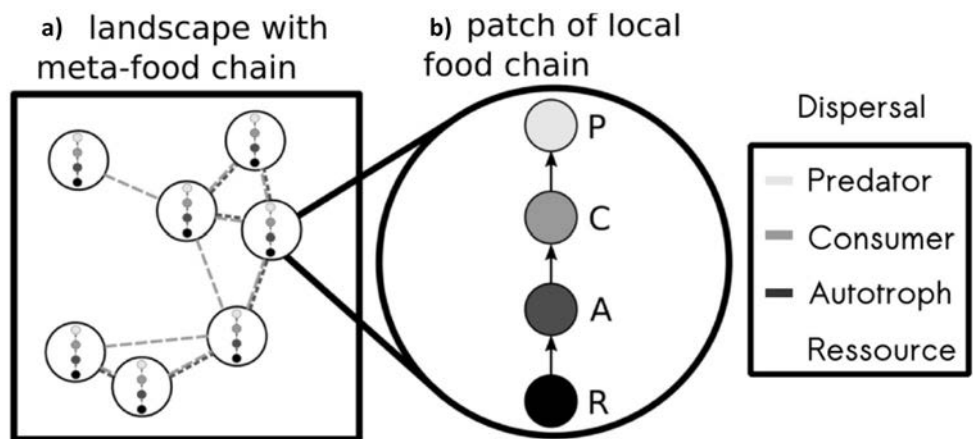
a) landscape with meta-food chain

b) patch of local food chain

P
C
A
R

Dispersal
— Predator
— Consumer
— Autotroph
Ressource

Table 1 Standard parameter set used in the model

Parameter	Description	Value
D	Resource turnover rate	0.5
R_0	Resource supply concentration	5
r_0	Intercept mass specific max. resource uptake rate	1
K	Half saturation density for resource uptake	0.2
c_C, c_P	Interference competition	0.6
e_C	Assimilation efficiency consumer (C)	0.45
e_P	Assimilation efficiency predator (P)	0.85
$x_{0,A}$	Intercept respiration rate plant (A)	0.138
$x_{0,C}, x_{0,P}$	Intercept respiration consumer (C) and predator (P)	0.314
a_{AC}	Attack rate consumer	105 or 170
a_{PC}	Attack rate predator	450 or 10000
h_0	Intercept handling time	0.1
D_0	Intercept maximum dispersal distance	[0.06: 0.5]
ϵ	Scaling exponent for maximum dispersal distance	0.05
μ_0	Scaling factor maximum emigration rate	2
b	Curvature of emigration function	25
Z	Number of habitat patches	30
σ	Fraction of habitat patches blinking	0.3
λ	Period length of blinking cycle	6000

maximum growth rate and respiration rates are assumed to decrease with a negative quarter-power law with body mass, i.e., $r = r_0 m_i^{-0.25}$ and $x_i = x_{0,i} m_i^{-0.25}$ (Yodzis and Innes 1992; Brose et al. 2006). Following Rall et al. (2012), handling times depend on the body masses of both consumer and resource with $h_{ij} = h_0 m_i^{-0.48} m_j^{-0.66}$. The same is true for the attack rates, but since these parameters were used to differentiate the contrasting states of top-down control, fixed values were used here (c.f. Table 1) that nevertheless obey the general trends found in Rall et al. (2012). Body masses increase by a factor of 100 per trophic level, a value commonly found in invertebrate communities and known to

have a stabilizing effect on population dynamics (Brose et al. 2006; Brose et al. 2006b). Freedom of choosing an appropriate set of units allows us to set the body mass of the autotroph to $m_A = 1$. In general, the model is parameterized such that the population dynamics of all species are oscillatory when dispersal is not accounted for (Table 1, Fig. 2).

Habitat network and dispersal

We use the same rules for modeling spatial interactions as in Ryser et al. (2019). Dispersal is considered for the autotroph, consumer and predator species in the model. The spatial

Fig. 2 Time series of the dynamics for the weak **A** and strong **B** trophic cascades on a single patch without dispersal dynamics. In case **A**, $a_{CA} = 105$ and $a_{PC} = 450$; in case **B**, $a_{CA} = 170$ and $a_{PC} = 10000$. All other parameters are listed in Table 1. Note the different scales of x- and y-axes in the two panels
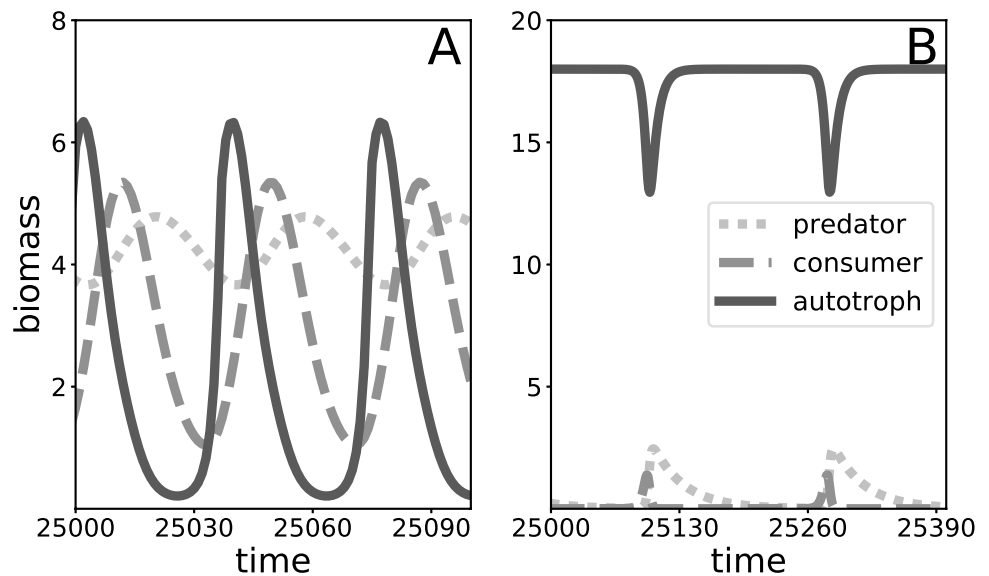
setting is implemented as a random geometric graph (RGG) (Penrose 2003), where each node of the spatial network represents a habitat patch for a local community (Urban and Keitt 2001). The (x, y)-coordinates of each patch were drawn at random from a bivariate uniform distribution over the interval $[0 : 1] \times [0 : 1]$. Dispersal links between the patches connect the local populations, enabling exchange of biomass between patches and thereby forming a meta-food chain (Fig. 1).

Each species perceives its individual dispersal network depending on its body mass m_i. A dispersal link for species i exists between two patches k and l only if the distance between them is less than the species-specific maximum dispersal distance

$$D_{max,i} = D_0 m_i^\epsilon . \tag{4}$$

The exponent ϵ is set to a positive value to account for increased mobility and thus improved dispersal abilities of species with a larger body mass (Hein et al. 2012; Peters 1983).

Dispersal itself is at least for animal species often an active process resulting in metabolic costs and potentially involving a higher risk of predation. To account for these costs (dispersal mortality), we assume that dispersal success $S_{i,lk}$ (i.e., the fraction of individuals *not* dying during dispersal) of species i, when moving between patches l and k, decreases linearly with the distance between the patches:

$$S_{i,lk} = \max \left(1 - d_{i,lk}, 0 \right) , \tag{5}$$

where $d_{i,lk} = \frac{d_{lk}}{D_{max,i}}$ is the distance between the patches relative to the maximum dispersal distance of species i. For passively dispersing plants, distance-depending costs can be caused by a decreasing probability of propagules finding by chance a suitable patch that is further away.

The fraction of individuals emigrating from a source patch k that move toward a target patch l is calculated using the weight function

$$W_{i,lk} = \frac{1 - d_{i,lk}}{\sum_p (1 - d_{i,pk})} , \tag{6}$$

where the sum in the denominator is taken over all potential target patches p that are within the maximum dispersal range of species i on patch k (i.e., those with $d_{pk} < D_{max,i}$). This weight function makes dispersal links between nearby patches stronger, implying that a larger proportion of emigrating biomass arrives there, than those between patches that are further apart. Note that while specific distances $d_{i,lk}$ and success terms $S_{i,lk}$ are symmetric for all pairs of patches, the weight function is not (i.e., $W_{i,lk} \neq W_{i,kl}$).

In general, the process of dispersal can be described as an exchange of biomass between habitat patches that is affecting the population dynamics of species i on patch l via emigration ($E_{i,l}$) from this patch and immigration ($I_{i,l}$) into the patch. The full population dynamics of species i on patch l, comprising both local, trophic dynamics, Eqs. (2), and dispersal dynamics, can thus be written as

$$\frac{dB_{i,l}}{dt} = g_{i,l} B_{i,l} - E_{i,l} + I_{i,l} . \tag{7}$$

Emigration is a complex process in nature possibly involving different environmental cues and species properties. Here, we assume an adaptive emigration rate that depends on the net per capita growth rate $g_{i,l}$ of species i on patch l, reflecting its current situation in this habitat. If a species' net growth is positive, there is little need for dispersal and emigration will be low. However, if the local environmental conditions deteriorate, e.g., due to low resource availability or high predation pressure, the emigration rate increases. This is captured by the following function:

$$E_{i,l} = \frac{\mu_i B_{i,l}}{1 + e^{b(g_{i,l} + x_i)}} . \tag{8}$$

The parameter $\mu_i = \mu_0 x_i$ determines the maximum per capita emigration rate and b determines how sensitively the emigration rate depends on the net growth rate (i.e., how quickly it drops when $g_{i,l}$ increases). Finally, immigration of species i into patch l depends on the amount of emigration from all neighboring patches k as well as on the specific dispersal network, encoded in the success and weight functions $S_{i,lk}$ and $W_{i,lk}$, according to

$$I_{i,l} = \sum_k S_{i,lk} W_{i,lk} E_{i,k} . \tag{9}$$

The parameters defining the dispersal dynamics are also summarized in Table 1.

Simulation setup

Static and dynamic landscapes

The baseline simulations are carried out using static landscapes, i.e., with RGG networks of $Z = 30$ habitat patches as described above, where all patches and dispersal links are permanently available. However, since the environmental conditions in nature are rarely completely constant, we also study dynamic landscapes in which a fraction σ of the patches becomes periodically unavailable as a habitat. This process is called "blinking" and has a period length $\lambda = 6000$. This period length encompasses several hundred generation times of the autotroph, thereby providing sufficient time for the food chain to recover between blinking events. Blinking patches are turned on and off synchronously and change their state every $\frac{\lambda}{2}$ time units. When the blinking

patches are turned off, the local food chains go extinct immediately. Furthermore, the dispersal network can be disrupted because these patches cannot be used as stepping stones for dispersal between patches that are too far apart for a direct dispersal link.

Patch isolation

To capture the effects of varying mean patch isolation, the intercept of the maximum dispersal distance, D_0, (Eq. (4)) is varied systematically between 0.06 and 0.5. This creates habitat networks that range from mostly isolated patches to systems where the predator can move in a single step between any two patches. The spatial network is quantified by the mean patch isolation of the predator's dispersal network,

$$I_{RGG,P} = 1 - \frac{L_P}{\frac{1}{2}Z \cdot (Z-1)}, \tag{10}$$

with L_P the number of undirected dispersal links of the predator and Z the number of habitat patches. Note that using the isolation of the dispersal network of any of the other species to define the mean patch isolation of the landscape would only rescale the x-axis of the results (Fig. 3), but not change them qualitatively.

Ecosystem stability

We evaluated ecosystem stability according to Wang and Loreau (2014) as α-, β-, and γ-variability of autotroph, consumer and predator. For the mean local or α-variability of a species, the coefficients of variation (CV, $\frac{\text{standard deviation}}{\text{mean}}$) of its local biomass densities on all patches are calculated and then averaged across patches (weighted with the respective local mean biomass density), while for the γ-variability (variability of the metapopulation) the CV of the total biomass density (sum over all patches) is evaluated. Similar to the α-, β-, and γ-diversity indices (Whittaker 1972), β-variability measures differences between the patches and can thus be used to determine how synchronously local biomass densities on the different patches oscillate. It is here defined as $\beta = \frac{\alpha}{\gamma}$. In contrast to the diversity indices, however, variability decreases with an increase in spatial scale, i.e., $\gamma \leq \alpha$ and thus $\beta \geq 1$. Spatially synchronous oscillations result in a low β-variability and a γ-variability that approaches the value of the α-variability. Perfect synchronicity is obtained at $\beta = 1$. The variability measures of a species do not change if it is permanently extinct on one or several patches. An intuitive example of two species, one with synchronous and one with asynchronous oscillations, is provided in the Online Resource (Fig. S1).

Numerical simulations

We simulated food chains that were parameterized to exhibit either a strong or a weak trophic cascade, corresponding to a very uneven or a relatively even distribution of biomass along the food chain, respectively. The weak trophic cascade was generated by relatively low attack rates of the consumer and predator species ($a_{CA} = 105$, $a_{PC} = 450$, Fig. 2a), while for the strong trophic cascade much higher attack rates were chosen ($a_{CA} = 170$, $a_{PC} = 10000$, Fig. 2b). The spatial networks were either static (all patches permanently available as habitats) or dynamic (30% of the patches periodically becoming unavailable as habitats). The mean patch isolation was constant for each individual simulation run, but was gradually varied between simulations by decreasing D_0 from 0.5 to 0.06 in steps of 0.01. Simulations were carried out with a full-factorial design and 30 replicates for each combination of parameters, resulting in a total of 5400 simulation runs. Replicates differed in the randomly chosen positions of 30 patches that formed the spatial networks. Time series were simulated for 90 000 time units and split in three sections of equal length. During the first section, the systems settled on the attractor and from the second section, mean biomass densities were calculated. These mean biomass densities were then used to calculate the variability coefficients from the third section of the time series. During the simulations, a species was considered extinct on a given patch if its local biomass density fell below 10^{-20}. Global extinction of a species from the entire meta-food chain was never observed. Numerical simulations of the ODE model were performed in C (source code adopted from (Schneider et al. 2016)) using the SUNDIALS CVODE solver (Hindmarsh et al. 2005) with absolute and relative error tolerances of 10^{-10}. Output data were analyzed using Python 2.7.11, 3.6 and several Python packages, in particular NumPy and Matplotlib (Oliphant 2015; Van der Walt et al. 2011; Hunter 2007).

Results

Food chain dynamics without dispersal

To capture how different parameterizations of trophic interactions affect the metacommunity dynamics, we analyzed two contrasting trophic cascades in the food chain that were created by assuming either low or high attack rates. The first type, called weak trophic cascade, is characterized by a weak predation pressure of the predator, a relatively even distribution of biomass along the food chain and a high oscillation frequency (note the different
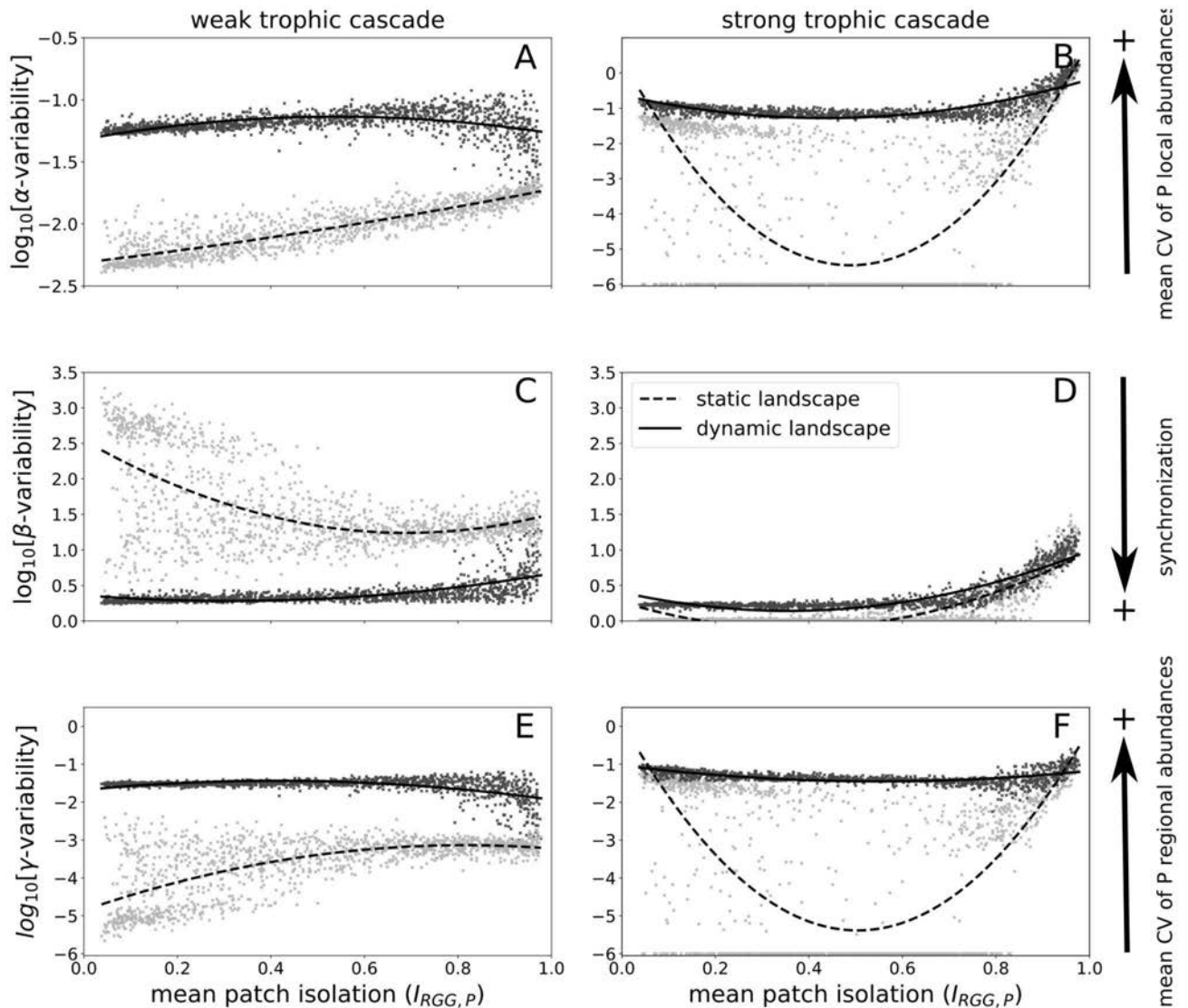
Fig. 3 Local (α-variability, top row), between patch (β-variability, middle row) and metapopulation dynamics (γ-variability, bottom row) of the predator for the weak (left column) and the strong trophic cascade (right column). Light gray data points and dashed trend lines (second order fit) indicate static landscapes, and dark gray data points and solid trend lines indicate dynamic landscapes. Each data point represents the result of one simulation run with a unique spatial network of habitat patches. All data points where the variability is below 10^{-6} are set to 10^{-6} as differences between them provide no meaningful information that close to the fixed point

scales of the x-axes of the two panels in Fig. 2). The strong trophic cascade is, in contrast, characterized by a very uneven distribution of biomass with a strong dominance of the autotroph (caused by the suppression of the consumer by the predator), a much lower oscillation frequency and much more drastic population cycles that drive both the predator and the consumer biomass densities repeatedly to very low values. The difference between the predator attack rates in the two cases had to be this pronounced as for intermediate values, the food chain is stable and the analysis of (meta-)population variabilities is not possible (Online Resource, Fig. S2).

Metacommunity dynamics

We evaluated the two different landscape scenarios (static vs. dynamic) for both the weak and strong trophic cascade over a gradient of the mean patch isolation. All scenarios are evaluated with respect to local (α-variability), between patch (β-variability) and metapopulation dynamics (γ-variability). The observed trends in population variabilities on the different spatial scales were always the same for all trophic levels. We therefore only show results for the predator species. Results for the autotroph and consumer species are in the Online Resource (Figs. S3 and S4).

Local dynamics: α-variability

In contrast to our expectations, increasing mean patch isolation amplifies biomass oscillations in static landscapes (increasing α-variability, Fig. 3a,b). This trend is particularly pronounced in the strong trophic cascade from intermediate mean patch isolation (where many systems even settle on a stable fixed point) to high mean patch isolation (Fig. 3b). Because α-variability has nonzero values at low mean patch isolation, the overall pattern is u-shaped. In the weak trophic cascade, α-variability monotonously increases with mean patch isolation. In dynamic landscapes, α-variability is higher than in static landscapes, but its main trends with mean patch isolation are significantly weaker than in static landscapes (cf. also Table 2).

Synchronization of patches: β-variability

On the regional scale, we evaluated to what extent the biomass dynamics between habitat patches synchronized (Fig. 3c,d). In line with our expectations, there is in most cases a clear trend toward decreased synchronization (increased β-variability, c.f. also Table 2) of the dynamics as mean patch isolation increases. The apparent limitation of synchronization in dynamic landscapes (minimal β-variability ≈ 2 for both weak and strong trophic cascades) is only a numerical effect due to the difference between constant and blinking patches.

Only the weak trophic cascade in static landscapes deviates from the general trend: Not only the β-variability is higher than in the other cases, but it also appears to decrease from low to intermediate mean patch isolation and only slightly increases at high mean patch isolation. The initial decrease is due to a separate cloud of data points with very high β-variabilities, which emerges for $I_{RGG,P} \lesssim 0.4$. This suggests that in this part of the parameter space a second attractor with even less synchronization between the patches exists. The bistability of the system is indeed confirmed by dedicated simulations using spatial networks with fixed coordinates of the patches (cf. Online Resource, Fig. S5)

Table 2 Summary of the trends of α-, β- and γ-variability with increasing mean patch isolation for the weak (WTC) or strong (STC) trophic cascade in static or dynamic landscapes

State of landscape	Type of effect	Trend for WTC	Trend for STC
Static	α-variability	$\uparrow$	U-shape
Static	β-variability	$\downarrow$ & $\nearrow$	$\uparrow$
Static	γ-variability	$\uparrow$ & $\rightarrow$	U-shape
Dynamic	α-variability	$\rightarrow$	$\nearrow$
Dynamic	β-variability	$\nearrow$	$\uparrow$
Dynamic	γ-variability	$\searrow$	$\rightarrow$

Metapopulation : γ-variability

For both the weak and strong trophic cascades, we find a relatively constant total biomass of the metapopulation (γ-variability $< 10^{-1}$, Fig. 3e,f). As expected, γ-variability is higher in dynamic landscapes than in static ones. Since local biomass oscillations are often highly synchronized, the trends in the metapopulation dynamics largely follow those already observed in the local dynamics (cf. also Table 2). As with the β-variability of the weak trophic cascade in static landscapes, at low mean patch isolation ($I_{RGG} \lesssim 0.4$) a small cloud of data points appears to be separated from the rest, which have a low γ-variability. Again, these data points can be attributed to an alternative attractor with less synchronized dynamics and correspondingly a lower γ-variability.

Discussion

The impact of habitat fragmentation on biodiversity and community dynamics is a subject of ongoing debate (Fahrig et al. 2019; Fletcher et al. 2018). Here, we evaluated the effect of mean patch isolation as one aspect of fragmentation on the population dynamics of two contrasting states of a meta-food chain in static and dynamic landscapes. Most intriguingly, we found that both local (α-) and metacommunity (γ-) variability increased with increasing mean patch isolation, despite the fact that synchronization among patches mostly decreased (β-variability increased) along the same gradient. Periodic environmental disturbances that rendered some patches regularly uninhabitable in dynamic landscapes weakened these trends, but at the prize of overall higher levels of α- and γ-variability.

Interactions between dispersal and local interactions drive the dynamics in static landscapes

Higher effective dispersal rates at low patch isolation have been shown to synchronize the dynamics of metacommunities (Gouhier et al. 2010), but our results suggest that the extent of this effect may depend on the local interactions between the populations. While our results largely confirm the negative correlation between mean patch isolation (and thus, by proxy, effective dispersal rate) and synchronization, we also observe a significant deviation from this trend in the weak trophic cascade at low mean patch isolation. There, an alternative attractor with very asynchronous population oscillations (high β-variability) emerges. However, α-variability is also relatively low on this attractor, which may explain the lack of synchronization: When the local populations do not oscillate much, their emigration rates are also almost constant over time, and there is consequently little potential for affecting the population oscillations on neighboring patches. This highlights the importance of details of

the local interactions between species (in this case low attack rates in the weak trophic cascade that limit α-variability) for collective phenomena like synchronization. Other theoretical studies also indicate a relevance of local interactions for the synchronization of population dynamics. Koelle and Vandermeer (2005) show, for example, opposing trends of synchronization between species in a food chain, which are due to an interaction between dispersal patterns and trophic interactions. Moreover, empirical studies provide evidence that dispersal may even alter biotic interactions between species directly (Walting and Donnelly 2006), further underlining the importance of local species interactions for our understanding of metapopulation dynamics.

Indirect effects of local trophic interactions also explain why our initial hypothesis, regarding decreasing α-variability at increasing mean patch isolation, turned out to be incorrect in the weak trophic cascade. The hypothesis was based on the "principle of energy flux" (Rip and McCann 2011), according to which an increasing (dispersal) mortality at higher mean patch isolation should weaken and consequently stabilize the trophic interactions along the food chain (and thus decrease α-variability). In contrast to this prediction, high dispersal mortality does not generally result in a lower α- or γ-variability in our model. We attribute this counter-intuitive trend to an indirect effect of dispersal mortality: Despite their superior dispersal abilities, higher trophic levels often suffer most from mean patch isolation because they are energetically more limited than the species on lower trophic levels (Ryser et al. 2019). In fact, we also find that the higher the mean patch isolation, the lower the mean biomass of the predator (see Online Resource, Fig. S6). This decreases the per-capita predation mortality of the consumer, which more than compensates for the increase in the consumer's dispersal mortality. In line with the principle of energy flux, this destabilizes the consumer–autotroph interaction. At high mean patch isolation, the α-variability of the predator thus increases because the dynamics of the predator is driven by the increasingly unstable consumer–autotroph interaction.

This apparent mismatch between increasing β-variability (more asynchronous dynamics) and simultaneously increasing γ-variability at high mean patch isolation has also implications for the so-called portfolio effect (Schindler et al. 2015), which is often considered in more applied contexts. Specifically, the spatial portfolio effect (Thorson et al. 2018) measures how much γ-variability is reduced relative to its theoretical maximum (here given by γ-variability = α-variability) due to asynchronous oscillations among different spatial locations. While we do observe such a reduction of γ-variability *relative to α-variability* when mean patch isolation increases, the indirect effect of dispersal mortality discussed above still leads to an increase in γ-variability in absolute terms. This underlines that assessing factors that affect the synchronization of population dynamics across space is not always sufficient to understand the variability of a population on the regional scale.

Bistability in the weak tropic cascade

In static landscapes, the weak trophic cascade is bistable for low-to-medium mean patch isolation. In this parameter range, in addition to the attractor with intermediate synchronicity, which exists for the entire range of mean patch isolation, a second attractor with very asynchronous dynamics between the patches exists. Interestingly, the bistability concerns only the synchronicity of the dynamics (and consequently the γ-variability). Local (α-) variability is not affected by whether the populations on different patches cycle more or less in synchrony (Fig. 3a).

Such bistability is relevant because it implies hysteresis (Scheffer et al. 1993): A small change in environmental conditions can drive the system away from one attractor, but for the system to return to it, a much larger change of the environmental conditions in the opposite direction will be necessary. This is particularly concerning here: The second attractor, which may be regarded as more desirable due to its lower metapopulation variability, loses its stability when the mean patch isolation increases beyond a certain threshold. However, the system may never return to it even when environmental conditions improve again, because the primary attractor never loses its stability.

A possible explanation for the occurrence of the alternative synchronization patterns we observe is the way the dispersal rate is modeled. Specifically, that the rate at which individuals emigrate from a given patch depends on the net growth rate they experience there. Emigration can thus be driven by a lack of resources (in which case emigration helps ending the unfavorable growth conditions and is thus self-limiting) or by an exceedingly high predation rate (in which case emigration actually intensifies the per-capita predation rate for the remaining individuals and becomes self-enforcing). Preliminary analyses suggest that dampening or amplification of net dispersal flows by synchronous and asynchronous oscillations, respectively, creates different feedback loops based on these different drivers of emigration, but more detailed analyses are required to understand how these contrasting states stabilize themselves.

Effect of periodic environmental disturbances

Periodic environmental disturbances have a stronger effect on population variability on all spatial scales than local interactions or mean patch isolation. We infer this from the observation that both weak and strong trophic cascades, which behave very differently in static landscapes, exhibit almost identical variability patterns in dynamic landscapes, with elevated levels of α- and γ-variability and low β-variability. Further, all three variability measures are almost constant over a wide range from low-to-medium mean patch

isolation. Only at high mean patch isolation, where the patch networks begin to decompose into several isolated components anyway, the effect of the periodic disruption of the patch networks by the blinking patches dwindles and the variability measures become more similar to their values in static landscapes again. Both the increase in α-variability and the synchronization of the patches, due to the periodic environmental disturbances, are of course not unexpected. The blinking of the patches increases α-variability by causing low-frequency biomass oscillations through the extinction and recolonization process and by decreasing the mean biomass densities on these patches. Similarly, environmental fluctuations have long been known to be able to synchronize ecological dynamics in coupled habitats (Moran 1953). More surprising is, however, the overruling strength of the effect of periodic environmental disturbances, considering that a blinking cycle (period length $\lambda = 6000$) is about 150 times slower than the period length of the population cycles in the weak trophic cascade.

Our approach of modeling periodic environmental disturbances as dynamic landscapes, where some patches become periodically uninhabitable, is inspired by the natural example of kettle holes that have a species-rich community during the colder and wetter seasons, but can run dry during the summer (Kalettka and Rudat 2006). Such periodic (in the example: seasonal) environmental disturbances are a common feature of ecological systems, since in most environments seasonally fluctuating climatic drivers exist (Fretwell 1972). Together with the above discussed surprisingly strong effect of even very rarely occurring disturbances, this may explain why empirically observed effects of patch isolation are often small and inconclusive (Fahrig 2003). Environmental disturbances (especially seasonal ones) of course do not always lead to the abrupt extinction of entire local communities, but could, for example, simply modify resource availability or mortality rates. An interesting avenue for future research might therefore be to explore whether such less drastic disturbances also have the potential to overrule the effects of local interactions and landscape configuration. Furthermore, resting stages can play a critical role in the recolonization of periodically uninhabitable patches (Wade 1990). Accounting for them in the model might decrease synchronicity, as they allow for an independent restart of the local communities.

Relevance and effects of dispersal assumptions

Details of the way species dispersal is implemented within a model can have major implications for the arising population dynamics. In nature, a multitude of causes affects an individual's decision to leave its home patch (Bowler and Benton 2005), among them being, for example, intraspecific competition (Herzig 1995), quality of food resources (Kuussaari et al. 1996) or top-down pressure through parasitism or predation (Sloggett and Weisser 2002). In our model, we use the net growth rate of a species in a given patch to determine its emigration rate. Since the net growth rate depends on both food availability and predation pressure, the model captures multiple of the above-mentioned causes of dispersal. However, we assume that individuals have only knowledge about the growth conditions in the patch they are currently in and not about the conditions in potential target patches. The dispersal rate between any two patches thus only depends on the local conditions in the source patch and on the spatial arrangement of the patches. Using a consumer-resource model with two patches, Abrams and Ruokolainen (2011) showed that when the dispersal rate depends on the difference of the growth rates between source and target patch, asynchronous (antiphase) cycles frequently occur, which promotes stability. With our approach, we only find asynchronous dynamics in static landscapes, but even then synchronous metacommunity dynamics frequently occur.

Conclusions

We conclude that due to indirect effects of local ecological interactions, dispersal is not necessarily a "double-edged sword" (Hudson and Cattadori 1999) (dubbed so because too much of it can synchronize metacommunity dynamics and increase the risk of correlated extinctions), but also that a portfolio effect due to asynchronous oscillations may not always result in reduced variability at the metacommunity level. Furthermore, in each unique landscape, comprising a multitude of abiotic factors, the impact of a periodic environmental disturbance has the potential to outweigh local interactions present in a community. The extent of the effect of mean patch isolation on the variability of population dynamics in a metacommunity thus may strongly depend on local environmental conditions which are relevant for reliable predictions. Whether this is also true for other aspects of fragmentation or habitat loss is an intriguing question for future investigations. Finally, the non-monotonous stability response curve of the strong trophic cascade shows that the effect of mean patch isolation on metacommunity dynamics may not be trivial and that there might be transitions where patch isolation might switch from having a positive to having a negative effect.

Declarations

Conflicts of interest The authors declare no conflict of interest.

References

Abrams PA (2007) Habitat choice in predator - prey systems: Spatial instability due to interacting adaptive movements. Am Nat 169(5):581–594. https://doi.org/10.1086/512688

Abrams PA, Ruokolainen L (2011) How does adaptive consumer movement affect population dynamics in consumer resource metacommunities with homogeneous patches? J Theor Biol 277(1):99–110. https://doi.org/10.1016/j.jtbi.2011.02.019

Beddington JR (1975) Mutual interference between parasites or predators and its effect on searching efficiency. J Anim Ecol 44(1):331–340. https://doi.org/10.2307/3866

Blasius B, Huppert A, Stone L (1999) Complex dynamics and phase synchronization in spatially extended ecological systems. Nature 399:354–359. https://doi.org/10.1038/20676

Bowler DE, Benton TG (2005) Causes and consequences of animal dispersal strategies: relating individual behaviour to spatial dynamics. Biol Rev 80(2):205–225. https://doi.org/10.1017/S1464793104006645

Briggs CJ, Hoopes MF (2004) Stabilizing effects in spatial parasitoid - host and predator - prey models: a review. Theor Popul Biol 65(3):299–315. https://doi.org/10.1016/j.tpb.2003.11.001

Brooks TM, Mittermeier RA, Mittermeier CG, Da Fonseca GAB, Rylands AB, Konstant WR, Flick P, Pilgrim J, Oldfield S, Magin G, Hilton-Taylor C (2002) Habitat loss and extinction in the hotspots of biodiversity. Conserv Biol 16(4):909–923. https://doi.org/10.1046/j.1523-1739.2002.00530.x

Brose U, Williams RJ, Martinez ND (2006) Allometric scaling enhances stability in complex food webs. Ecol Lett 9(11):1228–1236. https://doi.org/10.1111/j.1461-0248.2006.00978.x

Brose U, Jonsson T, Berlow EL, Warren P, Banasek-Richter C, Bersier LF, Blanchard JL, Brey T, Carpenter SR, Blandenier MFC, Cushing L, Dawah HA, Dell T, Edwards F, Harper-Smith S, Jacob U, Ledger ME, Martinez ND, Memmott J, Mintenbeck K, Pinnegar JK, Rall BC, Rayner TS, Reuman DC, Ruess L, Ulrich W, Williams RJ, Woodward G, Cohen JE (2006a) Consumer - resource body-size relationships in natural food webs. Ecol 87(10):2411–2417. https://doi.org/10.1890/0012-9658(2006)87[2411:CBRINF]2.0.CO;2

Butchart SHM, Walpole M, Collen B, van Strien A, Scharlemann JPW, Almond REA, Baillie JEM, Bomhard B, Brown C, Bruno J, Carpenter KE, Carr GM, Chanson J, Chenery AM, Csirke J, Davidson NC, Dentener F, Foster M, Galli A, Galloway JN, Genovesi P, Gregory RD, Hockings M, Kapos V, Lamarque JF, Leverington F, Loh J, McGeoch MA, McRae L, Minasyan A, Morcillo MH, Oldfield TEE, Pauly D, Quader S, Revenga C, Sauer JR, Skolnik B, Spear D, Stanwell-Smith D, Stuart SN, Symes A, Tierney M, Tyrrell TD, Vié JC, Watson R (2010) Global biodiversity: Indicators of recent declines. Sci 328(5982):1164–1168. https://doi.org/10.1126/science.1187512

Carter PE, Rypstra AL (1995) Top-down effects in soybean agroecosystems: Spider density affects herbivore damage. Oikos 72(3):433–439. https://doi.org/10.2307/3546129

De Meester L, Declerck S, Stoks R, Louette G, Van De Meutter F, De Bie T, Michels E, Brendonck L (2005) Ponds and pools as model systems in conservation biology, ecology and evolutionary biology. Aquat Conserv Mar Freshw Ecosyst 15(6):715–725. https://doi.org/10.1002/aqc.748

DeAngelis DL, Goldstein RA, O'Neill RV (1975) A model for tropic interaction. Ecol 56(4):881–892. https://doi.org/10.2307/1936298

Didham RK, Kapos V, Ewers RM (2012) Rethinking the conceptual foundations of habitat fragmentation research. Oikos 121:161–170. https://doi.org/10.1111/j.1600-0706.2011.20273.x

Duraiappah A, Naeem S, Agardy T, Ash N, Cooper H, Diaz S, Faith D, Mace G, McNeely J, Mooney H, Oteng-Yeboah A, Pereira H, Polasky S, Prip C, Reid W, Samper C, Schei P, Scholes R, Schutyser F, Van Jaarsveld A (2005) Ecosystems and human well-being: biodiversity synthesis; a report of the Millennium Ecosystem Assessment. World Resources Institute. Type: Report http://hdl.handle.net/20.500.11822/8755

Estes JA, Duggins DO (1995) Sea otters and kelp forests in alaska: Generality and variation in a community ecological paradigm. Ecol Monogr 65(1):75–100. https://doi.org/10.2307/2937159

Fahrig L (2003) Effects of habitat fragmentation on biodiversity. Ann Rev Ecol Evol Syst 34(1):487–515. https://doi.org/10.1146/annurev.ecolsys.34.011802.132419

Fahrig L (2017) Ecological responses to habitat fragmentation per se. Ann Rev Ecol Evol and Syst 48(1):1–23. https://doi.org/10.1146/annurev-ecolsys-110316-022612

Fahrig L, Arroyo-Rodrìguez V, Bennett JR, Boucher-Lalonde V, Cazetta E, Currie DJ, Eigenbrod F, Ford AT, Harrison SP, Jaeger JA, Koper N, Martin AE, Martin JL, Metzger JP, Morrison P, Rhodes JR, Saunders DA, Simberloff D, Smith AC, Tischendorf L, Vellend M, Watling JI (2019) Is habitat fragmentation bad for biodiversity? Biol Conserv 230:179–186. https://doi.org/10.1016/j.biocon.2018.12.026

Fletcher RJ, Burrell NS, Reichert BE, Vasudev D, Austin JD (2016) Divergent perspectives on landscape connectivity reveal consistent effects from genes to communities. Curr Landsc Ecol Rep 1(2):67–79. https://doi.org/10.1007/s40823-016-0009-6

Fletcher RJ, Didham RK, Banks-Leite C, Barlow J, Ewers RM, Rosindell J, Holt RD, Gonzalez A, Pardini R, Damschen EI, Melo FP, Ries L, Prevedello JA, Tscharntke T, Laurance WF, Lovejoy T, Haddad NM (2018) Is habitat fragmentation good for biodiversity? Biol Conserv 226:9–15. https://doi.org/10.1016/j.biocon.2018.07.022

Fretwell SD (1972) Populations in a seasonal environment. Monogr Popul Biol, 1972

Gotelli NJ (1991) Metapopulation models: The rescue effect, the propagule rain, and the core-satellite hypothesis. Am Nat 138(3):768–776. https://doi.org/10.2307/2462468

Gouhier TC, Guichard F, Gonzalez A (2010) Synchrony and stability of food webs in metacommunities. Am Nat 175(2):E16–E34. https://doi.org/10.1086/649579 (PMID: 20059366)

Hanski I (2015) Habitat fragmentation and species richness. J Biogeogr 42(5):989–993. https://doi.org/10.1111/jbi.12478

Hauzy C, Gauduchon M, Hulot FD, Loreau M (2010) Density-dependent dispersal and relative dispersal affect the stability of predator-prey metacommunities. J Theor Biol 266(3):458–469

Heckmann L, Drossel B, Brose U, Guill C (2012) Interactive effects of body-size structure and adaptive foraging on food-web stability. Ecol Lett 15(3):243–250. https://doi.org/10.1111/j.1461-0248.2011.01733.x

Hein AM, Hou C, Gillooly JF (2012) Energetic and biomechanical constraints on animal migration distance. Ecol Lett 15(2):104–110. https://doi.org/10.1111/j.1461-0248.2011.01714.x

Herzig AL (1995) Effects of population density on long-distance dispersal in the goldenrod beetle trirhabda virgata. Ecol 76(7):2044–2054. https://doi.org/10.2307/1941679

Hindmarsh AC, Brown PN, Grant KE, Lee SL, Serban R, Shumaker DE, Woodward CS (2005) SUNDIALS: Suite of nonlinear and differential/algebraic equation solvers. ACM Trans Math Soft (TOMS) 31(3):363–396

Holland MD, Hastings A (2008) Strong effect of dispersal network structure on ecological dynamics. Nature 456:792–794

Hudson PJ, Cattadori IM (1999) The moran effect: a cause of population synchrony. Trends Ecol Evol 14:1–2

Hunter JD (2007) Matplotlib: A 2d graphics environment. Comput Sci Eng 9(3):90–95. https://doi.org/10.1109/MCSE.2007.55

Jansen VA (2001) The dynamics of two diffusively coupled predator-prey populations. Theor Pop Biol 59(2):119–131. https://doi.org/10.1006/tpbi.2000.1506

Kahilainen A, van Nouhuys S, Schulz T, Saastamoinen M (2018) Metapopulation dynamics in a changing climate: Increasing spatial synchrony in weather conditions drives metapopulation synchrony of a butterfly inhabiting a fragmented landscape. Glob Change Biol 24(9):4316–4329. https://doi.org/10.1111/gcb.14280

Kalettka T, Rudat C (2006) Hydrogeomorphic types of glacially created kettle holes in north-east Germany. Limnol - Ecol Manag Inl Wat 36(1):54–64. https://doi.org/10.1016/j.limno.2005.11.001

Koelle K, Vandermeer J (2005) Dispersal-induced desynchronization: from metapopulations to metacommunities. Ecol Lett 8(2):167–175. https://doi.org/10.1111/j.1461-0248.2004.00703.x

Koenig WD (1999) Spatial autocorrelation of ecological phenomena. Trends Ecol Evol 14(1):22–26

Kuussaari M, Nieminen M, Hanski I (1996) An experimental study of migration in the glanville fritillary butterfly melitaea cinxia. J Anim Ecol 65(6):791–801. https://doi.org/10.2307/5677

LeCraw RM, Kratina P, Srivastava DS (2014) Food web complexity and stability across habitat connectivity gradients. Oecologia 176(4):903–915. https://doi.org/10.1007/s00442-014-3083-7

Levins R (1969) Some demographic and genetic consequences of environmental heterogeneity for biological control1. Bull Entomol Soc Am 15(3):237–240. https://doi.org/10.1093/besa/15.3.237

Moran P (1953) The statistical analysis of the canadian lynx cycle. Aust J Zool 1:291–298. https://doi.org/10.1071/ZO9530163

Oliphant TE (2015) Guide to NumPy, 2nd edn. CreateSpace Independent Publishing Platform, USA

Penrose M (2003) Random Geometric Graphs. Oxford University Press

Pereira HM, Leadley PW, Proença V, Alkemade R, Scharlemann JPW, Fernandez-Manjarrés JF, Araújo MB, Balvanera P, Biggs R, Cheung WWL, Chini L, Cooper HD, Gilman EL, Guénette S, Hurtt GC, Huntington HP, Mace GM, Oberdorff T, Revenga C, Rodrigues P, Scholes RJ, Sumaila UR, Walpole M (2010) Scenarios for global biodiversity in the 21st century. Sci 330(6010):1496–1501. https://doi.org/10.1126/science.1196624

Peters RH (1983) The Ecological Implications of Body Size: Cambridge University Press, vol 10., Cambridge

Pillai P, Gonzalez A, Loreau M (2011) Metacommunity theory explains the emergence of food web complexity. Proc Natl Acad Sci 108(48):19293–19298. https://doi.org/10.1073/pnas.1106235108

Pimm SL, Jenkins CN, Abell R, Brooks TM, Gittleman JL, Joppa LN, Raven PH, Roberts CM, Sexton JO (2014) The biodiversity of species and their rates of extinction, distribution, and protection. Sci 344(6187). https://doi.org/10.1126/science.1246752

Plitzko SJ, Drossel B (2015) The effect of dispersal between patches on the stability of large trophic food webs. Theor Ecol 8(2):233–244

Rall BC, Brose U, Hartvig M, Kalinkat G, Schwarzmüller F, Vucic-Pestic O, Petchey OL (2012) Universal temperature and body-mass scaling of feeding rates. Philos Trans R Soc B Biol Sci 367(1605):2923–2934. https://doi.org/10.1098/rstb.2012.0242

Ranta E, Kaitala V, Lindstrom J, Lindén H (1995) Synchrony in population dynamics. Proc R Soc B Biol Sci 262:113–118

Rip JMK, McCann KS (2011) Cross-ecosystem differences in stability and the principle of energy flux. Ecol Lett 14(8):733–740. https://doi.org/10.1111/j.1461-0248.2011.01636.x

Ryser R, Häussler J, Stark M, Brose U, Rall BC, Guill C (2019) The biggest losers: habitat isolation deconstructs complex food webs from top to bottom. Proc R Soc B Biol Sci 286(1908):20191177. https://doi.org/10.1098/rspb.2019.1177

Scheffer M, Hosper S, Meijer ML, Moss B, Jeppesen E (1993) Alternative equilibria in shallow lakes. Trends in Ecology & Evolution 8(8):275–279. https://doi.org/10.1016/0169-5347(93)90254-M

Schindler DE, Armstrong JB, Reed TE (2015) The portfolio concept in ecology and evolution. Frontiers in Ecology and the Environment 13(5):257–263. https://doi.org/10.1890/140275

Schneider FD, Brose U, Rall BC, Guill C (2016) Animal diversity and ecosystem functioning in dynamic food webs. Nat Commun 7(12718). https://doi.org/10.1038/ncomms12718

Sherratt TN, Lambin X, Petty SJ, Mackinnon JL, Coles CF, Thomas CJ (2000) Use of coupled oscillator models to understand synchrony and travelling waves in populations of the field vole Microtus agrestis in northern england. J Appl Ecol 37(Suppl. 1):148–158

Sloggett JJ, Weisser WW (2002) Parasitoids induce production of the dispersal morph of the pea aphid, acyrthosiphon pisum. Oikos 98(2):323–333. https://doi.org/10.1034/j.1600-0706.2002.980213.x

Thorson JT, Scheuerell MD, Olden JD, Schindler DE. Spatial heterogeneity contributes more to portfolio effects than species variability in bottom-associated marine fishes. Proc R Soc Lond B 285:20180915. https://doi.org/10.1098/rspb.2018.0915

Urban D, Keitt T (2001) Landscape connectivity: A graph-theoretical perspective. Ecol 82(5):1205–1218. https://doi.org/10.1890/0012-9658(2001)082[1205:LCAGTP]2.0.CO;2

Van der Walt S, Colbert SC, Varoquaux G (2011) The numpy array: A structure for efficient numerical computation. Comp Sci Eng 13:22–30. https://doi.org/10.1109/MCSE.2011.37

Wade PM (1990) The colonisation of disturbed freshwater habitats bycharaceae. Folia Geobot Phytotaxon 25(3):275–278. https://doi.org/10.1007/BF02913027

Walting JI, Donnelly MA (2006) Fragments as islands: a synthesis of faunal responses to habitat patchiness. Conservation Biology 20(4):1016–1025. https://doi.org/10.1111/j.1523-1739.2006.00482.x

Wang S, Loreau M (2014) Ecosystem stability in space: α-, β- and γ-variability. Ecol Lett 17(8):891–901. https://doi.org/10.1111/ele.12292

Whittaker RH (1972) Evolution and measurement of species diversity. Taxon 21(2/3):213–251. https://doi.org/10.2307/1218190

Yodzis P, Innes S (1992) Body size and consumer-resource dynamics. Am Nat 139(6):1151–1175. https://doi.org/10.2307/2462335

ECOLOGY LETTERS cnrs WILEY

Self-organised pattern formation increases local diversity in metacommunities

Christian Guill | **Janne Hülsemann** | **Toni Klauschies**

Institute of Biochemistry and Biology, University of Potsdam, Potsdam, Germany

Correspondence
Christian Guill, Am Neuen Palais 10, 14469 Potsdam, Germany.
Email: guill@uni-potsdam.de

Funding information
Deutsche Forschungsgemeinschaft, Grant/Award Number: GU 1645/1-1

Editor: Shaopeng Wang

Abstract

Self-organised formation of spatial patterns is known from a variety of different ecosystems, yet little is known about how these patterns affect the diversity of communities. Here, we use a food chain model in which autotroph diversity is described by a continuous distribution of a trait that affects both growth and defence against heterotrophs. On isolated patches, diversity is always lost over time due to stabilising selection, and the local communities settle on one of two alternative stable community states that are characterised by a dominance of either defended or undefended species. In a metacommunity context, dispersal can destabilise these states and complex spatio-temporal patterns in the species' abundances emerge. The resulting biomass-trait feedback increases local diversity by an order of magnitude compared to scenarios without self-organised pattern formation, thereby maintaining the ability of communities to adapt to potential future changes in biotic or abiotic environmental conditions.

KEYWORDS
biomass-trait feedback, fitness gradient, food chain, functional diversity, metacommunity, self-organisation, source–sink dynamics, spatio-temporal pattern, trait-based aggregate model, Turing instability

INTRODUCTION

Biodiversity is a key prerequisite for the functioning of natural communities and ecosystems (Cadotte et al., 2011; Tilman, 1999), the stable supply of ecosystem goods and services (Hooper et al., 2005) and the ability of communities to adapt to environmental change (Yachi & Loreau, 1999). The maintenance of diversity within individual habitats strongly relies on local processes and species interactions such as resource partitioning (Tilman, 1999), selective predation (Tirok & Gaedke, 2010) or neighbourhood-dependent selection (Vasseur et al., 2011), which may generate sufficient niche differentiation among coexisting species. However, local communities are naturally embedded in a larger biogeographic context, and thus connected to other communities of adjacent habitats (Leibold et al., 2004). Dispersal between the habitats of such metacommunities can substantially contribute to the maintenance of diversity within local communities, for example, through source–sink dynamics (Brown & Kodric-Brown, 1977) that enable the persistence of locally inferior competitors via immigration of conspecifics from other habitats (Leibold et al., 2004). A necessary condition for this mechanism is spatial heterogeneity that allows differently adapted species to coexist on a regional scale (Amarasekare, 2003).

Christian Guill and Janne Hülsemann contributed equally to this work.

Most previous studies on the influence of dispersal on local diversity rely, however, on the assumption that spatial heterogeneity in species abundances primarily results from differences in abiotic environmental conditions. This premise neglects that heterogeneous species abundances may also emerge purely as a consequence of local interactions of species and their movement in space, so-called self-organised pattern formation (Malchow, 1993). This process usually results from scale-dependent feedback, that is, a situation where positive and negative feedbacks between species occur at different spatial scales (Rietkerk and Van de Koppel, 2008). For example, producers can locally facilitate the growth of conspecifics by increasing the availability of a scarce, but mobile resource (e.g. surface run-off water in arid ecosystems, or dissolved nutrients in aquatic ecosystems) in a small area around themselves. This short-range positive feedback also creates a long-range negative feedback, as growth of producers is inhibited by the depletion of the resource in a certain region around areas where producers have already established (Figure 1a) (Kéfi et al., 2010).

Self-organised pattern formation through scale-dependent feedback was originally described by Turing (1952). The emerging patterns can either be stationary like the spot or stripe patterns of some animal fur coats or vary in time (oscillatory Turing patterns, (Hata et al., 2014)). Self-organised formation of spatial patterns in species abundances has been found in a variety of ecological systems such as vegetation (Klausmeier, 1999; Rietkerk and Van de Koppel, 2008), host–parasitoid (Hassell et al., 1994), plant–parasite (White & Gilligan, 1998) and plankton–fish systems (Medvinsky et al., 2002), and has been proposed as a potential explanation for patchy distribution of phytoplankton and herbivores

in the oceans (Levin & Segel, 1976). However, these previous studies only analysed the mechanism proposed by Turing in the context of pure biomass (or abundance) patterns. Recently, it has been shown that self-organised patterns in the abundance of a facilitator species can indirectly promote diversity by creating spatial niches with different environmental conditions for beneficiary species that are not involved in the pattern-forming process, but rely on this environmental heterogeneity for coexistence (Cornacchia et al., 2018). Nevertheless, it remains open to what extent self-organised spatial pattern formation in species abundances can directly influence the diversity of local communities (i.e. of the species directly involved in the pattern-forming process).

In the examples above, self-organised pattern formation was studied in spatially continuous systems, but the extension to networks of discrete habitat patches is well developed (Nakao & Mikhailov, 2010; Othmer & Scriven, 1971). In this case, it is not the patches themselves that emerge in a self-organised manner, but the species composition or biomass densities on these patches. One way in which we expect local diversity to be supported by spatial pattern formation in such network-organised metacommunities is via the generation of source–sink dynamics (Brown & Kodric-Brown, 1977; Shmida & Wilson, 1985). Spatially variable biomass densities of interacting species lead to heterogeneous biotic environments and thus to locally different selection pressures. Consequently, each habitat may possess a different species composition in the local community, which promotes between-patch diversity. As outlined above, this may positively affect the diversity of local communities by continuous immigration of species that cannot form persistent populations under the prevailing local conditions. In case of oscillatory
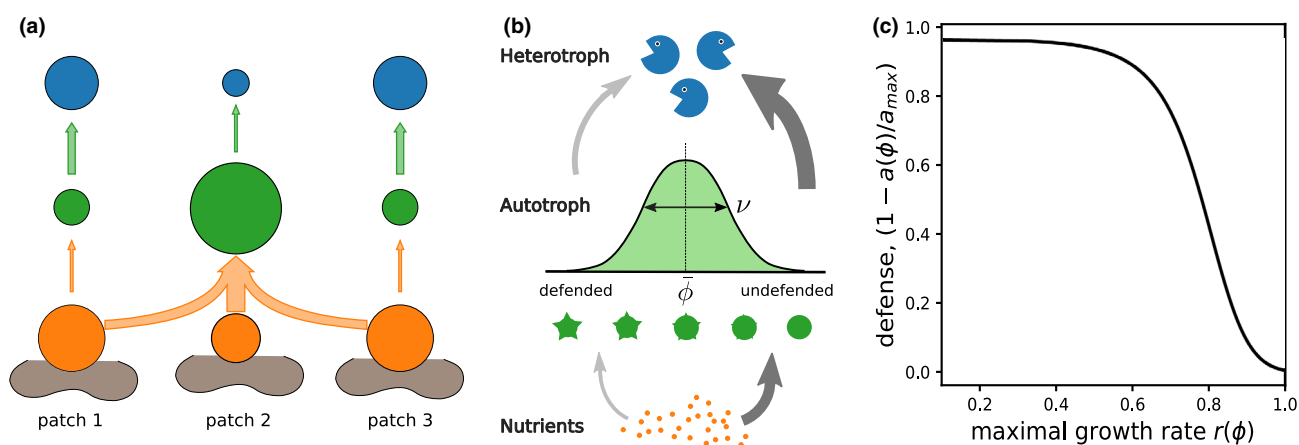

FIGURE 1 (a) Illustration of the basic mechanism for self-organised pattern formation in nutrients and biomasses. Autotrophs on the central patch 2 have grown to high density, which lowers the local nutrient concentration and leads to a net inflow of nutrients from neighbouring patches. This allows autotrophs on patch 2 to grow even further (positive short-range feedback), but suppresses their density on the neighbouring patches (negative long-range feedback). See Appendix S4 for details. (b) Conceptual representation of the local food chain model. The autotroph community exhibits a continuous (logit-normal) distribution of the trait ϕ, characterised by the mean $\bar{\phi}$ and the variance v. A low trait value signifies a low attack rate of the heterotrophs (due to high investment into defence by the autotrophs), at the cost of a low maximal growth rate (visualised by thin arrows), whereas a high trait value leads to a high attack rate but also a high maximal growth rate (thick arrows). (c) Shape of the trade-off between maximal growth rate $r(\phi)$ versus defence against predation, $1 - \frac{a(\phi)}{a_{\max}}$, mediated by the trait ϕ

Turing patterns, we also expect an interaction between source–sink dynamics and the emerging non-equilibrium dynamics, but it is not clear a priori whether this will have a positive or negative effect on local diversity. These mechanisms are particularly relevant for systems where the prevailing selection regime is stabilising and would—without self-organised pattern formation—promote the dominance of a single species.

In this study, we investigate a food chain model with abiotic nutrients, a community of autotrophic prey species and a heterotrophic predator in a spatial context. We explicitly resolve the diversity of the autotrophs by considering a continuous trait distribution within each local habitat. A network of habitat patches, each hosting a local food chain, is interconnected via dispersal and thereby forms a metacommunity on the regional scale. Under the premise of suitable dispersal rates, we expect to find self-organised formation of patterns in the biomasses, which we analyse regarding their potential to increase local and between-patch diversity, possibly beyond classical source–sink dynamics.

METHODS

The model consists of multiple food chains that are spatially distributed on a ring of n interconnected habitat patches with identical environmental conditions. The diversity of the autotroph communities is characterised by a logit-normally distributed trait ϕ ($\in [0, 1]$), which affects both defence and maximal growth rate (Figure 1b,c). We follow a trait-based aggregate approach for modelling diverse communities (Klauschies et al., 2018; Norberg et al., 2001; Wirtz & Eckhardt, 1996) that explicitly describes the temporal change in the trait distribution on each patch by differential equations for the mean trait, $\overline{\phi}$, and the trait variance, v. Together with the nutrient concentration N and total biomass densities A (autotrophs) and H (heterotrophs), the equations for the dynamics on a single patch are

$$\frac{dN}{dt}\bigg|_{\text{loc}} = D(S - N) - \overline{r(\phi)}\frac{N}{N_H + N}A \qquad (1)$$

$$\frac{dA}{dt}\bigg|_{\text{loc}} = \overline{G_A}A \qquad (2)$$

$$\frac{dH}{dt}\bigg|_{\text{loc}} = \left(e\overline{g(\phi)}A - D\right)H \qquad (3)$$

$$\frac{d\overline{\phi}}{dt}\bigg|_{\text{loc}} = v\frac{\partial G_A}{\partial \phi}\bigg|_{\overline{\phi}} \qquad (4)$$

$$\frac{dv}{dt}\bigg|_{\text{loc}} = v^2\left(\frac{\partial^2 G_A}{\partial \phi^2}\bigg|_{\overline{\phi}} + \frac{3(1 - 2\overline{\phi})}{\overline{\phi}(1 - \overline{\phi})}\frac{\partial G_A}{\partial \phi}\bigg|_{\overline{\phi}} - B(v)\right), \qquad (5)$$

where $|_{\text{loc}}$ means local dynamics without spatial interactions. The nutrients N follow chemostat dynamics with supply concentration S and dilution rate D. The nutrient uptake by the autotrophs follows Michaelis–Menten kinetics, with half-saturation constant N_H and average maximal growth rate $\overline{r(\phi)}$ (with $r(\phi) = (r_{\max} - r_{\min})\phi^s + r_{\min}$). The per capita net growth rate (fitness function) of the autotrophs is

$$G_A(\phi) = r(\phi)\frac{N}{N_H + N} - g(\phi)H - D, \qquad (6)$$

where the heterotroph's grazing rate follows a Type II functional response with attack rate $a(\phi) = a_{\max}\frac{e^{b(\phi-c)}}{e^{b(\phi-c)}+1}$ and handling time h:

$$g(\phi) = \frac{a(\phi)}{1 + h\overline{a(\phi)}A}. \qquad (7)$$

The heterotroph's growth is determined by the average grazing rate $\overline{g(\phi)}$ scaled by the conversion efficiency e and the total autotroph biomass A. Autotrophs and heterotrophs also experience losses due to dilution. The average of a function $f(\phi)$ (where f can be any of r, G_A, g or a) across the trait distribution is approximated up to the second order (Coutinho et al., 2016; Klauschies et al., 2018; Norberg et al., 2001):

$$\overline{f(\phi)} = f\left(\overline{\phi}\right) + \frac{v}{2}\frac{\partial^2 f}{\partial \phi^2}\bigg|_{\overline{\phi}}. \qquad (8)$$

The local fitness gradient $\frac{\partial G_A}{\partial \phi}\big|_{\overline{\phi}}$ at $\overline{\phi}$ (Equation (4)) drives changes in $\overline{\phi}$ in the direction that enhances the per capita net growth rate of the autotrophs. The speed of change is scaled by v, which reflects the diversity of the local autotroph community: The presence of many functionally different species (v large) enhances the capability of a community to adapt, while a lack of diversity (v small) slows down the adaptation process. Internal changes in v are predominantly determined by the local curvature of the fitness landscape around $\overline{\phi}$, $\frac{\partial^2 G_A}{\partial \phi^2}\big|_{\overline{\phi}}$, which accounts for stabilising or disruptive selection (reducing or enhancing v respectively). The second term in the parentheses in Equation (5) captures enhancing or reducing effects on v through potential skewness of the trait distribution (Klauschies et al., 2018). This keeps $\overline{\phi}$ in the range [0, 1] by reducing v (and thereby halting change in $\overline{\phi}$) when $\overline{\phi}$ approaches the limits of the trait range. Last, for numerical reasons, we included a boundary function $B(v) = \varepsilon/(v_{\max} - v)$ to ensure that, during transient dynamics, v does not exceed the hypothetical maximal value of $v_{\max} = 0.25$ of a distribution on the interval [0, 1].

The shape of the fitness landscape depends on the trade-off between growth and defence of the autotrophs

(Tirok et al., 2011), where a normalised measure for defence is given by $1 - \frac{a(\phi)}{a_{max}}$. High trait values denote high maximal growth rates, $r(\phi)$, but also weak defence against the heterotroph, and vice versa (Figure 1c). The trade-off between growth and defence ensures that defended species (low ϕ) will thrive when predators are abundant, but are at a disadvantage when predators are rare.

The movement of nutrients, autotrophs and heterotrophs between neighbouring patches is driven by differences in concentration or biomass density, respectively (diffusive movement). The local dynamics on a patch i (Equations (1) to (5)) are thus supplemented by terms describing the effects of diffusion on N_i, A_i and H_i (together summarised as B_i), as well as on $\overline{\phi}_i$ and v_i:

$$\frac{dB_i}{dt} = \frac{dB_i}{dt}\bigg|_{loc} + d_B(B_{i-1} + B_{i+1} - 2B_i) \quad (9)$$

$$\frac{d\overline{\phi}_i}{dt} = \frac{d\overline{\phi}_i}{dt}\bigg|_{loc} + \sum_{k=i\pm1} \frac{d_A A_k}{A_i}(\overline{\phi}_k - \overline{\phi}_i) \quad (10)$$

$$\frac{dv_i}{dt} = \frac{dv_i}{dt}\bigg|_{loc} + \sum_{k=i\pm1} \frac{d_A A_k}{A_i}[v_k - v_i + (\overline{\phi}_k - \overline{\phi}_i)^2] \quad (11)$$

with diffusion constants d_B ($B = N$, A, or H). If trait distributions differ between neighbouring patches, dispersal of the autotrophs also affects the change of $\overline{\phi}_i$ (Equation (10)) and v_i (Equation (11)) (Klauschies et al., 2018; Norberg et al., 2001). The change of the resident mean trait value is affected by the difference between mean trait values of resident and incoming species as well as by the ratio of incoming to resident biomass. The change of the trait variance is affected in a similar way by the difference between trait variances of resident and incoming species, and it increases if the mean trait of the incoming species differs from that of the residents (last term in Equation (11)).

Usually, diffusion acts to reduce spatial inhomogeneities, but for appropriate values of the diffusion constants, the system can undergo a bifurcation (a so-called Turing instability) and spatial patterns in the nutrient concentrations and biomass densities emerge in a self-organised manner (i.e. without requiring any externally imposed spatial heterogeneity). In order to mathematically determine whether a Turing instability occurs, one has to evaluate the dominant eigenvalue λ of a set of matrices $\mathbf{T_k}$ that combine the Jacobian matrix for the local dynamics of N, A and H with the diffusion constants and information on the spatial arrangement of the patches. See Brechtel et al. (2018), Othmer & Scriven (1971) and Appendix S2 for details.

As key metrics influencing the pattern formation process, we varied the diffusion constants d_N, d_A and d_H of nutrients, autotrophs and heterotrophs respectively. The other parameters were set to constant values oriented at planktonic systems (Table 1). For each combination of diffusion constants, 100–1000 replicates with random initial conditions were calculated. As measures for mean

TABLE 1 Description and values of the model parameters

Parameter	Description	Dimension	Value
S	Substrate supply concentration	mass area^{-1}	4.8
D	Dilution rate	time^{-1}	0.3
N_H	Half-saturation constant for nutrient uptake	mass area^{-1}	1.5
r_{max}	Maximum growth rate of the autotrophs	time^{-1}	1
r_{min}	Minimum growth rate of the autotrophs	time^{-1}	0.1
s	Shape parameter of the growth rate function	—	0.3
a_{max}	Maximum attack rate of the heterotroph	area (mass time^{-1})	1.3 or 2.0
B	Scaling parameter of the attack rate function	—	8
C	Scaling parameter of the attack rate function	—	0.4
H	Handling time for the autotrophs	time	0.53
e	Conversion efficiency of the heterotroph	—	0.33
ε	Scaling parameter of the boundary function	—	10^{-3}
v_{max}	Maximum value of the trait variance	—	0.25

local ($\overline{\alpha}$-) and between-patch (β-) diversity, we calculated the mean of $\langle v \rangle_t$ and the variance of $\langle \overline{\phi} \rangle_t$ across patches and replicates (where $\langle \cdot \rangle_t$ represents the temporal average of the respective variable per patch). Additionally, we calculated the probability of maintaining diversity as the fraction of replicates with regional (γ-) diversity (= $\overline{\alpha} + \beta$ -diversity) $>10^{-2}$. If γ-diversity fell below this threshold, it usually tended towards zero, but at a very slow rate. Further details on the output variables and the simulation process are provided in Appendix S1.

RESULTS

Local dynamics

We first describe the dynamics of the local food chain with trait dynamics (Appendix S4, Figures S3 and S4). Importantly, the model system is bistable: On one of the attractors, a high defence level ($\overline{\phi} \lesssim 0.4$) allows the autotrophs to achieve a high biomass density (hereinafter referred to as the defended attractor), while on the other, a low defence level ($\overline{\phi} \approx 1$) leads to lower autotrophic biomass density (hereinafter referred to as the undefended attractor). The nature of the undefended attractor depends on the maximum attack rate a_{max}. At low values of a_{max}, the attractor is a stable fixed point, but at $a_{max} \approx 1.35$, it undergoes a Hopf bifurcation and a limit cycle with

oscillations in nutrient concentration and biomass densities occurs. The defended attractor, conversely, is always a stable fixed point that is only marginally affected by changing a_{max}. On both attractors and irrespective of the Hopf bifurcation, the mean trait $\overline{\phi}$ settles at a constant value. Initially, selection can be disruptive, but eventually the trait variance v always slowly decays to 0 due to stabilising selection closer to the respective attractor, thereby preventing any further temporal change of $\overline{\phi}$.

Metacommunity dynamics

For the analysis of the metacommunity dynamics, we first established that the range of diffusion constants that lead to a Turing instability (TI) of the defended attractor is a proper subset of those that lead to a TI of the undefended attractor (Appendix S2, Figure S1). We also established that, in the parameter region of interest, the dominant eigenvalue of the matrices $\mathbf{T_k}$, Equation (S10), is always complex, implying that an oscillatory TI occurs and spatio-temporal patterns in the biomasses emerge. There are, thus, three different situations: no TI of any attractor, TI of only the undefended attractor and TI of both attractors. However, as diffusion constants for the third case have to be very high, the strong coupling between the patches homogenises the system: Both mean local ($\overline{\alpha}$-) and between-patch (β-) diversity are almost always lost as all patches settle on a single attractor. We, therefore, do not consider this case. The occurrence of a Hopf bifurcation and a Turing instability of the undefended attractor, thus, leaves us with four qualitatively different cases: (1) Undefended attractor is a fixed point and no TI occurs; (2) undefended attractor is a limit cycle and no TI occurs; (3) undefended attractor is a fixed point and a TI occurs; and (4) undefended attractor is a limit cycle and a TI occurs.

Figure 2 shows representative time series for the four cases in a system with $n = 6$ patches. Some trait variance is maintained in all local communities in all four cases (Figure 2i–l), even without TI (cases 1 and 2). In these cases, local trait variances v_i do not vanish because coupling of patches with defended and undefended autotroph communities leads to source–sink dynamics that ensure the local persistence of maladapted species (last term in Equation (11)). In case 2, the diffusive coupling also synchronises the biomass oscillations on patches that host an undefended autotroph community (Figure 2b). However, mean trait values $\overline{\phi}_i$ remain constant, as the low values of the v_i, which scale the adaptation speed (Equation 4), prevent keeping track of the varying selection pressure due to the comparably fast biomass oscillations.

In cases 3 and 4 (TI of the undefended attractor), complex spatio-temporal dynamics arise (Figure 2c and d). On a given patch, the biomass oscillations are notably slower than those induced by the Hopf bifurcation,

their amplitudes are larger and they now also affect the patches with a defended autotroph community. On most patches, trait variance v_i is now markedly greater than in the cases without TI, which leads to visible temporal dynamics in the mean traits $\overline{\phi}_i$. However, if only one of the attractors (defended or undefended) is present in the metacommunity, v_i decays to zero on all patches, despite pattern formation in nutrients and biomasses still occurring (Appendix S5, Figure S5).

The diffusion constant of the autotrophs (d_A) directly affects the trait dynamics within the metacommunity (cf. Equations (10) and (11)). Figure 3 shows the effect of d_A on $\overline{\alpha}$- and β-diversity as well as on the probability of preserving γ-diversity. Increasing d_A positively affects $\overline{\alpha}$-diversity, but has a neutral to negative effect on β-diversity. The latter is due to mean traits of communities on different patches becoming on average more similar when spatial coupling between them intensifies. Regarding $\overline{\alpha}$-diversity, clear and consistent differences between the four cases exist: without TI (cases 1 and 2), $\overline{\alpha}$-diversity is lowest and similar for the two cases. Case 3 exhibits an elevated level of $\overline{\alpha}$-diversity, especially towards higher values of d_A, and case 4 stands out by showing an increase in $\overline{\alpha}$-diversity by about an order of magnitude compared to the cases without TI. However, case 4 also exhibits the largest loss of β-diversity (mean traits of the communities on different patches become more similar as d_A increases) and the probability of retaining γ-diversity in the metacommunity strongly declines for $d_A > 10^{-5}$. (Note that $\overline{\alpha}$- and β-diversity, Figure 3a and b, were only calculated using the replicates in which γ-diversity was retained.)

Last, we demonstrate that the spatio-temporal pattern formation induced by the Turing instability is indeed the driving force behind the increased level of $\overline{\alpha}$-diversity. Comparing the dominant eigenvalue or Floquet multiplier (depending on whether the undefended attractor of the local dynamics is a fixed point or a limit cycle, cf. Appendix S2) of the matrices $\mathbf{T_k}$, which determines whether a TI occurred, with the level of preserved $\overline{\alpha}$-diversity over a wide range of values of the diffusion constants d_N and d_H shows that both metrics are coherently increasing with the distance of the diffusion constants from the Turing instability boundary (Figure 4). This visual inspection of their dependency is also quantitatively supported (Spearman rank-correlation $r_s = 0.82$ for stable local dynamics and $r_s = 0.85$ for oscillatory local dynamics; see Appendix S6).

DISCUSSION

Preserving diversity is essential for the functioning of ecosystems (Hooper et al., 2005; Tilman, 2001) and their persistence in the face of accelerated global change (Duraiappah et al., 2005). Recent studies have shown that locally (i.e. in a specific habitat), its maintenance
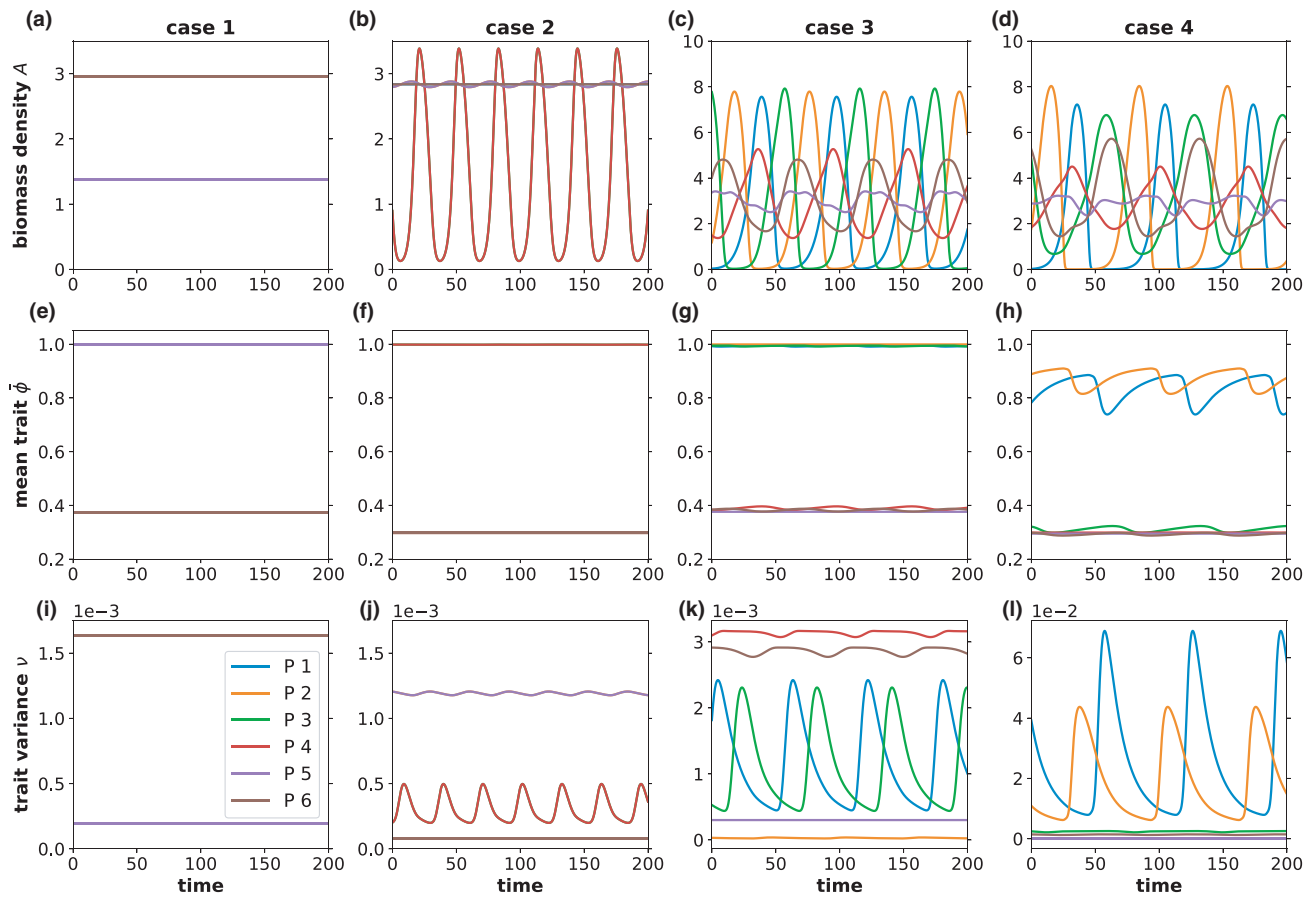
FIGURE 2 Exemplary time series of autotroph biomass densities (top row, a–d), mean traits $\overline{\phi}$ (middle row, e–h) and trait variances ν (bottom row, i–l, y-axes are scaled with the number at the top left corner of the panels) for spatial systems in cases 1–4 with 6 patches (labelled P1 through P6). In cases 1 and 2, no Turing instability (TI) occurs ($d_N = 10^{-2}$), in cases 3 and 4, a TI occurs ($d_N = 1$). In cases 1 and 3, the undefended attractor is a fixed point ($a_{max} = 1.3$), in cases 2 and 4, it is a limit cycle ($a_{max} = 2.0$). In all four cases, $d_A = 10^{-5}$ and $d_H = 10^{-3}$
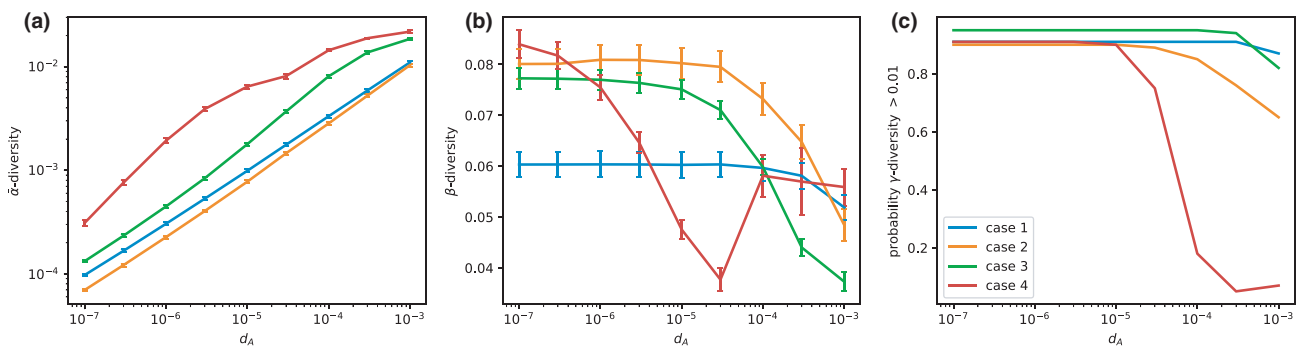
FIGURE 3 The degree of diversity maintenance on different spatial scales depends on the mobility of the autotrophs. In panel (a), the biomass-weighted mean trait variance $\langle \nu \rangle_t$ across six patches is shown as a measure of $\overline{\alpha}$-diversity; in (b), the biomass-weighted variance of mean trait values $\langle \overline{\phi} \rangle_t$ signifies β-diversity. Results were obtained as arithmetic means over 1000 simulation runs with randomised initial conditions. In panel (c), the fraction of simulation runs in which regional (γ-) diversity is maintained ($\overline{\alpha} + \beta > 10^{-2}$), is shown. In cases 1 and 2, $d_N = 10^{-2}$; in cases 3 and 4, $d_N = 1$. In all four cases, $d_H = 10^{-3}$

may strongly rely on the immigration of novel species (Klauschies et al., 2018; Norberg, 2004; Norberg et al., 2001). However, these studies did not explicitly account for the spatial context and, thus, potential interactions between mean local ($\overline{\alpha}$-) and between-patch (β-) diversity. In the present study, we overcome this limitation by investigating the potential impact of dispersal between different habitats on the diversity of local autotroph communities in a food chain through a novel mechanism based on self-organised pattern formation. For a wide range of dispersal rates, spatio-temporal patterns in the biomasses of the interacting species form, which feed

back on the distribution of a functional trait. If these local biomass-trait feedbacks interact with standing β-diversity, $\overline{\alpha}$-diversity increases up to tenfold compared to scenarios without self-organised pattern formation.

$\overline{\alpha}$-diversity without pattern formation

Our model reproduces several classic results when no self-organised formation of spatial biomass patterns occurs. If some source of β-diversity in the metacommunity exists, for example, due to environmental heterogeneity or, as is the case here, due to alternative stable local community states, dispersal of the autotrophs creates source–sink dynamics (Brown & Kodric-Brown, 1977; Shmida & Wilson, 1985). Permanent sink populations that contribute to $\overline{\alpha}$-diversity form if the locally maladapted species are reintroduced via dispersal faster than they are competitively excluded (Pulliam, 1988). This also explains the frequently made observation that $\overline{\alpha}$-diversity increases—at least up to a certain point—with dispersal rate (Grainger & Gilbert, 2016; Mouquet & Loreau, 2003). Conversely, $\overline{\alpha}$-diversity vanishes when the autotroph communities are completely isolated. In our model, stabilising selection leads to a dominance of either fast-growing, undefended species, or slow-growing, well-defended species, but the model precludes coexistence of the two strategies in one patch. Over time, the

isolated communities thus lose their ability to adapt to changing environmental conditions, which makes them susceptible to perturbations (Gunderson, 2000; Ceulemans et al., 2021).

Increase of $\overline{\alpha}$-diversity via self-organised pattern formation

When the dispersal rates of heterotrophs and autotrophs are at intermediate levels and the diffusion rate of the nutrients is high enough to induce a Turing instability, spatio-temporal patterns in the nutrients and biomasses form. These patterns create differences in consumption rates and nutrient availability, and thereby different selection pressures on the autotroph communities, which are fluctuating both in space and time. However, with no independent source of β-diversity, for example, due to the coexistence of defended and undefended communities in the landscape, these fluctuations in selection pressures proved not strong enough or to vary too quickly to overcome the general stabilising selection regime that over time eliminates $\overline{\alpha}$-diversity.

Nevertheless, if there is an additional source of β-diversity that is independent of the self-organised biomass patterns, $\overline{\alpha}$-diversity is maintained on a far higher level than could be expected from simple source–sink dynamics, and which now allows for continuing adaptation
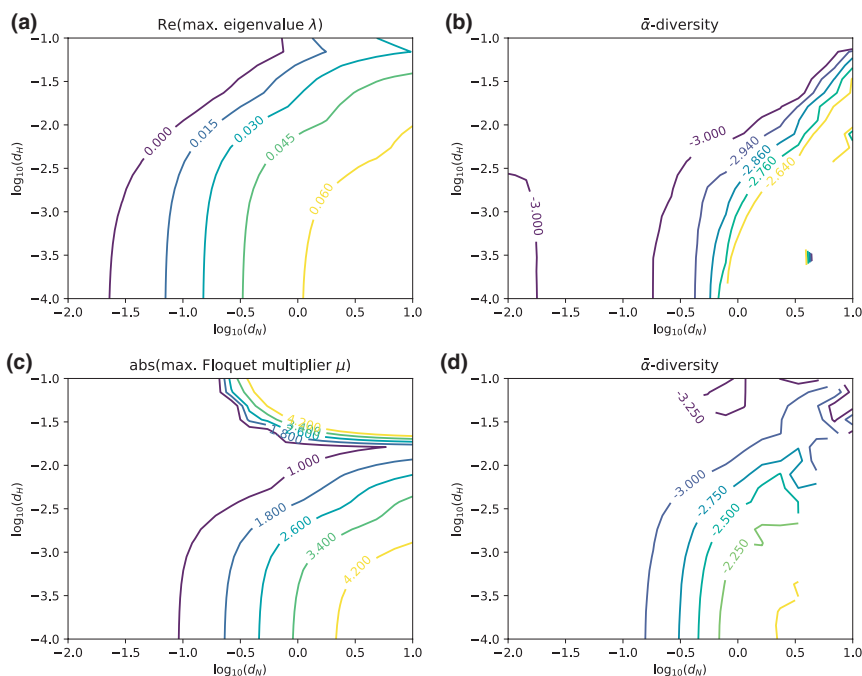

FIGURE 4 Correspondence between Turing instability and $\overline{\alpha}$-diversity. In panels a) and b), the undefended attractor is a fixed point ($a_{\max} = 1.3$). Panel (a) shows the real part of the dominant eigenvalue λ of the matrices $\mathbf{T_k}$ (Equation (S10)), while panel (b) shows on a logarithmic scale the mean trait variance ν (averaged over patches and simulation runs), that is, the $\overline{\alpha}$-diversity. In panels (c) and (d), the undefended attractor is a limit cycle ($a_{\max} = 2.0$). In this case, the matrices $\mathbf{T_k}$ are time dependent and periodic, and the relevant quantity that determines the occurrence of a Turing instability is now the dominant Floquet multiplier μ (panel (c), cf. Appendix S2 for details). Panel (d) shows the mean trait variance ν on a logarithmic scale for this case. For each combination of d_N and d_H, results were obtained as arithmetic means over 100 simulation runs with randomised initial conditions. In both cases, $d_A = 10^{-5}$

of the local communities. We suggest the following mechanism by which the interplay of the fluctuating selection pressure with the influx of external phenotypes supports $\overline{\alpha}$-diversity: When the mean trait of a local community is at its optimal value (maximising the fitness function G_A), the curvature of the fitness landscape is necessarily negative and the trait variance decreases. Under a fluctuating selection regime, however, the optimal trait value varies over time, which allows different species to thrive at different moments in time. Furthermore, the immigrating species will usually be maladapted, which in combination with the constantly changing biotic environment keeps the mean trait of the local community sufficiently far from its current optimal value that the curvature of the fitness landscape may be less negative or at times even positive. Thereby, local dynamics do not reduce trait variance as strongly and can be counterbalanced by the direct increase of trait variance by the immigration of species with different trait values. When additional temporal variability in the form of a limit cycle of the local population dynamics is present, $\overline{\alpha}$-diversity is increased even further. Finally, the standing β-diversity also generates spatial heterogeneity in the interaction rates, which has been shown to enhance the complexity of the emerging patterns (Krause et al., 2020). This increases the magnitude of the fluctuations in the selection pressure and may thus contribute to maintaining $\overline{\alpha}$-diversity.

We hypothesise that even without an independent source of β-diversity, it is possible that self-organised pattern formation and the entailing varying selection pressure induce permanent $\overline{\alpha}$-diversity. The first evidence for this was provided by Eigentler and Sherratt (2020), who analysed travelling waves of vegetation on sloped terrain in savanna ecosystems. They demonstrated that coexistence of two plant species (grasses and trees) is possible due to a colonisation–competition trade-off. In Eigentler (2021), these results were extended to cover a wider range of environmental conditions by including intraspecific competition. In general, conditions under which pattern formation might facilitate $\overline{\alpha}$-diversity include less strongly stabilising selection regimes, more flexible shapes of the local trait distributions (e.g. assuming a beta distribution instead of a transformed normal distribution (Klauschies et al., 2018)), or stationary instead of oscillatory Turing patterns. These stationary patterns would create selection pressures that only vary between habitats, but are constant over time in each habitat. This would allow the local communities to slowly adapt to the prevailing conditions and thereby create a certain amount of β-diversity in a self-organised manner, which in turn could increase $\overline{\alpha}$-diversity via source–sink dynamics.

Loss of $\overline{\alpha}$- and β-diversity at high dispersal rates

The amount of $\overline{\alpha}$-diversity maintained correlates strongly with the strength of the Turing instability, that is, the more pronounced the spatio-temporal patterns are, the higher is the $\overline{\alpha}$-diversity (Figure 4). Generally, this happens when the diffusion or dispersal rates increase, which leads to a higher exchange of nutrients, biomass and especially different species between the habitat patches.

However, we also observe that dispersal is indeed a 'double-edged sword' (Hudson & Cattadori, 1999), as very high dispersal rates eventually reduce diversity by homogenising the metacommunity. In fact, it has been observed before that stronger ecological coupling may decrease β-diversity (Mouquet & Loreau, 2003). This makes species that are exchanged between habitats increasingly similar, which reduces the stimulating effect of dispersal on $\overline{\alpha}$-diversity. In our system, this is of particular relevance since β-diversity directly relies on the coexistence of defended and undefended communities in the landscape. Progressive homogenisation thus has a strong effect since it increases the probability for all local communities to adopt the same strategy (fast-growing, undefended, or slow-growing, well-defended), corresponding to a complete loss of β-diversity and eventually also $\overline{\alpha}$-diversity.

Applicability in different ecosystem types

While we developed our model with a planktonic system in mind, the wide range of autotroph dispersal rates that leads to self-organised pattern formation (Figure 3) suggests that our findings may apply to a variety of different ecosystems. These range from aquatic environments with relatively mobile autotrophs (mid to upper end of the d_A spectrum) to terrestrial ecosystems with often very limited autotroph dispersal (lower end of the d_A spectrum).

In aquatic metacommunities, local habitats are given by ponds or lakes that are interconnected by dispersal, for example, through overflows and rivulets (Leibold et al., 2004; Vanormelingen et al., 2008). Furthermore, aquatic metacommunities can establish in larger waterbodies like large lakes, seas and oceans (Leibold & Norberg, 2004) where local communities form in confined areas like embayments or gyres and are interconnected by water currents. The autotrophic level mainly consists of phytoplankton which behave like particles in water and exhibit moderate mobility. Inorganic nutrients are considerably smaller particles with diffusion rates several orders of magnitude higher than the diffusion rates of phytoplankton. Due to active movement, herbivorous zooplankton can also achieve much higher dispersal rates than phytoplankton. Previous theoretical studies showed that self-organised pattern formation can occur in plankton systems (Malchow, 1993; Medvinsky et al., 2001, 2002; Ruan, 1998). However, to our knowledge, none of these studies considered pattern formation as an explanation for plankton diversity and as a potential mechanism contributing to resolving the paradox of the plankton (Hutchinson, 1961; Scheffer et al., 2003).

174

This mechanism will of course always interact with other mechanisms creating diversity in aquatic communities. Depending on the scale considered, even small systems like ponds can be internally structured with clear distinctions between littoral, pelagic and benthic zones. Furthermore, vertical stratification in lakes creates a structuring with sufficiently different environmental conditions that allow different communities to develop. On the one hand, this environmental heterogeneity may positively interact with the self-organised formation of biomass patterns (Krause et al., 2020), mutually increasing the potential of the respective mechanism to support diversity. On the other hand, seasonal mixing events temporally equalise diffusion rates, thereby eliminating a necessary condition for self-organised pattern formation.

In terrestrial systems, the autotroph level consists of sessile plants, which move only once in their lifetime during seed or propagule dispersal, while nutrient transportation (e.g. via ground water) and active herbivore movement are once again relatively fast. The dispersal rates of plants are consequently determined by their generation time as well as their dispersal strategy (Pueyo et al., 2008). Since both factors can vary greatly between terrestrial plant species, a variety of different autotroph dispersal rates exist in terrestrial metacommunities, which are covered by our results. Species diversity in terrestrial ecosystems is explained by several classical theories like the intermediate disturbance hypothesis (Connell, 1978) or the Janzen–Connell hypothesis (Hyatt et al., 2003). The former links plant diversity to non-equilibrium dynamics, while the latter traces it back to a reduced probability of seed survival near parent trees through enhanced predation pressure. In studies of savanna ecosystems, the coexistence of grass and tree species has also been linked to self-organised pattern formation (Baudena & Rietkerk, 2013; Gilad et al., 2007; Nathan et al., 2013). However, these studies usually assume that only one of the plant species is involved in the pattern-forming process (notable exceptions are Eigentler, 2021; Eigentler & Sherratt, 2020)), which then facilitates the persistence of the other species. The results of the present study suggest that self-organised pattern formation, especially when it interacts with pre-existing β-diversity (or spatial heterogeneity in general), might be an important mechanism complementing the well-established theories on plant diversity.

SUMMARY AND CONCLUSIONS

In line with previous studies (Mouquet & Loreau, 2003; Venail et al., 2008), our findings show that dispersal acts as a link between $\overline{\alpha}$- and β-diversity and that it can have both positive and negative effects on local diversity in a metacommunity. Besides having the potential to cause self-organised pattern formation in biomass densities, dispersal determines to what extent functionally different species are exchanged between local habitats and therefore how β-diversity affects $\overline{\alpha}$-diversity. Low dispersal rates that do not initiate pattern formation enhance $\overline{\alpha}$-diversity only marginally via source–sink dynamics. On the other side, strong dispersal tends to homogenise the landscape and thereby eliminates any differences between the habitats, which ultimately also leads to the loss of $\overline{\alpha}$-diversity. In contrast, intermediate dispersal leads to the highest amount of preserved diversity. It enhances $\overline{\alpha}$-diversity through an interplay of source–sink dynamics with variable selection pressures caused by self-organised pattern formation while preserving between-patch differences in the local trait distributions (i.e. β-diversity).

Our results indicate that self-organised pattern formation by the Turing mechanism alone is not necessarily sufficient to create $\overline{\alpha}$-diversity in the first place. However, this study shows for the first time in a generic food-web model that self-organised pattern formation can amplify $\overline{\alpha}$-diversity from the low levels created by, for example, source–sink dynamics in environmentally heterogeneous landscapes, to levels required for maintaining the ability of communities to adapt to changes in environmental conditions. To fully understand spatial and temporal variation of biodiversity, we thus argue that it is necessary to take regional processes like pattern formation and their effects on local dynamics into account. Since self-organised pattern formation occurs only for certain combinations of dispersal rates, factors like obstacles or corridors that reduce or enhance the flux of nutrients and organisms in nature potentially have strong effects on the diversity of natural metacommunities. This has important implications for decision-making in ecological management, as both facilitating or hindering dispersal can have adverse effects on pattern formation and thus the maintenance of biodiversity.

AUTHOR CONTRIBUTIONS
CG and TK conceived the study design. JH and CG wrote the computer code, performed the numerical simulations and evaluated the data. All authors interpreted and discussed the results. JH wrote the first draft of the manuscript (with contributions of CG), CG led the editing. All authors contributed critically to the drafts and gave final approval for publication.

PEER REVIEW
The peer review history for this article is available at https://publons.com/publon/10.1111/ele.13880.

DATA AVAILABILITY STATEMENT

The code and data required to reproduce the results is available at Zenodo.org with DOI https://doi.org/10.5281/zenodo.5235435.

ORCID

Christian Guill ⬥ https://orcid.org/0000-0002-5955-9998
Toni Klauschies ⬥ https://orcid.org/0000-0001-8609-931X

REFERENCES

Amarasekare, P. (2003) Competitive coexistence in spatially structured environments: a synthesis. *Ecology Letters*, 6, 1109–1122.

Baudena, M. & Rietkerk, M. (2013) Complexity and coexistence in a simple spatial model for arid savanna ecosystems. *Theoretical Ecology*, 6, 131–141.

Brechtel, A., Gramlich, P., Ritterskamp, D., Drossel, B. & Gross, T. (2018) Master stability functions reveal diffusion-driven pattern formation in networks. *Physical Review E*, 97(3).

Brown, J.H. & Kodric-Brown, A. (1977) Turnover rates in insular biogeography: effect of immigration on extinction. *Ecology*, 58, 445–449.

Cadotte, M.W., Carscadden, K. & Mirotchnick, N. (2011) Beyond species: functional diversity and the maintenance of ecological processes and services. *Journal of Applied Ecology*, 48, 1079–1087.

Ceulemans, R., Wojcik, L.A. & Gaedke, U. (2021). Functional diversity alters the effects of a pulse perturbation on the dynamics of tritrophic foodwebs. *bioRxiv*. https://doi.org/10.1101/2021.03.22.436420

Connell, J.H. (1978) Diversity in tropical rain forests and coral reefs. *Science*, 199, 1302–1310.

Cornacchia, L., van de Koppel, J., van der Wal, D., Wharton, G., Puijalon, S. & Bouma, T.J. (2018) Landscapes of facilitation: how self-organized patchiness of aquatic macrophytes promotes diversity in streams. *Ecology*, 99, 832–847.

Coutinho, R.M., Klauschies, T. & Gaedke, U. (2016) Bimodal trait distributions with large variances question the reliability of trait-based aggregate models. *Theoretical Ecology*, 9, 389–408.

Duraiappah, A., Naeem, S., Agardy, T., Ash, N., Cooper, H., Diaz, S. et al. (2005) *Ecosystems and human well-being: biodiversity synthesis; a report of the Millennium Ecosystem Assessment*. World Resources Institute.

Eigentler, L. (2021) Species coexistence in resource-limited patterned ecosystems is facilitated by the interplay of spatial self-organisation and intraspecific competition. *Oikos*, 130, 609–623.

Eigentler, L. & Sherratt, J. (2020) Spatial self-organisation enables species coexistence in a model for savanna ecosystems. *Journal of Theoretical Biology*, 487, 110122.

Gilad, E., Shachak, M. & Meron, E. (2007) Dynamics and spatial organization of plant communities in water-limited systems. *Theoretical Population Biology*, 72, 214–230.

Grainger, T.N. & Gilbert, B. (2016) Dispersal and diversity in experimental metacommunities: linking theory and practice. *Oikos*, 125, 1213–1223.

Gunderson, L.H. (2000) Ecological resilience – in theory and application. *Annual Review of Ecology and Systematics*, 31, 425–439.

Hassell, M.P., Comins, H.N. & May, R.M. (1994) Species coexistence and self-organizing spatial dynamics. *Nature*, 370, 290–292.

Hata, S., Nakao, H. & Mikhailov, A.S. (2014) Dispersal-induced destabilization of metapopulations and oscillatory turing patterns in ecological networks. *Scientific Reports*, 4, 3585.

Hooper, D.U., Chapin, F.S., Ewel, J.J., Hector, A., Inchausti, P., Lavorel, S. et al. (2005) Effects of biodiversity on ecosystem functioning: a consensus of current knowledge. *Ecological Monographs*, 75, 3–35.

Hudson, P.J. & Cattadori, I.M. (1999) The moran effect: a cause of population synchrony. *Trends in Ecology and Evolution*, 14, 1–2.

Hutchinson, G.E. (1961) The paradox of the plankton. *American Naturalist*, 95, 137–145.

Hyatt, L.A., Rosenberg, M.S., Howard, T.G., Bole, G., Fang, W., Anastasia, J. et al. (2003) The distance dependence prediction of the Janzen-Connell hypothesis: a meta-analysis. *Oikos*, 103, 590–602.

Kéfi, S., Eppinga, M.B., de Ruiter, P.C. & Rietkerk, M. (2010) Bistability and regular spatial patterns in arid ecosystems. *Theoretical Ecology*, 3, 257–269.

Klauschies, T., Coutinho, R.M. & Gaedke, U. (2018) A beta distribution-based moment closure enhances the reliability of trait-based aggregate models for natural populations and communities. *Ecological Modelling*, 381, 46–77.

Klausmeier, C.A. (1999) Regular and irregular patterns in semiarid vegetation. *Science*, 284, 1826–1828.

Krause, A.L., Klika, V., Woolley, T.E. & Gaffney, E.A. (2020) From one pattern into another: analysis of turing patterns in heterogeneous domains via WKBJ. *Journal of the Royal Society, Interface*, 17(162), 20190621.

Leibold, M.A., Holyoak, M., Mouquet, N., Amarasekare, P., Chase, J.M., Hoopes, M.F. et al. (2004) The metacommunity concept: a framework for multi-scale community ecology. *Ecology Letters*, 7, 601–613.

Leibold, M.A. & Norberg, J. (2004) Biodiversity in metacommunities: plankton as complex adaptive systems? *Limnology and Oceanography*, 49, 1278–1289.

Levin, S.A. & Segel, L.A. (1976) Hypothesis for origin of planktonic patchiness. *Nature*, 259, 659.

Malchow, H. (1993) Spatio-temporal pattern formation in nonlinear non-equilibrium plankton dynamics. *Proceedings of the Royal Society of London, Series B: Biological Sciences*, 251, 103–109.

Medvinsky, A.B., Petrovskii, S.V., Tikhonova, I.A., Malchow, H. & Li, B.L. (2002) Spatiotemporal complexity of plankton and fish dynamics. *SIAM Review*, 44, 311–370.

Medvinsky, A.B., Tikhonova, I.A., Aliev, R.R., Li, B.L., Lin, Z.S. & Malchow, H. (2001) Patchy environment as a factor of complex plankton dynamics. *Physical Review E*, 64, 021915.

Mouquet, N. & Loreau, M. (2003) Community patterns in source-sink metacommunities. *American Naturalist*, 162, 544–557.

Nakao, H. & Mikhailov, A.S. (2010) Turing patterns in network-organized activator–inhibitor systems. *Nature Physics*, 6, 544.

Nathan, J., Meron, E. & von Hardenberg, J. (2013) Spatial instabilities untie the exclusion principle constraint on species coexistence. *Journal of Theoretical Biology*, 335, 198–204.

Norberg, J. (2004) Biodiversity and ecosystem functioning: a complex adaptive systems approach. *Limnol. Oceanog*, 49, 1269–1277.

Norberg, J., Swaney, D.P., Dushoff, J., Lin, J., Casagrandi, R. & Levin, S.A. (2001) Phenotypic diversity and ecosystem functioning in changing environments: a theoretical framework. *Proceedings of the National Academy of Sciences of the United States of America*, 98, 11376–11381.

Othmer, H.G. & Scriven, L. (1971) Instability and dynamic pattern in cellular networks. *Journal of Theoretical Biology*, 32, 507–537.

Pueyo, Y., Kéfi, S., Alados, C. & Rietkerk, M. (2008) Dispersal strategies and spatial organization of vegetation in arid ecosystems. *Oikos*, 117, 1522–1532.

Pulliam, H.R. (1988) Sources, sinks, and population regulation. *American Naturalist*, 132, 652–661.

Rietkerk, M. & Van de Koppel, J. (2008) Regular pattern formation in real ecosystems. *Trends in Ecology and Evolution*, 23, 169–175.

Ruan, S. (1998) Turing instability and travelling waves in diffusive plankton models with delayed nutrient recycling. *IMA Journal of Applied Mathematics*, 61, 15–32.

Scheffer, M., Rinaldi, S., Huisman, J. & Weissing, F.J. (2003) Why plankton communities have no equilibrium: solutions to the paradox. *Hydrobiologia*, 491, 9–18.

Shmida, A. & Wilson, M.V. (1985) Biological determinants of species diversity. *Journal of Biogeography*, 12, 1–20.

Tilman, D. (1999) The ecological consequences of changes in biodiversity: a search for general principles 101. *Ecology*, 80, 1455–1474.

Tilman, D. (2001) Functional diversity. *Encyclopedia of Biodiversity*, 3, 109–120.

Tirok, K., Bauer, B., Wirtz, K. & Gaedke, U. (2011) Predator-prey dynamics driven by feedback between functionally diverse trophic levels. *PLoS ONE*, 6, e27357.

Tirok, K. & Gaedke, U. (2010) Internally driven alternation of functional traits in a multispecies predator–prey system. *Ecology*, 91, 1748–1762.

Turing, A.M. (1952) The chemical basis of morphogenesis. *Philosophical Transactions of the Royal Society of London. Series B: Biological Sciences*, 237, 37–72.

Vanormelingen, P., Cottenie, K., Michels, E., Muylaert, K., Vyverman, W. & De Meester, L. (2008) The relative importance of dispersal and local processes in structuring phytoplankton communities in a set of highly interconnected ponds. *Freshwater Biology*, 53, 2170–2183.

Vasseur, D.A., Amarasekare, P., Rudolf, V.H. & Levine, J.M. (2011) Eco-evolutionary dynamics enable coexistence via neighbor-dependent selection. *American Naturalist*, 178, E96–E109.

Venail, P.A., MacLean, R.C., Bouvier, T., Brockhurst, M.A., Hochberg, M.E. & Mouquet, N. (2008) Diversity and productivity peak at intermediate dispersal rate in evolving metacommunities. *Nature*, 452, 210.

White, K. & Gilligan, C. (1998) Spatial heterogeneity in three-species, plant-parasite-hyperparasite, systems. *Philosophical Transactions of the Royal Society of London. Series B: Biological Sciences*, 353, 543–557.

Wirtz, K.W. & Eckhardt, B. (1996) Effective variables in ecosystem models with an application to phytoplankton succession. *Ecological Modelling*, 92, 33–53.

Yachi, S. & Loreau, M. (1999) Biodiversity and ecosystem productivity in a fluctuating environment: the insurance hypothesis. *Proceedings of the National Academy of Sciences of the United States of America*, 96, 1463–1468.

SUPPORTING INFORMATION

Additional supporting information may be found in the online version of the article at the publisher's website.

Animal diversity and ecosystem functioning in dynamic food webs

Florian D. Schneider[1,2], Ulrich Brose[3,4], Björn C. Rall[3,4] & Christian Guill[5,6]

Species diversity is changing globally and locally, but the complexity of ecological communities hampers a general understanding of the consequences of animal species loss on ecosystem functioning. High animal diversity increases complementarity of herbivores but also increases feeding rates within the consumer guild. Depending on the balance of these counteracting mechanisms, species-rich animal communities may put plants under top-down control or may release them from grazing pressure. Using a dynamic food-web model with body-mass constraints, we simulate ecosystem functions of 20,000 communities of varying animal diversity. We show that diverse animal communities accumulate more biomass and are more exploitative on plants, despite their higher rates of intra-guild predation. However, they do not reduce plant biomass because the communities are composed of larger, and thus energetically more efficient, plant and animal species. This plasticity of community body-size structure reconciles the debate on the consequences of animal species loss for primary productivity.

[1] Institut des Sciences de l'Evolution (ISEM), Université Montpellier, CNRS, IRD, UMR 5554, C.C.065, 34095 Montpellier Cedex 05, France. [2] Senckenberg Biodiversity and Climate Research Centre (BiK-F), Senckenberganlage 25, 60325 Frankfurt am Main, Germany. [3] German Centre for Integrative Biodiversity Research (iDiv) Halle-Jena-Leipzig, Deutscher, Platz 5e, 04103 Leipzig, Germany. [4] Institute of Ecology, Friedrich Schiller Universtiy Jena, Dornburger-Strasse 159, 07743 Jena, Germany. [5] Institute for Biodiversity and Ecosystem Dynamics, University of Amsterdam, PO Box, 94248, 1090 GE Amsterdam, The Netherlands. [6] Institute of Biochemistry and Biology, University of Potsdam, Maulbeerallee 2, 14469 Potsdam, Germany. Correspondence and requests for materials should be addressed to F.D.S. (email: fd.schneider@senckenberg.de).

Although there is much evidence that ecosystem functioning is a product of organismal activity[1], the relationship between species diversity and ecosystem functioning remains enigmatic. Alarmed by the recent rates of species extinction across all ecosystems, much ecological research over the past two decades has been driven by the biodiversity effects on the magnitude and stability of ecosystem functions (the biodiversity-ecosystem functioning debate)[1–3]. While most of this research focused on variation in plant diversity[4,5], fewer studies addressed the consequences of declining animal diversity[6–8] despite the higher extinction risk at higher trophic levels[9]. Consequently, we lack a generalized understanding of the relationship between animal diversity and ecosystem functioning: Apparently idiosyncratic, positive as well as negative consequences for plant primary productivity in response to animal species loss from multi-trophic communities have been observed[10–14], which cannot be explained by species richness alone.

Partially, this dichotomy of effects may be explained by the ecosystem's balance between niche complementarity effects and community trophic cascades[15–17]. A simply structured animal community of a single trophic level is limited to cause direct negative effects on the trophic level below. Therefore, it would become more exploitative on the plant community, due to niche complementarity[18], as animal diversity increases. This mechanism is highly relevant when horizontal diversity, that is, diversity within a trophic level increases[8]. For instance, an increase in the number of obligate herbivorous species should result in higher absolute rates of herbivory. In contrast, predation among animals can generate indirect positive effects on the plant community: the predominant consumption of animal prey releases the basal community from top–down pressure due to trophic cascades. As vertical diversity increases through added trophic levels, the animal communities' total effect on the basal plant community would be reduced[8,10,15,19,20]. Accordingly, the net effect of increasing animal diversity on basal productivity could be negative or positive depending on the relative dominance of increased niche complementarity or trophic cascades, respectively[8].

In natural ecosystems, however, vertical and horizontal diversity are not independent of each other but are linked due to the complex feeding interactions within the animal community. As species number increases, animals cover larger parts of the resource niche space (horizontal diversity) and occupy new trophic levels (vertical diversity)[8,21,22]. Generalist feeding leads to omnivory (that is, feeding on resources across trophic levels) and causes intraguild predation (that is, feeding on resources of the same trophic group) to be more common in diverse food webs[23,24]. Consequently, any clear distinction between trophic levels would be lost[8], which has been hypothesized to make trophic cascades less likely[7,10,18–20,25].

These counteracting mechanisms inhibit any generalized predictions about how animal diversity affects the plant compartment and the processes and ecosystem functions related to it[6,16]. Usually in experimental studies, the plant biomass standing stock, rates of herbivore consumption and metabolism are assessed to quantify ecosystem functions. Therefore, in this study we employ dynamic simulations of complex food webs to assess general patterns in these community level quantities of ecosystem function in response to changes in animal diversity (Fig. 1).

Food-web models can scale individual and population level mechanisms to complex communities of interacting species[16] to make predictions about the consequences of altered diversity across trophic levels[26–29]. In previous applications, however, species richness within a trophic level (horizontal diversity) and

the number of trophic levels (vertical diversity) were investigated separately[3,16], with only few exceptions[28,30]. None of these models reflected the variability and complexity of natural food webs, which differ strongly in species richness and composition as well as the number and strength of their interactions. We fill this gap by extrapolating dynamic models based on allometric constraints[31], that have successfully been applied to predict population dynamics and consequences of species extinctions in simple modules, to the context of entire food webs[32–34].

Allometric, or body mass, constraints on multiple species traits like movement speed, reproduction rates, volume-to-surface ratios and metabolic rates have long been appreciated[35]. More recently, the implications of allometry for community level properties, such as feeding rates[36–40], niche differentiation[32,38,41,42] and food web structure[23,41,43,44], have been quantified. Therefore, we apply an allometric model that defines the consumer (that is, animal) species' feeding rates on its resource (that is, plants and other animals) as functions of consumer and resource body masses ('allometric functional response')[31,32,36–39]. The potential feeding rate is highest for an energetically optimal resource size, while smaller and larger resource species are less efficiently foraged for (Fig. 2, Methods section).

During the simulations, biomasses of species adjust dynamically and species extinctions occurr before a steady state is achieved. Thus, the species that comprise the final community were 'selected' by energetic processes among the allometrically defined species. While similarly sized species exploit the same resources and are vulnerable to the same consumers, which synchronizes their population dynamics, differently sized species
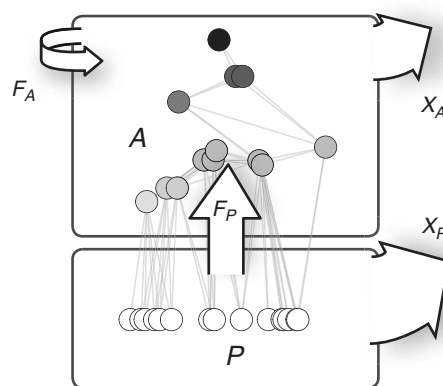

Figure 1 | Schematic diagram of the ecosystem model. The animal community, A, feeds on the plant community, P, with rate F_P but also on members of the own consumer guild with rate F_A. Both, plant and animal community, lose energy due to metabolic demands, X_P and X_A, respectively.
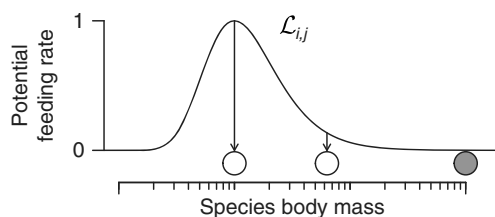

Figure 2 | Potential per-capita feeding rate of a consumer species on its resources. The feeding efficiency, $\mathcal{L}_{i,j}$ of a consumer (grey circle) on its resources (white circles), is maximized for an energetically optimal resource size relative to its own body mass. Larger or smaller resource species are consumed less efficiently.

contribute complementary features to the community, for example, exploit a resource that cannot be accessed by others. By occupying a spot in the upper range of our model's niche axis, particularly large animals would form a predatory trophic level on top of the primary consumer community. The observed levels of biomass of the animal and plant community as well as the process rates and energetic losses on the community level arise implicitly from the allometric constraints at the population level. Being based on well understood mechanisms at the population level, this is a generic approach to the functions provided at the ecosystem level[45] (Fig. 1).

Using this generic model framework, we investigate whether increasing animal diversity causes stronger top–down control on the plant community via enhanced direct feeding interactions and complementarity effects, or if it rather weakens top–down control due to the increase of intraguild predation among animals. We observe that despite increased intraguild predation in diverse animal communities, plants are not released from top–down pressure due to the plasticity of community size structure.

Results

Dynamic food-web model. We cast the concepts outlined above into a unifying ecological framework by applying a network-theoretic approach assuming that the species (nodes), connected by dynamic feeding interactions (edges), compose the higher level characteristics of ecosystems[3,14,16,18]. The potential feeding rate curves of all animal species thus define the network structure of the entire community. A consumer feeds on all species present in the local food web that are within a certain body-mass range, including other consumers (Fig. 3a,b)[41]. By this definition, similarly sized species are redundant (as species 13 and 14 in Fig. 3a,b), while differently sized species are complementary (as species 11 and 12 in Fig. 3a,b). Also, larger predators occupy a higher trophic position in the food web which forms distinct

trophic levels and induces cascading effects[46]. We believe that this model significantly reflects the major part of bioenergetic fluxes in ecosystems where body size is the dominant constraint on feeding rates and food web structure, such as marine and freshwater systems or terrestrial below-ground systems[38,39,41,44].

We applied the model to simulate population dynamics of 21,461 randomly sampled communities over a large gradient of animal species richness until a steady state was reached. We included 10–100 animal species of different body mass on top of 30 plant species to build plausible communities of variable vertical and horizontal diversity (Fig. 3c).

Ecosystem functions respond to animal diversity. We investigated how increasing animal diversity affects ecosystem functioning, defined as the summed biomass stocks of plant and animal species (P and A, respectively), the rates of consumption on the plant community (F_P) and within the animal community (that is, intraguild predation, F_A), as well as the energetic losses due to metabolism of both compartments (X_P and X_A; Fig. 1). We found that as the number of animal species increased, the total biomass of animals, A, increased as well (Fig. 4a; $a = 0.35$, and $\alpha = 1.2$ as least squares estimates of power-law relationship of the shape $A = aS_A^\alpha$ fitted as a linear model on log–log transformed data; Residual standard error on degrees of freedom: s.e. $= 0.012$; Goodness of fit as indicated by Coefficient of determination: $R^2 = 0.31$). In contrast, the total biomass of plants, P, stagnated (Fig. 4b; $a = 29.75$, and $\alpha = -0.08$, s.e. $= 0.005$, $R^2 = 0.01$). Along with the increase in animal biomasses, we observed an increase in intraguild predation rates, F_A (Fig. 4c, $a = 0.004$, and $\alpha = 0.92$, s.e. $= 0.012$, $R^2 = 0.2$). Despite the stable total biomass of plants, we found an increase in the consumption of plants by animals, F_P (Fig. 4d; $a = 0.1$ and $\alpha = 0.61$, s.e. $= 0.005$, $R^2 = 0.38$). Moreover, with increasing animal species richness the total animal metabolic rates, X_A, increased (Fig. 4e; $a = 0.05$ and $\alpha = 0.58$, s.e. $= 0.005$,
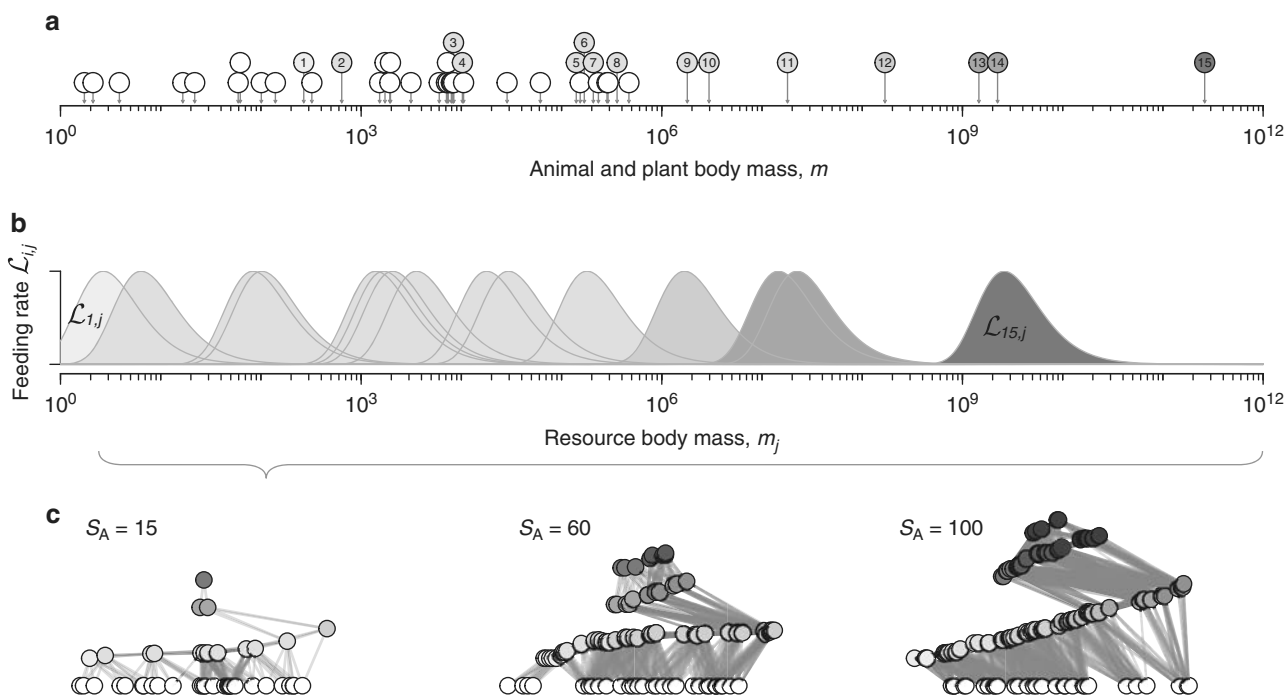
Figure 3 | Allometric constraints determine food-web structure. (**a**) Each simulated food web is initiated with S_A animal species (numbered grey circles) on 30 plant species (white circles) of randomly assigned body masses (here: $S_A = 15$). (**b**) The potential feeding efficiencies $\mathcal{L}_{i,j}$ (light curves and areas) of all consumers i over the size range m_j describe the functional niche coverage. (**c**) Static network representation of random food webs. A link is drawn if the consumer feeds on resource with $\mathcal{L}_{i,j} \geq 0.01$ (Methods section). Plant species are ordered by body mass, animal consumers are ordered by the average position of their direct resource species (x axis) and by their average trophic level (y axis).
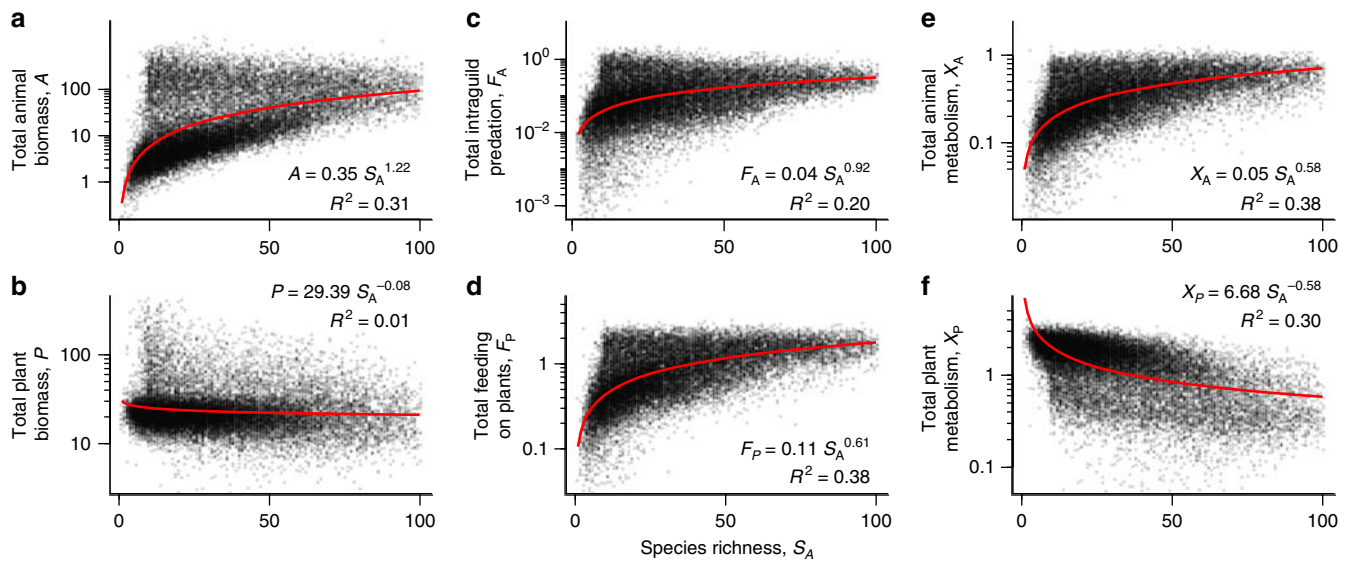
Figure 4 | Effect of species richness on ecosystem functions in dynamic communities. Shown are distributions of 21,461 randomly assembled food webs at equilibrium. Increasing species richness increased total animal biomass (**a**) but maintained biomass of the plant community at the same levels (**b**). Intraguild-consumption within the animal community was increased (**c**), as was the consumption on the plant species (**d**). Metabolic losses of animals increased (**e**), while losses of plant species decreased (**f**). Equations and red lines show fitted power-law models (Methods section). Coefficient of determination R^2 indicates goodness of fit.

$R^2 = 0.38$) while the total metabolic rates of plants, X_P, decreased (Fig. 4f; $a = 6.72$ and $\alpha = -0.54$, s.e. $= 0.006$, $R^2 = 0.3$).

Sensitivity to model parameters. For the patterns described above, we explored the sensitivity to parameter choice. The majority of the parameters were randomly drawn from normal distributions (allometric scaling parameters, hill-exponent of functional response, predator interference) and mostly had no visible effects on the relationship between animal diversity and ecosystem functions. Solely the allometric scaling exponent of consumer body mass in attack rates, β_i, had important leverage on the effect of species richness on plant biomass: low exponents resulted in positive effects and high exponents resulted in negative effects of animal species richness on plant biomass, but left other ecosystem functions unaffected (Supplementary Figs 1–6, Supplementary Methods). While higher plant species richness ($S_P = 50$) did not alter the observed patterns qualitatively, the total plant biomass in communities with lower plant species richness ($S_P = 10$) responded negatively to animal species richness along with a stronger reduction in plant respiration (Supplementary Fig. 7, Supplementary Methods). To assess the role of omnivore feeding as opposed to strict herbivory, we ran an alternative simulation where 50% of the animals were only consuming plants. This case of a more pronounced trophic structure strengthened the suppression of plant biomass with increasing diversity via increasing plant respiration (Supplementary Fig. 8, Supplementary Methods). Lower or higher rates of nutrient turnover did not influence the relationship qualitatively (Supplementary Fig. 9, Supplementary Methods), but had an effect on the quantity of biomasses, rates and losses, indicating that bottom–up control was left unimpaired by animal diversity. We conclude that the structural features of the model, rather than the precise parameter values, are responsible for the observed patterns.

Plasticity of community size structure. The dynamic reallocation of biomass within the animal and plant community towards larger species was responsible for the decoupling of feeding rates and plant biomass. This biomass shift translates into larger
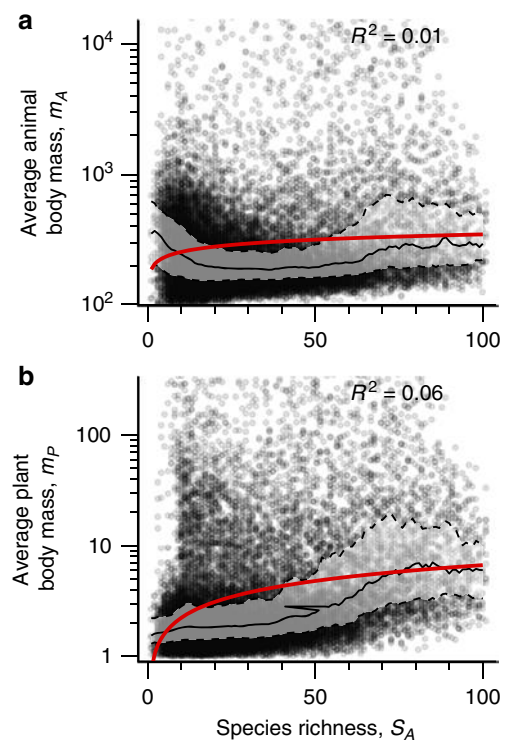

Figure 5 | Average individual body mass in response to animal species richness. Observed average individual body mass of (**a**) animals and (**b**) plants. Equations and red lines show fitted power-law models (Methods section); grey line shows median body mass (calculated as median of body mass at each $S_A \pm 2$ with 50%-inner quantile range). Coefficient of determination R^2 indicates goodness of fit. The y-axes were truncated to include 95% of simulated food webs.

average individual body masses of animals as species richness increased (Fig. 5a; $a = 187.91$, and $\alpha = 0.13$, s.e. $= 0.011$, $R^2 = 0.01$). On the basal trophic level, larger plants were favoured over smaller plants, and this effectively reduced total metabolic
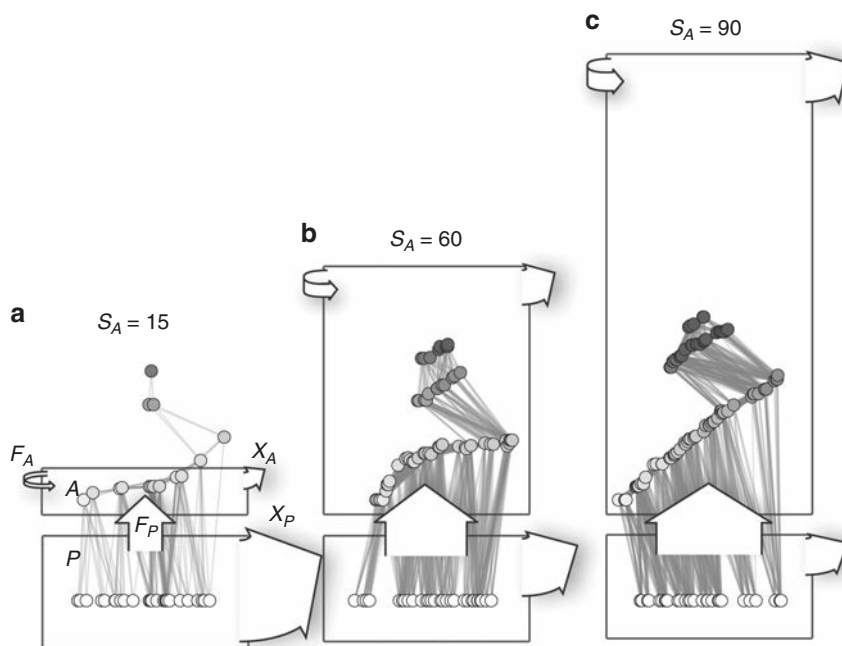
Figure 6 | Visualized changes of ecosystem functions at varying animal species richness. Communities visualized for (**a**) 15, (**b**) 60 and (**c**) 90 species (S_A). Arrow width at the base is proportional to biomass change per time; Area of boxes is proportional to biomass stocks. While animal biomass, A, increased along the gradient due to an increased turnover within the animal community (arrows F_P, F_A and X_A), biomass of plants, P, could be maintained at the same level owing of a slowing down of biomass turnover in the plant community (arrow X_P).

losses while allowing plant biomass to remain constant (Fig. 5b; $a = 0.75$ and $\alpha = 0.48$, s.e. $= 0.013$, $R^2 = 0.06$).

In summary, with increasing animal species richness and an accumulation of more biomass in the animal community (Fig. 6, compartment A) the total biomass of plants could nevertheless be maintained at the same level (Fig. 6, compartment P). The animals' consumption of plants (Fig. 6, rate F_P) increased, which enhanced the metabolic rate in the animal community (Fig. 6, compartment A, rates F_P and X_A). In the plant community, the increased loss of biomass to consumption was compensated by a reduction in community metabolism (X_P), which rendered the plant community more efficient in maintaining biomass.

Discussion

We applied a dynamic simulation approach to investigate the relationship between animal diversity and ecosystem functioning represented by standing stocks of biomasses and process rates at the community level. In our model simulation, increasing animal diversity led to an increase in biomass of the animal compartment of the ecosystem despite higher energetic losses of the animal community caused by higher rates of respiration and intraguild predation. Metabolic losses of animals increased proportionately to the gains via consumption on plants. The losses due to intraguild predation increased more strongly in relative terms, but at lower absolute values.

Our results corroborate the hypothesis that high animal diversity should lead to increased intraguild predation, with large species at the top of the food web accumulating more biomass, while small species are losing. However, the high level of intraguild feeding will not *per se* release plants from top–down control and increase plant biomass. Instead, a diverse animal community may be more exploitative without imposing stronger top–down control on plants. The reason for this lack of an effective top–down control is that the plant community also responds to the increased pressure by shifting the community

size structure towards larger species. These larger species compensate for higher losses due to herbivore consumption with their lower per unit biomass metabolic rates, which enables them to maintain their levels of biomass as animal diversity increases.

The allometric food web model applied in our study takes body mass as the only differentiating parameter for the particular set of feeding traits and physiological parameters of a species[32]. This simplification of ecological systems assumes that all animal species of equal body mass are equal, in contrast to neutral animal species models, which assume that all species are equal. At the cost of adding only one defining parameter, allometric models provide a much more realistic baseline for the investigation of systemic processes within food webs and may easily be extended to integrate phylogeny and other body-mass independent species traits[47] as well as the effects of temperature on individual metabolism[33,39,48]. Most importantly, the model drops the limiting distinction of vertical versus horizontal diversity[8,16]. The increase in total intraguild predation with increasing animal diversity is the consequence of the more complete niche coverage since allometry defines the resource range and feeding intensity of consumers on the body-mass axis relative to their own body mass, analogous to classical niche concepts[49]. For plant species and also for smaller and intermediately sized animals, this enhances the likelihood of top–down control by an animal consumer. Thus, allometric feeding rates produce niche complementarity[18,41], a concept that applies when varying horizontal diversity, that is, diversity within the trophic level[8]. Further, the allometric niche differentiation leads to intraguild predation and subsequent indirect effects[16], or trophic cascades within the food web. Thus, as species number increases the vertical diversity of the community increases[8], resulting in food webs with a 'taller' effective trophic height (Fig. 5). The model is consistent with the natural complexity of food webs that are rich in feeding interactions across and within trophic levels[44].

The model framework further assumes that communities respond dynamically to the quality and quantity of resource supply and consumption in the food web context. In this dynamic process, the biomasses of both animals and plants were allocated towards larger-sized species as animal species number increased. This systematic shift in community body mass structure had strong implications for the effective feeding interactions within the community. The advantage of large animals in species-rich communities led to a stronger limitation of smaller species' populations and enhanced the total direct feeding on plants. However, this increase in feeding was selective for smaller plant species, which resulted in large, slow-growing plant species dominating the community.

The spectrum of simulated communities that we observed at low species richness is relatively wide and heterogeneous, potentially allowing for multiple stable ecosystem states, depending on the feeding traits and food web context of the species present. In contrast, at high animal species richness this spectrum of possible ecosystem states narrows down and becomes more homogeneous with more complementary or redundant species (that is, insurance effects[50]) and a greater probability of including top-predator species of high trophic level (that is, sampling effects[16,51]). Thus, increasing diversity consolidates ecosystem function. The sensitivity analysis suggests that the scaling of attack rates with consumer body-mass may also be influential on the relationship between animal diversity and ecosystem function and encourages further exploration. Most importantly, it corroborates previous findings that species-rich communities will be less variable and more predictable in their functioning than communities with few species[52].

In summary, our food-web simulations indicate that increasing animal diversity, while fostering intraguild predation, does not necessarily release plant biomass from top–down control. Instead, more diverse animal communities favour larger-bodied animal and plant species which balances the effects on plant biomass. We therefore revisit a long-established hypothesis which assumes that increased amounts of intraguild feeding in diverse animal communities will relax the total pressure on plants. This traditional notion originated from static, structural concepts of food webs that neglected compensatory dynamics of complementary species and the resulting complexity of indirect effects. In contrast, the approach of this study offers a concept of body-size regulated community plasticity that reconciles the hypotheses regarding the relationship between animal diversity and plant biomass stock. The mechanisms that have been identified as major drivers of the biodiversity-ecosystem functioning relationship, such as niche complementarity or trophic complexity, are inherent to the allometric food-web model. The limiting assumptions of the model approach also represent important future directions of research that can be added to its flexible model framework to create tailored null hypotheses. Thus, our approach opens new possibilities for future studies of multi-trophic biodiversity and ecosystem functioning. We anticipate that such a mechanistic and dynamic concept of complex, multi-trophic communities is indispensable to overcome the unidirectional cause-consequence approach to biodiversity and ecosystem functioning and to truly understand the dynamic consequences of imminent species loss.

Methods

Food-web structure. The model food webs consisted of a basal plant compartment (P) and the consumer compartment ('animals', A; Fig. 1). We varied the initial animal species number, S_A, from 10 to 100 species with 300 replicates each. The plant community has been standardized to $S_P = 30$ species. The $\log_{10}$ body mass m_i of any species i was drawn from independent uniform distributions within the inclusive

limits $\mu_P = (10^0, 10^6)$ for plant species and $\mu_A = (10^2, 10^{12})$ for animals, constraining the smallest possible body mass of a plant species to 1 and the largest possible body mass of an animal species to 10^{12}. Trophic relations are defined by the success curve of consumers, that is, the probability of a consumer i to actually attack and capture an encountered resource j (which can be a plant or an animal),

$$\mathcal{L}_{i,j} = \left(\frac{m_i}{m_j R_{opt}} e^{1 - \frac{m_i}{m_j R_{opt}}} \right)^{\gamma}. \tag{1}$$

It is defined as an asymmetrical hump-shaped curve (Ricker function)[53] with width $\gamma = 2$, centred around an optimal consumer-resource body-mass ratio $R_{opt} = 100$ (Fig. 2)[37]. This success curve is subsequently termed the 'feeding efficiency'. Very weak links with $\mathcal{L}_{i,j} \leq 0.01$ were removed from the model networks, yielding food webs as depicted in Fig. 3c. Note, that in this model we use body mass as the only determinant of a generalist resource choice for both carnivorous and herbivorous feeding. We acknowledge that this simplifying assumption might not reflect the diversity of natural feeding relationships. Especially in terrestrial above-ground food webs, other species traits can be more relevant in determining a feeding link, for example, specialized insect herbivores feeding on large plants may be limited by plant defense or traits rather than size. However, universal body mass constraints on feeding are found in many aquatic and belowground terrestrial habitats[44]. Implementing additional, size-independent constraints on feeding and higher degrees of specialization might be an avenue for future investigations.

Feeding rates. The allometric model for the rate at which consumer i feeds on a resource j applies a multi-prey Holling-type functional response with variable Hill-exponent[54], and includes intra-specific consumer interference (Beddington–DeAngelis type)[32,55,56]. The feeding rate,

$$F_{ij} = \frac{\omega_i b_{ij} R_j^{1+q}}{1 + c A_i + \omega_i h_i \sum_k b_{ik} R_k^{1+q}} \cdot \frac{1}{m_i}, \tag{2}$$

of one unit of biomass of the consumer, i, (transformed from per capita feeding rates by dividing by individual body mass, m_i) is a function of the biomass density of the consumer, A_i, and biomass density of the resource, R_j, which can be an animal or a plant species (thus substitute A_j or P_j). It includes the resource specific capture coefficient,

$$b_{ij} = b_0 m_i^{\beta_i} m_j^{\beta_j} \mathcal{L}_{i,j}, \tag{3}$$

of a consumer species i on a resource species j, which scales the feeding efficiency $\mathcal{L}_{i,j}$ by a power function of consumer and resource body mass, assuming that the rate of encounters between consumer and resource scales with their respective movement speed. Thus, b_{ij} increases according to a power law with the body masses of consumer (m_i) and animal resource (m_j)[35]. For each food web replicate, the exponents β_i and β_j were sampled from normal distributions with mean $\mu_{\beta_i} = 0.47$, and s.d. $\sigma_{\beta_i} = 0.04$, and $\mu_{\beta_j} = 0.15$ and $\sigma_{\beta_j} = 0.03$, respectively[39]. Since plants do not move, we assumed a constant $m_j^{\beta_j} = 20$ for plant resources. We further assumed a constant $b_0 = 50$ for all capture coefficients. The relative consumption rate ω_i accounts for the fact that a consumer has to split its consumption if it has more than one resource species. It thus is defined as $\omega_i = 1/$(number of resource species of i). Further, the feeding rate includes the time lost due to consumer interference c, the proportion of time that a consumer spends encountering con-specifics[55], which is independent of body mass[15]. For each food-web replicate, c was drawn from a normal distribution ($\mu_c = 0.8$, $\sigma_c = 0.2$). The density-dependent change in search efficiency is implemented via the Hill-exponent $1 + q$, which reduces the feeding rate for low resource densities and varies the functional response between classic type II ($q = 0$) and type III ($q = 1$)[54,55]. The value of q was drawn for each replicate from a normal distribution ($\mu_q = 0.5$, $\sigma_q = 0.2$) within the inclusive limits of 0 and 1 (invalid draws were repeated), reflecting that different ecosystems provide specific levels of habitat heterogeneity that reduce feeding at low resource density, for instance by providing refuges[55]. Finally, the handling time,

$$h_i = h_0 m_i^{\eta_i} m_j^{\eta_j}, \tag{4}$$

depends on the body mass of the consumer to the power of η_i ($\mu_{\eta_i} = -0.48$, $\sigma_{\eta_i} = 0.03$) and the body mass of the resource to the power of η_j ($\mu_{\eta_j} = -0.66$, $\sigma_{\eta_j} = 0.02$), with the scaling constant $h_0 = 0.4$ (refs 31,39). All exponents were sampled within the exclusive limits of $\pm 3\sigma$. Invalid draws were repeated.

Population dynamics. The model food webs were energetically based on a dynamic nutrient model with two nutrients of different importance supplying the plant community[57,58]. On top, a variable number of consumers were feeding on the plant species and among each other as defined by the food-web structure.

The rate of change of the biomass density of an animal species j is defined as

$$\frac{dA_i}{dt} = e_P A_i \sum_j F_{ij} + e_A A_i \sum_k F_{ik} - \sum_k A_k F_{ki} - x_i A_i. \tag{5}$$

The first-term describes the summed gain by consumption of plant species j times

the conversion efficiency $e_P = 0.45$ typical for herbivory that determines the proportion of biomass of eaten resource that can be converted into own biomass[31]. The second term is identical, but refers to the summed gain by consumption of other animal species k times a conversion efficiency $e_A = 0.85$ for carnivorous consumption[31]. The third-term sums the mortality due to predation by other animal species k. The metabolic demands per unit biomass for animals are defined to scale allometrically with $x_i = x_A m_i^{-0.25}$ (that is, corresponding to a 34 power-law scaling of per capita metabolic rates)[31,58], using the scaling constant[31] $x_A = 0.314$.

Similarly, the rate of change of the biomass density of any plant species i is defined as

$$\frac{dP_i}{dt} = r_i G_i P_i - \sum_k A_k F_{ki} - x_i P_i. \qquad (6)$$

The first-term describes growth due to the uptake of nutrients (see below). The second-term describes mortality due to predation by animals, summed over all consumers k of plant species i. Finally, each plant species has metabolic demands, $x_i = x_P m_i^{-0.25}$, which scale allometrically with its body mass m_i, using $x_P = 0.138$ as a constant[31,58].

The growth of a plant species is limited by its intrinsic growth rate[59] $r_i = m_i^{-0.25}$ and by the species specific growth factor G_i which is determined dynamically by the concentration of the nutrient $l \in \{1, 2\}$ that is most limiting to i:

$$G_i = min\left(\frac{N_1}{K_{i1} + N_1}, \frac{N_2}{K_{i2} + N_2}\right). \qquad (7)$$

For high nutrient concentrations, the term in the minimum operator approaches 1. The half-saturation densities K_{il} determine the nutrient uptake efficiency and are assigned randomly for each plant species i and each nutrient l (uniform distribution within the inclusive limits of 0.1 and 0.2). This model makes plants compete for resources, which is an essential feature of dynamic ecosystem functions, and generates niche differentiation of the plant species[60], which reduces the risk of competitive exclusion[57,58]. The dynamic change of nutrient concentration N_l is defined by

$$\frac{dN_l}{dt} = D(S_l - N_l) - v_l \sum_i r_i G_i P_i, \qquad (8)$$

with a global turnover rate $D = 0.25$ that determines the rate by which nutrients are refreshed[58]. The supply concentration S_l determines the maximal nutrient level drawn at random from a normal distribution ($\mu_S = 10$, $\sigma_S = 2$) and is constrained to be larger than 0. The nutrient stock is diminished by the summed uptake by all plants i. The loss of a specific nutrient l is limited by its relative content in the plant species' biomass ($v_1 = 1$, $v_2 = 0.5$).

The population dynamics were calculated by integrating the system of differential equations implemented in C using procedures of the SUNDIALS-CVODE solver (backward differentiation formula; absolute and relative error tolerances of 10^{-10})[61,62]. Nutrient concentrations N_l were initialized with random values uniformly distributed between $S_l/2$ and S_l, animal and plant biomass densities were initialized with random values uniformly distributed between 0 (exclusive) and 10 (inclusive). The food webs were simulated until $t = 150,000$ to ensure that stationary dynamics were reached. Species were assumed to be permanently extinct from the food-web once their biomass fell below a threshold, that is, if A_i or $P_i \leq 10^{-6}$ it was immediately set to 0. Replicates that included consumer-free basal species at the end of the simulation time were discarded from the data set ($n = 5,839$, corresponding to 21% of the simulations initialized). The uncontrolled growth of such inedible basal species would outcompete other plants and reduce overall species richness drastically, leading to a fundamentally different type of ecosystem[28]. In total, 21,461 valid food webs were simulated.

Output parameters. The total biomass stocks of the animals, A, and the plants, P, were calculated as the average of the summed biomasses of all species over an evaluation period of 10,000 time steps after the population dynamics had reached a stationary state. Rates of biomass flow from plants to animals, F_P (herbivory), and among animals (carnivory or intraguild predation), F_A, were calculated as average biomass transfer per time step over the same evaluation period. Note, that these flows represent the rate of biomass production by plants and animals, respectively, since we calculated them before accounting for losses due to incomplete assimilation. Total metabolic rates of animals, X_A, and plants, X_P, were calculated as the sum of the metabolic rates multiplied with the average biomass densities of animal and plant species, respectively.

Statistical models. The basal and consumer stocks, rates and losses were statistically described as power laws of S_A of the form $response = a \cdot S_A^z$. A log–log-transformation yielded the linear model structure of the form $log(x) = log(a) + \alpha \, log(S_A)$ which was fitted using least squares (using the function lm() in R v3.2.2 (ref. 63)). We report the coefficient of determination, R^2, as a goodness of fit metric for the linear model. For the linear model predicting intraguild predation, replicates with value zero were omitted ($n = 28$; 0.1% of all replicates).

Data availability. All relevant computer codes and simulation results are available online[64] including the original simulation source code (written in C) as well as the code for the statistical analysis and figure generation (written in R); Code repository on GitHub: https://github.com/fdschneider/schneider_et_al_2016_animaldiversity.

References

1. Hooper, D. U. et al. Effects of biodiversity on ecosystem functioning: a consensus of current knowledge. Ecol. Monogr. **75**, 3–35 (2005).
2. Naeem, S., Loreau, M. & Inchausti, P. in Biodiversity and Ecosystem Functioning: Synthesis and Perspectives (eds Loreau, M., Naeem, S. & Inchausti, P.) (Oxford University Press, 2002).
3. Loreau, M. From Populations to Ecosystems: Theoretical Foundations for a New Ecological Synthesis (Princeton University Press, 2010).
4. Tilman, D. & Downing, J. A. Biodiversity and stability in grasslands. Nature **367**, 363–365 (1994).
5. Naeem, S., Thompson, L. J., Lawler, S. P., Lawton, J. H. & Woodfin, R. M. Declining biodiversity can alter the performance of ecosystems. Nature **368**, 734–737 (1994).
6. Sih, A., Englund, G. & Wooster, D. Emergent impacts of multiple predators on prey. Trends Ecol. Evol. **13**, 350–355 (1998).
7. Duffy, J. E. Biodiversity and ecosystem function: The consumer connection. Oikos **99**, 201–219 (2002).
8. Duffy, J. E. et al. The functional role of biodiversity in ecosystems: Incorporating trophic complexity. Ecol. Lett. **10**, 522–538 (2007).
9. Cardillo, M. et al. Multiple causes of high extinction risk in large mammal species. Science **309**, 1239–1241 (2005).
10. Halaj, J. & Wise, D. H. Terrestrial trophic cascades: How much do they trickle? Am. Nat. **157**, 262–281 (2001).
11. Mittelbach, G. G. et al. What is the observed relationship between species richness and productivity? Ecology **82**, 2381–2396 (2001).
12. Shurin, J. B. et al. A cross-ecosystem comparison of the strength of trophic cascades. Ecol. Lett. **5**, 785–791 (2002).
13. Letourneau, D. K., Jedlicka, J. A., Bothwell, S. G. & Moreno, C. R. Effects of natural enemy biodiversity on the suppression of arthropod herbivores in terrestrial ecosystems. Annu. Rev. Ecol. Evol. Syst. **40**, 573–592 (2009).
14. Reiss, J., Bridle, J. R., Montoya, J. M. & Woodward, G. Emerging horizons in biodiversity and ecosystem functioning research. Trends Ecol. Evol. **24**, 505–514 (2009).
15. DeLong, J. P., Hanley, T. C. & Vasseur, D. A. Predatorprey dynamics and the plasticity of predator body size. Funct. Ecol. **28**, 487–493 (2014).
16. Ives, A. R., Cardinale, B. J. & Snyder, W. E. A synthesis of subdisciplines: Predator-prey interactions, and biodiversity and ecosystem functioning. Ecol. Lett. **8**, 102–116 (2005).
17. Finke, D. L. & Snyder, W. E. Niche partitioning increases resource exploitation by diverse communities. Science **321**, 1488–1490 (2008).
18. Cardinale, B. J. et al. in Biodiversity, Ecosystem Functioning, & Human Wellbeing An Ecological and Economic Perspective 105–120 (Oxford University Press, 2009).
19. Strong, D. R. Are trophic cascades all wet? differentiation and donor-control in speciose ecosystems. Ecology **73**, 747–754 (1992).
20. Pace, M. L., Cole, J. J., Carpenter, S. R. & Kitchell, J. F. Trophic cascades revealed in diverse ecosystems. Trends Ecol. Evol. **14**, 483–488 (1999).
21. Finke, D. L. & Denno, R. F. Predator diversity dampens trophic cascades. Nature **429**, 407–410 (2004).
22. Finke, D. L. & Denno, R. F. Predator diversity and the functioning of ecosystems: the role of intraguild predation in dampening trophic cascades. Ecol. Lett. **8**, 1299–1306 (2005).
23. Digel, C., Riede, J. O. & Brose, U. Body sizes, cumulative and allometric degree distributions across natural food webs. Oikos **120**, 503–509 (2011).
24. Riede, J. O. et al. Scaling of food-web properties with diversity and complexity across ecosystems. Ecol. Netw. **42**, 139–170 (2010).
25. Polis, G. A. & Strong, D. R. Food web complexity and community dynamics. Am. Nat. **147**, 813–846 (1996).
26. Krivan, V. & Schmitz, O. J. Adaptive foraging and flexible food web topology. Evol. Ecol. Res. **5**, 623–652 (2003).
27. Thébault, E. & Loreau, M. Food-web constraints on biodiversityecosystem functioning relationships. Proc. Natl Acad. Sci. USA **100**, 14949–14954 (2003).
28. Thébault, E. & Loreau, M. The relationship between biodiversity and ecosystem functioning in food webs. Ecol. Res. **21**, 17–25 (2006).
29. Bauer, B., Vos, M., Klauschies, T. & Gaedke, U. Diversity, functional similarity, and top-down control drive synchronization and the reliability of ecosystem function. Am. Nat. **183**, 394–409 (2014).
30. Ives, A. R. & Cardinale, B. J. Food-web interactions govern the resistance of communities after non-random extinctions. Nature **429**, 174–177 (2004).
31. Yodzis, P. & Innes, S. Body size and consumer-resource dynamics. Am. Nat. **139**, 1151–1175 (1992).
32. Schneider, F. D., Scheu, S. & Brose, U. Body mass constraints on feeding rates determine the consequences of predator loss. Ecol. Lett. **15**, 436–443 (2012).

185

33. Fussmann, K. E., Schwarzmüller, F., Brose, U., Jousset, A. & Rall, B. C. Ecological stability in response to warming. *Nat. Clim. Change* **4**, 206–210 (2014).

34. Heckmann, L., Drossel, B., Brose, U. & Guill, C. Interactive effects of body-size structure and adaptive foraging on food-web stability. *Ecol. Lett.* **15**, 243–250 (2012).

35. Peters, R. H. *The ecological implications of body size* (Cambridge University Press, 1983).

36. Vucic-Pestic, O., Rall, B. C., Kalinkat, G. & Brose, U. Allometric functional response model: Body masses constrain interaction strengths. *J. Anim. Ecol.* **79**, 249–256 (2010).

37. Brose, U. *et al.* Foraging theory predicts predator-prey energy fluxes. *J. Anim. Ecol.* **77**, 1072–1078 (2008).

38. Kalinkat, G. *et al.* Body masses, functional responses and predator-prey stability. *Ecol. Lett.* **16**, 1126–1134 (2013).

39. Rall, B. C. *et al.* Universal temperature and body-mass scaling of feeding rates. *Philos. Trans. R. Soc. Lond. B Biol. Sci.* **367**, 2923–2934 (2012).

40. Pawar, S., Dell, A. I. & Savage, V.M. Dimensionality of consumer search space drives trophic interaction strengths. *Nature* **486**, 485–489 (2012).

41. Petchey, O. L., Beckerman, A. P., Riede, J. O. & Warren, P. H. Size, foraging, and food web structure. *Proc. Natl Acad. Sci. USA* **105**, 4191–4196 (2008).

42. Stouffer, D. B., Rezende, E. L. & Amaral, L. A. N. The role of body mass in diet contiguity and food-web structure. *J. Anim. Ecol.* **80**, 632–639 (2011).

43. Otto, S. B., Rall, B. C. & Brose, U. Allometric degree distributions facilitate food-web stability. *Nature* **450**, 1226–1229 (2007).

44. Riede, J. O. *et al.* Stepping in Elton's footprints: a general scaling model for body masses and trophic levels across ecosystems. *Ecol. Lett.* **14**, 169–178 (2011).

45. Woodward, G. *et al.* Body size in ecological networks. *Trends Ecol. Evol.* **20**, 402–409 (2005).

46. DeLong, J. P. *et al.* The body size dependence of trophic cascades. *Am. Nat.* **185**, 354–366 (2015).

47. Eklöf, A., Helmus, M. R., Moore, M. & Allesina, S. Relevance of evolutionary history for food web structure. *Proc. R. Soc. B Biol. Sci.* **279**, 1588–1596 (2011).

48. Binzer, A., Guill, C., Brose, U. & Rall, B. C. The dynamics of food chains under climate change and nutrient enrichment. *Philos. Trans. R. Soc. Lond. B Biol. Sci.* **367**, 2935–2944 (2012).

49. Williams, R. J. & Martinez, N. D. Simple rules yield complex food webs. *Nature* **404**, 180–183 (2000).

50. Yachi, S. & Loreau, M. Biodiversity and ecosystem productivity in a fluctuating environment: The insurance hypothesis. *Proc. Natl Acad. Sci. USA* **96**, 1463–1468 (1999).

51. Loreau, M. *et al.* Biodiversity and ecosystem functioning: current knowledge and future challenges. *Science* **294**, 804–808 (2001).

52. Berlow, E. L. *et al.* Simple prediction of interaction strengths in complex food webs. *Proc. Natl Acad. Sci. USA* **106**, 187–191 (2009).

53. Persson, L. *et al.* Ontogenetic scaling of foraging rates and the dynamics of a size-structured consumer-resource model. *Theor. Popul. Biol.* **54**, 270–293 (1998).

54. Real, L. A. The kinetics of functional response. *Am. Nat.* **111**, 289–300 (1977).

55. Skalski, G. T. & Gilliam, J. F. Functional responses with predator interference: viable alternatives to the Holling type II model. *Ecology* **82**, 3083–3092 (2001).

56. Brose, U., Williams, R. J. & Martinez, N. D. Allometric scaling enhances stability in complex food webs. *Ecol. Lett.* **9**, 1228–1236 (2006).

57. Huisman, J. & Weissing, F. J. Biodiversity of plankton by species oscillations and chaos. *Nature* **402**, 407–410 (1999).

58. Brose, U. Complex food webs prevent competitive exclusion among producer species. *Proc. R. Soc. B Biol. Sci.* **275**, 2507–2514 (2008).

59. Brown, J. H., Gillooly, J. F., Allen, A. P., Savage, V. M. & West, G. B. Toward a metabolic theory of ecology. *Ecology* **85**, 1771–1789 (2004).

60. Tilman, D. *Resource Competition and Community Structure* (Princeton University Press, 1982).

61. Hindmarsh, A. C. *et al.* SUNDIALS: suite of nonlinear and differential/algebraic equation solvers. *ACM Trans. Math. Softw.* **31**, 363–396 (2005).

62. Hindmarsh, A. C. & Serban, R. User Documentation for cvode v2.8.2 (sundials v2.6.2). Center for Applied Scientific Computing Lawrence Livermore National Laboratory UCRL-SM-208108 (2015) https://www.R-project.org/.

63. R Core Team. *R: A Language and Environment for Statistical Computing* (R Foundation for Statistical Computing, Vienna, Austria, 2015).

64. Schneider, F. & Guill, C. Animaldiversity: source code for article Schneider *et al. Nat. Commun.* doi:10.5281/zenodo.58183 (2016).

Acknowledgements

Author contributions

F.D.S., U.B., B.C.R. and C.G. designed the simulation experiment; C.G. and F.D.S. developed the simulation code; F.D.S., U.B., B.C.R. and C.G. wrote the paper.

Additional information

ORIGINAL PAPER

CrossMark

Accounting for activity respiration results in realistic trophic transfer efficiencies in allometric trophic network (ATN) models

Nadja J. Kath[1] · Alice Boit[1] · Christian Guill[1] · Ursula Gaedke[1]

Abstract

Allometric trophic network (ATN) models offer high flexibility and scalability while minimizing the number of parameters and have been successfully applied to investigate complex food web dynamics and their influence on food web diversity and stability. However, the realism of ATN model energetics has never been assessed in detail, despite their critical influence on dynamic biomass and production patterns. Here, we compare the energetics of the currently established original ATN model, considering only biomass-dependent basal respiration, to an extended ATN model version, considering both basal and assimilation-dependent activity respiration. The latter is crucial in particular for unicellular and invertebrate organisms which dominate the metabolism of pelagic and soil food webs. Based on metabolic scaling laws, we show that the extended ATN version reflects the energy transfer through a chain of four trophic levels of unicellular and invertebrate organisms more realistically than the original ATN version. Depending on the strength of top-down control, the original ATN model yields trophic transfer efficiencies up to 71% at either the third or the fourth trophic level, which considerably exceeds any realistic values. In contrast, the extended ATN version yields realistic trophic transfer efficiencies ≤ 30% at all trophic levels, in accordance with both physiological considerations and empirical evidence from pelagic systems. Our results imply that accounting for activity respiration is essential for consistently implementing the metabolic theory of ecology in ATN models and for improving their quantitative predictions, which makes them more powerful tools for investigating the dynamics of complex natural communities.

Introduction

The metabolic theory of ecology relates biological rates to body size and serves to predict metabolic activity from the individual to the community level (Brown et al. 2004). Allometrically scaled trophic network (ATN) models implement this theory in a food web context by linking consumers to their resources in food webs. Yodzis and Innes (1992) parameterized the first ATN model which is the theoretical basis

of a fruitful series of ATN modeling studies for ecological theory building, e.g., contributing to the diversity-stability debate (Benoît and Rochet 2004; Brose et al. 2006; Heckmann et al. 2012), coexistence theory (Brose 2008), hypotheses on biodiversity-ecosystem functioning (Schneider et al. 2016), and for investigating biodiversity loss (Berlow et al. 2009; Schneider et al. 2012). The main advantage of ATN models is their scalability from small modules to large and complex food webs in a widely applicable approach with only few assumptions.

The ATN approach builds upon the fact that material ingested by a consumer is either excreted or allocated to respiration or production (Fig. 1). The assimilation efficiency differs for carnivores and herbivores because of the respective food's quality and stoichiometry. Regarding losses to respiration, all previous studies with ATN models except for Boit et al. (2012) and Kuparinen et al. (2016) considered

✉ Nadja J. Kath
nkath@uni-potsdam.de

1 Institut für Biochemie und Biologie, Universität Potsdam,
Maulbeerallee 2, 14469 Potsdam, Germany

② Springer

Fig. 1 The carbon (surrogate for energy) flow scheme implemented in the ATN model approach. The original version by Yodzis and Innes (1992) does not separate activity from basal respiration, but assumes that all respiration is proportional to biomass. The missing part of activity respiration proportional to assimilation (box) is added to the original ATN model in this study. Model parameters are e assimilation efficiency, f_a factor accounting for activity respiration, f_m factor accounting for basal respiration, x metabolic rate, B biomass, and I ingestion (for details see Table 1 and "Methods")
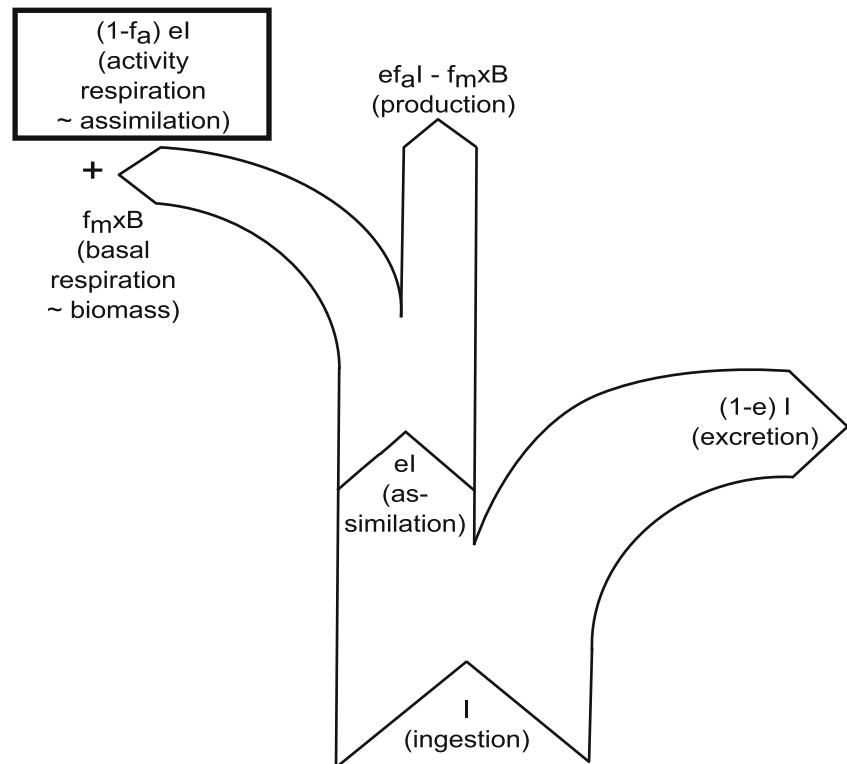
only respiration proportional to biomass, here called basal respiration, whereas respiratory losses due to activity, hereafter called activity respiration, were not specifically accounted for. This approximation may apply to homoiothermic mammals and birds with high maintenance costs. However, it appears less suitable for modeling pelagic and soil food webs, which mostly consist of unicellular and invertebrate organisms with low basal respiration, but high activity respiration, which is proportional to food uptake (Anderson 1992). The study by Boit et al. (2012) on the seasonal plankton succession in Lake Constance already indicated that the ATN model successfully reproduced general community patterns only if the important physiological process of activity respiration was accounted for. In contrast, the original ATN model considerably overestimated heterotrophic production if activity respiration was ignored (Boit et al. 2012). Kuparinen et al. (2016) used the ATN model as extended by Boit et al. (2012) to successfully model the effects of fishing on a food web and the fish life-history traits. These two studies called for the in-depth evaluation of ATN model energetics which we present in this work. To differentiate between the two model versions, we employ the terms "original" (Yodzis and Innes 1992) and "extended" ATN model (Boit et al. 2012).

To quantify and evaluate model energetics, we determine the trophic transfer efficiency (TTE) between four ascending trophic levels (autotrophs, herbivores, carnivores, and top predators) for both the original and the extended ATN

versions. We find that only by accounting for activity respiration, the ATN model achieves realistic TTE towards the higher trophic levels. To explain this model behavior, we additionally compared biomasses, respiration, and production of both model versions for different levels of top predator mortality. The latter elucidates the influence of top-down vs. bottom-up control on the TTE and the formation of trophic cascades. We discuss our findings in the context of previous modeling studies and observations from pelagic systems to promote the inclusion of activity respiration in future ATN models. Achieving more realistic energetics and improving quantitative predictions will make ATN models more powerful tools to investigate complex natural food webs in order to better serve their purpose in ecological theory building.

Methods

Allometric trophic network (ATN) models represent consumer-resource relationships based on allometric scaling of key physiological rates (e.g., ingestion) with individual body mass, which achieves minimum data necessity for model parameterization (Yodzis and Innes 1992). Ingested carbon serves as surrogate for energy and is allocated to either excretion, respiration, or production (Fig. 1, Begon et al. 2006). The original ATN model formulation does not differentiate between basal respiration proportional to the biomass, and

activity respiration proportional to the amount of assimilated food (Fig. 1).

General ATN model equations and parameters

We applied the ATN model equations to a linear chain of four trophic levels from autotrophs (A) and herbivores (H) to carnivores (C) and top predators (T). In order to facilitate comparability between studies, our notation and parameterization closely follow that of previous ATN modeling studies (Brose et al. 2006; Boit et al. 2012). Growth of the autotrophs is modeled by a logistic function (Eq. 1), and consumption by all consumers is described by a Holling type II functional response (Eqs. 1–4, Holling 1959). Together, the rates of change of the biomasses B_i (i = A, H, C, T) at the four trophic levels are given by the following ordinary differential equations:

$$\frac{dB_A}{dt} = rB_A\left(1-\frac{B_A}{K}\right) - yx_H\frac{B_A}{B_0+B_A}B_H \tag{1}$$

$$\frac{dB_H}{dt} = f_a e_h yx_H\frac{B_A}{B_0+B_A}B_H - yx_C\frac{B_H}{B_0+B_H}B_C - f_m x_H B_H \tag{2}$$

$$\frac{dB_C}{dt} = f_a e_c yx_C\frac{B_H}{B_0+B_H}B_C - yx_T\frac{B_C}{B_0+B_C}B_T - f_m x_C B_C \tag{3}$$

$$\frac{dB_T}{dt} = f_a e_c yx_T\frac{B_C}{B_0+B_C}B_T - f_m x_T B_T - dB_T^2. \tag{4}$$

The maximum growth rate of the autotrophs is described by r and their carrying capacity by K. The functional responses for consumption are expressed by the metabolic rate of the respective consumer, x_H, x_C, x_T, the maximum ingestion rate y normalized by the respective metabolic rate, and the half-saturation constant B_0. The assimilation efficiency for

herbivores is denoted as e_h, the one for carnivorous predators as e_c, the fraction of assimilated carbon not respired is defined by f_a, i.e., (1-f_a) is the fraction of carbon lost by activity respiration, and the fraction of maintenance respiration linked to biomass is f_m. The metabolic rates x_i scale allometrically with body mass m_i with an allometric exponent of -0.25 (Yodzis and Innes 1992). The autotrophs' body mass is set to 1 and the consumer-resource body-mass ratio is 1000 for all trophic levels. The standard values of all parameters are given in Table 1. The death rate constant of the top predator is given by d (Eq. 4, Table 1), and it was varied between 0 and 0.05 in steps of 0.0001. The term dB_T represents the top predator's per capita death rate. The case $d = 0$ represents an extreme case as it leads to a massive accumulation of top predator biomass which in nature would attract pathogens, parasites, or another carnivore, which all induce mortality.

Calculation of central rates

All central rates, i.e., ingestion, excretion, basal and activity respiration, and production have the same dimension mass × volume^{-1} × time^{-1}. The total ingestion rate I_i of the consumer species on trophic level i with biomass B_i is given by

$$I_i = yx_i\frac{B_{i-1}}{B_0+B_{i-1}}B_i. \tag{5}$$

Multiplied with the assimilation constant e_i and the activity respiration factor f_a, the term I_i constitutes the first term in Eqs. 2–4. The total excretion rate E_i of trophic level i is proportional to its ingestion rate and is given by

$$E_i = (1-e_i)I_i = (1-e_i)yx_i\frac{B_{i-1}}{B_0+B_{i-1}}B_i. \tag{6}$$

The assimilation efficiency e_i describes the fraction of the ingested material that is assimilated and not lost by excretion. It is higher for carnivores than for herbivores

Table 1 Parameter values. If the original and extended ATN versions are differently parameterized, their values are labeled with $^{orig.}$ and $^{ext.}$, respectively. Dimensionless units are labeled as [−]

Parameter name	Abbreviation	Value [dimension]	Literature
Mass-specific maximum growth rate of the autotrophs	r	1 [$\frac{1}{\text{time}}$]	(Brose et al. 2006)
Carrying capacity	K	1 [$\frac{\text{mass}}{\text{volume}}$]	(Brose et al. 2006)
Metabolic rate	x_i	0.314 mass$_i^{-0.25}$ [$\frac{1}{\text{time}}$]	(Brose et al. 2006)
Maximum ingestion rate relative to metabolic rate	y	8 [−]	(Brose et al. 2006)
Half-saturation constant	B_0	0.5 [$\frac{\text{mass}}{\text{volume}}$]	(Brose et al. 2006)
Fraction of assimilated carbon used for production	f_a	1^{orig} /0.4^{ext} [−]	(Boit et al. 2012)
Factor for maintenance respiration	f_m	1^{orig} /0.1^{ext} [−]	Boit et al. 2012)
Assimilation efficiency for herbivorous species	e_h	0.45 [−]	(Yodzis and Innes 1992)
Assimilation efficiency for carnivorous species	e_c	0.85 [−]	(Yodzis and Innes 1992)
Death rate constant of top predator	d	[0, 0.05] [$\frac{\text{volume}}{\text{time mass}}$]	Varied in this study

(Table 1) since the former consume high-quality food of similar biochemical composition as themselves, whereas plants often contain nutrient-poor material which is hard to digest.

Basal respiration is the energy lost due to maintenance processes. It is analog to the basal metabolic rate defined for homoiotherms (Gessaman 1973) as measured in the thermoneutral zone where homoiotherms have very low costs for thermoregulation and are most similar to ectotherms in this regard. Basal respiration $R_{b,i}$ is defined as

$$R_{b,i} = f_m x_i B_i \tag{7}$$

and is therefore proportional to the standing stock biomass. Activity respiration is the energy spent for processes related to the production of new biomass (including locomotion, foraging, food handling and digestion, ontogenetic processes, and reproduction). We call f_a the fraction of energy not lost due to activity processes. Following Boit et al. (2012), the activity respiration $R_{a,i}$ is calculated as

$$R_{a,i} = (1-f_a)\, e_i\, I_i = (1-f_a) e_i y x_i \frac{B_{i-1}}{B_0 + B_{i-1}} B_i. \tag{8}$$

This part is neglected in the original ATN model, i.e. $f_a = 1$.

The production summarizes all processes that lead to creation of new biomass (somatic and reproductive growth). On average, the production at trophic level i compensates for losses by predation, i.e., the ingestion by trophic level $i + 1$. If we neglect non-grazing mortality, which typically plays a minor role in pelagic systems (Gaedke et al. 2002), the production P_i can either be calculated as ingestion of the next higher trophic level I_{i+1} or as ingestion at trophic level i minus excretion E_i and total respiration $R_i = R_{a,i} + R_{b,i}$,

$$P_i = I_{i+1} = I_i - E_i - R_{a,i} - R_{b,i}. \tag{9}$$

For the top predator, the ingestion by a higher trophic level is replaced by its death rate dB_T^2 (Eq. 4). These different ways to calculate the production (Eq. 9) enable us to infer the trophic transfer efficiencies.

Trophic transfer efficiency

The trophic transfer efficiency (TTE) is defined as the ratio of the production of two adjacent trophic levels and is therefore dimensionless. It is used to quantify the fraction of energy passed on to the next trophic level. To calculate the maximum TTE, it is crucial to remember that ingested carbon can only be excreted, respired, or invested into new production (Fig. 1). When one of the first two rates increases, the production decreases. Following Yodzis and Innes (1992), carnivores are assumed to have an assimilation efficiency of 85% and

herbivores of 45% (Table 1). From physiological considerations based on a comprehensive data set across different taxonomic groups (Humphreys 1979; Hendriks 1999), it can be estimated that at most half of the assimilated carbon can be allocated to production (Fig. 1), which yields an upper limit to the maximum feasible TTE_i between trophic level i and $i + 1$:

$$\text{Maximum feasible } TTE_{i \to i+1} \le 0.5 \frac{e_{i+1} I_{i+1}}{P_i}. \tag{10}$$

This results in a maximum feasible TTE of at most 42.5% of the ingested carbon for carnivores and of 22.5% for herbivores (cf. Table 2). Note that this is a very conservative estimation. Most taxa have considerably higher respiratory losses and thus lower production to assimilation ratios, resulting in a lower maximum feasible TTE.

One way to calculate the TTE to the next trophic level in the model is

$$TTE_{i \to i+1} = \frac{P_{i+1}}{P_i} = \frac{e_{i+1} I_{i+1} - (R_{a,i+1} + R_{b,i+1})}{I_{i+1}}$$
$$= \frac{f_a e_{i+1} y \dfrac{B_i}{B_h + B_i} - f_m}{y \dfrac{B_i}{B_h + B_i}}. \tag{11}$$

This expression has an upper limit that is reached for unlimited food supply $B_i \to \infty$. For this limit, the rightmost part of Eq. 11 can be simplified to

$$TTE_{i \to i+1} < \frac{f_a e_{i+1} y - f_m}{y} \tag{12}$$

as an expression for the upper bound of the TTE inherent in the ATN model (Eqs. 1–4). When calculating this model-inherent maximum TTE from the first to the second trophic level, the autotrophs' maximum biomass is their capacity K and not infinity, and Eq. 11 is used for the calculation instead of Eq. 12.

To differentiate the inherent TTE (upper bound of the TTE in the ATN model) from the actually obtained TTE during the dynamic simulations, the latter will thereafter be called obtained TTE.

Simulations

Biomasses and resulting values are mean values of the last 50,000 time steps of a 100,000 step time series. All calculations and figures were made using Python 2.7.6. For integration of the ordinary differential equations, the adaptive step-size lsoda solver was used with absolute and relative error tolerances $\varepsilon_{abs} = \varepsilon_{rel} = 10^{-13}$.

Table 2 Three trophic transfer efficiencies (TTE) are given, the maximum feasible TTE according to the given assimilation efficiencies (Table 1) and assuming that production equals respiration (Humphreys 1979) (Eq. 10), the maximum inherent TTE assuming maximum food concentration (Eq. 12), and the maximum TTE obtained from the simulations for both the original and the extended ATN versions for the three trophic levels in %

|	Max. feasible TTE	Max. inherent TTE		Max. obtained TTE	
		Original	Extended	Original	Extended
$TTE_{3\rightarrow4}$	42.5	72.5	32.8	50.5	30.1
$TTE_{2\rightarrow3}$	42.5	72.5	32.8	44.5	30.2
$TTE_{1\rightarrow2}$	22.5	26.3	16.1	14.1	13.2

Results

We first evaluated the maximum inherent trophic transfer efficiency (TTE) assuming unlimited food supply. We found a value of 32.5% for the herbivores and 72.5% for the carnivores and top predators in the original ATN model, which exceeds by far the maximum feasible TTE of 22.5% for herbivores and 42.5% for carnivores and top predators (Eqs. 10, 12, Table 2). In the extended ATN

version, the maximum inherent TTE was 16.1% for the herbivores and 32.8% for the carnivores and top predators (Eq. 12, Table 2). The maximum inherent TTE was smaller in the extended version as more carbon is respired instead of transported through the food chain to the upper trophic levels.

As a second and more practical step, we investigated the TTE obtained in dynamic simulations of a four trophic-level food chain using both the original and extended ATN versions over a gradient of the top predator's death rate constant d. In the extended ATN version, which accounts for activity and basal respiration separately, the maximum obtained TTE at trophic level 3 and 4 never exceeded the maximum feasible TTE (Fig. 2, Table 2, Eq. 10). In contrast, in the original ATN model the obtained TTE at trophic level 4 exceeded the maximum feasible TTE of 42.5% for $d > 0.0029$ (Fig. 2, maximum observed value 50.5%). At trophic level 3, the TTE of the carnivores in the original ATN model exceeded the maximum feasible TTE for small values of d ($d < 0.0006$, Fig. 2). The consistently lower obtained TTE in the extended ATN version indicates that this model version represents the energy transfer towards the higher trophic level more realistically than the original ATN model.

Fig. 2 Trophic transfer efficiency (TTE) obtained in simulations (in percent, defined as the production ratio of upper vs. lower trophic level) of the top predator (top panel), carnivore (center), and herbivore (bottom) in the original (dashed lines) and extended (solid lines) ATN versions for different top predator's death rate constants d. Gray vertical lines indicate the position of the biomass pyramids provided in Fig. 3. The horizontal lines indicate the maximum feasible TTE (see "Trophic transfer efficiency," Table 2)
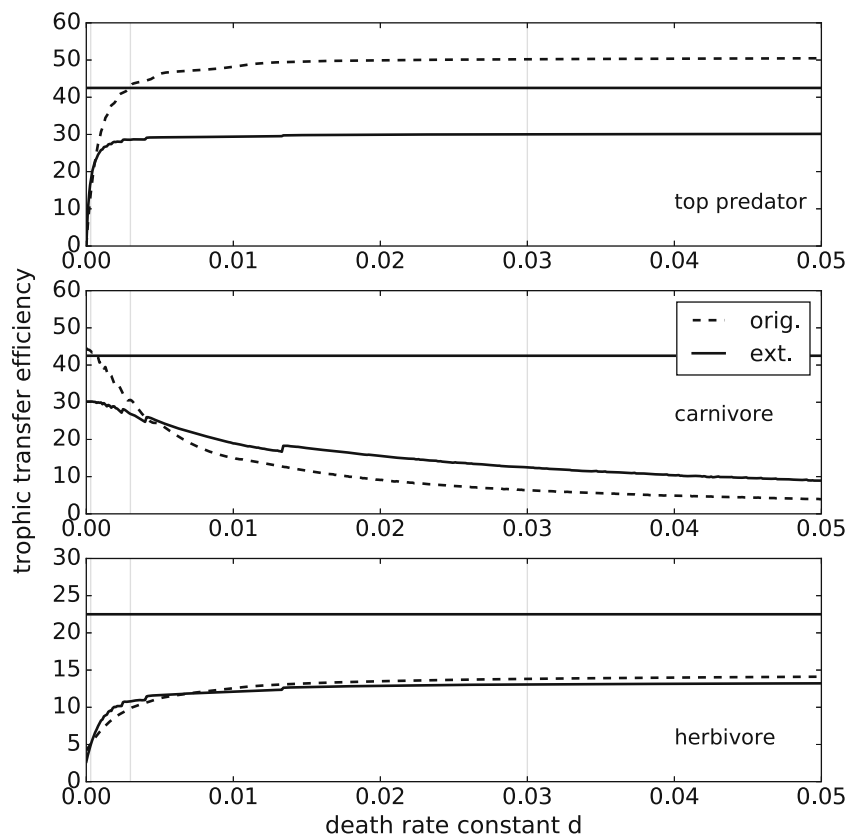
With an increasing death rate constant d of the top predator, its own as well as the herbivore's obtained TTE increased, whereas the carnivore's obtained TTE decreased (Fig. 2). This alternating pattern of increasing and decreasing obtained TTE with increasing d resulted from a trophic cascade: Higher values of d lowered the top predator's biomass, which in turn lowered its total ingestion. Released from top-down control, the carnivore's biomass, and thus, its ingestion increased. This pattern propagated down to the herbivores and autotrophs. Since the TTE is a monotonously increasing function of the biomass on the respective lower trophic level (Eq. 11, Appendix, Fig. 7), this alternating pattern of decreasing and increasing biomasses translates directly to the TTEs on the different trophic levels.

The herbivore's obtained TTE remained below the maximum feasible TTE of 22.5% (Eq. 10) in both model versions (Fig. 2). The reason is the nonlinear dependence of the autotroph's production on its carrying capacity and its interaction with the nonlinear grazing function of the herbivore. When assuming a chain of three trophic levels where the carnivore as the highest trophic level experiences a quadratic death term, the herbivore was under strong top-down control and exceeded its maximum feasible TTE by up to a factor of 1.1 (Appendix, Figs. 5 and 6).

Depending on the top predator's death rate, the models exhibited different trophic cascade patterns. For small d (0.0003), the herbivore and the top predator accumulated high biomasses resulting in a top-heavy trophic cascade (Fig. 3a, d). For larger d (0.0030), the biomasses resembled roughly a column (Fig. 3b, e), and for higher d, a bottom-heavy trophic cascade occurred (Fig. 3c, f).

To further elucidate the reason for the inconsistencies between the obtained TTE of the original ATN model and physiological considerations and realistic estimates, we analyzed the carbon fluxes in the bottom-heavy trophic cascade (Fig. 3c, f) in more detail (Fig. 4, Table 3). The alternating biomasses indicate where the inconsistencies are most obvious. In the original ATN model, the top predator's respiration was small compared to its ingestion, resulting in a large production per ingested unit of carbon (Table 3). This led to a production being 33% higher than the respiration (Fig. 4b) and an obtained TTE of 50% (Fig. 4b, Table 3). In contrast, in the extended ATN version, the respiration per ingested unit of carbon was higher due to the activity respiration, which resulted in a lower production and an obtained TTE of 30% (Fig. 4a).

In the original ATN model, respiration per ingestion and production per ingestion varied considerably more between trophic levels than in the extended ATN version. This was due to the overemphasis of basal respiration and neglecting of the activity respiration: Only a high biomass (here, of the carnivore) resulted in respiration losses of substantially more than 50% of the assimilation and, thus, a realistic TTE in the original ATN model. In the extended ATN version, respiration per ingestion and production per ingestion did not vary that much across trophic levels even in the presence of a strong trophic cascade because respiration is not solely coupled to the standing biomass stock, but also to the assimilation. As low biomasses are connected with high per capita rates in the ATN models, a low biomass-related basal respiration is counteracted by high activity respiration and vice versa.

Discussion

Allometric trophic network (ATN) models are an important tool to analyze dynamics of food webs (Boit et al. 2012; Hudson and Reuman 2013; Schuwirth and Reichert 2013; Kuparinen et al. 2016) and their diversity and stability (Brose et al. 2006; Rall et al. 2008; Berlow et al. 2009; Heckmann et al. 2012). Despite their frequent use, the ATN energetics was not yet explicitly addressed, though it decisively influences dynamic patterns of the model (Boit et al. 2012). Here, we compared the energetics of the original ATN model (Yodzis and Innes 1992; Brose et al. 2006) which considers only basal respiration, and an extended ATN version (Boit et al. 2012) including both basal and activity respiration. We found that the trophic transfer efficiency (TTE) could become unrealistically high in the original ATN model in both static calculations and dynamic simulations, whereas it always fell into a physiologically and ecologically realistic range in the extended ATN version. The reason for the more realistic energy transfer is the inclusion of the activity respiration that depends on the amount of assimilated carbon in the extended ATN version.

The threshold above which we consider a TTE unrealistically high was set very conservatively and followed from the assumption that the energy allocated to production can at most be equal to respiration (Humphreys 1979). This yields a maximum feasible TTE of 22.5% for herbivores and 42.5% for carnivores (Eq. 10). These upper theoretical limits are usually not reached in natural communities even when dominated by unicellular organisms or invertebrates, except when a trophic level is under high predation pressure. Empirically established maximum TTE ranges between 13% and around 30% for both herbivores and carnivores from pelagic systems and including small to large fish (Straile 1997; Jennings et al. 2002; Barnes et al. 2010). The extended ATN version reflects these natural energetic constraints well by keeping the obtained TTE in a realistic range up to 30% (cf. Fig. 2). In contrast, the original ATN model led to an obtained TTE up to 51% (cf. Fig. 2) which overestimates the empirical values of at most 30% by a factor of 1.7.
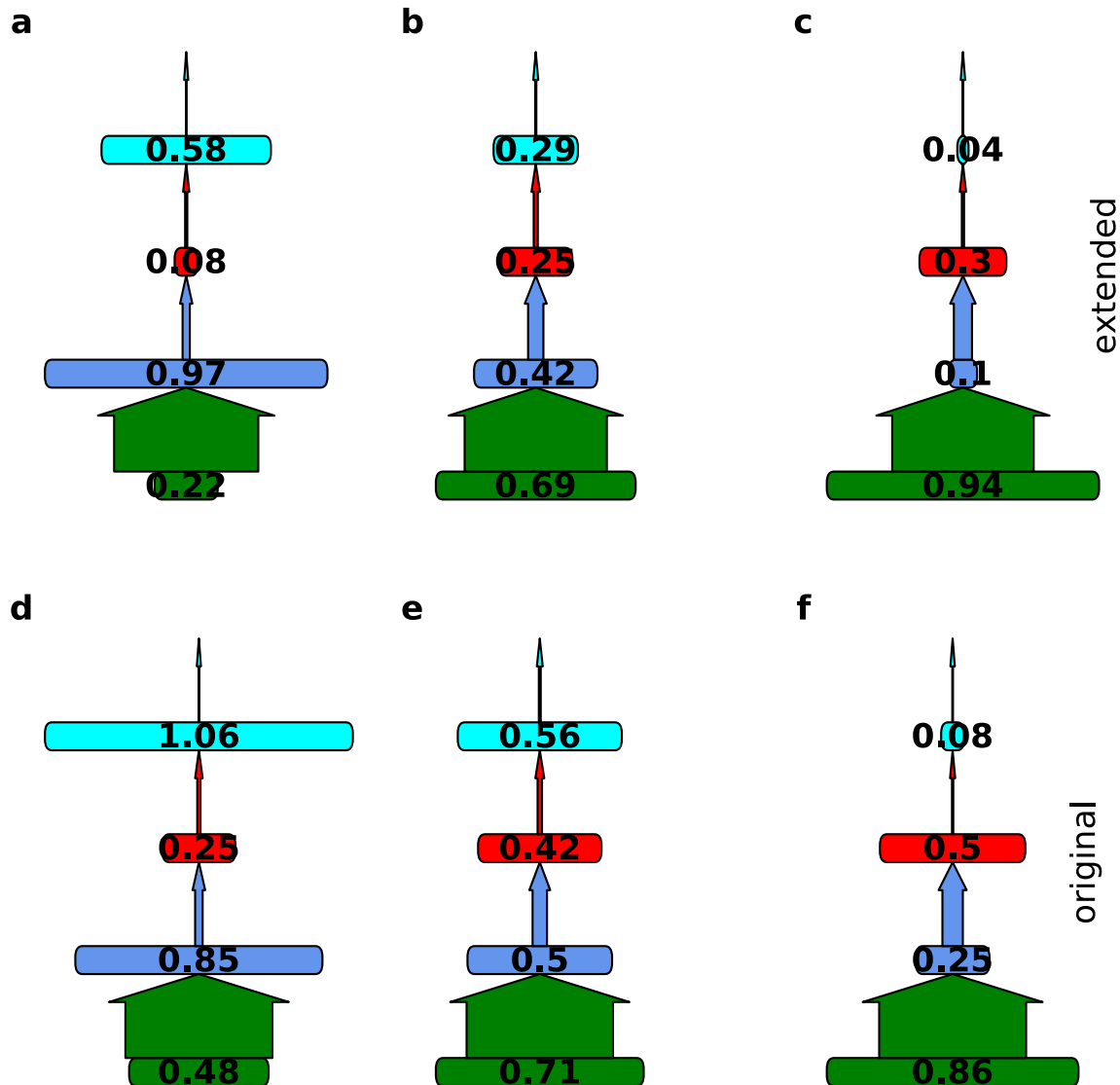
Fig. 3 Comparison of the mean biomasses (bold numbers) within the food chain of the extended ATN version including activity respiration (**a**–**c**) and the original ATN model (**d**–**f**), for different top predator's death rate constants $d = 0.0003$ (**a**, **d**), $d = 0.003$ (**b**, **e**), and $d = 0.03$ (**c**, **f**). Arrows indicate production rates. Their width is scaled to autotroph's production as 100%. Box widths are scaled with the species' biomasses

The metabolic theory of ecology does not differentiate between basal respiration proportional to the standing biomass stock and activity respiration (Brown et al. 2004). Brown et al. (2004) stated that the metabolic rate generally depends only on biomass and that the field metabolic rate, analog to our activity respiration, is a "fairly constant multiple of the basal rate" and therefore also depends only on the biomass. A similar assumption also served as basis for the ATN models accounting only for basal respiration proportional to the biomass. This assumption is reasonable if resource levels are fairly constant; however, biomasses and ingestion rates vary in nature and dynamic models and so does, ultimately, also the TTE (Appendix, Fig. 7).

The different patterns of trophic cascades illustrate the problematic consequences of linking respiration only to

biomass. The amount of top-down control exerted by the top predator or the carnivore, and thus the strength of the trophic cascade were modulated by the death rate constant d. For small d, the top predator had a high biomass and controlled the carnivore. The carnivore's obtained TTE then became unrealistically high in the original ATN model, and the food web became (too) top heavy. The link between a high TTE and top heavy food webs is also described in a review of 23 food webs (McCauley et al. 2018). For intermediate d, the biomasses were approximately equally distributed across different trophic levels which is in line with the flat biomass distribution established for pelagic systems (Gaedke 1992). For higher d, the top predator was top-down controlled by its death rate and released the carnivore from grazing pressure, but
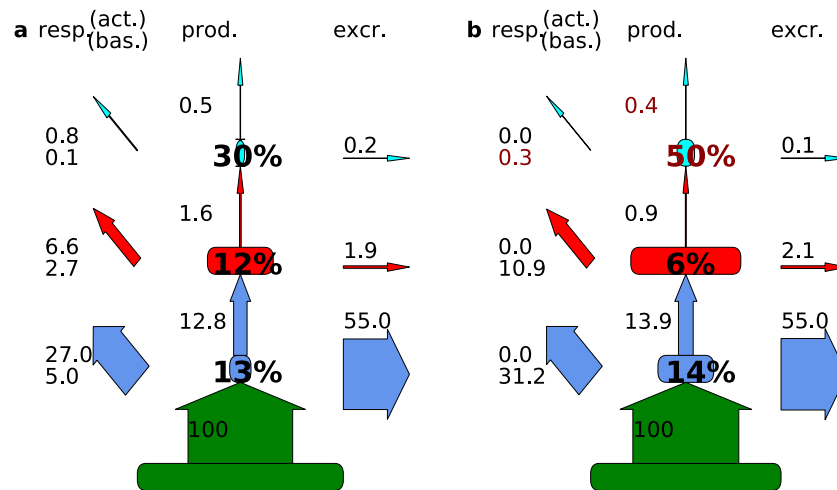
Fig. 4 Comparison of the energy transfer within the food chain of the extended ATN version including activity respiration (**a**), and the original ATN model (**b**). The biomass pyramids are based on the same data as Fig. 3c, f, i.e., $d = 0.03$. Included values are basal and activity respiration (numbers on the left, activity above basal respiration), production (numbers in the middle to the left of the upward arrows), trophic transfer efficiency (bold large numbers), and excretion (numbers above the right arrows). All fluxes are standardized to autotroph's production as 100%, so that wider arrows indicate larger values. Box widths are scaled with the species' biomasses. Red values point out inconsistencies with the physiological considerations that respiration is equal to or less than production (Humphreys 1979)

in this case, the top predator's obtained TTE became unrealistically high. In any case, the obtained TTE was too high at one particular trophic level within a pronounced trophic cascade because the top-down controlled trophic levels had a low biomass and thus a low basal respiration. Thus, the assumption of Brown et al. (2004) that activity respiration and field metabolic rate are proportional to a standing biomass stock only holds for equally distributed biomasses, but not for unequally distributed biomasses in trophic cascades.

The link between activity respiration and ingestion as we introduced it here to the ATN model allows for a more flexible reaction to dynamic instead of constant biomasses. This is important when modeling large food webs with rapidly changing dynamics such as pelagic systems. ATN and other food web models are known to form trophic cascades (Carpenter et al. 2016) which are observed in many ecosystems (Carpenter et al. 1985; Pace et al. 1999; Shurin et al. 2002) and, as we showed here, strongly affects the TTE. Other ATN models dampened the trophic cascades with mechanism such as predator interference or type III functional response which obfuscates this underlying energetic problem to some extent (Rall et al. 2008). However, they do not solve it, as the model-inherent TTE is independent of these mechanisms. The ATN approach has also been used to parameterize large-scale ecosystem models such as the Madingley model (Harfoot et al. 2014). In this model, neglecting activity respiration seems to have contributed to unrealistically top heavy biomass distributions as well, underlining the importance of more accurate assumptions regarding basic energetic processes than the original ATN provides. The pronounced trophic cascades as seen in our study are due to the structurally simplistic food chain and would be dampened in natural systems, e.g., by a higher trophic connectance via omnivory.

Other models, like Rosenzweig-MacArthur-type predator-prey models (Rosenzweig and MacArthur 1963; Weitz and Levin 2006), incorporate respiration losses only by a constant factor named conversion efficiency related to ingestion and production; thus, this type of model only accounts for (what we call here) activity respiration. Basal respiration may be implicitly considered in a death rate proportional to the biomass. Anderson (1992) pointed out the difference between basal and activity respiration

Table 3 Respiration to ingestion ratio (R/I) and production to ingestion ratio (P/I ≙ obtained TTE since non-grazing mortality was not included in the ATN model for the 1st–3rd trophic level; thus, the production of the trophic level below is ingested entirely, see "ATN model equations") for both the original (orig.) and extended (ext.) ATN versions with the top predator's death rate constant $d = 0.03$. Autotrophic respiration is already included in the growth rate and therefore not listed here. Values were calculated from the biomass, respiration, and production values shown in Figs. 3f and 4b for the original ATN model, and in Figs. 3c and 4a for the extended ATN version, respectively

	R/I		P/I ≙ TTE	
	orig. (%)	ext. (%)	orig. (%)	ext. (%)
Top predator	35	55	50	30
Carnivore	79	72	6	12
Herbivore	31	32	14	13

especially for unicellular organisms and invertebrates whose activity respiration exceeds the basal respiration as they are poikilotherms with low maintenance costs when inactive. In our extended ATN version, we combined both respiration rates and implemented these ideas by introducing the factor f_a in the formulation of assimilation (cf. Eq. 8, "Methods," Fig. 1), thereby making activity respiration proportional to the amount of assimilated carbon.

Following Boit et al. (2012), we set the parameter $f_a = 0.4$ for all consumers assuming that respiration is slightly larger than production (Humphreys 1979). Although this conservative estimate satisfies fundamental energetic constraints, a more differentiated picture may emerge when defining a more empirically grounded value range for f_a for different taxa. In the same way, the parameter $f_m = 0.1$ (following Boit et al. (2012)) may be adapted to fit different taxa. As a recent meta-analysis reveals that the differences in respiration rates between taxonomic groups are not only due to consumer type (e.g., herbivore or carnivore) (Lang et al. 2017), future research could aim to entangle the influences of taxonomic group, activity, and food availability on respiration rates. Until then, due to the scarcity of experimental data on activity vs. basal respiration rates of invertebrates, the parameterization of f_a and f_m in a specific food web context remains a challenge for future modeling studies with ATNs.

The complexity of the model did not increase from a mathematical point of view even though we introduced two additional parameters (f_a and f_m) in the extended ATN version. The number of effective parameters that independently determine model dynamics is the same in the original and the extended ATN versions. This becomes obvious when we introduce new parameters for the extended ATN model: $e_{\mathrm{prod},i} = e_i f_a$ as the production efficiency (equivalent to e_i in the original model) and $x_{b,i} = f_m x_i$ (equivalent to x_i in the original model) as the per capita basal metabolic rate. When aiming for a concise mathematical description of the model, we recommend to use these effective parameters. Here, however, we chose not to do so in order to emphasize the underlying biological processes. In the same vein, we argue that we do not merely propose to use different values for some parameters of the ATN model, but stress the conceptual advancement of the ATN model by clearly distinguishing between basal and activity respiration, which is essential for improving quantitative predictions about ecosystem energetics.

To conclude, basal and activity respiration depend on different processes and should both be considered explicitly in models covering metabolic processes. Including activity respiration in the ATN model lowers the obtained TTE to realistic values in comparison to empirically derived values. Especially

for food webs mainly based on unicellular organisms and invertebrates or modeling ecosystems prone to trophic cascading, we recommend using the extended ATN version to achieve more realistic energetics. Far more than a mere modeling fix, reflecting the energy flux through food webs in a realistic way is indispensable for upscaling and integrating smaller modules to larger community networks or even large-scale ecosystem models. ATN models will then be ready for quantitatively linking trophic interactions in biodiverse communities to ecosystem-level biomass dynamics and biogeochemical cycling.

Appendix

We also modeled a three trophic-level food chain in which the carnivore has a density-dependent death rate equivalent to the top predator in the chain of four trophic levels (Eq. 4). With this model setup, we examined the herbivore's obtained TTE when being released from top-down control due to increasing the carnivore's death rate.
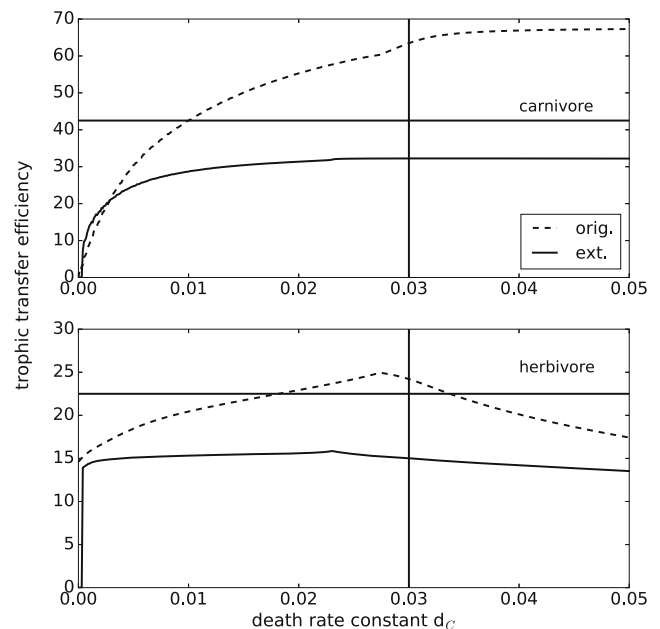

Fig. 5 Trophic transfer efficiency (obtained TTE, defined as the production ratio of upper vs. lower trophic level) of the carnivore (upper panel) and herbivore (bottom) in the original (dashed lines) and extended (solid lines) ATN versions for different carnivore's death rate constants d. For one parameter value (vertical line), the biomass pyramids are provided in Fig. 6. The horizontal lines indicate the maximum feasible TTE (Eq. 10, Table 2)
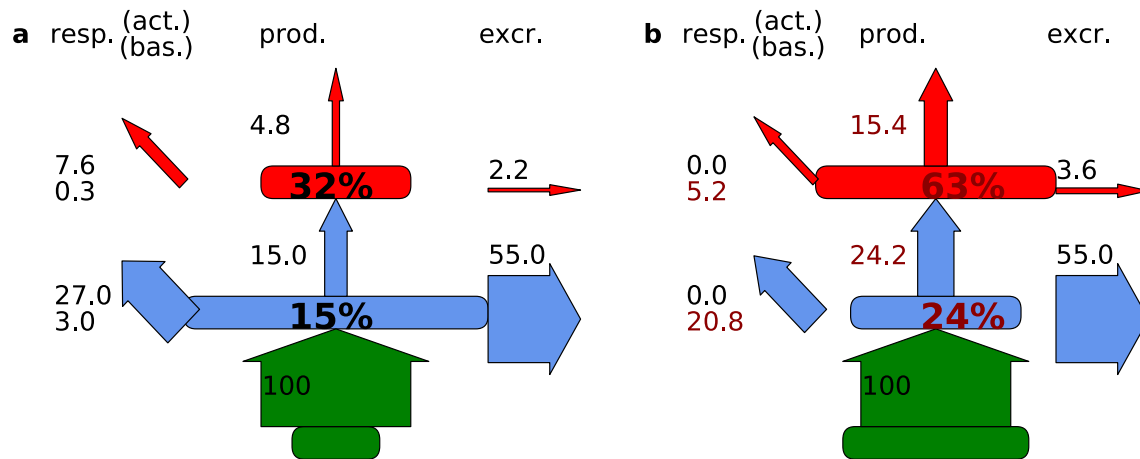
Fig. 6 Comparison of the energy transfer within a three trophic-level food chain of the extended ATN version including activity respiration (**a**) and the original ATN model (**b**). The biomass pyramids are based on the parameter indicated in Fig. 5, i.e., $d = 0.03$. Included values are basal and activity respiration (numbers on the left, activity above basal respiration), production (numbers in the middle to the left of the upward arrows), trophic transfer efficiency (bold large numbers), and excretion (numbers above the right arrows). All fluxes are standardized to autotroph's production as 100%, so that wider arrows indicate larger values. Box widths are scaled with the species' biomasses. Red values point out inconsistencies with the physiological considerations that respiration is equal to or less than production (Humphreys 1979)
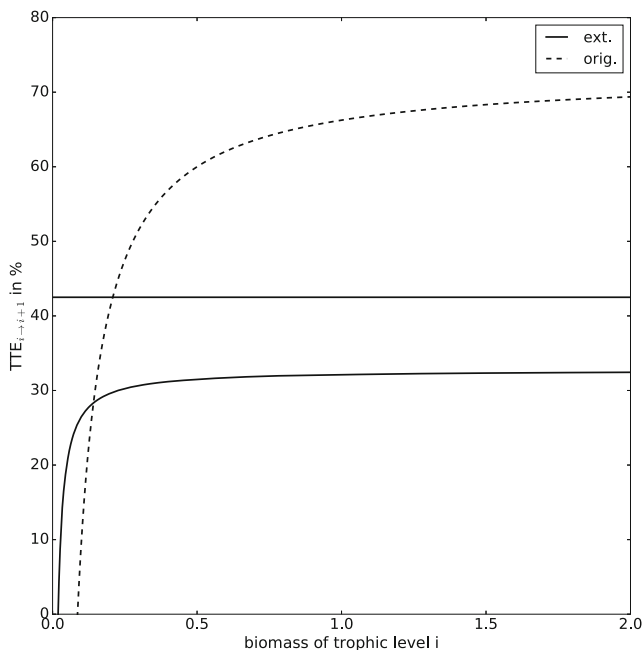

Fig. 7 Trophic transfer efficiency (obtained TTE in %, defined as the production ratio of upper vs. lower trophic level) of a trophic level $i + 1$ (here, parameterized for both the carnivore and the top predator as they have the same assimilation efficiency) in the original (dashed line) and extended (solid line) ATN versions for different food quantities (biomass of the lower trophic level i). The horizontal line indicates the maximum feasible TTE (Eq. 10, Table 2)

References

Anderson TR (1992) Modelling the influence of food C:N ratio, and respiration on growth and nitrogen excretion in marine zooplankton and bacteria. J Plankton Res 14:1645–1671. https://doi.org/10.1093/plankt/14.12.1645

Barnes C, Maxwell D, Reuman DC, Jennings S (2010) Global patterns in predator-prey size relationships reveal size dependency of trophic transfer efficiency. Ecology 91:222–232. https://doi.org/10.1890/08-2061.1

Begon M, Townsend CR, Harper JL (2006) Ecology—from individuals to ecosystems, 4th edn. Blackwell Publishing Malden, Mass

Benoît E, Rochet M-J (2004) A continuous model of biomass size spectra governed by predation and the effects of fishing on them. J Theor Biol 226:9–21. https://doi.org/10.1016/S0022-5193(03)00290-X

Berlow EL, Dunne JA, Martinez ND, Stark PB, Williams RJ, Brose U (2009) Simple prediction of interaction strengths in complex food webs. Proc Natl Acad Sci 106:187–191. https://doi.org/10.1073/pnas.0806823106

Boit A, Martinez ND, Williams RJ, Gaedke U (2012) Mechanistic theory and modelling of complex food-web dynamics in Lake Constance. Ecol Lett 15:594–602. https://doi.org/10.1111/j.1461-0248.2012.01777.x

Brose U (2008) Complex food webs prevent competitive exclusion among producer species. Proc Biol Sci 275:2507–2514. https://doi.org/10.1098/rspb.2008.0718

Brose U, Williams RJ, Martinez ND (2006) Allometric scaling enhances stability in complex food webs. Ecol Lett 9:1228–1236. https://doi.org/10.1111/j.1461-0248.2006.00978.x

Brown JH, Gillooly JF, Allen AP, Savage VM, West GB (2004) Toward a metabolic theory of ecology. Ecology 85:1771–1789. https://doi.org/10.1890/03-9000

Carpenter SR, Kitchell JF, Hodgson JR (1985) Cascading trophic interactions and lake productivity. Bioscience 35:634–639. https://doi.org/10.1525/bio.2010.60.10.17

Carpenter SR, Cole JJ, Pace ML, Wilkinson GM (2016) Response of plankton to nutrients, planktivory and terrestrial organic matter: a

model analysis of whole-lake experiments. Ecol Lett 19:230–239. https://doi.org/10.1111/ele.12558

Gaedke U (1992) The size distribution of plankton biomass in a large lake and its seasonal variability. Limnol Oceanogr 37:1202–1220

Gaedke U, Hochstädter S, Straile D (2002) Interplay between energy limitation and nutritional deficiency: empirical data and food web models. Ecol Monogr 72:251–270. https://doi.org/10.1890/0012-9615(2002)072[0251:IBELAN]2.0.CO;2

Gessaman JA (1973) Methods of estimating the energy cost of free existence. In: Logan UT (ed) Ecological energetics of homeotherms. Utah State University Press, Logan, Utah, pp 3–31

Harfoot MBJ, Newbold T, Tittensor DP, Emmott S, Hutton J, Lyutsarev V, Smith MJ, Scharlemann JPW, Purves DW (2014) Emergent global patterns of ecosystem structure and function from a mechanistic general ecosystem model. PLoS Biol 12:e1001841. https://doi.org/10.1371/journal.pbio.1001841

Heckmann L, Drossel B, Brose U, Guill C (2012) Interactive effects of body-size structure and adaptive foraging on food-web stability. Ecol Lett 15:243–250. https://doi.org/10.1111/j.1461-0248.2011.01733.x

Hendriks AJ (1999) Allometric scaling of rate, age and density parameters in ecological models. Oikos 86:293–310. https://doi.org/10.2307/3546447

Holling CS (1959) Some characteristics of simple types of predation and parasitism. Can Entomol 91:385–398

Hudson LN, Reuman DC (2013) A cure for the plague of parameters: constraining models of complex population dynamics with allometries. Proc R Soc B Biol Sci 280:20131901. https://doi.org/10.1098/rspb.2013.1901

Humphreys WF (1979) Production and respiration in animal populations. J Anim Ecol 48:427–453. https://doi.org/10.2307/4171

Jennings S, Warr KJ, Mackinson S (2002) Use of size-based production and stable isotope analyses to predict trophic transfer efficiencies and predator-prey body mass ratios in food webs. Mar Ecol Prog Ser 240:11–20. https://doi.org/10.3354/meps240011

Kuparinen A, Boit A, Valdovinos FS, Lassaux H, Martinez ND (2016) Fishing-induced life-history changes degrade and destabilize harvested ecosystems. Sci Rep 6:1–9. https://doi.org/10.1038/srep22245

Lang B, Ehnes RB, Brose U, Rall BC (2017) Temperature and consumer type dependencies of energy flows in natural communities. Oikos 4:1–9. https://doi.org/10.1111/oik.04419

McCauley DJ, Gellner G, Martinez ND et al (2018) On the prevalence and dynamics of inverted trophic pyramids and otherwise top-heavy communities. Ecol Lett 21:439–454. https://doi.org/10.1111/ele.12900

Pace ML, Cole JJ, Carpenter SR, Kitchell JF (1999) Trophic cascades revealed in diverse ecosystems. Trends Ecol Evol 14:483–488. https://doi.org/10.1016/S0169-5347(99)01723-1

Rall B, Guill C, Brose U (2008) Food-web connectance and predator interference dampen the paradox of enrichment. Oikos 117:202–213. https://doi.org/10.1111/j.2007.0030-1299.15491.x

Rosenzweig MI, MacArthur RH (1963) Graphical representation and stability conditions of predator-prey interactions. Am Nat 97:209–223. https://doi.org/10.1086/662677

Schneider FD, Scheu S, Brose U (2012) Body mass constraints on feeding rates determine the consequences of predator loss. Ecol Lett 15:436–443. https://doi.org/10.1111/j.1461-0248.2012.01750.x

Schneider FD, Brose U, Rall BC, Guill C (2016) Animal diversity and ecosystem functioning in dynamic food webs. Nat Commun 7:12718. https://doi.org/10.1038/ncomms12718

Schuwirth N, Reichert P (2013) Bridging the gap between theoretical ecology and real ecosystems: modeling invertebrate community composition in streams. Ecology 94:368–379. https://doi.org/10.1890/12-0591.1

Shurin JB, Borer ET, Seabloom EW, Anderson K, Blanchette CA, Broitman B, Cooper SD, Halpern BS (2002) A cross-ecosystem comparison of the strength of trophic cascades. Ecol Lett 5:785–791. https://doi.org/10.1046/j.1461-0248.2002.00381.x

Straile D (1997) Gross growth efficiencies of protozoan and metazoan zooplankton and their dependence on food concentration, predator-prey weight ratio, and taxonomic group. Limnol Oceanogr 42:1375–1385. https://doi.org/10.4319/lo.1997.42.6.1375

Weitz JS, Levin SA (2006) Size and scaling of predator-prey dynamics. Ecol Lett 9:548–557. https://doi.org/10.1111/j.1461-0248.2006.00900.x

Yodzis P, Innes S (1992) Body size and consumer-resource dynamics. Am Nat 139:1151–1175. https://doi.org/10.1086/285380
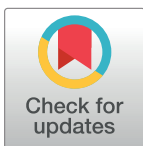
Non-trophic interactions strengthen the diversity—functioning relationship in an ecological bioenergetic network model

Vincent Miele[1], Christian Guill[2], Rodrigo Ramos-Jiliberto[3], Sonia Kéfi[4]*

1 Université de Lyon, F-69000 Lyon; Université Lyon 1; CNRS, UMR5558, Laboratoire de Biométrie et Biologie Évolutive, F-69622 Villeurbanne, France, **2** Institut für Biochemie und Biologie, Universität Potsdam, Potsdam, Germany, **3** GEMA Center for Genomics, Ecology & Environment, Faculty of Sciences, Universidad Mayor, Huechuraba, Santiago, Chile, **4** Institut des Sciences de l'Evolution de Montpellier, CNRS, Université de Montpellier, IRD, EPHE, Montpellier, France

* sonia.kefi@umontpellier.fr

Abstract

Ecological communities are undeniably diverse, both in terms of the species that compose them as well as the type of interactions that link species to each other. Despite this long recognition of the coexistence of multiple interaction types in nature, little is known about the consequences of this diversity for community functioning. In the ongoing context of global change and increasing species extinction rates, it seems crucial to improve our understanding of the drivers of the relationship between species diversity and ecosystem functioning. Here, using a multispecies dynamical model of ecological communities including various interaction types (e.g. competition for space, predator interference, recruitment facilitation in addition to feeding), we studied the role of the presence and the intensity of these interactions for species diversity, community functioning (biomass and production) and the relationship between diversity and functioning.Taken jointly, the diverse interactions have significant effects on species diversity, whose amplitude and sign depend on the type of interactions involved and their relative abundance. They however consistently increase the slope of the relationship between diversity and functioning, suggesting that species losses might have stronger effects on community functioning than expected when ignoring the diversity of interaction types and focusing on feeding interactions only.

Author summary

The question of how species diversity contributes to the functioning of ecological communities has intrigued ecologists for decades, and is especially relevant in the current context of species extinctions. Ecological communities are not only diverse in terms of the species that compose them but also in terms of the way they interact with each other: for example, species compete for space and for food, eat and facilitate each other. The diversity of ways species interact has rarely been taken into account in the study of ecological communities, although widely acknowledged. Here we show that the diversity of interaction types

199

matters: it affects species diversity, community functioning and the relationship between them by strengthening this relationship. This means that when the diversity of interaction types is taken into account, species losses have stronger impacts on the functioning of ecological communities. Our results therefore suggest that species loss may have more important consequences than expected based on classical models that do not take the diversity of interaction types into account.

Introduction

Despite the wide recognition of the coexistence of multiple interaction types linking species in nature [1–3], research on ecological networks has been massively dominated by studies on a single interaction at a time (e.g. trophic, competitive or mutualistic; e.g. [4–6]). The implications of the diversity of interactions for ecological community dynamics and resilience remains therefore largely unknown, despite a recent growing interest in the ecological literature [7–10].

Among interaction types, feeding has massively dominated the literature [2], leading to the analysis of the structural properties of food webs on data sets and to the use of modeling to investigate the functional consequences of these structures (e.g. [4, 11–16]). Early on, Arditi and colleagues [17] proposed to integrate non-trophic interactions in such dynamical models as modifications of trophic interactions (so-called 'rheagogies'). Building on that idea, Goudard and Loreau [18] investigated the effect of rheagogies on the relationship between biodiversity and ecosystem functioning (BEF) in a tri-trophic model. They showed that ecosystem biomass and production depended not only on species richness but also on the connectance and magnitude of the non-trophic interactions.

Several studies have investigated the role of incorporating specific interactions in food webs. For example, incorporating interspecific facilitation in a resource-consumer model allowed species coexistence in communities of plants consuming a single resource [19]. This increase in species diversity also happens in ecological communities with higher trophic levels including both trophic and facilitative interactions [3]. In the same model, intra- and interspecific predator interference increased species coexistence as well in multi-trophic webs, although to a lesser extent than facilitation among plants [3].

More generally, the joint effect of several interaction types is expected to affect community functioning and stability. Extending May's work, Allesina and Tang [20] showed that communities including a mixture of mutualistic and competitive interactions with equal probability were less likely to be stable than random ones (i.e. where interactions between species are randomly chosen), themselves being less stable than predator–prey communities (i.e. in which interactions come in pairs of opposite sign). Using a similar approach, Suweis and colleagues [21] explored the effect of mixing mutualistic and predator-prey interactions on stability, and showed that, without making any further hypothesis, increasing the proportion of mutualistic interactions tend to destabilize the community. Conversely, in a spatially explicit model including both mutualism and antagonism, Lurgi *et al*. [9] found that increasing the proportion of mutualism increased the stability of the communities. Addressing the relationship between structure and stability, Sauve *et al*. [8] showed that the role of nestedness and modularity—structural properties that were shown to promote stability in their single interaction types networks (more specifically in mutualistic networks for nestedness and in antagonistic networks for modularity)—was weakened in networks combining mutualistic and antagonistic

interactions. Note that this result contrasts with Allesina and Tang [20]'s result on community matrices who showed that, for mutualistic interactions, nested matrices were less likely to be stable than unstructured matrices.

Combining dynamical models with an empirical network analysis including all known non-trophic interactions between the species of intertidal communities in central Chile [22], Kéfi *et al.* [10] found that the specific ways in which the different layers of interactions are structured in the data increased community biomass, species persistence and tend to improve community resilience to species extinction compared to randomized counter-parts. More recently, García-Callejas *et al.* [23] used a dynamical model to investigate the effect of the relative frequency of different interaction types on species persistence and showed that persistence was more likely in species-poor communities if positive interactions were present, while this role of positive interactions was less important in species-rich communities.

Altogether, these studies suggest that the joint effect of several interaction types could alter fundamental properties of ecological systems—such as species coexistence, production and community stability—with however a clear lack of consensus on how. So far, most studies have addressed these questions with specific subsets of non-trophic interactions [3, 8, 18, 19], in small species modules [24, 25], in networks with limited numbers of trophic levels [19] or with unrealistic trophic structure [18]. Only a few studies have extended these approaches to complex networks of interactions with a diversity of interaction types (see e.g. [9, 23, 26]). We therefore still lack a clear view on the overall role of the diversity of interaction types *per se* for species diversity and community functioning, and especially how they may affect the relationship between diversity and functioning.

In the 90ies, because of the raising awareness of the increase in species extinction rates, the long-lasting interest on the origin and maintenance of species diversity shifted toward the study of the consequences of biodiversity, and especially of its loss, for ecosystem functioning [27]. This became an entire sub-field of ecology referred to as 'Biodiversity and Ecosystem Functioning' (so-called BEF) and lead to decades of experimental and theoretical research investigating how diversity affects functioning (see [28–33] for reviews). Results of experimental studies suggests that more diverse communities generally produce more biomass than less diverse ones [34, 35]. Theoretically, the question has been addressed as well; models have long focused on plant communities (i.e. a single trophic level) (e.g. [36]), but have more recently started to expand these investigations to more complex, realistic communities (e.g. [37–39]). Until now, as far as we know, studies had not specifically investigated the role of the diversity of interactions types on the shape of the BEF.

Here, using a bioenergetics resource-consumer model in which broad categories of non-trophic interactions were introduced [3], we systematically investigated the functioning of 'multiplex' ecological networks, i.e. how multiple interactions (their abundance and intensity) affect species coexistence, community functioning (biomass and production), and the relationship between diversity and functioning. Our model includes, in addition to the consumer-resource interactions, competition for space among sessile species, predator interference, refuge provisioning, recruitment facilitation as well as effects that increase or decrease mortality.

Methods

The dynamical model

The trophic model. We used an allometric-scaling dynamic food web model [12, 40]. These models have been used extensively to explore the dynamics and stability of complex ecological networks [12, 13, 41].

The food web model consisted of plants (primary producers, at the base of the network, which consume nutrients not explicitly modeled here), and consumers (animals which eat plants and other consumers). The number of species (plants and consumers) and the structure of the web (who eats whom) were initially determined based on the niche model [42] (for details see section 'Simulated networks' in the 'Numerical simulations' part). We mapped dynamical equations to that food web skeleton. The change in species i's biomass density B_i (in $\frac{[mass]}{[area]}$) was described by an ordinary differential equation of the general form:

$$\frac{dB_i}{dt} = r_i G_i B_i + B_i \sum_{j\in prey} \epsilon_{o_j} F_{ij} - \sum_{k\in pred} B_k F_{ki} - x_i B_i - d_i B_i, \tag{1}$$

where the first term describes plant growth; the second term describes the biomass gained by the consumption of other species j; the third term describes mortality due to predation, summed over all consumers k of species i; the fourth term represents the metabolic demands of species i; the last term is the natural mortality of species i. More precisely:

- r_i is the intrinsic growth rate of primary producers (in $[time]^{-1}$; r_i is positive for primary producers and null for other species);

- G_i is the growth term described in Eq (2) below;

- ϵ_{o_j} is a conversion efficiency (dimensionless) which determines how much biomass eaten of resource j is converted into biomass of consumer i;

- F_{ij} is the functional response, i.e. the rate at which consumer i feeds on resource j (see Eq (3) below; in $[time]^{-1}$);

- x_i is the metabolic demand of consumer species i (in $[time]^{-1}$); note that for basal species, metabolic demand is already taken into account in the intrinsic growth rate r_i;

- d_i the natural mortality rate (in $[time]^{-1}$).

Plant growth. We assumed a logistic growth for basal species:

$$G_i = \left(1 - \frac{B_i}{K_i}\right) \tag{2}$$

with K_i the carrying capacity of the environment for species i (in $\frac{[mass]}{[area]}$).

Functional response. We used a multi-prey Holling-type functional response. The feeding rate of species i on species j is expressed as:

$$F_{ij} = \frac{w_i a_{ij} B_j^{1+q}}{m_i(1 + w_i \sum_{k\in prey} a_{ik} h_{ik} B_k^{1+q})}, \tag{3}$$

where:

- w_i is the relative consumption rate of predator i on its prey, which accounts for the fact that a consumer has to split its consumption between its different resources (dimensionless);

- a_{ij} is the capture coefficient in $\frac{[area]}{[time]} \cdot \frac{[area]^q}{[mass]^q}$ (the attack rate here is $a_{ij}B_j^q$ which has the unit $\frac{[area]}{[time]}$).

- $1+q$ is the Hill-exponent, where the Hill-coefficient q makes the functional response vary gradually from a type II ($q = 0$) to a type III ($q = 1$) [43] (dimensionless);

202

- h_{ij} is the handling time in $\frac{[time]}{[mass]}$.

- Note that m_i, the body mass of species i, is needed here for model and unit consistency [39].

Introducing non-trophic interactions. We introduced in this model a number of non-trophic effects found to be frequent ones mentioned in the literature [3, 10, 22]. We made the relevant parameters of the trophic model become a function of the density of the species source of the effect [3, 18]. As a first approximation, we assume all such dependencies to have a similar, linear shape.

Competition for space. We add a space-dependent term, g_i, which affects species' net growth rate:

$$\frac{dB_i}{dt} = g_i \left(r_i G_i + \sum_{j \in prey} \epsilon_{o_j} F_{ij} - x_i \right) B_i - \sum_{k \in pred} B_k F_{ki} - d_i B_i \tag{4}$$

$$g_i = (1 - c_0 \sum_{l \in comp} \gamma_{il} B_l) \tag{5}$$

where g_i—the competition for space term—is evaluated as in Eq (5), l refers to all the species that potentially compete for space with each other, which need to be sessile (excluding intra-specific competition, i.e. l different from i), c_0 is the overall intensity of competition for space and γ_{il} is the strength of competition exerted by species l on species i, which is assumed to increase with the amount of space occupied by each individual of species l (see upcoming subsection on 'Parameter values used' in the 'Numerical simulations' part). Note that the element γ_{il} is zero if either i or l is non-sessile and even if both species are sessile it is non-zero only with a certain probability (see 'Simulated networks' in 'Numerical simulations' part). This makes competition for space asymmetric, as some species can have a large negative effect on others but are not negatively affected themselves. Also note that because plants have a higher probability of being sessile than other species in the web (see upcoming subsection on 'Simulated networks' in the 'Numerical simulations' part) competition for space occurs more frequently among plants than among other species of the network. Finally, note that if γ_{il} is null for all l, Eq (4) is identical to Eq (1).

Competition for space was assumed to only operate if the net growth rate of the target species (the first term in between brackets in Eq (4)) is positive, i.e. if $(r_i G_i + \sum_{j \in prey} \epsilon_{o_j} F_{ij} - x_i) > 0$. 0therwise, g_i is set to 1.

Predator interference. We introduced predator interference in the feeding rate as follows:

$$F_{ij_{new}} = \frac{w_i a_{ij} B_j^{1+q}}{m_i (1 + i_0 \sum_{s \in pred} \delta_{si} B_s + w_i \sum_{k \in prey} a_{ik} h_{ik} B_k^{1+q})}, \tag{6}$$

where s denotes all the predators of prey j and δ_{si} is the strength of interference competition between predators s and i (Beddington-DeAngelis type, [12, 44]). Again, even if two predators share a prey, this term is non-zero only with a certain probability, and its values is assumed to depend on the differences of the body mass of the two predators (see upcoming subsection on 'Parameter values used' in the 'Numerical simulations' part). The constant i_0 is the overall intensity of predator interference.

Effects on mortality. A number of negative interactions lead to a decrease in the survival of the target species i (e.g. whiplash). Some species might also increase the survival of target

203

species (e.g. improvement of local environmental conditions). We summarized these two types of effects on the mortality rate, d_i as follows:

$$d_{i_{new}} = d_i \left(\frac{1 + n_0 \sum_k n_{ki} B_k}{1 + p_0 \sum_k p_{ki} B_k} \right), \tag{7}$$

with n_0 and p_0 the overall intensities of negative and facilitative effects on mortality (i.e. resp. increase and decrease in mortality), and n and p the interaction matrices containing zeros and ones.

Refuge provisioning from predators.   Refuge provisioning can happen in different ways: a species can protect another from abiotic stress (e.g. decreasing its mortality—see previous example) but a species can also protect another from its predator (e.g. affecting the attack rate of the predator). A refuge provision from species k to species j from its predators can be modeled as follows. For all the predator species i of j:

$$a_{ij_{new}} = \frac{a_{ij}}{1 + r_0 \sum_k \phi_{kj} B_k}, \tag{8}$$

where $a_{ij_{new}}$ tends to 0 in the presence of facilitators, r_0 is the intensity of the refuge effect and ϕ is the interaction matrix containing zeros and ones.

Effects on recruitment.   Species may increase (e.g. habitat amelioration) the recruitment of new plants in the community. We therefore created the term e_i which is multiplied by the growth rate of the species:

$$e_i = \left(1 + e_0 \sum_k \eta_{ki} B_k \right) \tag{9}$$

$$r_{i_{new}} = r_i e_i \tag{10}$$

with e_0 the overall intensity of facilitative effects on recruitment, and η the interaction matrices containing zeros and ones. Note that this term only applies to plants.

Numerical simulations

Simulated networks.   Trophic networks were generated with the niche model [42] starting with 100 species including a fixed number of 20 plants (primary producers) and a connectance of 0.06 (i.e. about 600 trophic links per network) [45]. Cannibalism was allowed but trophic networks containing cycles were discarded.

We imposed a fixed number of 33 sessile species in each network: for each species, we uniformly drew a 'mobility' trait with probability 0.2 for plants and 0.8 for other species, and we repeated the procedure until the network contained 33 sessile species. As a consequence of this choice of probability, plants have a much higher chance of being sessile in our networks than other species in the web.

The location of the non-trophic links was chosen randomly in the trophic web, but following a number of basic rules inspired from the Chilean data set [10, 22]. Competition for space was drawn between two sessile species, interference between two mobile predators that have at least one prey in common, refuge provisioning from a sessile species to a prey (i.e. a species that has at least one consumer), and recruitment facilitation from any species to a plant. Effects on mortality were drawn between any pair of species (i.e. no constraint). Non-trophic links were drawn only between different species because we focused on the role of inter-specific

204

interactions. Note however that our simulations all include intra-specific interference with $i_{0-intra} = 0.8$, as in [39], without which the species diversity at steady state is much lower.

With the previous rules satisfied, the interaction probability (i.e. the probability for a non-zero element of the corresponding non-trophic interaction matrix) between two species was respectively set to 0.098, 0.15, 0.01, 0.01, 0.033 and 0.063 for competition, interference, increase and decrease in mortality, refuge provisioning and recruitment facilitation. These settings allowed to get, on average, 100 non-trophic links for any of the six types of non-trophic interactions (because of the imposed rules, the probabilities need to be different for each interaction type). This means that a simulation started with about 600 trophic and 100 non-trophic links of a given non-trophic interaction type.

Simulations setup. In the first part (Fig 1; see also S1 and S2 Figs), simulations were first run with trophic links only, and 100 trophic networks were selected in which no disconnected plant (i.e. plants that have no consumer) was present at the end of the dynamics (as in [39]). For each of these trophic networks, we drew 50 non-trophic networks of each non-trophic interaction type (to study the effect of each type of non-trophic interaction individually). Again, we only kept the networks in which no disconnected plant was present at the end of the dynamics with the non-trophic links. For each non-trophic interaction type, we defined a range of non-trophic intensity values as follows. We started from a minimum non-trophic intensity value, and we linearly increased this value to a maximum. The minimum (resp. maximum) values were selected so that they correspond to a 2.5% (resp. 10%) variation in species diversity at the end of the simulation in the case with compared to without NTIs. This was the case for all NTIs except for positive effects on mortality for which reaching an effect of 10% change in diversity was not possible even for very high values of p_0 (see colored lines in Fig 1). With this procedure, we put all non-trophic interactions on equal footing, which allowed comparing their effect on outcome variables. This procedure allowed us to compute the slope of the effect of the non-trophic interaction intensity on final species diversity using a linear regression, which is an indicator of the strength of the non-trophic interaction. The slope of this regression is displayed on top of each panel of Fig 1.

In the second part (Figs 2 and 3; see also S4 Fig), decrease in mortality (also referred to as 'positive effects on mortality' in the text) were discarded because of their lack of significant effect on species diversity. For the other five non-trophic interaction types, we selected 1000 simulated trophic networks (again with no disconnected plants), and for each of these networks, we repeated the following procedure 100 times: we drew five non-trophic networks (one per non-trophic interaction type), with one quarter of the previous interaction probabilities for the four negative non-trophic interaction types. This way, we ensure that we have added an equal number of positive and negative links in the networks (i.e. there are as many positive as negative links in the networks studied). We uniformly drew the non-trophic interaction intensities in the same range of values as in the first part (see above). Hence, in this set of simulations, we started with about 600 trophic links, 100 positive (facilitation for recruitment) and 100 negative non-trophic links (about 25 for each of the four types: competition for space, interference, refuge and increase in mortality). In the sensitivity analysis (S5 Fig), we reproduced the same procedure for each of the parameter values investigated (namely the Hill coefficient, *expo* and capture coefficient a_0—see after).

In the same vein, we did another set of simulations in which the intensities of the non-trophic interactions were fixed (to the values leading to 10% variation in species diversity; $i_0 = 3$, $r_0 = 1.75$, $c_0 = 0.012$, $e_0 = 1.8$ and $n_0 = 3$), but we varied the number of links of each of the non-trophic interaction type (S3 Fig). We simulated 100 trophic networks with no disconnected plants and, for each trophic network, we drew 100 non-trophic interaction networks for each non-trophic interaction type of varying size: by modulating the previously mentioned

205
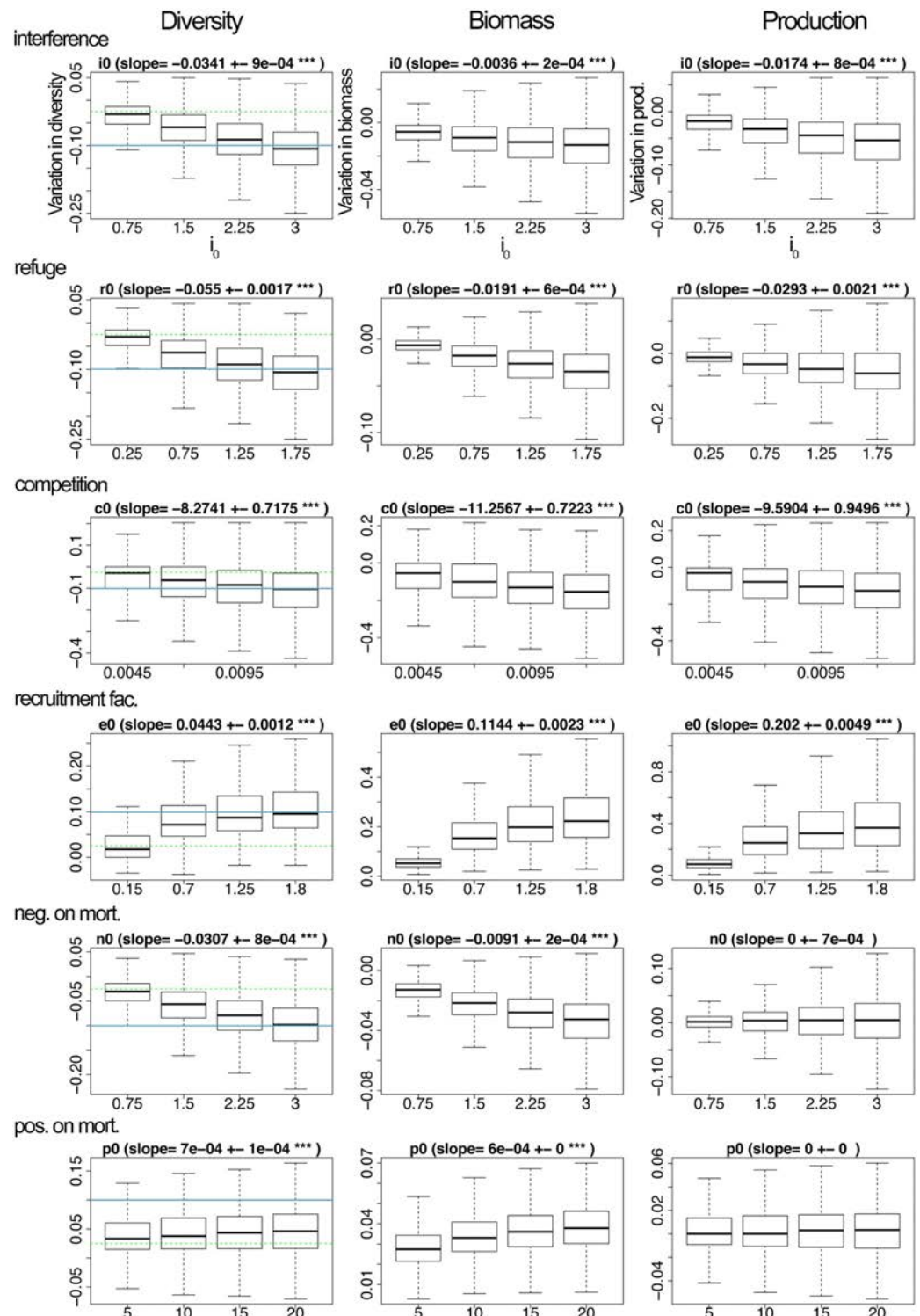
Fig 1. Changes in species diversity, biomass and production (in columns) as a function of the intensity of the NTI along the x-axis for each of the 6 NTIs (in rows). Values along the y-axis are evaluated at steady state in networks with NTIs compared to ones without NTIs. Values on the x-axis correspond to values of the parameters i_0 for interference, r_0 for refuge provisioning, c_0 for competition for space, e_0 for recruitment facilitation, n_0 for increase in mortality (i.e. negative effects on mortality), p_0 for decrease in mortality (i.e. positive effects on mortality). For each NTI, their minimum and maximum values

206

along the x-axis were chosen such that it lead to a ±2.5% (green dashed line; minimum value of the parameter range) to ±10% (blue line; maximum value of the parameter range) change in species diversity, relatively to the case without NTI. Note that the y-axes of the different panels differ. The NTIs were categorized into 'positive' (i.e. beneficial, recruitment facilitation) vs 'negative' (i.e. detrimental; interference, refuge provisioning, competition for space and increase in mortality) based on their effect on diversity.

interaction probabilities, we created setups with 100 positive links and 100 negative links (100 of one type or about 25 for each of the four types), 50 and 100, or 100 and 50 respectively. Again we only retained networks with no disconnected plant at the end of the dynamical simulations with trophic and non-trophic links.

Simulation runs. We used the GNU Scientific Library (https://www.gnu.org/software/gsl/) solver with the embedded Runge-Kutta-Fehlberg (4,5) method. For each network, numerical simulations were run until steady state was reached (we set a maximum time $t = 5000$ which we observed to be sufficient). During the dynamics, we set a species to extinction when its biomass was very small (<1e-6). To fairly compare results with and without non-trophic interactions, we used the same initial conditions in both cases. At steady state, we measured: diversity, i.e. the number of surviving species (biomass> = 1e-6), total biomass (sum of the biomass of all surviving species at steady state) and total production (the sum of the intrinsic growth of basal species and food uptake minus the respiration of consumers, over all surviving species, i.e. first term in Eq (4)). We also evaluated the normalized ratio of each of
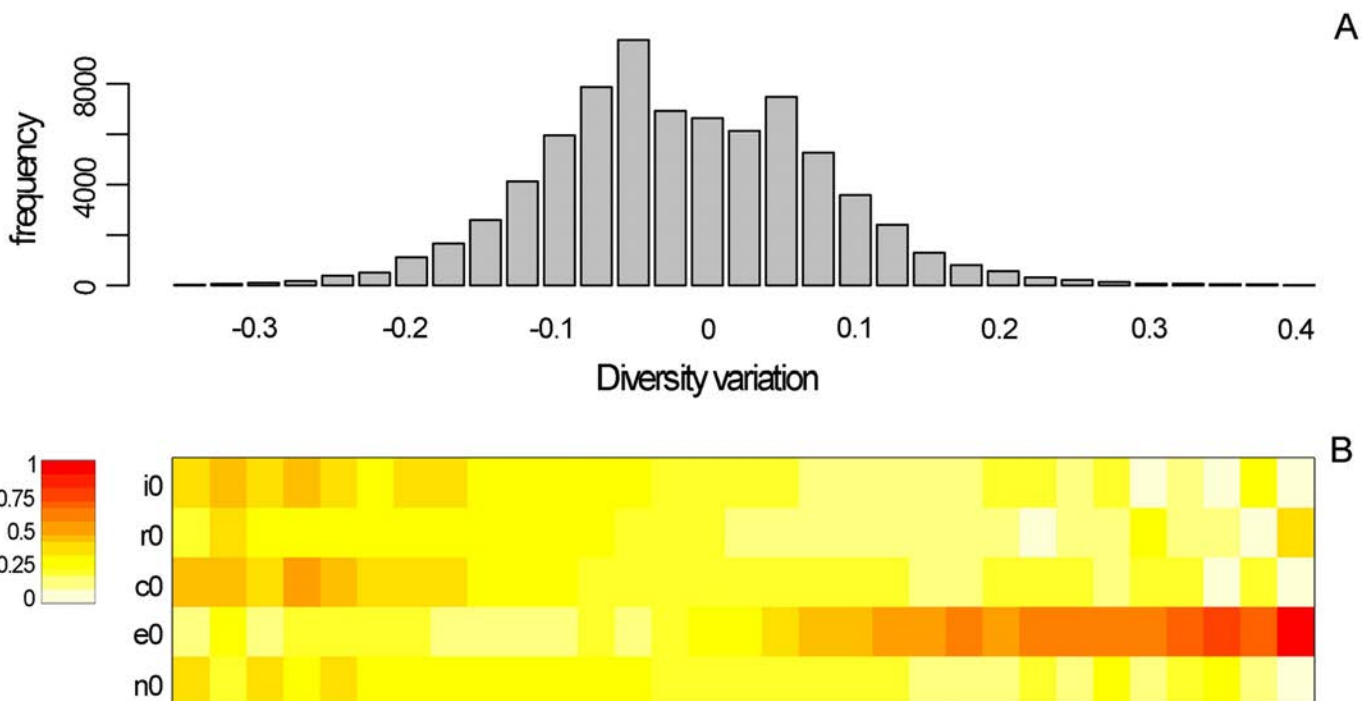

Fig 2. Effect of the NTIs on diversity ratio. A) Frequency of simulations leading to a given variation of diversity (x-axis) in networks with trophic links only compared to those with both trophic and non-trophic links. In these simulations, NTI intensities were picked randomly at the start of the simulation in the ranges defined in Fig 1. B) Average values of each of the NTI parameters corresponding to the simulations of A (mean parameter value used for the simulations leading to each of the bar in A). Colors range from light yellow for small average values to red for strong average values. i_0: intensity of interference among predators, r_0: intensity of refuge provisioning, c_0: intensity of competition for space, e_0: intensity of facilitation for recruitment, n_0: intensity of increase in mortality. Insert on the top left of panel B represents the normalized color range of the parameter value used (1 for the maximal value used, and 0 for the minimum value used within the parameter ranges defined in Fig 1).
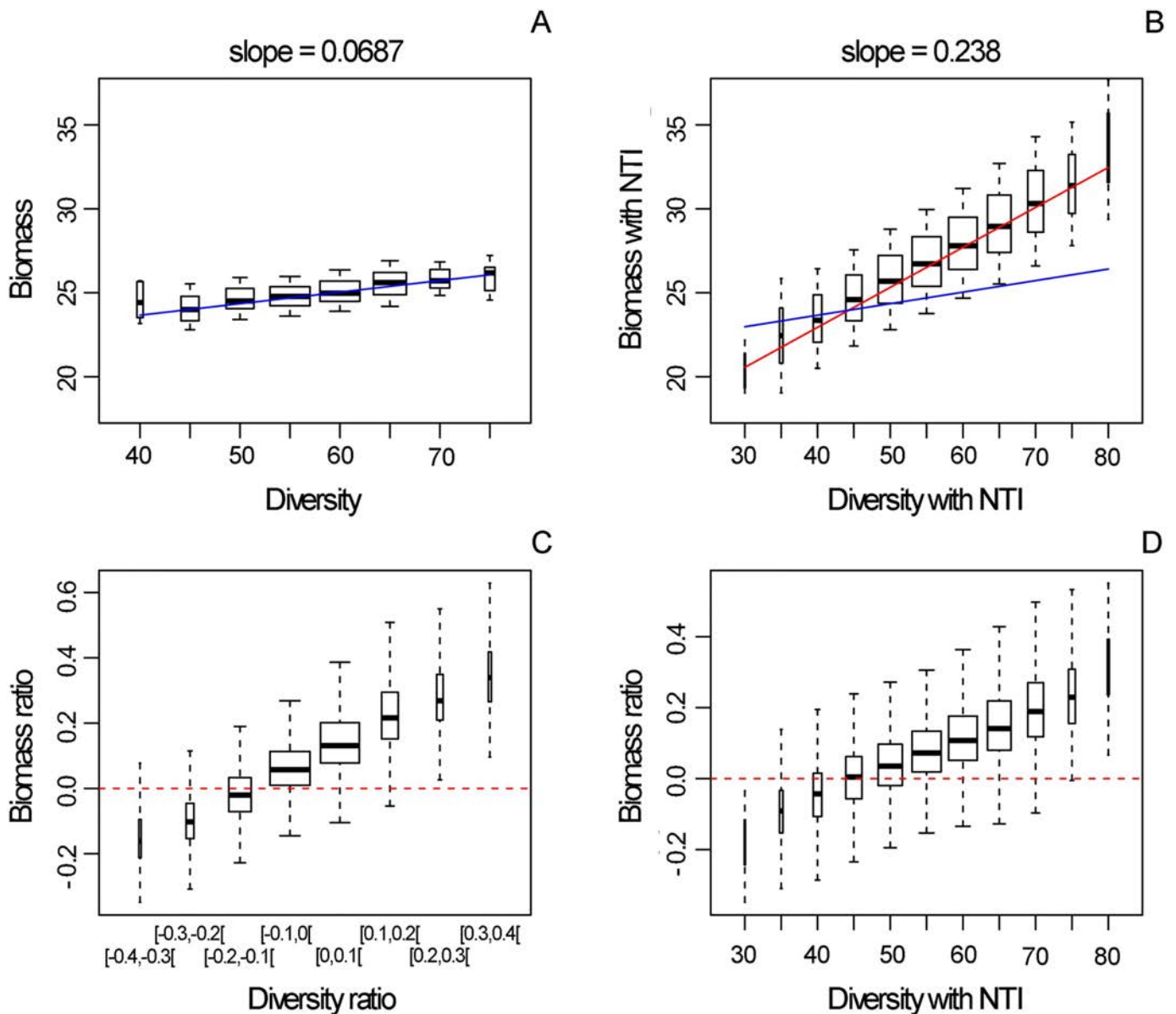
207

Fig 3. Relationships between species diversity and biomass in networks with compared to without NTIs. Values of all NTIs intensities were taken randomly in a given range (see Methods). A) Biomass as a function of species diversity (number of species) in networks with trophic interactions only (regression line in blue). B) Same as A in networks with NTIs (regression line in red; regression line from A) is also superimposed in blue). C) Variation in biomass (in networks with NTIs compared to networks with TI only; see Methods) as a function of the variation in species diversity (in networks with NTIs compared to networks with TI only; see Methods). D) Variation in biomass as a function of species diversity in networks with NTIs.

these metrics in the case with and without non-trophic interactions. For instance, we call *diversity ratio* (in particular in the legends of the figures) the difference between the diversity with and without non-trophic interactions divided by the diversity without non-trophic interactions.

Parameter values used.

- ϵ_{0_j} was set to 0.45 if the resource j is a plant and to 0.85 otherwise;

208

- r_i is the intrinsic growth rate of plant species with $r_i = r_0 m_i^{-0.25}$ if species i is a plant, and $r_i = 0$ for consumer species [46]; The unit of r_i is $[time]^{-1}$ and r_0 is a scaling parameter which is the same for all species and has the unit $\frac{[mass]^{0.25}}{[time]}$ (it defines the time scale of the system). $r_0 = 1$.

- x_i is the metabolic demand of species i. If i is not a plant $x_i = x_{species} m_i^{-0.25}$ with $x_{species} = 0.314$.

- d_i the natural mortality of species i is assumed to be $d_0 x_{species} m_i^{-0.25}$ with $d_0 = 0.1$ and $x_{species} = 0.138$ if i is a plant and 0.314 otherwise.

- K_i the carrying capacity of the environment for species i (in $\frac{[g]}{[area]}$); $K_i = K_0 m_i^{0.25}$ with $K_0 = 1$.

- w_i, the relative consumption rate; it is defines as 1/(number of resources of species i);

- a_{ij} is the capture coefficient, such that if i and j are both mobile species: $a_{ij} = a_0 m_i^{exp1} m_j^{exp2}$ [47] with $exp1 = 0.45$, $exp2 = 0.15$ and $a_0 = 50$; if i is sessile and j is mobile: $a_{ij} = a_{0_{sesscons}} m_j^{exp2}$ with $a_{0_{sesscons}} = 50$; if i is mobile and j is sessile: $a_{ij} = a_{0_{sessres}} m_i^{exp1}$ with $a_{0_{sessres}} = 50$.

- $1 + q$ is the Hill-exponent; $1 + q = 1.5$.

- h_{ij} is the handling time in $[time]$, with $h_i = h_0 m_i^{-0.48} m_j^{-0.66}$ and $h_0 = 0.3$ [40, 48].

- γ_{ij}, the effect strength of competition for space of species j on species i, is assumed to depend on body mass such that $\gamma_{ij} = \gamma_0 m_j^{\frac{2}{3}}$, with $\gamma_0 = 1$.

- δ_{ij} is the term of interference between predator i and predator j; we assume that the more similar the body masses of the two predators, the stronger the interference between them, such that $\delta_{ij} = \frac{1}{1 + abs(log(m_i) - log(m_j))}$.

- We make the non-trophic interaction intensities vary in the following ranges: $0.75 \leq i_0 \leq 3$ for inter-specific interference, and $i_0 = 0.8$ for intra-specific interference [39]), $0.25 \leq r_0 \leq 1.75$, $0.0045 \leq c_0 \leq 0.012$, $0.15 \leq e_0 \leq 1.8$, $0.75 \leq n_0 \leq 3$ and $5 \leq p_0 \leq 20$.

- Body mass of each of the species in the networks were determined based on the trophic level: $m_i = expo^{(TL_i - 1)}$, with $expo = 50$, TL_i the trophic level of species i.

Parameter values used in the sensitivity analysis. In order to perform the sensitivity analysis shown in S5 Fig, we varied the most influential parameters in the model:

- the Hill exponent was tested with $q = 0.3$ and 0.7 (in addition to the value 0.5 used for the main simulation)

- we tested $a_0 = a_{0_{sesscons}} = a_{0_{sessres}} = 10$ (in this case, we had to set $h_0 = 0.1$ to avoid massive extinctions) and 250 (in addition to the value 50 used for the main simulation)

- the parameter $expo$ was set to 25 and 75 (in addition to the value 50 used for the main simulation)

We focused on these three parameters because they are linked with both the largest variation in real ecological systems and the largest measurement uncertainties. Also, they are known to strongly affect biomass flow patterns and dynamical stability in food webs. Others parameters of the bioenergetics model are either fixed by defining the scales for time and biomass density (e.g. r_0) or do not show much variation in natural systems (e.g. the assimilation efficiencies).

209

The ranges over which the parameters were varied in the sensitivity analysis were chosen as broad as possible, but with the constraint of still enabling enough species survival in the food webs (i.e. in the networks without NTIs). This restriction is useful as the aim of this study is not to explore conditions for persistence in food web models, but to focus on the effect NTIs have on diversity, ecosystem functioning, and the relationship between both.

Results

In what follows, we use NTI(s) to refer to non-trophic interaction(s).

Effect of the presence and intensity of each NTI

We ran community dynamics with or without NTIs, and evaluated the relative difference in community characteristics at steady state obtained in the presence compared to in the absence of each NTI. This allowed comparing the effects of the different NTI types (for a range of interaction intensities; see Methods). At steady state, the measured characteristics of the communities were: species diversity (the number of species which survived at steady-state, i.e. whose biomass was above a threshold level), total biomass (the sum of the biomass of all surviving species at steady state) and total production (the sum of the intrinsic growth of basal species and food uptake minus respiration of consumers, over all surviving species; first term in Eq (4) in Methods, 'The dynamical model').

The following NTIs were introduced, one at a time, in the consumer-resource model: i) predator interference, which can occur between two predators which share at least one prey, ii) refuge provisioning which can happen if a species protects another from its predator (e.g. affecting the attack rate of the predator), iii) competition for space which occurs predominantly between sessile species, iv) recruitment facilitation which happens when some species increase the recruitment of new plants in the community (e.g. by habitat amelioration), v) increases in mortality when some species decrease the survival of others (e.g. because of whiplash) and vi) decreases in mortality when some species increase the survival of others (e.g. by improving the local environmental conditions).

We found that interference had a negative effect on diversity and community production and a weak (negative) effect on biomass (1st row of Fig 1). Through time, interference decreased the consumption of some of the predators; this initially favored some of the basal and intermediate species (that were less consumed), and eventually lead to the extinction of some of the intermediate and top predators, as well as to a decrease in their total biomass (1st rows in S1 and S2 Figs). Primary producers, some of which were relieved from consumers, exhibited a slight gain in biomass.

Refuge provisioning had similar overall effects, but with a larger effect on biomass than the one of interference (2nd row of Fig 1). In this case, species benefiting from refuges remained in the system but were less accessible resources. This lead to a loss of biomass and subsequent extinctions of some consumers (which could not access their prey; especially top predators), while their resources remained under protection and gained a bit of biomass (except for those whose protector went extinct) (see S1 and S2 Figs, 2nd row).

Competition for space had a strong negative effect on all variables (which affected all trophic levels), while recruitment facilitation had a positive effect on all community characteristics (but affected only consumer and predator species; 3rd and 4th rows of Fig 1 and S2 Fig). Through time, these effects tend to first affect the basal species, then the intermediate and eventually the top predators (see S1 Fig).

Modifications of mortality rates produced very weak effects overall. Increasing mortality had a negative effect on diversity and biomass and no effect on production (5th row of Fig 1).

Decreasing mortality had a very weak positive effect on diversity and biomass and no effect on production (6th row of Fig 1).In what follows, we did not consider decreases in mortality (also referred to as 'positive effects on mortality') which was the weakest of all NTIs considered overall and focused instead on the five remaining NTIs, namely interference among predators, refuge provisioning, competition for space, recruitment facilitation, and increase in mortality (also referred to as 'negative effects on mortality').

Overall, the most influential NTIs among the ones studied were competition for space and recruitment facilitation, in terms of both diversity and functioning (see slopes linking the parameter values to see the extent of the effects in Fig 1). The effect of competition for space on diversity was two orders of magnitude larger than those of all the other NTIs (namely interference, refuge provisioning, recruitment facilitation and increase in mortality). Regarding biomass, the effect of competition for space was two orders of magnitude larger than the one of recruitment facilitation, which was itself an order of magnitude larger than the one of all the other NTIs (namely interference, refuge provisioning, and increase in mortality).

For all NTIs except for competition for space, effects seemed to be stronger on intermediate and top trophic levels at steady state (see S2 Fig). Regarding species diversity, this was partly due to the fact that plant species already all persisted with trophic interactions only, and—besides competition for space (and to a much lesser extent increases in mortality)—the other NTIs were not able to lead to plant extinctions, because their effects either corresponded to a decrease in plants consumption (interference, refuge) or to a positive effect on plants (recruitment facilitation, decrease in mortality). Therefore, the NTIs studied here had very little opportunities for affecting plant species diversity. Conversely, the NTIs studied had more leverage on intermediate and higher trophic levels where species did not all persist in webs with trophic interactions only, and where they could therefore either increase or decrease species diversity. Regarding biomass, effects seemed to first affect basal species but then climb up the food web to eventually affect the top predators more strongly (see S1 Fig).

This first set of simulations helped us categorize the NTIs studied into 'positive' (i.e. beneficial; recruitment facilitation) vs 'negative' (i.e. detrimental; interspecific predator interference, refuge provisioning, competition for space and increase in mortality) based on their effect on diversity.

Combined effects of the NTIs on species diversity

Next we mixed the five remaining NTIs together, with NTI intensities picked at random within predefined ranges to study the joint effect of the NTIs considered. These predifined ranges were chosen so that each NTI increases or decreases the diversity of the system by 2.5% to 10% compared to the case without NTI (see Methods and Fig 1). Pre-defining these ranges for each of the NTI taken individually allows to put all NTIs on comparable grounds.

Not unexpectedly, the effect of the presence of the NTIs depended on the relative number of links of the different NTIs and on their intensities. When all interaction types were together with an equal proportion of positive and negative NTIs, networks with NTIs tended to have a smaller species diversity than networks without NTIs (Fig 2A). In other words, NTIs lead to extinctions of species compared to simulations run with feeding interactions alone. There were also quite a few number of cases where the net effect on diversity was null.

There was nonetheless a large fraction of cases where NTIs tended to enhance species diversity; these were clearly cases where beneficial NTIs were present and strong (orange and red areas on Fig 2B). It was noteworthy that the NTI values were all chosen at random for each of the simulations, so all combinations of intensity values were possible and present across

211

simulations, but our results showed that positive effects of NTIs on diversity always happened when the beneficial NTI (recruitment facilitation) was strong while the detrimental NTIs were weaker.

Now fixing the intensities of all NTI links to their maximum value (corresponding to a 10% effect on diversity ratio; see Fig 1) and focusing on their relative abundance, we found that a greater number of recruitment facilitation links tend to favor positive effects on diversity while increasing the number of interference, refuge or competitive links pushed toward negative effects on diversity (S3 Fig).

Combined effects of NTIs on the Biodiversity-Ecosystem functioning relationship

How did these effects on species diversity translate into community functioning? Using the previous simulations where NTI intensities were picked at random, we found that both in food webs (i.e. in ecological networks without NTIs) and in ecological networks with NTIs, the relationship between species diversity and biomass at steady state was positive (Fig 3A and 3B; this was also the case for production: see S4 Fig)Strikingly, in presence of NTIs, the relationship was significantly stronger than in their absence (ANCOVA p-value<1e-16; comparing slopes in Fig 3A and 3B). We checked that this result was robust to changes in the value of major parameters of the model (namely the Hill exponent which determines the shape of the functional response, the parameter *expo* which determines how species body mass depends on their trophic level, and the capture coefficient a_0 of consumers; S5 Fig).

Plotting the biomass ratio (i.e. the variation in biomass with NTIs compared to without NTIs) as a function of the species diversity ratio suggested that when NTIs contributed to a gain in species, this generally translated into a gain in biomass as well (Fig 3C). Actually, networks with NTIs tended to gain biomass (compared to networks without NTIs) even when there was no gain (or even a weak loss) in diversity (see boxes at diversity ratios of -0.1 and 0 in Fig 3C).When there was a small loss of diversity in presence of NTI (-0.1–0), the remaining species took advantage of these extinctions and gained biomass. When there was a gain in species diversity compared to the case without NTIs, this was often happening because of the presence of beneficial NTIs (Fig 2B), and those beneficial links lead to a considerable increase in biomass as well. There was, however, a large variability around these trends due to the fact that each simulation corresponded to a different combination of NTI intensities.

Discussion

Using a bioenergetic model in which six types of NTIs were incorporated, we found that these NTIs in isolation and jointly affected significantly species diversity and community functioning (biomass and production), consistently with previous studies addressing the role of the diversity of interaction types in module or network contexts [3, 10, 17–20, 23].

Overall, when taken together and with a balanced number of beneficial and detrimental interactions (as defined by their individual effects on diversity), the presence of NTIs tended to have a slightly negative effect on species diversity. This is in agreement with Goudard and Loreau [18] who studied NTIs that are modifications of feeding links; with equal numbers of positive and negative effects, they found a decrease in the total number of species when NTIs are incorporated. In our case, we did not expect this result since the range of NTI intensities spanned was selected such that each interaction type had equivalent effects on diversity when taken individually. Yet, despite controlling for both the number and the intensities of NTIs, the joint effect of the NTIs, when simultaneously incorporated in the model, tended to be negative for the species diversity of the resulting communities. It is noteworthy that the only

212

beneficial NTI studied in this model, recruitment facilitation, operates on a single trophic level, namely the plants. When considered alone (i.e. without any other NTI), we showed that the positive effect of recruitment facilitation on diversity of the entire networks was entirely due to indirect effects on consumer species (trophic level > 2, S2 Fig). Thus, the negative joint effect of NTIs on diversity suggests that recruitment facilitation has less leverage on diversity than the other NTIs, and more specifically, that the fact that its positive effect on diversity comes about only by indirectly affecting species on higher trophic levels, does not allow it to compensate for the more direct negative diversity effects of some of the detrimental NTIs.

Surprisingly, we found interference between predators to have a negative impact on diversity, which contrasts with other studies reporting stabilizing effects on population dynamics and positive effects on diversity [12, 49, 50] when interference is included via a Beddington-DeAngelis functional response [51, 52]. However, these studies included interference either as a purely intra-specific effect or assumed that intra-specific interference was stronger than inter-specific interference. Here, intra-specific interference was present in all simulations at a fixed value, and our aim was to study the effect of changes in the intensity of inter-specific interference. In this sense, our result that interference reduces diversity is reflecting classic results from competition theory, namely that competition is destabilizing if it is stronger between species than within species [53]. As interference was only included for predators that are already competing for at least one common prey species, the decline in diversity can be attributed to an increased effect of the competitive exclusion principle [54]. It has to be noted, however, that the complex network structure of trophic and non-trophic interactions provides a plethora of niches, which reduces the direct applicability of this principle [13].

Interestingly, we found that NTIs affected the relationship between diversity and functioning, and this result seems to be robust to changes in the value of key parameters of our model. Despite the array of possible effects from the NTIs, individually and combined, the relationship between species diversity and biomass was found to be significantly stronger in networks with NTIs than in networks without them. Again, this was not necessarily expected since simulations were run with all NTIs together, whose intensity values were picked at random in a range such that their effects on diversity was controlled; we could therefore have expected, e.g. compensatory or negative effects since most of the NTIs studied here tended to have negative effects on diversity (Fig 1). The effect of NTIs on the slope of the diversity-biomass relationship means that when species-rich networks gain even more species, that goes with a disproportionately higher gain in biomass in the presence than in the absence of NTIs. This also means that, conversely, species-poor communities lose more biomass with additional species loss with than without NTI. This is due to the fact that species-rich communities are communities in which beneficial interactions are present and strong, while species-poor communities are communities where detrimental NTIs operate. This result is interesting in that it suggests that species loss may have stronger consequences on community functioning than expected if ignoring non-feeding interactions. Further work is needed to see if this result extends to other models as well as to real ecosystems.

Of course, our study presents a number of limitations. The strongest NTIs studied here, namely competition for space and facilitation for recruitment, both affect mainly plants in our model. It is therefore unclear whether these NTI types appear to exert stronger effects because plants are the affected species. This could be a topic of further investigations.

Moreover, we have focused on a selection of six NTIs that are the major ones found to occur in the Chilean web [10, 22], but other interaction types not present in this data set are known to be frequent and important in nature. Examples include parasitism, effects on resource availability, plant dispersal or animal movement. Further work could introduce these other interactions in a single framework.

213

We also assumed here the intensity of the interactions between pairs of species to be constant through time. Some interactions may however be context-dependent (beyond the biomass or abundance of other species). For example, adaptive inducible defenses are a form of phenotypic plasticity that affects the strength of predator-prey interactions [55]. Changes in morphological, behavioral, or life-historical traits in response to chemical, mechanical or visual signals from predators have been reported in the literature for a number of organisms [56]. These responses can moreover occur with a lag, given that the expression of defenses may involve considerable time, relative to the organisms life-cycle [57]. The intensity, and even the type of interactions, could also change with e.g. changes in abiotic factors such as climate.

We have no information regarding the relative importance or intensities of the different interaction types. We proposed a way of putting all interaction types on equal footing regarding their effect on species diversity. This is however a debatable choice—we could for example have chosen to make NTIs comparable regarding their effect on biomass. In nature, it is likely that interaction intensities are not equivalent and that some of them are much stronger than others. Making progress along these lines requires experimental work aiming at quantifying different interactions types, which involves a number of challenges [1].

In this study, NTIs were plugged in the food web randomly although with a number of constraints based on our knowledge of the Chilean web [10, 22]. We did not explicitly investigate the role of the structure of the NTI network, despite the fact that previous studies have suggested that it might play an important role [10, 58]. This remains a difficult task since it can be necessary to take into account the dependency between the structure of the different layers (e.g. NTI types, as observed in [10]); however this is a promising avenue of future research.

Previous studies have used the community matrix approach focused on net effects between species to investigate the role of the diversity of interaction types [7, 20]. This approach has a number of advantages, including the fact that it allows analytical predictions and generalizations. Here, we chose to focus on a more mechanistic approach, starting from the mechanism of the NTIs without assuming their net effect. For example, we had initially assumed that refuge provisioning would be a beneficial NTI, meaning that it would have a positive effect on species diversity. We however found the opposite in the model simulations—indeed, refuge provisioning protects prey from their consumers but it also deprives consumers from their resource and it seems that this latter effect has stronger consequences at the community scale. In a dynamical model, Gross [19] showed that interspecific facilitation among plants allowed the maintenance of species diversity despite the fact that the net effects measured among plants remained negative. These results highlight that insights gained from the analysis of few-species systems cannot be easily translated into the dynamics of complex communities. Focusing on the net effects between species may conceal important coexistence mechanisms when species simultaneously engage in both detrimental and beneficial interactions and stresses the importance of working with mechanistic models to better understand the consequences of NTIs for community diversity and functioning. Nonetheless, a more mechanistic approach implies, for each of the NTI identified, to model it in one specific way, matching our knowledge of how these interactions operate in nature (in our case here, having the Chilean web in mind [10, 22]). For example, regarding refuge provisioning, alternative ways of how it could affect trophic interactions are certainly conceivable. It could increase the Hill coefficient of all predators of the protected prey, e.g. to mimic the fact that prey at low density would become better protected, but if prey density is too high, the predators would still see them. This could have a different effect on diversity than found here.

Our study is a step toward getting a better understanding of the dynamics of multiplex ecological networks (i.e. including several interaction types among a set of species), and more precisely of the role of NTIs on community functioning. Our model results suggest that, when

214

simultaneously included, and assembled according to simple rules reflecting observations in nature, NTIs tend to mechanically strengthen the BEF, making the dependency between the number of species present in the community and the functioning of this community (in terms of biomass or production) stronger. This result has important consequences for predicting the consequences of species loss on community functioning.

Supporting information

S1 Fig. Relative change in species diversity (left column) and biomass (right column) per trophic level through time for 500 simulations for the main NTI types (5 first rows) and the NTI all together (6th row). Each simulation starts with 600 trophic links and 100 non-trophic links. Note that on the *x*-axis, time is on a log-scale. Green: TL = 1, yellow: TL between 2 and 3, red: TL> 3. TL refers to the prey-averaged trophic level measured as one plus the mean trophic level of all the species resources, where the trophic level of a resource is the chain length from the resource to a basal species [59]. Species whose TL is 1 are primary producers.
(PDF)

S2 Fig. Relative change in each of the measured variables (3 columns) as a function of the intensity of the NTI by trophic level, for each NTI type (6 rows). Note that each NTI has its own y-axis. Green: TL = 1, yellow: TL between 2 and 3, red: TL> 3. TL refers to the prey-averaged trophic level measured as one plus the mean trophic level of all the species resources, where the trophic level of a resource is the chain length from the resource to a basal species [59]. Species whose TL is 1 are primary producers. Note that the y-axis differ for the different NTIs.
(PDF)

S3 Fig. Frequency of simulations leading to a given diversity ratio, i.e. variation in species diversity in the case with compared to without NTI links. (to match the term defined in the Methods**).** The intensity of each NTI type is now fixed and we vary the relative number of links of different NTI types when put together. The left column correspond to situations where there are twice more detrimental than beneficial links, the middle column shows results with equal number of beneficial and detrimental links, and the right column correspond to cases where there are twice more beneficial than detrimental links. The panels correspond to different combinations of NTIs: I for interference, E for recruitment facilitation, N for negative effects on mortality, R for refuge, C for competition. At fixed intensity and with equal number of links, detrimental links tend to take over (slightly). There are configurations of relative abundance of the different types of NTIs in which positive and negative effects can balance each other.
(PDF)

S4 Fig. Changes in production as a function of species diversity in networks with NTIs. Same as [Fig 3B](Fig 3B) but for production instead of biomass. The slope obtained by linear regression of the relationship is indicated on top of the panel.
(PDF)

S5 Fig. Sensitivity analysis of the result of [Fig 3A and 3B](Fig 3A and 3B) **to changes in the value of major parameters of the model, namely the Hill coefficient, which determines the shape of the functional response, the parameter *expo* which determines how species body masses depend on their trophic level, and the capture coefficient a_0 of the consumers.** See Methods, part 'The dynamical model', for more details about the parameters and how they contribute to

215

the dynamical equations. Independently of the combinations of parameter values found, the slope of the BEF is stronger in the presence than in the absence of NTIs.
(PDF)

Acknowledgments

Author Contributions

Conceptualization: Vincent Miele, Christian Guill, Rodrigo Ramos-Jiliberto, Sonia Kéfi.

Formal analysis: Vincent Miele, Sonia Kéfi.

Methodology: Vincent Miele, Christian Guill, Rodrigo Ramos-Jiliberto, Sonia Kéfi.

Software: Vincent Miele, Christian Guill, Sonia Kéfi.

Validation: Vincent Miele, Sonia Kéfi.

Visualization: Vincent Miele, Sonia Kéfi.

Writing – original draft: Sonia Kéfi.

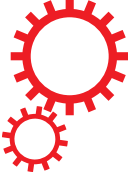**Writing – review & editing:** Vincent Miele, Christian Guill, Rodrigo Ramos-Jiliberto.

References

1. Berlow EL, Neutel AM, Cohen JE, de Ruiter PC, Ebenman B, Emmerson M, et al. Interaction strengths in food webs: issues and opportunities. Journal of Animal Ecology. 2004; 73:585–598. https://doi.org/10.1111/j.0021-8790.2004.00833.x

2. Ings TC, Montoya JM, Bascompte J, Blüthgen N, Brown L, Dormann CF, et al. Review: Ecological networks—beyond food webs. Journal of Animal Ecology. 2009; 78(1):253–269. https://doi.org/10.1111/j.1365-2656.2008.01460.x

3. Kéfi S, Berlow E, a Wieters E, Navarrete S, Petchey O, Wood S, et al. More than a meal: integrating non-feeding interactions into food webs. Ecology Letters. 2012; p. 291–300. https://doi.org/10.1111/j.1461-0248.2011.01732.x

4. de Ruiter PC, Neutel AM, Moore JC. Energetics, Patterns of Interaction Strengths, and Stability in Real Ecosystems. Science. 1995; 269:1257–1260. https://doi.org/10.1126/science.269.5228.1257 PMID: 17732112

5. Bascompte J, Jordano P, Melián CJ, Olesen JM. The nested assembly of plant–animal mutualistic networks. Proceeding of the National Academy of Sciences. 2003; 100:9383–9387. https://doi.org/10.1073/pnas.1633576100

6. Brose U, Berlow EL, Martinez ND. Scaling up keystone effects from simple to complex ecological networks. Ecology Letters. 2005; 8:1317–1325. https://doi.org/10.1111/j.1461-0248.2005.00838.x

7. Mougi A, Kondoh M. Diversity of Interaction Types and Ecological Community Stability. Science. 2012; 337(6092):349–351. https://doi.org/10.1126/science.1220529 PMID: 22822151

8. Sauve AMC, Fontaine C, Thébault E. Structure–stability relationships in networks combining mutualistic and antagonistic interactions. Oikos. 2014; 123(3):378–384. https://doi.org/10.1111/j.1600-0706.2013.00743.x

9. Lurgi M, Montoya D, Montoya JM. The effects of space and diversity of interaction types on the stability of complex ecological networks. Theoretical Ecology. 2016; 9(1):3–13. https://doi.org/10.1007/s12080-015-0264-x

10. Kéfi S, Miele V, Wieters EA, Navarrete SA, Berlow EL. How structured is the entangled bank? The surprisingly simple organization of multiplex ecological networks leads to increased persistence and resilience. PLOS Biology. 2016; 14:e1002527. https://doi.org/10.1371/journal.pbio.1002527 PMID: 27487303

11. McCann K, Hastings A, Huxel GR. Weak trophic interactions and the balance of nature. Nature. 1998; 395:794–798. https://doi.org/10.1038/27427

216

12. Brose U, Williams RJ, Martinez ND. Allometric scaling enhances stability in complex food webs. Ecology Letters. 2006; 9:1228–1236. https://doi.org/10.1111/j.1461-0248.2006.00978.x PMID: 17040325

13. Brose U. Complex food webs prevent competitive exclusion among producer species. Proceedings of the Royal Society B: Biological Sciences. 2008; 275:2507–2514. https://doi.org/10.1098/rspb.2008.0718 PMID: 18647714

14. Neutel AM, Heesterbeek JAP, de Ruiter PC. Stability in Real Food Webs: Weak Links in Long Loops. Science. 2002; 296(5570):1120–1123. https://doi.org/10.1126/science.1068326 PMID: 12004131

15. Neutel AM, Heesterbeek JAP, van de Koppel J, Hoenderboom G, Vos A, Kaldeway C, et al. Reconciling complexity with stability in naturally assembling food webs. Nature. 2007; 449:599–602. https://doi.org/10.1038/nature06154 PMID: 17914396

16. Stouffer DB, Bascompte J. Compartmentalization increases food-web persistence. Proceedings of the National Academy of Sciences. 2011; 108(9):3648–3652. https://doi.org/10.1073/pnas.1014353108

17. Arditi R, Michalski J, Hirzel AH. Rheagogies: Modelling non-trophic effects in food webs. Ecological Complexity. 2005; 2:249–258. https://doi.org/10.1016/j.ecocom.2005.04.003

18. Goudard A, Loreau M. Nontrophic Interactions, Biodiversity, and Ecosystem Functioning: An Interaction Web Model. The American Naturalist. 2008; 171(1):91–106. https://doi.org/10.1086/523945 PMID: 18171154

19. Gross K. Positive interactions among competitors can produce species–rich communities. Ecology Letters. 2008; 11(9):929–936. https://doi.org/10.1111/j.1461-0248.2008.01204.x

20. Allesina S, Tang S. Stability criteria for complex ecosystems. Nature. 2012; 483(7388):205–208. https://doi.org/10.1038/nature10832 PMID: 22343894

21. Suweis S, Grilli J, Maritan A. Disentangling the effect of hybrid interactions and of the constant effort hypothesis on ecological community stability. Oikos. 2014; 123(5):525–532. https://doi.org/10.1111/j.1600-0706.2013.00822.x

22. Kéfi S, Berlow EL, Wieters EA, Joppa LN, Wood SA, Brose U, et al. Network structure beyond food webs: mapping non-trophic and trophic interactions on Chilean rocky shores. Ecology. 2015; 96:291–303. https://doi.org/10.1890/13-1424.1

23. García-Callejas D, Molowny-Horas R, Araújo MB. The effect of multiple biotic interaction types on species persistence. Ecology. 2018; 99(10):2327–2337. https://doi.org/10.1002/ecy.2465 PMID: 30030927

24. González-Olivares E, Ramos-Jiliberto R. Dynamic consequences of prey refuges in a simple model system: more prey, fewer predators and enhanced stability. Ecological Modelling. 2003; 166(1):135–146. https://doi.org/10.1016/S0304-3800(03)00131-5

25. Garay-Narváez L, Ramos-Jiliberto R. Induced defenses within food webs: The role of community trade-offs, delayed responses, and defense specificity. Ecological Complexity. 2009; 6(3):383–391. https://doi.org/10.1016/j.ecocom.2009.03.001

26. Lin Y, Sutherland WJ. Color and degree of interspecific synchrony of environmental noise affect the variability of complex ecological networks. Ecological Modelling. 2013; 263:162–173. https://doi.org/10.1016/j.ecolmodel.2013.05.007

27. Loreau M. From populations to ecosystems: theoretical foundations for a new ecological synthesis. Princeton University Press; 2010.

28. Tilman D. The ecological consequences of changes in biodiversity: a search for general principles. Ecology. 1999; 80:1455–1474. https://doi.org/10.1890/0012-9658(1999)080%5B1455:TECOCI%5D2.0.CO;2

29. McCann KS. The diversity–stability debate. Nature. 2000; 405:228–233. https://doi.org/10.1038/35012234

30. Loreau M. Biodiversity and ecosystem functioning: Current knowledge and future challenges. Science. 2001; 294:804–808. https://doi.org/10.1126/science.1064088 PMID: 11679658

31. Naeem S. Ecosystem consequences of biodiversity loss: The evolution of a paradigm. Ecology. 2002; 83:1537–1552. https://doi.org/10.1890/0012-9658(2002)083%5B1537:ECOBLT%5D2.0.CO;2

32. Hooper DU. Effects of biodiversity on ecosystem functioning: A consensus of current knowledge. Ecological Monographs. 2005; 75:3–35. https://doi.org/10.1890/04-0922

33. Cardinale BJ, Duffy JE, Gonzalez A, Hooper DU, Perrings C, Venail P, et al. Biodiversity loss and its impact on humanity. Nature. 2012; 486:59–67. https://doi.org/10.1038/nature11148 PMID: 22678280

34. Tilman D, Reich PB, Knops J, Wedin D, Mielke T, Lehman C. Diversity and productivity in a long-term grassland experiment. Science. 2001; 294:843–845. https://doi.org/10.1126/science.1060391 PMID: 11679667

217

35. Spehn EM, Hector A, Joshi J, Scherer-Lorenzen M, Schmid B, Bazeley-White E, et al. Ecosystem effects of biodiversity manipulations in European grasslands. Ecological Monographs. 2005; 75(1):37–63. https://doi.org/10.1890/03-4101

36. Loreau M. Biodiversity and ecosystem functioning: A mechanistic model. Proceedings of the National Academy of Sciences. 1998; 95(10):5632–5636. https://doi.org/10.1073/pnas.95.10.5632

37. Thébault E, Loreau M. Food-web constraints on biodiversity–ecosystem functioning relationships. Proceedings of the National Academy of Sciences. 2003; 100(25):14949–14954. https://doi.org/10.1073/pnas.2434847100

38. Thébault E, Loreau M. Trophic Interactions and the Relationship between Species Diversity and Ecosystem Stability. The American Naturalist. 2005; 166(4):E95–E114. https://doi.org/10.1086/444403 PMID: 16224699

39. Schneider FD, Brose U, Rall BC, Guill C. Animal diversity and ecosystem functioning in dynamic food webs. Nature Communications. 2016; 7:12718. https://doi.org/10.1038/ncomms12718 PMID: 27703157

40. Yodzis P, Innes S. Body size and consumer-resource dynamics. The American Naturalist. 1992; 139:1151–1175. https://doi.org/10.1086/285380

41. Williams RJ, Martinez ND. Stabilization of chaotic and non-permanent food-web dynamics. The European Physical Journal B—Condensed Matter and Complex Systems. 2004; 38(2):297–303. https://doi.org/10.1140/epjb/e2004-00122-1

42. Williams RJ, Martinez ND. Simple rules yield complex food webs. Nature. 2000; 404:180–183. https://doi.org/10.1038/35004572 PMID: 10724169

43. Real LA. The kinetics of functional response. The American Naturalist. 1977; 111:289–300. https://doi.org/10.1086/283161

44. Skalski GT, Gilliam JF. Functional responses with predator interference: viable alternatives to the holling type II model. Ecology. 2001; 82:3083–3092. https://doi.org/10.1890/0012-9658(2001)082%5B3083:FRWPIV%5D2.0.CO;2

45. Dunne JA, Williams RJ, Martinez ND. Food-web structure and network theory: The role of connectance and size. Proceedings of the National Academy of Science of the United States of America. 2002; 99:12917–12922. https://doi.org/10.1073/pnas.192407699

46. Brown JH, Gillooly JF, Allen AP, Savage VM, West GB. Toward a metabolic theory of ecology. Ecology. 2004; 85:1771–1789. https://doi.org/10.1890/03-9000

47. Peters RH. The ecological implications of body size. Cambridge University Press; 1983.

48. Rall BC, Brose U, Hartvig M, Kalinkat G, Schwarzmüller F, Vucic-Pestic FO, Petchey OL. Universal temperature and body-mass scaling of feeding rates. Philosophical Transactions of the Royal Society B. 2012; 367(1605):2923–2934. https://doi.org/10.1098/rstb.2012.0242

49. Rall BC, Guill C, Brose U. Food-web connectance and predator interference dampen the paradox of enrichment. Oikos. 2008; 217:202–213. https://doi.org/10.1111/j.2007.0030-1299.15491.x

50. Guill C, Drossel B. Emergence of complexity in evolving niche-model food webs. Journal of Theoretical Biology. 2008; 251:108–120. https://doi.org/10.1016/j.jtbi.2007.11.017 PMID: 18164730

51. Beddington JR. Mutual interference between parasites or predators and its effect on searching efficiency. Journal of Animal Ecology. 1975; 44:331–340. https://doi.org/10.2307/3866

52. DeAngelis DL, Goldstein RA, O'Neill RV. A model for tropic interaction. Ecology. 1975; 56:881–892. https://doi.org/10.2307/1936298

53. Gause GF. The struggle for existence. The Williams and Wilkins Company, Baltimore; 1934. https://doi.org/10.5962/bhl.title.4489

54. Hardin G. The competitive exclusion principle. Science. 1960; 131:1292–1297. https://doi.org/10.1126/science.131.3409.1292 PMID: 14399717

55. Valdovinos FS, Ramos-Jiliberto R, Garay-Narváez L, Urbani P, Dunne JA. Consequences of adaptive behaviour for the structure and dynamics of food webs. Ecology Letters. 2010; 13(12):1546–1559. https://doi.org/10.1111/j.1461-0248.2010.01535.x PMID: 20937057

56. Aránguiz-Acuña A, Ramos-Jiliberto R, Bustamante RO. Experimental evidence that induced defenses promote coexistence of zooplanktonic populations. Journal of Plankton Research. 2010; 33(3):469–477.

57. Aránguiz-Acuña A, Ramos-Jiliberto R, Sarma N, Sarma Sss, Bustamante R, Toledo V. Benefits, costs and reactivity of inducible defences: an experimental test with rotifers. Freshwater Biology. 2010; 55(10):2114–2122. https://doi.org/10.1111/j.1365-2427.2010.02471.x

58. Melián CJ, Bascompte J, Jordano P, Krivan V. Diversity in a complex ecological network with two interaction types. Oikos. 2009; 118(1):122–130. https://doi.org/10.1111/j.1600-0706.2008.16751.x

59. Williams RJ, Martinez ND. Trophic levels in complex food webs: theory and data. American Naturalist. 2004; 163:458–468. https://doi.org/10.1086/381964

218

SCIENTIFIC REPORTS

OPEN

The effects of functional diversity on biomass production, variability, and resilience of ecosystem functions in a tritrophic system

Ruben Ceulemans, Ursula Gaedke, Toni Klauschies & Christian Guill

Diverse communities can adjust their trait composition to altered environmental conditions, which may strongly influence their dynamics. Previous studies of trait-based models mainly considered only one or two trophic levels, whereas most natural system are at least tritrophic. Therefore, we investigated how the addition of trait variation to each trophic level influences population and community dynamics in a tritrophic model. Examining the phase relationships between species of adjacent trophic levels informs about the strength of top-down or bottom-up control in non-steady-state situations. Phase relationships within a trophic level highlight compensatory dynamical patterns between functionally different species, which are responsible for dampening the community temporal variability. Furthermore, even without trait variation, our tritrophic model always exhibits regions with two alternative states with either weak or strong nutrient exploitation, and correspondingly low or high biomass production at the top level. However, adding trait variation increased the basin of attraction of the high-production state, and decreased the likelihood of a critical transition from the high- to the low-production state with no apparent early warning signals. Hence, our study shows that trait variation enhances resource use efficiency, production, stability, and resilience of entire food webs.

Functional diversity has proven to be important for linking community structure to ecosystem functions such as biomass production and resource use efficiency[1–4]. Our understanding of the multifaceted impact of functional diversity on ecosystem functioning, and on the dynamics of populations and communities has been greatly advanced by adopting a trait-based point of view[5,6]. In particular, functional traits link morphological, physiological or phenological features of a species to a certain community or ecosystem function[7]. A prevalent example is simply body size, which is related to several functions such as growth (larger organisms tend to grow slower), prey preference (predators tend to be larger than their prey), or nutrient uptake (larger cells have higher nutrient demands)[8–11]. Trait-based models of simple food web modules have facilitated detailed mechanistic understanding of dynamics observed in the laboratory[12] and in the field[13]. For example, observed anti-phase predator-prey cycles between zooplankton and algae have been attributed to the co-occurrence of fast-growing undefended and slow growing, well defended prey phenotypes[14,15].

However, such trait-based models have mainly been restricted to describing trait variation on one or two trophic levels[13,16–18]. Likewise, only up until recently, empirical studies on functional diversity have been limited to considering trait variation in only autotrophs (plants or algae)[19,20], or both autotrophs and herbivores[21,22], with few exceptions[23]. This strongly contrasts with the fact that natural food webs are in general complex multitrophic networks[24]. Focusing only on direct, bitrophic predator-prey interactions neglects the intricate effects of more complex, partly indirect interactions spanning multiple trophic levels, such as trophic cascades[25]. These multi-trophic effects may be very important factors affecting the relevant ecosystem functions[26–28]. For instance, the total number of trophic levels may strongly influence the efficiency of nutrient exploitation[29]. In addition, as predation is an important factor in many food webs, trait variation on the predator level is expected to have an important influence on ecosystem functioning[4,20,30]. Hence, including additional trophic levels with functional diversity is a very natural step towards improving the accuracy and descriptive power of trait-based models.

Institute of Biochemistry and Biology, University of Potsdam, Maulbeerallee 2, Potsdam, 14469, Germany. Correspondence and requests for materials should be addressed to R.C. (email: ceulemans@uni-potsdam.de)
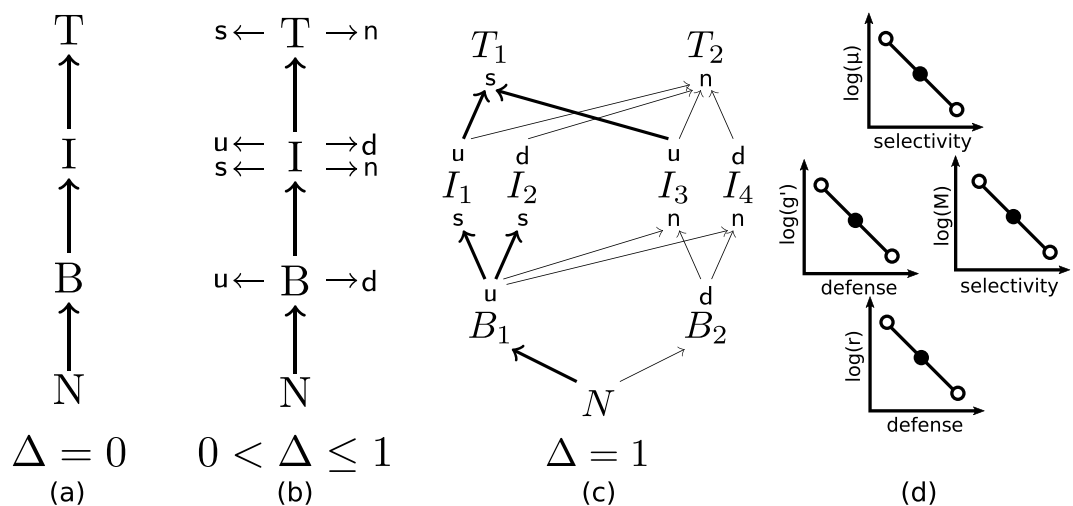
219

Figure 1. (**a**) A simple linear tritrophic chain, where nutrients N are taken up by a basal species B, which is grazed by an intermediate species I, which in turn is consumed by a top species T. (**b**) Gradually introducing trait variation, where species can be undefended (u) or defended (d) against predators, and/or selective (s) or non-selective (n) consumers, starting from a linear chain. (**c**) Maximally trait-separated food web model. The basal and top species have only one trait, but the intermediate species have two. The thickness of the arrows indicates the intensity of the trophic interaction, reflecting that selective consumers can exploit their limited resources spectrum more efficiently. (**d**) Schematic shape of the trade-off curves for the top species (top row), intermediate species (middle row), and basal species (bottom row). The solid circles indicate that for $\Delta = 0$, all species on a given trophic level have the same trait values, whereas the open circles demonstrate how the trait values between the species differ as Δ is increased to one.

We developed a tritrophic model to study the effects of trait variation at all trophic levels on food web dynamics. Particularly, the dynamics of a simple tritrophic linear food chain will be compared to a tritrophic food web where prey species are either defended or undefended, and predator species are either selective or non-selective feeders. Trade-offs between these traits are explicitly built in such that defended prey have a lower growth rate, and selective feeders have a lower half-saturation constant to allow for efficient feeding at low prey densities[13,31,32]. Our model structure allows for a gradual increase of the trait differences between the species at each trophic level, from a simple linear chain up to a fully separated food web with maximal trait differences (Fig. 1). As the trait differences increase, the species will fulfill increasingly different functions; in this way, we are able to link trait differences to functional diversity.

We use the tritrophic model to investigate how an increasing degree of trait variation affects:

- the production of the system;
- the efficiency of the energy transfer towards the higher trophic levels;
- the temporal biomass variability at the population and community level; and
- the dynamic properties and the resilience of alternative stable system states.

Our results provide theoretical evidence that trait variation has a significant impact on all of these properties. To the best of our knowledge, we present the first systematic, multi-trophic study which mechanistically explains such patterns and explicitly discusses their relevance to ecosystem functions and stability.

Methods

We developed a tritrophic model where basal species are consumed by intermediate species, which in turn are consumed by top species. The species biomass densities are denoted by B, I, and T, respectively. In addition, the uptake of a limiting nutrient with concentration N (in this case nitrogen) by the basal species is modeled explicitly. We assume a chemostat environment, which causes all nutrients and biomass of species to be washed out at an equal rate, δ, the dilution rate. The washed out volume is replaced by new medium rich in nutrients.

Model equations. As in[13,33], we include two relevant functional traits. The prey species B and I may be defended against predation: specifically, there will be defended (d) and undefended (u) species. Investing in a defense strategy requires sacrificing a certain amount of resources which could have otherwise been put into growth. Hence, the defended species have a lower growth rate than the undefended species, but are rewarded by being insusceptible to certain consumers. The consumer species I and T are able to specialize feeding on a certain prey species, leading to selective (s) and non-selective (n) species. Here, the non-selective consumer species consume all species on the trophic level below. In contrast, the selective species are only able to consume the undefended prey species, but they are able to exploit low food densities at a higher rate, reflected in a lower half-saturation constant.

Representing each possible trait combination on all trophic levels by one species leads to a food web with two basal species, four intermediate species and two top species (Fig. 1c). In order to write down the equations compactly, the following equivalence is explicitly stated:

$$B^{\mathrm{u}} \equiv B_1, \quad B^{\mathrm{d}} \equiv B_2, \quad I_{\mathrm{s}}^{\mathrm{u}} \equiv I_1, \quad I_{\mathrm{s}}^{\mathrm{d}} \equiv I_2 \tag{1}$$

$$I_{\mathrm{n}}^{\mathrm{u}} \equiv I_3, \quad I_{\mathrm{n}}^{\mathrm{d}} \equiv I_4, \quad T_{\mathrm{s}} \equiv T_1, \quad T_{\mathrm{n}} \equiv T_2. \tag{2}$$

In their most general form, the equations used have the following shape:

$$
\begin{cases}
\dot{N} &= \delta(N_0 - N) - \dfrac{c_N}{c_C}\sum_i r_i B_i \\
\dot{B}_i &= r_i B_i - \sum_j g_{ji} I_j - \delta B_i \\
\dot{I}_j &= e\sum_i g_{ji} I_j - \sum_i \gamma_{ij} T_i - \delta I_j \\
\dot{T}_i &= \varepsilon \sum_j \gamma_{ij} T_i - \delta T_i
\end{cases}
\tag{3}
$$

with $i \in \{1, 2\}$, $j \in \{1, 2, 3, 4\}$, where N_0 denotes the incoming nutrient concentration. Following typical experimental conditions, we assume nitrogen as the limiting nutrient (N). Hence, the nutrients are measured in nitrogen concentration, as compared to carbon for biomass, therefore, the nitrogen-to-carbon weight ratio (c_N/c_C) is required to scale the basal (B_i) growth terms. Moreover, the basal growth rate r_i is described by a Monod function[34,35], with maximum growth rate r'_i and a nutrient-uptake half-saturation constant h_N. The intermediate and top species have a generalized Holling-type-III functional response, with maximum growth rates g'_j and γ'_i, half-saturation constants M and μ, and Hill coefficients h and η, respectively[36,37]. This means:

$$r_i = r'_i \frac{N}{N + h_N} \tag{4}$$

$$g_{ji} = g'_j \frac{(p_{ji} B_i)^h}{\sum_{i'} (p_{ji'} B_{i'})^h + 1} \tag{5}$$

$$\gamma_{ij} = \gamma'_i \frac{(\phi_{ij} I_j)^{\eta}}{\sum_{j'} (\phi_{ij'} I_{j'})^{\eta} + 1}, \tag{6}$$

and,

$$
p = \begin{array}{c} \quad B^{\mathrm{u}} \quad\quad B^{\mathrm{d}} \\ \begin{pmatrix} \frac{1}{M_{\mathrm{u,s}}} & \frac{1}{M_{\mathrm{d,s}}} \\ \frac{1}{M_{\mathrm{u,s}}} & \frac{1}{M_{\mathrm{d,s}}} \\ \frac{1}{M_{\mathrm{u,n}}} & \frac{1}{M_{\mathrm{d,n}}} \\ \frac{1}{M_{\mathrm{u,n}}} & \frac{1}{M_{\mathrm{d,n}}} \end{pmatrix} \begin{array}{l} I_{\mathrm{s}}^{\mathrm{u}} \\ I_{\mathrm{s}}^{\mathrm{d}} \\ I_{\mathrm{n}}^{\mathrm{u}} \\ I_{\mathrm{n}}^{\mathrm{d}} \end{array} \end{array},
\qquad
\phi = \begin{array}{c} \quad I_{\mathrm{s}}^{\mathrm{u}} \quad\; I_{\mathrm{s}}^{\mathrm{d}} \quad\; I_{\mathrm{n}}^{\mathrm{u}} \quad\; I_{\mathrm{n}}^{\mathrm{d}} \\ \begin{pmatrix} \frac{1}{\mu_{\mathrm{u,s}}} & \frac{1}{\mu_{\mathrm{d,s}}} & \frac{1}{\mu_{\mathrm{u,s}}} & \frac{1}{\mu_{\mathrm{d,s}}} \\ \frac{1}{\mu_{\mathrm{u,n}}} & \frac{1}{\mu_{\mathrm{d,n}}} & \frac{1}{\mu_{\mathrm{u,n}}} & \frac{1}{\mu_{\mathrm{d,n}}} \end{pmatrix} \begin{array}{l} T_{\mathrm{s}} \\ T_{\mathrm{n}} \end{array} \end{array}
\tag{7}
$$

such that e.g. $M_{\mathrm{u,s}}$ indicates the half saturation constant of the undefended species being grazed by the selective species, etc.

Finally, our model includes a parameter, Δ, which explicitly controls the species' trait values. Abstract traits such as defense and selectivity are linked to concrete and measurable parameters describing the species' interactions. For the basal species, their maximal growth rate r'_i is linked to their position on the defense axis (Fig. 1d). The intermediate species have two trait values: defense is again linked to their maximal growth rate $e \cdot g'_j$, and the half saturation constant M_i is determined by their degree of selectivity; both of these traits affect the overall growth rate of the intermediate consumers. The top species have only one trait, selectivity, which is linked to their half saturation constant μ_i. As will be shown below, the equations are parametrized in a way such that for $\Delta = 0$ the linear chain system, where all species per trophic level are functionally identical, will be described (Fig. 1a). As Δ is increased, the system changes in a continuous way, where some prey species gradually become more and more defended (Fig. 1b), such that they can be preyed on less and less by the selective species. In addition, the selective species are gradually able to feed more efficiently on the undefended species. Finally, for $\Delta = 1$ the trait differences are maximal, as is the case in Fig. 1c: the selective species do not feed on the defended prey anymore.

221

Body mass ratio between adjacent trophic levels	$m_I/m_B = m_T/m_I = 10^3$
Allometric scaling exponent	$\lambda = -0.15$
Inflow nutrient concentration	$N_0 = 1120\,\mu gN/l$
Dilution rate	$\delta = 0.055$
Nutrient half-saturation const. of B	$h_n = 10\,\mu gN/l$
Nitrogen to carbon ratio of B	$c_N/c_C \approx 0.175$
B^u max. growth rate	$r'_1 = 1/day$
B^d max. growth rate	$r'_2 = 0.66/day$
I conversion efficiency	$e = 0.33$
I^u max. grazing rate	$g'_{1,3} \approx 1.08/day$
I^d max. grazing rate	$g'_{2,4} \approx 0.70/day$
I_s half-saturation const.	$M_{1,2} = 300\,\mu gC/l$
I_n half-saturation const.	$M_{3,4} = 600\,\mu gC/l$
T conversion efficiency	$\varepsilon = 0.33$
T max. grazing rate	$\gamma'_{1,2} \approx 0.38/day$
T_s half-saturation const.	$\mu_1 = M_{1,2} = 300\,\mu gC/l$
T_n half-saturation const.	$\mu_2 = M_{3,4} = 600\,\mu gC/l$

Table 1. Standard parameter values used in this study when the trait differences are maximal, i.e., $\Delta = 1$.

The parameter values are set to vary logarithmically with Δ. This implies that parameter changes occur proportional to the starting value in both directions, since r'_i and g'_i appear as linear factors in the differential equations. For consistency, the elements of p and ϕ are also varied logarithmically. Concretely, this means that:

$$\log[\theta(\Delta)] = \log\theta_0 + \Delta \cdot (\log\theta_1 - \log\theta_0) \tag{8}$$

where θ is r'_u, r'_d, g'_u, g'_d or any of p_{ij} or ϕ_{ji}. In this way, $\Delta = 0$ implies $\theta = \theta_0$ such that all the trait values are equal in the following manner:

$$r'_u(\Delta = 0) = r'_0 = r'_d(\Delta = 0), \tag{9}$$

$$g'_u(\Delta = 0) = g'_0 = g'_d(\Delta = 0), \tag{10}$$

$$\frac{1}{M_{u,s}}(\Delta = 0) = \frac{1}{M_0} = \frac{1}{M_{u,n}}(\Delta = 0), \tag{11}$$

and similarly for the other elements of p or ϕ. We define the parameter values θ_0 of the $\Delta = 0$ system as arithmetic averages of the extreme values θ_1 in the $\Delta = 1$ system, on a logarithmic scale, e.g.:

$$\log r'_0 = \frac{\log[r'_d(\Delta = 1)] + \log[r'_u(\Delta = 1)]}{2}, \tag{12}$$

and similarly for the other parameters. These extreme values are shown in Table 1.

As the logarithm of 0 is undefined, this requires the elements of p and ϕ related to the defended-selective species' interactions for $\Delta = 1$ to be nonzero. In this case 10^{-4} was taken, which is low enough not to affect our results (see Fig. A1, Appendix A). Note also that the set of 9 equations in equation (3), when the species on each trophic level are exactly equal ($\Delta = 0$), is mathematically equivalent to a linear chain system with 4 equations, up to a slight parameter transformation. Specifically, the 9-equation food web system corresponds to a 4-equation food chain by setting $M \to 2^{(h-1)/h}M$ and $\mu \to 4^{(h-1)/h}\mu$. For details of the derivation, see Appendix B.

Model parametrization and analysis. In order to decrease the number of free parameters, and simultaneously increase the realism of the model, the species' growth rates were scaled allometrically to their body mass[10,38]:

$$\frac{\text{intermediate growth rate}}{\text{basal growth rate}} = \left[\frac{m_I}{m_B}\right]^{\lambda}, \tag{13}$$

with body masses m and the exponent λ given typical for planktonic systems[39] (Table 1). The same relationship holds true for the ratio between the maximum growth rates of the intermediate and the top species.

This model was developed as a chemostat model, with an eye towards potential experimental application. Chemostat experiments have been very successful in identifying and understanding ecological and evolutionary interactions of planktonic[40], and many other microbiological systems[41]. In such experiments, many factors influencing dynamics in question, such as nutrient supply, light supply, temperature, etc., are kept constant and/or closely monitored. This procedure greatly facilitates observation of the interactions of interest between species in the chemostat. For this reason, extra care was taken to have empirically motivated and realistic values of

the remaining model parameter values (Table 1). Specifically, the parameter values we use are representative for planktonic chemostats. However, this does not mean that our results apply only to planktonic systems. In fact, as we show in Appendix A, similar results are obtained when the model parametrization is more adapted towards terrestrial food webs, for example.

To get a better understanding of how much certain values of Δ sets the species on the three trophic levels apart, we here consider a few exemplary cases. At $\Delta = 0$, the varied parameters are identical (and so are the species), while at $\Delta = 0.2$, maximal growth and grazing rates of the undefended species are 9% higher than those of defended species, and half saturation constants of non-selective species are 15% higher than selective species. At $\Delta = 0.5$, the differences are 23% and 42%, respectively; at $\Delta = 1$ they are 50 and 100%.

For simplicity and to reduce the dimensionality of the system somewhat, in the rest of the text it will be assumed that

$$h = \eta, \text{ and } M = \mu. \tag{14}$$

Hence, h will denote the Hill exponent, and M the half-saturation constant, of the functional response between both the first and the second, and between the second and the third trophic level. Additional narrowing of parameter ranges was achieved by requiring coexistence of the species in both the chain and the maximally separated food web. More information on the size of the range for which all species are able to coexist, as well as generalizations of our results for different model structures can be found in Appendix A.

To characterize the differences between the different attractors, the different phase relationships between predator-prey pairs were investigated. These phase relationships were obtained by calculating the Discrete Fourier Transform (DFT) of the simulated time series. Due to the non-sinusoid shape of the biomass oscillations, a signal with only a single frequency will generate an infinite amount of peaks in the frequency spectrum. These are necessarily multiples of the original frequency f, and the height of the peaks will scale as $1/f^2$[42]. This means they are easily identified in the frequency spectra when shown on a log-scale, by the linear decay in peak height.

The solutions of the differential equations presented were obtained numerically in C using the SUNDIALS CVODE solver[43], with relative and absolute tolerances of 10^{-10}. Output data were studied using Python and several Python packages; in particular NumPy, SciPy and Matplotlib[44,45].

Results

Firstly, we compare the biomass dynamics of the linear chain to the dynamics of the maximally trait-separated food web, where trait differences within each trophic level are maximal. Secondly, we study certain properties of the system, such as the temporal variability of population and community biomasses, and the relative abundances of species, while gradually increasing the amount of standing trait variation at each trophic level from a linear food chain to the maximally trait-separated food web.

The amount of trait variation is described by Δ ranging continuously from 0 to 1. When $\Delta = 0$ we describe the linear chain without trait variation, and when $\Delta = 1$ we describe the maximally trait-separated food web. This fully separated food web consists of defended and undefended prey species, which are being preyed upon by non-selective and/or selective predator species (Fig. 1c). The benefits and costs of the different offense-defense strategies are linked to each other through predefined trade-offs (see Methods). The defended species have a lower growth rate than the undefended species, but in turn, they are not preyed upon by the selective species of the next trophic level in the fully separated web. Similarly, the selective species, while unable to prey on the defended species, are able to graze the undefended species more efficiently at low prey concentrations than their non-selective counterparts.

Our results are first summarized schematically in Fig. 2, subsequent mechanistic details are presented in the sections and figures below. We observe two alternative stable states with low vs. high total production (State 1 and 2 in Fig. 2) in both the linear chain (low trait variation) and the maximally separated food web (high trait variation). In the low-production state, the high mean concentration of free nutrients corresponds to a low amount of total biomass and consequently, a low total production. In the high-production state, in contrast, the low mean nutrient concentration implies that most of the nutrients are stored in the biomass which implies a high total production. Note that at equilibrium, the total amount of nutrients in the system is always constant because the chemostat model's dilution rate δ is constant for all species.

In the food chain without trait variation (left part of the biomass pyramids in Fig. 2), the population-level biomass dynamics for the low-production state (Fig. 3a) exhibit pronounced predator-prey cycles, while the high-production state exhibits slower cycles with lower amplitudes (Fig. 3b). The respective phase relationships of these oscillations (right part in Figs 2 and 3c,d) may inform about the ecological mechanism behind the two different states (for details, see section 3.1). In the low-production state, fast cycles with high amplitudes occur due to the strong coupling between adjacent trophic levels. Such a strong interaction between predators and their prey is indicated by the quarter-cycle phase lags (henceforth referred to as ¼-lag cycles) (Fig. 3c). In the high-production state the top and intermediate level still exhibit ¼-lag cycles, but the phase difference between the intermediate and basal level is significantly larger (Fig. 3d). This offset in the phase-relationship indicates that the top-down control over the intermediate level is so strong in the high-production state that the intermediate level's dynamics are less closely coupled to the basal level than in the low-production state. The basal level is then free to fully exploit the available nutrients.

The decoupling of the intermediate and basal level results in a lower temporal variability, especially at the basal level, and hence, reduces times of strong basal suppression during which the nutrients can almost reach their capacity as observed in the low-production state. In the high-production state, the overall higher primary production combined with the lower temporal variability between the basal and the intermediate level enhances the energy transfer through the food chain and results in a top-heavy biomass pyramid.
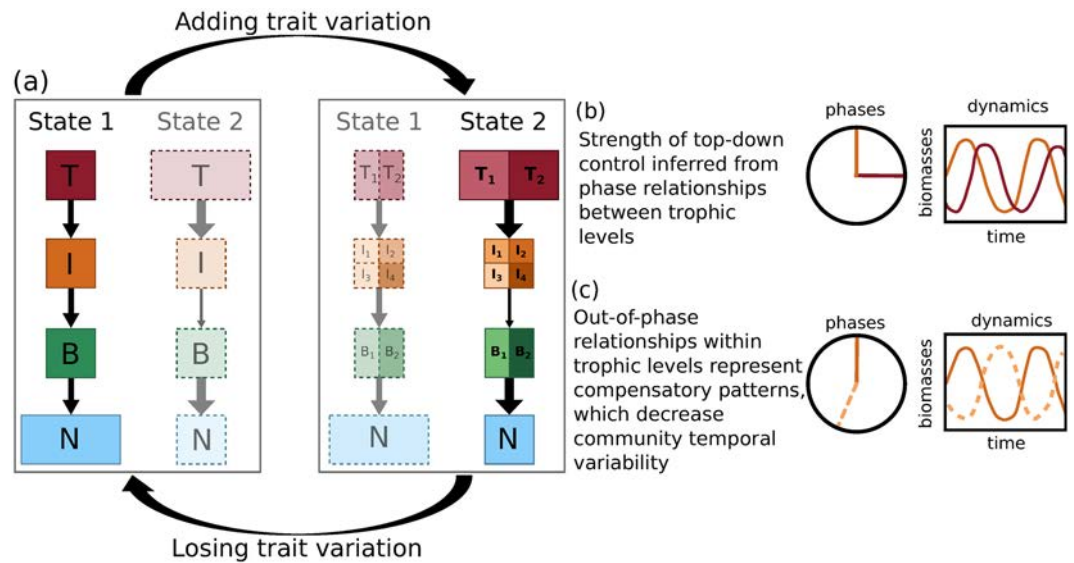
Figure 2. Schematic overview of our results. (**a**) The model system (with *B* basal species, *I* intermediate consumers and *T* top predators) always exhibits two alternative stable states, State 1 (low-production) and 2 (high-production), for both low and high amounts of trait variation. As trait variation is added, the system tends toward the high-production state with the top-heavy biomass pyramid (solidly drawn states have a larger basin of attraction than grayed out states). (**b**) The phase differences between predators and their prey inform about the intensity of top-down control in the system as indicated by arrow width in (a), i.e. ¼-lag cycles indicate strong coupling between predator and prey. (**c**) Within trophic level out-of-phase cycles indicate compensatory dynamical patterns, where the different species exploit different temporal niches, and hence, reduce the community temporal variability.
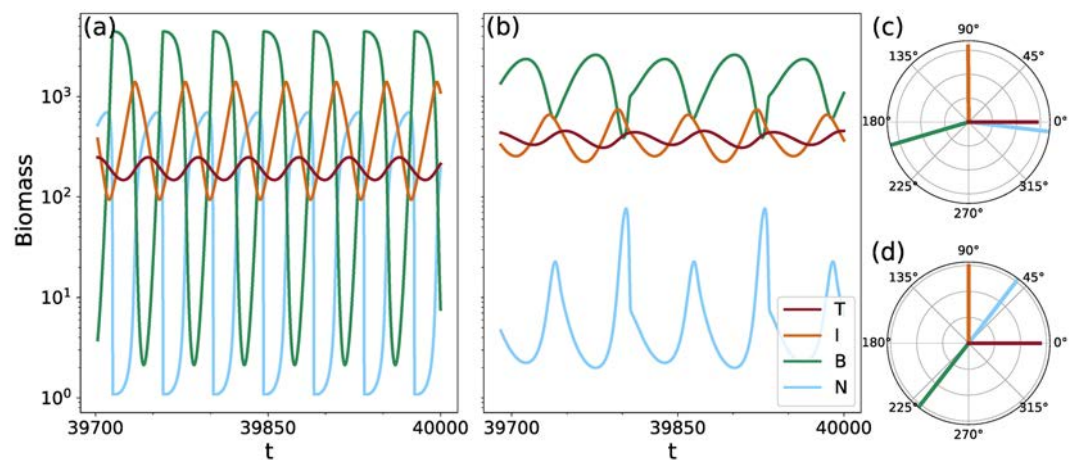

Figure 3. Biomass and nutrient dynamics on the two different states for the tritrophic chain for $h = 1.1$ ($=\eta$), and their corresponding phase relationships. (N = nutrients, B = basal species, I = intermediate species and T = top species). The relative phases of the low-production state shown in (**a**) (mean nutrient level $\approx 250 \, \mu g \text{N}/l$) are plotted in panel (c). The phases of the high-production state shown in (**b**) (mean nutrient level $\approx 10 \, \mu g \text{N}/l$) are plotted in panel (d). In both cases the phases relative to the top species are shown.

When the food chain becomes a food web by adding trait variation (right part of the biomass pyramids in Fig. 2), the biomass dynamics of the low-production (Fig. 4a) and high-production state (Fig. 4b) as well as their respective phase-relationships (Fig. 4c–f) become more complex because a slow and a fast timescale underlie the oscillations (see Section 3.1 for details). Information regarding intensity of top-down control is only deduced from the phase-relationships of the oscillatory mode that explains most of the observed variation, i.e. the fast timescale of the low-production state (Fig. 4d) and the slow timescale of the high-production state (Fig. 4e). Similar to the food chain without trait variation, the strong top-down control by the top level and subsequently, the decoupling of the intermediate and basal level in the high production state again results in lower temporal variability, a temporally more balanced nutrient use, and a more efficient energy transfer towards the top level. Importantly, the high-production state becomes more likely than the low-production state with increasing trait
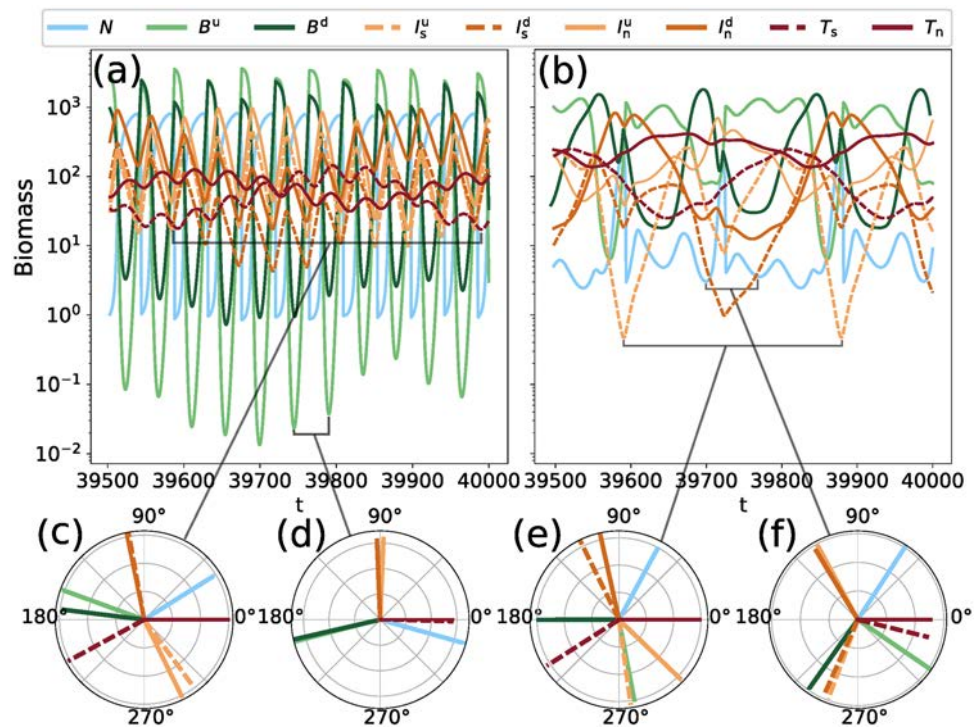
Figure 4. The dynamics of the maximally separated food web (see Fig. 1c for structure and species names), for $h = 1.05$ $(=\eta)$. (**a,b**) Show the biomass time series on the low- and high-production state, respectively. The phase relationships (relative to $\top_n$) of the two main temporal modes on the states are shown in panels (c,e) (slow) and (d,f) (fast). (See Fig. 5 and its explanation in the text for why the chosen value of $h = 1.05$ is different from the one used to compare the two states on the chain in Fig. 3).
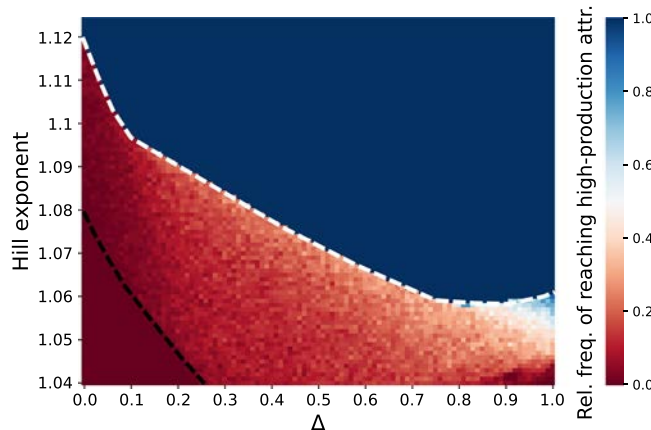

Figure 5. Relative frequency of reaching the high-production state, as a function of the trait difference Δ and the Hill-exponents $h = \eta$. Each of the points in the 101×85 grid shows the relative frequency of reaching the high-production state, sampling 200 random initial conditions. The black dashed line shows the approximate location of the boundary crisis of the high-production state. The low-production attractor also undergoes a boundary crisis, the approximate location of which is indicated by the white dashed line.

variation, i.e., its basin of attraction increases, making it more resilient against external disturbances (for details, see Fig. 5 and Section 3.2).

As trait variation (Δ) increases, selective and non-selective consumers at the top level exploit different temporal niches and force the intermediate level to split up into two distinct groups comprising the defended and the undefended species, respectively. As both groups include both selective and non-selective consumers, this further weakens the interaction between the intermediate and basal levels, strengthening the aforementioned mechanisms that stabilize the high-production state. Notably, the mean population biomasses stay relatively constant as trait variation increases (cf. Fig. 6c,d), while the community temporal variability decreases (Fig. 6e,f, gray lines). This effect could also be predicted from the phase relationship diagrams, which show that with increasing
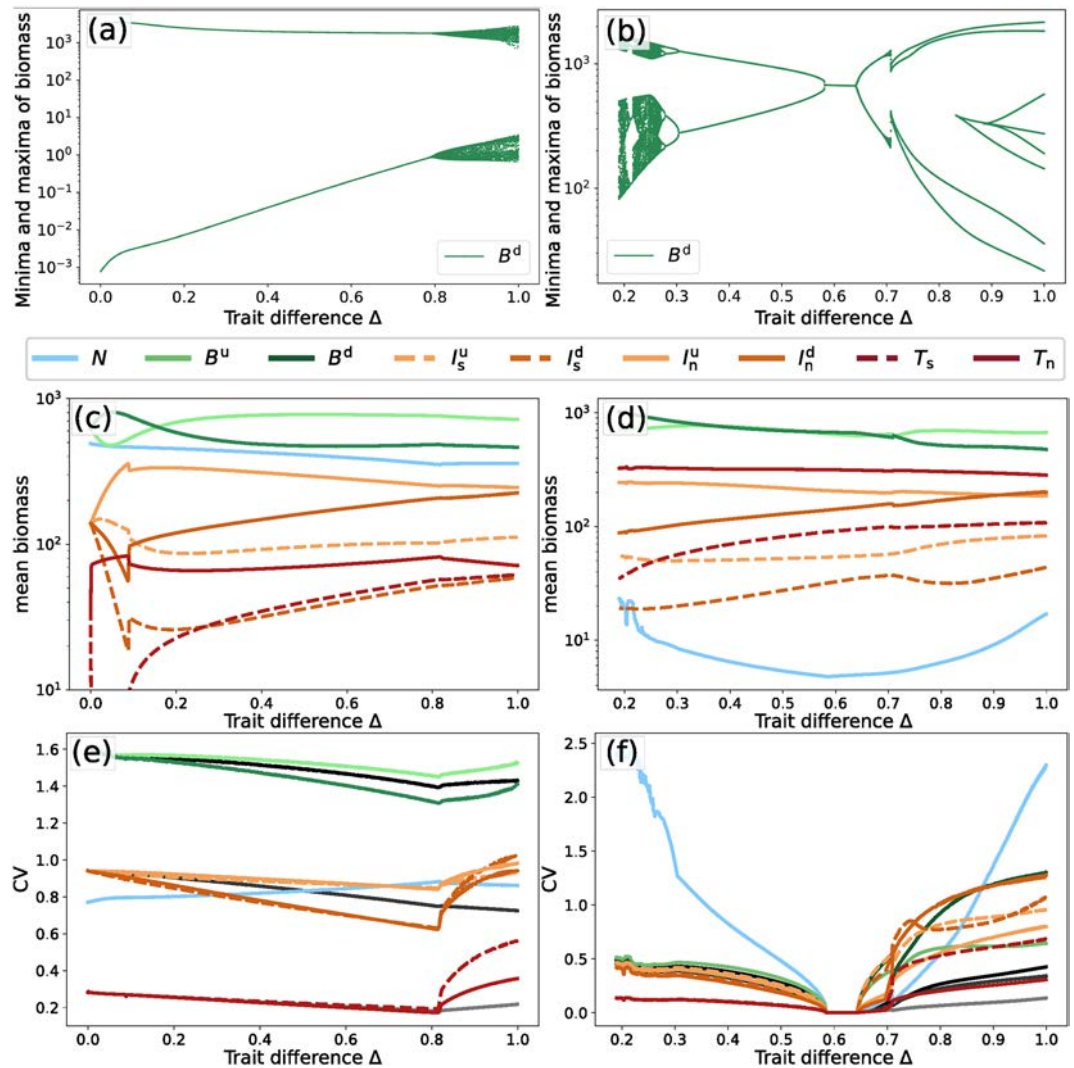
Figure 6. Bifurcation diagrams of the defended basal species, B^d (**a,b**), mean biomasses (**c,d**), and CV (**e,f**) of all the species in the system, for the low-production (left) and the high-production (right) attractors, for $h = 1.05$. For the bifurcation diagrams of the other species see Appendix C. The CV of the selective top predator is not plotted for the region where it goes extinct ($0 \lessgtr \Delta \lessgtr 0.1$ in panel (e)). In panels (e,f), the black to gray lines respectively denote the CV of the first, second, and third trophic level as a whole. Note the different scales on the x- and y-axes.

trait variation, competing species within the same trophic level move out-of-phase with each other (Fig. 4c,e,f). Such out-of-phase cycles indicate compensatory dynamical patterns with potentially high amplitudes at the population level. However, because the different species are able to exploit different temporal niches, the community temporal variability is kept low.

In summary, adding trait variation safeguards the high-production state which is characterized by a high top-level biomass resulting from an efficient transfer of energy towards the higher trophic levels, and low temporal variability due to weak coupling between the intermediate and basal levels and prominent compensatory dynamics within the lower trophic levels. Contrarily, losing trait variation increases the risk of an irreversible transition to the low-production state, which is characterized by a lower top-level biomass resulting from the less efficient transfer of energy towards the higher trophic levels, and higher temporal variability. With trait variation added, primary production increases from the low- to the high production state by a factor of 1.5 and the efficiency of the energy transfer towards the top level increases by a factor of 2 (See Table C1 in Appendix C). Hence, adding trait variation results in a more productive and energy-efficient food web.

More details about the above-mentioned results are presented in the respective sections below.

Phase relationships as a way to identify underlying mechanisms. In order to understand how to use the phase relationships between different populations of a complex food web, such as the maximally trait-separated web (Fig. 1c), to uncover the mechanisms driving their dynamics, let us first look at the simpler linear chain containing only three species (Fig. 1a). As mentioned above, the state shown in Fig. 3a with a

mean nutrient concentration of about 250 μgN/l will be called the low-production state, relative to the other state (Fig. 3b) which has a much lower mean nutrient concentration of around 10 μgN/l and therefore will be called the high-production state.

Closer inspection of the time series reveals the origin of the difference in mean free nutrient levels between the two states. In the low-production state (Fig. 3a) the intermediate level is able to grow to sufficiently high densities to graze the bottom level down significantly, despite the predation pressure imposed by the top species. Hence, the nutrient uptake is strongly reduced for a considerable amount of time leading to a relatively high mean nutrient level. Conversely, in the high-production state (Fig. 3b), the higher biomass at the top level implies a stronger grazing pressure on the intermediate level. The intermediate species are thus not able to grow to the density levels reached on the low-production state, and in turn, do not graze the basal level down to low densities. Hence, the mean nutrient level is much lower. Here, we define top-down effects simply as effects arising from the terms linking a species to the trophic level above it, and vice-versa for bottom-up effects. In this way, increased grazing pressure constitutes an increase in top-down control.

Using this definition, we could conclude that the overall control exerted by the top level is higher in the high-production state than on the low-production state. Such an observation cannot be made as straightforwardly by inspecting only the mean biomass levels, as the temporal averages of the intermediate and basal biomasses are quite similar in both states and thus, they do not inform about potential changes in the production at each level. Therefore, examining the degree of top-down or bottom-up control in the case of non-static dynamics requires information about the oscillations themselves.

Interestingly, the phase differences between the different trophic levels contain sufficient information to reach the same conclusions regarding the strength of top-down control in the two states. In the low-production state, the phase differences between the top and intermediate level, and intermediate and bottom level, are about a ¼-cycle Fig. 3c), reflecting the presence of clear predator-prey oscillations, i.e., cyclic change between top-down and bottom-up control, between both the top and intermediate level, and the intermediate and basal level. In contrast, in the high-production state, the phase lag between the intermediate and basal level is significantly more than a ¼-cycle (Fig. 3d), indicating rather weak interactions between these two different trophic levels.

With this in mind, we now investigate the fully trait-separated food web ($\Delta = 1$, Fig. 1c), whose dynamics are shown in Fig. 4a,b. Just as the linear chain, the system settles down to a stable limit cycle. While the dynamics are visually much more complex when compared to the linear chain, the basic properties and differences between the two states remain the same. However, in contrast to the chain, the discrete Fourier frequency spectra (cf. Appendix C, Fig. C3) reveal two distinct frequencies at substantially different timescales. Despite this increase in complexity, our results clearly show that the phase relationships between distinct populations of adjacent trophic levels provide substantial information about the regulations of trophic interactions and changes therein. The absence of qualitatively different interaction types (e.g., omnivory) allows us to meaningfully compare the phase relationship between each individual predator-prey pair in our trait-separated food web to its expected value in isolation[12].

The low-production state of the maximally separated food web (Fig. 4a) exhibits two important timescales governing the overall dynamics. First, the same high-frequency oscillations as were observed for the food chain are present, with the ¼-lag cycles indicative of predator-prey oscillations (Fig. 4d). Second, oscillations on a slower timescale are found. Their phase relationships show that they arise from the trait differences between species (Fig. 4c). Here, the top species are almost completely out of phase relative to each other. Consider first the selective predator T_s, which preys only on the undefended intermediate species I_s^u and I_n^u. The phase relationship diagram shows that these species precede T_s by the regular ¼-lag. The same is true for T_n, which is preceded by a quarter-cycle by the defended intermediate species I_s^d and I_n^d. Quarter-lag cycles are not observed between the basal and intermediate trophic level, which indicates that the trait differences within the top trophic level influence the intermediate level more strongly as those on the intermediate level influence the basal level. As the two alternating groups of defended and undefended intermediate species contain a selective and non-selective grazer on the basal species, they exert together approximately the same grazing pressure on both types of basal species. Consequently, no clear phase relationship between the intermediate and basal level is found. However, visual inspection combined with analysis of the Discrete Fourier Transform (DFT) spectrum (Appendix C, Fig. C3) shows that the high-frequency component is the dominant one, explaining most of the observed variation in the biomass. Hence, the biomass dynamics reflect an overall balance between top-down and bottom-up interactions in the low-production state, similar to the simple linear chain.

In the high-production state of the maximally separated food web (Fig. 4b), the difference in dynamics as compared to the linear chain is even more pronounced. The basal species exhibit a clear compensatory dynamical pattern, with alternating biomass peaks of defended and undefended species. While the dynamics appear highly irregular, the frequency spectrum shows that they are also mainly driven by two frequencies. On the lower of these frequencies, which explains most of the variation observed in this state, the phase relationships resemble those of the low frequency in the low-production state (Fig. 4e vs. 4c), with the exception of the basal species, which now cycle out of phase. The selective and non-selective top species also move out of phase, which leads the groups of defended and undefended intermediate species to behave similarly, as they each precede their respective main predator. As in the low-production state, no further relationship can be identified between the intermediate and the basal level.

However, the high frequency roughly corresponding to that of the chain also has an influential component in the Fourier spectrum. On this frequency, the phase relationships show that the basal species also move out-of-phase. In contrast to the dominant lower frequency, the intermediate species are now split into two groups according to their main prey type. The non-selective intermediate species follow the defended basal species, and the selective intermediate species the undefended basal species, by a ¼-lag. As each of these two groups

of intermediate species contains both a defended and undefended type, no further relationship can be drawn between the phases of the intermediate and the top level.

In summary, the strength of top-down control across trophic levels may be inferred from the phase relationships in both the linear chain and the maximally separated food web. The phase-relationships further reveal compensatory dynamics within trophic levels in the fully separated web.

Trait variation increases resilience of the high-production state.
Recall that trait differences between the modeled species at each trophic level, determined by Δ (equation (8)), can be varied continuously. Varying Δ between $\Delta = 0$ (chain) and $\Delta = 1$ (maximally separated web) reveals the intermediate region between the two extremes considered so far.

In this intermediate region, the food web is not yet completely separated as is the case for Fig. 1c, although there are already trait differences between different species at each trophic level. That is, the selective predator species are not yet fully specialized: they are still able to prey on the defended species albeit with a lower efficiency than the undefended species. Accordingly, the undefended species are not fully defended against the selective predators. The difference in growth rates between defended and undefended species is thus gradually increased to its maximum value, which is obtained when $\Delta = 1$. In this way the trade-offs between defense and growth rate, and between selectivity and prey grazing efficiency, are explicitly built into the model.

To investigate the effect of trait variation on the likelihood of the system adopting either of the two alternative stable states, we determined the size of the basin of attraction of the high-production state. Figure 5 shows the relative frequency of a random initial value falling in this basin of attraction, as Δ is varied. The random initial values were sampled from the set of all potentially accessible biomass configurations of the chemostat system, i.e., the total carbon content in the system does not exceed the maximum possible carbon content attainable by the incoming nutrient concentration N_0.

The region of intermediate frequency values confirms that the bistability is an important aspect of the system. The typical behavior when varying Δ from 0 to 1 is an increasing probability of reaching the high-production state. Furthermore, the graph shows an important dependency on the predator-prey functional responses' Hill coefficient h: increasing the exponent also increases the probability of reaching the high-production state. Investigating the effect of other model parameters on the presence of bistability reveals that it is quite common for this type of model structure, and that the trends presented here are not limited to this particular part of the parameter space. For details, see Appendix A.

Over the whole range of Δ, there is a very sharp transition between the region where only the high-production state exists (dark blue), and the region where both states exist, indicated by the white dashed line (Fig. 5). Notably, the border decreases steeply as the trait difference Δ is increased, indicating the much lower dependence on low-density grazing suppression for higher amounts of standing trait variation. The sharp border between the two regions is an indication that the low-production state undergoes a catastrophic bifurcation, where it suddenly disappears. Similar behavior is observed for the high-production state, indicated by the black dashed line. This transition is of particular ecological interest as it implies the sudden disappearance of the high-production, low-temporally-variable state. The region for $h < 1.04$ was not considered, as the amount of extinctions was too high. However, the graph indicates that the probability of reaching the high-production state decreases further.

Dynamical properties of the alternative stable states under gradual changes in trait variation.
Consider now $h = 1.05$ as a representative value catching the most complex region in Fig. 5, to study the possible effects of varying Δ on the system's dynamics. In this case, the low-production state exists over the whole range of Δ, its bifurcation diagram for the defended basal species B^{d} is shown in Fig. 6a. The qualitative features of the diagram are representative for the other species in the network, whose bifurcation diagrams are shown in Appendix C, Figs. C1 and C2.

For $\Delta = 0$, the oscillations are simple, in the sense that they are governed by a single timescale and have a constant amplitude, as the maxima and respectively minima each fall on the same position. As Δ increases, this situation remains unchanged, up until the species become different enough for the second timescale to emerge, in which they exhibit a compensatory dynamical pattern. This explains the variation of the values of the extrema as the two timescales interact destructively and constructively.

The mean biomasses of the species (Fig. 6c) reveal that the selective top predator goes extinct for low values of Δ. In this case, the species are too similar to stably coexist due to a lack of niche differences, and the non-selective predator outcompetes the selective species. However, it quickly recovers as Δ is increased and the species become more different. While this event causes some disturbances in the mean biomasses of the other species, outside of this range the values are more or less constant.

Disregarding the initial region of Δ where the selective top predator goes extinct, all species' *CV* exhibit a gradual decrease as Δ is increased, up to the point where the second timescale enters the system (Fig. 6e). At this point, a sharp increase is observed as the complexity is enhanced by the interaction of the two timescales. The black to gray lines, depicting the *CV* of the biomasses at each trophic level as a whole, show that the sharp increase is not present on the trophic-level-scale. Hence, the increase in *CV* for each of the species can be solely attributed to the introduction of the second, slower timescale. As discussed above, species with different traits may move out of phase on this timescale, and thus the effects of the slower timescale on the temporal variability for the trophic level as a whole cancel out.

The bifurcation diagram for the high-production attractor (Fig. 6b) does not cover the full range of $0 \leq \Delta \leq 1$ for $h = 1.05$, as it only exists on the right side of the black dashed line in Fig. 5. Furthermore, the attractor exhibits a much richer structure as Δ is varied than the low-production attractor. Multiple bifurcations occur in which the dynamics are altered. In particular, lowering Δ sufficiently the system undergoes a series of period-doubling bifurcations which lead to chaotic dynamics. Eventually the attractor undergoes a boundary crisis, as indicated by

228

both the sudden disappearance of the then chaotic attractor and the presence of a chaotic transient (Appendix C, Fig. C4).

The species' mean biomass on the high-production state (Fig. 6d) reveal a similar monotonicity as those on the low-production state (Fig. 6c). A notable observation is the very low mean nutrient level along the whole range of Δ. The nutrients show a very high CV (Fig. 6f), which can be attributed to their low mean value. In addition, the CV for each of the species is higher on the right side of the Hopf-bifurcations (higher Δ), as compared to the left side for lower values of Δ. However, just as for the low-production state, these increases are buffered when looking at the temporal variability of the trophic levels as a whole (black to gray lines). This reflects the compensatory dynamical pattern of the high-production state, where some of the species move out of phase, which leads to a reduction in temporal variability on the entire trophic level.

Discussion

We developed a generic tritrophic model to investigate the effect of varying degrees of trait variation on the dynamics of multitrophic food webs and their associated ecosystem functions such as the mean resource use efficiency, biomass production, temporal variability and resilience. By increasing the trait difference parameter Δ from 0, the system increases in complexity while it changes gradually from a simple chain without trait variation to a complex web with selective and non-selective consumers, and correspondingly defended and undefended prey. The relevant parameters affecting these traits (growth rate, edibility, food preference, and half saturation constant) are closely linked to the functions of the individual species in the food web. Hence, increasing Δ also increases the functional differences between the species, and thus, the functional diversity of the system. For $\Delta > 0$ but low, the trait differences are small which means the species are very similar, hence, the functional diversity at each trophic level is low. Correspondingly, for Δ close to one, the functional diversity of the system is high, even though the number of species is kept constant. Therefore, varying Δ is a means to study the effects of changing functional diversity on all three trophic levels on the dynamics of the whole system without potentially confounding effects of changing the number of species. The different aspects of how trait variation impacts the food web dynamics are discussed in detail below.

Phase relationships help unravel complex trophic interactions.

Traditionally, effects of multi-trophic interactions such as trophic cascades and the degree of bottom-up or top-down control were studied using a rigid linear chain in equilibrium[46,47]. However, natural systems are usually not simple chains, but highly complex webs with functionally diverse species at all trophic levels[48,49]. Moreover, their dynamics may not evolve towards an equilibrium fixed point, but rather to a limit cycle[50], or a strange attractor[51] where they will perpetually exhibit oscillatory behavior. This phenomenon can be separated from stochastic noise and has been observed in natural communities[52]. Such oscillatory behavior gives rise to certain phase relationships between the biomass dynamics of the different species.

Additionally, in the maximally trait-separated food web (Fig. 1c), calculation of the Discrete Fourier Spectrum clearly exposes the two timescales at which major driving mechanisms take place. The emergence of a second timescale does not rely on the addition of a third trophic level as this feature has already been found in bitrophic models that considered multiple species or phenotypes at only one[53] or both trophic levels[13]. However, our treatment highlights how the phase relationships may shed light on the mechanisms driving complex systems by disentangling the different timescales at which these mechanisms may act.

Strength of trophic interactions. We found that the main dynamical differences between the two alternative stable states present in our system can be explained by an increased top-down control of the top level on the intermediate level. When the intermediate level is strongly controlled, such as is the case on the high-production state, its species are unable to control the basal level. The basal level is in turn able to fully exploit the available nutrients, increasing the overall production in the system (See Appendix C, Table C1).

This result holds independent of the amount of trait variation present, and is in line with previous studies showing that reduced top-down control may result in an increased phase difference between predator and prey[14,15]. Importantly, the larger than ¼-cycle phase difference between the basal prey and intermediate predator observed in our system with only one species per trophic level (Fig. 1a) shows that the common conception of anti-phase cycles as a "smoking gun" for the presence of evolution, or other mechanisms causing trait changes[12,54] does not hold any longer when considering multitrophic systems in which the intermediate predator faces strong top-down control by the top predator.

Role of compensatory dynamics. When a community consists of functionally diverse populations, a decline in one functional group can be accompanied by an increase of another[55]. In this way, even though the individual populations exhibit high temporal variability in their biomasses in our model, the variability of the community biomass per trophic level remains low (Fig. 6f). Such an effect has been observed before in studies investigating the effect of standing trait variation or phenotypic plasticity on population dynamics[33,56], and it is often made possible through compensatory dynamics between the species[57–59]. Hence, compensatory dynamics can be understood as a mechanism by which ecosystem functions such as biomass production can stay rather constant while individual populations may be highly variable[1,33]. Compensatory dynamics are observed in both the high- and low-production state, for sufficiently high Δ (Fig. 4a,b). When present, they effectively decrease the biomass CV of the trophic level as whole, even though the CVs of the species' individual biomass may be relatively high (Fig. 6e,f). These compensatory dynamical patterns naturally keep species within a trophic level moving out-of-phase relative to each other, and thus, can also be inferred by analyzing phase relationship diagrams.

Notably, the compensatory dynamics on the low-production state are only present at the slower timescale related to the trait dynamics (Fig. 4c). The dominant faster timescale does not exhibit compensatory dynamics

(Fig. 4d), and thus, given substantial variation in the biomass of the individual populations, the *CV* at the community level remains relatively high (Fig. 6e). Even so, the sharp increase in temporal variation on the population level for high trait variation is buffered on the community scale, through the compensatory dynamics taking place on a different timescale than the dominant one. Our time-scale dependent phase-relationships between populations are in line with empirical observations showing that phytoplankton populations may exhibit compensatory dynamics on the sub-annual scale, likely associated with trophic interactions, combined with synchronous dynamics on the annual, externally driven timescale[58]. Similarly, zooplankton dynamics may be governed by two distinct timescales: seasonal variation and experimentally varied environmental conditions[60]. Hence, unraveling the different timescales governing the population dynamics may help to understand the major processes driving them.

Trait variation promotes high production at the top-level.

In line with our results, bistability has been observed in other food chain models[18,61–63], ontogenetic growth models[27,64], and in other, broader ecological contexts[65]. The presence of two alternative states in our system is an important feature as it may have far-reaching consequences regarding the stability and perseverance of food webs when confronted with external perturbations. A commonly made distinction when studying the effects of perturbations is whether they consist of a change to the state variables, or to the actual model parameters[65,66]. The first kind, for example a sudden decrease in one of the species' biomass, is often called a pulse perturbation because of its short duration. The second kind is called a press perturbation, because the change to the perturbed parameters is permanent, such as a decrease in the nutrient inflow concentration. In a multistable system, pulse perturbations, particularly when they are large, might push the system over the edge of one basin of attraction into another, where the dynamics are potentially completely different. Press perturbations may produce a similar outcome by causing large changes to an attractor's basin of attraction, or by crossing a bifurcation point where the dynamics change significantly. Therefore, the size of the basin of attraction may be used as a measure of resilience[65]. A highly resilient system will nearly always return to its original state, hence its basin of attraction must be very large. Conversely, a non-resilient or fragile system is easily pushed out of one basin of attraction into another one.

Recall that the two states in our system have very different dynamical properties: the low-production state with low top biomass production and high variability, compared to the high-production state with high top biomass production and low variability. From an ecosystem function perspective, low variability or high biomass in higher trophic levels are beneficial for e.g. fish yield. Therefore, it may be desirable to keep the system on the high-production state.

While biomass production of a community is known to be mostly positively correlated with its functional diversity[67,68], we also found the high-production state in the food chain. This corresponds to, e.g., modern agricultural systems, which typically consist of monocultures with a low functional diversity, but a high biomass production available for higher trophic levels. However, even though such monocultures may produce more biomass than some functionally highly diverse mixtures, they are very fragile against external disturbances[69,70]. In this way, functional diversity is regarded as an insurance against external perturbations. We clearly observed such an effect in our system, for both pulse and press perturbations, as illustrated by Fig. 5. Since the basin of attraction of the high-production attractor increases in size with Δ, the system becomes less likely to be pushed out of the basin of attraction by a pulse perturbation. This trend is persistent when varying not only the Hill exponents, but also the dilution rate, and the nutrient inflow concentration (Appendix A, Fig. A3), and is thus not limited to a particular part of the model's parameter space. In addition, the boundary crisis causing the sudden disappearance of high-production attractor (Fig. 5, black dashed line) is only present for low values of Δ. Hence, functional diversity also protects the high-production state from suddenly disappearing under a press perturbation.

Typical for a boundary crisis, as the high-production state undergoes when decreasing Δ, are the long transients that are still present near the crisis point[71] (Appendix C, Fig. C4). In an ecological context this could be problematic as such a long transient implies there is no way to know exactly when the crisis point has been passed and the basin of attraction no longer exists, until the system eventually accelerates towards the only remaining attractor. Such regime shifts were empirically observed and predicted by a variety of ecosystem models in different contexts[72], such as woodlands threatened by fires turning into grasslands[73], and shallow lakes threatened by eutrophication turning from a macrophyte to a phytoplankton dominated state[74]. The key idea is that a small perturbation near the bifurcation point may move the system to an alternative stable state, but once this has happened, a much larger perturbation is needed in order to return back to the original state. It has been argued that, under certain circumstances, one may be able to observe early-warning signals that a transition is imminent[75–77]. For example, near some types of bifurcations a dampening of the speed-of-return after a pulse perturbations may be observed, called critical slowing down[75,78]. In the case of a boundary crisis, showing the existence of any early-warning signals has proven to be difficult[79,80]. However, even if their existence could be shown mathematically, they will almost certainly be very difficult or impossible to detect in a real-life setting, where the exact chaotic dynamics may be obscured by measurement noise. Our results reveal that maintaining sufficient trait variation provides protection from boundary crises, with their often ecologically and economically undesirable consequences.

These conclusions rely on the presence of alternative stable states in our model. This is a prominent property in tritrophic systems, present in even a simple tritrophic chain with Holling-type-II functional responses and logistic growth of the basal species[61]. However, there always exist parameter regions where there is only one non-trivial stable state. We find that also in such cases, production at the top level and temporal stability both increase with Δ, as the attractor changes from resembling the low-production to resembling the high-production state in a gradual way (See Appendix A, Fig. A6).

Influence of a sigmoidal functional response. The use of sigmoidal functional responses such as the (generalized) Holling type-III ($h = \eta > 1$) has been an active area of discussion for quite some time. Sigmoidal functional responses are praised for their favorable effects on food web dynamics such as an increased dynamical stability[36,81]. Such an increase is justified by the apparent discrepancy between the observed stability of natural ecosystems, and the highly unstable nature of ecosystem models describing them[82]. While experimental evidence has traditionally mainly supported hyperbolic functional response shapes, such as Holling type-II ($h = \eta = 1$)[83,84], sigmoidal functional responses such as Holling-type-III provide models with additional stability which may overcome this discrepancy. Recent experiments studies have found evidence for sigmoidal functional response shapes[37,85,86], or otherwise have shown the difficulty in distinguishing Holling type-II from type-III functional response shapes[87]. Furthermore, sigmoidal shapes account for natural processes not captured by the model such as spatial heterogeneity, refuges, formation of resting shapes, etc. Hence, Hill exponents close to—but higher than—one are likely to be relevant, and thus, the requirement of at least some grazing suppression at low densities for all species to coexist adds to the realism of the model. Even in the highly-controlled environment of the chemostat, some of the proposed mechanisms giving rise to the predation dampening at low prey densities, such as prey clumping[88] or other induced defenses[89], may well be of importance. In addition, while a Hill exponent larger than 1 does facilitate coexistence, it is not guaranteed. For example, Fig. 6c shows that one of the top predators is not able to survive for $0 \lessgtr \Delta \lessgtr 0.1$.

Nonetheless, Fig. 5 also shows a significant, decreasing dependence on low prey density grazing suppression in order to reach the high-production state. For most of the range of Δ, the sharp border between the bistable region and the region where only the high-production state exists occurs at a lower value of the Hill-exponent as Δ is increased. Hence, while the grazing suppression at low prey densities is necessary to reach the high-production state, it becomes a less important factor as Δ is increased.

Concluding remarks. Despite the higher dynamical complexity of the resulting food web, the introduction of trait variation at all trophic levels to a linear food chain increased the overall reliability of ecosystem functions, such as resource use efficiency and high biomass production. Our results highlight that functional diversity on different trophic levels can reduce the overall temporal variability at the community level through compensatory dynamics among functionally different species within a trophic level. Investigating the phase relationships between the different species of adjacent trophic levels enabled us to identify the regulation of trophic interactions, such as changes in top-down or bottom-up control, in oscillatory dynamical regimes. Accordingly, we observed that strong deviations from the expected ¼-lag between predator and prey are possible in a tritrophic system, even without any trait variation. Hence, observation of such deviations do not necessarily indicate the presence of eco-evolutionary dynamics as is often assumed. Furthermore, independent of the presence or absence of trait variation, our tritrophic model shows two alternative states with the top predator exhibiting either a relatively low or high biomass. However, while the high-production state is attainable in a tritrophic food chain, its basin of attraction is very small. It becomes more resilient when trait variation is added, underlining the role of functional diversity as an insurance against sudden pulse perturbations. In addition, as trait variation decreases, this state may suddenly disappear through a boundary crisis. Hence, high functional diversity also protects the high-production state under press perturbations. We thus highlight the importance of functional diversity regarding resilience against external perturbations, low community temporal variability, resource use efficiency, and maintenance of biomass in higher trophic levels.

Data Availability
The numerical datasets generated and analyzed during the current study are available from the corresponding author on reasonable request.

References
1. Hooper, D. U. *et al.* Effects of biodiversity on ecosystem functioning: A consensus of current knowledge. *Ecological Monographs* **75**, 3–35, https://doi.org/10.1890/04-0922 (2005).
2. Tilman, D., Reich, P. B. & Knops, J. M. H. Biodiversity and ecosystem stability in a decade-long grassland experiment. *Nature* **441**, 629–632, https://doi.org/10.1038/nature04742 (2006).
3. Worm, B. *et al.* Impacts of Biodiversity Loss on Ocean Ecosystem Services. *Science* **314**, 787–790, https://doi.org/10.1126/science.1132294 (2006).
4. Schneider, F. D., Brose, U., Rall, B. C. & Guill, C. Animal diversity and ecosystem functioning in dynamic food webs. *Nature Communications* **7**, 12718, https://doi.org/10.1038/ncomms12718 (2016).
5. Hillebrand, H. & Matthiessen, B. Biodiversity in a complex world: Consolidation and progress in functional biodiversity research. *Ecology Letters* **12**, 1405–1419, https://doi.org/10.1111/j.1461-0248.2009.01388.x (2009).
6. Krause, S. *et al.* Trait-based approaches for understanding microbial biodiversity and ecosystem functioning. *Frontiers in Microbiology* **5**, 251, https://doi.org/10.3389/fmicb.2014.00251 (2014).
7. Violle, C. *et al.* Let the concept of trait be functional! *Oikos* **116**, 882–892, https://doi.org/10.1111/j.2007.0030-1299.15559.x (2007).
8. Weithoff, G. The concepts of 'plant functional types' and 'functional diversity' in lake phytoplankton – a new understanding of phytoplankton ecology? *Freshwater Biology* **48**, 1669–1675 (2003).
9. Brown, J. H., Gillooly, J. F., Allen, A. P., Savage, V. M. & West, G. B. Toward a metabolic theory of ecology. *Ecology* **85**, 1771–1789 (2004).
10. Brose, U., Williams, R. J. & Martinez, N. D. Allometric scaling enhances stability in complex food webs. *Ecology Letters* **9**, 1228–1236, https://doi.org/10.1111/j.1461-0248.2006.00978.x (2006).
11. Litchman, E., Klausmeier, C. A., Schofield, O. M. & Falkowski, P. G. The role of functional traits and trade-offs in structuring phytoplankton communities: Scaling from cellular to ecosystem level. *Ecology Letters* **10**, 1170–1181, https://doi.org/10.1111/j.1461-0248.2007.01117.x (2007).
12. Ellner, S. P. & Becks, L. Rapid prey evolution and the dynamics of two-predator food webs. *Theoretical Ecology* **4**, 133–152, https://doi.org/10.1007/s12080-010-0096-7 (2011).
13. Tirok, K. & Gaedke, U. Internally driven alternation of functional traits in a multispecies predator- prey system. *Ecology* **91**, 1748–1762, https://doi.org/10.1890/09-1052.1 (2010).

14. Yoshida, T., Jones, L. E., Ellner, S. P., Fussmann, G. F. & Hairston, N. G. Rapid evolution drives ecological dynamics in a predator-prey system. *Nature* **424**, 303–306, https://doi.org/10.1038/nature01767 (2003).

15. Becks, L., Ellner, S. P., Jones, L. E. & Hairston, N. G. Jr. Reduction of adaptive genetic diversity radically alters eco-evolutionary community dynamics. *Ecology Letters* **13**, 989–997, https://doi.org/10.1111/j.1461-0248.2010.01490.x (2010).

16. Abrams, P. A. & Matsuda, H. Fitness minimization and dynamic instability as a consequence of predator-prey coevolution. *Evolutionary Ecology* **10**, 167–186, https://doi.org/10.1007/BF01241783 (1996).

17. Litchman, E. & Klausmeier, C. A. Trait-Based Community Ecology of Phytoplankton. *Annual Review of Ecology, Evolution, and Systematics* **39**, 615–639, https://doi.org/10.1146/annurev.ecolsys.39.110707.173549 (2008).

18. Erbach, A., Lutscher, F. & Seo, G. Bistability and limit cycles in generalist predator-prey dynamics. *Ecological Complexity* **14**, 48–55, https://doi.org/10.1016/j.ecocom.2013.02.005 (2013).

19. Duffy, J. E. Biodiversity and ecosystem function: The consumer connection. *Oikos* **99**, 201–219, https://doi.org/10.1034/j.1600-0706.2002.990201.x (2002).

20. Gamfeldt, L. *et al.* Marine biodiversity and ecosystem functioning: What's known and what's next? *Oikos* **124**, 252–265, https://doi.org/10.1111/oik.01549 (2015).

21. Steiner, C. F. *et al.* The influence of consumer diversity and indirect facilitation on trophic level biomass and stability. *Oikos* **110**, 556–566, https://doi.org/10.1111/j.0030-1299.2005.13665.x (2005).

22. Filip, J. *et al.* Multitrophic diversity effects depend on consumer specialization and species-specific growth and grazing rates. *Oikos* **123**, 912–922, https://doi.org/10.1111/oik.01219 (2014).

23. Rasher, D. B., Hoey, A. S. & Hay, M. E. Consumer diversity interacts with prey defenses to drive ecosystem function. *Ecology* **94**, 1347–1358, https://doi.org/10.1890/12-0389.1 (2013).

24. Digel, C., Curtsdotter, A., Riede, J., Klarner, B. & Brose, U. Unravelling the complex structure of forest soil food webs: Higher omnivory and more trophic levels. *Oikos* **123**, 1157–1172, https://doi.org/10.1111/oik.00865 (2014).

25. Levine, J. M., Bascompte, J., Adler, P. B. & Allesina, S. Beyond pairwise mechanisms of species coexistence in complex communities. *Nature* **546**, 56–64, https://doi.org/10.1038/nature22898 (2017).

26. Peet, A. B., Deutsch, P. A. & Peacock-López, E. Complex dynamics in a three-level trophic system with intraspecies interaction. *Journal of Theoretical Biology* **232**, 491–503, https://doi.org/10.1016/j.jtbi.2004.08.028 (2005).

27. Nakazawa, T. Ontogenetic niche shift, food-web coupling, and alternative stable states. *Theoretical Ecology* **4**, 479–494, https://doi.org/10.1007/s12080-010-0090-0 (2011).

28. Golubski, A. J., Westlund, E. E., Vandermeer, J. & Pascual, M. Ecological Networks over the Edge: Hypergraph Trait-Mediated Indirect Interaction (TMII) Structure. *Trends in Ecology and Evolution* **31**, 344–354, https://doi.org/10.1016/j.tree.2016.02.006 (2016).

29. Wang, S. & Brose, U. Biodiversity and ecosystem functioning in food webs: the vertical diversity hypothesis. *Ecology Letters* **21**, 9–20, https://doi.org/10.1111/ele.12865 (2018).

30. Tilman, D., Isbell, F. & Cowles, J. M. Biodiversity and Ecosystem Functioning. *Annual Review of Ecology, Evolution, and Systematics* **45**, 471–493, https://doi.org/10.1146/annurev-ecolsys-120213-091917 (2014).

31. Coutinho, R. M., Klauschies, T. & Gaedke, U. Bimodal trait distributions with large variances question the reliability of trait-based aggregate models. *Theoretical Ecology* **9**, 389–408, https://doi.org/10.1007/s12080-016-0297-9 (2016).

32. Van Velzen, E. & Gaedke, U. Disentangling eco-evolutionary dynamics of predator-prey coevolution: The case of antiphase cycles. *Scientific Reports* **7**, 17125, https://doi.org/10.1038/s41598-017-17019-4 (2017).

33. Bauer, B., Vos, M., Klauschies, T. & Gaedke, U. Diversity, Functional Similarity, and Top-Down Control Drive Synchronization and the Reliability of Ecosystem Function. *The American Naturalist* **183**, 394–409, https://doi.org/10.1086/674906 (2014).

34. Monod, J. La technique de culture continue, theorie et applications. *Ann d'Institute Pasteur* **79**, 390–410, https://doi.org/10.1016/B978-0-12-460482-7.50023-3 (1950).

35. Tilman, D., Kilham, S. S. & Kilham, P. Phytoplankton Community Ecology: The Role of Limiting Nutrients. *Annual Review of Ecology and Systematics* **13**, 349–372, https://doi.org/10.1146/annurev.es.13.110182.002025 (1982).

36. Williams, R. J. & Martinez, N. D. Stabilization of chaotic and non-permanent food-web dynamics. *European Physical Journal B* **38**, 297–303, https://doi.org/10.1140/epjb/e2004-00122-1 (2004).

37. Kalinkat, G. *et al.* Body masses, functional responses and predator-prey stability. *Ecology Letters* **16**, 1126–1134, https://doi.org/10.1111/ele.12147 (2013).

38. De Castro, F. & Gaedke, U. The metabolism of lake plankton does not support the metabolic theory of ecology. *Oikos* **117**, 1218–1226, https://doi.org/10.1111/j.0030-1299.2008.16547.x (2008).

39. Moloney, C. L. & Field, J. G. General allometric equations for rates of nutrient uptake, ingestion, and respiration in plankton organisms. *Limnology and Oceanography* **34**, 1290–1299, https://doi.org/10.4319/lo.1989.34.7.1290 (1989).

40. Fussmann, G. F. *et al.* Ecological and Evolutionary Dynamics of Experimental Plankton Communities. *Advances in Ecological Research* **37**, 221–243, https://doi.org/10.1016/S0065-2504(04)37007-8 (2005).

41. Elena, S. F. & Lenski, R. E. Evolution experiments with microorganisms: The dynamics and genetic bases of adaptation. *Nature Reviews Genetics* **4**, 457–469, https://doi.org/10.1038/nrg1088 (2003).

42. Bracewell, R. N. *The Fourier Transform and its Applications*. Electrical engineering series, 3rd edn. (McGraw Hill International Editions, 1999).

43. Hindmarsh, A. C. *et al.* Sundials. *ACM Transactions on Mathematical Software* **31**, 363–396, https://doi.org/10.1145/1089014.1089020 (2005).

44. Van Der Walt, S., Colbert, S. C. & Varoquaux, G. The NumPy array: A structure for efficient numerical computation. *Computing in Science and Engineering* **13**, 22–30, https://doi.org/10.1109/MCSE.2011.37 (2011).

45. Hunter, J. D. Matplotlib: A 2D graphics environment. *Computing in Science and Engineering* **9**, 99–104, https://doi.org/10.1109/MCSE.2007.55 (2007).

46. Carpenter, S. R., Kitchell, J. F. & Hodgson, J. R. Cascading Trophic Interactions and Lake Productivity. *BioScience* **35**, 634–639, https://doi.org/10.2307/1309989 (1985).

47. Pace, M. L., Cole, J. J., Carpenter, S. R. & Kitchell, J. F. Trophic cascades revealed in diverse ecosystems. *Trends in Ecology and Evolution* **14**, 483–488, https://doi.org/10.1016/S0169-5347(99)01723-1 (1999).

48. Boit, A., Martinez, N. D., Williams, R. J. & Gaedke, U. Mechanistic theory and modelling of complex food-web dynamics in Lake Constance. *Ecology Letters* **15**, 594–602, https://doi.org/10.1111/j.1461-0248.2012.01777.x (2012).

49. Wollrab, S., Diehl, S. & De Roos, A. M. Simple rules describe bottom-up and top-down control in food webs with alternative energy pathways. *Ecology Letters* **15**, 935–946, https://doi.org/10.1111/j.1461-0248.2012.01823.x (2012).

50. May, R. M. Limit Cycles in Predator-Prey Communities. *Science* **177**, 900–902 (1972).

51. Hastings, A., Hom, C. L., Ellner, S., Turchin, P. & Godfray, H. C. J. Chaos in Ecology: Is Mother Nature s Strange Attractor? *Annual Review of Ecology and Systematics* **24**, 1–33 (1993).

52. Kendall, B. E. Estimating the magnitude of environmental stochasticity in survivorship data. *Ecological Applications* **8**, 184–193, https://doi.org/10.1890/1051-0761(1998)008[0184:ETMOES]2.0.CO;2 (1998).

53. Yamamichi, M., Yoshida, T. & Sasaki, A. Comparing the Effects of Rapid Evolution and Phenotypic Plasticity on Predator-Prey Dynamics. *The American Naturalist* **178**, 287–304, https://doi.org/10.1086/661241 (2011).

54. Hiltunen, T., Hairston, N. G., Hooker, G., Jones, L. E. & Ellner, S. P. A newly discovered role of evolution in previously published consumer-resource dynamics. *Ecology Letters* **17**, 915–923, https://doi.org/10.1111/ele.12291 (2014).

232

55. Klug, J. L., Fischer, J. M., Ives, A. R. & Dennis, B. Compensatory Dynamics in Planktonic Community Responses to pH Perturbations. *Ecology* **81**, 387–398 (2000).
56. Kovach-Orr, C. & Fussmann, G. F. Evolutionary and plastic rescue in multitrophic model communities. *Philosophical Transactions of the Royal Society B: Biological Sciences* **368**, 20120084, https://doi.org/10.1098/rstb.2012.0084 (2013).
57. Micheli, F. *et al.* The Dual Nature of Community Variability. *Oikos* **85**, 161–169, https://doi.org/10.2307/3546802 (1999).
58. Vasseur, D. A. & Gaedke, U. Spectral analysis unmasks synchronous and compensatory dynamics in plankton communities. *Ecology* **88**, 2058–2071, https://doi.org/10.1890/06-1899.1 (2007).
59. Gonzalez, A. & Loreau, M. The causes and consequences of compensatory dynamics in ecological communities. *Annual Review of Ecology, Evolution, and Systematics* **40**, 393–414, https://doi.org/10.1146/annurev.ecolsys.39.110707.173349 (2009).
60. Keitt, T. H. & Fischer, J. Detection of scale-specific community dynamics using wavelets. *Ecology* **87**, 2895–2904, https://doi.org/10.1890/0012-9658(2006)87[2895:DOSCDU]2.0.CO;2 (2006).
61. Abrams, P. A. & Roth, J. D. The effects of enrichment of three-species food chains with nonlinear functional responses. *Ecology* **75**, 1118–1130, https://doi.org/10.2307/1939435 (1994).
62. Letellier, C. & Aziz-Alaoui, M. A. Analysis of the dynamics of a realistic ecological model. *Chaos, Solitons and Fractals* **13**, 95–107, https://doi.org/10.1016/S0960-0779(00)00239-3 (2002).
63. Van Voorn, G. A. K., Kooi, B. W. & Boer, M. P. Ecological consequences of global bifurcations in some food chain models. *Mathematical Biosciences* **226**, 120–133, https://doi.org/10.1016/j.mbs.2010.04.005 (2010).
64. Guill, C. Alternative dynamical states in stage-structured consumer populations. *Theoretical Population Biology* **76**, 168–178, https://doi.org/10.1016/j.tpb.2009.06.002 (2009).
65. Beisner, B. E., Haydon, D. T. & Cuddington, K. Alternative stable states in ecology. *Frontiers in Ecology and the Environment* **1**, 376–382, https://doi.org/10.1890/100071 (2003).
66. Bender, E. A., Case, T. J. & Gilpin, M. E. Perturbation experiments in community ecology: theory and practice. *Ecology* **65**, 1–13, https://doi.org/10.2307/1939452 (1984).
67. Tilman, D. *et al.* The influence of functional diversity and composition on ecosystem processes. *Science* **277**, 1300–1302, https://doi.org/10.1126/science.277.5330.1300 (1997).
68. Naeem, S., Duffy, J. E. & Zavaleta, E. The functions of biological diversity in an age of extinction. *Science* **336**, 1401–1406, https://doi.org/10.1126/science.1215855 (2012).
69. Yachi, S. & Loreau, M. Biodiversity and ecosystem productivity in a fluctuating environment: The insurance hypothesis. *Proceedings of the National Academy of Sciences* **96**, 1463–1468, https://doi.org/10.1073/pnas.96.4.1463 (1999).
70. Loreau, M. *et al.* Biodiversity and ecosystem functioning: Current knowledge and future challenges. *Science* **294**, 804–808, https://doi.org/10.1126/science.1064088 (2001).
71. Grebogi, C., Ott, E. & Yorke, J. A. Chaotic attractors in crisis. *Physical Review Letters* **48**, 1507–1510, https://doi.org/10.1103/PhysRevLett.48.1507 (1982).
72. Scheffer, M. & Carpenter, S. R. Catastrophic regime shifts in ecosystems: Linking theory to observation. *Trends in Ecology and Evolution* **18**, 648–656, https://doi.org/10.1016/j.tree.2003.09.002 (2003).
73. Dublin, H. T., Sinclair, A. & McGlade, J. Elephants and Fire as Causes of Multiple Stable States in the Serengeti-Mara Woodlands. *The Journal of Animal Ecology* **59**, 1147–1164, https://doi.org/10.2307/5037 (1990).
74. Scheffer, M., Hosper, S. H., Meijer, M. L., Moss, B. & Jeppesen, E. Alternative equilibria in shallow lakes. *Trends in Ecology and Evolution* **8**, 275–279, https://doi.org/10.1016/0169-5347(93)90254-M (1993).
75. Scheffer, M. *et al.* Early-warning signals for critical transitions. *Nature* **461**, 53–59, https://doi.org/10.1038/nature08227 (2009).
76. Carpenter, S. R. *et al.* Early warnings of regime shifts: A whole-ecosystem experiment. *Science* **332**, 1079–1082, https://doi.org/10.1126/science.1203672 (2011).
77. Kéfi, S. *et al.* Early warning signals of ecological transitions: Methods for spatial patterns. *PLoS One* **9**, e92097, https://doi.org/10.1371/journal.pone.0092097 (2014).
78. Wissel, C. A universal law of the characteristic return time near thresholds. *Oecologia* **65**, 101–107, https://doi.org/10.1007/BF00384470 (1984).
79. Hastings, A. & Wysham, D. B. Regime shifts in ecological systems can occur with no warning. *Ecology Letters* **13**, 464–472, https://doi.org/10.1111/j.1461-0248.2010.01439.x (2010).
80. Boettiger, C. & Hastings, A. Early warning signals and the prosecutor's fallacy. *Proceedings of the Royal Society B: Biological Sciences* **279**, 4734–4739, https://doi.org/10.1098/rspb.2012.2085 (2012).
81. Kalinkat, G., Rall, B. C., Vucic-Pestic, O. & Brose, U. The allometry of prey preferences. *PLoS One* **6**, e25937, https://doi.org/10.1371/journal.pone.0025937 (2011).
82. McCann, K. S. The diversity–stability debate. *Nature* **405**, 228–233, https://doi.org/10.1038/35012234 (2000).
83. DeMott, W. R. Feeding selectivities and relative ingestion rates of Daphnia and Bosmina. *Limnology and Oceanography* **27**, 518–527, https://doi.org/10.4319/lo.1982.27.3.0518 (1982).
84. Murdoch, A. W. W., Nisbet, R. M., Mccauley, E., deRoos, A. M. & Gurney, W. S. C. Plankton Abundance and Dynamics across Nutrient Levels: Tests of Hypotheses. *Ecology* **79**, 1339–1356 (1998).
85. Sarnelle, O. & Wilson, A. E. Type III functional response in Daphnia. *Ecology* **89**, 1723–1732, https://doi.org/10.1890/07-0935.1 (2008).
86. Morozov, A. Y. Emergence of Holling type III zooplankton functional response: Bringing together field evidence and mathematical modelling. *Journal of Theoretical Biology* **265**, 45–54, https://doi.org/10.1016/j.jtbi.2010.04.016 (2010).
87. Seifert, L. I. *et al.* Heated relations: Temperature-mediated shifts in consumption across trophic levels. *PLoS One* **9**, e95046, https://doi.org/10.1371/journal.pone.0095046 (2014).
88. Oaten, A. & Murdoch, W. W. Functional response and stability in predator-prey systems. *The American Naturalist* **109**, 289–298, https://doi.org/10.1086/282998 (1975).
89. Lurling, M. & Beekman, W. Palmelloids formation in Chlamydomonas reinhardtii: defence against rotifer predators? *Annales de Limnologie - International Journal of Limnology* **42**, 65–72, https://doi.org/10.1051/limn/2006010 (2006).

Acknowledgements

Author Contributions

Theoretical work and numerical simulations were carried out by R.C., under joint supervision of C.G. and U.G. The initial project outline was developed by U.G., C.G. and T.K. The manuscript was written by R.C., in close cooperation with T.K., and with valuable comments and feedback by C.G. and U.G.

233

Additional Information

Supplementary information accompanies this paper at https://doi.org/10.1038/s41598-019-43974-1.

Competing Interests: The authors declare no competing interests.

Publisher's note: Springer Nature remains neutral with regard to jurisdictional claims in published maps and institutional affiliations.

Top predators govern multitrophic diversity effects in tritrophic food webs

Ruben Ceulemans [iD],[1] Christian Guill, and Ursula Gaedke

Institute of Biochemistry and Biology, University of Potsdam, Am Neuen Palais 10, Potsdam 14469 Germany

Abstract. It is well known that functional diversity strongly affects ecosystem functioning. However, even in rather simple model communities consisting of only two or, at best, three trophic levels, the relationship between multitrophic functional diversity and ecosystem functioning appears difficult to generalize, because of its high contextuality. In this study, we considered several differently structured tritrophic food webs, in which the amount of functional diversity was varied independently on each trophic level. To achieve generalizable results, largely independent of parametrization, we examined the outcomes of 128,000 parameter combinations sampled from ecologically plausible intervals, with each tested for 200 randomly sampled initial conditions. Analysis of our data was done by training a random forest model. This method enables the identification of complex patterns in the data through partial dependence graphs, and the comparison of the relative influence of model parameters, including the degree of diversity, on food-web properties. We found that bottom-up and top-down effects cascade simultaneously throughout the food web, intimately linking the effects of functional diversity of any trophic level to the amount of diversity of other trophic levels, which may explain the difficulty in unifying results from previous studies. Strikingly, only with high diversity throughout the whole food web, different interactions synergize to ensure efficient exploitation of the available nutrients and efficient biomass transfer to higher trophic levels, ultimately leading to a high biomass and production on the top level. The temporal variation of biomass showed a more complex pattern with increasing multitrophic diversity: while the system initially became less variable, eventually the temporal variation rose again because of the increasingly complex dynamical patterns. Importantly, top predator diversity and food-web parameters affecting the top trophic level were of highest importance to determine the biomass and temporal variability of any trophic level. Overall, our study reveals that the mechanisms by which diversity influences ecosystem functioning are affected by every part of the food web, hampering the extrapolation of insights from simple monotrophic or bitrophic systems to complex natural food webs.

Key words: food-web efficiency; functional diversity; machine learning; nutrient exploitation; production; random forest; temporal variability; top predator; trait diversity.

Introduction

In the face of rapid global biodiversity loss (Pimm et al. 2014), investigating the influence of biodiversity on ecosystem functioning is a highly important area of research. It has become clear that biodiversity is a predominant factor in determining relevant functions of ecosystems such as biomass production, resource use efficiency, and stability (Hooper et al. 2005, Tilman et al. 2006, Worm et al. 2006). A major factor affecting the link between biodiversity and these ecosystem functions is functional diversity, that is, the range of differences between the functions of species contained within the ecosystem (Petchey and Gaston 2006).

Mechanistically motivated studies into the role of functional diversity have mainly been performed in the context of simple communities consisting only of one or, at best, two trophic levels. Many of these studies restricted their focus to primary producer diversity, and were able to show its correlation with relevant ecosystem functions (reviewed by Cardinale et al. 2011). However, during the last two decades, more sophisticated theoretical and experimental studies linking both plant and consumer diversity to these ecosystem functions were conducted (see Thébault and Loreau 2003, Tirok and Gaedke 2010, Borer et al. 2012, Filip et al. 2014, Klauschies et al. 2016, Schneider et al. 2016, Seabloom et al. 2017, Flöder et al. 2018, and reviews by Duffy et al. 2007, Griffin et al. 2013, Barnes et al. 2018). In a recent experimental study, Wohlgemuth et al. (2017) demonstrated that producer diversity effects on the biomass distribution and production at higher trophic levels crucially depends on particular traits of the consumer level,

such as specialization and selectivity. Such studies highlight how the links between multitrophic functional diversity and ecosystem functioning are difficult to generalize, because of their high contextuality. The specific food webs that are studied, and the theoretical models used to study them, are often too different to enable a meaningful attempt at synthesis of their findings (Thébault and Loreau 2003, Barnes et al. 2018).

For this reason there is a clear need to understand the effects of diversity on ecosystem functions in a setting that is as general and context-free as possible. In addition, the high degree of interplay already observed between diversity of the primary producer and herbivore consumer level underlines the importance of including diversity of even higher trophic levels. In this study, we want to advance our understanding of how functional diversity affects ecosystem functioning in model communities by including a diverse third trophic level. Although it has often been highlighted how important the effects of the third trophic level on ecosystem functions are (Bruno and O'Connor 2005, Duffy et al. 2007, Abdala-Roberts et al. 2019, Daam et al. 2019, Ehrlich and Gaedke 2020), relatively few studies have attempted to take these effects into account explicitly. Ceulemans et al. (2019) showed that functional diversity increases the biomass production, temporal stability, and biomass transfer efficiency to higher trophic levels of a tritrophic food web, when diversity is increased simultaneously at all three trophic levels. This model analyzed one particular food-web structure in detail, which raises the question of whether the observed trends are to be expected in general, or whether they are context dependent as well.

Our study tackles this issue by investigating several different tritrophic food web configurations with respect to the same ecosystem functions. Such a method has been applied successfully in the past (Gilman et al. 2010, Kovach-Orr and Fussmann 2013, Poisot et al. 2013), but this study is the first where the diversity can be independently controlled on three trophic levels. We investigated eight different food-web configurations (Fig. 1), which differ in the trophic location at which functional diversity

may be present. We measured functional diversity of a trophic level by the difference between the functional traits of the two species residing there: when the trait difference between the species is large, so is the functional diversity, and vice versa. In this way, we were able to change the functional diversity of a trophic level without changing the number of species. Adopting such a trait-based rather than species-specific approach by analyzing functional diversity through trait differences, instead of using nonfunctional metrics of biodiversity such as species number, allows us to produce results of high generality (McGill et al. 2006, Hillebrand and Matthiessen 2009, Krause et al. 2014). Furthermore, the relatively simple and general structure of our food webs (see Fig. 1) makes our results accessible for verification by experimental studies, as they are often limited in how much complexity can be included.

Our model rests on few very general assumptions. The first is allometry, which states that larger organisms tend to grow slower than smaller ones (Kalinkat et al. 2013). Combined with the assumption that consumers tend to be larger than their prey, we obtain the general property that the mean growth rate should decrease as the trophic level increases. This strictly holds for pelagic systems (Gaedke and Kamjunke 2006), but also for other ones, except for the plant–herbivore interface (Brose et al. 2006). The third basic assumption is the frequently established trade-off between growth rate and defense (Herms and Mattson 1992; Hillebrand et al. 2000, Kneitel and Chase 2004, Ehrlich et al. 2017, 2020). It implies that slow-growing species are generally less affected by grazing than faster-growing species, which invest less in defense mechanisms because of energetic limitations. In addition, the nongrazing mortality terms (see Eq. 8) are of general nature and may be due to several different processes, such as basal respiration, the influence of parasites and viruses, or outflow in an experimental microcosm.

Importantly, food-web dynamics do not only depend on the topology of the food web, but also on the specific parametrization used, regarding both external environmental parameters as well as internal parameters such as growth rates, attack rates, and handling times. To
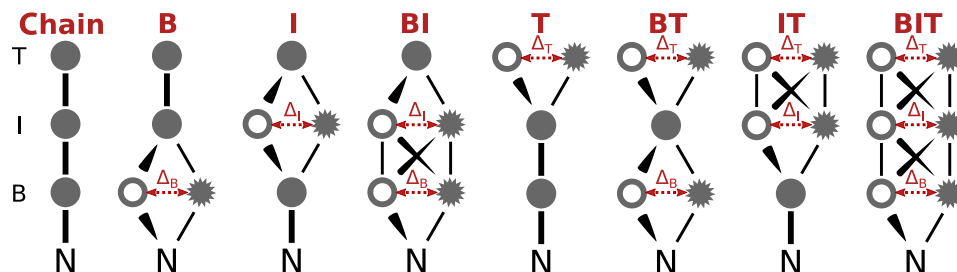

FIG. 1. Schematic overview of the eight different food webs compared in this study, which differ by the trophic levels (*B* for basal, *I* for intermediate, and *T* for top) on which diversity is possible (indicated above). In this way, chain refers to the linear chain that contains no diversity, *B* to the food web on which only the basal level is diverse, and so on, and finally *BIT* denotes the food web that contains diversity on all trophic levels. The thickness of the connections between the nodes illustrates the comparative intensity of the trophic interaction, which is determined by the amount of diversity, or the trait difference, between the species on each trophic level (Δ_B, Δ_I, and Δ_T). Each of these food webs are analyzed as generally as possible, with independently varying amounts of trait differences and parameters drawn randomly from biologically plausible intervals.

TABLE 1. Name and meaning of the parameters that were used in the study, along with the range from which they were sampled. For example, the nutrient inflow concentration N_0 was randomly sampled from the interval $[1/2, 2] \cdot 1{,}120 \approx [560, 2{,}240]$ µg N/l. In this table, $B\text{-}I$ refers to the functional response between the basal (B) and the intermediate (I) trophic level, and $I\text{-}T$ to the intermediate and top (T) level. The bottom three parameters were kept at fixed values.

Parameter	Meaning	Range
N_0	Nutrient inflow concentration	$[1/2, 2] \cdot 1{,}120$ µg N/l
h_N	Nutrient uptake half-saturation const.	$[1/2, 2] \cdot 10$ µg N/l
r'_0	Basal growth rate	$[1/2, 2] \cdot 1/\mathrm{d}$
a_0	$B\text{-}I$ attack rate	$[1/2, 2] \cdot 1.04 \times 10^{-3}/$ (d µg C/l)
h_0	$B\text{-}I$ handling time	$[1/2, 2] \cdot 1.15 \cdot \mathrm{d}$
α_0	$I\text{-}T$ attack rate	$[1/2, 2] \cdot 4.48 \times 10^{-4}/$ (d µg C/l)
η_0	$I\text{-}T$ handling time	$[1/2, 2] \cdot 2.62 \cdot \mathrm{d}$
δ	Inflow rate	$[0.03, 0.06] \cdot 1/\mathrm{d}$
a_{scale}	Cross link scaling factor	$[1, 500]$
n	$B\text{-}I$ Hill exponent	$[1, 2]$
ν	$I\text{-}T$ Hill exponent	$[1, 2]$
e	Biomass conversion efficiency	0.33 (not varied)
c_N/c_C	Basal nitrogen-to-carbon ratio	0.175 (not varied)
τ_{inc}	Maximal trait increase	$1/2$ (not varied)

capture the potentially high variation in biomass dynamics sufficiently, we randomly selected a total of 128,000 parameter combinations from ecologically plausible intervals for the eight different food webs, as well as tested 200 initial conditions per parameter combination. These parameter values were drawn from intervals geometrically centered around values that are particularly relevant for planktonic systems (Ceulemans et al. 2019), but are sufficiently wide to capture the behavior of many different types of food webs (see Table 1). This procedure allows us to obtain results of high generality, as they apply to the average behavior of tritrophic systems, independent of its parametrization.

METHODS

The numerical data used in our study were obtained by storing the mean biomasses and coefficients of variation (CVs) of the following ordinary differential equation model:

$$
\begin{cases}
\dot{N} = \delta(N_0 - N) - \dfrac{c_N}{c_C}\sum_i r_i B_i \\[2mm]
\dot{B}_i = r_i B_i - \sum_j g_{ji} I_j - d_{B_i} B_i \\[2mm]
\dot{I}_i = e\sum_j g_{ij} I_i - \sum_j \gamma_{ji} T_j - d_{I_i} I_i \\[2mm]
\dot{T}_i = e\sum_j \gamma_{ij} T_i - d_{T_i} T_i
\end{cases}
\tag{1}
$$

where the indices $i, j \in \{1, 2\}$. N describes the free inorganic nutrients in the system, with the inflow concentration N_0, inflow rate δ, and nutrient-to-carbon ratio c_N/c_C. The loss rates d_{B_i}, d_{I_i}, and d_{T_i} represent losses proportional to the biomass present, such as basal respiration, sedimentation, or washout. The basal species' B_i uptake rate r_i is described by their maximal growth rate r'_i and nutrient uptake half-saturation constant h_N:

$$
r_i = r'_i \frac{N}{N + h_N}.
\tag{2}
$$

The interaction between the intermediate species I_i and the basal species B_j is described by a Holling–Type-III functional response that is determined by the attack rate a_{ij}, handling time h_{ij}, and the Hill exponent n:

$$
g_{ij} = a_{ij} \frac{B_j^n}{\sum_{j'} a_{ij'} h_{ij'} B_{j'}^n + 1}.
\tag{3}
$$

In the same way, the interaction between top species T_i and intermediate species I_j is given by

$$
\gamma_{ij} = \alpha_{ij} \frac{I_j^\nu}{\sum_{j'} \alpha_{ij'} \eta_{ij'} I_{j'}^\nu + 1}
\tag{4}
$$

with attack rate α_{ij}, handling time η_{ij}, and Hill exponent ν. Finally, the biomass conversion efficiency for the intermediate and top species is described by e.

Influence of trait differences on trait parameters

The parameters r'_i, h_{ij}, a_{ij}, η_{ij}, α_{ij}, and all death rates are determined by the trait differences Δ_B, Δ_I, and Δ_T, which each can vary from 0 (the two species at each trophic level are equal) to 1 (maximal trait differences). As trait differences increase, the species B_1, I_1, and T_1 will be metabolically more active, whereas B_2, I_2, and T_2 will be less active through modifying their maximal feeding rates (which equal the inverse of the handling times h_{ij} and η_{ij} for the intermediate and top species).

In our model, trait differences affect the relevant species' parameters symmetrically, such that an increase for species 1 leads to a decrease for species 2 by the same factor. Explicitly

$$
r'_1 = r'_0 \cdot B_{\mathrm{inc}} \quad h_{1i} \sim \frac{h_0}{I_{\mathrm{inc}}} \quad \eta_{1i} \sim \frac{\eta_0}{T_{\mathrm{inc}}}
$$
$$
r'_2 = \frac{r'_0}{B_{\mathrm{inc}}} \quad h_{2i} \sim h_0 \cdot I_{\mathrm{inc}} \quad \eta_{2i} \sim \eta_0 \cdot T_{\mathrm{inc}}
\tag{5}
$$

with

$$
B_{\mathrm{inc}} = 1 + \Delta_B \cdot \tau_{\mathrm{inc}} \quad I_{\mathrm{inc}} = 1 + \Delta_I \cdot \tau_{\mathrm{inc}} \quad T_{\mathrm{inc}} = 1 + \Delta_T \cdot \tau_{\mathrm{inc}}
\tag{6}
$$

so that they are unity for $\Delta_i = 0$, leaving the species' parameters unaffected, and maximal for $\Delta_i = 1$, where

τ_{inc} determines their maximal increase. Note that the handling times h_{ij} and η_{ij} depend on the trait differences of both the predator and the prey level, hence the proportional relationship ($\sim$) instead of equality (more information is provided; cf. Eqs. 7 and 9).

The universality of trade-offs in natural systems (Kneitel and Chase 2004, Ehrlich et al. 2017) implies that for any increase or decrease in growth rates, the species' loss rates must change correspondingly. Time and/or energy that is invested towards a certain defense strategy cannot be used for resource uptake, and thus, comes at the cost of a lower growth rate (and thus a higher handling time). Conversely, investing in a higher growth rate (lower handling time) tends to make a species more vulnerable to predation, as it leaves less time and/or energy for employing defense strategies. For simplicity, the loss rates are affected in the same way as the growth rates. Thus, B_{inc} affects the handling times h_{ij} as well as the death rates d_{B_i}, I_{inc} affects η_{ij} and d_{I_i}, and T_{inc} affects d_{T_i}, in the following way:

$$h_{i1} \sim \frac{h_0}{B_{inc}} \qquad \eta_{i1} \sim \frac{\eta_0}{I_{inc}}$$
$$h_{i2} \sim h_0 \cdot B_{inc} \quad \eta_{i2} \sim \eta_0 \cdot I_{inc} \tag{7}$$

and

$$d_{B_1} = \delta \cdot B_{inc} \quad d_{I_1} = \delta \cdot I_{inc} \quad d_{T_1} = \delta \cdot T_{inc}$$
$$d_{B_2} = \frac{\delta}{B_{inc}} \qquad d_{I_2} = \frac{\delta}{I_{inc}} \qquad d_{T_2} = \frac{\delta}{T_{inc}} . \tag{8}$$

The handling times h_{ij} and η_{ij} are thus dependent on both B_{inc} and I_{inc}, or I_{inc} and T_{inc}, respectively. Although the linear relationship that describes this dependence is almost certainly a simplification of biological reality, specifying a more complex relationship might make our model unnecessarily more complicated. As described in the next section, multiple parameter combinations will be investigated, which means that our approach is not limited to one single distinct trade-off curve.

Summarizing:

$$h = h_0 \begin{pmatrix} \dfrac{1}{B_{inc}I_{inc}} & \dfrac{B_{inc}}{I_{inc}} \\[2ex] \dfrac{I_{inc}}{B_{inc}} & B_{inc}I_{inc} \end{pmatrix}, \quad \eta = \eta_0 \begin{pmatrix} \dfrac{1}{I_{inc}T_{inc}} & \dfrac{I_{inc}}{T_{inc}} \\[2ex] \dfrac{T_{inc}}{I_{inc}} & I_{inc}T_{inc} \end{pmatrix}. \tag{9}$$

The interaction between predator–prey pairs is not only determined by the handling times h_{ij} and η_{ij}, but also by the attack rates a_{ij} and α_{ij}. In our model, these are responsible for determining the relative strength of the "cross" links between two adjacent trophic levels (e.g., $B_1 \rightarrow I_2$, etc.). As the functional diversity of adjacent trophic levels increases, these cross links will decrease in strength relative to the "parallel" links (e.g., $B_1 \rightarrow I_1$, etc.). The rate at which their strength decreases

is determined by the attack-rate scaling parameter a_{scale}. For details see Appendix S1. In this way, it is possible to describe a tightly linked food web for $a_{scale} \approx 1$, two largely separated tritrophic chains for $a_{scale} \gg 1$, or an intermediate situation.

Parameter selection

In order to capture a high diversity of dynamical outcomes, within a plausible ecological setting, the parameters of the food web were sampled uniformly from certain intervals determined by a standard value from which the boundaries are calculated (Table 1). These standard values are based on Ceulemans et al. (2019), and describe an ecologically realistic planktonic system with three trophic levels. In particular, the maximal growth rates (r'_0, e/h_0 and e/η_0) were set to correspond to an allometrically scaled food chain with the body mass ratios between adjacent trophic levels of 10^3, with an allometric scaling exponent of -0.15. However, because of the spread of the intervals the actual ratio between body masses (assuming the same scaling exponent λ) can vary between approximately 1 and 10,000,000 (for details, see Appendix S2). In this way, a good balance is made between capturing a high amount of dynamical variation, while still being ecologically realistic.

The trait-difference parameters can take the following values:

$$\Delta_B \in \{0, 0.25, 0.5, 0.75, 1\}$$
$$\Delta_I \in \{0, 0.25, 0.5, 0.75, 1\} \tag{10}$$
$$\Delta_T \in \{0, 0.25, 0.5, 0.75, 1\}$$

so that there are 125 combinations possible. These determine both the specific food-web topology and the amount of functional diversity present. For example, $\Delta_B = 1$, $\Delta_I = 0.25$, and $\Delta_T = 0$ implies that we are investigating the *BI* food web (Fig. 1), where the basal level is highly diverse, but the species on the intermediate level are still relatively similar.

In order to sample a large part of all the possible dynamical outcomes that can be exhibited by our model, we randomly sampled 1,024 different parameter combinations, for each selection of Δ_B, Δ_I, and Δ_T (Eq. 10). Moreover, for every parameter combination, 200 different initial conditions were tested to capture potential alternative stable states. These initial values were randomly sampled such that the total amount of biomass in the initial state did not exceed $2 \cdot N_0$. The system was allowed to relax to its attractor before the mean biomasses and the CV of each species, and of each trophic level, were recorded for a sufficiently long time period. More detailed information on this procedure can be found in Appendix S3. Numerical integration of the ordinary differential equations in Eq. 1 was done in *C* with the SUNDIALS CVODE solver version 2.7.0 (Hindmarsh et al. 2005). Subsequent analysis of the

food-web data was performed in Python 3.6 using NumPy (Van Der Walt et al. 2011), pandas (McKinney 2010), and Matplotlib (Hunter 2007). Further details on our computational procedure, as well as the code itself and the data required to produce Figs. 3–6 and various Appendix figures can be found in Data S1 (Ceulemans et al. 2020).

Random forest model

In order to simplify the presentation of our results, and to extract additional relevant information easily, we trained a random forest model on our data set. A detailed description of how this works can be found in Appendix S3. Essentially, random forests are a class of machine learning models that are popularly used because of their relatively simple structure and high versatility (Breiman 2001, Cutler et al. 2007, Thomas et al. 2018).

For each quantity of interest (see Results), an extremely random forest consisting of 2,000 trees was trained using the Scikit-learn (Pedregosa et al. 2011) package in Python. Using only those parameter combinations that lead to coexistence of all species in the food web, the training data set consisted of the 14 different parameters (see Table 1 and Eq. 10) as input values, and the mean biomass and CVs of each trophic level as output values. During training, the random forest algorithm performed cross-validation by calculating the out-of-bag (OOB) score, to estimate its accuracy. After training the random forest model, we used it to investigate how the basal, intermediate, and top diversity (Δ_B, Δ_I, and Δ_T) affect the quantities of interest, independently of all other parameters, by examining the partial dependency graphs. Finally, the random forest also provided us with a measure of the importance of each of the input parameters in determining the desired outcome (relative importance).

Results

In order to understand in which ways diversity of different trophic levels affects tritrophic systems, we analyzed the solutions of the ordinary differential equation model presented in Methods (Eq. 1) for 128,000 different parameter combinations. For each parameter combination, we saved the mean nutrient concentration and biomass density (in short biomass) and CV of each individual population and trophic level over a long period of time (see also Appendix S3). In the main text, we will focus in particular on diversity effects on:

- the nutrient concentration N and biomass per trophic level B_B, B_I, B_T (see Fig. 3); and
- the CV of the nutrient concentration and biomass per trophic level CV_N, CV_B, CV_I, CV_T (see Fig. 4).

Based on the mean biomasses, we also calculated several quantities related to the flow of energy through the food web. The following ones are shown in the main text (see Fig. 5, and Eq. 1 and Appendix S5 for more information):

- the biomass production on the top level $P_T = \sum_i d_{T_i} T_i$;
- the amount of basal biomass flowing upward to the intermediate level B_{up};
- the production to biomass ratio of the basal level $(P/B)_B = (B_{up} + \sum_i d_{B_i} B_i)(\sum_i B_i)$; and
- the food-web efficiency, defined as the ratio between the biomass production at the top and the basal level: P_T/P_B.

Figs. 3–5 are partial dependence graphs revealing how trait differences on the basal (Δ_B), intermediate (Δ_I), and top (Δ_T) level affect the quantity of interest. Such partial dependence graphs are calculated from the random forest model trained on the food-web data, and show the average value of the quantity of interest, independent of all other model parameters (see *Methods*). This presentation allows us to capture the full behavior of all food webs concisely, as they each occupy a certain location in the partial dependency graphs (Fig. 2). A concise summary of our main findings is presented in Table 2.

In most cases the OOB scores, which measure the accuracy of the random forest models, were above 0.60, with some exceptions (Table 3). Such scores indicate a sufficient model accuracy, as we focus on the average trends in the predicted quantity as a function of the functional diversity of different trophic levels, rather than on predictions for specific parameter values.
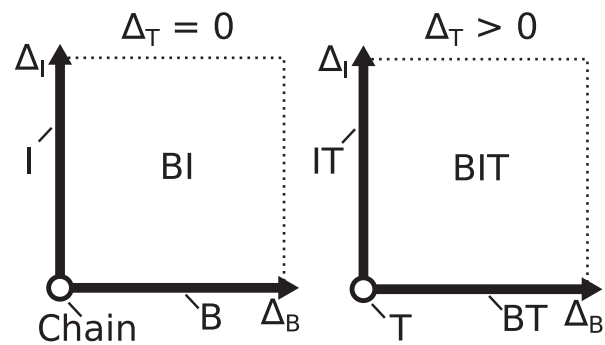

Fig. 2. Pictorial representation of the location of the different food webs (Fig. 1) in the partial dependence graphs in Figs. 3–5. On the left-side graph ($\Delta_T = 0$, that is, no diversity at the top level), the chain is on the point (0, 0) ($\Delta_B = \Delta_I = 0$), the B food web is located on the line $\Delta_I = 0$, the I food web is located on the line $\Delta_B = 0$, and the BI web is located in the plane where both Δ_B and Δ_I are nonzero. Similarly, on the right-side graph where $\Delta_T > 0$ (either low or high in Figs. 3–5), the T web is located on the point (0, 0) ($\Delta_B = \Delta_I = 0$), the BT food web is located on the line $\Delta_I = 0$, the IT food web is located on the line $\Delta_B = 0$, and finally the BIT web is located in the plane where Δ_B, Δ_I, and Δ_T are nonzero.

TABLE 2. Comparison of established knowledge of the link between the functional diversity and certain ecosystem functions of communities consisting of one or two trophic levels (see text for references), to our model where diversity can be changed at three trophic levels (see Fig. 1). Δ_i, B_i, and P_i refer to the diversity, biomass, and biomass production at trophic level $i \in \{B, I, T\}$, respectively (see Fig. 1 and Results), and the arrows indicate the direction in which these quantities are changing ($\uparrow$: increase, $\nearrow$: moderate increase, $\approx$: approximately constant, $\downarrow$: decrease). Our model enables us to understand the mechanisms responsible for top-down and bottom-up effects that simultaneously cascade through the food web.

Established knowledge	In our diverse tritrophic system	Shown
Top predators are often keystone species.	Confirmed, Δ_T and trophic interactions between I and T are most decisive for the biomasses, CVs, and energetics at all trophic levels.	Fig. 6
More diverse consumers exploit resources more efficiently.	Confirmed, diversity must be high throughout the whole food web for efficient exploitation.	Fig. 5
For a single trophic level in isolation: $\Delta_B \uparrow$ implies: $B_B \uparrow$, $P_B \uparrow$	Effects of changing Δ_i depend on the diversity of other trophic levels.	
For bitrophic systems: Δ_B and $\Delta_I \uparrow$: context-dependent effects on biomasses and production	However, when all $\Delta_i \uparrow$: $B_B \downarrow$, $B_I \uparrow$, $B_T \uparrow$ $P_B \approx$, $P_I \nearrow$, $P_T \uparrow$	Fig. 3 Fig. 5
For a single trophic level in isolation: $\Delta \uparrow$ implies: CV $\downarrow$	Effects of changing Δ_i depend on $\Delta_{j \neq i}$; however, all CVs first decrease, and then increase, with increasing Δ_T.	Fig. 4

TABLE 3. Out-of-bag (OOB) scores estimating the accuracy of the random forest model, for all outcome quantities. An OOB score of 1 represents a perfect model prediction, whereas an OOB score of 0 means that the model is as accurate as simply predicting the mean outcome value every time.

Outcome variable	Out-of-bag score
Nutrient density	0.44
Basal biomass	0.65
Intermediate biomass	0.92
Top biomass	0.77
Nutrient CV	0.26
Basal CV	0.73
Intermediate CV	0.68
Top CV	0.70
P_T/P_B	0.83
B_{up}	0.86
$(P/B)_B$	0.34
P_T	0.78

The quantities of interest were only examined for those initial conditions and parameter combinations that actually led to coexistence of all species originally present (see Fig. 1). Interestingly, there were only very few parameter combinations that led to coexistence for the top (T) (1 combination) and basal top (BT) (8 combinations) food webs (see Fig. 1, and Appendix S4). One of the two top species almost always outcompeted the other in these webs. As we cannot reliably investigate the behavior of these food webs in general, we did not include these parameter combinations in our data set. This implies that our data set contains no data points with $\Delta_T > 0$, $\Delta_I = 0$, and therefore, the region below $\Delta_I = 0.25$ for $\Delta_T > 0$ in Figs. 3–5 remains empty.

Nutrient concentration and biomasses

The partial dependency graphs of the free nutrient concentration and the biomasses on each trophic level on the trait differences Δ_B, Δ_I, and Δ_T (Fig. 3) reveal strong differences between the simple chain without any diversity ($\Delta_B = \Delta_I = \Delta_T = 0$), and the food web with high trait differences at every trophic level ($\Delta_B = \Delta_I = 1$ and $\Delta_T =$ high). Comparing these two points shows that the linear chain has a higher average free nutrient concentration and a lower intermediate and top biomass than the diverse food web.

In between these two extremes, the tritrophic structure of our model gives rise to several interesting patterns. Comparing the chain and the B, I and BI food webs (i.e., $\Delta_T = 0$; Fig. 3, left panels) shows that when Δ_I is 0 or low, increasing Δ_B leads to a decrease in basal biomass, whereas if Δ_I is high, this pattern reverses as the basal biomass increases with Δ_B. In other words, if functional diversity is only present on the basal level, basal biomass tends to decrease with Δ_B. However, taking consumer diversity into consideration in the BI food web shows that this pattern is not general and strongly depends on the actual level of consumer diversity (Δ_I).

Investigating the effect of Δ_I and Δ_T on the intermediate and top-level biomasses shows exactly the same pattern. When Δ_T is 0, intermediate biomass tends to decrease as Δ_I increases, whereas when Δ_T is high, it increases with Δ_I (independently of Δ_B). Additionally, it is clear that top biomass increases with Δ_T in a gradual fashion.

The location and strength of trophic cascading in the food web is also affected by the amount of functional diversity present on the different trophic levels. For example, when Δ_T is zero, an inverse relationship between the biomass on the intermediate and basal level can be observed, whereas the top-level biomass seems hardly affected by Δ_B and Δ_I (Fig. 3). When Δ_T is low, biomasses at the top and intermediate levels are strongly negatively correlated, indicating that a diverse top level is able to exert a stronger influence on the whole food web as compared to a nondiverse top level. This negative relationship does not cascade downwards to the basal
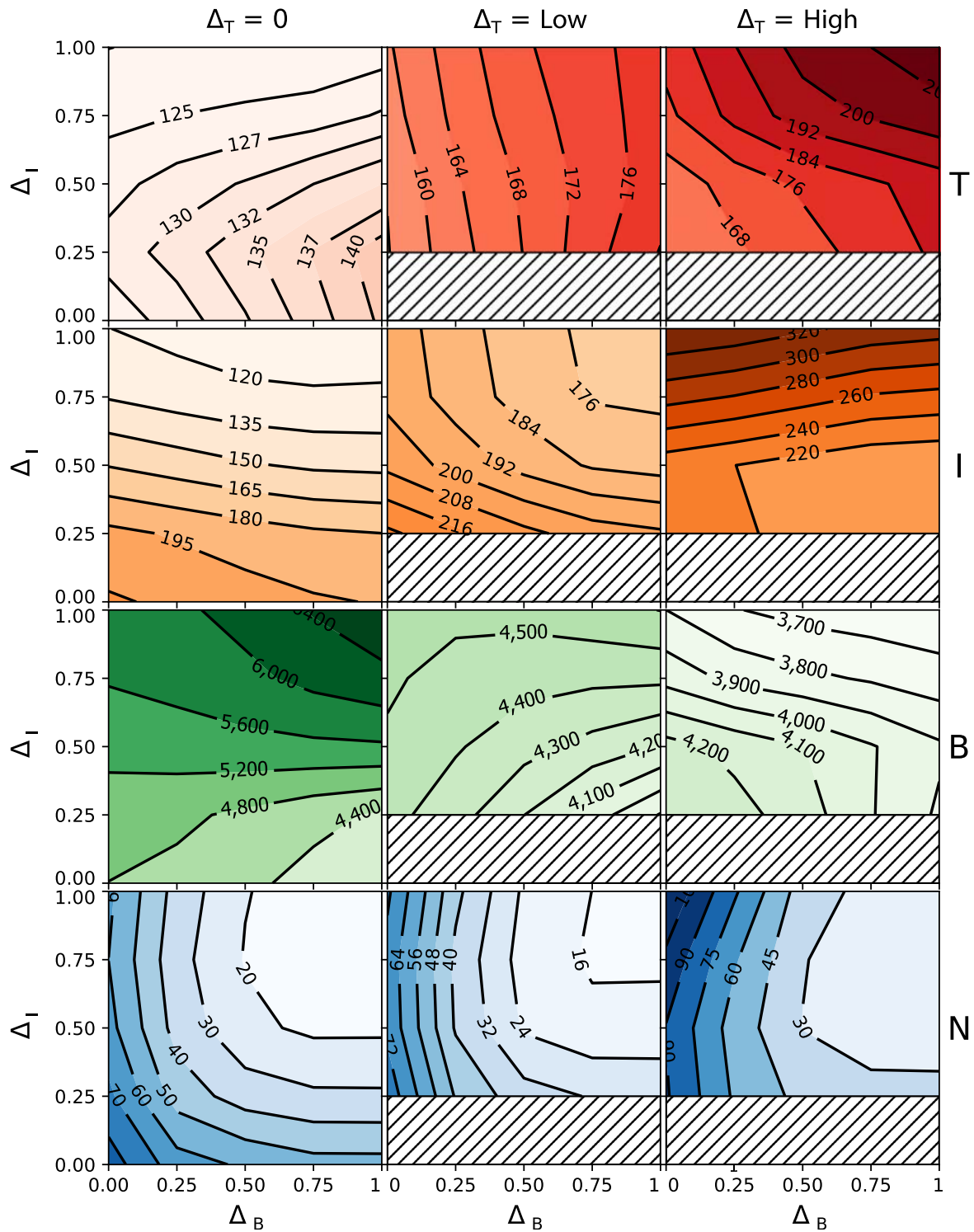
Fig. 3. Effect of trait differences at the basal (Δ_B), intermediate (Δ_I), and top (Δ_T) trophic levels on the free nutrient concentration (N, blue), and the biomasses on the basal (B, green), intermediate (I, orange), and top (T, red) trophic level, displayed as partial dependence graphs. To simplify the presentation, the effects of Δ_B and Δ_I are shown separately for three levels of Δ_T: $\Delta_T = 0$ (left), low Δ_T (0.25 and 0.5, middle), and high Δ_T (0.75 and 1, right). Fig. 2 shows a detailed explanation on how to read this figure. These graphs show the expected trends of N, B, I, and T as the amount of diversity of any trophic level is varied (for more information see Methods and Appendix S5). For example, in the chain (lower left corner of each subplot for $\Delta_T = 0$), T is expected to be much lower than in the highly diverse BIT web (upper right corner for $\Delta_T =$ high). When Δ_T is nonzero, the region below $\Delta_I = 0.25$ (T and BT webs) cannot be shown, as no coexisting parameter combination exists here because of the two distinct top species share only one resource.

level, potentially because of the buffering properties of a diverse intermediate level. However, for $\Delta_T =$ high, the strong inverse relationship between top and intermediate biomass is replaced by a rather positive one, because of the sharp increase in intermediate biomass as Δ_I is increased.

Temporal variation

We also examined how the functional diversity at each trophic level (Δ_B, Δ_I, and Δ_T) influences the temporal variation of the nutrients and biomasses per trophic level, by calculating the CV (Fig. 4). One clear overarching pattern is the covariation of the CVs along the different trophic levels. Temporal fluctuations at any trophic level propagate through the whole food web, affecting all other levels.

The left column shows how Δ_B and Δ_I affect the CVs of the food webs without top diversity ($\Delta_T = 0$). In this case, the CV of any trophic level depends almost solely on Δ_I. Only the CV of the nutrient concentration depends strongly on Δ_B.

These results are strongly affected by the top diversity. By increasing Δ_T from 0 to low, all CVs are considerably dampened. However, this trend reverses as Δ_T is increased further, as all CVs tend to increase again ($\Delta_T =$ high). Hence, while comparing the simple chain ($\Delta_B = \Delta_I = \Delta_T = 0$) to the food web with high trait differences ($\Delta_B = \Delta_I = 1$ and $\Delta_T =$ high) does not immediately show any notable differences, it is clear that temporal variability is strongly affected in an intricate way by the amount of functional diversity at the different trophic levels.

Additionally, there is a strong correlation between the CV of the basal trophic level, and the free-nutrient concentration (Fig. 3, bottom row). A low temporal variability on the basal level leads to a strong increase in nutrient exploitation efficiency, and therefore low nutrient concentrations.

Biomass production and food-web energetics

We also analyzed metrics related to biomass production and food-web energetics: biomass production on the top level P_T, basal biomass flowing to the intermediate level B_{up}, basal biomass to production ratio $(P/B)_B$, and the food-web efficiency P_T/P_B (Fig. 5, and Appendix S5 for more information on these quantities). Examining these (and related; see Appendix S5) quantities helped us to understand why the biomass at the top level is highest when functional diversity everywhere is high (top right corner in Fig. 3 for $\Delta_T =$ high). Importantly, we can infer the quantities P_I (total biomass production of the intermediate level) and I_{up} (biomass flowing from the intermediate to the top level) from B_{up} and P_T: $P_I = e \cdot B_{up}$, and $I_{up} = P_T/e$ (see also Appendix S5).

The biomass production by the basal level P_B varies only little, as this quantity is completely determined by

the interaction with the free nutrients (see Appendix S6). This property lies at the basis for explaining the increase in top biomass and food-web efficiency as functional diversity increases everywhere.

When $\Delta_T = 0$, the absence of a diverse top trophic level creates a slight relative advantage for the fast-growing species I_1 (see Appendix S7: Fig. S1). Its effects on the basal level strongly depend on Δ_I. For high Δ_I, the fast growing B_1 is heavily suppressed and the basal biomass is concentrated in B_2, which is less edible for the prominent I_1. For low Δ_I (i.e., I_1 and I_2 are functionally similar and less specialized), the dominant I_1 can also graze significantly on the slow-growing B_2, which strongly promotes the fast-growing B_1. The higher growth rate of B_1 causes strong fluctuations of the basal biomass (Fig. 4), which, in turn, leads to less efficient nutrient exploitation (Fig. 3). Thus, for both low and high intermediate diversity, the basal level is unevenly exploited, which leads to a relatively high proportion of basal biomass being lost from the system, instead of being transferred up the food web (see also Appendix S7: Fig. S5). The rather low basal biomass that is transferred to the intermediate level supports only a modest amount of intermediate biomass, and hence, a low biomass and biomass production on the top level, and a low food-web efficiency.

In contrast, when the top level is highly diverse ($\Delta_T =$ high), the intermediate level is more evenly exploited, leading to a balanced presence of both intermediate species. In turn, this leads to an efficient exploitation of the basal level, especially when Δ_I is also high, which is reflected by high values of $(P/B)_B$ (Fig. 5). Even though P_B remains roughly the same (Appendix S5: Fig. S2, and Appendix S6), B_{up} is increased (Fig. 5) which leads to a significantly higher intermediate biomass and biomass production (Fig. 3; Appendix S5: Fig. S2), and, ultimately an increase in biomass on the top level. This increase subsequently explains the increase in food-web efficiency through an increased top biomass production (Fig. 5).

Relative importance of parameters

The random forest model provides an estimate for the importance of each of the food-web parameters in predicting the outcome (see *Methods*). Fig. 6 shows them for the different biomasses and CVs for each of the 14 model parameters (for the relative importance of the different production metrics, see Appendix S5: Fig. S4).

The parameters are grouped by their mean importance in descending order in each graph. For example, the Hill exponent of the functional response describing the intermediate–top interaction (ν) has the highest mean relative importance for predicting the biomasses on each trophic level (Fig. 6, top). In particular, it is very important for predicting the biomass on the top and intermediate level. On the other hand, the nutrient-uptake half saturation constant h_N is the least important.
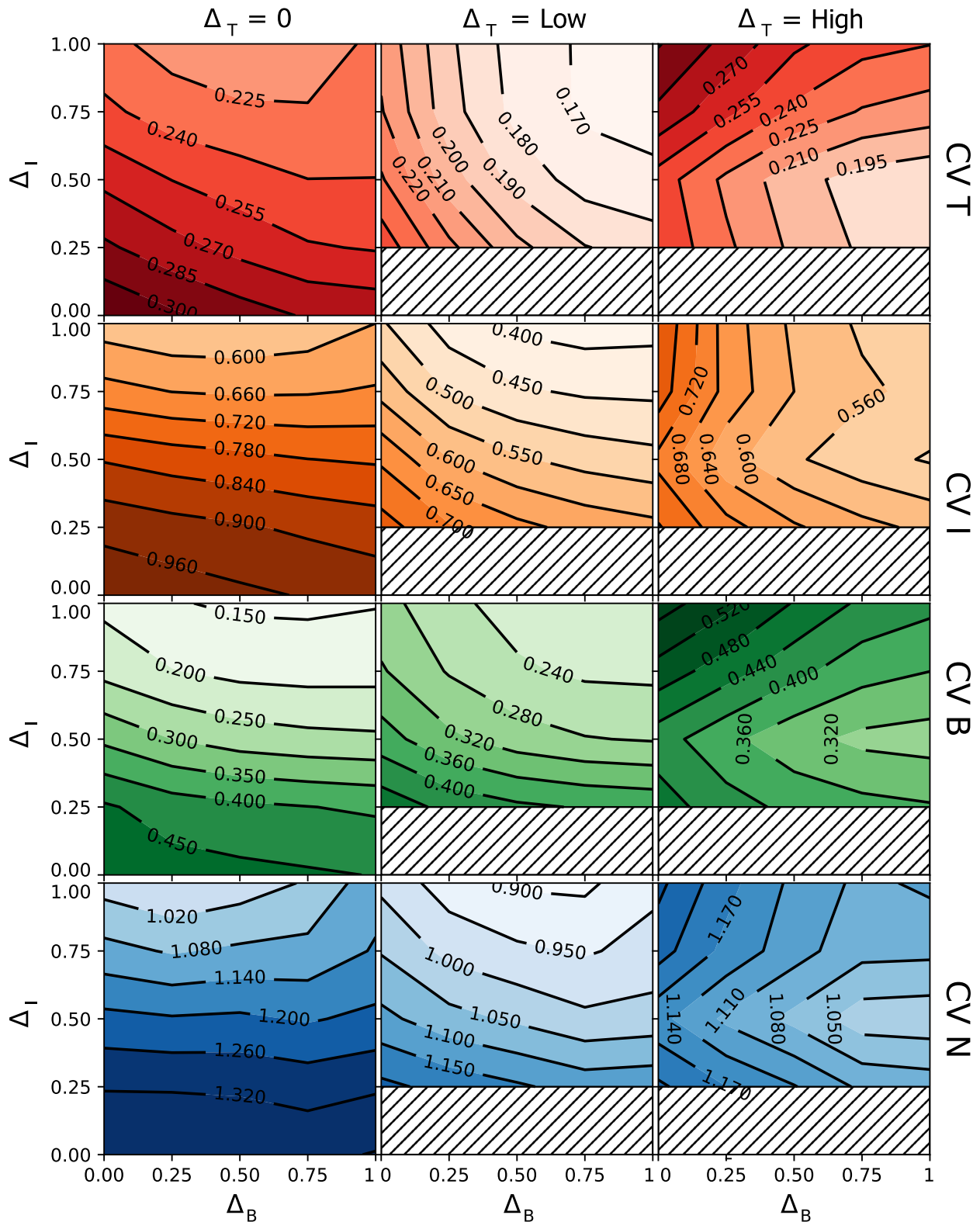
Fig. 4. Effect of trait differences at the basal (Δ_B), intermediate (Δ_I), and top (Δ_T) trophic level on the coefficient of variation of the free nutrient concentration (N, blue), the total biomass at the basal (B, green), intermediate (I, orange), and top (T, red) trophic levels, displayed as partial dependence graphs. Consult Figs. 2 and 5 for a detailed description on how to read this figure. Strikingly, we can see that Δ_T has a nonmonotonous effect on the temporal variability of the whole food web: a moderate amount of top predator diversity tends to decrease the temporal variation, but adding yet more diversity to the food web causes it to increase again.

One important observation in all three panels is that although the three possible trait differences Δ_B, Δ_I, and Δ_T have a strong influence on all the different quantities we have investigated (see Figs. 3–5), they are never among the most important parameters. However, this is not very surprising given the nature of the other parameters in our model: For example, it is very natural that increasing the nutrient inflow concentration N_0 has a very strong influence on species' biomasses.

Our results also show a balance between the relative importance of parameters affecting the external environment (such as the nutrient inflow concentration N_0 and the inflow rate δ), and internal parameters affecting the ecological dynamics within the food web (such as the handling times h_0, η_0, and Hill exponents n, ν). Remarkably, parameters affecting the intermediate–top interaction (ν, η_0, α_0) are of higher importance than their intermediate–basal analogues (n, h_0, a_0). In particular, the importances of the different diversity measures Δ_T, Δ_I, Δ_B are consistently ranked by trophic level. In this way, it is clear that food-web parameters affecting the top level of are of highest importance.

DISCUSSION

The food-web model analyzed in this manuscript was built with the aim of being as general as possible, while still being ecologically realistic. Given the expansive range of different environmental and ecological situations that are effectively covered by the model, we did not intend to answer research questions about specific environmental or ecological conditions. Rather, we focused on how the *average* behavior of tritrophic systems depends on the diversity of each trophic level separately. In particular, we studied how functional diversity in tritrophic food webs affects the biomass distribution, temporal variability, and production, on average. The partial dependence graphs provided by training a random forest model on our data served as an ideal tool to answer these questions. Given the high number of parameters that were randomly sampled, it is to be expected that the output data have a high degree of variation. For example, parameters like the inflow nutrient concentration N_0, or the inflow rate δ naturally have a very strong influence on the trophic-level biomasses and temporal variation. Partial dependence graphs revealed how the predicted outcome changes as a function of one particular parameter, on average, that is, independently of all other model parameters (cf. Table 2).

Absence of coexistence in some webs

In two of the food webs we investigated, *T* and *BT* (see Fig. 1), coexistence of all species was extremely rare (see Appendix S4). In almost every case, one of the two top species outcompeted the other one, as expected when applying the competitive exclusion principle (Hardin 1960, Armstrong and McGehee 1980, Klauschies and

Gaedke 2019). For only <0.1% of the parameter combinations did both top species still co-occur at the end of the simulation time. The structure of these two food webs entails that the two top species are competing with each other for only one resource, *I*, with no other density-dependent interaction.

In contrast, all species frequently coexisted in the intermediate (*I*) and intermediate top (*IT*) food webs (see Fig. 1), even though the two intermediate species also share a single resource, *B*. This is because of an additional density-dependent interaction acting on the intermediate species, by the presence of the top level (which may or may not be diverse). Therefore, more than one species can exist at the intermediate level without the necessity of fine-tuning their interaction parameters (Huntly 1991, Brose 2008, van Velzen 2020).

Viewed in this way, it is clear that the amount of functional diversity of one trophic level can drastically influence that of other trophic levels: a loss of functional diversity at the intermediate level in the *IT* or basal intermediate top (*BIT*) food webs (see Fig. 1) leads to a loss of functional diversity at the top level as well. It is therefore crucial to safeguard functional diversity of lower trophic levels to maintain diversity at higher trophic levels.

Relative parameter importance

The random forest model trained on the output data of our simulations (see Methods) provides information on which of the input parameters (see Table 1) are most important for estimating the predicted biomasses, CVs, and production metrics. In short, a parameter is of high importance when it tends to appear high up in many different trees in the forest. Conversely, when a parameter only appears near the end of the trees, it is of low importance in estimating the desired outcome. These relative importances are ranked from highest to lowest in Fig. 6.

Remarkably, parameters directly affecting the top trophic level tend to be of high importance, whereas parameters influencing the nutrient uptake by the basal species are all situated near the bottom end. The different diversity indices Δ_B, Δ_I, and Δ_T are also ranked by trophic level. This hierarchy shows how important the higher trophic levels are in determining the biomass distributions, temporal variation of biomass dynamics, and energetics of whole food webs. Our model is thus able to support mechanistically the general observation that changing the diversity of the top trophic level often has far-reaching consequences (Ripple et al. 2014).

In addition to most of the parameters governing the trophic interactions of the top trophic level, the nutrient inflow rate δ and concentration N_0 are also of high importance. As δ determines the death rates of all the species in the model (see Eq. 8), and in particular those of the top level, it has a strong influence on the quantities we have investigated (Kath et al. 2018). The nutrient inflow concentration is unsurprisingly also of high
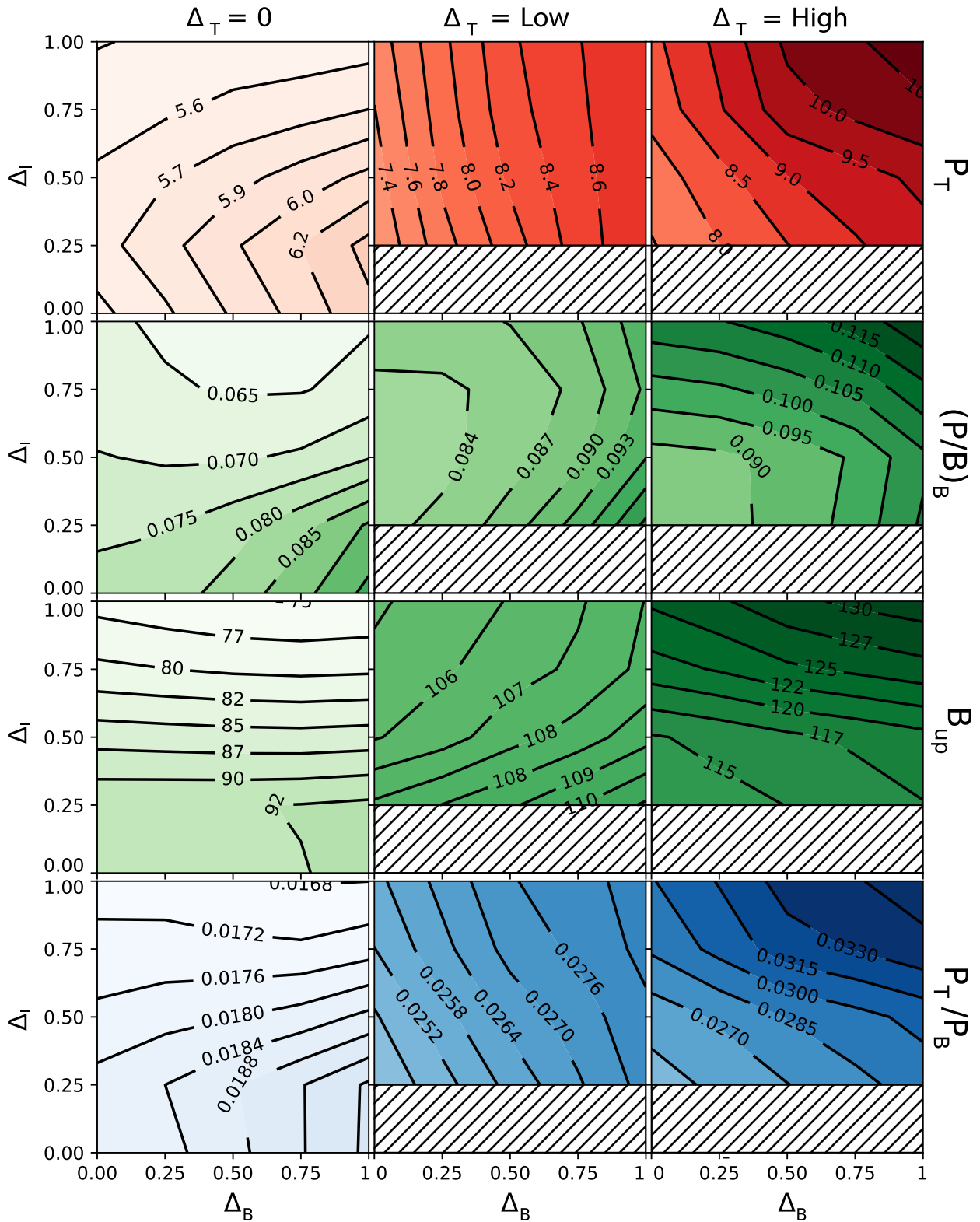
FIG. 5. Effect of trait differences at the basal (Δ_B), intermediate (Δ_I), and top (Δ_T) trophic level on several different metrics related to the flow of biomass and energy through the food web, displayed as partial dependence graphs. From top to bottom: top biomass production P_T, basal production to biomass ratio ($(P/B)_B$), basal biomass flowing to I (B_{up}), and the food web efficiency P_T/P_B. Consult the Results and Appendix S5 for more information on these quantities, and Figs. 2 and 3 for a detailed description on how to read this figure. In the chain (lower left corner for $\Delta_T = 0$), we observe for example a much lower P_T/P_B than in the highly diverse *BIT* web (upper right corner for Δ_T = high), which means biomass produced by the basal trophic level is transferred much more efficiently to the top level.

importance in estimating these quantities. Its level, representing the total biomass carrying capacity of our system, affects the basal trophic level most strongly (Fig. 6), which is in line with field observations (Gaedke 1998).

This analysis shows that the relative importance measures provided by the random forest model provide useful information to uncover the underlying mechanisms that govern the dynamics of more complex models. Our results clearly show how external and internal food-web parameters do not overpower each other. Information on both types is required for accurately predicting biomasses, biomass variability, and food-web energetics.

The complex relationships between diversity and ecosystem functioning

Our results show that functional diversity robustly increases biomass and production efficiency (Fig. 5) at high trophic levels (Fig. 3), and generally decreases temporal variation (Fig. 4), as summarized by Table 2. In addition, we reveal intricate and complicated interactions between the degree of diversity at different trophic levels and these ecosystem functions. These interactions complicate the comparison of studies on the links between diversity and functioning in a bitrophic context (Filip et al. 2014, Wohlgemuth et al. 2017, Flöder et al. 2018, Daam et al. 2019).

For instance, our model shows that the effect of increasing producer diversity on the biomasses of each trophic level highly depends on the amount of functional diversity of the other trophic levels (Fig. 3). When the top level is not functionally diverse ($\Delta_T = 0$), the direction of the effect of Δ_B on the basal biomass is determined by the amount of functional diversity of the intermediate level (Δ_I). When Δ_I is low, basal and intermediate biomasses tend to decrease with increasing Δ_B, whereas this trend reverses as Δ_I becomes higher. A recent experimental study revealed that the effects of producer diversity on food-web functioning also depend on the trait values on the consumer level in a bitrophic system (Wohlgemuth et al. 2017). Our results indicate that this interdependency is of a very general nature, and moreover, is expected to hold for higher trophic levels as well, which are less manageable in experimental settings. Indeed, our model shows a similar pattern when investigating the effect of Δ_I and Δ_T on the intermediate and top biomasses. Starting from $\Delta_T = 0$, increasing Δ_I leads to a reduction in intermediate biomass, in contrast to an increase in intermediate biomass when Δ_T is high.

Our tritrophic food-web comparison also shows that, when functional diversity is increased everywhere, the biomass of the intermediate and top species increases significantly, whereas the basal biomass stays roughly constant. The same pattern was found in a modeling study comparing food webs of up to 100 animal species (Schneider et al. 2016). This correspondence gives credibility to considering the effects of biodiversity on food-web functioning through changing the functional diversity in simpler food webs, instead of changing the species number, which significantly increases food-web complexity.

The effect of functional diversity on the temporal variability (CV) of the biomasses at the different trophic levels also exhibited a complex dependency on the functional diversity of every single trophic level (Fig. 4). One particularly robust result, however, is the non-monotonous relationship between top diversity (Δ_T) and the CV of any trophic level. When Δ_T is increased from 0 to low, the CVs often strongly decreased. Such a reduction in the CV with increasing diversity has often been observed (Tilman 1996), and attributed to the presence of compensatory dynamical patterns (Gonzalez and Loreau 2009, Bauer et al. 2014). However, as Δ_T is increased further from low to high, the CV of each trophic level increased again. Hence, additional mechanisms governing the dynamics must also have a strong influence of the trophic level CVs. In Ceulemans et al. (2019), we observed a similar pattern in the trophic level CVs, which could be explained by the increased relevance of an additional dynamical timescale at high Δ_T: the biomasses not only varied rapidly within predator–prey cycles, but also because of slower trait changes. As this slower timescale became more dominant, the CV increased again. Because of the similar model structure, this mechanism may be responsible for the increase in CV here as well. This result suggests that mechanisms for dampening community temporal variability established for simple but functionally diverse systems, such as compensatory dynamics arising from competition for a joint resource, may be counteracted by destabilizing effects in more complex—and thus more realistic—systems.

Examining how the functional composition at each trophic level and ecosystem functions are linked allows us to understand mechanistically why the biomass and biomass production on higher trophic levels is maximal when every trophic level is diverse, and why the diversity of the top level plays such a crucial role. This becomes particularly obvious when comparing the trends of the different metrics related to biomass production within the food web (see Results, Fig. 5, and Appendix S5: Fig. S4).

A functionally diverse consumer community leads to an efficient exploitation of the production at the prey level because of their functional complementarity (Gamfeldt et al. 2005). In our model, this mechanism is present between both the top and intermediate, as well as between the intermediate and basal level: a diverse top community efficiently exploits the intermediate production, which in turn results in the basal production being efficiently exploited. In contrast, when the top community is not functionally diverse, potentially functionally diverse intermediate and basal communities adjust in species composition so that they escape efficient predation (Filip et al. 2014, Seiler et al. 2017). As a
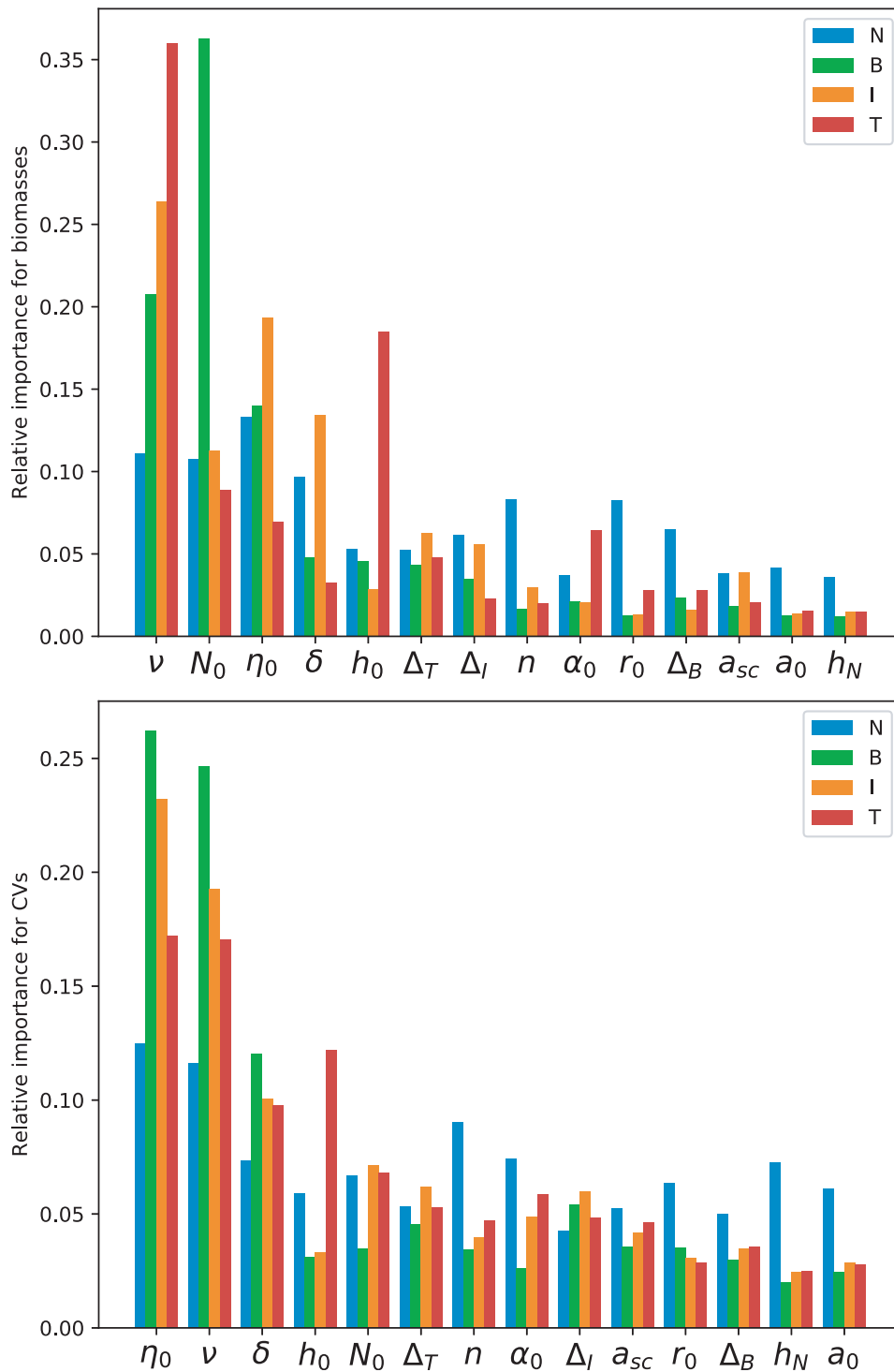
Fig. 6.   Relative importance of the different model parameters (see Table 1) on determining the biomasses and CVs of the different trophic levels. The relative importance quantifies how important the value of a certain parameter is to predict the desired quantity accurately, and they sum up to 1. The higher the relative importance of a parameter, the more relevant it is to make a prediction. In these graphs, the model parameters are ordered by their mean importance for each group of quantities (biomasses and CVs); for each parameter, the individual bars are ordered by trophic level.

consequence, a higher proportion of the production is lost from the system by nongrazing mortality rather than transferred up to the level above. In this way, the

effects of functional diversity of different trophic levels synergize to make the food web with diversity everywhere the most efficient configuration in transferring

biomass from the basal to the top level (Fig. 5, P_T/P_B, and Appendix S5: Fig. S2). Importantly, analysis of the individual populations' biomasses (Appendix S7: Fig. S1) confirms that the trade-offs function as intended and prevent any one species from dominating others on average. This provides additional evidence that the patterns we observe are caused by changes in trait differences between the species on each trophic level; that is, they are due to diversity effects.

The importance of considering multitrophic diversity has been emphasized before (Gamfeldt et al. 2005, Filip et al. 2014, Lefcheck et al. 2015, Soliveres et al. 2016, Barnes et al. 2018, Ceulemans et al. 2019). With these complex interactions between functional diversity of different trophic levels clearly exhibited by our model, it is not surprising that studies focusing on a single food-web structure or a single parametrization sometimes find incommensurable results. For example, increased primary producer diversity had often been linked to an increased producer biomass or biomass production (Tilman et al. 1997, Cardinale et al. 2011). Our results show that this relationship not only depends on the trait values of the consumer level (Seabloom et al. 2017, Wohlgemuth et al. 2017), but crucially also on the top level. Hence, we reveal considerable variation in the behavior of differently structured food webs with respect to the relationship between diversity and ecosystem functioning, explaining the incommensurable results arising from studies of specific systems. Nevertheless, we are able to identify clear trends and uncover mechanisms governing the behavior of tritrophic systems, even when considering a large range of different parameter combinations.

Concluding remarks

Understanding the link between functional diversity and the functioning of complex food webs is crucial to predict accurately how losses in functional diversity will affect the functions of natural food webs everywhere around us. Considerable detailed knowledge about this link has been gained in communities comprising one or two trophic levels. Partly, the knowledge gained from bitrophic systems helps us to understand tritrophic ones, such as the enhanced exploitation of resources by a more diverse consumer community. However, accounting for the third trophic level clearly shows that a restriction to two trophic levels may yield misleading results for complex natural food webs. The present comparison of several different food webs consisting of three trophic levels reveals simultaneously operating bottom-up and top-down cascading effects over three trophic levels. We uncover how food-web functioning may be affected differently, depending on the amount of functional diversity of every trophic level, which explains the incommensurable results from past studies based on a specific food-web structure. Importantly, we find that functional diversity at lower trophic levels is essential to

support diversity at higher trophic levels. At high functional diversity throughout the whole food web, functional shifts within the individual trophic levels result in a high food-web efficiency and biomass on higher trophic levels, and a high degree of nutrient exploitation. Additionally, we show that the functional diversity of the top level is a strongly regulating factor for the biomass, temporal variability, and biomass production efficiency of any trophic level. Therefore, to prevent drastic reduction of important functions, as well as potentially irreversible transitions, it is of crucial importance to increase our efforts in conserving diversity of higher trophic levels, despite the often large operational problems involved.

LITERATURE CITED

Abdala-Roberts, L., et al. 2019. Tri-trophic interactions: bridging species, communities and ecosystems. Ecology Letters 22:2151–2167.

Armstrong, R. A., and R. McGehee. 1980. Competitive exclusion. American Naturalist 115:151–170.

Barnes, A. D., M. Jochum, J. S. Lefcheck, N. Eisenhauer, C. Scherber, M. I. O'Connor, P. de Ruiter, and U. Brose. 2018. Energy flux: The link between multitrophic biodiversity and ecosystem functioning. Trends in Ecology and Evolution 33:186–197.

Bauer, B., M. Vos, T. Klauschies, and U. Gaedke. 2014. Diversity, functional similarity, and top-down control drive synchronization and the reliability of ecosystem function. American Naturalist 183:394–409.

Borer, E. T., E. W. Seabloom, and D. Tilman. 2012. Plant diversity controls arthropod biomass and temporal stability. Ecology Letters 15:1457–1464.

Breiman, L. 2001. Random forests. Machine Learning 45:5–32.

Brose, U. 2008. Complex food webs prevent competitive exclusion among producer species. Proceedings of the Royal Society B: Biological Sciences 275(1650):2507–2514.

Brose, U., R. J. Williams, and N. D. Martinez. 2006. Allometric scaling enhances stability in complex food webs. Ecology Letters 9:1228–1236.

Bruno, J. F., and M. I. O'Connor. 2005. Cascading effects of predator diversity and omnivory in a marine food web. Ecology Letters 8:1048–1056.

Cardinale, B. J., K. L. Matulich, D. U. Hooper, J. E. Byrnes, E. Duffy, L. Gamfeldt, P. Balvanera, M. I. O'Connor, and A. Gonzalez. 2011. The functional role of producer diversity in ecosystems. American Journal of Botany 98:572–592.

Ceulemans, R., U. Gaedke, T. Klauschies, and C. Guill. 2019. The effects of functional diversity on biomass production, variability, and resilience of ecosystem functions in a tri-trophic system. Scientific Reports 9. https://doi.org/10.1038/s41598-019-43974-1

Ceulemans, R., C. Guill, and U. Gaedke. 2020. Top predators govern multitrophic diversity effects: Data S1. https://doi.org/10.5281/zenodo.4672681.

Cutler, D. R., et al. 2007. Random forests for classification in ecology. Ecology 88:2783–2792.

Daam, M. A., H. Teixeira, A. I. Lillebø, and A. J. Nogueira. 2019. Establishing causal links between aquatic biodiversity and ecosystem functioning: Status and research needs. Science of the Total Environment 656:1145–1156.

Duffy, J. E., B. J. Cardinale, K. E. France, P. B. McIntyre, E. Thébault, and M. Loreau. 2007. The functional role of biodiversity in ecosystems: Incorporating trophic complexity. Ecology Letters 10:522–538.

Ehrlich, E., L. Becks, and U. Gaedke. 2017. Trait-fitness relationships determine how trade-off shapes affect species coexistence. Ecology 98:3188–3198.

Ehrlich, E., and U. Gaedke. 2020. Coupled changes in traits and biomasses cascading through a tritrophic plankton food web. Limnology and Oceanography 65(10):2502–2514.

Ehrlich, E., N. J. Kath, and U. Gaedke. 2020. The shape of a defense–growth trade off governs seasonal trait dynamics in natural phytoplankton. ISME Journal 14:1451–1462.

Filip, J., B. Bauer, H. Hillebrand, A. Beniermann, U. Gaedke, and S. D. Moorthi. 2014. Multitrophic diversity effects depend on consumer specialization and species-specific growth and grazing rates. Oikos 123:912–922.

Flöder, S., L. Bromann, and S. Moorthi. 2018. Inter- and intraspecific consumer trait variations determine consumer diversity effects in multispecies predator–prey systems. Aquatic Microbial Ecology 81:243–256.

Gaedke, U. 1998. The response of the pelagic community of a large and deep lake (L. Constance) to reoligotrophication: evidence for scale-dependent hierarchical patterns. Advances in Limnology 53:317–333.

Gaedke, U., and N. Kamjunke. 2006. Structural and functional properties of low- and high-diversity planktonic food webs. Journal of Plankton Research 28:707–718.

Gamfeldt, L., H. Hillebrand, and P. R. Jonsson. 2005. Species richness changes across two trophic levels simultaneously affect prey and consumer biomass. Ecology Letters 8:696–703.

Gilman, S. E., M. C. Urban, J. Tewksbury, G. W. Gilchrist, and R. D. Holt. 2010. A framework for community interactions under climate change. Trends in Ecology and Evolution 25:325–331.

Gonzalez, A., and M. Loreau. 2009. The causes and consequences of compensatory dynamics in ecological communities. Annual Review of Ecology, Evolution, and Systematics 40:393–414.

Griffin, J. N., J. E. K. Byrnes, and B. J. Cardinale. 2013. Effects of predator richness on prey suppression: A meta-analysis. Ecology 94:2180–2187.

Hardin, G. 1960. The competitive exclusion principle. Science 131:1292–1297.

Herms, D. A., and W. J. Mattson. 1992. The dilemma of plants: To grow or defend. Quarterly Review of Biology 67:283–335.

Hillebrand, H., and B. Matthiessen. 2009. Biodiversity in a complex world: Consolidation and progress in functional biodiversity research. Ecology Letters 12:1405–1419.

Hillebrand, H., B. Worm, and H. K. Lotze. 2000. Marine microbenthic community structure regulated by nitrogen loading and grazing pressure. Marine Ecology Progress Series 204:27–38.

Hindmarsh, A. C., P. N. Brown, K. E. Grant, S. L. Lee, R. Serban, D. E. Shumaker, and C. S. Woodward. 2005. Sundials. ACM Transactions on Mathematical Software 31:363–396.

Hooper, D. U., et al. 2005. Effects of biodiversity on ecosystem functioning: A consensus of current knowledge. Ecological Monographs 75:3–35.

Hunter, J. D. 2007. Matplotlib: A 2D graphics environment. Computing in Science and Engineering 9:99–104.

Huntly, N. 1991. Herbivores and the dynamics of communities and ecosystems. Annual Review of Ecology and Systematics 22:477–503.

Kalinkat, G., F. D. Schneider, C. Digel, C. Guill, B. C. Rall, and U. Brose. 2013. Body masses, functional responses and predator–prey stability. Ecology Letters 16:1126–1134.

Kath, N. J., A. Boit, C. Guill, and U. Gaedke. 2018. Accounting for activity respiration results in realistic trophic transfer efficiencies in allometric trophic network (ATN) models. Theoretical Ecology 11:453–463.

Klauschies, T., and U. Gaedke. 2019. Nutrient retention by predators undermines predator coexistence on one prey. Theoretical Ecology 13:183–208.

Klauschies, T., D. A. Vasseur, and U. Gaedke. 2016. Trait adaptation promotes species coexistence in diverse predator and prey communities. Ecology and Evolution 6:4141–4159.

Kneitel, J. M., and J. M. Chase. 2004. Trade-offs in community ecology: Linking spatial scales and species coexistence. Ecology Letters 7:69–80.

Kovach-Orr, C., and G. F. Fussmann. 2013. Evolutionary and plastic rescue in multitrophic model communities. Philosophical Transactions of the Royal Society B 368:20120084.

Krause, S., X. Le Roux, P. A. Niklaus, P. M. Van Bodegom, J. T. Lennon, S. Bertilsson, H.-P. Grossart, L. Philippot, and P. L. E. Bodelier. 2014. Trait-based approaches for understanding microbial biodiversity and ecosystem functioning. Frontiers in Microbiology 5:251.

Lefcheck, J. S., J. E. Byrnes, F. Isbell, L. Gamfeldt, J. N. Griffin, N. Eisenhauer, M. J. Hensel, A. Hector, B. J. Cardinale, and J. E. Duffy. 2015. Biodiversity enhances ecosystem multifunctionality across trophic levels and habitats. Nature Communications 6. https://doi.org/10.1038/ncomms7936

McGill, B. J., B. J. Enquist, E. Weiher, and M. Westoby. 2006. Rebuilding community ecology from functional traits. Trends in Ecology and Evolution 21:178–185.

McKinney, W. 2010. Data structures for statistical computing in python. Proceedings of the 9th Python in Science Conference 1697900:51–56.

Pedregosa, F., et al. 2011. Scikit-learn: Machine learning in Python. Journal of Machine Learning Research 12:2825–2830.

Petchey, O. L., and K. J. Gaston. 2006. Functional diversity: Back to basics and looking forward. Ecology Letters 9:741–758.

Pimm, S. L., C. N. Jenkins, R. Abell, T. M. Brooks, J. L. Gittleman, L. N. Joppa, P. H. Raven, C. M. Roberts, and J. O. Sexton. 2014. The biodiversity of species and their rates of extinction, distribution, and protection. Science 344:1246752.

Poisot, T., N. Mouquet, and D. Gravel. 2013. Trophic complementarity drives the biodiversity–ecosystem functioning relationship in food webs. Ecology Letters 16:853–861.

Ripple, W. J., et al. 2014. Status and ecological effects of the world's largest carnivores. Science 343:1241484.

Schneider, F. D., U. Brose, B. C. Rall, and C. Guill. 2016. Animal diversity and ecosystem functioning in dynamic food webs. Nature Communications 7:12718.

Seabloom, E. W., L. Kinkel, E. T. Borer, Y. Hautier, R. A. Montgomery, and D. Tilman. 2017. Food webs obscure the strength of plant diversity effects on primary productivity. Ecology Letters 20:505–512.

Seiler, C., E. van Velzen, T. R. Neu, U. Gaedke, T. U. Berendonk, and M. Weitere. 2017. Grazing resistance of bacterial

biofilms: A matter of predators' feeding trait. FEMS Microbiology Ecology 93:1–9.

Soliveres, S., et al. 2016. Biodiversity at multiple trophic levels is needed for ecosystem multifunctionality. Nature 536:456–459.

Thébault, E., and M. Loreau. 2003. Food-web constraints on biodiversity–ecosystem relationships. Proceedings of the National Academy of Sciences 100:14949–14954.

Thomas, M. K., S. Fontana, M. Reyes, M. Kehoe, and F. Pomati. 2018. The predictability of a lake phytoplankton community, over time-scales of hours to years. Ecology Letters 21:619–628.

Tilman, D. 1996. Biodiversity: population versus ecosystem stability. Ecology 77:350–363.

Tilman, D., C. L. Lehman, and K. T. Thomson. 1997. Plant diversity and ecosystem productivity: Theoretical considerations. Proceedings of the National Academy of Sciences 94:1857–1861.

Tilman, D., P. B. Reich, and J. M. H. Knops. 2006. Biodiversity and ecosystem stability in a decade-long grassland experiment. Nature 441:629–632.

Tirok, K., and U. Gaedke. 2010. Internally driven alternation of functional traits in a multispecies predator–prey system. Ecology 91:1748–1762.

Van DerWalt, S., S. C. Colbert, and G. Varoquaux. 2011. The NumPy array: A structure for efficient numerical computation. Computing in Science and Engineering 13:22–30.

van Velzen, E. 2020. Predator coexistence through emergent fitness equalization. Ecology 101:1–10.

Wohlgemuth, D., J. Filip, H. Hillebrand, and S. D. Moorthi. 2017. Prey diversity effects on ecosystem functioning depend on consumer identity and prey composition. Oecologia 184:653–661.

Worm, B., et al. 2006. Impacts of biodiversity loss on ocean ecosystem services. Science 314:787–790.

Supporting Information

Open Research